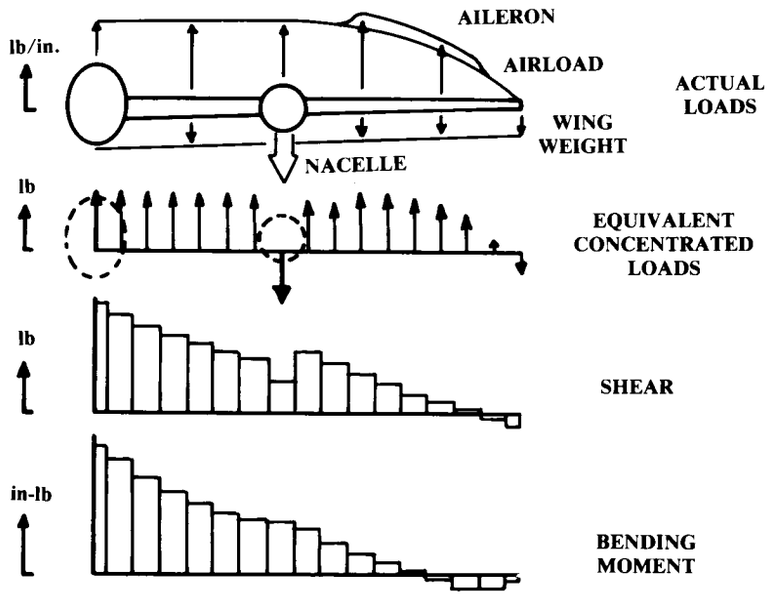

Fig. 14.38 Wing loads, shear, and bending moment.

The moments produced by the vertical loads must be balanced by a moment at the cut cross section. This moment is equal to the summation of the discrete loads times their distance from the cut station, or the integral of a distributed load with respect to the distance from the cut.

Figure 14.38 shows the typical loads on a wing. This shows the critical case of a rolling pullup, with the additional lift load of full aileron deflection. The lift and wing-weight loads are distributed, while the nacelle weight is concentrated. Remember that wing and nacelle weights are multiplied by the aircraft load factor to determine the load on the wing.

The easiest way to calculate the shear and moment distribution along a wing is to replace the distributed loads (lift and wing weight) by concentrated loads. The lift distribution can be determined with Schrenk's Approximation, described above. The wing weight will be determined in the next chapter, and can be assumed to be distributed proportional to the chord length.

Figure 14.39 shows the trapezoidal approximation for a distributed load, giving the total equivalent force and the spanwise location of that force. About ten to twenty spanwise stations will provide an accurate enough approximation for initial design purposes.

Once the distributed loads are replaced by concentrated loads, determination of the shear and bending moment distributions is easy. The shear at each span station is the sum of the vertical loads outboard of that station. The shear is found by starting at the wing tip and working inward, adding the load at each station to the total of the outboard stations.

The bending moment can be found for each span station by multiplying the load at each outboard station times its distance from the span station.

However, it is easier to graphically integrate by starting at the tip and working inward, adding to the total the area under the shear distribution at that station.

Referring back to Fig. 14.37, the bending moment at a cross-sectional cut is opposed by a combination of tension and compression forces in the spanwise direction. For a positive bending moment such as shown, the internal forces produce compression on the upper part of the beam and tension on the lower part. The vertical location in the beam at which there is no spanwise force due to bending is called the "neutral axis," and is at the centroid of the cross-sectional shape.

As long as the stresses remain within the elastic limit, the stresses vary linearly with vertical distance from the neutral axis regardless of the cross-sectional shape. These compression or tension stresses are found from Eq. (14.35) (for derivation, see Ref. 55), where M is the bending moment at the spanwise location and z is the vertical distance from the neutral axis. The maximum stresses due to bending are at the upper and lower surfaces.

$$\sigma_x = Mz/I_y \tag{14.35}$$

The vertical shear stresses within a beam are not evenly distributed from top to bottom of the cross section, so the maximum shear stress within the material can not be calculated simply as the total shear divided by the cross-sectional area.

Referring back to Fig. 14.20, it should be remembered that the vertical shear stresses on an element are balanced by and equal to the horizontal shear stresses. One cannot exist without the other. Therefore, the vertical shear distribution must be related to the horizontal shears in the beam.

Figure 14.40 shows a beam in bending, with the vertical distribution of compression and tension stresses. The total horizontal force on any element is the horizontal stress at the element's vertical location times the elemental

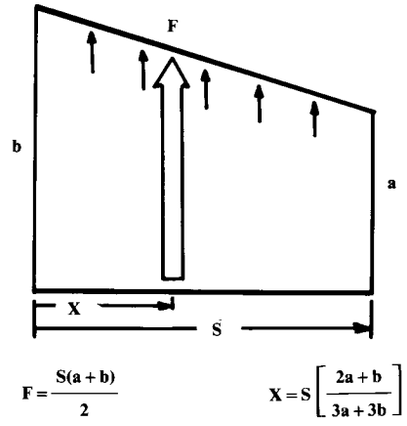

Fig. 14.39 Trapezoidal approximation for distributed loads.

area. If this beam is split lengthwise as shown, the upper section has only leftward forces, so a shear force must be exerted along the cut.

This shear force must be the sum of the horizontal stresses times the elemental areas above the cut. This reaches a maximum at the neutral axis. At the upper and lower surfaces, this shear force is zero.

The bottom of Fig. 14.40 shows the resulting vertical distribution of shear forces, expressed as magnitude toward the right. (Don't be confused by this presentation; the shear forces are exerted in a vertical direction, but we show the magnitude to the right to illustrate the distribution of magnitude from top to bottom.)

$$\tau = \frac{V}{bI_y} \int_{z1}^{h/2} z \, dA \tag{14.36}$$

Equation (14.36) describes this mathematically, where the integral term represents the area above the cut located at $z = z_1$. Note that the distribution of shear stresses depends upon the shape of the cross section. For a beam of rectangular cross section, the maximum shearing stress (at the neutral axis) is 1.5 times the averaged shearing stress (total shear divided by cross-sectional area). For a solid circular cross section, the maximum shearing stress is 1.33 times the averaged value.

Figure 14.41 shows a typical aircraft wing spar consisting of thick "spar caps" separated by a thin "shear web." The cross-sectional area of the

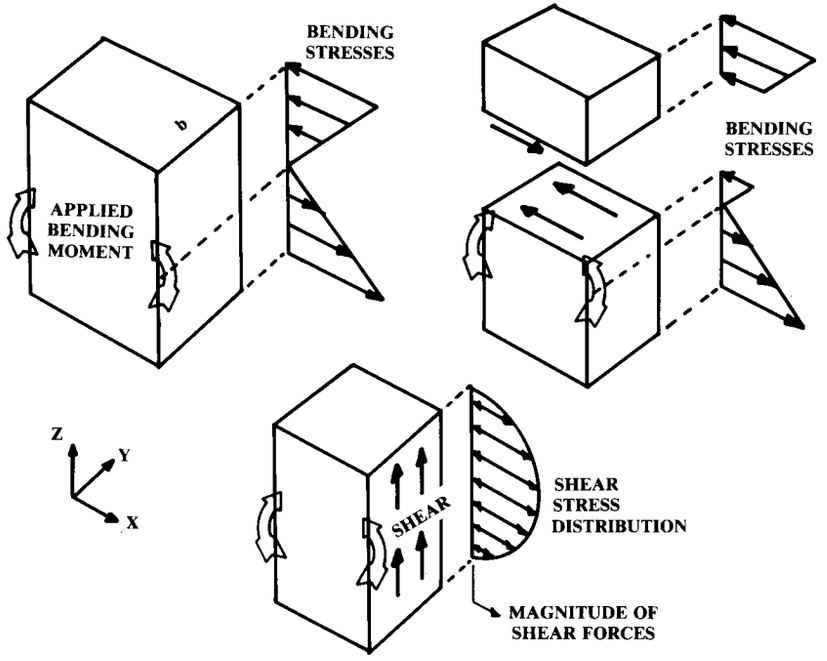

Fig. 14.40 Relationship between shear and bending.

shear web is insignificant compared to the area of the spar caps, so the caps absorb virtually all of the bending force (stress times area). The shear stress depends upon the cross-sectional area above the point of interest, and is therefore essentially constant within the thin shear web, as shown to the right.

In aircraft wing spar analysis it is common to assume that the caps absorb all of the bending stresses and that the web (extended to the full depth of the spar) absorbs all of the shear. This is shown at the bottom of Fig. 14.41. It is also assumed that the shear is constant within the web and therefore the maximum shear stress equals the average shear stress (shear divided by web area).

The shear web will fail in buckling long before the material maximum shear stress is reached. Equation (14.37) defines the critical buckling shear stress for a shear web. The value of K is obtained from Fig. 14.42.

$$F_{\text{shear buckle}} = KE(t/b)^2 \tag{14.37}$$

Braced-Wing Analysis

A wing braced with a strut will have the bending moments greatly reduced compared to a fully cantilevered wing. However, the analysis is more complex because of the spanwise compression loads exerted upon the wing by the strut. This can increase the bending moment by as much as a third compared to an analysis that ignores this compression effect.

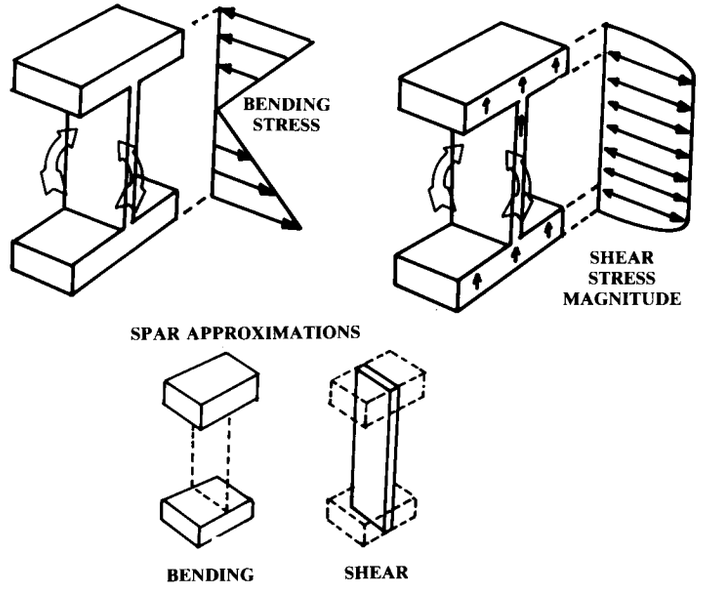

Fig. 14.41 Typical aircraft spar in bending and shear.

area. If this beam is split lengthwise as shown, the upper section has only leftward forces, so a shear force must be exerted along the cut.

This shear force must be the sum of the horizontal stresses times the elemental areas above the cut. This reaches a maximum at the neutral axis. At the upper and lower surfaces, this shear force is zero.

The bottom of Fig. 14.40 shows the resulting vertical distribution of shear forces, expressed as magnitude toward the right. (Don't be confused by this presentation; the shear forces are exerted in a vertical direction, but we show the magnitude to the right to illustrate the distribution of magnitude from top to bottom.)

$$\tau = \frac{V}{bI_y} \int_{z1}^{h/2} z \, dA \tag{14.36}$$

Equation (14.36) describes this mathematically, where the integral term represents the area above the cut located at $z = z_1$. Note that the distribution of shear stresses depends upon the shape of the cross section. For a beam of rectangular cross section, the maximum shearing stress (at the neutral axis) is 1.5 times the averaged shearing stress (total shear divided by cross-sectional area). For a solid circular cross section, the maximum shearing stress is 1.33 times the averaged value.

Figure 14.41 shows a typical aircraft wing spar consisting of thick "spar caps" separated by a thin "shear web." The cross-sectional area of the

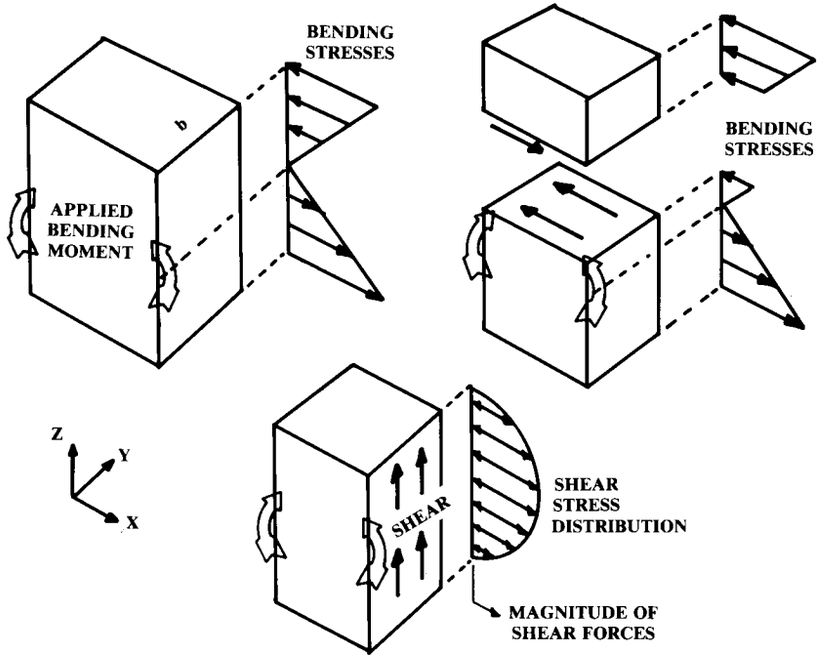

Fig. 14.40 Relationship between shear and bending.

shear web is insignificant compared to the area of the spar caps, so the caps absorb virtually all of the bending force (stress times area). The shear stress depends upon the cross-sectional area above the point of interest, and is therefore essentially constant within the thin shear web, as shown to the right.

In aircraft wing spar analysis it is common to assume that the caps absorb all of the bending stresses and that the web (extended to the full depth of the spar) absorbs all of the shear. This is shown at the bottom of Fig. 14.41. It is also assumed that the shear is constant within the web and therefore the maximum shear stress equals the average shear stress (shear divided by web area).

The shear web will fail in buckling long before the material maximum shear stress is reached. Equation (14.37) defines the critical buckling shear stress for a shear web. The value of K is obtained from Fig. 14.42.

$$F_{\text{shear buckle}} = KE(t/b)^2 \tag{14.37}$$

Braced-Wing Analysis

A wing braced with a strut will have the bending moments greatly reduced compared to a fully cantilevered wing. However, the analysis is more complex because of the spanwise compression loads exerted upon the wing by the strut. This can increase the bending moment by as much as a third compared to an analysis that ignores this compression effect.

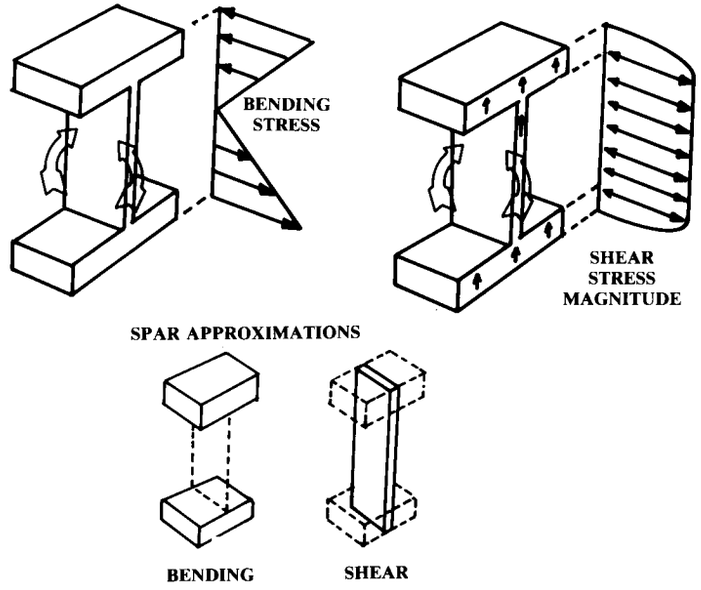

Fig. 14.41 Typical aircraft spar in bending and shear.

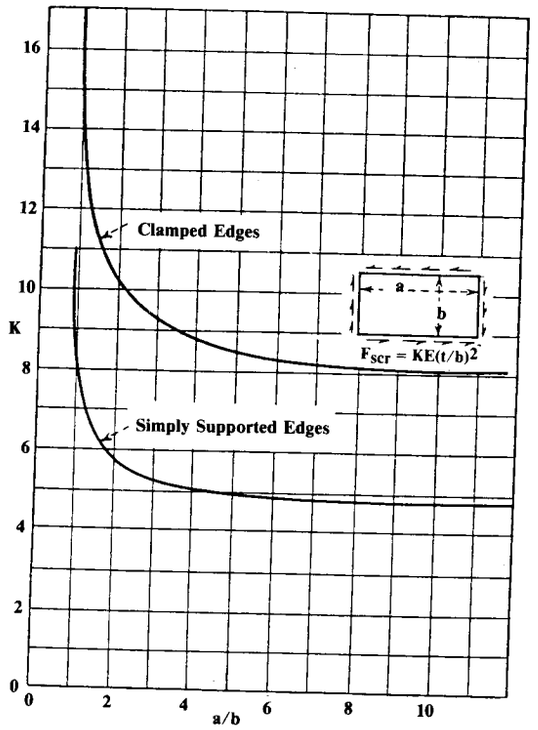

Fig. 14.42 Shear web buckling. (NACA TN3781)

Figure 14.43 shows a typical braced wing. The compression load P is the horizontal component of the force on the strut (S). The vertical component of S is found from summing the moments about the pin at the wing root, using the equivalent concentrated lift loads as discussed earlier.

The shear loads of the braced wing are analyzed as before, taking into account the large concentrated vertical load of the strut. The bending moment must be analyzed with special equations provided below.

The portion of the wing outboard of the strut is analyzed as before, and the bending moment at the strut location is determined (M_2). The root bending moment (M_1) is usually zero unless the hinge point is above or below the neutral axis, causing a bending moment due to the compression load P.

The lift distribution on the portion of the wing inboard of the strut must be approximated by a uniform load distribution (w). This is usually a reasonable approximation inboard of the strut. The following equations describe bending-moment distribution, maximum bending moment, and spanwise location of the maximum bending moment (Ref. 60):

$$M(x) = C_1 \sin(x/j) + C_2 \cos(x/j) + wj^2 \tag{14.38}$$

$$M_{max} = \frac{D_1}{\cos(x/j)} + wj^2 \tag{14.39}$$

$$\tan\left(\frac{x_m}{j}\right) = \frac{D_2 - D_1 \cos(L/j)}{D_1 \sin(L/j)} \tag{14.40}$$

where

$$j = \sqrt{EI/P} \tag{14.41}$$

$$C_1 = \frac{D_2 - D_1 \cos(L/j)}{\sin(L/j)} \tag{14.42}$$

$$C_2 = D_1 = M_1 - wj^2 \tag{14.43}$$

$$D_2 = M_2 - wj^2 \tag{14.44}$$

Torsion

Figure 14.44 shows a solid circular shaft in torsion. The applied torque T produces a twisting deformation ϕ that depends upon the length of the shaft. As shown at the right of the figure, the torque is resisted by shearing stresses that increase linearly with distance from the center—if the stresses remain within the elastic limit.

The shear stresses due to torsion are calculated with Eq. (14.45), and are at a maximum at the surface of the shaft ($r = R$). The angular deflection in

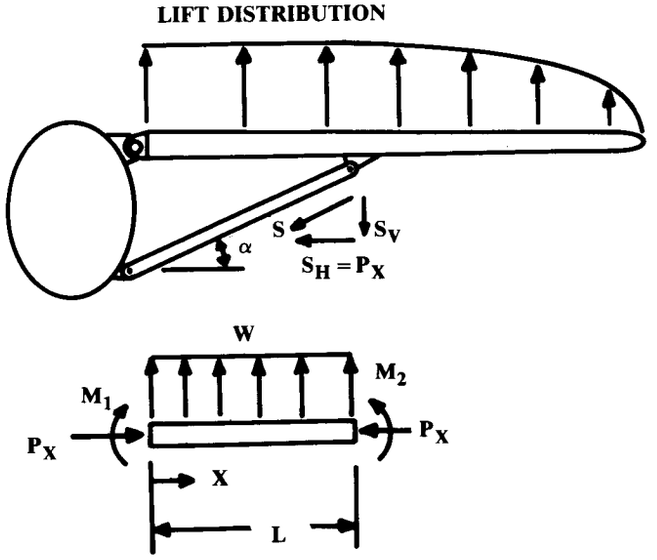

Fig. 14.43 Braced wing analysis.

radians is determined from Eq. (14.46). These equations also apply to circular tubing under torsion, using the appropriate value of Ip as provided previously.

$$\tau = Tr/I_p \tag{14.45}$$

$$\phi = TL/GI_p \tag{14.46}$$

For a noncircular member under torsion, the analysis is generally much more complex. Several special cases can be readily solved. A thin-walled, closed cross-sectional member with constant wall thickness t, total cross-sectional area A, and cross-sectional perimeter s has shear stress and angular deflection as defined by Eqs. (14.47) and (14.48).

$$\tau = T/2At \tag{14.47}$$

$$\phi = \frac{TL}{G}\left(\frac{s}{4A^2t}\right) \tag{14.48}$$

Solid rectangular members may be analyzed with Eqs. (14.49) and (14.50) using the values from Table 14.7, where t is the thickness of the member and

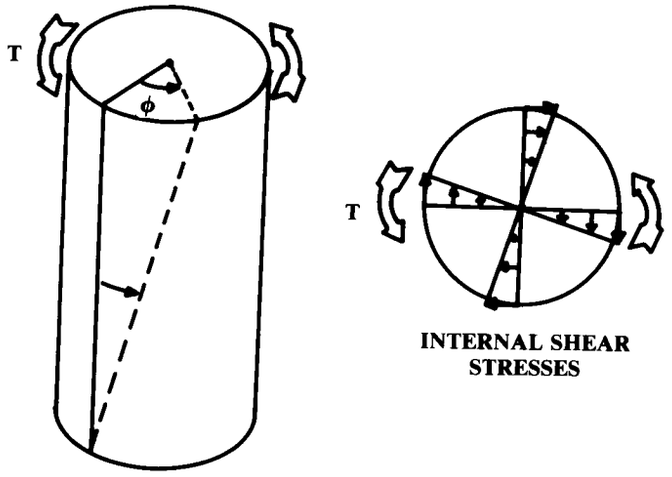

Fig. 14.44 Solid circular shaft in torsion.

Table 14.7 Torsion constants

t	1.00	1.50	1.75	2.00	2.50	3.00	4	6	8	10	∞
	0.208	0.231	0.239	0.246	0.258	0.267	0.282	0.299	0.307	0.313	0.3
	0.141	0.196	0.214	0.229	0.249	0.263	0.281	0.299	0.307	0.313	0.3

b is its width. These equations may also be applied to members bent up from flat sheet metal by "unwrapping" the member to find the total effective width.

$$\tau = \frac{T}{\alpha bt^2} \tag{14.49}$$

$$\phi = \frac{TL}{\beta bt^3 G} \tag{14.50}$$

Analysis of the torsional stresses in a complex shape such as a multicelled wing box goes beyond the scope of this book. See Ref. 60 for a discussion of such analysis.

14.11 FINITE-ELEMENT STRUCTURAL ANALYSIS

The structural-analysis methods described above, along with extensive handbooks and nomograms, have been used for many years for aircraft structural design. Today these methods are a dying art. Instead, virtually all major structural analysis is now performed using finite-element computer programs. Even today's homebuilders have access to finite-element programs using personal computers that are as powerful as the mainframe computers of the 1960's.

The Finite Element Method (FEM) is based upon the concept of breaking the structure of the aircraft into numerous small "elements," much like the gridding of the air-mass for CFD. Equations describing the structural behavior of these finite elements are prepared using various approximations of the end-constraints and deflection shapes for the element.

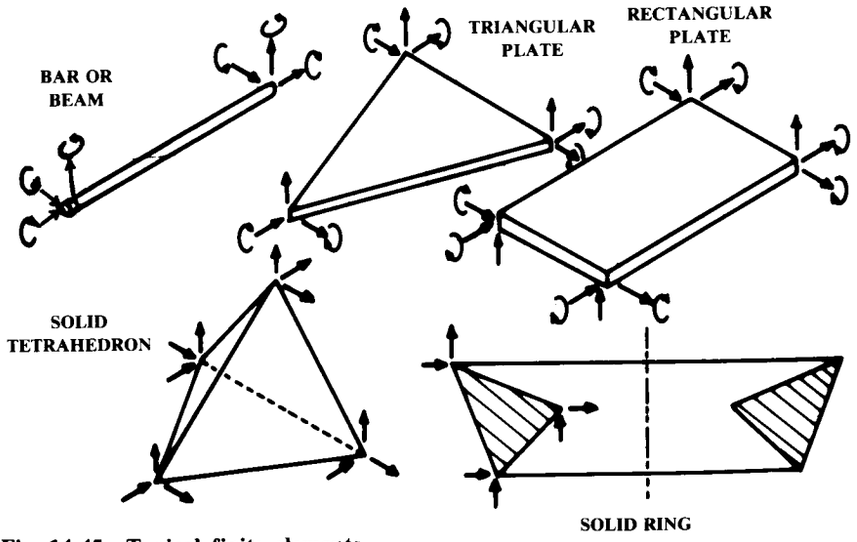

Fig. 14.45 Typical finite elements.

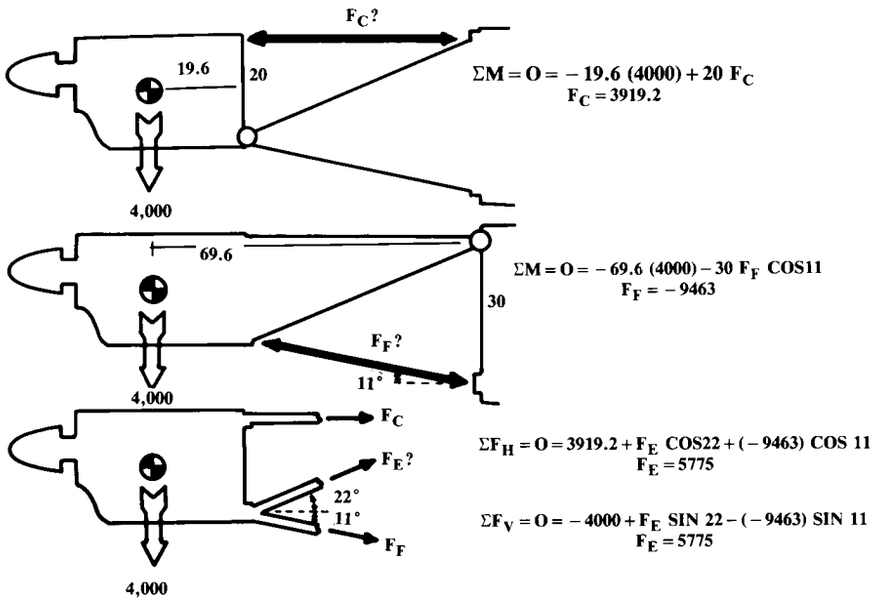

Fig. 14.36 Method of moments/method of shears.

The lower illustration of Fig. 14.36 shows the use of the method of shears to solve for the inner strut. This method involves severing the structure along a plane which cuts only three members, the upper and lower strut and the inner strut under analysis.

The severed part of the structure is analyzed as a free body, summing either the vertical and horizontal forces, which must total zero. Note that by calculating the unknown strut force both ways (vertical and horizontal summation), a check of your result can be made. This example gives a result of 5775 lb.

These methods are only applicable if the truss structure is "statically determinate." In general, a truss is statically determinate if every strut can be cut by some plane that cuts only two other struts. This insures that there is always a joint with only two unknown struts, permitting solution by the method of joints. For "indeterminate" trusses, more complicated methods based upon deflection analysis must be used (see Refs. 54 and 60).

Once the loads in each member of the truss are known, the struts can be analyzed using the equations presented above for tension or compression. Use the appropriate effective length for welded, riveted, or bolted columns from Fig. 14.31. To provide an extra margin of safety, it is customary to assume that welded steel-tube motor mounts act as though the ends were pinned ($L_e = L$).

The 3-D trusses, or "space structures," are solved similarly to the 2-D truss. Square cross section 3-D trusses, such as a typical welded-tube fuselage, can sometimes be solved separately in side view and top view as 2-D structures. The resulting strut loads are then summed for the various members. This is permitted provided that the combined loads on all struts are within the elastic range.

For more complicated 3-D trusses, the method of joints can be applied using three equations and three unknown strut loads. This involves simultaneous solution of equations, e.g., with a simple computer iteration program. In some cases the moments about some selected point can be used to obtain the solution with less effort. Space structures are discussed in detail in Ref. 54.

Beam Shear and Bending

A common problem in aircraft design is the estimation of the shear and bending stresses in the wing spars or fuselage. This is a two-step process. First, the shear and bending moment distributions must be determined; then the resulting stresses must be found.

Figure 14.37 shows a simple beam with a distributed vertical load. The beam is shown cut to depict internal forces. The right side of the beam being a free body, the sum of the vertical forces and the sum of the moments must equal zero.

If the severed part of the beam is to remain in vertical equilibrium, the externally applied vertical forces must be opposed by a vertical shear force within the cross section of the material, as shown. Thus, for any span station the shear force is simply the sum of the vertical loads outboard of that station, or the integral of a distributed load.

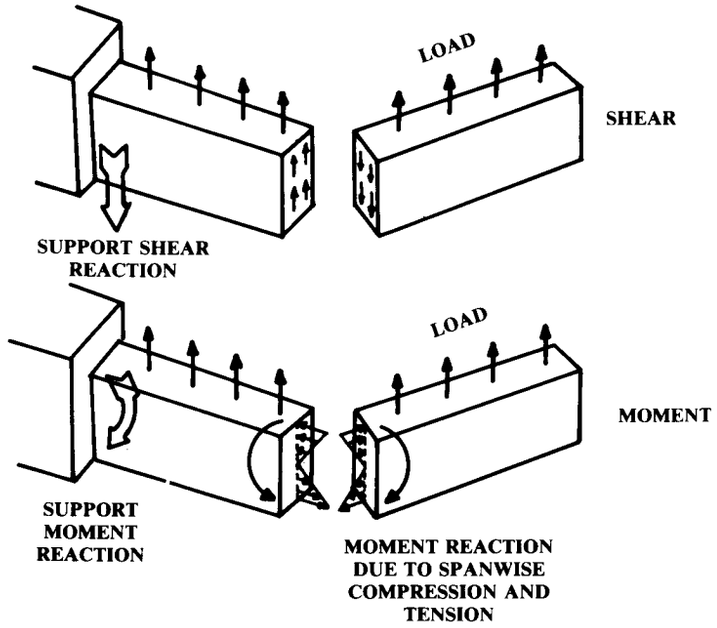

Fig. 14.37 Shear and moment in beams.

The element equations are then linked together using matrix algebra so that the entire structure's response to a given external loading condition can be determined. The huge size of the matrices used for FEM analysis requires computers for solution of all but the most trivial cases.

Figure 14.45 illustrates the more commonly used finite elements. The aircraft structure must be modeled as a connected collection of one or more of these finite-element shapes.

Selection of which element type to use is a matter of engineering judgment. Unfortunately, the selection of the element type can influence the results. Also, the selection of the size of the elements requires experience. As a general rule, the size of the elements should be reduced anywhere that the stress is expected to vary greatly. An example of this would be in the vicinity of a corner.

Figure 14.46 shows an FEM example in which the major structural members of a propfan research aircraft are modeled using the rectangular-plate finite element. As is the case for CFD gridding, the modeling of a complex structure for FEM analysis can be very time-consuming.

Detailed derivations of the equations for the various finite-element types shown in Fig. 14.45 are beyond the scope of this book (see Refs. 84 and 85).

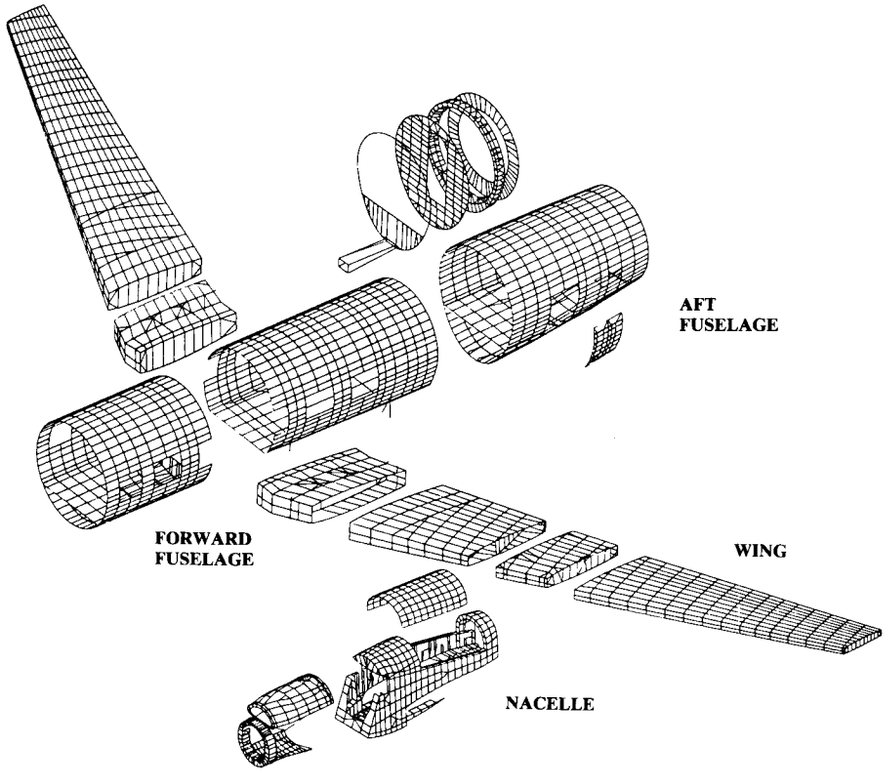

Fig. 14.46 Typical finite element model. (Courtesy Lockheed)

A simple example, the one-dimensional (1-D) bar, will be developed to illustrate the principles involved.

Figure 14.47 depicts a simple 1-D bar element with end-loadings P_1 and P_2, and end-deflections u_1 and u_2. For a static structural analysis, P_1 must equal the negative of P_2, although this is not true in a dynamic analysis. The cross-sectional area of the bar is shown as A. Note that while this example is a 1-D case, the deflected position is depicted slightly offset for clarity.

The strain ϵ is defined earlier in this chapter as the change in length divided by the original length L, as shown in Eq. (14.51). The stress σ is defined as the load divided by the cross-sectional area, and Young's Modulus E is defined as the stress divided by the strain. This results in Eq. (14.52).

$$\epsilon = (u_1 - u_2)/L \tag{14.51}$$

$$E = \sigma/\epsilon = (P/\mathrm{A})/[(u_1 - u_2)/L] \tag{14.52}$$

or

$$P = \frac{E\mathrm{A}}{L}(u_1 - u_2) \tag{14.53}$$

Applying a load P_1 yields Eq. (14.54). Similarly, applying a load P_2 results in Eq. (14.55). The change in signs of the deflections in Eq. (14.55) is due to the assumed directions of the two loads as drawn in the figure.

$$P_1 = \frac{EA}{L}(u_1 - u_2) \tag{14.54}$$

$$P_2 = \frac{EA}{L}(-u_1 + u_2) \tag{14.55}$$

Equations (14.54) and (14.55) can be combined into matrix form as shown in Eqs. (14.56) and (14.57). The k matrix is called the "stiffness matrix" because it relates the amount of deflection to the applied loads. The values within the k matrix are called "stiffness coefficients."

The u matrix containing the deflection terms is called the "displacement vector." The P matrix is the "force vector." (Letters other than P and u are

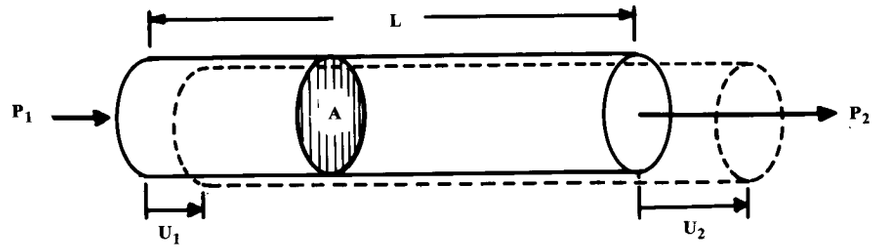

Fig. 14.47 Simple 1-D bar element.

frequently used for these terms, but for some reason k is almost always used for the stiffness matrix.)

$$\begin{Bmatrix} P_1 \\ P_2 \end{Bmatrix} = \begin{bmatrix} EA/L & -EA/L \\ -EA/L & EA/L \end{bmatrix} \begin{Bmatrix} u_1 \\ u_2 \end{Bmatrix} \tag{14.56}$$

$$\{P\} = [k]\ \{u\} \tag{14.57}$$

The values E, A, and L are known, so the stiffness matrix is known. By inverting the stiffness matrix, the deflections can be found for any loading condition.

This simple example could easily be solved by classical structure techniques. The power of FEM is in the assemblage of numerous finite elements.

Figure 14.48 shows a two-element assemblage using the 1-D bar element developed above. Two bars of different length and cross-sectional area are connected. The point where two (or more) finite elements are connected is called a "node" and is distinguished by the fact that at a node, the displacements of the connected finite elements are the same. Thus, u_2 represents both the displacement of the right end of the first element and the displacement of the left end of the second element.

From Eq. (14.56), the matrix equations for the left- and right-side elements can be written as Eqs. (14.58) and (14.59).

$$\begin{Bmatrix} P_1 \\ P_2 \end{Bmatrix} = \begin{bmatrix} EA_1/L_1 & -EA_1/L_1 \\ -EA_1/L_1 & EA_1/L_1 \end{bmatrix} \begin{Bmatrix} u_1 \\ u_2 \end{Bmatrix} \tag{14.58}$$

$$\begin{Bmatrix} P_2 \\ P_3 \end{Bmatrix} = \begin{bmatrix} EA_2/L_2 & -EA_2/L_2 \\ -EA_2/L_2 & EA_2/L_2 \end{bmatrix} \begin{Bmatrix} u_2 \\ u_3 \end{Bmatrix} \tag{14.59}$$

Now the matrices can be assembled by merging the element matrices. This is shown in Eq. (14.60). Note that the "overlapping" terms at the node result from the nodal condition of identical deflection (u_2 in this case). These overlapping terms are added in forming the assembled matrix.

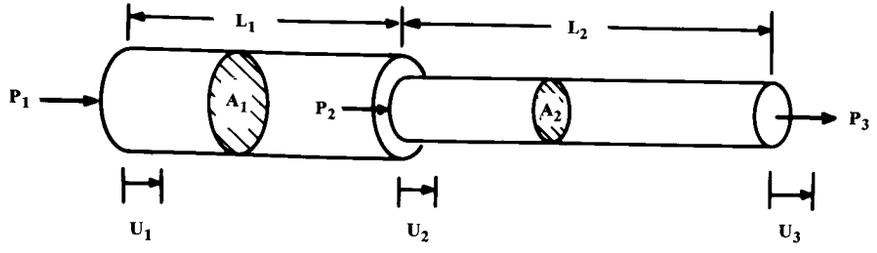

Fig. 14.48 1-D bar FEM assembly.

$$\begin{Bmatrix} P_1 \\ P_2 \\ P_3 \end{Bmatrix} = \begin{bmatrix} EA_1/L_1 & -EA_1/L_1 & 0 \\ -EA_1/L_1 & (EA_1/L_1 + EA_2/L_2) & -EA_2/L_2 \\ 0 & -EA_2/L_2 & EA_2/L_2 \end{bmatrix} \begin{Bmatrix} u_1 \\ u_2 \\ u_3 \end{Bmatrix} \tag{14.60}$$

This completes the FEM development for this example. The remaining work is strictly computation based upon the actual values of the variables in a given design problem. For example, Fig. 14.49 shows a two-bar structure in which the right side attaches to a wall, loads are as shown, and the dimensional and material values are as indicated. This produces the following:

$$\begin{Bmatrix} P_1 \\ P_2 \\ P_3 \end{Bmatrix} = \begin{bmatrix} (2.5 \times 10^7) & (-2.5 \times 10^7) & 0 \\ (-2.5 \times 10^7) & (3.4 \times 10^7) & (-9.2 \times 10^6) \\ 0 & (-9.2 \times 10^6) & (9.2 \times 10^6) \end{bmatrix} \begin{Bmatrix} u_1 \\ u_2 \\ u_3 \end{Bmatrix} \tag{14.61}$$

The 3×3 stiffness matrix in Eq. (14.61) can be inverted to find the deflections for any loading. This would first require determining the unknown wall-reaction load P_3.

Alternatively, we can simplify the FEM matrix solution by noting that the deflection at the wall u_3 is zero, so we can eliminate the third row and the third column from the matrix. This produces Eq. (14.62) with a 2×2 stiffness matrix.

$$\begin{Bmatrix} P_1 \\ P_2 \end{Bmatrix} = \begin{bmatrix} (2.5 \times 10^7) & (-2.5 \times 10^7) \\ (-2.5 \times 10^7) & (3.4 \times 10^7) \end{bmatrix} \begin{Bmatrix} u_1 \\ u_2 \end{Bmatrix} \tag{14.62}$$

$$\begin{bmatrix} (1.5 \times 10^{-7}) & (1.1 \times 10^{-7}) \\ (1.1 \times 10^{-7}) & (1.1 \times 10^{-7}) \end{bmatrix} \begin{Bmatrix} P_1 \\ P_2 \end{Bmatrix} = \begin{Bmatrix} u_1 \\ u_2 \end{Bmatrix} \tag{14.63}$$

$$\begin{Bmatrix} 0.093 \\ 0.077 \end{Bmatrix} = \begin{Bmatrix} u_1 \\ u_2 \end{Bmatrix} \tag{14.64}$$

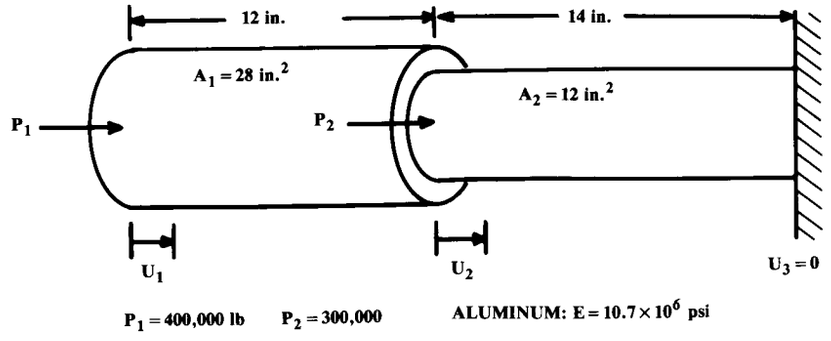

Fig. 14.49 FEM example.

In Eq. (14.63) we have found the inverse of the reduced k matrix. By substituting the actual values of the loadings P we determine the deflections as provided in Eq. (14.64). We can then use the deflections of the nodes to solve for the strain and stress, as follows:

$$\epsilon_1 = (0.093 - 0.077)/12 = 0.0013 \tag{14.65}$$

$$\epsilon_2 = (0.077 - 0)/14 = 0.0055 \tag{14.66}$$

$$\sigma_1 = 14{,}267 \text{ psi} \tag{14.67}$$

$$\sigma_2 = 58{,}850 \text{ psi} \tag{14.68}$$

This 1-D example does not illustrate the complications caused by 3-D geometry. For this simple example the deflections at the nodes produce identical changes in the length of the bars. Were the bars connected at some angle, the identical nodal deflections would produce different changes in bar lengths. Matrix direction-cosine terms must be used to keep track of these 3-D effects.

Most finite-element analyses use surface elements rather than simple bar elements. The triangle element shown in Fig. 14.45 is typical, and allows a complicated structure to be broken into numerous connected elements. These elements are assumed to be connected at the nodes (corners) where the deflections are identical.

Equations are prepared in matrix form describing how each element responds to loadings at its nodes. The element stiffness matrices are combined using appropriate direction cosine terms to account for 3-D geometry, and the combined matrix is inverted to solve for the deflections for a given loading.

For dynamic analysis, mass and damping terms are developed using matrix methods. These greatly increase the number of inputs required for the analysis.

Fortunately, working structural engineers do not need to develop their own FEM program every time they wish to analyze a structure. There are numerous "canned" FEM programs available, ranging from simple personal-computer ones to million-line programs.

The industry-standard FEM program is the "NASTRAN (NAsa STRuctural ANalysis)" program, developed years ago for NASA and continuously enhanced both by NASA and various private companies. NASTRAN handles virtually everything, but requires substantial experience to insure that the results are meaningful. However, for complex structural analysis, some variant of NASTRAN will probably be in use for many years to come.

15 WEIGHTS

15.1 INTRODUCTION

The estimation of the weight of a conceptual aircraft is a critical part of the design process. The weights engineer interfaces with all other engineering groups, and serves as the "referee" during the design evolution.

Weights analysis per se does not form part of the aerospace engineering curriculum at most universities. It requires a broad background in aerospace structures, mechanical engineering, statistics, and other engineering disciplines.

There are many levels of weights analysis. Previous chapters have presented crude statistical techniques for estimating the empty weight for a given takeoff weight. These techniques estimate the empty weight directly and are only suitable for "first-pass" analysis.

More sophisticated weights methods estimate the weight of the various components of the aircraft and then sum for the total empty weight. In this chapter, two levels of component weights analysis will be presented.

The first is a crude component buildup based upon planform areas, wetted areas, and percents of gross weight. This technique is useful for initial balance calculations and can be used to check the results of the more detailed statistical methods.

The second uses detailed statistical equations for the various components. This technique is sufficiently detailed to provide a credible estimate of the weights of the major component groups. Those weights are usually reported in groupings as defined by MIL-STD-1374, or some similar groupings defined by company practice. MIL-STD-1374 goes into exhaustive detail (taxi lights, for example!), but at the conceptual level the weights are reported via a "Summary Group Weight Statement." A typical summary format appears as Table 15.1, where the empty weight groups are further classified into three major groupings (structure, propulsion, and equipment).

The structures group consists of the load-carrying components of the aircraft. Note that it includes the inlet (air-induction-system) weight, as well as the nacelle (engine-section) weight including motor mounts and firewall provisions—despite their obvious relationship to the engine. The propulsion group contains only the engine-related equipment such as starters, exhaust, etc. The as-installed engine includes the propeller, if any.

Armament is broken down into fixed items, which are in the equipment groups, and expendable items, which are in the useful load. Sometimes a judgement call is required. For example, a gun may be considered to be fixed equipment, or it may be viewed as readily removable and unimportant to flight and therefore a part of the useful load.

The takeoff gross weight—the sum of the empty weight and the useful load—reflects the weight at takeoff for the normal design mission. The flight design gross weight represents the aircraft weight at which the structure will withstand the design load factors. Usually this is the same as the takeoff weight, but some aircraft are designed assuming that maximum loads will not be reached until the aircraft has taken off and climbed to altitude, burning off some fuel in the process.

"DCPR" stands for "Defense Contractors Planning Report." The DCPR weight is important for cost estimation, and can be viewed as the weight of the parts of the aircraft that the manufacturer makes, as opposed to buys and installs. DCPR weight equals the empty weight less the weights of the wheels, brakes, tires, engines, starters, cooling fluids, fuel bladders, instruments, batteries, electrical power supplies/converters, avionics, armament, fire-control systems, air conditioning, and auxiliary power unit. DCPR weight is also referred to as "AMPR" weight (Aeronautical Manufacturers Planning Report).

Table 15.1 Group weight format

Group	Group
STRUCTURES GROUP	EQUIPMENT GROUP
Wing	Flight controls
Tail-horizontal/canard	APU
vertical	Instruments
ventral	Hydraulic
Body	Pneumatic
Alighting gear-main	Electrical
auxiliary	Avionics
arresting gear	Armament
catapult gear	Furnishings
Nacelle/engine section	Air conditioning/ECS
Air induction system	Anti-icing
	Photographic
	Load and handling
PROPULSION GROUP	TOTAL WEIGHT EMPTY
Engine—as installed	USEFUL LOAD GROUP
Accessory gearbox and drive	
Exhaust system	Crew
Cooling provisions	Fuel-usable
Engine controls	-trapped
Starting system	Oil
Fuel system/tanks	Passengers
	Cargo/baggage
	Guns
	Ammunition
	Pylons and racks
	Expendable weapons
	Flares/chaff
	TAKEOFF GROSS WEIGHT
	Flight design gross weight
	Landing design gross weight
	DCPR weight

In a Group Weight Statement, the distance to the weight datum (arbitrary reference point) is included, and the resulting moment is calculated. These are summed and divided by the total weight to determine the actual center-of-gravity (c.g.) location. The c.g. varies during flight as fuel is burned off and weapons expended.

To determine if the c.g. remains within the limits established by an aircraft stability and control analysis, a "c.g.-envelope" plot is prepared (Fig. 15.1).

The c.g. must remain within the specified limits as fuel is burned, and whether or not the weapons are expended. It is permissible to "sequence" the fuel tanks, selecting to burn fuel from different tanks at different times to keep the c.g. within limits. However, an automated fuel-management system must be used, and that imposes additional cost and complexity.

Note that the allowable limits on the c.g. vary with Mach number. At supersonic speeds the aerodynamic center moves rearward, so the forward-c.g. limit may have to move rearward to allow longitudinal trim at supersonic speeds. However, the aft-c.g. limit is often established by the size of the vertical tail, which loses effectiveness at supersonic speeds. This prevents moving the aft limit rearwards at supersonic speeds, forcing a very narrow band of allowable limits.

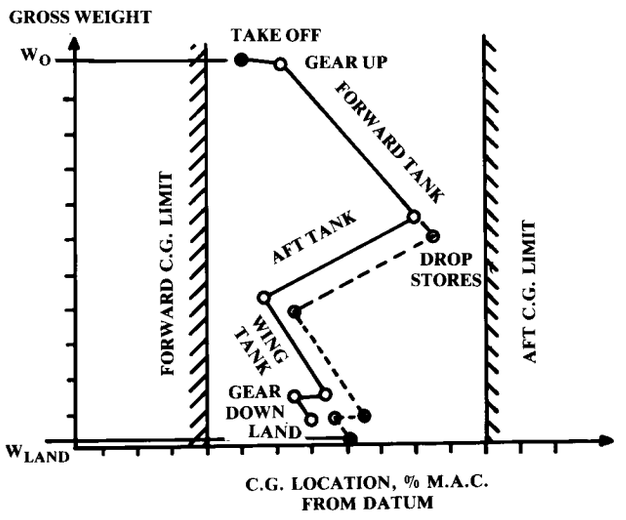

Fig. 15.1 C.G. envelope diagram.

Table 15.2 Approximate empty weight buildup

Item	Fighters	Transports and bombers	General aviation	Multiplier[a]	Approximate location
Wing	9.0	10.0	2.5	$S_{\text{exposed planform ft}^2}$	40% MAC
Horizontal tail	4.0	5.5	2.0	$S_{\text{exposed planform ft}^2}$	40% MAC
Vertical tail	5.3	5.5	2.0	$S_{\text{exposed planform ft}^2}$	40% MAC
Fuselage	4.8	5.0	1.4	$S_{\text{wetted area ft}^2}$	40–50% length
Landing gear[b]	.033 .045 Navy	.043	.057	TOGW (lb)	–
Installed engine	1.3	1.3	1.4	Engine weight (lb)	–
"All-else empty"	.17	.17	.10	TOGW (lb)	40–50% length

[a]Results are in pounds.
[b]15% to nose gear; 85% to main gear.

15.2 APPROXIMATE GROUP WEIGHTS METHOD

Early in design it is desirable to do a rough c.g. estimate. Otherwise, substantial rework may be required after the c.g. is properly estimated. A rough c.g. estimate can be done with a crude statistical approach as provided in Table 15.2.

The wing and tail weights are determined from historical values for the weight per square foot of exposed planform area. The fuselage is similarly based upon its wetted area. The landing gear is estimated as a fraction of the takeoff gross weight. The installed engine weight is a multiple of the uninstalled engine weight. Finally, a catch-all weight for the remaining items of the empty weight is estimated as a fraction of the takeoff gross weight.

This technique also applies the approximate locations of the component c.g. as given in Table 15.2. The resulting c.g. estimate can then be compared to the desired c.g. location with respect to the wing aerodynamic center. Also, these approximate component weights can be used as a check of the more detailed statistical equations provided below.

15.3 STATISTICAL GROUP WEIGHTS METHOD

A more refined estimate of the group weights applies statistical equations based upon sophisticated regression analysis. Development of these equations represents a major effort, and each company develops its own equations.

To acquire a statistical database for these equations, weights engineers must obtain group-weight statements and detailed aircraft drawings for as many current aircraft as possible. This sometimes requires weights engineers to trade group-weight statements much like baseball cards ("I'll trade you a T-45 for an F-16 and a C-5B"!)

The equations presented below typify those used in conceptual design by the major airframe companies, and cover fighter/attack, transport, and general-aviation aircraft. They have been taken from Refs. 62–64 and other sources. Definitions of the terms follow the equations.

It should be understood that there are no "right" answers in weights estimation until the first aircraft flies. However, these equations should provide a reasonable estimate of the group weights. Other, similar weights equations may be found in Refs. 10, 11, and 23. It's a good idea to calculate the weight of each component using several different equations and then select an average, reasonable result.

Reference 11 tabulates group-weight statements for a number of aircraft. These can also be used to help select a reasonable weight estimate for the components by comparing the component weights as a fraction of the empty weight for a similar aircraft.

Table 15.3 tabulates various miscellaneous weights.

When the component weights are estimated using these or similar methods, they are tabulated in a format similar to that of Table 15.1 and are summed to determine the empty weight. Since the payload and crew weights are known, the fuel weight must be adjusted to yield the as-drawn takeoff weight that is the sum of the empty, payload, crew, and fuel weights. If the empty weight is higher than expected, there may be insufficient fuel to

Table 15.3 Miscellaneous weights (approximate)

Missiles	
Harpoon (AGM-84 A)	1200 lb
Phoenix (AIM-54 A)	1000 lb
Sparrow (AIM-7)	500 lb
Sidewinder (AIM-9)	200 lb
Pylon and launcher	.12 $W_{missile}$
M61 Gun	
Gun	250 lb
940 rds ammunition	550 lb
Seats	
Flight deck	60 lb
Passenger	32 lb
Troop	11 lb
Instruments	
Altimeter, airspeed, accelerometer, rate of climb, clock, compass, turn & bank, Mach, tachometer, manifold pressure, etc.	1–2 lb each
Gyro horizon, directional gyro	4–6 lb each
Heads-up display	40 lb
Lavatories	
Long range aircraft	1.11 $N_{pass}^{1.33}$
Short range aircraft	0.31 $N_{pass}^{1.33}$
Business/executive aircraft	3.90 $N_{pass}^{1.33}$
Arresting gear	
Air Force-type	.002 W_{dg}
Navy-type	.008 W_{dg}
Catapult gear	
Navy carrier-based	.003 W_{dg}
Folding Wing	
Navy carrier based	.06 W_{wing}

complete the design mission. This must be corrected by resizing and optimizing the aircraft as described in Chapter 19, *not* by simply increasing fuel weight for the as-drawn aircraft (which would invalidate the component weight predictions that were based on the as-drawn takeoff weight).

Fighter/Attack Weights

$$W_{wing} = 0.0103 K_{dw} K_{vs} (W_{dg} N_z)^{0.5} S_w^{0.622} A^{0.785} (t/c)_{root}^{-0.4} \times (1+\lambda)^{0.05} (\cos\Lambda)^{-1.0} S_{csw}^{0.04} \quad (15.1)$$

$$W_{horizontal\ tail} = 3.316\left(1+\frac{F_w}{B_h}\right)^{-2.0}\left(\frac{W_{dg}N_z}{1000}\right)^{0.260} S_{ht}^{0.806} \quad (15.2)$$

$$W_{vertical\ tail} = 0.452 K_{rht}(1+H_t/H_v)^{0.5}(W_{dg}N_z)^{0.488} S_{vt}^{0.718} M^{0.341} \times L_t^{-1.0}(1+S_r/S_{vt})^{0.348} A_{vt}^{0.223}(1+\lambda)^{0.25}(\cos\Lambda_{vt})^{-0.323} \quad (15.3)$$

$$W_{fuselage} = 0.499 K_{dwf} W_{dg}^{0.35} N_z^{0.25} L^{0.5} D^{0.849} W^{0.685} \quad (15.4)$$

$$W_{\substack{main\ landing\\ gear}} = K_{cb} K_{tpg} (W_l N_l)^{0.25} L_m^{0.973} \quad (15.5)$$

$$W_{\substack{nose\ landing\\ gear}} = (W_l N_l)^{0.290} L_n^{0.5} N_{nw}^{0.525} \quad (15.6)$$

$$W_{\substack{engine\\ mounts}} = 0.013 N_{en}^{0.795} T^{0.579} N_z \quad (15.7)$$

$$W_{firewall} = 1.13 S_{fw} \quad (15.8)$$

$$W_{\substack{engine\\ section}} = 0.01 W_{en}^{0.717} N_{en} N_z \quad (15.9)$$

$$W_{\substack{air\ induction\\ system}} = 13.29 K_{vg} L_d^{0.643} K_d^{0.182} N_{en}^{1.498} (L_s/L_d)^{-0.373} D_e \quad (15.10)$$

where K_d and L_s are from Fig. 15.2.

$$W_{tailpipe} = 3.5 D_e L_{tp} N_{en} \quad (15.11)$$

$$W_{\substack{engine\\ cooling}} = 4.55 D_e L_{sh} N_{en} \quad (15.12)$$

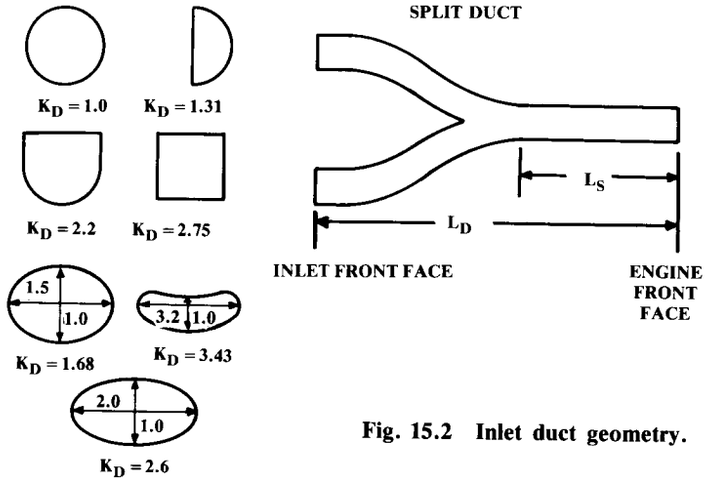

Fig. 15.2 Inlet duct geometry.

$$W_{\text{oil cooling}} = 37.82 N_{\text{en}}^{1.023} \tag{15.13}$$

$$W_{\substack{\text{engine}\\\text{controls}}} = 10.5 N_{\text{en}}^{1.008} L_{\text{ec}}^{0.222} \tag{15.14}$$

$$W_{\substack{\text{starter}\\\text{(pneumatic)}}} = 0.025\, T_e^{0.760} N_{\text{en}}^{0.72} \tag{15.15}$$

$$W_{\substack{\text{fuel system}\\\text{and tanks}}} = 7.45\, V_t^{0.47}\left(1 + \frac{V_i}{V_t}\right)^{-0.095}\left(1 + \frac{V_p}{V_t}\right) N_t^{0.066} N_{\text{en}}^{0.052}\left(\frac{T \cdot \text{SFC}}{1000}\right)^{0.249} \tag{15.16}$$

$$W_{\substack{\text{flight}\\\text{controls}}} = 36.28 M^{0.003} S_{\text{cs}}^{0.489} N_s^{0.484} N_c^{0.127} \tag{15.17}$$

$$W_{\text{instruments}} = 8.0 + 36.37 N_{\text{en}}^{0.676} N_t^{0.237} + 26.4(1 + N_{ci})^{1.356} \tag{15.18}$$

$$W_{\text{hydraulics}} = 37.23 K_{\text{vsh}} N_u^{0.664} \tag{15.19}$$

$$W_{\text{electrical}} = 172.2 K_{mc} R_{\text{kva}}^{0.152} N_c^{0.10} L_a^{0.10} N_{\text{gen}}^{0.091} \tag{15.20}$$

$$W_{\text{avionics}} = 2.117\, W_{\text{uav}}^{0.933} \tag{15.21}$$

$$W_{\text{furnishings}} = 217.6 N_c \tag{15.22}$$

$$W_{\substack{\text{air conditioning}\\\text{and anti-ice}}} = 201.6[(W_{\text{uav}} + 200\, N_c)/1000]^{0.735} \tag{15.23}$$

$$W_{\substack{\text{handling}\\\text{gear}}} = 3.2 \times 10^{-4} W_{\text{dg}} \tag{15.24}$$

Cargo/Transport Weights

$$W_{\text{wing}} = 0.0051 (W_{\text{dg}} N_z)^{0.557} S_w^{0.649} A^{0.5} (t/c)_{\text{root}}^{-0.4} (1 + \lambda)^{0.1} \times (\cos\Lambda)^{-1.0} S_{\text{csw}}^{0.1} \tag{15.25}$$

$$W_{\substack{\text{horizontal}\\\text{tail}}} = 0.0379 K_{\text{uht}} (1 + F_w/B_h)^{-0.25} W_{\text{dg}}^{0.639} N_z^{0.10} S_{\text{ht}}^{0.75} L_t^{-1.0} \times K_y^{0.704} (\cos\Lambda_{\text{ht}})^{-1.0} A_h^{0.166} (1 + S_e/S_{\text{ht}})^{0.1} \tag{15.26}$$

$$W_{\substack{\text{vertical}\\\text{tail}}} = 0.0026 (1 + H_t/H_v)^{0.225} W_{\text{dg}}^{0.556} N_z^{0.536} L_t^{-0.5} S_{\text{vt}}^{0.5} K_z^{0.875} \times (\cos\Lambda_{\text{vt}})^{-1} A_v^{0.35} (t/c)_{\text{root}}^{-0.5} \tag{15.27}$$

$$W_{\text{fuselage}} = 0.3280 K_{\text{door}} K_{\text{Lg}} (W_{\text{dg}} N_z)^{0.5} L^{0.25} S_f^{0.302} (1 + K_{\text{ws}})^{0.04} (L/D)^{0.10} \tag{15.28}$$

$$W_{\substack{\text{main landing}\\\text{gear}}} = 0.0106 K_{\text{mp}} W_l^{0.888} N_l^{0.25} L_m^{0.4} N_{\text{mw}}^{0.321} N_{\text{mss}}^{-0.5} V_{\text{stall}}^{0.1} \tag{15.29}$$

$$W_{\substack{\text{nose landing}\\\text{gear}}} = 0.032 K_{np} W_l^{0.646} N_l^{0.2} L_n^{0.5} N_{nw}^{0.45} \tag{15.30}$$

$$W_{\substack{\text{nacelle}\\\text{group}}} = 0.6724 K_{ng} N_{Lt}^{0.10} N_w^{0.294} N_z^{0.119} W_{\text{ec}}^{0.611} N_{\text{en}}^{0.984} S_n^{0.224} \quad \text{(includes air induction)} \tag{15.31}$$

$$W_{\substack{\text{engine}\\\text{controls}}} = 5.0 N_{\text{en}} + 0.80 L_{\text{ec}} \tag{15.32}$$

$$W_{\substack{\text{starter}\\\text{(pneumatic)}}} = 49.19\left(\frac{N_{\text{en}} W_{\text{en}}}{1000}\right)^{0.541} \tag{15.33}$$

$$W_{\substack{\text{fuel}\\\text{system}}} = 2.405\, V_t^{0.606} (1 + V_i/V_t)^{-1.0} (1 + V_p/V_t) N_t^{0.5} \tag{15.34}$$

$$W_{\substack{\text{flight}\\\text{controls}}} = 145.9 N_f^{0.554} (1 + N_m/N_f)^{-1.0} S_{cs}^{0.20} (I_y \times 10^{-6})^{0.07} \quad (15.35)$$

$$W_{\substack{\text{APU}\\\text{installed}}} = 2.2\, W_{\substack{\text{APU}\\\text{uninstalled}}} \quad (15.36)$$

$$W_{\text{instruments}} = 4.509 K_r K_{tp} N_c^{0.541} N_{en} (L_f + B_w)^{0.5} \quad (15.37)$$

$$W_{\text{hydraulics}} = 0.2673 N_f (L_f + B_w)^{0.937} \quad (15.38)$$

$$W_{\text{electrical}} = 7.291 R_{kva}^{0.782} L_a^{0.346} N_{gen}^{0.10} \quad (15.39)$$

$$W_{\text{avionics}} = 1.73 W_{uav}^{0.983} \quad (15.40)$$

$$W_{\text{furnishings}} = 0.0577 N_c^{0.1} W_c^{0.393} S_f^{0.75} \quad (15.41)$$

$$W_{\substack{\text{air}\\\text{conditioning}}} = 62.36 N_p^{0.25} (V_{pr}/1000)^{0.604} W_{uav}^{0.10} \quad (15.42)$$

$$W_{\text{anti-ice}} = 0.002 W_{dg} \quad (15.43)$$

$$W_{\substack{\text{handling}\\\text{gear}}} = 3.0 \times 10^{-4} W_{dg} \quad (15.44)$$

$$W_{\substack{\text{military cargo}\\\text{handling system}}} = 2.4 \times (\text{cargo floor area, ft}^2) \quad (15.45)$$

General-Aviation Weights

$$W_{\text{wing}} = 0.036 S_w^{0.758} W_{fw}^{0.0035} \left(\frac{A}{\cos^2\Lambda}\right)^{0.6} q^{0.006} \lambda^{0.04} \left(\frac{100\ t/c}{\cos\Lambda}\right)^{-0.3} (N_z W_{dg})^{0.49} \quad (15.46)$$

$$W_{\substack{\text{horizontal}\\\text{tail}}} = 0.016 (N_z W_{dg})^{0.414} q^{0.168} S_{ht}^{0.896} \left(\frac{100\ t/c}{\cos\Lambda}\right)^{-0.12} \times \left(\frac{A}{\cos^2\Lambda_{ht}}\right)^{0.043} \lambda_h^{-0.02} \quad (15.47)$$

$$W_{\substack{\text{vertical}\\\text{tail}}} = 0.073 \left(1 + 0.2 \frac{H_t}{H_v}\right) (N_z W_{dg})^{0.376} q^{0.122} S_{vt}^{0.873} \left(\frac{100\ t/c}{\cos\Lambda_{vt}}\right)^{-0.49} \times \left(\frac{A}{\cos^2\Lambda_{vt}}\right)^{0.357} \lambda_{vt}^{0.039} \quad (15.48)$$

$$W_{\text{fuselage}} = 0.052\ S_f^{1.086} (N_z W_{dg})^{0.177} L_t^{-0.051} (L/D)^{-0.072} q^{0.241} + W_{\text{press}} \quad (15.49)$$

$$W_{\substack{\text{main landing}\\\text{gear}}} = 0.095 (N_l W_l)^{0.768} (L_m/12)^{0.409} \quad (15.50)$$

$$W_{\substack{\text{nose landing}\\\text{gear}}} = 0.125 (N_l W_l)^{0.566} (L_n/12)^{0.845} \quad (15.51)$$

$$W_{\substack{\text{installed engine}\\\text{(total)}}} = 2.575 W_{en}^{0.922} N_{en} \quad (15.52)$$

$$W_{\text{fuel system}} = 2.49 V_t^{0.726} \left(\frac{1}{1 + V_i/V_t}\right)^{0.363} N_t^{0.242} N_{en}^{0.157} \quad (15.53)$$

$$W_{\substack{\text{flight}\\\text{controls}}} = 0.053 L^{1.536} B_w^{0.371} (N_z W_{dg} \times 10^{-4})^{0.80} \quad (15.54)$$

$$W_{\text{hydraulics}} = 0.001 W_{dg} \quad (15.55)$$

$$W_{\text{electrical}} = 12.57 (W_{\text{fuel system}} + W_{\text{avionics}})^{0.51} \quad (15.56)$$

$$W_{\text{avionics}} = 2.117 W_{uav}^{0.933} \quad (15.57)$$

$$W_{\substack{\text{air conditioning}\\\text{and anti-ice}}} = 0.265 W_{dg}^{0.52} N_p^{0.68} W_{\text{avionics}}^{0.17} M^{0.08} \quad (15.58)$$

$$W_{\text{furnishings}} = 0.0582\ W_{dg} - 65 \quad (15.59)$$

Weights Equations Terminology

A = aspect ratio
B_h = horizontal tail span, ft
B_w = wing span, ft
D = fuselage structural depth, ft
D_e = engine diameter, ft
F_w = fuselage width at horizontal tail intersection, ft
H_t = horizontal tail height above fuselage, ft
H_t/H_v = 0.0 for conventional tail; 1.0 for "T" tail
H_v = vertical tail height above fuselage, ft
I_y = yawing moment of inertia, lb-ft^2 (see Chap. 16)

K_{cb} = 2.25 for cross-beam (F-111) gear; = 1.0 otherwise
K_d = duct constant (see Fig. 15.2)
K_{door} = 1.0 if no cargo door; = 1.06 if one side cargo door; = 1.12 if two side cargo doors; = 1.12 if aft clamshell door; = 1.25 if two side cargo doors and aft clamshell door
K_{dw} = 0.768 for delta wing; = 1.0 otherwise
K_{dwf} = 0.774 for delta wing aircraft; = 1.0 otherwise
K_{Lg} = 1.12 if fuselage-mounted main landing gear; = 1.0 otherwise
K_{mc} = 1.45 if mission completion required after failure; = 1.0 otherwise
K_{mp} = 1.126 for kneeling gear; = 1.0 otherwise
K_{ng} = 1.017 for pylon-mounted nacelle; = 1.0 otherwise
K_{np} = 1.15 for kneeling gear; = 1.0 otherwise
K_p = 1.4 for engine with propeller or 1.0 otherwise
K_r = 1.133 if reciprocating engine; = 1.0 otherwise
K_{rht} = 1.047 for rolling tail; = 1.0 otherwise
K_{tp} = 0.793 if turboprop; = 1.0 otherwise
K_{tpg} = 0.826 for tripod (A-7) gear; = 1.0 otherwise
K_{tr} = 1.18 for jet with thrust reverser or 1.0 otherwise
K_{uht} = 1.143 for unit (all-moving) horizontal tail; = 1.0 otherwise
K_{vg} = 1.62 for variable geometry; = 1.0 otherwise
K_{vs} = 1.19 for variable sweep wing; = 1.0 otherwise
K_{vsh} = 1.425 if variable sweep wing; = 1.0 otherwise
K_{ws} = $0.75[1 + 2\lambda)/(1 + \lambda)]\ (B_w \tan\Lambda/L)$
K_y = aircraft pitching radius of gyration, ft ($\cong 0.3L_t$)
K_z = aircraft yawing radius of gyration, ft ($\cong L_t$)
L = fuselage structural length, ft (excludes radome, tail cap)
L_a = electrical routing distance, generators to avionics to cockpit, ft
L_d = duct length, ft
L_{ec} = length from engine front to cockpit—total if multiengine, ft
L_f = total fuselage length
L_m = length of main landing gear, in.
L_n = nose gear length, in.
L_s = single duct length (see Fig. 15.2)
L_{sh} = length of engine shroud, ft
L_t = tail length; wing quarter-MAC to tail quarter-MAC, ft
L_{tp} = length of tailpipe, ft
M = Mach number
N_c = number of crew
N_{ci} = 1.0 if single pilot; = 1.2 if pilot plus backseater; = 2.0 pilot and copassenger
N_{en} = number of engines
N_f = number of functions performed by controls (typically 4–7)
N_{gen} = number of generators (typically = N_{en})
N_l = ultimate landing load factor; = $N_{gear} \times 1.5$
N_{Lt} = nacelle length, ft
N_m = number of mechanical functions (typically 0–2)
N_{mss} = number of main gear shock struts
N_{mw} = number of main wheels
N_{nw} = number of nose wheels

N_p = number of personnel onboard (crew and passengers)
N_s = number of flight control systems
N_t = number of fuel tanks
N_u = number of hydraulic utility functions (typically 5–15)
N_w = nacelle width, ft
N_z = ultimate load factor; = 1.5 × limit load factor
q = dynamic pressure at cruise, lb/ft^2
R_{kva} = system electrical rating, kv · A (typically 40–60 for transports, 110–160 for fighters & bombers)
S_{cs} = total area of control surfaces, ft^2
S_{csw} = control surface area (wing-mounted), ft^2
S_e = elevator area, ft
S_f = fuselage wetted area, ft^2
S_{fw} = firewall surface area, ft^2
S_{ht} = horizontal tail area
S_n = nacelle wetted area, ft^2
S_r = rudder area, ft^2
S_{vt} = vertical tail area, ft^2
S_w = trapezoidal wing area, ft^2
SFC = engine specific fuel consumption—maximum thrust
T = total engine thrust, lb
T_e = thrust per engine, lb
V_i = integral tanks volume, gal
V_p = self-sealing "protected" tanks volume, gal
V_{pr} = volume of pressurized section, ft^3
V_t = total fuel volume, gal
W = fuselage structural width, ft
W_c = maximum cargo weight, lb
W_{dg} = design gross weight, lb
W_{ec} = weight of engine and contents, lb (per nacelle), $\cong 2.331\ W_{engine}^{0.901}\ K_p K_{tr}$
W_{en} = engine weight, each, lb
W_{fw} = weight of fuel in wing, lb
W_l = landing design gross weight, lb
W_{press} = weight penalty due to pressurization, $= 11.9 + (V_{pr}P_{delta})^{0.271}$, where P_{delta} = cabin pressure differential, psi (typically 8 psi)
W_{uav} = uninstalled avionics weight, lb (typically = 800–1400 lb)
Λ = wing sweep at 25% MAC

15.4 ADDITIONAL CONSIDERATIONS IN WEIGHTS ESTIMATION

These statistical equations are based upon a database of existing aircraft. They work well for a "normal" aircraft similar to the various aircraft in the database. However, use of a novel configuration (canard pusher) or an advanced technology (composite structure) will result in a poor weights estimate when using these or similar equations. To allow for this, weights engineers adjust the statistical-equation results using "fudge factors" (defined as the variable constant that you multiply your answer by to get the right answer!)

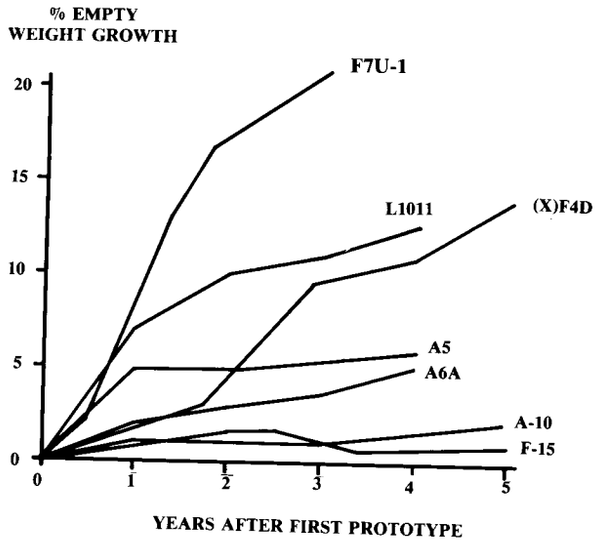

Fig. 15.3 Aircraft weight growth.

Table 15.4 Weights estimation "fudge factors"

Category	Weight group	Fudge factor (multiplier)
Advanced composites	Wing	0.85
	Tails	0.83
	Fuselage/nacelle	0.90
	Landing gear	0.95
	Air induction system	0.85
Braced wing	Wing	0.82
Wood fuselage	Fuselage	1.60
Steel tube fuselage	Fuselage	1.80
Flying boat hull	Fuselage	1.25

Fudge factors are also required to estimate the weight of a class of aircraft for which no statistical equations are available. For example, there have been too few Mach 3 aircraft to develop a good statistical database. Weights for a new Mach 3 design can be estimated by selecting the closest available equations (probably the fighter/attack equations) and determining a "fudge factor" for each type of component.

This is done using data for an existing aircraft similar to the new one (such as the XB-70 for a Mach 3 design) and calculating its component weights using the selected statistical equations. Fudge factors are then determined by dividing the actual component weights for that aircraft by the calculated component weights.

To estimate the component weights for the new design, these fudge factors are multiplied by the component weights as calculated using the selected statistical equations.

Fudge factors for composite-structure, wood or steel-tube fuselages, braced wings, and flying-boat hulls are provided in Table 15.4. These should be viewed as rough approximations only and subject to heated debate. For example, there are those who claim that a properly-designed steel-tube fuselage can be lighter than an aluminum fuselage.

One final consideration in aircraft-weights estimation is the weight growth that most aircraft experience in the first few years of production. This growth in empty weight is due to several factors, such as increased avionics capabilities, structural fixes (such as replacing an aluminum fitting with steel to prevent cracking), and additional weapons pylons.

Figure 15.3 shows the empty-weight growth of a number of aircraft. In the past, a weight growth of 5% in the first year was common. Today's better design techniques and analytical methods have reduced that to less than 2% in the first year. Still, some allowance for weight growth should be made in the conceptual-design weight estimation.

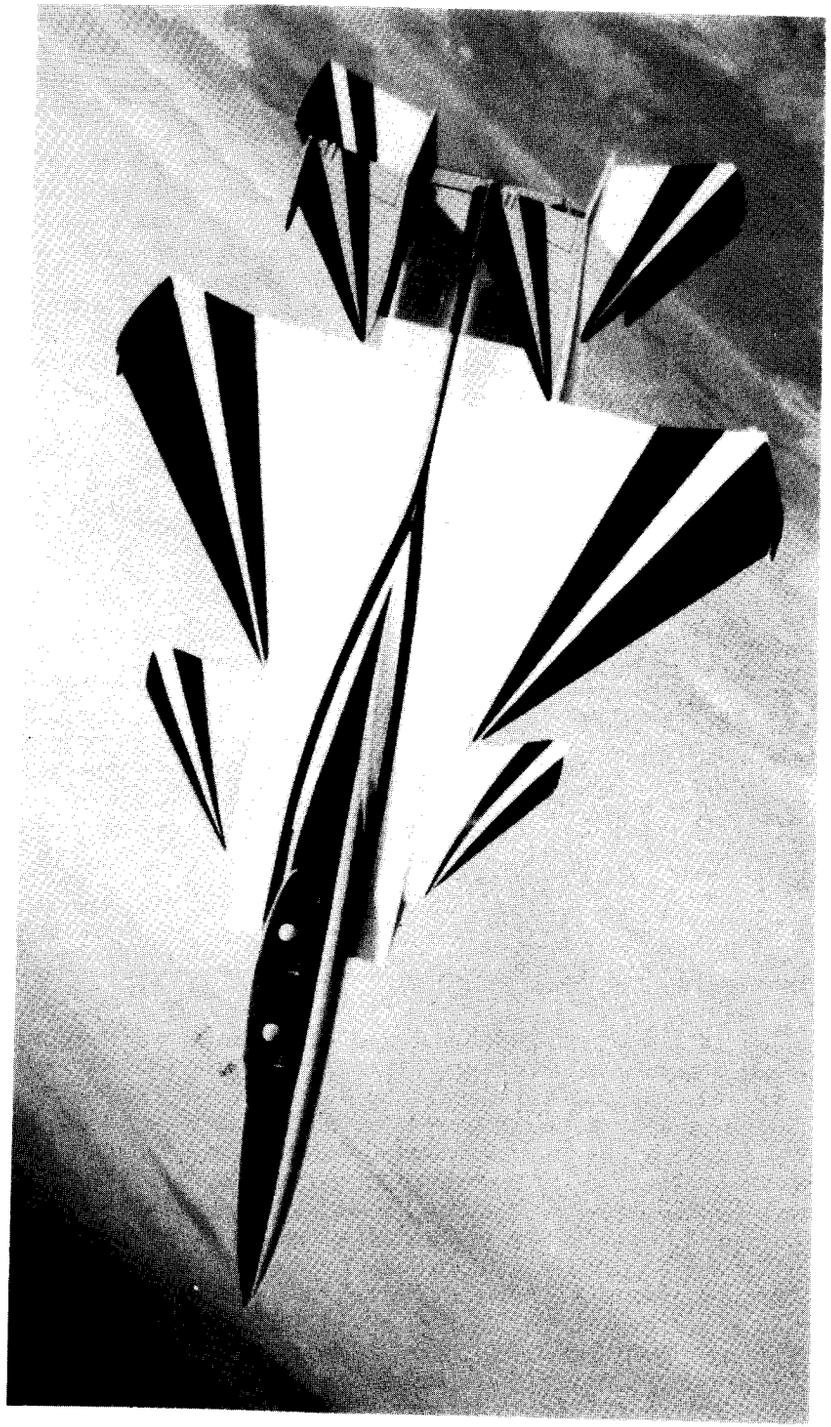

F-15 STOL Test Aircraft

16
STABILITY, CONTROL, AND HANDLING QUALITIES

16.1 INTRODUCTION

During early conceptual design, the requirements for good stability, control, and handling qualities are addressed through the use of tail volume coefficients and through location of the aircraft center of gravity (c.g.) at some percent of the wing mean aerodynamic chord (MAC), as discussed in Chapter 6. In larger aircraft companies, the aircraft is then analyzed by the controls experts, probably using a six-degree-of-freedom (6-DOF) aircraft-dynamics computer program to determine the required c.g. location and the sizes of the tails and control surfaces.

An understanding of the important stability and control design parameters can be attained through study of simpler methods, which are also suitable for use by homebuilders and designers at smaller companies.

This chapter introduces the key concepts and equations for stability, control, and handling qualities evaluation. These are based upon classical controls methods, many of which were developed by NACA in the period from 1925–1945. For derivations and additional detail on these methods, see Refs. 7, 37, 65, 66, and especially 67 and 4.

The basic concept of stability is simply that a stable aircraft, when disturbed, tends to return by itself to its original state (pitch, yaw, roll, velocity, etc.). "Static stability" is present if the forces created by the disturbed state (such as a pitching moment due to an increased angle of attack) push in the correct direction to return the aircraft to its original state.

If these restoring forces are too strong the aircraft will overshoot the original state and will oscillate with greater and greater amplitude until it goes completely out of control. Although static stability is present, the aircraft does not have "dynamic stability."

Dynamic stability is present if the dynamic motions of the aircraft will eventually return the aircraft to its original state. The manner in which the aircraft returns to its original state depends upon the restoring forces, mass distribution, and "damping forces." Damping forces slow the restoring rates. For example, a pendulum swinging in air is lightly damped and will oscillate back and forth for many minutes. The same pendulum immersed in water is highly damped and will slowly return to vertical with little or no oscillation.

Figure 16.1 illustrates these concepts for an aircraft disturbed in pitch. In Fig. 16.1a, the aircraft has perfectly neutral stability and simply remains at

whatever pitch angle the disturbance produces. While some aerobatic aircraft are nearly neutral in stability, few pilots would care to fly such an aircraft on a long trip in gusty conditions.

Illustration Fig. 16.1b shows static instability. The forces produced by the greater pitch angle actually cause the pitch angle to further increase. Pitchup is an example of this.

In Fig. 16.1c, the aircraft shows static stability with very high damping. The aircraft slowly returns to the original pitch angle without any overshoot.

Illustration Fig. 16.1d shows a more typical aircraft response; the aircraft returns to its original state, but experiences some converging oscillation. This is acceptable behavior provided the time to converge is short.

In Fig. 16.1e, the restoring forces are in the right direction so the aircraft is statically stable. However, the restoring forces are high and the damping forces are relatively low, so the aircraft overshoots the original pitch angle by a negative amount greater than the pitch angle produced by the disturbance. Restoring forces then push the nose back up, overshooting by an even greater amount. The pitch oscillations continue to increase in amplitude until the aircraft "diverges" into an uncontrolled flight mode such as a spin.

Note that dynamic instability is not always unacceptable provided that it occurs slowly. Most aircraft have at least one dynamic-instability mode, the spiral divergence. This divergence mode is so slow that the pilot has plenty of time to make the minor roll correction required to prevent it. In fact, pilots are generally unaware of the existence of the spiral-divergence mode because the minor corrections required are no greater than the roll corrections required for gusts.

Dynamic-stability analysis is complex and requires computer programs for any degree of accuracy. Most of the stability-analysis methods presented in this chapter evaluate static stability. For conventional aircraft configura-

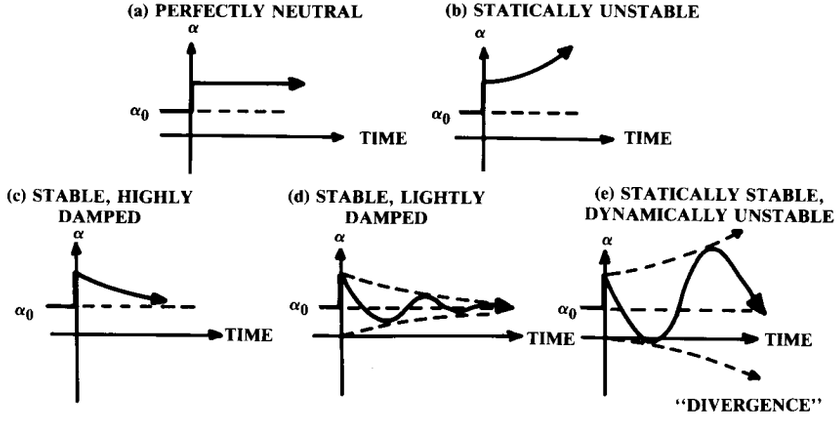

Fig. 16.1 Static and dynamic stability.

tions, satisfaction of static-stability requirements will probably give acceptable dynamic stability in most flight modes. Rule-of-thumb methods are presented for stall departure and spin recovery, the dynamic-stability areas of greatest concern.

16.2 COORDINATE SYSTEMS AND DEFINITIONS

Figure 16.2 defines the two axis systems commonly used in aircraft analysis. The "body-axis system" is rigidly fixed to the aircraft, with the X axis aligned with the fuselage and the Z axis upward. The origin is at an arbitrary location, usually the nose. The body-axis system is more "natural" for most people, but suffers from the variation of the direction of lift and drag with angle of attack. (Remember that lift, by definition, is perpendicular to the wind direction.)

The "wind axis" system solves this problem by orienting the X-axis into the relative wind regardless of the aircraft's angle of attack α or sideslip β. The aircraft is not fixed to the axis system, so the axis projections of the various lengths (such as the distance from the wing MAC to the tail) will vary for different angles of attack or sideslip. This variation in moment arms is usually ignored in stability analysis since the angles are usually small.

The "stability" axis system, commonly used in stability and control analysis, is a compromise between these two. The X-axis is aligned at the aircraft angle of attack, as in the wind axis system, but is not offset to the yaw angle. Directions of X, Y, and Z are as in the wind axis system.

Note that the rolling moment is called L. This is easily confused with lift. Also, the yawing moment is called N, which is the same letter used for the normal-force coefficient. The aerodynamics crowd must have used up all the good letters by the time the stability folks developed their equations!

Wing and tail incidence angles are denoted by i, which is relative to the body-fixed reference axis. The aircraft angle of attack α is also with respect to this reference axis, so the wing angle of attack is the aircraft angle of attack plus the wing angle of incidence.

Tail angle of attack is the aircraft angle of attack plus the tail angle of incidence, minus the downwash angle (ϵ) which is discussed later. In this

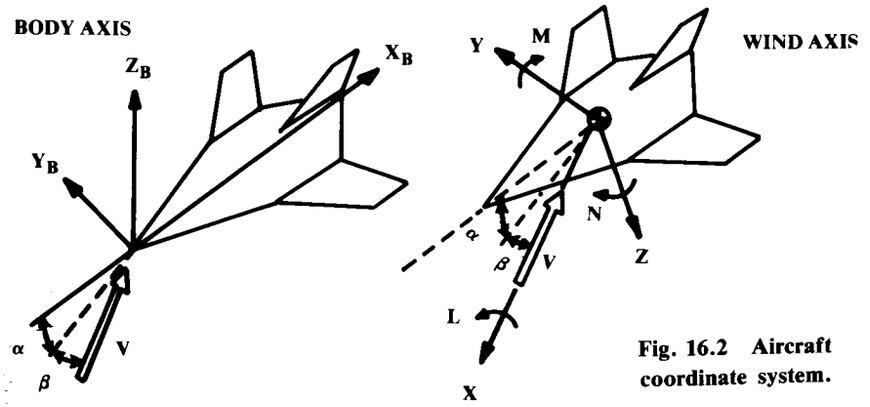

Fig. 16.2 Aircraft coordinate system.

chapter, angles of attack are measured from the zero-lift angle, which was discussed in Chapter 12.

Nondimensional coefficients for lift and drag have been previously defined by dividing by dynamic pressure and wing area. For stability calculations, the moments about the three axes (M, N, and L) must also be expressed as nondimensional coefficients.

Since the moments include a length (the moment arm) they must be divided by a quantity with dimension of length as well as by the dynamic pressure and wing area. This length quantity is the wing MAC chord for pitching moment and the wing span for yawing and rolling moments, as shown in Eqs. (16.1–16.3). Positive moment is nose up or to the right.

$$c_m = M/qS\bar{c} \tag{16.1}$$

$$c_n = N/qSb \tag{16.2}$$

$$c_\ell = L/qSb \tag{16.3}$$

Stability analysis is largely concerned with the response to changes in angular orientation, so the derivatives of these coefficients with respect to angle of attack and sideslip are critical. Subscripts are used to indicate the derivative. For example, C_{n_β} is the yawing moment derivative with respect to sideslip, a very important parameter in lateral stability.

Similarly, subscripts are used to indicate the response to control deflections, indicated by δ. Thus, $C_{m_{\delta_e}}$ indicates the pitching-moment response to an elevator deflection.

Unless otherwise indicated, all sweep angles in this chapter are quarter-chord sweeps, and all chord lengths c are the wing MAC. Also, all angles are in radians unless otherwise mentioned. Angle terms that are not estimated in radians must be converted to radians before use in stability equations.

16.3 LONGITUDINAL STATIC STABILITY AND CONTROL

Pitching-Moment Equation and Trim

Most aircraft being symmetrical about the centerline, moderate changes in angle of attack will have little or no influence upon the yaw or roll. This permits the stability and control analysis to be divided into longitudinal (pitch only) and lateral-directional (roll and yaw) analysis.

Figure 16.3 shows the major contributors to aircraft pitching moment about the c.g., including the wing, tail, fuselage, and engine contributions. The wing pitching-moment contribution includes the lift through the wing aerodynamic center and the wing moment about the aerodynamic center. Remember that the aerodynamic center is defined as the point about which pitching moment is constant with respect to angle of attack. This constant moment about the aerodynamic center is zero only if the wing is uncambered and untwisted. Also, the aerodynamic center is typically at 25% of the MAC in subsonic flight.

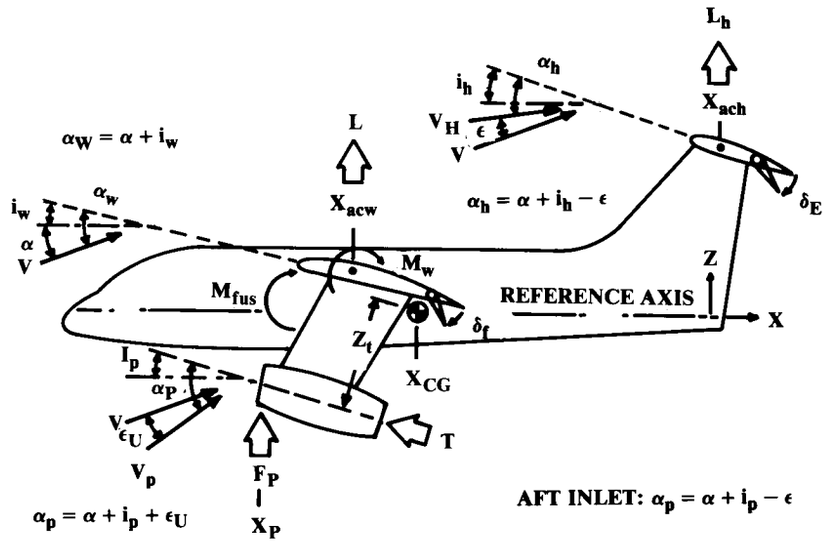

Fig. 16.3 Longitudinal moments.

Another wing moment term is the change in pitching moment due to flap deflection. Flap deflection also influences the wing lift, adding to that term. Flap deflection has a large effect upon downwash at the tail, as discussed later.

Drag of the wing and tail produces some pitching moment, but these values are negligibly small. Also, the pitching moment of the tail about its aerodynamic center is small and can be ignored.

On the other hand, the long moment arm of the tail times its lift produces a very large moment that is used to trim and control the aircraft. While this figure shows tail lift upward, under many conditions the tail lift will be downward to counteract the wing pitching moment.

A canard aircraft has a "negative" tail moment-arm that should be applied in the equations that follow. If an aircraft is tailless, the wing flap must be used for trim and control. Due to the short moment arm of such a control, the trim drags will be substantially higher for off-design c.g. locations.

The fuselage and nacelles produce pitching moments that are difficult to estimate without wind-tunnel data. These moments are influenced by the upwash and downwash produced by the wing.

The engine produces three contributions to pitching moment. The obvious term is the thrust times its vertical distance from the c.g. Less obvious is the vertical force F_p produced at the propeller disk or inlet front face due to the turning of the freestream airflow. Also, the propwash or jet-induced flowfield will influence the effective angle of attack of the tail and possibly the wing.

Equation (16.4) expresses the sum of these moments about the c.g. The effect of elevator deflection is included in the tail lift term. Equation (16.5)

expresses the moments in coefficient form by dividing all terms by (qS_wc) and expressing the tail lift in coefficient form. Note that, to facilitate understanding, these equations are defined in the body-axis coordinate system rather than the stability-axis system.

$$M_{cg} = L(X_{cg} - X_{acw}) + M_w + M_{w\delta_f}\delta_f + M_{fus} - L_h(X_{ach} - X_{cg}) - Tz_t + F_p(X_{cg} - X_p) \tag{16.4}$$

This produces a term representing the ratio between the dynamic pressure at the tail and the freestream dynamic pressure, which is defined in Eq. (16.6) as η_h. This ranges from about 0.85–0.95, with 0.90 as the typical value.

To simplify the equations, all lengths can be expressed as a fraction of the Wing mean chord c. These fractional lengths are denoted by a bar. Thus, $\bar{X}_{cg}$ represents X_{cg}/c. This leads to Eq. (16.7).

$$C_{m_{cg}} = C_L\left(\frac{X_{cg} - X_{acw}}{c}\right) + C_{m_w} + C_{m_{w_{\delta_f}}}\delta_f + C_{m_{fus}} - \frac{q_h S_h}{qS_w} C_{L_h}\left(\frac{X_{ach} - X_{cg}}{c}\right) - \frac{Tz_t}{qS_w c} + \frac{F_p(X_{cg} - X_p)}{qS_w c} \tag{16.5}$$

$$\eta_h = q_h/q \tag{16.6}$$

$$C_{m_{cg}} = C_L(\overline{X_{cg}} - \overline{X_{acw}}) + C_{m_w} + C_{m_{w_{\delta_f}}}\delta_f + C_{m_{fus}} - \eta_h \frac{S_h}{S_w} C_{L_h}(\overline{X_{ach}} - X_{cg}) - \frac{T}{qS_w}\overline{Z}_t + \frac{F_p}{qS_w}(\overline{X_{cg}} - \overline{X_p}) \tag{16.7}$$

For a static "trim" condition, the total pitching moment must equal zero. For static trim, the main flight conditions of concern are during the takeoff and landing with flaps and landing gear down and during flight at high transonic speeds. Trim for the high-g pullup is actually a dynamic problem (discussed later). Usually the most forward c.g. position is critical for trim. Aft-c.g. position is most critical for stability, as discussed below.

Equation (16.7) can be set to zero and solved for trim by varying some parameter, typically tail area, tail lift coefficient (i.e., tail incidence or elevator deflection), or sometimes c.g. position. The wing drag and tail trim drag can then be evaluated. Methods for the first-order evaluation of the terms of Eq. (16.7) are presented later.

Static Pitch Stability

For static stability to be present, any change in angle of attack must generate moments which oppose the change. In other words, the derivative of pitching moment with respect to angle of attack [Eq. (16.8)] must be negative. Note that the wing pitching moment and thrust terms have dropped out as they are essentially constant with respect to angle of attack.

Due to downwash effects, the tail angle of attack does not vary directly with aircraft angle of attack. A derivative term accounts for the effects of wing and propeller downwash, as described later. A similar derivative is provided for the propeller or inlet normal-force term F_p.

$$C_{m_\alpha} = C_{L_\alpha}(\overline{X}_{cg} - \overline{X}_{acw}) + C_{m_{\alpha fus}} - \eta_h \frac{S_h}{S_w} C_{L_{\alpha_h}} \frac{\partial \alpha_h}{\partial \alpha}(\overline{X}_{ach} - \overline{X}_{cg}) + \frac{F_{p_\alpha}}{qS_w}\frac{\partial \alpha_p}{\partial \alpha}(\overline{X}_{cg} - \overline{X}_p) \tag{16.8}$$

Equation (16.8) seems to offer no mechanism for stabilizing a tailless aircraft. In fact, the tailless aircraft must be stabilized in the first term by providing that the wing aerodynamic center is behind the c.g., making the first term negative.

The magnitude of the pitching-moment derivative [Eq. (16.8)] changes with c.g. location. For any aircraft there is a c.g. location that provides no change in pitching moment as angle of attack is varied. This "airplane aerodynamic center," or neutral point X_{np} represents neutral stability (Fig. 16.1a) and is the most-aft c.g. location before the aircraft becomes unstable.

Equation (16.9) solves Eq. (16.8) for the neutral point ($C_{m_\alpha} = 0$). Equation (16.10) then expresses the pitching moment derivative in terms of the distance in percent MAC from the neutral point to the c.g. This percent distance, called the "static margin," is the term in parenthesis in Eq. (16.10).

$$\overline{X}_{np} = \frac{C_{L_\alpha}\overline{X}_{acw} - C_{m_{\alpha fus}} + \eta_h \frac{S_h}{S_w} C_{L_{\alpha_h}} \frac{\partial \alpha_h}{\partial \alpha}\overline{X}_{ach} + \frac{F_{p_\alpha}}{qS_w}\frac{\partial \alpha_p}{\partial \alpha}\overline{X}_p}{C_{L_\alpha} + \eta_h \frac{S_h}{S_w} C_{L_{\alpha_h}} \frac{\partial \alpha_h}{\partial \alpha} + \frac{F_{p_\alpha}}{qS_w}} \tag{16.9}$$

$$C_{m_\alpha} = -C_{L_\alpha}(\overline{X}_{np} - \overline{X}_{cg}) \tag{16.10}$$

If the c.g. is ahead of the neutral point (positive static margin), the pitching-moment derivative is negative so the aircraft is stable (this is yet another confusing terminology!) At the most-aft c.g. position, a typical transport aircraft has a positive static margin of 5–10%.

Current fighters typically have positive static margins of about 5%, but new fighters such as the F-16 are being designed with "relaxed static stability (RSS)" in which a negative static margin (zero to −15%) is coupled with a computerized flight control system that deflects the elevator to provide artificial stability. This reduces trim drag substantially.

It is common to neglect the inlet or propeller force term F_p in Eq. (16.9) to determine "power-off" stability. This removes any strong dependence of X_{np} on velocity (q) in the subsonic flight regime. Power effects are then accounted for using a static margin allowance based upon test data for a

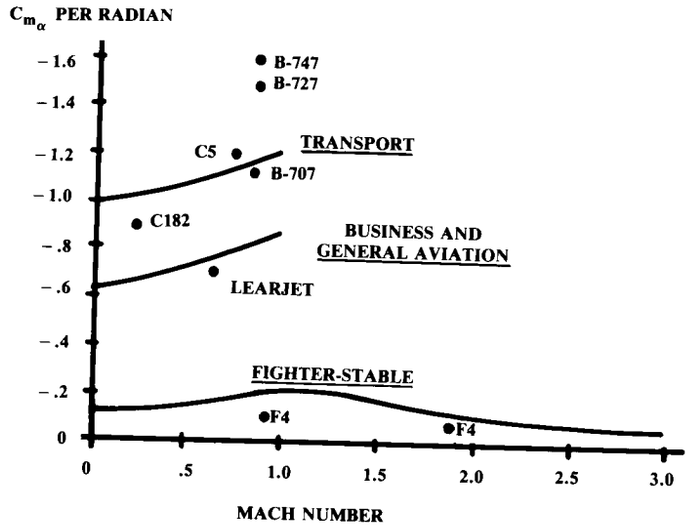

Fig. 16.4 Typical pitching moment derivative values.

similar aircraft. Typically these allowances for power-on will reduce the static margin by about 4–10% for propeller aircraft and 1–3% for jets.

Figure 16.4 illustrates pitching-moment-derivative values for several classes of aircraft. These may be used as targets for conceptual design. Dynamic analysis during later stages of design may revise these targets.

The evaluation of the terms in Eqs. (16.7–16.9) is difficult without wind-tunnel data. Various semi-empirical methods are presented below, primarily based upon Refs. 4, 37, 67, and 68. Note that these methods are considered crude by the stability and control community, and are only suitable for conceptual design estimates and for student design projects.

Aerodynamic Center

A critical term in Eq. (16.7) is X_{acw}, the location of the wing aerodynamic center. For a high-aspect-ratio wing the subsonic aerodynamic center will be located at the percent MAC of the airfoil aerodynamic center. For most airfoils this is the quarter-chord point (plus or minus 1%). At supersonic speeds the wing aerodynamic center typically moves to about 45% MAC.

Figure 16.5a–c provides graphical methods for aerodynamic center estimation (Refs. 67 and 37). Note that poor results are obtained at transonic speeds. These methods are also used for estimating the tail aerodynamic center.

Wing and Tail Lift, Flaps, and Elevators

The lift-curve slopes of the wing and tail are obtained with the methods presented in Chapter 12. The tail lift curve slope should be reduced about 20% if the elevator gap is not sealed.

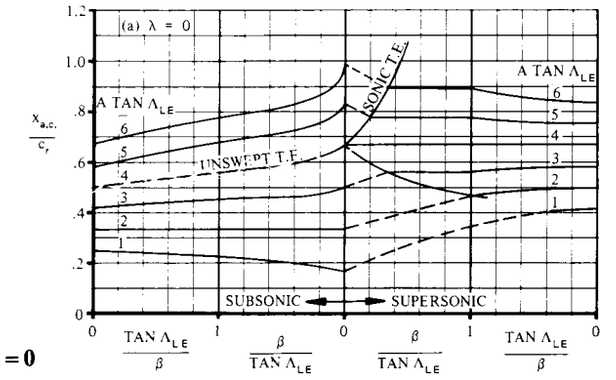

a) $\lambda = 0$

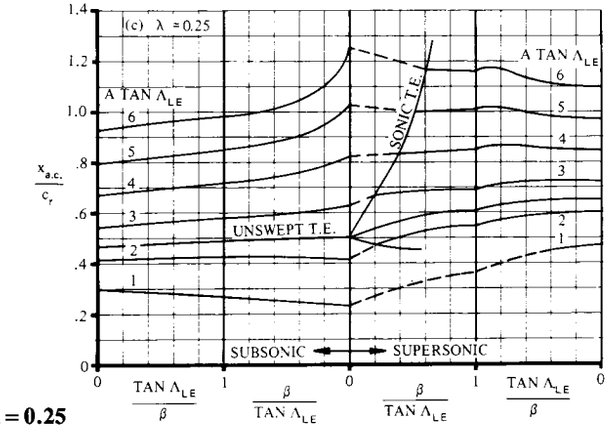

b) $\lambda = 0.25$

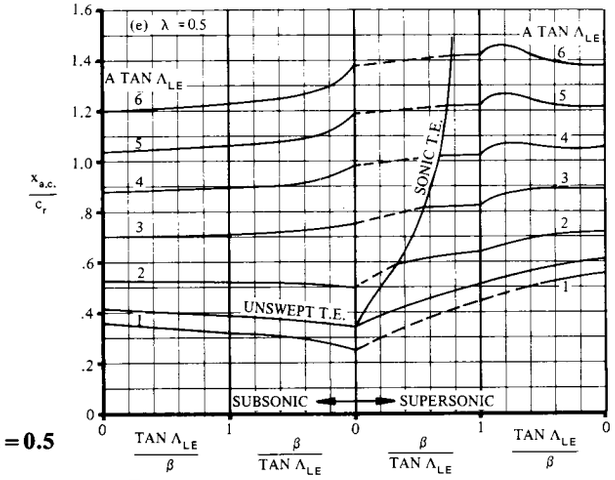

c) $\lambda = 0.5$

Fig. 16.5 Wing aerodynamic center. (Ref. 37)

The lift coefficients for the wing and tail are simply the lift-curve slopes times the wing or tail angle of attack (measured with respect to the zero-lift angle). These are defined in Eqs. (16.11) and (16.12) based upon the angle of attack definitions from Fig. 16.3. Note that for cambered airfoils, the zero-lift angle is a negative value. Also, the tail angle of attack must account for the downwash effect ϵ, which will be estimated later.

$$C_L = C_{L_\alpha}(\alpha + i_w - \alpha_{OL}) \tag{16.11}$$

$$C_{L_h} = C_{L_{\alpha_h}}(\alpha + i_h - \epsilon - \alpha_{OL_h}) \tag{16.12}$$

where α_{OL} is the angle of attack for zero lift, which is a negative value for a wing or tail with positive camber and/or downwards flap/elevation deflection.

The elevator acts as a flap to increase the tail lift. Flap deflection at moderate angles of attack does not change the lift-curve slope, so the lift increment due to flaps can be accounted for by a reduction in the zero-lift angle (i.e., more negative). This reduction in zero-lift angle is equal to the increase in lift coefficient due to flap deflection divided by the lift-curve slope:

$$\Delta\alpha_{OL} = -\frac{\Delta C_L}{C_{L_\alpha}} \tag{16.13}$$

For the complicated high-lift devices seen on most transport wings, the increase in lift coefficient can be approximated using the methods in Chapter 12 or from Fig. 5.3. The change in zero-lift angle can then be determined from Eq. (16.13) and applied to Eq. (16.11).

Plain flaps are used for a modest increase in wing lift and as the control surfaces (elevator, aileron, and rudder) for most aircraft. The change in zero-lift angle due to a plain flap is expressed in Eq. (16.14), where the lift increment with flap deflection is expressed in Eq. (16.15). The 0.9 factor is an approximate adjustment for flap tip losses.

$$\Delta\alpha_{0L} = -\frac{1}{C_{L_\alpha}}\frac{\partial C_L}{\partial \delta_f}\delta_f \tag{16.14}$$

where

$$\frac{\partial C_L}{\partial \delta_f} = 0.9K_f\left(\frac{\partial C_\ell}{\partial \delta_f}\right)'\frac{S_{\text{flapped}}}{S_{\text{ref}}}\cos\Lambda_{\text{H.L.}} \tag{16.15}$$

Figures 16.6 and 16.7 provide the theoretical airfoil lift increment for flaps at small deflections and an empirical adjustment for larger deflections. A typical flap used for control will have a maximum deflection of about 30 deg. Flap deflection must be converted to radians for use in Eq. (16.14). (Note that L is lift in these equations.)

Figure 16.8 defines the geometry for these equations. H.L. refers to the flap hinge-line sweep, S_{flapped} refers to the portion of the wing area with the

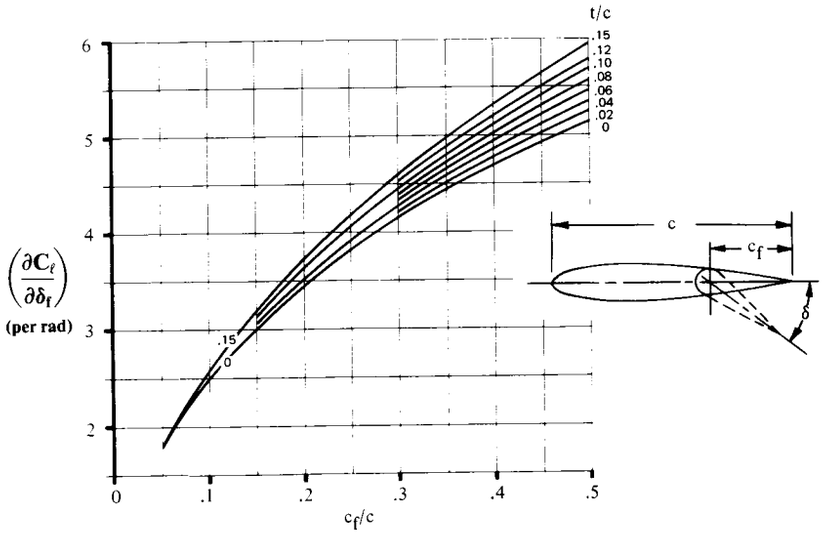

Fig. 16.6 Theoretical lift increment for plain flaps. (Ref. 37)

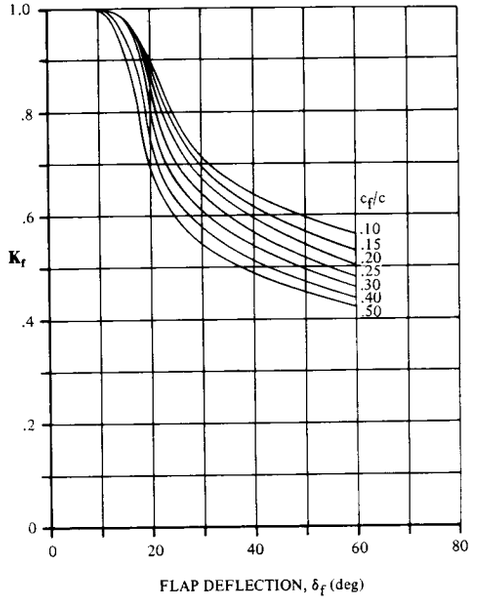

Fig. 16.7 Empirical correction for plain lift increment. (Ref. 37)

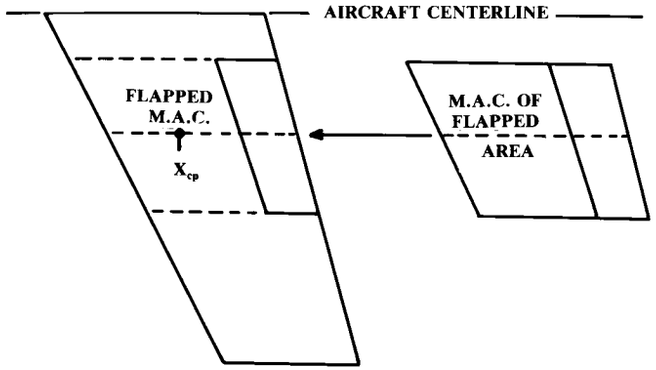

Fig. 16.8 Flapped area and flapped M.A.C. (C′).

flap or control surface. The MAC of the flapped portion of the wing or tail (c') is determined geometrically by considering the flapped portion as a separate surface.

If a flap, elevator, rudder, or aileron has an unsealed hinge gap the effectiveness will be reduced due to the air leaking through the opening. This reduction will be approximately 15% of the lift increment due to flap deflection.

Wing Pitching Moment

The wing pitching moment about the aerodynamic center is largely determined by the airfoil pitching moment. Equation (16.16) provides an adjustment for wing aspect ratio and sweep for a straight wing or an untwisted swept wing at low subsonic speeds. The wing twist adds an increment of approximately (-0.01) times the twist (in degrees) for a typical swept wing. A more detailed estimation of the wing twist effect is available in Ref. 37. Transonic effects increase the magnitude of the wing pitching moment by about 30% at Mach 0.8.

$$C_{m_w} = C_{m_{0_{\text{airfoil}}}}\left(\frac{A\cos^2\Lambda}{A+2\cos\Lambda}\right) \tag{16.16}$$

The pitching-moment increment due to flap deflection is approximated as the lift increment due to the flap times the moment arm from the center of pressure of the flap lift increment to the c.g. [Eq. (16.17)]. The center of pressure of the flap lift increment (X_{cp}) is determined as a percent of the flapped MAC (c') using Fig. 16.9.

For a highly swept wing the center of pressure of the flap lift increment can be ahead of the c.g., creating a positive moment increment. This reduces the download required by the tail. Conversely, a canard configuration will put the center of pressure of the flap lift increment well behind the c.g., requiring a huge balancing force.

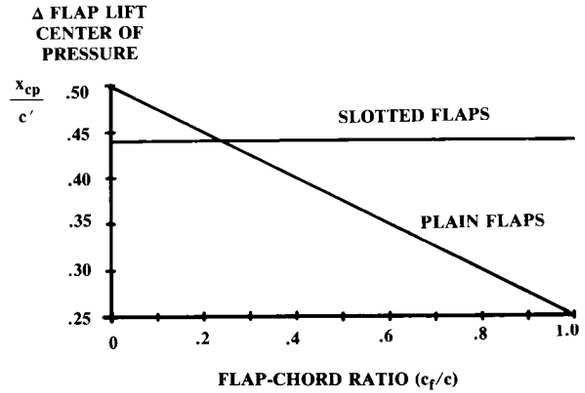

Fig. 16.9 Center of pressure for lift increment due to flaps. (after Ref. 37)

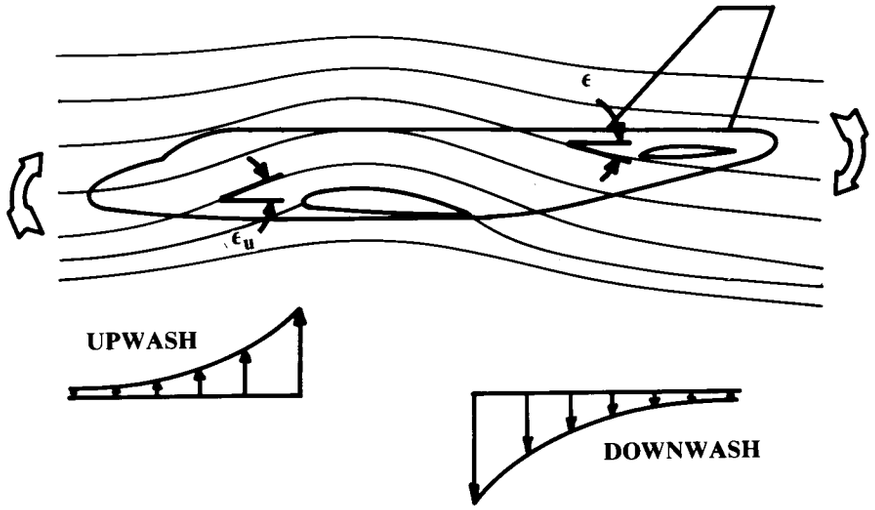

Fig. 16.10 Wing flowfield effect on pitching moment.

$$C_{m_{w_{\delta_f}}} = K_f \frac{\partial C_L}{\partial \delta_f}(\overline{X}_{cp} - \overline{X}_{cg}) \tag{16.17}$$

Downwash and Upwash

The remaining terms in Eq. (16.7) are strongly influenced by the wing flowfield, as shown in Fig. 16.10. Ahead of the wing, the air in subsonic flight is pulled upwards by the pressures about the wing. This upwash pushes upwards on the fuselage forebody and also turns the flow prior to reaching a propeller or inlet located ahead of the wing.

Behind the wing, the flow has an initial downward direction theoretically equal to the wing angle of attack. This downwash angle diminishes aft of the wing to a value of approximately half the wing angle of attack at the tail of a typical aircraft. Also, the downwash varies across the span and approaches zero near the wing tips.

The downwash reduces the tail angle of attack and pushes downward on the aft fuselage, contributing to the fuselage pitching moment. Downwash is strongly affected by the propwash.

The upwash-angle (ϵ_u) derivative with respect to wing angle of attack is determined from Fig. 16.11. The downwash angle (ϵ) derivative is determined from Fig. 16.12 at subsonic speeds. The spanwise variation in downwash behind the wing reduces the average downwash experienced by the tail by approximately 5%. The additional downwash due to flap deflection is determined from Fig. 16.13 in which h is the tail height above the wing.

At transonic speeds (around Mach 0.9) the downwash-angle derivative increases by about 30–40% then reduces at higher speeds. Equation (16.18) provides a rough approximation of the downwash at supersonic speeds.

$$\frac{\partial \epsilon}{\partial \alpha} = \frac{1.62 C_{L_\alpha}}{\pi A} \tag{16.18}$$

The resulting angle of attack considering the effect of upwash or downwash is determined by adding an upwash or subtracting a downwash from the freestream angle of attack. The angle-of-attack derivatives are therefore

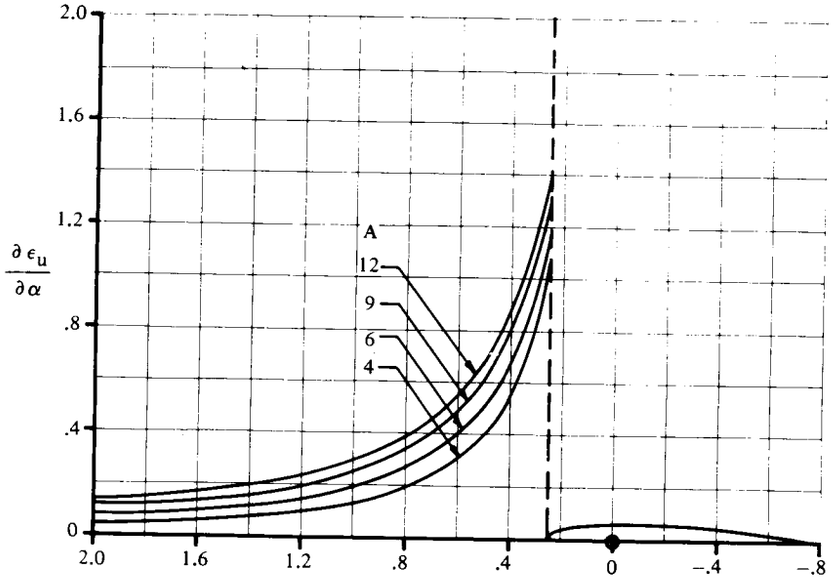

Fig. 16.11 Upwash estimation (subsonic only). (Ref. 37)

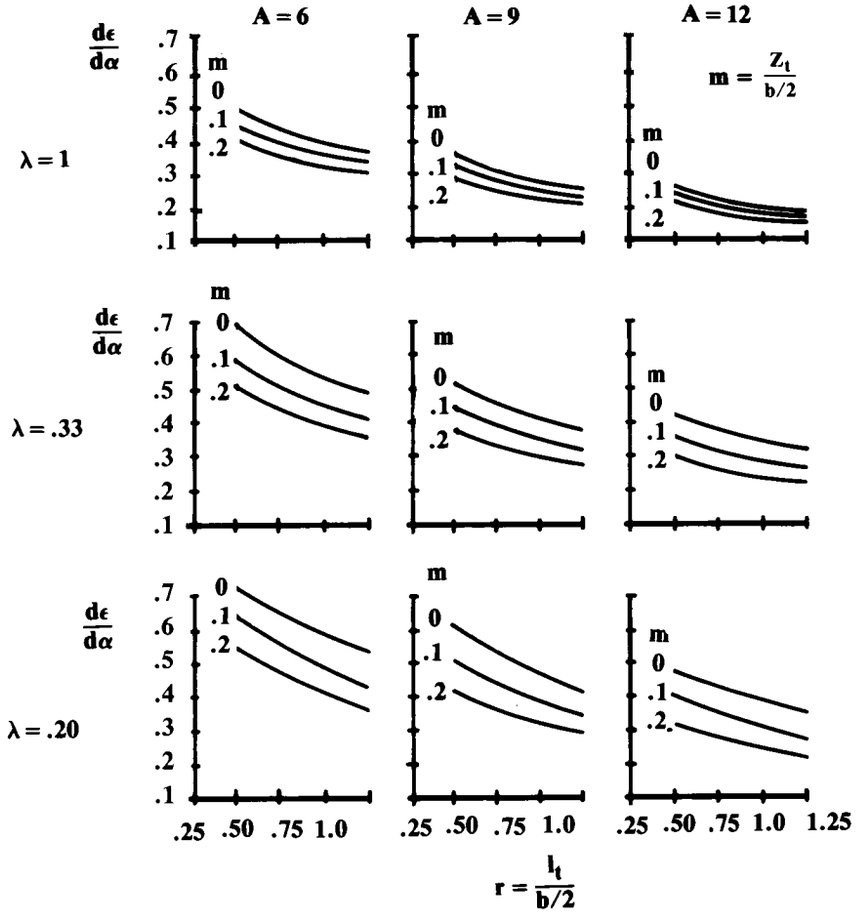

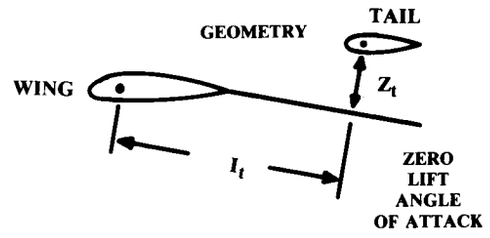

Fig. 16.12 Downwash estimation. (after Ref. 4)

as expressed in Eqs. (16.19) and (16.20). Equation (16.20) is the tail angle of attack derivative from Eq. (16.8), called β in many texts, which is easily confused with yaw angle. The downwash derivative is with respect to the wing angle of attack, so the tail angle of attack can now be determined as shown in Eq. (16.21).

$$\text{Upwash:} \quad \frac{\partial \alpha_u}{\partial \alpha} = 1 + \frac{\partial \epsilon_u}{\partial \alpha} \tag{16.19}$$

$$\text{Downwash:} \quad \frac{\partial \alpha_h}{\partial \alpha} = 1 - \frac{\partial \epsilon}{\partial \alpha} \tag{16.20}$$

$$\alpha_h = (\alpha + i_w)\left(1 - \frac{\partial \epsilon}{\partial \alpha}\right) + (i_h - i_w) \tag{16.21}$$

A canard will obviously experience no downwash from the wing, but its own downwash will influence the wing. The estimation of the effect of canard downwash on the wing is very difficult because the downwash varies across the canard span and because the canard tip vortices actually create an upwash on the wing outboard of the canard.

The effect of canard downwash on the wing may be crudely approximated by assuming that the canard downwash as calculated with these methods uniformly affects the wing inboard of the canard tips. This reduces the angle of attack at the wing root.

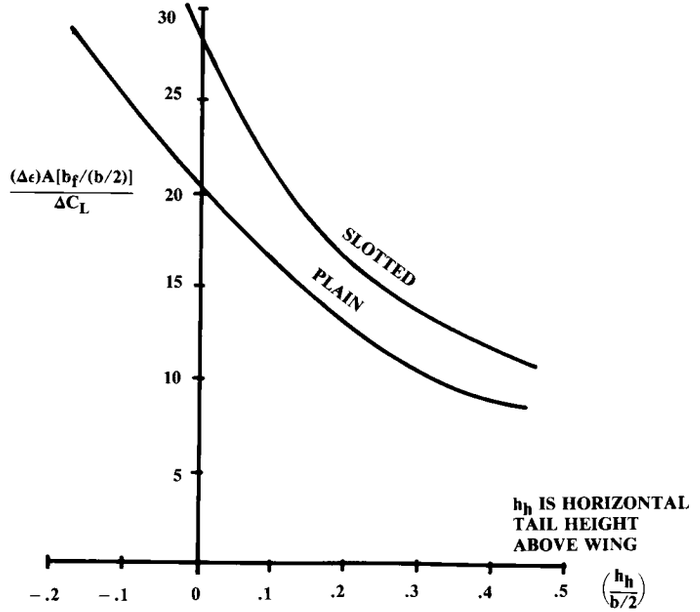

Fig. 16.13 Downwash increment due to flaps.

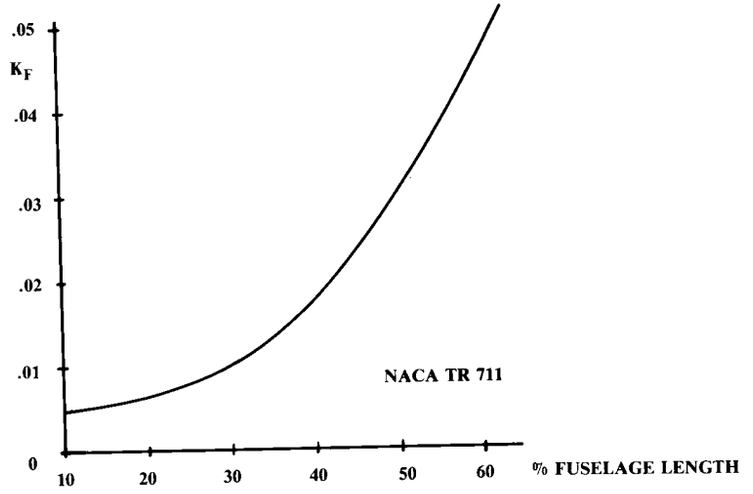

Fig. 16.14 Position of ¼ root chord.

Fuselage and Nacelle Pitching-Moment

The pitching-moment contributions of the fuselage and nacelles can be approximated by Eq. (16.22) from NACA TR 711. The W_f is the maximum width of the fuselage or nacelle and L_f is the length. Figure 16.14 provides the empirical pitching moment factor K_f.

$$C_{m_{\alpha_{\text{fuselage}}}} = \frac{K_f W_f^2 L_f}{c S_w}, \text{ per deg} \tag{16.22}$$

Thrust Effects

The remaining terms in Eq. (16.7) are thrust effects upon pitching moment. Thrust has three effects, namely the direct moment of the thrust, the propeller or inlet normal force due to turning of the air, and the influence of the propwash or jet-induced flows upon the tail, wing, and aft fuselage.

The direct moment of the thrust is simply the thrust times the moment arm about the c.g., as defined in Eq. (16.7). If the thrust axis passes through or near the c.g. this term may be ignored.

The normal force due to the turning of the air at an inlet front face F_p can be calculated from momentum considerations. This normal force equals the massflow into the inlet times the change in vertical velocity. Since the angles are small, the change in vertical velocity is approximately the turning angle (α_p—see Fig. 16.3) times the aircraft velocity [Eq. (16.23)]. The engine mass-flow can be approximated by assuming a capture-area ratio of one [Eq. (16.24)] if installed engine mass-flow data is unavailable. Note that mass flow is in slugs per second, which equals pounds per second divided by 32.2.

$$F_p = \dot{m}V \tan\alpha_p \cong \dot{m}V\alpha_p \tag{16.23}$$

$$\dot{m} \cong \rho V A_{\text{inlet}}, \text{ slugs/s} \tag{16.24}$$

$$F_{p_\alpha} = \dot{m}V \tag{16.25}$$

The derivative of the normal force with respect to angle of attack is the mass flow times the velocity [Eq. (16.25)]. The derivative of α_p with respect to angle of attack [see Eq. (16.9)] is the upwash derivative Eq. (16.19) if the inlet is ahead of the wing, and the downwash derivative Eq. (16.20) if the inlet is behind the wing. For an inlet mounted under the wing, the wing turns the flow before it reaches the inlet front face so the normal force is approximately zero.

For a propeller-powered aircraft, a normal force contribution to pitching moment is also produced by the momentum change caused by the turning of the airstream. Unlike the jet inlet, the actual turning angle is not apparent because the propeller does not fully turn the airflow to align with the propeller axis.

Equation (16.26) is an empirical method for estimation of the propeller normal force based upon charts in Ref. 68; N_B is the number of blades per propeller, A_p is the area of one propeller disk. The derivative term is the normal force exerted by one blade when the propeller is operating at zero thrust, found in Fig. 16.15 as a function of advance ratio. The function $f(T)$ adjusts for non-zero thrust and is found in Fig. 16.16.

$$F_{p_\alpha} = qN_B A_p \frac{\partial C_{N_{\text{blade}}}}{\partial\alpha} f(T) \tag{16.26}$$

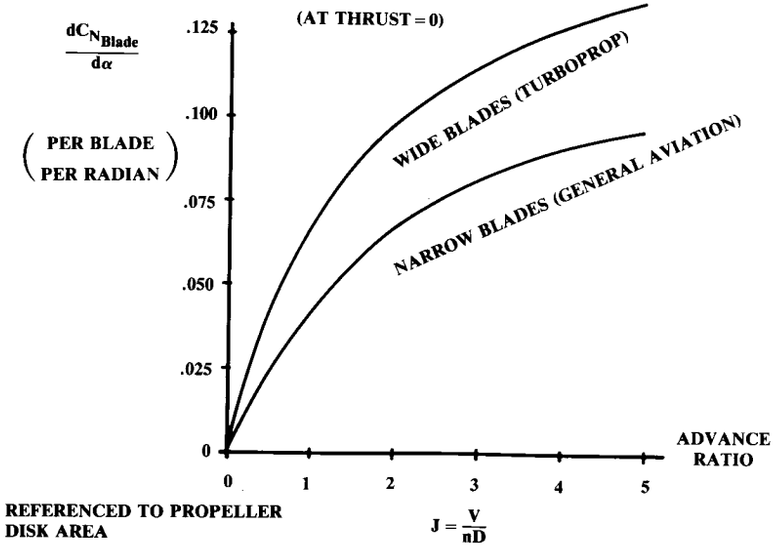

Fig. 16.15 Propeller normal force coefficient. (after Ref. 68)

Note in Eq. (16.7) that a propeller mounted aft of the c.g. is stabilizing. This is one of the advantages of the pusher-propeller configuration.

The propwash affects the downwash seen by the horizontal tail and reduces the tail's effectiveness. Equation (16.27) estimates this propeller downwash effect as a derivative that is added to the wing downwash derivative. The constant terms come from Fig. 16.17.

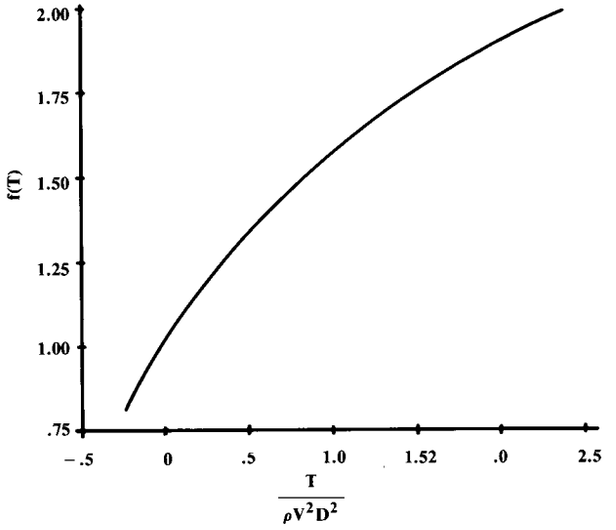

Fig. 16.16 Propeller normal force factor. (after Ref. 68)

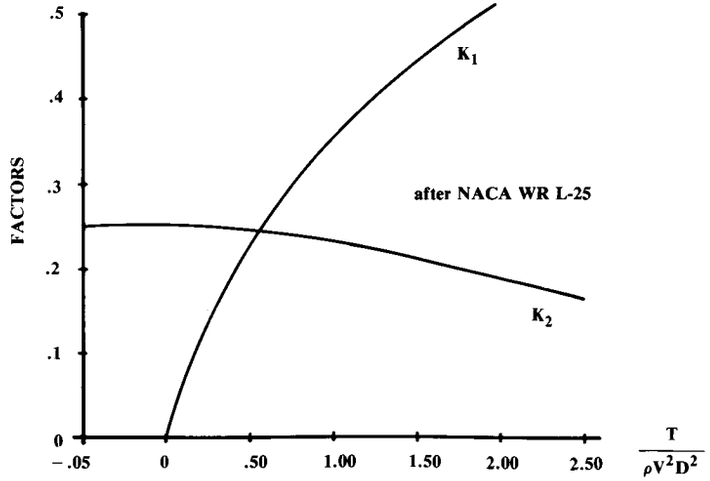

Fig. 16.17 Propeller downwash factors. (after Ref. 68)

$$\frac{\partial \epsilon_p}{\partial \alpha} = K_1 + K_2 N_B \frac{\partial C_{N_{\text{blade}}}}{\partial \alpha}\left(\frac{\partial \alpha_p}{\partial \alpha}\right) \tag{16.27}$$

If largely in the propwash, the tail will experience an increased dynamic pressure, as shown in Eq. (16.28). The tail dynamic pressure ratio η_h for zero thrust is approximately 0.9. If the tail is only partly in the propwash the right-side term in the parenthesis should be reduced proportionally. This term can also be applied to estimate increase in dynamic pressure at the wing, which may especially affect the pitching moment due to flap deflection.

$$\eta_h = \eta_{h_{T=0}}\left(1 + \frac{T}{qA_p}\right) \tag{16.28}$$

The increase in dynamic pressure at the tail will increase the magnitude of the tail lift which, being downward in most cases, causes a nose-up trim change with application of power. It is not uncommon in single-engined propeller aircraft to incline the propeller axis several degrees downward to counteract the power effect upon trim.

Trim Analysis

We now have all the information required for trim analysis. Trim requires that the total moment about the c.g. [Eq. (16.7)] equals zero. For a given flight condition, we can determine the values in the equation and see if they sum to zero. If not, we can vary the tail lift by changing elevator deflection or tail incidence until the total moment is zero.

However, the change in tail lift will change the aircraft total lift, which must equal the weight. Therefore, as the tail lift changes, the aircraft angle of attack must change. This can be solved by a computerized iterative process or by a graphical technique.

For the graphical solution, arbitrarily assumed aircraft angles of attack and elevator deflection angles (δ_E) are used to calculate the total-pitching-moment coefficient ($C_{m_{cg}}$) using Eq. (16.7). Equation (16.29) is used to determine the tail-lift term.

$$C_{L_h} = C_{L_{\alpha_h}}\left[(\alpha + i_w)\left(1 - \frac{\partial \epsilon}{\partial \alpha}\right) + (i_h - i_w) - \alpha_{OL_h}\right] \tag{16.29}$$

$$C_{L_{\text{total}}} = C_{L_\alpha}[\alpha + i_w] + \eta_h \frac{S_h}{S_w} C_{L_h} \tag{16.30}$$

For the arbitrarily assumed angles of attack and elevator deflection, the total lift coefficient $C_{L_{\text{total}}}$ can be estimated using Eq. (16.30). This equation sums the wing and tail lift coefficients, including the effects of dynamic pressure at the tail. Remember that by definition an upload on the tail is positive. If a download exists on the tail, the tail lift reduces the total lift.

The total-pitching-moment coefficient is then plotted vs the total lift coefficient for the various elevator-deflection angles. The elevator deflection

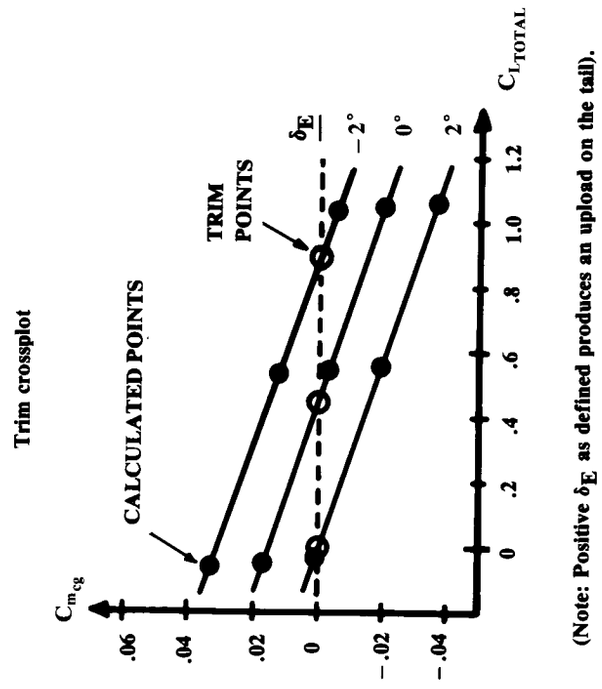

(Note: Positive δ_E as defined produces an upload on the tail).

Fig. 16.18 Graphical trim analysis.

Calculation table			
	$\delta_E = -2°$	0°	2°
$\alpha = 0°$	$C_{m_{cg}} = 0.033$	0.018	0.002
	$C_{L_{TOTAL}} = -0.07$	−0.05	−0.03
$\alpha = 5°$	$C_{m_{cg}} = 0.012$	−0.004	−0.02
	$C_{L_{TOTAL}} = 0.53$	0.54	0.56
$\alpha = 10°$	$C_{m_{cg}} = -0.005$	−0.021	−0.038
	$C_{L_{TOTAL}} = 1.03$	1.04	1.06

for trim is determined by interpolating for zero pitching moment at the required total lift coefficient. This is illustrated in Fig. 16.18.

The total induced drag including trim-drag effects can now be calculated at the trim angle of attack and elevator deflection angle using Eq. (16.31). Note that the term K_h is the drag-due-to-lift factor for the horizontal tail. This is determined using the methods of Chapter 12, treating the horizontal tail as a wing. Since the tail's induced drag is much smaller than the wing induced drag, it is permissible to use the simpler empirical methods for K (or e) rather than the leading-edge-suction method.

$$C_{D_{i_{\text{trimmed}}}} = K[C_{L_\alpha}(\alpha + i_w)]^2 + \eta_h \frac{S_h}{S_w} K_h \, [C_{L_h}]^2 \tag{16.31}$$

Due to the amount of computation involved, it is common in early conceptual design to calculate the trim condition without including the thrust effects unless the thrust axis is well above or below the c.g.

For an all-moving tail, the tail incidence angle is varied rather than elevator angle. For a tailless configuration, the wing flap acts as the elevator. Otherwise the procedure is similar.

(Most stability-and-control textbooks introduce a secondary derivative term $C_{m_{\delta_E}}$ that directly relates the elevator deflection to its influence upon pitching moment. I choose to leave the elevator effect as a change in tail lift to avoid further complexity in terminology and to leave the tail moment as a clearly-understood "force-times-distance" term. This understanding is especially important in conceptual design because the designer still has the freedom to change the "distance.")

Ground Effect on Trim Calculation

The trim Eq. (16.7) is strongly affected by ground effect (Chapter 12). When the aircraft approaches the ground to within about 20% of the span, the wing and tail lift-curve slopes will increase by about 10%. Furthermore, the downwash is reduced to about half of the normal value, which requires a greater elevator deflection to hold the nose up.

The aircraft must have sufficient elevator effectiveness to trim in ground effect with full flaps and full-forward c.g. location, at both power-off and full power. Some additional elevator authority must then be available for control.

Take-Off Rotation

Sometimes the elevator of an aircraft is sized by the requirement for takeoff rotation. For a tricycle-gear aircraft the elevator should be powerful enough to rotate the nose at 80% of takeoff speed with the most-forward c.g. For a taildragger aircraft the elevator should be powerful enough to lift the tail at half the takeoff speed with the most-aft c.g. (Ref. 66).

For rotation analysis, Eq. (16.7) may be employed with the addition of two landing-gear terms. The analysis assumes that the nosewheel or tailwheel is just resting on the ground without carrying any of the weight. The weight on the wheels is the aircraft weight minus the total lift at that angle

of attack. This exerts a vertical force with a moment arm equal to the distance from the main gear to the c.g. as measured parallel to the ground.

The rolling friction of the mainwheels exerts a rearward force equal to the weight on the wheels times the rolling friction coefficient (0.03 is typical). This rolling friction force acts through a moment arm equal to the vertical height of the c.g. above the ground.

These additional moments due to the vertical and rearward landing gear forces must be converted to moment coefficients by dividing them by (qS_wc).

The previously-described changes in lift-curve slopes and downwash angles due to ground effect must be considered in takeoff rotation analysis.

Velocity Stability

This brief discussion of longitudinal stability and control has focused upon the angle-of-attack stability derivatives. The aircraft must also have velocity stability, implying that an increase in velocity must produce forces which slow the aircraft down, usually by raising the nose. For most contributors to pitching moment, angle-of-attack stability implies velocity stability as well.

One additional term which affects velocity stability is the variation in thrust with velocity. For propellers, the thrust reduces with increased aircraft velocity. If the propeller is mounted substantially above the c.g., an increase in velocity will reduce the thrust, causing the aircraft to pitch nose-up. This produces a slight climb which will reduce the velocity, so a high-mounted propeller is stabilizing.

Roughly speaking, the static margin increases one-quarter of a percent for every 1% MAC that the thrust axis is above the c.g. Conversely, a propeller mounted below the c.g. is destabilizing by the same amount.

The stability advantage of the high-mounted propeller must be weighed against the large trim force required to counter the nose-down pitching moment of the high thrust axis. The high-mounted propeller is usually used only to provide water clearance in a seaplane.

For jet aircraft, the velocity effect upon thrust being negligible, engine vertical position has little effect upon velocity stability.

16.4 LATERAL-DIRECTIONAL STATIC STABILITY AND CONTROL

Yaw/Roll Moment Equations and Trim

In many ways the lateral-directional analysis resembles the longitudinal analysis. However, the lateral-directional analysis really embraces two closely-coupled analyses: the yaw (directional) and the roll (lateral).

It is important to realize that both are driven by the yaw angle β, and that the roll angle ϕ actually has no direct effect upon any of the moment terms! Furthermore, the deflection of either rudder or aileron will produce moments in both yaw and roll. (Note: to reduce verbiage, "lateral" is used synonymously with "lateral-directional" in the discussion below.)

The geometry for lateral analysis is illustrated in Fig. 16.19, showing the major contributors to yawing moment N and rolling moment L. By defini-

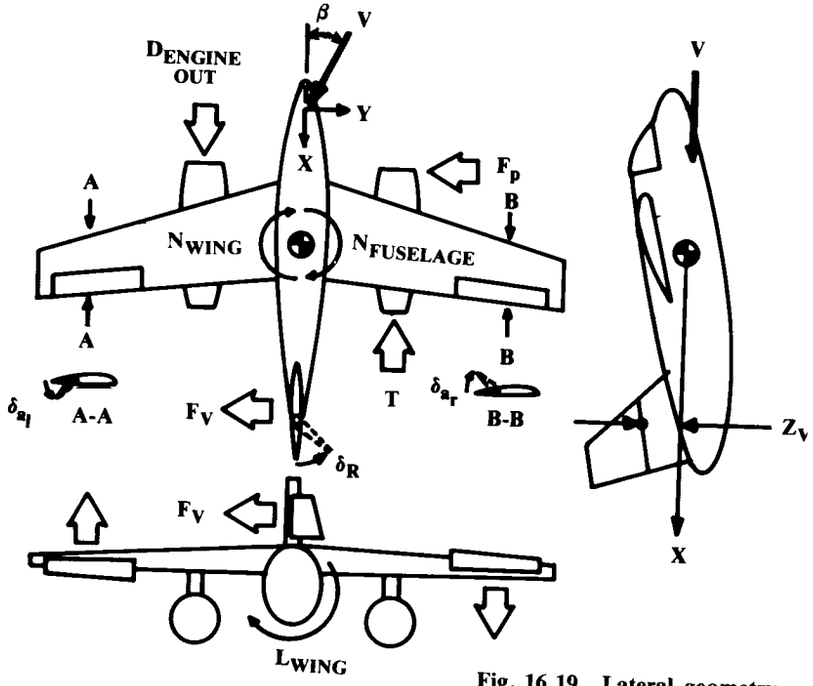

Fig. 16.19 Lateral geometry.

tion, yaw and roll are positive to the right. Note that unlike the longitudinal terms, most of these terms have a zero value when the aircraft is in straight and level flight. Also, by the sign conventions used for β and yaw, a positive value of yawing moment derivative with respect to β is stabilizing. However, a negative value of the rolling moment derivative with respect to β is stabilizing (dihedral effect).

The major yawing moment is due to the lateral lift of the vertical tail, denoted by F_v. This counteracts the fuselage yawing moment, which is generally negative to the sense shown in the figure. Rudder deflection acts as a flap to increase the lateral lift of the vertical tail.

A vertical tail immersed in the propwash experiences an additional force. The air in the propwash has a rotational component caused by the propeller and in the same direction that the propeller rotates. A propeller usually rotates clockwise when seen from behind. For a vertical tail above the fuselage, the propwash rotational component causes the angle of sideslip at the tail to become more negative, thus yawing the nose of the aircraft to the left. Called "p-effect," this is difficult to predict. Many single-engined aircraft have 1 or 2 deg of incidence built into the vertical tail to counteract p-effect. Alternatively, some aircraft have the propeller axis angled to the right.

The wing yawing moment can be visualized as an increase in drag on the side of the wing that is more nearly perpendicular to the oncoming flow. If the wing is swept aft, this yawing moment is stabilizing as shown.

Another wing yawing moment occurs with aileron deflection. The wing with increased lift due to aileron deflection has more induced drag, so the yawing moment is in the opposite direction from the rolling moment due to the aileron deflection. This is known as "adverse yaw."

The engines have the same three effects upon lateral moments that they have on longitudinal moments (direct thrust, normal force, and propwash or jet-induced flowfield effects). In yaw, the thrust is balanced unless an engine fails. Then the remaining engine(s) create a huge yawing moment which is made worse by the drag of the failed engine.

The inlet front face or propeller disk has the same normal-force term discussed for longitudinal stability. As in pitch, this is destabilizing in yaw if the inlet or propeller is in front of the c.g.

The propwash or jet-induced flowfield effects are generally negligible in yaw unless the vertical tail is in the propwash or near the jet exhaust. In this case the dynamic pressure and angle of sideslip at the tail will be affected much as the horizontal tail is affected by propwash.

In roll, the major influence is the wing rolling moment due to dihedral effect. As discussed in Chapter 4, this rolling moment tends to keep the aircraft level because it sideslips downward whenever a roll is introduced. The dihedral effect rolls the aircraft away from the sideslip direction.

The ailerons, the primary roll-control device, operate by increasing lift on one wing and reducing it on the other. The aileron deflection δ_a is defined as the average of the left and right aileron deflections in the directions shown. (Some texts define aileron deflection as the total of left and right.) Positive aileron deflection rolls the aircraft to the right.

"Spoilers" are an alternative roll-control device. These are plates that rise up from the top of the wing, usually just aft of the maximum-thickness point. This disturbs the airflow and "spoils" the lift, dropping the wing on that side. Spoiler deflection also increases drag, so the wing yaws in the same direction that it rolls ("proverse yaw").

The vertical tail contributes positively to the roll stability because it is above the c.g.. Note that the moment arm for the vertical tail roll contribution is from the vertical tail MAC to the X-axis in the stability (wind) axis system. This X-axis is through the c.g. and is aligned with the relative wing. Thus, this term changes substantially with angle of attack.

The major thrust effect on static roll moments is the engine-out case. The air in the propwash has higher dynamic pressure and thus produces more lift on the wing. With propwash on only one side of the wing there is a difference in lift between the left and right wing. This can frequently be ignored because the resulting roll moment is so much less than the engine-out yaw moment. The equivalent jet-induced effect on roll is negligible unless the jet exhaust impinges upon the flaps, as in the YC-15.

Propwash can also alter the wing dihedral effect. When the aircraft yaws, one side of the wing gets more propwash than the other, producing a destabilizing roll moment. This is more severe for single-engined aircraft where the propeller is way in front of the wing.

There will be a thrust normal force contribution to rolling moment at angle of sideslip if the engines are substantially above or below the c.g. A high-mounted engine would be stabilizing. This is usually negligible.

$$N = N_{\text{wing}} + N_{w_{\delta_a}}\delta_a + N_{\text{fus}} + F_v(X_{acv} - X_{\text{cg}}) - TY_p - DY_p - F_p(X_{\text{cg}} - X_p) \tag{16.32}$$

$$L = L_{\text{wing}} + L_{w_{\delta_a}}\delta_a - F_v(Z_v) \tag{16.33}$$

These yaw and roll moments are summed in Eqs. (16.32) and (16.33) for a twin-engined aircraft with one engine out. Similar equations for other engine arrangements should be obvious from inspection of Fig. 16.19. These are strictly static equations. Dynamic terms will be considered in a later section.

The lateral lift force on the vertical tail appears in both equations. This is much like the horizontal-tail lift, and must be calculated using the local dynamic pressure and angle of sideslip. The local angle of sideslip is less than the freestream sideslip angle because of a "sidewash" effect largely due to the fuselage. Propwash can also reduce the effective angle of sideslip. Equation (16.34) expresses the lateral lift force on the vertical tail. Note that the tail lateral-lift-force derivative C_{F_β} is equivalent to C_{L_α} in longitudinal notation and is calculated the same way.

$$F_v = q_v S_v C_{F_{\beta_v}} \frac{\partial \beta_v}{\partial \beta} \beta \tag{16.34}$$

The yaw- and roll-moment equations are expressed in coefficient form by dividing through by $(qS_w b)$, as shown in Eqs. (16.35) and (16.37). Lengths are expressed as a fraction of wing span using the "bar" notation. Thus, $(\bar{Y}_v)$ denotes (Y_v/b).

Lateral-Trim Analysis

The main static lateral-trim condition of concern is the engine-out case on takeoff. The vertical tail with rudder deflected must produce sufficient yawing moment to keep the aircraft at zero angle of sideslip at takeoff speed (1.1 times the stall speed) with one engine out and at the aftmost c.g. location. Rudder deflection should probably be no more than 20 deg to allow additional deflection for control.

Another lateral-trim condition which should be checked is the crosswind-landing case. The aircraft must be able to operate in crosswinds equal to 20% of takeoff speed, which is equivalent to holding an 11.5-deg sideslip at takeoff speed. Again, no more than 20 deg of rudder should be used.

If the vertical tail cannot provide sufficient force to produce zero yawing moment in Eq. (16.35) for either of these cases, there are several approaches to correct the problem. The brute-force method simply increases the vertical-tail size, but this penalizes aircraft weight and drag.

The rudder chord and/or span can be increased to improve the rudder effectiveness. This can also be increased by using a double-hinged rudder, as seen on the DC-10. An all-moving vertical tail as seen on the F-107 and SR-71 provides the greatest "rudder" control power for a given tail area, but is heavy.

Sometimes the engines may be moved inward to reduce the engine-out moment. However, this increases wing structural weight as discussed.

The rudder deflection and propwash effects for the engine-out case will also cause a rolling moment. Usually this is small enough to be ignored, but a short-coupled aircraft with widely-separated engines may require excessive aileron deflections to counter the rolling moments. The adverse yaw of

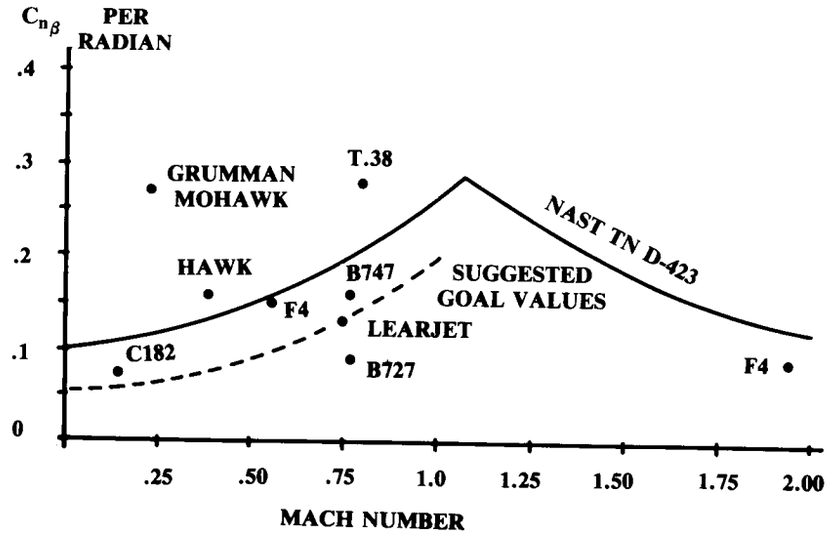

Fig. 16.20 Typical yaw moment derivative values.

Figure 16.20 provides suggested goal values for C_{n_β}. These are somewhat less than those suggested by the NASA curve. C_{l_β} should be of negative sign with magnitude about half that of the C_{n_β} value at subsonic speeds, and about equal to it at transonic speeds.

Final selection of these values requires dynamic analysis based upon wind-tunnel data, and it is not unheard of for the vertical-tail size or wing dihedral to be changed after the prototype flies (F-100, B-25).

The following sections provide crude estimation procedures for the terms of these lateral equations. Many of these terms are identical to longitudinal terms as previously discussed, and the reader should refer back to that material. These include the tail aerodynamic center, tail-force (lift) curve slope, rudder (flap) effectiveness, and propeller or inlet normal-force.

Wing Lateral-Directional Derivatives

Reference 37 provides an empirical expression for the wing yawing moment due to sideslip [Eq. (16.41)].

$$C_{n_{\beta_w}} = C_L^2 \left\{ \frac{1}{4\pi A} - \left[\frac{\tan\Lambda}{\pi A (A + 4\cos\Lambda)} \right] \left[\cos\Lambda - \frac{A}{2} - \frac{A^2}{8\cos\Lambda} + \frac{6(\bar{X}_{acw} - \bar{X}_{cg})\sin\Lambda}{A} \right] \right\} \tag{16.41}$$

The rolling moment due to sideslip, or dihedral effect, is proportional to the dihedral angle but also includes the effects of sweep and wing vertical position on the fuselage; C_{l_β} for a straight wing is approximately 0.0002

times the dihedral angle in deg, so 1 deg of "effective dihedral" is defined to be a C_{l_β} of 0.0002 per deg, or 0.0115 per radian.

Figure 16.21 (replotted from Ref. 10) provides an estimate of the wing dihedral effect due to sweep for a wing with no geometric dihedral. Two taper ratios are provided, requiring interpolation or extrapolation for other taper ratios. The values from the figure are per unit lift coefficient, so the final value is obtained by multiplying by the wing C_L.

Equation (16.42) from Ref. 37 estimates the effect of the geometric dihedral angle (radians). Equation (16.43) from Ref. 68 determines the effect of wing vertical placement on the fuselage; Z_{wf} is the vertical height of the wing above the fuselage centerline, D_f and W_f are the depth and width of the fuselage.

These two additional dihedral contributions are added to the value from Fig. 16.21, as shown in Eq. (16.44). All terms should be negative except that the wing vertical placement term will be positive (destabilizing) for a low wing.

$$(C_{l_\beta})_\Gamma = -\frac{C_{L_\alpha}\Gamma}{4}\left[\frac{2(1+2\lambda)}{3(1+\lambda)}\right] \tag{16.42}$$

$$C_{l_{\beta_{wf}}} = -1.2\frac{\sqrt{A}\, Z_{wf}(D_f + W_f)}{b^2} \tag{16.43}$$

$$C_{l_{\beta_w}} = \left(\frac{C_{l_{\beta_w}}}{C_L}\right)C_L + (C_{l_\beta})_\Gamma + C_{l_{\beta_{wf}}} \tag{16.44}$$

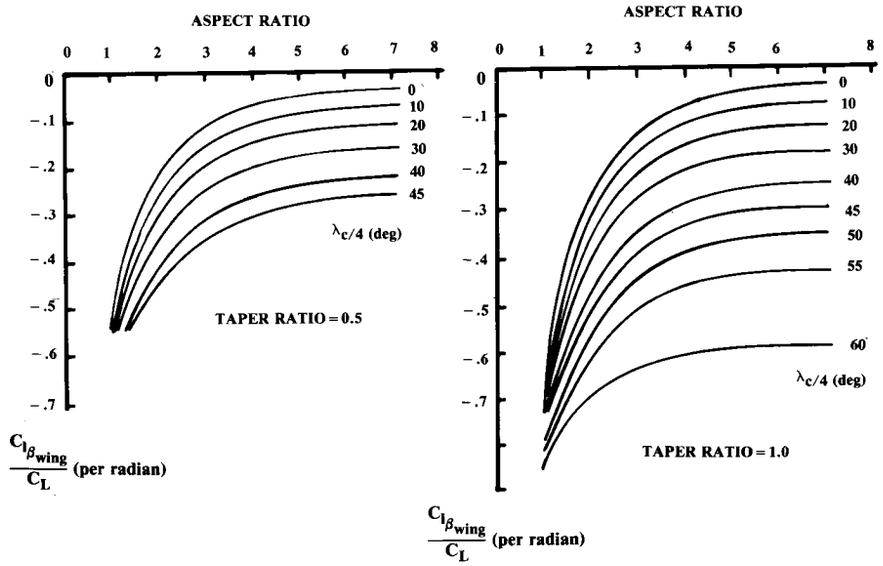

Fig. 16.21 Dihedral effect of sweep. (Ref. 10)

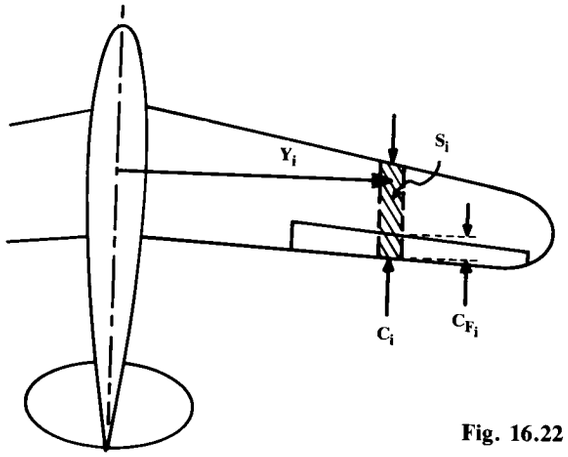

Fig. 16.22 Aileron strip geometry.

The aileron control power can be approximated using a strip method. The portion of the wing having the aileron is broken into strips as shown in Fig. 16.22. The lift increment due to aileron deflection is estimated as a flap effect using the method presented in Eq. (16.15). This lift increment is then multiplied by the strip's moment arm from the aircraft centerline (Y_1), as shown in Eq. (16.45), where K_f and the lift derivative with flap deflection come from Figs. 16.6 and 16.7. Remember to reduce the aileron effectiveness about 15% if the hinge gap is not sealed.

$$C_{\ell_{\delta_a}} = \frac{2\Sigma K_f \left(\frac{\partial C_L}{\partial \delta_f}\right)' Y_i S_i \cos\Lambda_{\text{H.L.}}}{S_w b} \tag{16.45}$$

$$C_{n_{\delta_a}} = -0.2 C_L C_{\ell_{\delta_a}} \tag{16.46}$$

The yawing moment due to aileron deflection depends upon the spanwise distribution of induced drag with the aileron deflected. This varies with the wing lift-coefficient as well as the aileron deflection. Yawing moment due to aileron deflection can be approximated by Eq. (16.46), a simplification of the method from Ref. 37; C_L is the wing lift-coefficient.

Fuselage and Nacelle Lateral-Directional Derivatives

The yawing moment due to sideslip is expressed in Eq. (16.47) as a function of the fuselage or nacelle volume, depth, and width. The fuselage contribution to roll is usually negligible except for its influence upon the wing effective dihedral, as previously discussed.

$$C_{n_{\beta_{\text{fus}}}} = -1.3 \frac{\text{volume}}{S_w b}\left(\frac{D_f}{W_f}\right) \tag{16.47}$$

Lateral-Directional Derivatives

The vertical-tail lateral derivatives were expressed above in Eqs. (16.36) and (16.38). The lateral lift-curve slope is found using the methods in Chapter 12. The vertical-tail aspect ratio should be increased for the end-plate effects of the fuselage and horizontal tail. Typically the effective aspect ratio will be about 55% higher than the actual aspect ratio. Also, the lateral lift-curve slope should be reduced by about 20% if the rudder hinge gap is not sealed.

The remaining unknowns in Eq. (16.36) and (16.38) are the local dynamic pressure ratio and sideslip derivative. These can be estimated in an empirical Eq. (16.48) from Ref. 37; S'_{vs} is the area of the vertical tail extended to the fuselage centerline.

$$\left(\frac{\partial \beta_v}{\partial \beta}\eta_v\right) = 0.724 + \frac{3.06\frac{S'_{vs}}{S_w}}{1+\cos\Lambda} - 0.4\frac{Z_{wf}}{D_f} + 0.009 A_{\text{wing}} \tag{16.48}$$

Thrust Effects on Lateral-Directional Trim and Stability

The thrust effects on the lateral trim and stability are similar to the longitudinal effects. There are direct-thrust moments, normal-force moments, and propwash or jet-induced effects.

When all engines are running, the direct-thrust moments cancel each other. The normal-force moments of the engines are additive.

When one engine fails, the remaining engine(s) produce a substantial yawing moment. Also, the failed engine contributes an additional drag term as previously presented in Chapter 13.

The propwash dynamic pressure effect is estimated using Eq. (16.28). The propwash effect upon sidewash can be estimated using Eqs. (16.27) and (16.20) then be applied to the result from Eq. (16.48).

(With the exception of rudder sizing for engine-out, the lateral analysis is frequently ignored in early conceptual design. To obtain good lateral results usually requires 6-DOF analysis using wind-tunnel data. During early conceptual design, previous aircraft data and rule-of-thumb methods such as the tail volume coefficient are relied upon to select tail areas, dihedral angle, and the rudder and aileron areas.)

16.5 STICK-FREE STABILITY

The preceding analysis has assumed that the control surfaces are rigidly held to the desired deflection. This "stick-fixed" assumption is reasonable for most modern fighters and large transports that employ fully powered flight-control systems.

Many smaller aircraft use purely manual or simply boosted control systems in which the airloads upon the control surfaces cause them to change deflection angle as the angles of attack and sideslip vary. Such a case requires a "stick-free" stability analysis.

A worst-case analysis for stick-free longitudinal stability would assume that the elevator "floats" up so much that it contributes nothing to the tail

lift. In this case the percent reduction in total tail lift-curve slope would equal the elevator's area as a percent of total tail area.

This is generally not the case, and the elevator will usually float to a lesser angle depending upon the airfoil pressure distribution and the amount of "aerodynamic balance" (i.e., the portion of the elevator ahead of the hinge line). Data in Ref. 70 indicates that a typical free elevator with aerodynamic balance will reduce the total tail lift-curve slope by approximately 50% of the elevator's area as a percent of total tail area. Thus, a stick-free elevator which is 40% of the total tail area will experience a reduction in the tail slope of the lift curve of about 20%.

In fact, the elevator can be "overbalanced" so that it floats into the relative wind and therefore adds to the stability. However, this may produce unusual control forces. Due to the strong effect of the boundary layer, control-surface float is difficult to predict even with wind-tunnel data.

References 4 and 67 provide detailed methods for analyzing the stick-free stability based upon test data for control surface hinge moments. Typically the stick-free neutral point is 2–5% ahead of the stick-fixed neutral point.

Stick-free directional stability is also reduced as a result of rudder float. This can be approximated using the percent reduction in tail slope of the lift curve described above.

16.6 EFFECTS OF FLEXIBILITY

The preceding discussion also assumes that the aircraft is rigid. In fact, many aircraft are quite flexible, especially in fuselage longitudinal bending, wing spanwise bending, and wing torsional deflection. These can have a major effect upon the stability characteristics.

If the fuselage is flexible in longitudinal bending, the horizontal-tail incidence angle will reduce when the aircraft angle of attack is increased. This reduces the effectiveness of the tail as a restoring force for pitch stability. The vertical tail experiences the same effectiveness reduction due to lateral fuselage bending.

Similarly, a swept flexible wing will deflect such that the wingtips have a reduced angle of attack compared to the rigid aircraft. This reduces the slope of the lift curve and moves the wing aerodynamic center forward, destabilizing the aircraft. These effects are shown in Fig. 16.23.

A typical swept-wing transport at high subsonic speeds will experience a reduction in wing lift-curve slope of about 20%, a reduction in tail pitching moment contribution of about 30%, and a reduction in elevator effectiveness of about 50% due to flexibility effects. The wing aerodynamic center will shift forward about 10% MAC due to flexibility.

In addition, the aileron effectiveness may be reduced by 50 to over 100%! At high dynamic pressures the ailerons will produce torsional moments on the wing that twist it in the opposite direction from the aileron deflection. This wing twist produces a rolling moment in the opposite direction from the desired rolling moment.

If the wing twists enough, this effect may overpower the aileron forces, producing "aileron reversal." To retain roll authority, many jet transports lock the outboard ailerons at high speeds and rely upon spoilers or small inboard ailerons.

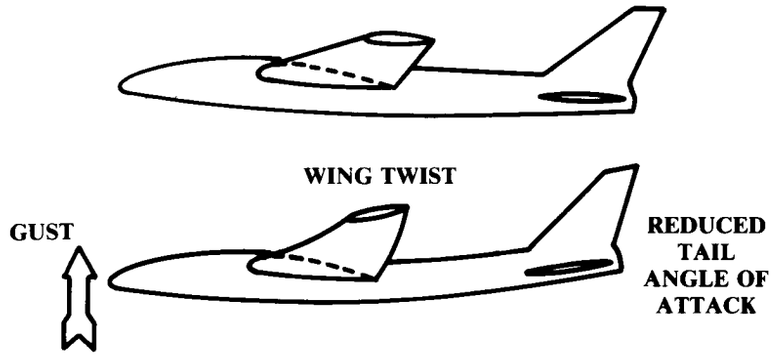

Fig. 16.23 Effects of flexibility on stability.

These effects are functions of dynamic pressure, with the greatest impact seen at the low-altitude, high-speed condition. A "stiffer" aircraft such as a fighter, with a low wing aspect ratio and a short fuselage, will have less impact on its static stability derivatives due to flexibility.

16.7 DYNAMIC STABILITY

Dynamic stability concerns the motions of the aircraft, so two new classes of force must be considered; the inertia forces and the damping forces.

Mass Moments of Inertia

Inertia forces derive from the tendency of mass to resist accelerations. The mass for rotational accelerations is represented by "mass moment of inertia" terms, denoted by I. Mass moment of inertia describes a body's resistance to rotational accelerations, and is calculated by integrating the products of mass elements and the square of their distance from the Ref. axis (units of slug-ft^2).

For aircraft dynamic analysis, the mass moments of inertia about the three principal axes must be determined: I_{xx} about the roll axis, I_{yy} about the pitch axis, and I_{zz} about the yaw axis.

These can be initially determined using historical data based upon the nondimensional radii of gyration ($\bar{R}$), as described in Ref. 11. Equations (16.49–16.51) are used with typical $\bar{R}$ values from Table 16.1.

$$I_{xx} = \frac{b^2 W \bar{R}_x^2}{4g} \tag{16.49}$$

$$I_{yy} = \frac{L^2 W \bar{R}_y^2}{4g} \tag{16.50}$$

$$I_{zz} = \left(\frac{b+L}{2}\right)^2 \frac{W \bar{R}_z^2}{4g} \tag{16.51}$$

Table 16.1 Nondimensional radii of gyration[a]

Aircraft class	$\overline{R}_x$	$\overline{R}_y$	$\overline{R}_z$
Single-engine prop	0.25	0.38	0.39
Twin-engine prop	0.34	0.29	0.44
Business jet twin	0.30	0.30	0.43
Twin turboprop transport	0.22	0.34	0.38
Jet transport—Fuselage-mounted engines	0.24	0.36	0.44
—2 wing-mounted engines	0.25	0.38	0.46
—4 wing-mounted engines	0.31	0.33	0.45
Military jet trainer	0.22	0.14	0.25
Jet fighter	0.23	0.38	0.52
Jet heavy bomber	0.34	0.31	0.47
Flying wing (B-49 type)	0.32	0.32	0.51
Flying boat	0.25	0.32	0.41

[a]Typical values see Ref. 11 for examples.

Damping Derivatives

Aerodynamic damping forces resist motion. The rotational damping forces are proportional to the pitch rate q', roll rate p and yaw rate r. (The q-prime notation avoids confusing q' with dynamic pressure, q).

These damping forces arise because of a change in effective angle of attack due to the rotational motion, as shown in Fig. 16.24 for the lift on the horizontal tail during a steady pitchup and for the lift on a segment of the wing during a steady roll. The lateral lift on a vertical tail in a steady yawing motion would change similarly to the horizontal tail.

The change in effective angle of attack, and hence the change in lift, is directly proportional to the rotation rate and the distance from the c.g. The moment is proportional to the lift times the distance from the c.g. Rotational damping moment is therefore proportional to the rotational rate and the square of the distance from the c.g.

Equations (16.52) and (16.53) provide first-order estimates of the pitch- and yaw-damping derivatives. The wing drag term in Eq. (16.53) accounts for the yaw-damping effect of the wing. Dynamic pressure ratios (η) for horizontal and vertical tails can be approximated as 0.9.

Roll damping is estimated with Fig. 16.25, based upon data in NACA 1098 covering the lower aspect ratios and NACA 868 covering the higher aspect ratios. The sweep factor is multiplied times the unswept damping derivative.

$$C_{m_{q'}} = -2.2\eta_h \frac{S_h}{S_w} C_{L_{\alpha_h}} \left(\frac{X_{ach} - X_{cg}}{c}\right)^2 \tag{16.52}$$

$$C_{n_r} = -2.0\eta_v \frac{S_v}{S_w} C_{F_{\beta_v}} \left(\frac{X_{acv} - X_{cg}}{c}\right)^2 - \frac{C_{D\,\text{wing}}}{4} \tag{16.53}$$

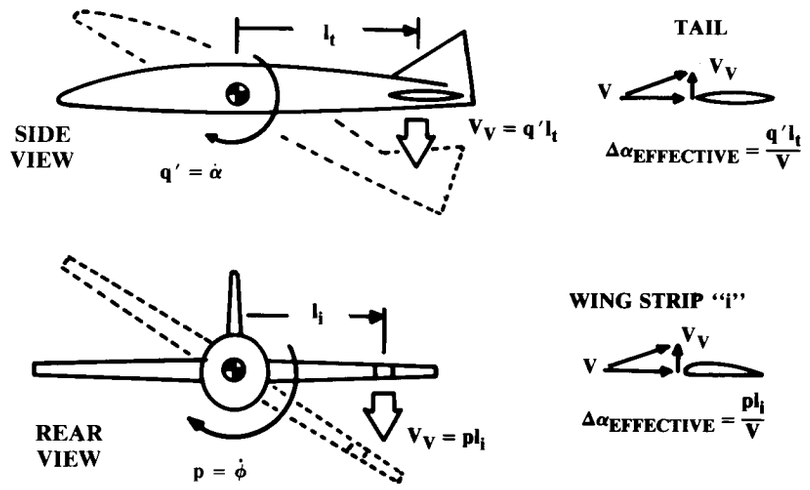

Fig. 16.24 Origin of damping forces.

There are also "cross-derivative" damping terms. The yaw rate will affect the roll moment, and the roll rate will affect the yaw moment. These are both functions of wing lift-coefficient. As a rough approximation, the rolling moment due to yaw rate C_{l_r} is about $C_L/4$ and the yawing moment due to roll rate C_{n_p} is about $-C_L/8$.

1-DOF Dynamic Equations

A 6-DOF analysis is required to fully evaluate aircraft dynamic stability and control. The 6-DOF allows simultaneous rotations in pitch, yaw, and roll, and allows the aircraft velocity to change in the vertical, lateral, and longitudinal directions. All these motions affect each other, requiring a tremendous number of cross-derivatives to account fully for all forces and moments. References 37 and 67 are recommended for the equations for 6-DOF analysis.

The 1-DOF equations may be used for initial analysis of several flight conditions, such as pullup and steady roll. The 1-DOF rotation equations are based upon the fact that the rotational acceleration times the mass moment of inertia equals the sum of the applied moments (which includes the damping moments). Equations (16.54–16.56 provide these:

$$\text{Pitch:} \quad I_{yy}\dot{q}' = qS_w c C_{m_\alpha}\alpha + qS_w c C_{m_{q'}} q' \tag{16.54}$$

$$\text{Yaw:} \quad I_{zz}\dot{r} = qS_w b C_{n_\beta}\beta + qS_w b C_{n_r} r \tag{16.55}$$

$$\text{Roll:} \quad I_{xx}\dot{p} = qS_w b C_\ell + qS_w b C_{\ell_p} p \tag{16.56}$$

These are second-order differential equations since q', r, and p are the derivative with time of pitch, yaw, and roll. Note that there is no first-order

term in the roll equation since the roll angle does not affect the roll moments if the sideslip remains zero.

Aircraft Dynamic Characteristics

With proper input data, these 1-DOF equations may be solved for time history after a given disturbance. However, the results will be incorrect since real aircraft motions always involve more than 1-DOF. Longitudinal analysis requires a minimum of 3-DOF to account for the interplay between pitch angle, vertical velocity, and changes in horizontal velocity. An additional equation is required for elevator deflection in a stick-free analysis.

Lateral analysis with stick fixed also requires a minimum of 3-DOF, which account for lateral velocity, sideslip angle, and rolling angle. For stick-free lateral analysis, two additional equations are required to account for the aileron and rudder deflections. A full 6-DOF (9-DOF for stick-free) is preferable because of the interplay between lift coefficient and the lateral derivatives, especially at higher angles of attack.

Analytical techniques for 3- or 6-DOF simulations are beyond the scope of this book, but a few comments on typical results are in order. Longitudinally, there are two oscillatory solutions to the equations of motion. One is a short-period mode, which is typically heavily damped, and provides the desired dynamic stability in response to a pitch disturbance. The other solution is a long-period lightly-damped mode called the "pitch phugoid." This involves a slow pitch oscillation over many seconds in which energy is exchanged between vertical and forward velocity. Many aircraft have a slight unnoticeable pitch phugoid. An excessive phugoid should be avoided.

The lateral equations of motion yield three solutions to a yaw disturbance. One is the desired heavily-damped direct convergence. The spiral-divergence mode, another solution, involves an increasing bank angle with the aircraft turning tighter and tighter until control is lost. However, the time to diverge is so long that pilots can easily correct for spiral divergence.

The third lateral solution, a short-period oscillation called "Dutch Roll," sees the aircraft waddle from side to side, exchanging yaw and roll. If the Dutch Roll is excessive, this oscillation will be objectionable to passengers and crew. Dutch Roll is largely caused by the dihedral effect.

Dutch Roll damping is determined mainly by the size of the vertical tail, and is usually the driving criteria for tail sizing other than engine-out control. For this reason, vertical-tail size should not be reduced below the size indicated by the tail volume coefficient method until a 6-DOF analysis has been conducted, preferably with wind-tunnel data for the dynamic derivatives.

Dutch Roll is aggravated by flexibility effects at high speeds. Most large, swept-wing aircraft use a powered rudder mechanized with a gyro to deflect into a yaw, thus increasing the effective Dutch Roll damping.

16.8 QUASI-STEADY STATE

Setting the rotational accelerations in Eqs. (16.54–16.56) to zero yields "quasi-steady state" equations. These represent a steady pitch, yaw, or roll

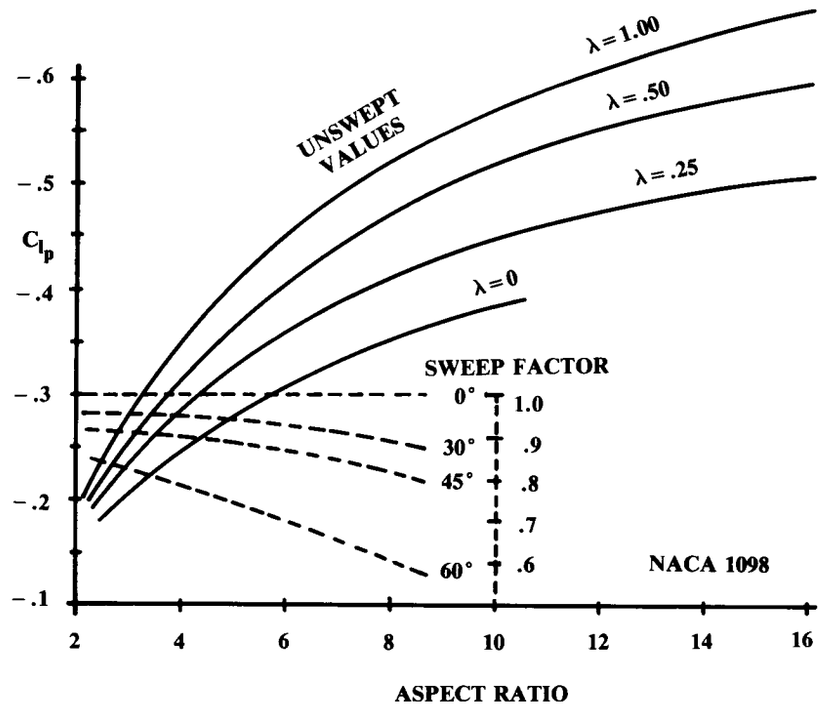

Fig. 16.25 Roll damping parameter.

rate and are identical to the steady-state trim equations presented earlier, but with the addition of damping terms.

Pullup

Pullup is a quasi-steady-state trim condition in which the aircraft accelerates vertically at a load factor n. Level flight implies that $n = 1$. The longitudinal-trim equation previously presented [Eq. (16.7)], with the addition of the pitch damping moment (C_{m_q} times q'), is solved to provide a total aircraft lift equal to n times the aircraft weight. The required elevator deflection is then determined from the required tail lift. The pitch rate q' is related to the load factor in a pullup as follows:

$$q' = \frac{g(n-1)}{V} \tag{16.57}$$

Level Turn

A level turn is similar to the pullup in that the aircraft experiences an increased load factor and a steady pitch rate. Note that the sideslip remains zero during a coordinated turn so that the level turn is strictly a longitudinal problem! The load factor due to a bank angle ϕ is obtained from Eq. (16.58), and the resulting pitch rate is obtained from Eq. (16.59).

Table 16.2 MIL-F-8785 B roll requirements

Class	Aircraft type	Required roll
I	Light utility, observation, primary trainer	60° in 1.3 s
II	Medium bomber, cargo, transport, ASW, recce.	45° in 1.4 s
III	Heavy bomber, cargo, transport	30° in 1.5 s
IV A	Fighter-attack, interceptor	90° in 1.3 s
IV B	Air-to-air dogfighter	90° in 1.0 s 360° in 2.8 s
IV C	Fighter with air-to-ground stores	90° in 1.7 s

$$n = 1/\cos\phi \tag{16.58}$$

$$q' = \frac{g}{V}\left(n - \frac{1}{n}\right) \tag{16.59}$$

Steady Roll

The steady roll is found by setting Eq. (16.56) to zero. Equation (16.37) C_l indicates that the only rolling-moment term that remains when the sideslip equals zero is the roll due to aileron deflection. This leads to Eq. (16.60), which is solved for roll rate (radians) as a function of aileron deflection in Eq. (16.61).

$$I_{xx}\dot{p} = 0 = qS_w bC_{\ell_{\delta_a}}\delta_a + qS_w bC_{\ell_p}p \tag{16.60}$$

$$p = -\left(\frac{C_{\ell_{\delta_a}}}{C_{\ell_p}}\right)\delta_a \tag{16.61}$$

For many years the roll-rate requirement was based upon the wing helix angle $pb/2V$. NACA flight tests (NACA 715) determined that most pilots consider an aircraft to have a good roll rate if the wing helix angle is at least equal to 0.07 (0.09 for fighters).

Military specifications (MIL-F-8785B or Mil Std 1797) require that the aircraft reach a certain roll angle in a given number of seconds, as noted in Table 16.2. These assume that the aircraft is in level flight upon initiation of the roll, so the rotational acceleration should be accounted for. However, aircraft generally reach maximum roll rate quickly; the quasi-steady-state roll rate therefore may be used initially to estimate the time to roll.

16.9 INERTIA COUPLING

The F-100 prototype, the first fighter capable of level supersonic flight, featured a thin swept wing and long heavy fuselage compared to previous fighters. During flight testing, a series of high-speed rolls suddenly diverged in angle of attack and sideslip, much to the surprise of all concerned. Detailed analysis and simulation discovered the cause to be "inertia coupling."

Figure 16.26 shows a typical fighter in roll. The mass of the forebody and aft-fuselage are concentrated like a barbell for illustrative purposes.

Like all objects, the fighter tends to roll about its principal (longitudinal) axis. However, if the fighter rolled 90 deg about its longitudinal axis, the angle of attack would be exchanged with the angle of yaw, as shown. The C_{n_β} effect of the vertical tail would oppose this increase in yaw angle with roll.

In addition, the aileron rolling moments are about the wind axis. The aircraft thus actually rolls around an axis somewhere between the principal axis and the wind axis.

The masses of the forebody and aft-fuselage are above and below this actual roll axis. Centrifugal force tends to pull them away from the roll axis, creating a nose-up pitching moment. The combination of the increase in yaw angle with roll and the nose-up pitching moment due to inertia is called inertia coupling.

Inertia coupling becomes a problem only when the moments produced by the inertia forces are stronger than the aerodynamic restoring moments. This is most likely to happen at high altitudes (lower air density) and at high Mach numbers where the tail loses lift effectiveness.

The solution to inertia coupling in the F-100 was a larger vertical tail. This remains the typical solution. For this reason the vertical-tail area should not be reduced below the statistical tail-volume-method result until a more detailed analysis is available.

16.10 HANDLING QUALITIES

Cooper-Harper Scale

Aircraft handling qualities are a subjective assessment of the way the plane feels to the pilot. Few modern pilots fully appreciate the great ad-

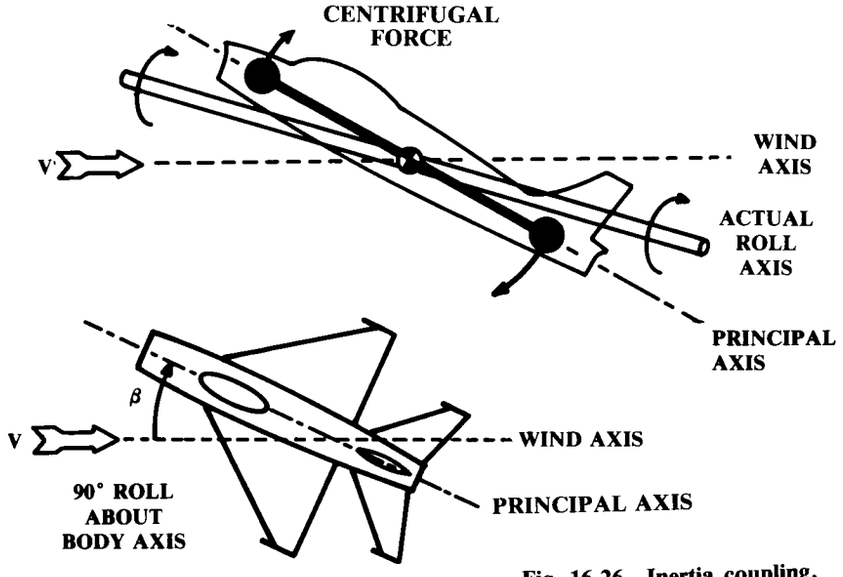

Fig. 16.26 Inertia coupling.

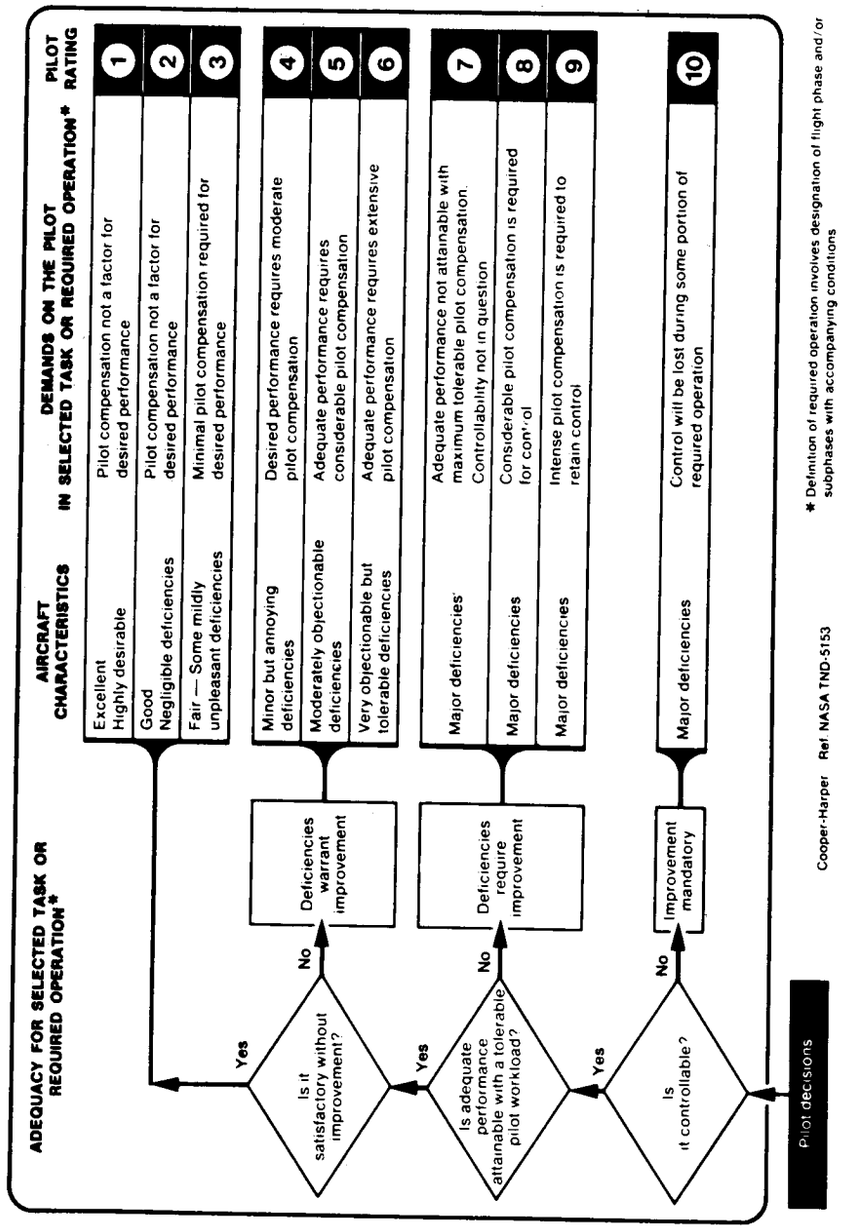

Fig. 16.27 Cooper-Harper handling qualities rating scale.

vances in handling qualities made since the dawn of aviation. Early fighters such as the Fokker Eindecker had handling qualities which were so poor that the pilots felt that without constant attention, the aircraft would "turn itself inside out or literally swap ends" (movie stunt pilot Frank Tallman, quoted from Ref. 71).

A number of "goodness" criteria such as the wing helix angle have already been discussed. It is important that the aircraft have a nearly linear response to control inputs and that the control forces be appropriate for the type of aircraft. The control forces required due to flap deflection or power application should be small and predictable.

These handling qualities criteria are generally considered later in the design cycle. Figure 16.27 illustrates the Cooper-Harper Handling Qualities Rating Scale, which is used by test pilots to categorize design deficiencies (Ref. 72). Handling qualities are discussed in detail in Ref. 69.

Departure Criteria

One of the most important aspects of handling qualities is the behavior of the aircraft at high angles of attack.

As the angle of attack increases, a "good" airplane experiences mild buffetting to warn the pilot, retains control about all axes, and stalls straight ahead with immediate recovery and no tendency to enter a spin. If a spin is forced, the "good" airplane can be immediately recovered.

A "bad" airplane loses control in one or more axis as angle of attack increases. A typical bad characteristic is the loss of aileron roll control and an increase in aileron adverse yaw. When the aircraft is near the stall angle of attack, any minor yaw resulting from aileron deflection may slow down one wing enough to stall it. With only one wing generating lift, the "bad" airplane will suddenly depart into a spin or other uncontrolled flight mode.

Design features for good departure and spin characteristics have been discussed in earlier chapters. There have been many criteria proposed for good departure characteristics. Several aerodynamic coefficients are important to departure characteristics, especially C_{n_β}, $C_{n_{\delta_a}}$, C_{l_β}, and $C_{l_{\delta_a}}$.

These are combined in the lateral control departure parameter (LCDP), sometimes called the lateral control spin parameter or the aileron-alone divergence parameter [Eq. (16.62)]. The LCDP focuses upon the relationship between adverse yaw and directional stability.

Equation (16.63) shows another departure parameter, $C_{n_{\beta_{\text{dynamic}}}}$, which includes the effects of the mass moments of inertia. Both of these parameters should be positive for good departure resistance. A typical goal is to have $C_{n_{\beta_{\text{dynamic}}}}$ greater than 0.004.

$$\text{LCDP} = C_{n_\beta} - C_{\ell_\beta} \frac{C_{n_{\delta a}}}{C_{\ell_{\delta_a}}} \tag{16.62}$$

$$C_{n_{\beta_{\text{dynamic}}}} = C_{n_\beta} \cos\alpha - \frac{I_{zz}}{I_{xx}} C_{\ell_\beta} \sin\alpha \tag{16.63}$$

Figure 16.28 shows a crossplot of the LCDP and $C_{n_{\beta_{dynamic}}}$ with increase in angle of attack. In Ref. 73 the boundaries for acceptable departure resistance were determined from high-g simulator tests using experienced pilots. The earlier Weissman criteria is also shown.

Note the departure-parameter crossplot for the F-5. This aircraft is widely considered to be one of the best fighters at high angle of attack. Both departure parameters are increasing with angle of attack.

On the other hand, the F-4 has poor departure characteristics. Its departure-parameter crossplot starts in the acceptable zone, but crosses into the unacceptable zone as angle of attack increases.

The HiMat fighter shows that even an advanced supersonic canard configuration can have good departure characteristics. The HiMat has highly-cambered outboard wing leading edges and has large twin tails with a substantial portion below the wing.

Unfortunately, the stability derivatives used to calculate these departure parameters become very nonlinear near the stall. First-order estimation techniques used in conceptual design may not give usable results for departure estimation. However, the configuration designer can expect to be instructed to "fix it" when the first wind-tunnel data is available!

There are a few design rules which can be applied during early configuration layout. The fuselage forebody shape has a huge effect upon the stability characteristics at high angles of attack. An elliptical nose cross section that has width greater than height is desirable.

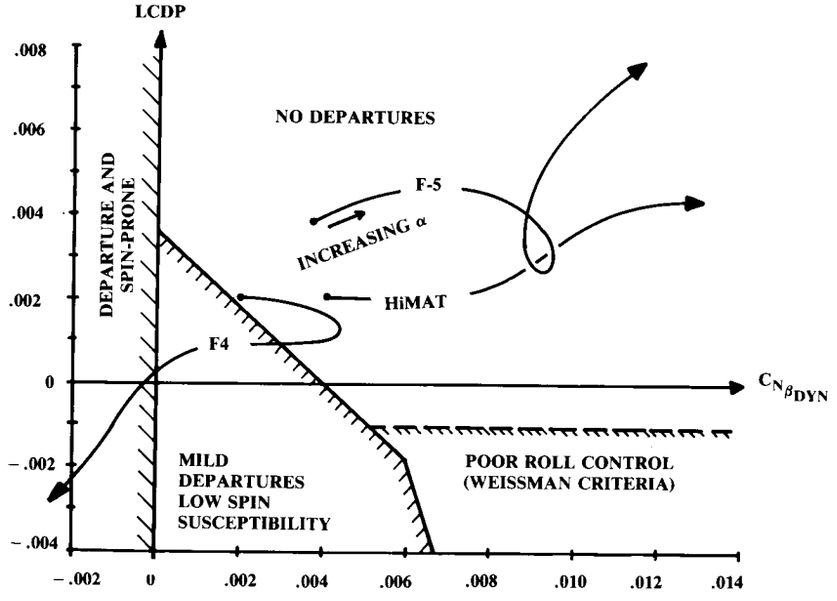

Fig. 16.28 Departure susceptibility.

Wing-tip stalling should be prevented by the use of wing twist, fences, notches, or movable leading-edge devices. It is also desirable for departure prevention to have a substantial ventral-tail surface.

Spin Recovery

After stall, a spin will develop in a "bad" airplane or a good airplane severely abused. Figure 16.29 shows the forces acting in a fully developed spin. The fuselage and wing masses are represented by barbells. The centrifugal forces acting on the fuselage tend to raise the nose, further increasing the wing stall.

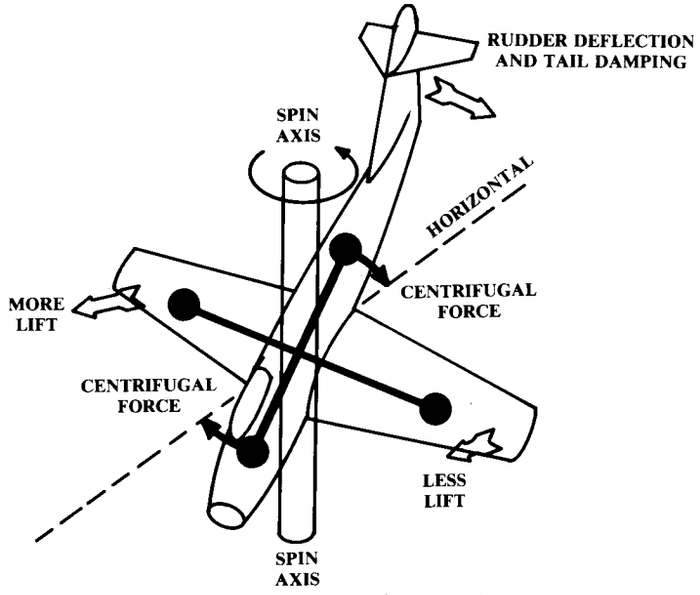

Fig. 16.29 Forces in spin.

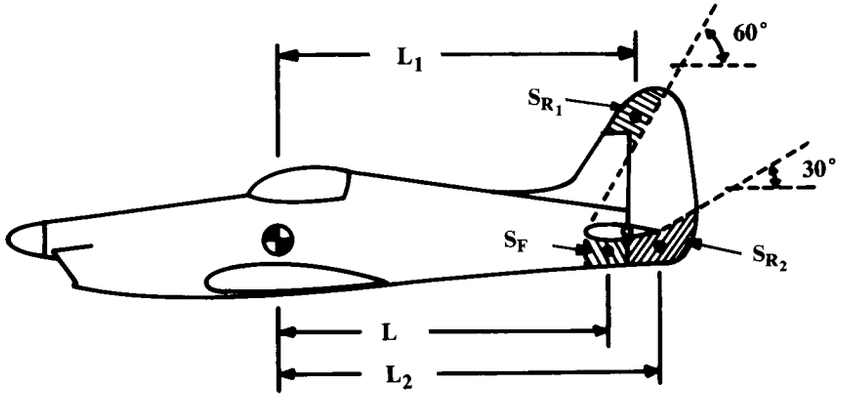

Fig. 16.30 Geometry for spin recovery estimation.

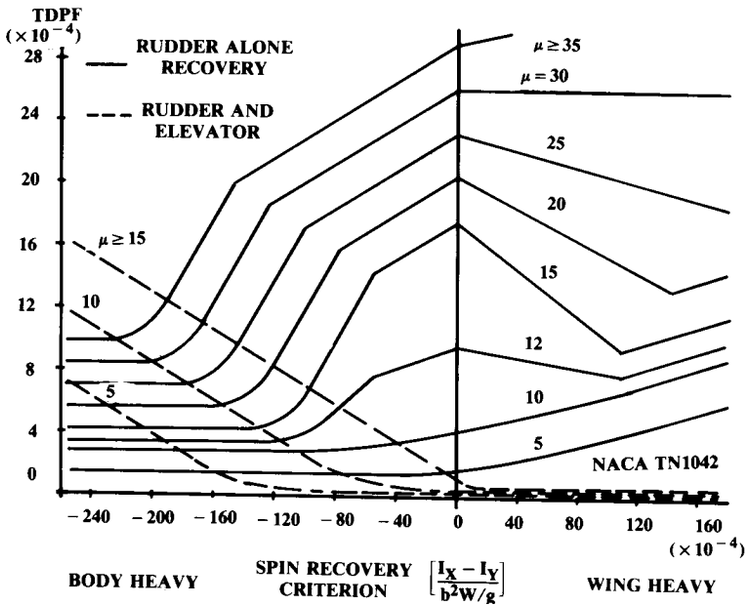

Fig. 16.31 Spin recovery criteria.

The spin is primarily driven by the difference in lift between the outer, faster wing and the inner, slower wing, which is more fully stalled. The spin is opposed by damping forces, primarily from portions of the aft fuselage and vertical tail underneath the horizontal tail (S_F—see Fig. 16.30).

For recovery, the rudder is deflected against the spin. However, only the part of the rudder not blanketed by the stalled air from the horizontal tail will aid the recovery (S_{R_1} and S_{R_2}).

Figure 16.31 presents an empirical estimation of the required tail damping and rudder area for spin recovery for straight-winged aircraft (Ref. 74). This determines the minimum allowable tail-damping power factor (TDPF), defined in Eq. (16.64) where TDR is the tail damping ratio [Eq. (16.65)] and URVC is the unshielded rudder volume coefficient [Eq. (16.66)]. The airplane relative density parameter (μ) is defined in Eq. (16.67).

$$\text{TDPF} = (\text{TDR})(\text{URVC}) \tag{16.64}$$

$$\text{TDR} = \frac{S_F L^2}{S_w (b/2)^2} \tag{16.65}$$

$$\text{URVC} = \frac{S_{R_1} L_1 + S_{R_2} L_2}{S_w (b/2)} \tag{16.66}$$

$$\mu = \frac{W/S}{\rho g b} \tag{16.67}$$

17
PERFORMANCE AND FLIGHT MECHANICS

17.1 INTRODUCTION AND EQUATIONS OF MOTION

The last chapter discussed stability and control, which largely concern the rotational motions of the aircraft in pitch, yaw, and roll. This chapter introduces flight mechanics, the study of aircraft translational motions. The geometry for flight mechanics is shown in Fig. 17.1.

The climb angle γ is the angle between horizontal and the wind (stability) X-axis (Xs). The "climb gradient" (G), the tangent of the climb angle, represents the vertical velocity divided by the horizontal velocity.

Summing forces in the Xs and Zs directions yields Eqs. (17.1) and (17.2). The resulting accelerations on the aircraft in the Xs and Zs directions are determined as these force summations divided by the aircraft mass (W/g):

$$\Sigma F_x = T\cos(\alpha + \phi_T) - D - W\sin\gamma \tag{17.1}$$

$$\Sigma F_z = T\sin(\alpha + \phi_T) + L - W\cos\gamma \tag{17.2}$$

$$\dot{W} = -CT \tag{17.3}$$

$$C = C_{\text{bhp}} \frac{V}{550\,\eta_p} \tag{17.4}$$

$$T = 550\ \text{bhp}\ \eta_p / V \tag{17.5}$$

Equation (17.3) defines the time rate of change in aircraft weight as the specific fuel consumption (C) times the thrust. For a piston-propeller engine, Eq. (17.4) determines the equivalent C based upon the piston-engine definition of C_{bhp} (see Chapter 5), and Eq. (17.5) determines the thrust of the propeller.

These simple equations are the basis of the most detailed sizing and performance programs used by the major airframe companies. The angle of attack and thrust level are varied to give the required total lift (including load factor) and the required longitudinal acceleration depending upon what maneuver the aircraft is to perform (level cruise, climb, accelerate, turn, etc.). Angle of attack and lift are restricted by the maximum lift available. The thrust level is restricted to the available thrust, as obtained from a table of installed engine thrust vs altitude and velocity (or Mach number).

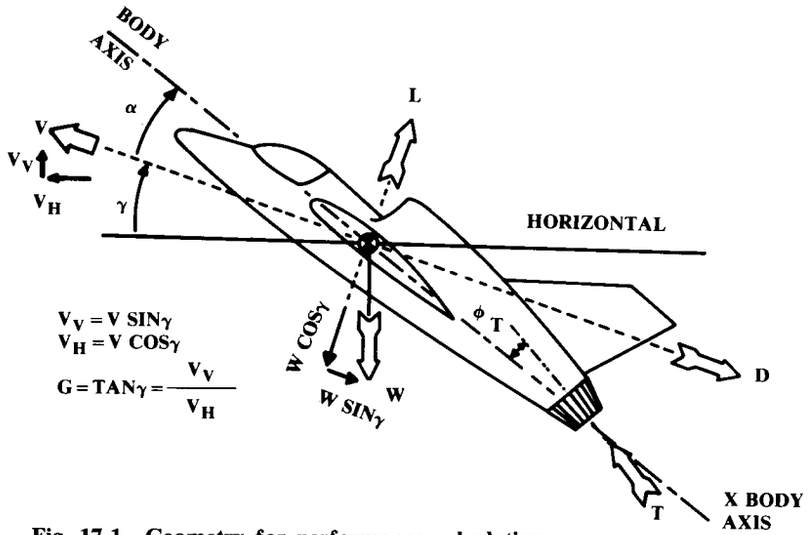

Fig. 17.1 Geometry for performance calculation.

What makes the sizing and performance programs complicated is not the actual calculation of the aircraft response to the forces at a given angle of attack and thrust level. The complications arise in determining what the angle of attack and thrust level should be to perform some maneuver.

For example, the rate of climb varies with velocity. What combination of velocity and thrust setting will allow an airliner to climb to cruise altitude with the least fuel consumption over the total mission? This chapter will address such performance issues.

For most aircraft the thrust axis has little incidence with respect to the wind axis under most flight conditions. This is by design, and permits simplifying Eqs. (17.1) and (17.2) to the forms shown in Eqs. (17.6) and (17.7).

$$\Sigma F_x = T - D - W \sin\gamma \tag{17.6}$$

$$\Sigma F_z = L - W \cos\gamma \tag{17.7}$$

(A word of caution: Be especially careful with units in the performance calculations. Apply each equation to the units of the data you are using to be sure that all units cancel leaving you with the units of the desired answer. Be wary of equations involving horsepower. Anytime the constant "550" appears in an equation, the other units must be converted to feet, pounds, and seconds (One bhp = 550 ft-lb/s). Another "gotcha" is the specific fuel consumption C, which is usually given in units of hours^{-1}. This must be divided by 3600 to yield seconds^{-1}.)

17.2 STEADY LEVEL FLIGHT

If the aircraft is flying in unaccelerated level flight, then γ equals zero and the sum of the forces must equal zero. This leads to Eqs. (17.8) and (17.9), the most simple versions of the translational equations of motion. They state simply that in level flight, thrust equals drag and lift equals weight. These are expressed using aerodynamic coefficients for the analysis which follows.

$$T = D = qS(C_{D_0} + KC_L^2) \tag{17.8}$$

$$L = \mathrm{W} = qSC_L \tag{17.9}$$

$$V = \sqrt{\frac{2}{\rho C_L}\left(\frac{W}{S}\right)} \tag{17.10}$$

From Eq. (17.9), the velocity in level flight can be expressed as a function of wing loading, lift coefficient, and air density [Eq. (17.10)].

These equations imply that the actual T/W in level flight must be the inverse of the L/D at that flight condition [Eq. (17.11)]. The T/W and L/D in level flight can be expressed in terms of the wing loading and dynamic pressure by substituting Eq. (17.9) into Eq. (17.8), as follows:

$$\frac{T}{W} = \frac{1}{L/D} = \frac{qC_{D0}}{(W/S)} + \left(\frac{W}{S}\right)\frac{K}{q} \tag{17.11}$$

Minimum Thrust Required for Level Flight

From Eq. (17.11) it follows that the condition for minimum thrust at a given weight is also the condition for maximum L/D. To find the velocity at which thrust is minimum and L/D is maximum, the derivative with respect to velocity of Eq. (17.11) is set to zero. This is shown in Eq. (17.12), and solved in Eq. (17.13) for the velocity at which the required thrust is minimum and the L/D is at a maximum.

$$\frac{\partial(T/W)}{\partial V} = \frac{\rho V C_{D_0}}{W/S} - \frac{W}{S}\frac{2K}{\frac{1}{2}\rho V^3} = 0 \tag{17.12}$$

$$V_{\substack{\text{min thrust}\\ \text{or drag}}} = \sqrt{\frac{2W}{\rho S}}\sqrt{\frac{K}{C_{D_0}}} \tag{17.13}$$

$$C_{L_{\substack{\text{min thrust}\\ \text{or drag}}}} = \sqrt{\frac{C_{D_0}}{K}} \tag{17.14}$$

Substituting this velocity into Eq. (17.9) yields the lift coefficient for minimum drag in level flight [Eq. (17.14)]. This optimal lift coefficient is

only dependent upon the aerodynamic parameters. At any given weight, the aircraft can be flown at the optimal lift coefficient for minimum drag by varying velocity or air density (altitude).

If the lift coefficient for minimum drag is substituted back into the total-drag Eq. (17.8), the induced-drag term will equal the zero-lift drag term. The total drag at the lift coefficient for minimum drag will then be exactly twice the zero-lift drag [Eq. (17.15)].

$$D_{\substack{\text{min thrust}\\ \text{or drag}}} = qS\left[C_{D_0} + K\left(\sqrt{\frac{C_{D_0}}{K}}\right)^2\right] = qS(C_{D_0} + C_{D_0}) \tag{17.15}$$

Minimum Power Required for Level Flight

The conditions for minimum thrust and minimum power required are not the same. Power is force times velocity, which in steady level flight equals the drag times the velocity as shown in Eq. (17.16). Substituting the lift coefficient in level flight from Eq. (17.9) yields Eq. (17.17).

$$P = DV = qS(C_{D_0} + KC_L^2)V = \tfrac{1}{2}\rho V^3 S(C_{D_0} + KC_L^2) \tag{17.16}$$

$$P = \tfrac{1}{2}\rho V^3 S C_{D_0} + \frac{KW^2}{\tfrac{1}{2}\rho VS} \tag{17.17}$$

The velocity for flight on minimum power is obtained by setting the derivative of Eq. (17.17) to zero, as shown in Eqs. (17.18) and (17.19). Substituting this into Eq. (17.9) yields the lift coefficient for minimum power, Eq. (17.20). Substituting this into Eq. (17.8) gives the drag at minimum power required [Eq. (17.21)]:

$$\frac{\partial P}{\partial V} = \frac{3}{2}\rho V^2 S C_{D_0} - \frac{KW^2}{\tfrac{1}{2}\rho V^2 S} = 0 \tag{17.18}$$

$$V_{\substack{\min\\ \text{power}}} = \sqrt{\frac{2W}{\rho S}}\sqrt{\frac{K}{3C_{D_0}}} \tag{17.19}$$

$$C_{L_{\substack{\min\\ \text{power}}}} = \sqrt{\frac{3C_{D_0}}{K}} \tag{17.20}$$

$$D_{\substack{\min\\ \text{power}}} = qS(C_{D_0} + 3C_{D_0}) \tag{17.21}$$

Note that the velocity for minimum power required is approximately 0.76 times the velocity for minimum thrust [Eq. (17.13)]. The aircraft is flying at a lift coefficient for minimum power, which is about 73% higher than the lift coefficient for minimum drag [Eq. (17.14)].

The induced drag at the lift coefficient for minimum power is exactly three times the zero-lift drag, so the total drag is four times the zero-lift drag [Eq. (17.21)]. This drag coefficient is twice as high as at minimum drag [Eq. (17.15)].

Remember that at the minimum-power condition the aircraft is flying at a slower speed (reduced dynamic pressure) than at the minimum-drag condition. The actual drag increase will thus be less than the factor of two indicated by the drag coefficients. The actual drag increase is 2.0 times the ratio of dynamic pressures (0.76^2), or only 15.5% higher than the total drag at minimum-drag conditions. Thus, the L/D when flying at the velocity for minimum power required is 1/1.155, or 0.866 times the maximum L/D.

Graphical Analysis for Thrust and Power Required

The analytical optimizations in the last two sections depend upon the assumptions that the zero-lift drag is constant with velocity, that the drag due to lift follows the parabolic approximation, and that K is constant with velocity. As seen in Chapter 12, these assumptions are not very good other than for an aircraft with a high-aspect-ratio wing which is flying at low Mach numbers.

To determine the actual thrust (or horsepower) required for level flight, the aerodynamic results are plotted vs velocity or Mach number and compared to the engine data.

For piston-powered aircraft, horsepower is virtually constant with velocity. The only horsepower variation with velocity is due to ram pressure in the intake manifold. For jet aircraft, equivalent horsepower varies widely with velocity but thrust is roughly constant with velocity.

It is therefore common practice to graph the propulsive requirements of an aircraft vs velocity (or Mach number), using thrust for jet aircraft and using horsepower for propeller aircraft. These are shown in Fig. 17.2. The horsepower required is found by multiplying the drag by the velocity (divided by 550 to make the units come out as horsepower). The equivalent thrust for the propeller aircraft is also shown for illustration, but is not commonly plotted.

The velocities for minimum thrust and minimum power are shown. Note that the minimum-power-required velocity is about 86.6% of the minimum-thrust-required velocity, as predicted in the last section. Also, the superiority of the jet engine for high-speed flight should be clear from this illustration.

The excess thrust at full throttle is determined simply by subtracting the thrust required from the thrust available. This excess can be used to accelerate or climb, as discussed later.

Such a plot of thrust or horsepower vs velocity is different at each altitude.

Range

The range of an aircraft is its velocity multiplied by the amount of time it can remain in the air. Time in the air equals the amount of fuel carried

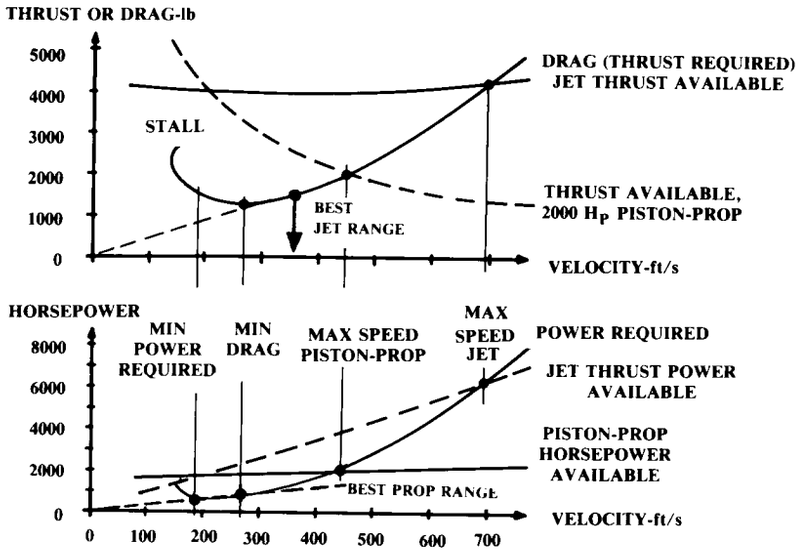

Fig. 17.2 Thrust and power.

divided by the rate at which the fuel is burned. This in turn is the required thrust multiplied by the specific fuel consumption.

Unfortunately, the simple equation implied by the last paragraph is complicated by the fact that the aircraft weight drops as fuel is burned. This changes the drag, which then changes the thrust required. Net result: the aircraft goes farther but the calculation is more difficult!

However, the "instantaneous range" derivative can be calculated using the simple relationship described above, which is expressed in Eq. (17.22). This describes the additional distance the aircraft will travel with the next incremental amount of fuel burned. This can also be expressed in terms of the L/D and weight, as shown. Instantaneous range is a commonly-used measure of merit and is usually discussed in units of nautical miles per pound of fuel.

$$\frac{dR}{dW} = \frac{V}{-CT} = \frac{V}{-CD} = \frac{V(L/D)}{-CW} \tag{17.22}$$

$$R = \int_{W_i}^{W_f} \frac{V(L/D)}{-CW}\,dW = \frac{V}{C}\frac{L}{D}\ln\left(\frac{W_i}{W_f}\right) \tag{17.23}$$

Integrating the instantaneous range with respect to the change in aircraft weight yields the "Breguet range equation" [Eq. (17.23)]. This integration assumes that the velocity, specific fuel consumption, and L/D are approximately constant.

These assumptions require that the aircraft hold lift coefficient constant. To hold the lift coefficient constant as the aircraft becomes lighter requires reducing the dynamic pressure. Since velocity is also being held constant, the only way to reduce dynamic pressure is to reduce air density by climbing. This results in a flight path known as the "cruise-climb," which maximizes range.

The cruise-climb is not normally permitted for transport aircraft because of the desire by air-traffic control to keep all aircraft at a constant altitude and airspeed. It is possible to develop a rather messy range equation under these assumptions.

However, the Breguet range equation can be applied with little loss of accuracy by breaking the cruise legs into several shorter mission-segments, using the appropriate L/D values as aircraft weight drops.

On a long flight, air traffic control may permit a "stairstep" flight path in which the aircraft climbs to a more optimal altitude several times during the cruise as fuel is burned off.

Range Optimization—Jet

The Breguet range equation can be applied equally well to jets or propeller aircraft, with the use of Eq. (17.4) to determine an equivalent thrust specific fuel consumption for the propeller aircraft. However, the conditions for maximum range differ for jets and props because of the effect of velocity on thrust for the propeller.

The terms in the Breguet range equation that do not involve the weight change [i.e., $(V/C)(L/D)$] are known as the "range parameter" and are a measure of the cruising performance. For subsonic jet aircraft the specific fuel consumption is essentially independent of velocity and the range parameter can be expanded as shown in Eq. (17.24).

Setting the derivative of Eq. (17.24) with respect to velocity equal to zero yields Eq. (17.25), the velocity for best range for a jet. The resulting lift coefficient and drag are given in Eqs. (17.26) and (17.27).

$$\frac{V}{C}\left(\frac{L}{D}\right) = \frac{V}{C}\left(\frac{C_L}{C_{D_0} + KC_L^2}\right) = \frac{2W/\rho VS}{CC_{D_0} + (4KW^2C)/(\rho^2V^4S^2)} \tag{17.24}$$

$$V_{\substack{\text{best}\\\text{range}}} = \sqrt{\frac{2W}{\rho S}}\sqrt{\frac{3K}{C_{D_0}}} \tag{17.25}$$

$$C_{L_{\substack{\text{best}\\\text{range}}}} = \sqrt{\frac{C_{D_0}}{3K}} \tag{17.26}$$

$$D_{\substack{\text{best}\\\text{range}}} = qS\left(C_{D_0} + \frac{C_{D_0}}{3}\right) \tag{17.27}$$

Note that the drag coefficient for best range for a jet is 1.33 times the zero-lift drag. This is a lower drag coefficient than the drag coefficient for

This method minimizes time to climb with no constraint on ending velocity. To climb to a given altitude with a specified ending velocity, the optimal trajectory is flown until the aircraft reaches the energy-height curve of the desired ending condition. Then that energy-height curve is followed to the ending altitude and velocity, by either climbing or diving.

$$t_{1\text{-}2} \cong \frac{\Delta h_e}{(P_s)_{\text{average}}} \tag{17.90}$$

The actual time to climb is determined by numerically integrating along the optimal trajectory using Eq. (17.89). The time to change energy height is approximately expressed in Eq. (17.90) as the change in energy height divided by the average P_s during the change. As always, accuracy is improved with smaller integration steps.

Note that the time to follow lines of constant energy-height is usually negligible for a first-order analysis.

Minimum Fuel-to-Climb Trajectory

The energy equations can be modified to determine the climb trajectory that minimizes fuel consumption. The "fuel specific energy" (f_s) is defined as the change in specific energy per change in fuel weight. This is shown in Eq. (17.91) to equal the P_s divided by the fuel flow, which is the thrust times the specific fuel consumption.

Like P_s, the f_s values can be calculated and plotted vs Mach number for each altitude and then cross-plotted as contour lines on a Mach number vs altitude chart, as shown in Fig. 17.15.

$$f_s = \frac{\mathrm{d}h_e}{\mathrm{d}W_f} = \frac{\mathrm{d}h_e/\mathrm{d}t}{\mathrm{d}W_f/\mathrm{d}t} = \frac{P_s}{CT} \tag{17.91}$$

$$W_{f_{1\text{-}2}} = \int_{h_{e_1}}^{h_{e_2}} \frac{1}{f_s}\,\mathrm{d}h_e \tag{17.92}$$

In Eq. (17.92), Eq. (17.91) is rearranged and integrated to yield the change in fuel weight for a change in energy height (h_e). Note that this is minimized when f_s is maximized for each energy height. This implies that the minimum-fuel-to-climb trajectory passes through those points for which f_s contours are exactly tangent to the h_e contours. This is shown in Fig. 17.15, which greatly resembles the chart used to determine the minimum-time-to-climb trajectory.

$$W_{f_{1\text{-}2}} \cong \frac{\Delta h_e}{(f_s)_{\text{average}}} \tag{17.93}$$

The fuel consumed during the climb is determined by numerically integrating along the minimum-fuel trajectory, using Eq. (17.93) as an approximation.

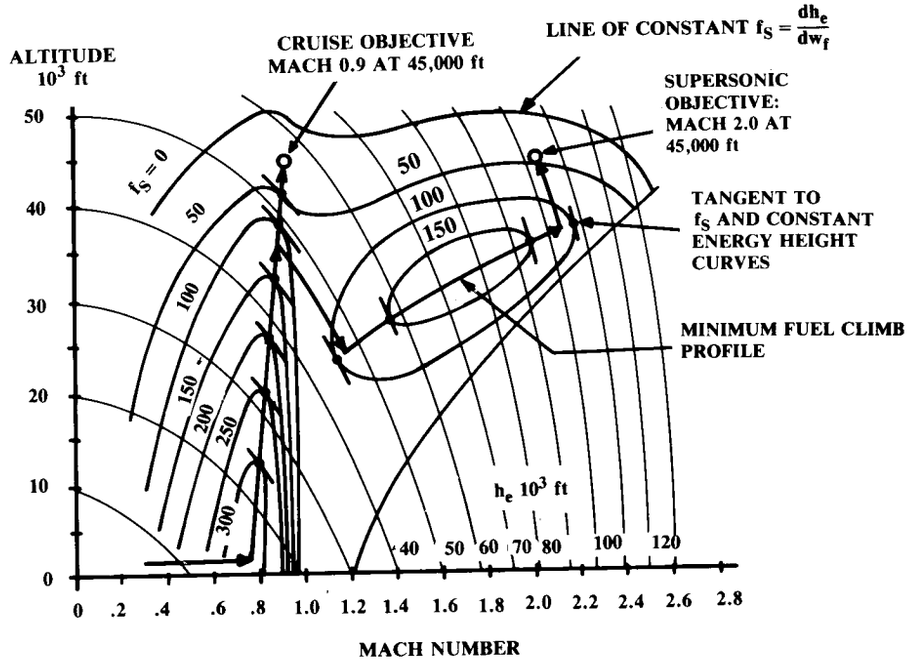

Fig. 17.15 Minimum fuel to climb.

Energy Method for Mission-Segment Weight Fraction

Equation (17.94) is an expression of the mission-segment weight fraction for any flight maneuver involving an increase in energy height. This can be used for climbs or accelerations or combinations of the two. Remember that the mission-segment weight fraction expresses the total aircraft weight at the end of the mission segment divided by the total aircraft weight at the beginning of the mission segment. This is used for sizing as discussed in earlier chapters.

$$\frac{W_{i+1}}{W_i} = \exp\left[\frac{-C\Delta h_e}{V(1-D/T)}\right] \tag{17.94}$$

Unfortunately, a maneuver involving a reduction in energy height cannot create fuel as would be implied by putting a negative value for the change in h_e into Eq. (17.94)!

17.7 OPERATING ENVELOPE

The aircraft "operating envelope" or "flight envelope" maps the combinations of altitude and velocity that the aircraft has been designed to withstand. The "level-flight operating envelope" has the further restriction that the aircraft be capable of steady level flight.

The rate of climb, or vertical velocity, is the velocity times the sine of the climb angle [Eq. (17.37)].

$$T = D + W\sin\gamma \tag{17.34}$$

$$L = W\cos\gamma \tag{17.35}$$

$$\gamma = \sin^{-1}\left(\frac{T-D}{W}\right) = \sin^{-1}\left(\frac{T}{W} - \frac{\cos\gamma}{L/D}\right) \cong \sin^{-1}\left(\frac{T}{W} - \frac{1}{L/D}\right) \tag{17.36}$$

$$V_v = V\sin\gamma = V\left(\frac{T-D}{W}\right) \cong V\left(\frac{T}{W} - \frac{1}{L/D}\right) \tag{17.37}$$

The velocity for steady climbing flight can now be derived from Eq. (17.35), as shown in Eq. (17.38).

The thrust-to-weight ratio is no longer the inverse of the lift-to-drag ratio as was the case for level flight. Solving Eq. (17.36) for T/W yields Eq. (17.39), the thrust-to-weight ratio required for a steady climb at angle γ.

$$V = \sqrt{\frac{2}{\rho C_L}\left(\frac{W}{S}\right)\cos\gamma} \tag{17.38}$$

$$\frac{T}{W} = \frac{\cos\gamma}{L/D} + \sin\gamma \cong \frac{1}{L/D} + \sin\gamma \tag{17.39}$$

Graphical Method for Best Angle and Rate of Climb

Two climb conditions especially concern the aircraft designer: the "best rate of climb," which provides the maximum vertical velocity (V_v), and the "best angle of climb," which provides a slightly lower vertical velocity but at a reduced horizontal speed, so that the angle of climb is maximized.

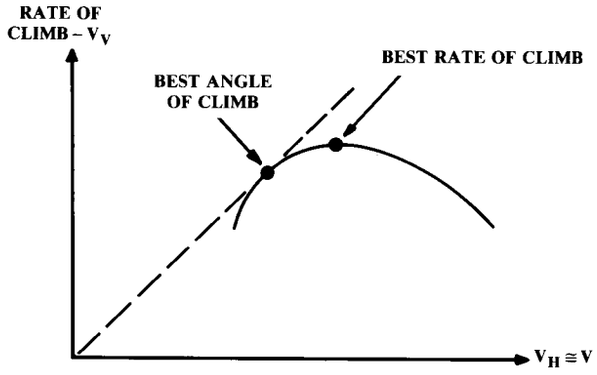

Fig. 17.3 Graphical method for best climb.

Therefore, the aircraft gains more altitude for a given horizontal distance; important for clearing mountains!

The most accurate way to determine best rate and angle of climb is to plot the rate of climb vs velocity, using Eq. (17.37) and the actual thrust and drag data as shown in Fig. 17.3. The best rate of climb is obviously the peak of the curve. The best angle of climb is the point of tangency to a line from the origin. The angle of climb is the arctangent of the vertical velocity divided by the horizontal velocity at that point.

Best Angle and Rate of Climb—Jet

Analytical optimization of velocity for best angle and rate of climb can be messy. Graphical analysis is more reliable, but doesn't give an analytical feeling for the key variables.

For a jet aircraft, the thrust is essentially constant with velocity so Eq. (17.36) can be directly maximized for the conditions for best climb angle. Since the T/W term is constant with velocity, the velocity for best L/D should be selected to maximize climb angle. This velocity was determined in Eq. (17.13).

To determine the velocity for best rate of climb of a jet aircraft, Eq. (17.37) must be maximized. Equation (17.40) is obtained from Eq. (17.37) by expanding the drag term and assuming that γ is small enough that lift approximately equals weight:

$$V_v = V\left(\frac{T-D}{W}\right) = V\left(\frac{T}{W}\right) - \frac{\rho V^3 C_{D_0}}{2(W/S)} - \frac{2K}{\rho V}\left(\frac{W}{S}\right) \tag{17.40}$$

$$\frac{\partial V_v}{\partial V} = 0 = \frac{T}{W} - \frac{3\rho V^2 C_{D_0}}{2(W/S)} + \frac{2K}{\rho V^2}\left(\frac{W}{S}\right)$$

$$V = \sqrt{\frac{W/S}{3\rho C_{D_0}}\left[T/W + \sqrt{(T/W)^2 + 12C_{D_0}K}\right]} \tag{17.41}$$

In Eq. (17.41), the derivative of the vertical velocity with respect to aircraft velocity is set to zero and solved for velocity for best climb.

Note that if the thrust is zero this equation collapses to the equation for the velocity for minimum power required [Eq. (17.19)], which serves as a lower boundary on the solution. The effect of nonzero thrust is a significant increase in the velocity for best climb rate with increasing thrust.

The velocity for best climb rate including the effects of thrust may be on the order of twice the velocity for minimum power. Velocities of 300–500 knots are not uncommon for the best climb speed for a jet. The XB-70 has a best climb speed of 583 knots!

This climb optimization will only determine the velocity for the best rate of climb at some altitude. It will not tell you what the complete climb profile should be to minimize time to a given altitude. For many supersonic aircraft, minimizing total time to climb requires leveling off or even diving as the aircraft accelerates through transonic speeds to minimize the time spent at these high-drag conditions. In a later section, the "specific excess power"

method will be presented as a means for determining the climb profile that minimizes total time to climb.

Best Angle and Rate of Climb—Prop

Equation (17.42) expresses the climb angle of a propeller aircraft, as obtained by substituting Eq. (17.5) into Eq. (17.36). This equation can be expanded and the derivative taken with respect to velocity:

$$\gamma = \sin^{-1}\left[\frac{550\text{bhp}\ \eta_p}{VW} - \frac{D}{W}\right] \tag{17.42}$$

However, the theoretical optimal velocities obtained with the resulting equation tend to be too low (sometimes lower than the stall speed) for the parabolic drag approximation to be valid, because of the separation drag at high angles of attack. Also, the thrust no longer follows Eq. (17.5) which implies that thrust is infinite at zero airspeed.

If thrust and drag data are available at low speeds, the graphical method will produce good results. Most propeller aircraft have a best angle-of-climb speed about 85–90% of the best rate-of-climb speed. This can be used for an initial estimate.

Best rate of climb for a propeller aircraft is obtained by substituting Eq. (17.5) into Eq. (17.37). This yields Eq. (17.43); simply the power available minus the power required, divided by aircraft weight. Therefore the best rate of climb occurs at the velocity for minimum power required, as defined in Eq. (17.19):

$$V_v = V\sin\gamma = \frac{550\text{bhp}\ \eta_p}{W} - \frac{DV}{W} \tag{17.43}$$

Time to Climb and Fuel to Climb

The time to climb to a given altitude is the change in altitude divided by the vertical velocity (rate of climb), as shown in Eq. (17.44) for an incremental altitude change. Fuel burned is the product of the thrust, specific fuel consumption, and time to climb [Eq. (17.45)].

$$\mathrm{d}t = \frac{\mathrm{d}h}{V_v} \tag{17.44}$$

$$\mathrm{d}W_f = -CT\,\mathrm{d}t \tag{17.45}$$

The air density, aircraft weight, drag, thrust, specific fuel consumption, and best climb velocity all change during the climb. A good approximation over small changes in altitude is that the rate of climb at a given weight and constant-thrust setting and constant velocity will reduce linearly with the altitude. This is shown in Eq. (17.46), where the linear constant a is determined from the rates of climb at any two altitudes h_1 and h_2 [Eq. (17.47)]. These two altitudes used to determine a should be near the beginning and ending altitudes of the climb being analyzed, but need not be exactly the same altitudes.

$$V_v = V_{v_i} - a(h_{i+1} - h_i) \tag{17.46}$$

$$a = \frac{V_{v_2} - V_{v_1}}{h_2 - h_1} \tag{17.47}$$

If the climb is broken into short segments (less than 5000 ft in altitude gain), the fuel burned will be an insignificant portion of the total aircraft weight and can be ignored in the time integration. Substituting Eq. (17.46) into Eq. (17.44) and integrating yields Eq. (17.48), the time to climb from altitude i to altitude $i + 1$.

Oddly enough, the change in altitude has dropped out of the equation! However, the change in altitude is implicit in the change in rate of climb (V_v) due to change in altitude. The fuel burned will then be described by Eq. (17.49).

$$t_{i+1} - t_i = \frac{1}{a}\ln\left(\frac{V_{v_i}}{V_{v_{i+1}}}\right) \tag{17.48}$$

$$\Delta W_{\text{fuel}} = (-CT)_{\text{average}}\,(t_{i+1} - t_i) \tag{17.49}$$

If desired, the accuracy of Eq. (17.48) can be improved upon by iteration. The rate of climb at the end of the climb segment can be recalculated using the reduced aircraft weight obtained by subtracting the fuel burned [Eq. (17.49)] from the original weight. This revised rate of climb can then be applied back into Eq. (17.48).

17.4 LEVEL TURNING FLIGHT

In level turning flight, the lift of the wing is canted so that the horizontal component of the lift exerts the centripetal force required to turn. The total lift on the wing is n times the aircraft weight W, where n is the load factor. Since the vertical component of lift must be W, the horizontal component of lift must be W times the square root of $(n^2 - 1)$. The geometry of a level turn is shown in Fig. 17.4.

$$\dot{\psi} = \frac{W\sqrt{n^2 - 1}}{(W/g)V} = \frac{g\sqrt{n^2 - 1}}{V} \tag{17.50}$$

Turn rate ($\mathrm{d}\psi/\mathrm{d}t$) equals the radial acceleration divided by the velocity, as shown in Eq. (17.50). Turn rate is usually expressed in degrees per second. Equation (17.50) yields radians per second, which must be multiplied by 57.3 to get degrees per second.

Instantaneous Turn-Rate

If the aircraft is allowed to slow down during the turn ("instantaneous turn"), the load factor n will be limited only by the maximum lift coeffi-

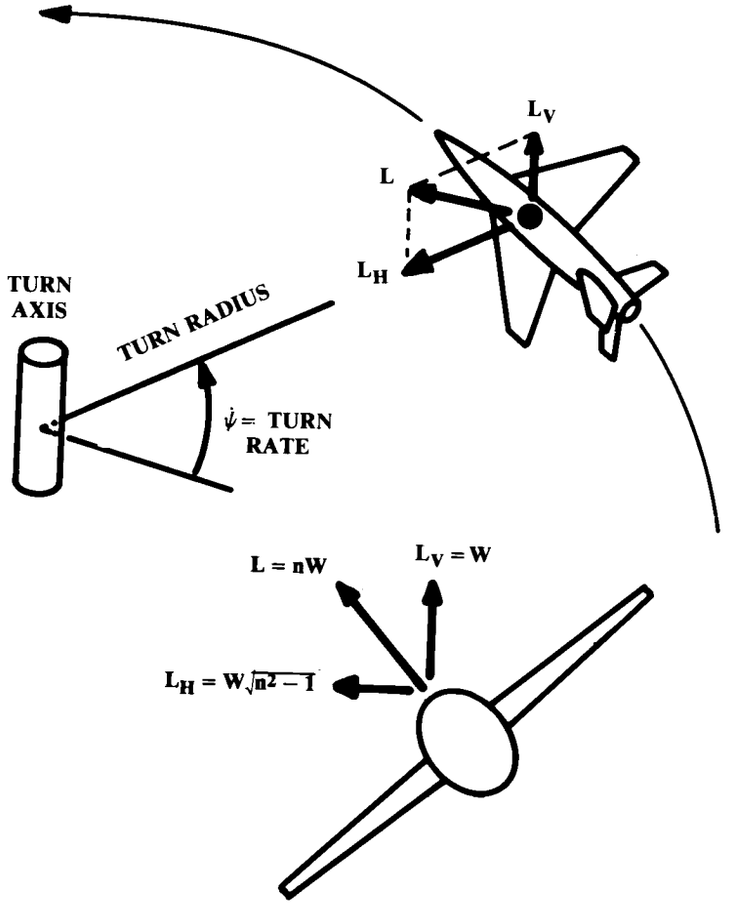

Fig. 17.4 Level turn geometry.

cient or structural strength of the aircraft. Figure 17.5 shows these stall and structural limits expressed as turn rate vs velocity for a typical fighter aircraft.

The intersection of the stall limit and the structural limit defines the "corner speed," which is the velocity for maximum instantaneous turn-rate. For a typical fighter, corner speed is about 300–350 knots. In a classical turning dogfight, opponents will try to get to their own corner speed as quickly as possible.

Sustained Turn-Rate

In a "sustained turn," the aircraft is not permitted to slow down or lose altitude during the turn. In a sustained turn the thrust must equal the drag and the lift must equal load factor n times the weight. Thus the maximum load factor for sustained turn can be expressed as the product of the thrust-to-weight and lift-to-drag ratios [Eq. (17.51)], assuming that the thrust axis is approximately aligned with the flight direction.

To solve for the sustained load factor in terms of the basic aerodynamic coefficients, the drag is expanded using ($C_L = nW/qS$) and set equal to the thrust. This leads to Eq. (17.52), which defines the maximum available sustained load factor for a given flight condition.

Note that the drag-due-to-lift factor (K) is a function of lift coefficient, as described in Chapter 12. Since n is also a function of lift coefficient, iteration is required to solve Eq. (17.52).

$$n = (T/W)(L/D) \tag{17.51}$$

$$n = \sqrt{\frac{q}{K(W/S)}\left(\frac{T}{W} - \frac{qC_{D_0}}{W/S}\right)} \tag{17.52}$$

Equation (17.51) implies that the sustained-turn load factor can be optimized by flying at the lift coefficient for maximum L/D, which was determined in Eq. (17.14). Using this lift coefficient and setting lift equal to n times W leads to Eq. (17.53). This can be readily solved for either velocity or wing loading to obtain the maximum sustained-turn load factor.

$$L = nW = qS\sqrt{\frac{C_{D_0}}{K}} \tag{17.53}$$

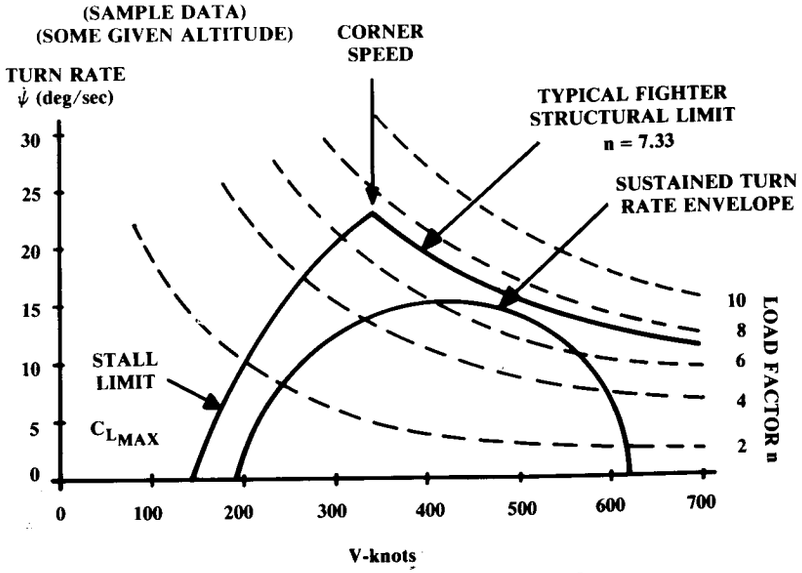

Fig. 17.5 Turn rate and corner speed.

Figure 17.5 showed the "sustained turn-rate envelope." This is derived using Eq. (17.50) to determine the turn-rates provided by the sustained load factors available at the various flight conditions.

Turn Rate with Vectored Thrust

Vectored thrust offers improved turn performance for future fighters, and is already used in the VSTOL Harrier fighter to maximize turn-rate. The direction the thrust should be vectored depends upon whether instantaneous or sustained turn-rate is to be maximized.

In a level turn with vectored thrust, the load factor times the weight must equal the lift plus the contribution of the vectored thrust, as shown in Eq. (17.54).

The maximum load factor (and turn rate) is obtained by taking the derivative with respect to vector angle and setting it to zero [Eq. (17.55)]. This yields Eq. (17.56), which states simply that the thrust vector for maximum instantaneous turn-rate should be perpendicular to the flight direction.

$$nW = L + T\sin(\alpha + \phi_T) \tag{17.54}$$

$$\frac{\partial n}{\partial \phi_T} = \frac{\partial}{\partial \phi_T}\left(\frac{L}{W} + \frac{T}{W}\sin(\alpha + \phi_T)\right) = \left(\frac{T}{W}\right)\cos(\alpha + \phi_T) = 0 \tag{17.55}$$

$$\phi_T = 90 \text{ deg} - \alpha \tag{17.56}$$

Since none of the thrust is propelling the aircraft forward, it will slow down very rapidly! British pilots in combat have used the 90-deg vectoring of the Harrier to generate a high turn-rate while decelerating, causing pursuing pilots to overshoot.

In a sustained turn with vectored thrust, the drag equals the thrust times the cosine of the total thrust angle, so the load factor n is expressed as in Eq. (17.57). Setting the derivative with respect to thrust-vector angle equal to zero [Eq. (17.58)] yields Eq. (17.59).

$$n = \left(\frac{T\cos(\alpha + \phi_T)}{W}\right)\left(\frac{L}{D}\right) \tag{17.57}$$

$$\frac{\partial n}{\partial \phi_T} = \frac{T}{W}\sin(\alpha + \phi_T)\left(\frac{L}{D}\right) = 0 \tag{17.58}$$

$$\phi_T = -\alpha \tag{17.59}$$

Equation (17.59) implies that the thrust vector for maximum sustained turn rate should be aligned with the flight direction. If the aircraft is at a positive angle of attack, the thrust should be vectored upward (relative to the fuselage axis) to align it with the freestream! However, this calculation ignores the jet flap effect which may produce a drag reduction with slight downward deflection if the nozzles are located near the wing trailing edge.

17.5 GLIDING FLIGHT

Straight Gliding Flight

Gliding flight is similar to climbing flight with the thrust set to zero. Equations (17.34) and (17.35) become Eqs. (17.60) and (17.61). The direction of the gliding angle γ is assumed to be reversed from that used for climb.

$$D = \text{W}\sin\gamma \tag{17.60}$$

$$L = \text{W}\cos\gamma \tag{17.61}$$

$$\frac{L}{D} = \frac{W\cos\gamma}{W\sin\gamma} = \frac{1}{\tan\gamma} \cong \frac{1}{\gamma} \tag{17.62}$$

The lift-to-drag ratio is the inverse of the tangent of the glide angle [Eq. (17.62)]. In sailplane terminology, the "glide ratio" is the ratio between horizontal distance travelled and altitude lost, and is equal to the lift-to-drag ratio. A high-performance sailplane with a glide ratio of 40 will travel over seven statute miles for every thousand feet of altitude lost.

(Cultural note: In sailplane terminology, a "sailplane" is an expensive, high-performance unpowered aircraft. A "glider" is a crude, low-performance unpowered aircraft!)

To maximize range from a given altitude, the glide ratio should be maximized. This requires flying at the velocity for maximum L/D as found in Eq. (17.13), repeated below as Eq. (17.63). The lift coefficient for maximum L/D is repeated as Eq. (17.64). The resulting maximum L/D (glide ratio) is determined from Eq. (17.15), as shown in Eq. (17.65).

$$V_{\max L/D} = \sqrt{\frac{2W}{\rho S}}\sqrt{\frac{K}{C_{D_0}}} \tag{17.63}$$

$$C_{L\max L/D} = \sqrt{\frac{C_{D_0}}{K}} \tag{17.64}$$

$$\left(\frac{L}{D}\right)_{\max} = \frac{1}{2\sqrt{C_{D_0}K}} = \frac{1}{2}\sqrt{\frac{\pi Ae}{C_{D_0}}} \tag{17.65}$$

The time a glider may remain in the air is determined by the "sink rate"; the vertical velocity V_v, which is negative in this case. Sink rate is the aircraft velocity times the sine of the glide angle, as expressed in Eq. (17.66).

$$V_v = V\sin\gamma = \sin\gamma\sqrt{\left(\frac{W}{S}\right)\frac{2\cos\gamma}{\rho C_L}} \tag{17.66}$$

$$\sin\gamma = \frac{D}{L}\cos\gamma = \frac{C_D}{C_L}\cos\gamma \tag{17.67}$$

$$V_v = \sqrt{\frac{W}{S}\frac{2\cos^3\gamma C_D^2}{\rho C_L^3}} \cong \sqrt{\frac{W}{S}\frac{2}{\rho(C_L^3/C_D^2)}} \tag{17.68}$$

Equation (17.66) contains both sine and cosine terms. In Eq. (17.67) the sine of the glide angle is expressed in cosine terms to allow substitution into Eq. (17.66), as shown in Eq. (17.68). For typical, small glide angles the cosine term may be ignored.

The lift coefficient for minimum sink rate is solved for by maximizing the term involving C_L and C_D. This is shown in Eq. (17.69), with the result in Eq. (17.70). Note that this is also the lift coefficient for minimum power required, so the velocity can be expressed as in Eq. (17.71). The L/D at minimum sink speed is given by Eq. (17.72).

$$\frac{\partial}{\partial C_L}\left(\frac{C_L^3}{C_D^2}\right) = \frac{\partial}{\partial C_L}\left(\frac{C_L^3}{(C_{D_0} + KC_L^2)^2}\right) = 0 \tag{17.69}$$

$$C_{L\,\text{min sink}} = \sqrt{\frac{3C_{D_0}}{K}} \tag{17.70}$$

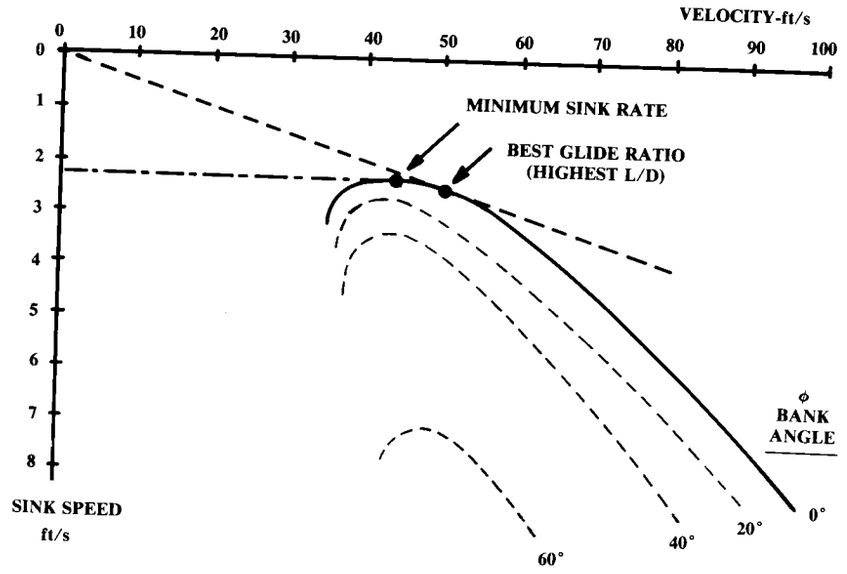

Fig. 17.6 Sailplane sink rate.

$$V_{\text{min sink}} = \sqrt{\frac{2W}{\rho S}\sqrt{\frac{K}{3C_{D_0}}}} \tag{17.71}$$

$$\left(\frac{L}{D}\right)_{\text{min sink}} = \sqrt{\frac{3}{16KC_{D_0}}} = \sqrt{\frac{3\pi Ae}{16C_{D_0}}} \tag{17.72}$$

The velocity for minimum sink rate is 76% of the velocity for best glide ratio. Sailplane pilots fly at minimum sink speed when they are in "lift" (i.e., in an airmass moving upwards). When the lift "dies," they accelerate to the velocity for best glide ratio to cover the most ground while looking for the next lift. An instrument called a "variometer" tells the sailplane pilots when they are in lift.

Figure 17.6 shows a graphical representation of sink rate for a sailplane. This is known as a "speed-polar," or "hodograph," and can be used to graphically determine the velocities for minimum sink rate and best glide ratio.

Turning Gliding Flight

When sailplane pilots find lift, they turn in a small circle to stay within the lifting airmass. Due to the additional wing lift required to turn, the sailplane will experience higher drag and a greater sink rate. Equation (17.61) must be modified to account for the bank angle ϕ [Eq. (17.73)].

$$L\cos\phi = W\cos\gamma \cong W \tag{17.73}$$

Turn-rate is equal to the centripetal acceleration divided by the velocity, and is also equal to the velocity divided by the turn radius [Eq. (17.74)]. This allows the centripetal acceleration to be expressed as the velocity squared divided by the turn radius [Eq. (17.75)]. In Eq. (17.76), the turning force due to the lateral component of wing lift is equal to the aircraft mass times the centripetal acceleration.

$$\dot{\psi} = a/V = V/R \tag{17.74}$$

$$a = V^2/R \tag{17.75}$$

$$L\sin\phi = \frac{WV^2}{gR} = W\sqrt{n^2 - 1} \tag{17.76}$$

$$R = \frac{V^2}{g\tan\phi} = \frac{V^2}{g\sqrt{n^2 - 1}} \tag{17.77}$$

Equation (17.76) can be solved for turn radius as expressed in terms of either bank angle or load factor [Eq. (17.77)].

The vertical velocity (sink rate) can be determined by substituting $C_L\cos\phi$ for C_L in Eq. (17.68). This yields Eq. (17.78), which is simply the previous

result divided by the cosine of ϕ, raised to the 3/2 power. The radius of the turn is found by substituting Eq. (17.73) into Eq. (17.77), as shown in Eq. (17.79):

$$V_v = \frac{1}{\cos^{3/2}\phi}\sqrt{\frac{W}{S}\frac{2}{\rho(C_L^3/C_D^2)}} \tag{17.78}$$

$$R = \frac{2W}{\rho S C_L g \sin\phi} \tag{17.79}$$

Since the ϕ term in Eq. (17.78) does not vary with velocity, the prior results for the velocities for best glide ratio and minimum sink rate can be applied.

One unique problem for a slow-flying sailplane in a turn is the variation in velocity across the long span of the wing. The wing on the inside of the turn may stall due to the lower velocity. This is shown in Fig. 17.7. The velocity across the span varies linearly with distance from the axis of the turn. Also, the bank angle shortens the wing span when seen from above.

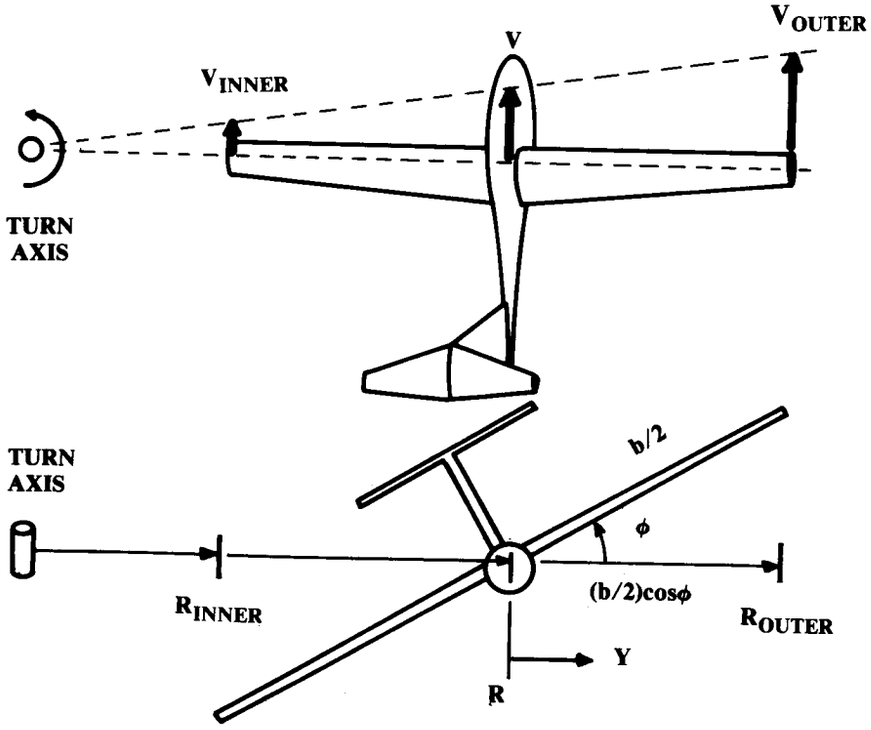

Fig. 17.7 Turn radius effect on wingtip velocity.

These effects are shown in Eq. (17.80):

$$V = V_{cg}\left[1 + \frac{Y}{R}\cos\phi\right] \tag{17.80}$$

$$V_{inner} = V_{cg}\left[1 - \frac{b}{2R}\cos\phi\right] \tag{17.81}$$

In Eq. (17.81), the velocity at the inner wing tip is shown as a function of wing span, turn radius, and bank angle. In normal flight this velocity difference is easily corrected with a little aileron to increase the lift coefficient on the inner wing. However, when flying near the stall at even a moderate bank angle, this can reduce the velocity of the inner wing tip enough to create a one-wing stall, which leads to a spin.

17.6 ENERGY-MANEUVERABILITY METHODS

Energy Equations

Fighter pilots have always known that management of energy is critical to survival and success. In World War I the experienced pilots always tried to enter a dogfight from above. They could then exchange the potential energy of altitude for the kinetic energy of speed or turn rate.

Jet-fighter dogfight maneuvers largely rely upon the exchange of potential and kinetic energy to attain a positional advantage. For example, the "High Speed Yo-Yo" maneuver is used when overtaking a slower aircraft in a hard turn. The attacker pulls up, trading kinetic energy for potential energy and slowing to allow a higher turn rate. After turning, the attacker rolls partially inverted and pulls down astern of the opponent, now exchanging potential energy back for speed.

Fighter pilots understand that potential and kinetic energy can be exchanged, and that the sum of the aircraft energy must be managed to attain success. This intuitive measure of goodness can be analytically developed and applied to aircraft design.

$$E = Wh + \frac{1}{2}\left(\frac{W}{g}\right)V^2 \tag{17.82}$$

$$h_e = \frac{E}{W} = h + \frac{1}{2g}V^2 \tag{17.83}$$

$$P_{s_{used}} = \frac{dh_e}{dt} = \frac{dh}{dt} + \frac{V}{g}\frac{dV}{dt} \tag{17.84}$$

At any point in time, the total energy of an aircraft (the "energy state") is the sum of the potential and kinetic energy, as shown in Eq. (17.82). Dividing by aircraft weight gives the "specific energy" [Eq. (17.83)].

Specific energy has units of distance (feet), and is also called the "energy height" (h_e) because it equals the aircraft altitude if the velocity is zero.

Power is the time rate of energy usage, so the "specific power" $(P_s)_{used}$ can be defined as the time rate at which the aircraft is gaining altitude or velocity [Eq. (17.84)]. Since specific energy has units of distance (feet), specific power has units of distance per time (feet per second).

This power being used by the aircraft to gain height or velocity has to come from somewhere. In the discussions of power required vs power available, it was pointed out that the excess power could be used to climb or accelerate. This excess power is the excess thrust $(T - D)$ times the velocity [Eq. (17.85)].

The "specific excess power" (P_s) is the excess power divided by the weight, and equals the specific power used, as shown in Eq. (17.86).

$$P = V(T - D) \tag{17.85}$$

$$P_s = \frac{V(T-D)}{W} = \frac{dh}{dt} + \frac{V}{g}\frac{dV}{dt} \tag{17.86}$$

$$P_s = V\left[\frac{T}{W} - \frac{qC_{D_0}}{W/S} - n^2\frac{K}{q}\frac{W}{S}\right] \tag{17.87}$$

Drag, and therefore P_s, is a function of the aircraft load factor. The higher the load factor, the greater the drag, and thus the less excess power available. Equation (17.86) can be expanded in terms of the load factor and the aerodynamic coefficients as shown in Eq. (17.87). Note that T/W and W/S are at the given flight condition, not the takeoff values!

Specific excess power P_s has units of feet per second, just like rate of climb. In fact, Eq. (17.86) is identical to the rate-of-climb equation if the longitudinal acceleration (dV/dt) is zero. The P_s at a load factor of one is actually the rate of climb that would be available if the pilot chose to use all of the excess power for climbing at constant velocity.

When P_s equals zero, the drag of the aircraft exactly equals the thrust so there is no excess power. This does not necessarily mean that the aircraft isn't climbing or accelerating. However, if the sum of the energy usage equals zero, then the aircraft must be flying level, or climbing and decelerating, or descending and accelerating.

Equations (17.86) and (17.87) assume that the thrust axis is approximately aligned with the flight direction. If this is not the case, the thrust term should be multiplied by the cosine of $(\alpha + \phi t)$.

P_s Plots

For any given altitude, P_s can be calculated using Eq. (17.87) for varying Mach numbers and load factors once the aerodynamic coefficients and installed thrust data are available. Design specifications for a new fighter will have a large number of "must meet or exceed" P_s points, such as "$P_s = 0$ at $n = 5$ at Mach 0.9 at 30,000 ft."

P_s values are calculated and plotted against Mach number as shown in Fig. 17.8 for a number of altitudes. Computers are especially handy for this "number crunching."

From the P_s charts at the various altitudes (Fig. 17.8), several additional charts can be prepared by cross-plotting.

The level turn-rate can be determined for the various load factors at a given altitude and Mach number, and plotted vs P_s (Fig. 17.9). This is compared to the data for a threat aircraft at that altitude and Mach number. With an equivalent P_s at a higher turn-rate, the new fighter would always be able to turn inside the opponent without losing relative energy. A turn-rate advantage of 2 deg/s is considered significant.

In Fig. 17.10, $P_s = 0$ contours are plotted for different load factors on a Mach number vs altitude chart. This is a major tool for the evaluation of new fighters, and permits comparisons between two aircraft for all Mach numbers and altitudes on one chart. To win a protracted dogfight, an aircraft should have $P_s = 0$ contours that envelop those of an opponent.

In Fig. 17.11, contour lines of constant P_s at a given load factor are plotted onto a Mach number vs altitude chart. A separate chart is prepared for each load factor. The chart for load factor equals one is especially important because it provides the rate of climb and the aircraft ceiling, and because it is used to determine an optimal climb trajectory.

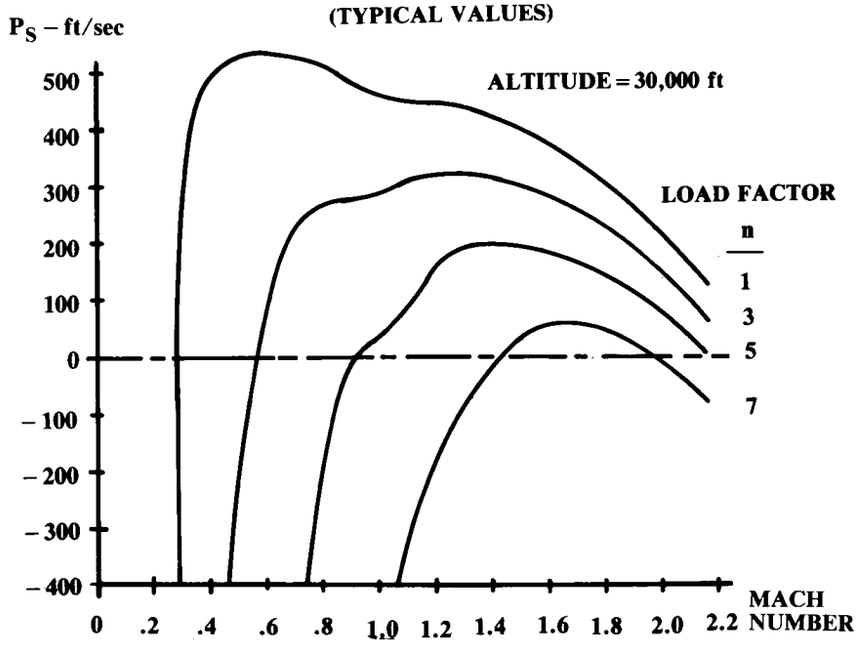

Fig. 17.8 P_S vs Mach number and load factor.

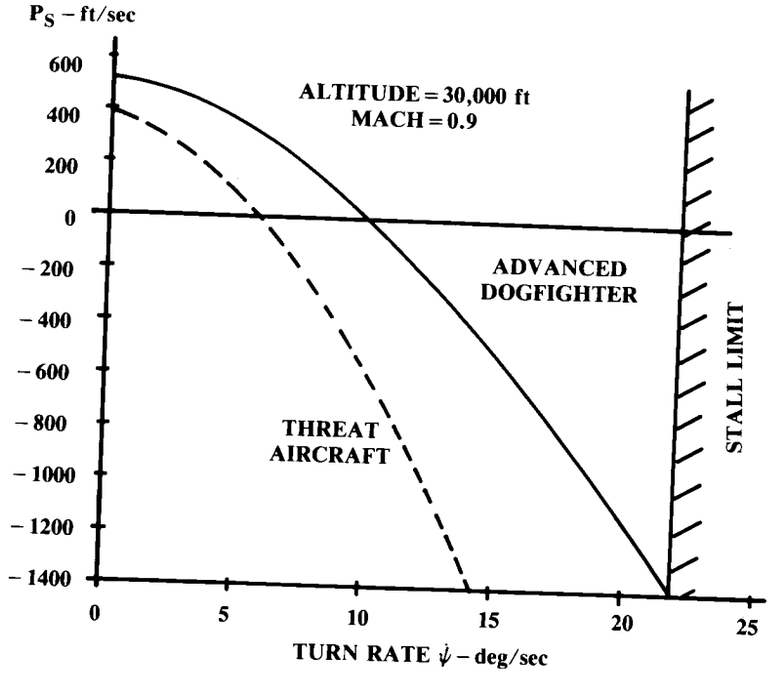

Fig. 17.9 Turn rate vs P_S.

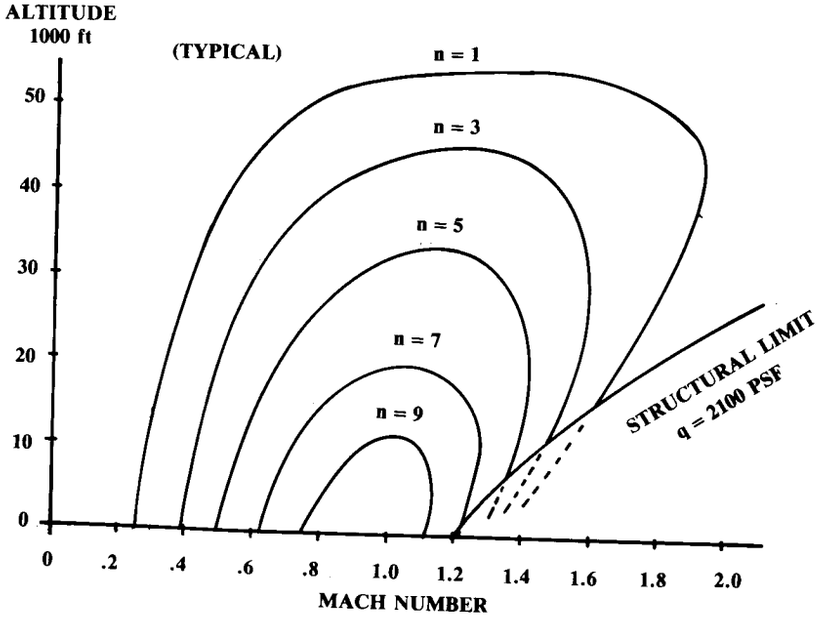

Fig. 17.10 $P_S = 0$ contours.

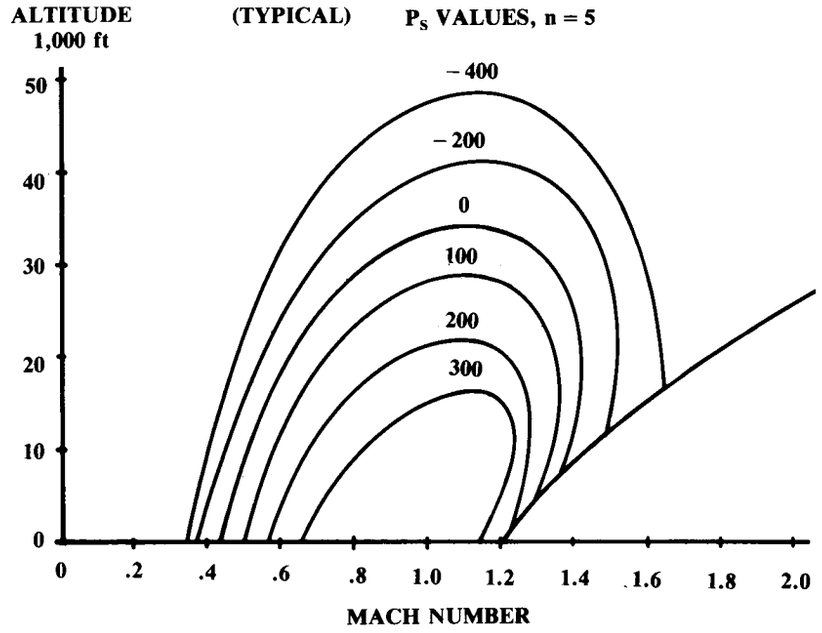

Fig. 17.11 P_S contours, constant load factor.

Minimum Time-to-Climb Trajectory

Figure 17.12 is a plot of energy height vs Mach number and altitude. This is merely a graphical representation of Eq. (17.83), and has nothing to do with the particulars of any one aircraft. An F-16 or a Boeing 747 would have an energy height of 42,447 ft if flying at Mach 0.9 at 30,000 ft.

$$dt = \frac{dh_e}{P_s} \tag{17.88}$$

$$t_{1\text{-}2} = \int_{h_{e_1}}^{h_{e_2}} \frac{1}{P_s}\, dh_e \tag{17.89}$$

Equation (17.84) can be rearranged into Eq. (17.88) which expresses the incremental time to change energy height (h_e) as the change in energy height divided by the P_s at that flight condition. This is then integrated in Eq. (17.89) for the time to change energy height.

Equation (17.89) shows that the time to change energy height is minimized if the P_s is maximized at each energy height. This occurs at those points on the Mach number vs altitude plot of 1-g P_s (Fig. 17.11) where the P_s curve is exactly tangent to an energy-height curve (Fig. 17.12).

In Fig. 17.13, the 1-g P_s curves for a typical current-technology-high-thrust fighter are superimposed on the h_e curves of Fig. 17.12. The trajectory for minimum time to climb is shown as passing through the dots repre-

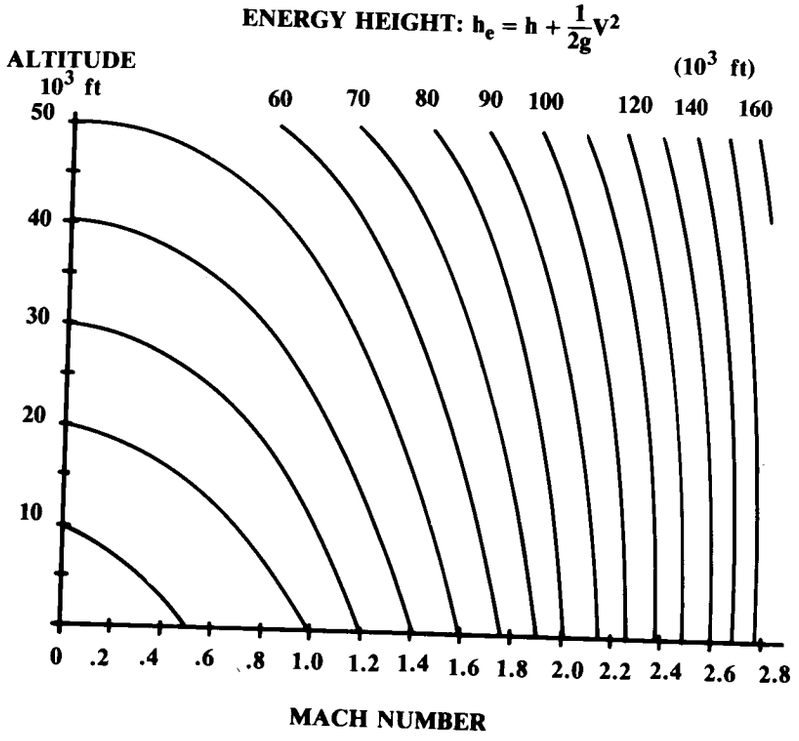

Fig. 17.12 Lines of constant energy height.

senting the points where the P_s curves are tangent to h_e curves. For such a fighter, the minimum time to climb is obtained by staying low and accelerating to transonic speeds, then pitching up into a steep climb at approximately constant indicated airspeed (i.e., dynamic pressure), as shown by the optimal trajectory.

Figure 17.14 shows the 1-g P_s curves for a typical 1960's era jet fighter. These fighters had significantly less thrust, and suffered a "thrust pinch" at transonic speeds—in which the thrust minus drag would reduce to almost zero. This causes the P_s contours to form "bubbles."

The minimum-time-to-climb trajectory requires jumping from one bubble to the other. This is done by diving or climbing along lines of constant energy height tangent to P_s lines of the same numerical value for both bubbles, as shown in Fig. 17.14.

Note that Fig. 17.14 requires diving through Mach 1.0 to minimize time to climb for this aircraft. This was common in earlier jets, and makes sense intuitively. Since thrust minus drag is nearly zero at transonic speeds, acceleration will be slow and the aircraft will spend a lot of time in transonic acceleration. Diving reduces this time. The altitude lost is easily regained at higher speeds where the drag is less.

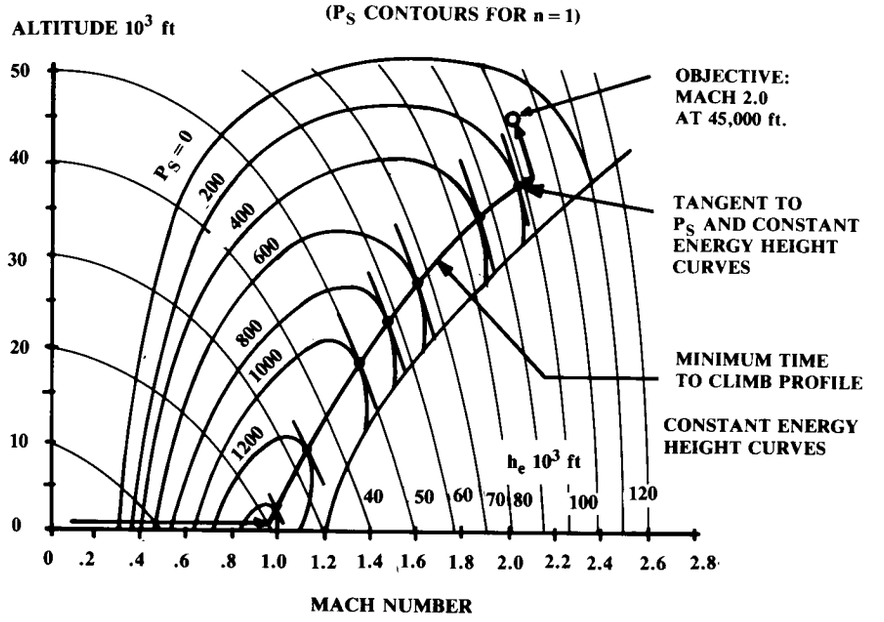

Fig. 17.13 Minimum time-to-climb trajectory, high-thrust fighter.

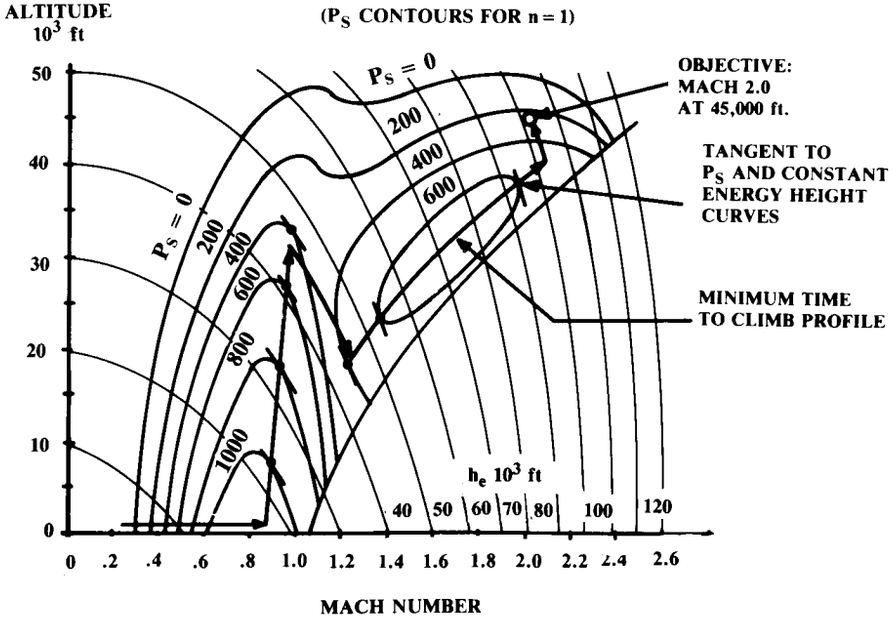

Fig. 17.14 Minimum time-to-climb, low thrust fighter (circa 1960).

This method minimizes time to climb with no constraint on ending velocity. To climb to a given altitude with a specified ending velocity, the optimal trajectory is flown until the aircraft reaches the energy-height curve of the desired ending condition. Then that energy-height curve is followed to the ending altitude and velocity, by either climbing or diving.

$$t_{1\text{-}2} \cong \frac{\Delta h_e}{(P_s)_{\text{average}}} \tag{17.90}$$

The actual time to climb is determined by numerically integrating along the optimal trajectory using Eq. (17.89). The time to change energy height is approximately expressed in Eq. (17.90) as the change in energy height divided by the average P_s during the change. As always, accuracy is improved with smaller integration steps.

Note that the time to follow lines of constant energy-height is usually negligible for a first-order analysis.

Minimum Fuel-to-Climb Trajectory

The energy equations can be modified to determine the climb trajectory that minimizes fuel consumption. The "fuel specific energy" (f_s) is defined as the change in specific energy per change in fuel weight. This is shown in Eq. (17.91) to equal the P_s divided by the fuel flow, which is the thrust times the specific fuel consumption.

Like P_s, the f_s values can be calculated and plotted vs Mach number for each altitude and then cross-plotted as contour lines on a Mach number vs altitude chart, as shown in Fig. 17.15.

$$f_s = \frac{\mathrm{d}h_e}{\mathrm{d}W_f} = \frac{\mathrm{d}h_e/\mathrm{d}t}{\mathrm{d}W_f/\mathrm{d}t} = \frac{P_s}{CT} \tag{17.91}$$

$$W_{f_{1\text{-}2}} = \int_{h_{e_1}}^{h_{e_2}} \frac{1}{f_s}\,\mathrm{d}h_e \tag{17.92}$$

In Eq. (17.92), Eq. (17.91) is rearranged and integrated to yield the change in fuel weight for a change in energy height (h_e). Note that this is minimized when f_s is maximized for each energy height. This implies that the minimum-fuel-to-climb trajectory passes through those points for which f_s contours are exactly tangent to the h_e contours. This is shown in Fig. 17.15, which greatly resembles the chart used to determine the minimum-time-to-climb trajectory.

$$W_{f_{1\text{-}2}} \cong \frac{\Delta h_e}{(f_s)_{\text{average}}} \tag{17.93}$$

The fuel consumed during the climb is determined by numerically integrating along the minimum-fuel trajectory, using Eq. (17.93) as an approximation.

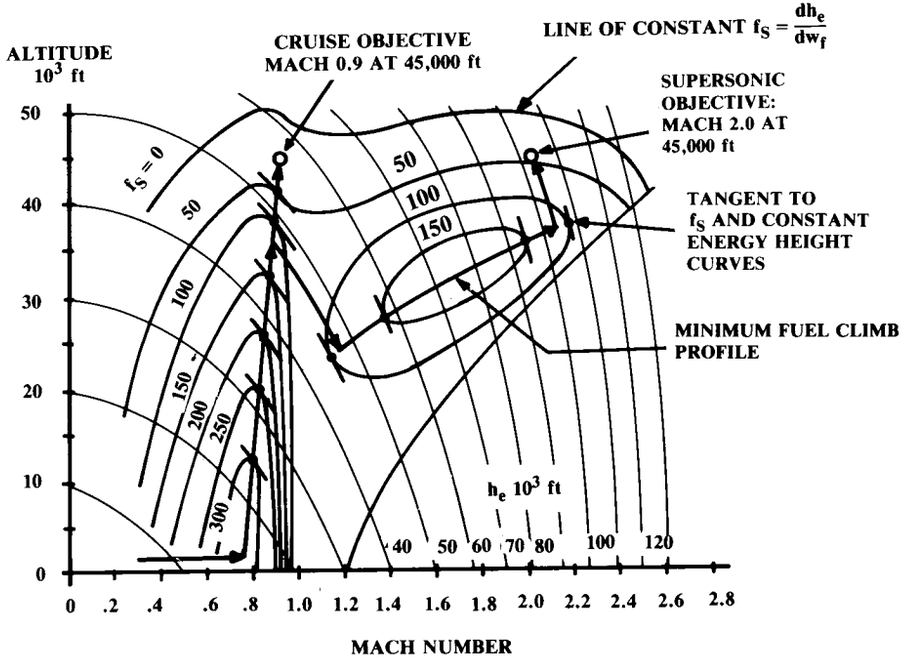

Fig. 17.15 Minimum fuel to climb.

Energy Method for Mission-Segment Weight Fraction

Equation (17.94) is an expression of the mission-segment weight fraction for any flight maneuver involving an increase in energy height. This can be used for climbs or accelerations or combinations of the two. Remember that the mission-segment weight fraction expresses the total aircraft weight at the end of the mission segment divided by the total aircraft weight at the beginning of the mission segment. This is used for sizing as discussed in earlier chapters.

$$\frac{W_{i+1}}{W_i} = \exp\left[\frac{-C\Delta h_e}{V(1-D/T)}\right] \tag{17.94}$$

Unfortunately, a maneuver involving a reduction in energy height cannot create fuel as would be implied by putting a negative value for the change in h_e into Eq. (17.94)!

17.7 OPERATING ENVELOPE

The aircraft "operating envelope" or "flight envelope" maps the combinations of altitude and velocity that the aircraft has been designed to withstand. The "level-flight operating envelope" has the further restriction that the aircraft be capable of steady level flight.

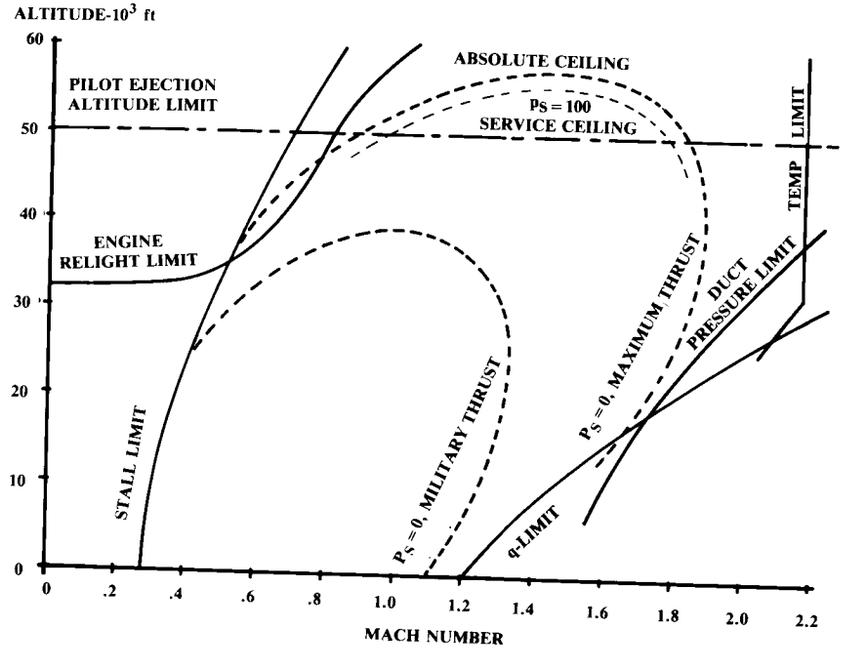

Fig. 17.16 Operating envelope.

The operating envelope for a typical fighter is shown in Fig. 17.16. Fighter operating envelopes are the most complicated and contain all the elements of the operating envelopes of other classes of aircraft.

The level-flight operating envelope is determined from the $P_s = 0$ and stall limit lines. The $P_s = 0$ limit is usually shown for both maximum thrust and for military (nonafterburning) thrust.

Since the $P_s = 0$ and stall lines vary with aircraft weight, some assumption about aircraft weight must be made. Typically the operating envelope is calculated at takeoff weight, cruise weight, or combat weight.

The "absolute ceiling" is determined by the highest altitude at which $P_s = 0$. Some small rate of climb capability (i.e., P_s) is required at the "service ceiling." FAR's require 100 fpm for propeller aircraft and 500 fpm for jets. Military specifications require 100 fpm at the service ceiling.

For some jet aircraft, the limitation on usable ceiling is the pilot. The odds of surviving an ejection above 50,000 ft are rather small without an astronaut-type pressure suit or some type of capsule. This limits the usable ceiling as shown.

Another limitation to the level flight envelope of many jet aircraft is the low-q engine operating limit. At low velocities and high altitudes there may not be enough air available to restart the engine in the event of a flameout. It may also be impossible to operate or light the afterburner. These limits are provided by the engine manufacturer.

The remaining limits shown in Fig. 17.16 are structural. The external-flow dynamic pressure q as defined in Eq. (17.95) has a direct impact upon the structural loads. A maximum q limit is specified in the design requirements and used by the structural designers for stress analysis. Typical fighter aircraft have a q limit of 1800–2200 psf. This corresponds to transonic speeds at sea level.

$$q = \tfrac{1}{2}\rho_\infty V_\infty^2 = 0.7 P_{\text{static}} M^2 \tag{17.95}$$

$$P_{T_0} = P_{\text{static}}[1 + 0.2M^2]^{3.5} \tag{17.96}$$

The airload pressures exerted within the inlet duct are greater than the freestream pressures because the inlet slows the air down (typically to about Mach 0.4–0.5 at the engine front-face). The total pressure of the oncoming air is determined from Eq. (17.96), using the static atmospheric pressure at that altitude from the Standard Atmosphere Table A.2.

The total pressure within the duct equals the outside total pressure times the inlet-duct pressure recovery, as discussed in Chapter 13. Equation (17.96) is used again for the flow within the duct and solved for the static pressure at the Mach number at the engine front-face. This is the maximum wall pressure exerted within the inlet duct, and may easily be three times the outside dynamic pressure. As shown in Fig. 17.16, the inlet-duct pressure limit does not follow the same slope as the dynamic-pressure limit.

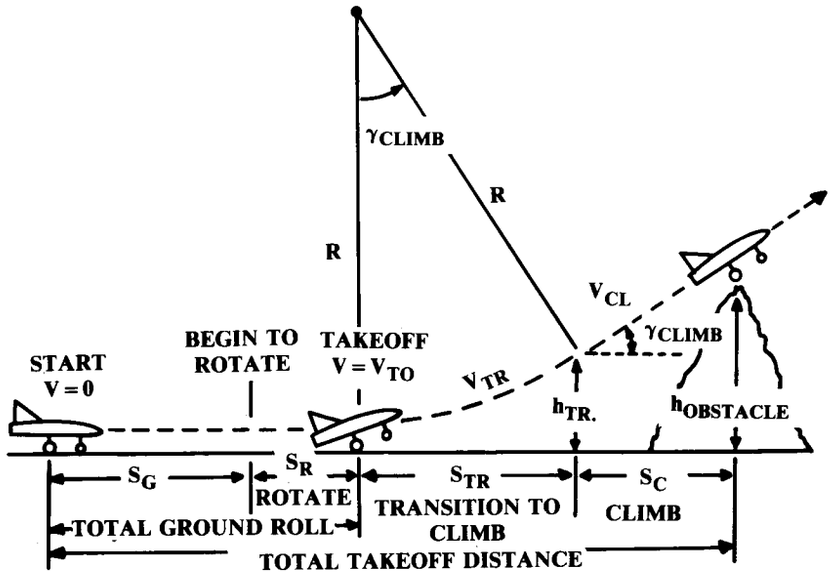

Fig. 17.17 Takeoff analysis.

The remaining operating envelope limit is the temperature limit due to skin aerodynamic heating. This depends upon the selected structural materials. A design chart for skin temperature vs Mach number and altitude was presented in Chapter 14.

17.8 TAKEOFF ANALYSIS

An empirical chart for determining takeoff distance has been presented. Later in the design process, a more detailed analysis breaks the takeoff into segments for more accurate analysis.

Figure 17.17 illustrates the segments of the takeoff analysis. The ground roll includes two parts, the level ground-roll and the ground roll during rotation to the angle of attack for liftoff. After rotation, the aircraft follows an approximately circular arc ("transition") until it reaches the climb angle.

Ground Roll

During the ground roll, the forces on the aircraft are the thrust, drag, and rolling friction of the wheels, this last being expressed as a rolling friction coefficient μ times the weight on the wheels (W-L). A typical μ value for rolling resistance on a hard runway is 0.03. Values for various runway surfaces are presented in Table 17.1.

The resulting acceleration of the aircraft, as expressed by Eq. (17.97), can be expanded in terms of the aerodynamic coefficients. This requires evaluating the lift and drag of the aircraft in ground effect and with landing gear down and flaps in the takeoff position, as discussed in Chapter 12. The lift coefficient is based on the wing angle of attack on the ground (measured to the zero lift-angle), and is typically less than 0.1 unless large takeoff flaps are deployed.

$$a = \frac{g}{W}\left[T - D - \mu(W - L)\right] = g\left[\left(\frac{T}{W} - \mu\right) + \frac{\rho}{2W/S}\left(-C_{D_0} - KC_L^2 + \mu C_L\right)V^2\right] \tag{17.97}$$

Table 17.1 Ground rolling resistance

Surface	μ-typical values	
	Rolling (brakes off)	Brakes on
Dry concrete/asphalt	0.03–0.05	0.3–0.5
Wet concrete/asphalt	0.05	0.15–0.3
Icy concrete/asphalt	0.02	0.06–0.10
Hard turf	0.05	0.4
Firm dirt	0.04	0.3
Soft turf	0.07	0.2
Wet grass	0.08	0.2

$$S_G = \int_{V_i}^{V_f} \frac{V}{a}\,dV = \frac{1}{2}\int_{V_i}^{V_f} \frac{1}{a}\,d(V^2) \tag{17.98}$$

The ground-roll distance is determined by integrating velocity divided by acceleration, as shown in Eq. (17.98). Note the mathematical trick that simplifies the integration by integrating with respect to V^2 instead of V.

The takeoff velocity must be no less than 1.1 times the stall speed, which is found by setting maximum lift at stall speed equal to weight and solving for stall speed. The maximum lift coefficient is with the flaps in the takeoff position. Remember that landing gear geometry may limit maximum angle of attack (and hence lift coefficient) for takeoff and landing.

Equation (17.98) is integrated for ground-roll distance from V_{initial} to V_{final} in Eq. (17.99), where the terms K_T and K_A are defined in Eqs. (17.100) and (17.101). K_T contains the thrust terms and K_A contains the aerodynamic terms.

$$S_G = \frac{1}{2g}\int_{V_i}^{V_f} \frac{d(V^2)}{K_T + K_A V^2} = \left(\frac{1}{2gK_A}\right)\ln\left(\frac{K_T + K_A V_f^2}{K_T + K_A V_i^2}\right) \tag{17.99}$$

$$K_T = \left(\frac{T}{W}\right) - \mu \tag{17.100}$$

$$K_A = \frac{\rho}{2(W/S)}\left(\mu C_L - C_{D_0} - KC_L^2\right) \tag{17.101}$$

Equation (17.99) integrates ground roll from any initial velocity to any final velocity. For takeoff, the initial velocity is zero and the final velocity is V_{TO}. Since the thrust actually varies somewhat during the ground roll, an averaged thrust value must be used. Since we integrate with respect to velocity squared, the averaged thrust to use is the thrust at about 70% (1/square-root 2) of V_{TO}.

For greater accuracy the ground roll can be broken into smaller segments and integrated using the averaged thrust for each segment in Eq. (17.99). The averaged thrust is the thrust at 70% of the velocity increase for that segment. Also, K may be reduced due to ground effect (Chapter 12).

The time to rotate to liftoff attitude depends mostly upon the pilot. Maximum elevator deflection is rarely employed. A typical assumption for large aircraft is that rotation takes three seconds. The acceleration is assumed to be negligible over that short time interval, so the rotation ground-roll distance S_R is approximated by three times V_{TO}. For small aircraft the rotational time is on the order of 1 s, and $S_R = V_{TO}$.

Transition

During the transition, the aircraft accelerates from takeoff speed (1.1 V_{stall}) to climb speed (1.2 V_{stall}). The average velocity during transition is therefore about 1.15 V_{stall}. The average lift coefficient during transition can be assumed to be about 90% of the maximum lift coefficient with takeoff flaps. The average vertical acceleration in terms of load factor can then be

found from Eq. (17.102):

$$n = \frac{L}{W} = \frac{\frac{1}{2}\rho S(0.9C_{L_{max}})(1.15V_{stall})^2}{\frac{1}{2}\rho S C_{L_{max}} V_{stall}^2} = 1.2 \tag{17.102}$$

$$n = 1.0 + \frac{V_{TR}^2}{Rg} = 1.2 \tag{17.103}$$

$$R = \frac{V_{TR}^2}{g(n-1)} = \frac{V_{TR}^2}{0.2g} \cong 0.205 V_{stall}^2 \tag{17.104}$$

The vertical load factor must also equal 1.0 plus the centripetal acceleration required to cause the aircraft to follow the circular transition-arc. This is shown in Eq. (17.103), and solved for the radius of the transition-arc in Eq. (17.104).

The climb angle γ at the end of the transition is determined from Eq. (17.105). The climb angle is equal to the included angle of the transition-arc (see Fig. 17.17), so the horizontal distance traveled during transition can be determined from Eq. (17.106). The altitude gained during transition is determined from the geometry of Fig. 17.17 to be as indicated in Eq. (17.107).

$$\sin\gamma_{climb} = \frac{T-D}{W} \cong \frac{T}{W} - \frac{1}{L/D} \tag{17.105}$$

$$S_T = R\sin\gamma_{climb} = R\left(\frac{T-D}{W}\right) \cong R\left(\frac{T}{W} - \frac{1}{L/D}\right) \tag{17.106}$$

$$h_{TR} = R(1 - \cos\gamma_{climb}) \tag{17.107}$$

If the obstacle height is cleared before the end of the transition segment, then Eq. (17.108) is used to determine the transition distance.

$$S_T = \sqrt{R^2 - (R - h_{TR})^2} \tag{17.108}$$

Climb

Finally, the horizontal distance travelled during the climb to clear the obstacle height is found from Eq. (17.109). The required obstacle clearance is 50 ft for military and small civil aircraft and 35 ft for commercial aircraft.

$$S_c = \frac{h_{obstacle} - h_{TR}}{\tan\gamma_{climb}} \tag{17.109}$$

If the obstacle height was cleared during transition, then S_c is zero.

Balanced Field Length

The "balanced field length" (discussed in Chapter 5) is the total takeoff distance including obstacle clearance when an engine fails at "decision speed" V_1, the speed at which, upon an engine failure, the aircraft can either brake to a halt or continue the takeoff in the same total distance. If the engine fails before decision speed, the pilot can easily brake to a halt. If the engine fails after decision speed, the pilot must continue the takeoff.

An empirical method for balanced field-length estimation was presented in Chapter 5. A more detailed equation, as developed in Ref. 23, takes this form:

$$\text{BFL} = \frac{0.863}{1 + 2.3G}\left(\frac{W/S}{\rho g C_{L_{climb}}} + h_{obstacle}\right)\left(\frac{1}{\frac{T_{av}}{W} - U} + 2.7\right) + \left(\frac{655}{\sqrt{\frac{\rho}{\rho_{SL}}}}\right) \tag{17.110}$$

$$\text{JET: } T_{av} = 0.75\, T_{\substack{takeoff \\ static}}\left[\frac{5 + \text{BPR}}{4 + \text{BPR}}\right] \tag{17.111}$$

$$\text{PROP: } T_{av} = 5.75\ \text{bhp}\left[\frac{(\rho/\rho_{SL})N_e D_p^2}{\text{bhp}}\right]^{1/3} \tag{17.112}$$

where

BFL	= balanced field length (ft)
G	= $\gamma_{climb} - \gamma_{min}$
γ_{climb}	= arcsine $[(T\text{-}D)/W]$, 1-engine-out, climb speed
γ_{min}	= 0.024 2-engine; 0.027 3-engine; 0.030 4-engine
$C_{L_{climb}}$	= C_L at climb speed (1.2 V_{stall})
$h_{obstacle}$	= 35 ft commercial, 50 ft military
U	= 0.01 $C_{L_{max}}$ + 0.02 for flaps in takeoff position
BPR	= bypass ratio
bhp	= engine brake horsepower
N_e	= number of engines
D_p	= propeller diameter (ft)

For a more accurate determination of the balanced field length, the takeoff roll should be integrated with an engine failure at an assumed V_1, and compared with a braking analysis at that V_1 using the methods in the next section. The assumed V_1 should be iterated until the total takeoff distance including a 35-ft-obstacle clearance equals the total distance with braking.

It is usually assumed that the pilot waits one second before recognizing the engine failure and applying the brakes. Also, the use of reverse thrust is not permitted for the balanced field length calculations.

17.9 LANDING ANALYSIS

Landing is much like taking off, only backwards! Figure 17.18 illustrates the landing analysis, which contains virtually the same elements as the takeoff. Note that the aircraft weight for landing analysis is specified in the design requirements, and ranges from the takeoff value to about 85% of

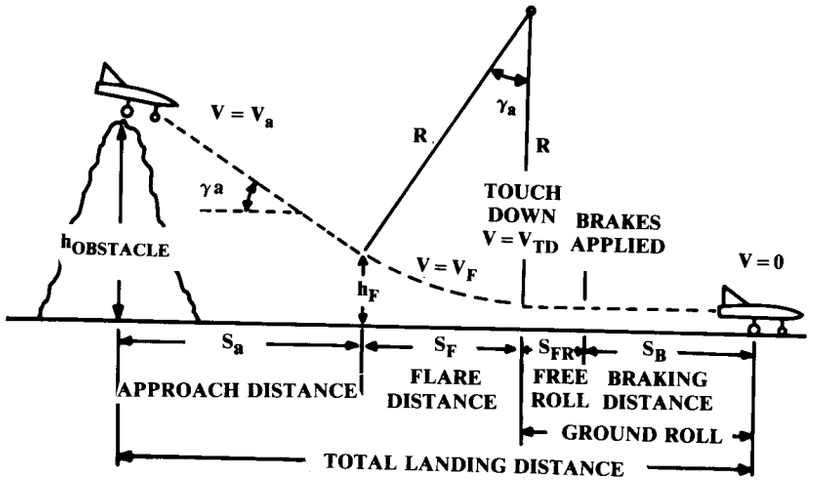

Fig. 17.18 Landing analysis.

takeoff weight. Landing weight is not the end-of-mission weight, because this would require dumping large amounts of fuel to land immediately after takeoff in the event of an emergency.

Approach

The approach begins with obstacle clearance over a 50-ft object. Approach speed V_a is 1.3 V_{stall} (1.2 V_{stall} for military). The steepest approach angle can be calculated from Eq. (17.105), with idle thrust and drag with full flaps deflected.

For transport aircraft the approach angle should be no steeper than 3 deg (0.052 rad), which may require more than idle thrust. Approach distance is determined from Eq. (17.109) using the flare height h_f.

Flare

Touchdown speed V_{TD} is 1.15 V_{stall} (1.1 V_{stall} for military). The aircraft decelerates from V_a to V_{TD} during the flare. The average velocity during the flare V_f is therefore 1.23 V_{stall} (1.15 V_{stall} for military). The radius of the flare circular arc is found by Eq. (17.104) using V_f, and where $n = 1.2$ for a typical aircraft.

The flare height can now be found from Eq. (17.107), and the horizontal distance during flare can be found from Eq. (17.106).

Although the deceleration from V_a to V_{TD} would imply additional energy and thus additional distance, this is negligible because the pilot usually pulls off all remaining approach power when the flare is begun.

Ground Roll

After touchdown, the aircraft rolls free for several seconds before the pilot applies the brakes. The distance is V_{TD} times the assumed delay (1–3 s).

The braking distance is determined by the same equation used for takeoff ground roll [Eq. (17.99)]. The initial velocity is V_{TD}, and the final velocity is zero.

The thrust term is the idle thrust. If a jet aircraft is equipped with thrust reversers, the thrust will be a negative value approximately equal to 40 or 50% of maximum forward thrust.

Thrust reversers cannot be operated at very slow speeds because of reingestion of the exhaust gases. Thrust reverser "cutoff speed" is determined by the engine manufacturer, and is typically about 50 knots (85 ft/s). The ground roll must be broken into two segments using Eq. (17.99) and the appropriate values for thrust (negative above cutoff speed, positive idle thrust below cutoff speed).

Reversible propellers produce a reverse thrust of about 40% of static forward thrust (60% for turboprops), and can be used throughout the landing roll.

The drag term may include the additional drag of spoilers, speed brakes, or drogue chutes. Drogue chutes have drag coefficient of about 1.4 times the inflated frontal area, divided by the wing reference area.

The rolling resistance will be greatly increased by the application of the brakes. Typical μ values for a hard runway surface are about 0.5 for civil and 0.3 for military aircraft. Values for various surfaces are provided in Table 17.1.

The FAA requires that an additional two-thirds be added to the total landing distance of commercial aircraft to allow for pilot technique. Thus the "FAR Field Length" is equal to 1.666 times the sum of the approach, flare, and total ground roll.

17.10 OTHER FIGHTER PERFORMANCE MEASURES OF MERIT

The standard measures of merit for fighter aircraft including turn rate, corner speed, load factor, and specific excess power P_s do not completely distinguish between a good and a not-so-good fighter. For example, two fighters with exactly the same turn-rate vs P_s will be widely different in combat effectiveness if one aircraft has unpredictable and uncontrollable behavior at high angle of attack. There is now great interest in defining new fighter measures of merit that can account for such differences.

There are several key deficiencies in current measures of merit. First, they focus on steady-state performance abilities, whereas a real dogfight is characterized by continuous change in aircraft state. In the High Speed Yo-Yo discussed earlier, the aircraft quickly pitches up, then rolls and turns at approximately corner speed for a few seconds, then rolls to almost inverted flight, pitches up (down) again, and then rolls out and dives.

While turn-rate at corner speed is important, the ability to rapidly execute these changes in state is also very important. Furthermore, these changes of state are usually being executed simultaneously (such as pitching and rolling at the same time, known affectionately as "bank and yank").

Another deficiency is that the current measures of merit are oriented around the classical gun attack in which a tail chase with your opponent in front is the desired outcome. Modern missiles are getting so good that in

future combat the first aircraft to point its nose at the opponent will win, regardless of energy state.

It must be remembered, however, that missiles are expensive and that each fighter can only carry a few of them. Future fighters must also have good classical dogfighting abilities.

Current measures of merit also fail to address the importance of what is called "decoupled energy management" to permit nonstandard fighter manuevers. "Coupled energy management" refers to manuevers in which potential and kinetic energy are exchanged. In the High Speed Yo-Yo, kinetic energy is exchanged for potential energy in the initial climb, and the potential energy is then exchanged back for kinetic energy after the turn. This makes the aircraft predictable.

In decoupled energy management, the potential and kinetic energy are changed independently. For example, speed may be reduced rapidly and without gaining altitude by using large speed brakes and/or in-flight thrust reversing.

Figure 17.19 shows a proposed new performance measure of merit. In this extended version of energy manueverability, the maximum and minimum (most negative) P_s values obtainable are plotted vs turn-rate. If suitable controls over thrust and drag are available, the pilot can manage his energy state by selecting any P_s level within the envelope at a given turn-rate. In the traditional evaluation of Fig. 17.9, only the maximum P_s obtainable is considered.

Note from Fig. 17.19 that an aircraft controllable after the stall has the option of developing a tremendous drag force for reduction of energy state. Under certain combat conditions this can be used to force the opponent to overshoot.

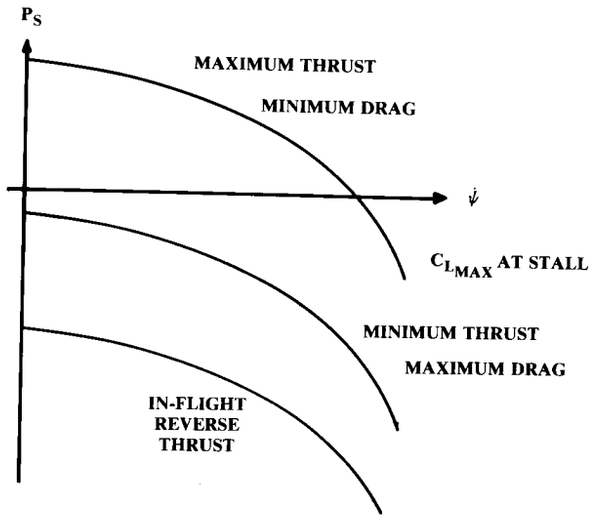

Fig. 17.19 Energy management envelope.

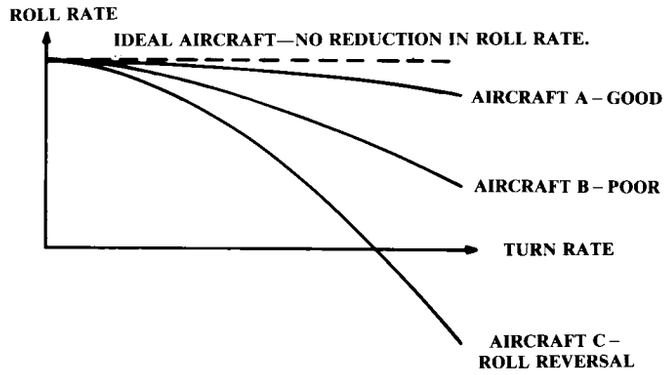

Fig. 17.20 Loaded roll comparison.

Also, turn-rate is inversely proportional to velocity. If an aircraft can be momentarily slowed to extremely low speeds, well below stall, the turn-rate can greatly exceed that in conventional flight. This may allow a missile first-shot opportunity. This "post-stall manuevering" (Ref. 75) is employed on the X-31 test aircraft.

Another proposed measure of merit deals with the effect of angle of attack on roll performance. A number of existing fighters lose their roll ability at high load-factors due to aeroelastic effects, adverse yaw, and aileron flow separation. An aircraft sluggish in roll during a high-g turn will be at a clear disadvantage. Figure 17.20 illustrates this comparison for a "good" aircraft, a "fair" aircraft, and an aircraft that experiences complete roll reversal.

Reference 76 defines a number of proposed fighter measures of merit. These have not yet been widely adopted; but they or similar measures of merit can be expected to be important in the future evaluation of fighter designs.

Supermaneuver and Post-Stall Maneuver

There has been tremendous attention paid recently to capabilities variously called post-stall maneuver (PSM), enhanced fighter maneuver, and supermaneuver. With the successful flight test of the X-31, and the YF-22's demonstration of 60-deg angle-of-attack operation, these capabilities have finally come of age. A supermaneuver capability allows a fighter to point its nose at an opponent more rapidly, getting the first missile shot in a "face-to-face" dogfight. This is attained primarily by the combination of thrust-induced turning and dynamic turning, usually involving high angles of attack as described below.

Contrary to science-fiction movies, a rocket can turn in space only by thrusting in a direction perpendicular to the flight path (Fig. 17.21). This produces a turn load factor (n) which is the component of thrust perpendicular to the flight path, divided by the weight of the vehicle. Turn rate can then be expressed simply as equal to (gn/V).

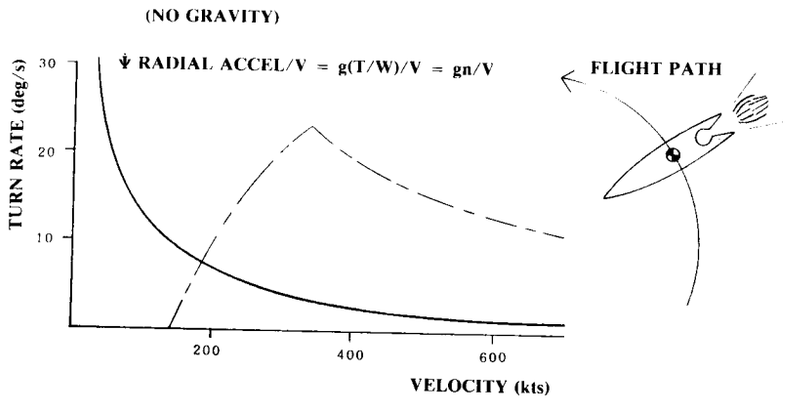

Fig. 17.21 Thrust-induced turning.

Note that at zero velocity, turn rate seems to go to infinity! While limited by pitch rate capability, a rocket could attain extremely high turn rates if it slowed to a very low speed.

An aircraft can also turn using thrust, provided that its thrust can be angled to have a substantial component perpendicular to the flight path. This can be done in three ways.

Figure 17.22 shows one way to direct the aircraft thrust perpendicular to the flight path, namely by providing thrust vectoring nozzles at or near the aircraft center of gravity. This allows the pilot to vector thrust at will, without concern for thrust-produced pitching moments. Such vectoring is available on the Harrier, and is proposed for the Reverse-Installation Vectored Engine Thrust ("RIVET") VSTOL concept (Ref. 93).

For such a design, the turn rate plot and the vectored thrust-induced turn rate plot are essentially summed. The wing can be kept at the angle of attack

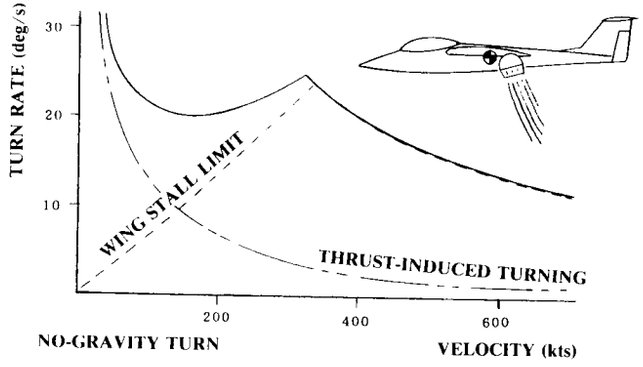

Fig. 17.22 Thrust vectoring at center of gravity.

for maximum lift, while the nozzles are directed approximately perpendicular to the flight path for maximum instantaneous turn rate as proven in Eq. (17.56).

Note that the wing stall limit line of Fig. 17.22 goes to zero rather than the level-flight stall speed. This indicates that we are momentarily ignoring gravity, going to a 90-deg bank to maximize instantaneous turn rate. Obviously, this can only be done for a few seconds!

Another option for vectoring the thrust perpendicular to the flight path is the addition of a thrust-vectored nozzle at the rear. This is a relatively easy feature to add to a design, and in fact the F-22 has such a nozzle already. However, the F-22 nozzles cannot be used for thrust-induced turning because the downward vectoring of thrust produces a large nose-down pitching moment. To be useful for thrust-induced turning, this pitching moment must be balanced by some nose-up moment, which can be attained by the addition of a large canard as seen on the F-15 STOL/Maneuver demonstrator.

This approach, the aft-nozzle-plus-canard, allows the aircraft to retain the full turning ability due to wing lift, plus the additional vectored thrust-induced turning, down to the speed at which the canard stalls (Fig. 17.23). By selecting canard size, the designer can select the lowest turning speed available. However, the larger the canard, the greater the weight and drag impact on the design.

In the third option, the aircraft acts like a rocket, pointing its fuselage at a very high angle to the flight path (Fig 17.24). Note that whereas a nearly 90-deg angle of attack is shown, substantial thrust turning is available at lesser angles.

In this option the aircraft angle of attack is well past the stall angle (hence "post-stall maneuvering"). This clearly requires that the aircraft not just have flying abilities at post-stall angles, but that it also retain good controllability and acceptable air quality into the inlet duct so that the engine continues running.

This post-stall thrust-induced turning, used by X-31, has several problems. It is difficult for the pilots, because the airplane is flying in a direction

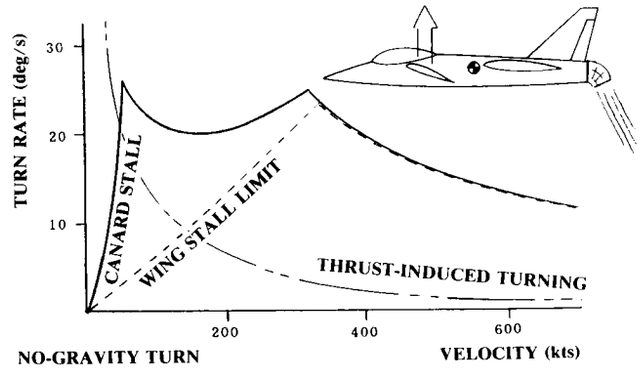

Fig. 17.23 Aft nozzle plus canard.

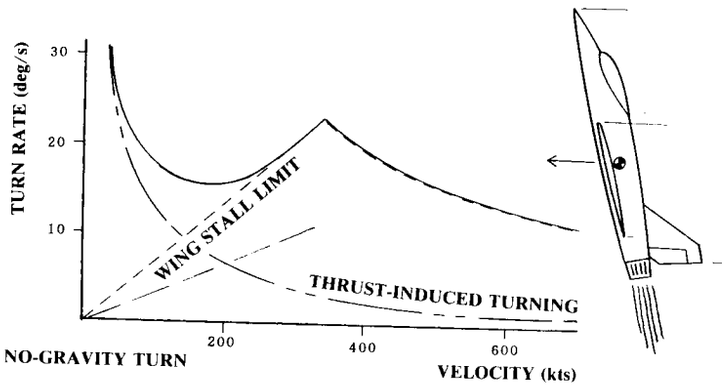

Fig. 17.24 Fuselage pointing.

downwards through the floorboards! The pilot is blind in the direction of flight. A roll about the velocity vector looks like a yaw to the pilot, and so disorientation is very possible.

Also, flight into the post-stall region means just that—the wing is stalled, and hence is producing only a fraction of its maximum lift. However, if velocity is slow enough, the jet thrust alone ensures that turn rate will be high anyway.

In any case the drag at extreme angle of attack will be very high, and the thrust component in the flight direction very small, so that the aircraft will decelerate very rapidly and may reach velocities near zero if the pilot is not careful.

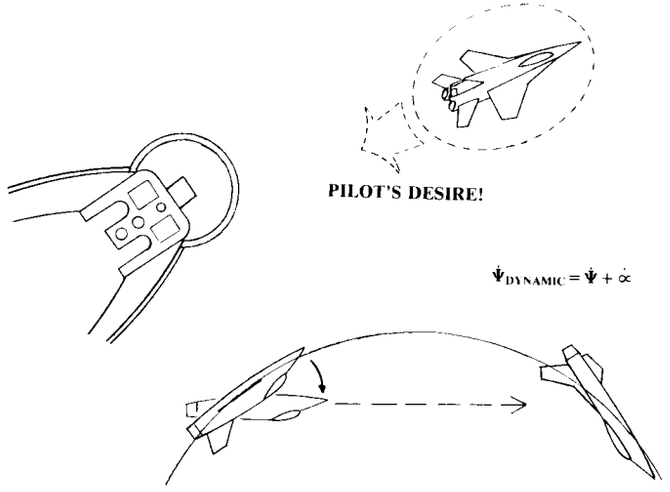

Fig. 17.25 Dynamic turn.

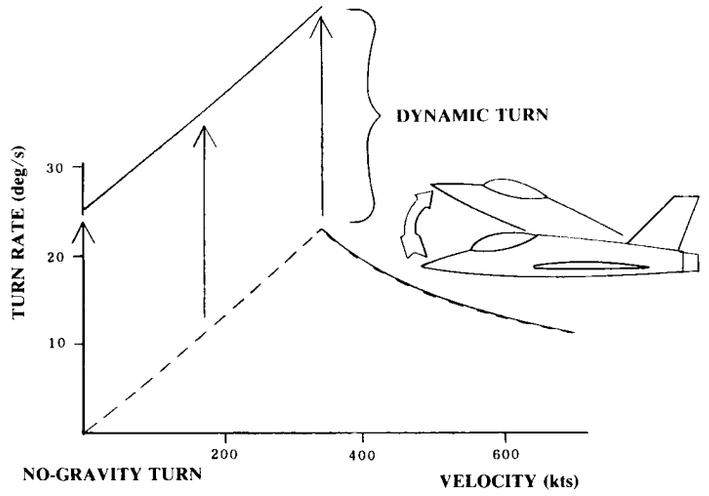

Fig. 17.26 Dynamic turn on the turn rate plot.

However, this option requires far less compromise to the design than the options above, and a substantial number of studies have verified that pilots can be trained to fly and fight at these extreme angles of attack.

Figure 17.25 shows a frustrating moment for the fighter pilot—the opponent is almost, but not quite, in his sight! If he could just lift the nose a little more...

To the pilot, pitch rate looks like turn rate in such a situation. With a normal aircraft the pilot should not pitch up faster than the aircraft turn rate or the aircraft will stall. With a PSM aircraft, however, that is not a problem. The pilot can just pull the nose up past stall, take the shot, and put the nose back down in a quick, smooth motion.

While the nose is coming up, there appears to be a much greater "turn rate," equal to the actual aircraft turn rate plus the available pitching rate at that condition. This is shown in Fig. 17.26.

This "dynamic turn" depends only upon the pitch rate capability of the aircraft and can be virtually as rapid as the pilots desire. For a modern, relaxed-stability fighter, the aircraft is always trying to pitch up anyway and the computer must fight to prevent it! Therefore, pitch-up can occur at 90 deg/s or more, and will be limited only to make the airplane less sensitive to fly. However, pitch-down from a high angle of attack is more difficult to obtain and is often the limiting case for control surface sizing.

Dynamic turning is not the result of a turning of the velocity vector and so does not produce increased load factor on the airplane. Thus, the apparent violation of the structural limit line is permissible—the aircraft doesn't see any additional g force.

Realize, though, that this dynamic turn can be used for only a brief period of time before the aircraft reaches its maximum angle of attack, even if that limit is 90 degrees. Also, as the aircraft pitches past the stall angle of

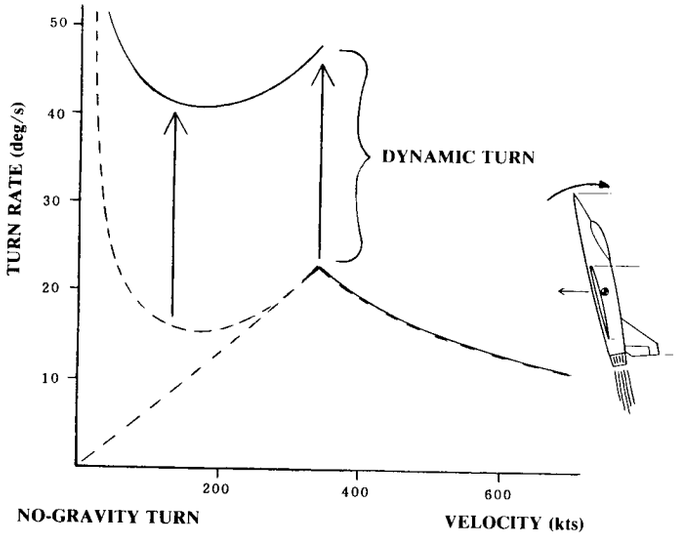

Fig. 17.27 Combined dynamic and PSM turning.

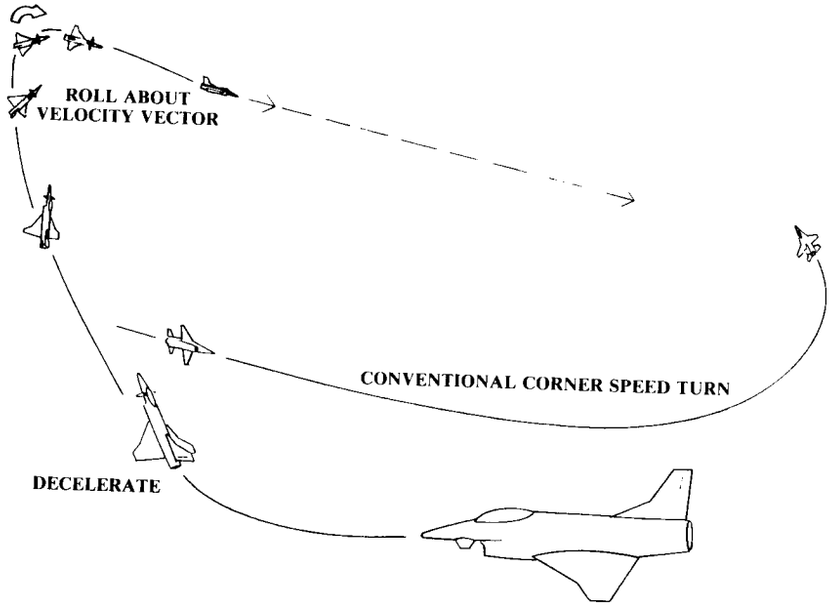

Fig. 17.28 X-31 Supermaneuver.

attack, the conventional turn rate will sharply decrease. Drag will go up, and speed and energy will reduce. This dynamic turn maneuver must take place rapidly or the PSM airplane will wind up at a large energy disadvantage should the opponent fail to die as planned.

Figure 17.27 illustrates the effects of combining post-stall dynamic turning with thrust-induced turning. As can be seen, such designs have ample capability to exceed the turn rates predicted by the classic turn rate plot for a brief period of time (Ref. 94).

Figure 17.28 shows a combined supermaneuver developed for the X-31 program which minimizes total time to reach a shot opportunity. Here the aircraft pitches up and bleeds off speed, slowing to extremely low speeds while initiating the turn.

At the top of the maneuver, the aircraft is rapidly turned using engine thrust until the velocity vector is roughly 90 degrees to the target aircraft. Meanwhile, the aircraft is also rolled approximately 90 degrees around the velocity vector, which looks like a 90-deg yaw to the pilot due to the high angle of attack. This results in the nose pointing at the target aircraft! Although the velocity vector is not yet pointed at the target aircraft, the pilot can take the shot, then accelerate out of the high angle of attack condition.

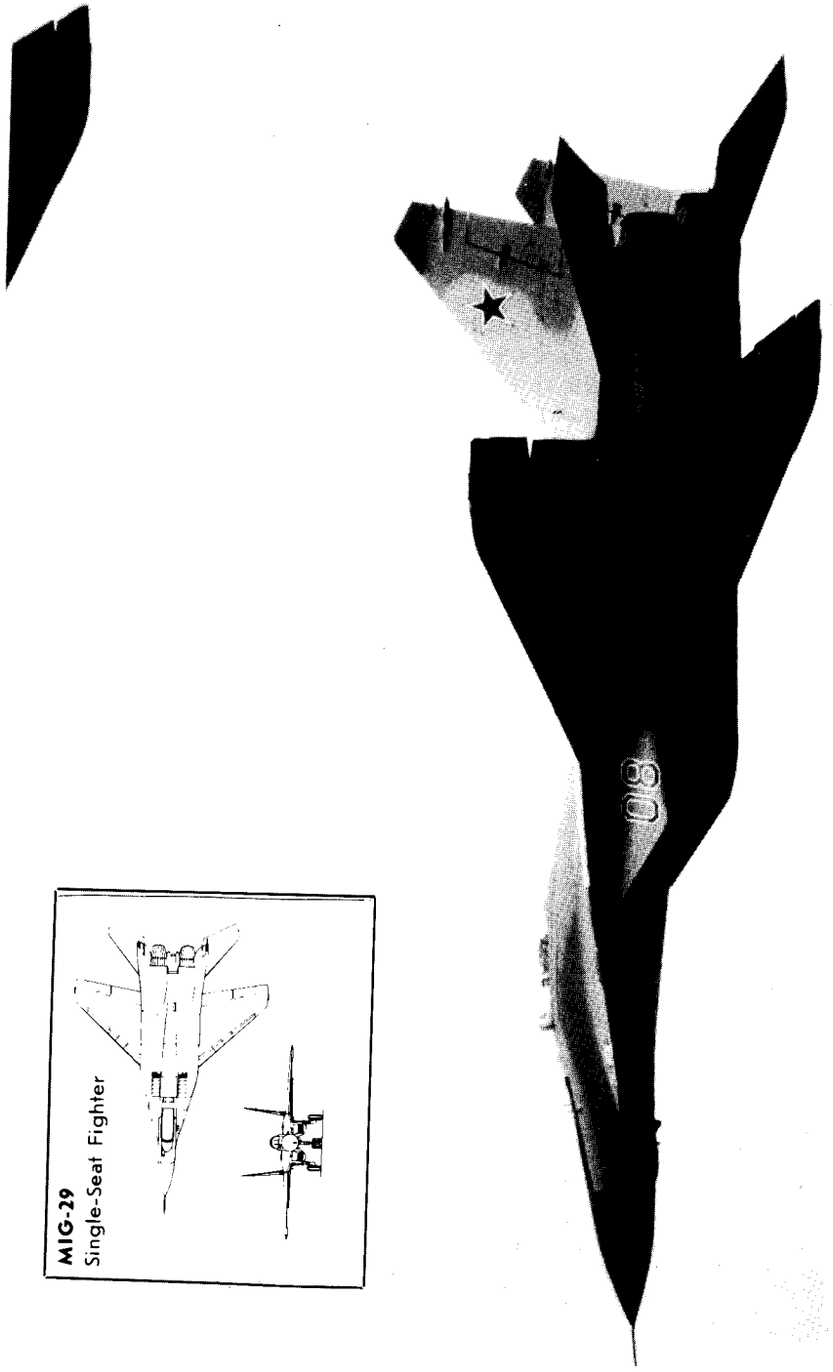

Mikoyan Mig-29

18
COST ANALYSIS

18.1 INTRODUCTION

When the aircraft manufacturers submit their proposals for a new aircraft, the customer faces a problem. All of the proposed aircraft will meet the design requirements! This is insured by the methods of this book and the much more in-depth methods used by the aircraft companies.

The customer must use some criteria other than aircraft performance to select the best proposal. While there will be some differences in technical credibility, data substantiation, and intrinsic design qualities, the final contractor selection will probably hinge on cost.

Aircraft cost estimation occupies the fuzzy gray area between science, art, and politics. Cost estimation is largely statistical, and in the final analysis we predict the cost of a new aircraft based on the actual costs of prior aircraft. However, it is very difficult to determine how much a prior aircraft really did cost in terms that are meaningful to the next aircraft.

For example, anybody attempting to use the B-1B actual costs to predict the costs of a similar future bomber would have a terrible time establishing a meaningful baseline cost. The B-1B began as the B-1A, which was cancelled before entering production. Rockwell stored a warehouse full of B-1A parts and tooling, some of which (but not all) were usable in the B-1B program when it was started. The new requirements for the B-1B required substantial re-engineering, especially in the nacelle and avionics areas.

The cost estimation for a future bomber should not be based upon the sum of all of the costs in the B-1A and B-1B programs. Hopefully, a future aircraft would be designed and produced without the inefficient stop-and-restart experienced by the B-1B. It would be virtually impossible, though, to try to determine an equivalent program cost for the B-1B had it been designed from the ground up.

While the B-1B case is extreme, other aircraft programs pose similar problems in establishing a baseline program-cost. For political reasons most military aircraft production programs are stretched out. To reduce "this year's" defense budget, the number of aircraft produced per year may be reduced well below the optimal production rate. In some cases, production rates are less than one per month.

This will greatly increase the cost per aircraft. Should this be included in cost estimation for the next aircraft? Or should the actual cost be adjusted to determine a cost baseline at the optimal production rate? This approach insures a cost overrun when the new aircraft's production rate is slowed.

In fact, it is very difficult to compare costs for two aircraft that are already in production. Part of the problem hinges upon what type of money to use. Program cost-comparisons can be made in "then-year" or "constant-year" dollars. Then-year dollars are the actual dollars spent in each year of the program, past, present, and future. For future program costs, an estimate of the inflation rate must be made.

For comparison of program costs and for establishing a cost baseline for new aircraft cost-prediction, constant-year dollars should be used (the actual dollars spent, ratioed by inflation factors to some selected year). However, budgeting in Congress is done in then-year dollars, so most cost data are prepared in then-year dollars.

As an example, Ref. 77 quotes from Congressional testimony the actual costs per aircraft of $17.6 million for the F-15 and $10.8 million for the F-16. Considering the far-greater capabilities of the F-15, it would seem a better bargain at only 60% more than the F-16. But, these are in then-year dollars for procurements during different years! In constant 1978 dollars, the costs were $18.8 million for the F-15 and $8.2 million for the F-16, so the F-15's actually cost 130% more in constant dollars.

Another problem in cost comparison is the aircraft production quantity and rates. The more aircraft produced, the more the manufacturer learns and the cheaper the next aircraft can be produced. This is known as the "learning curve" effect.

Roughly speaking, every time the production quantity is doubled the labor cost per aircraft goes down 20% (i.e., an "80% learning curve").

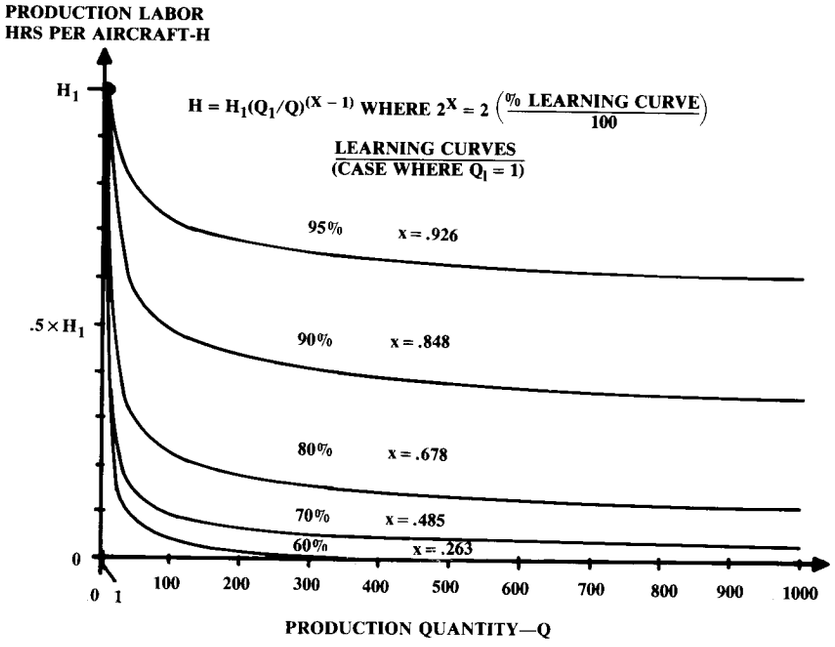

Fig. 18.1 Production learning curve.

Aircraft production typically follows a 75–85% learning curve (see Fig. 18.1.)

Due to the learning-curve effect, cost comparisons are not meaningful between a new aircraft just entering production and an old aircraft already produced in the hundreds or thousands.

Still another problem in cost comparison is that different costs are used, frequently without proper identification. Comparing the flyaway cost of one aircraft to the program or life-cycle cost of another is meaningless.

18.2 ELEMENTS OF LIFE-CYCLE COST

When you buy a car, the "cost" is what the dealer charges you to drive it home. Most car buyers today are somewhat influenced by the expected cost of ownership (gas mileage and maintenance), but would never consider that as an actual part of the purchase price. However, a typical $15,000 car will cost at least 25 cents per mile to operate (in 1988), which adds another $25,000 to the probable "life-cycle cost" of the car!

Figure 18.2 shows the elements which make up aircraft life cycle cost (LCC). The sizes of the boxes are roughly proportional to the magnitude of the costs for a typical aircraft.

"RDT&E" stands for research, development, test, and evaluation, which includes all the technology research, design engineering, prototype fabrication, flight and ground testing, and evaluations for operational suitability. The cost of aircraft conceptual design as discussed in this book is included in the RDT&E cost.

RDT&E includes certification cost for civil aircraft. For military aircraft, RDT&E includes the costs associated with the demonstration of airworthiness, mission capability, and compliance with Mil-Specs. RDT&E costs are essentially fixed ("nonrecurring") regardless of how many aircraft are ultimately produced.

The aircraft "flyaway" (production) cost covers the labor and material costs to manufacture the aircraft, including airframe, engines, and avionics. This cost includes production tooling costs. Note that "cost" includes the manufacturer's overhead and administrative expenses. Production costs are "recurring" in that they are based upon the number of aircraft produced. The cost per aircraft is reduced as more aircraft are produced due to the learning curve effect.

The purchase price for a civil aircraft is set to recover the RDT&E and production costs, including a fair profit. Since the RDT&E costs are fixed, some assumption must be made as to how many aircraft will be produced to determine how much of the RDT&E costs each sale must recover.

For military aircraft, the RDT&E costs are paid directly by the government during the RDT&E phase, so these costs need not be recovered during production. Military-aircraft "procurement cost" (or "acquisition cost") includes the production costs as well as the costs of required ground support equipment, such as flight simulators and test equipment, and the cost of the initial spare parts during operational deployment. For civil aircraft, these are normally purchased separately.

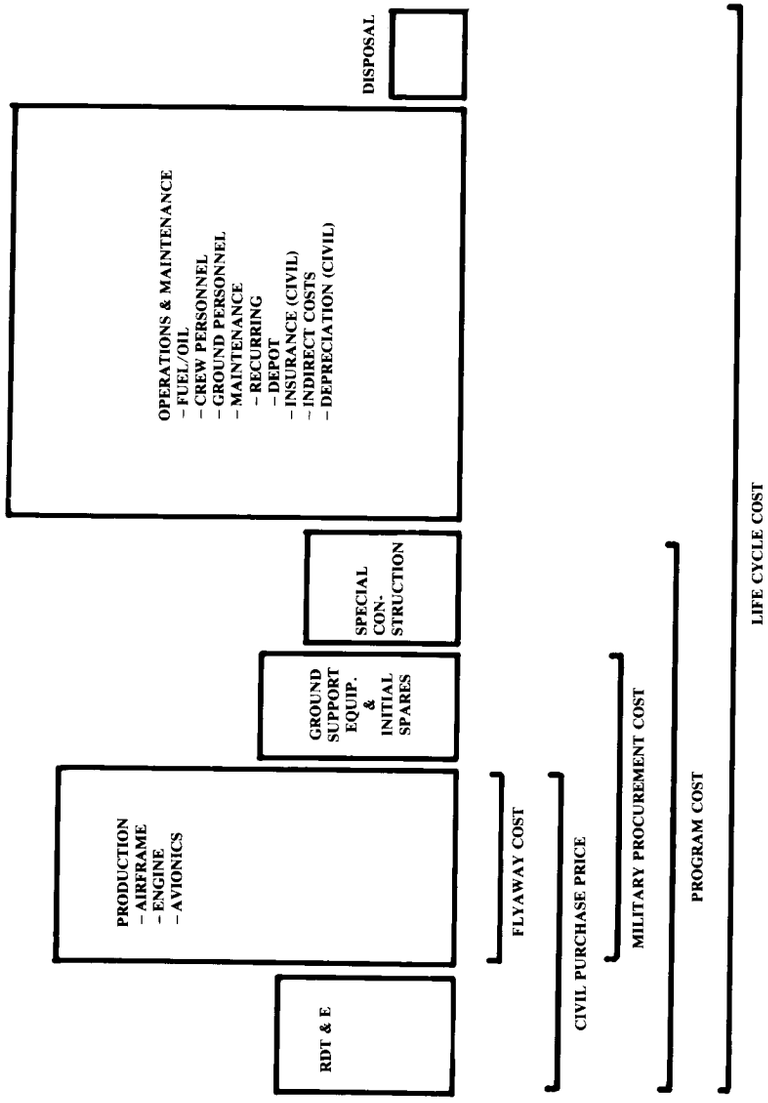

Fig. 18.2 Elements of life cycle cost.

One recent trend in military aircraft procurement is called "cost sharing"; the contractor is invited to share some of the RDT&E costs with the expectation of recovering them later during production. It remains to be seen whether future administrations will permit full cost recovery at a later date.

"Program cost" covers the total cost to develop and deploy a new aircraft into the military inventory. Some aircraft require special ground facilities for operational deployment. For example, a fighter/attack aircraft with a large wing span may not fit into the existing bombproof shelters in Europe. The cost of constructing new shelters would be included in the total program cost along with the RDT&E and procurement costs.

"Operations and Maintenance" (O&M) costs are usually much larger than development and production costs. O&M covers fuel, oil, aircrew, maintenance, and various indirect costs. For civil aircraft, insurance will be part of operations cost.

For the operators of commercial aircraft, the depreciation of the aircraft based upon purchase price is also considered to be a part of the operating cost. "Depreciation" is an accounting term that refers to the allocation of the purchase price out over a number of years, using some depreciation schedule.

The simplest depreciation schedule is a straight-line formula, in which each year's depreciation is the purchase price divided by the number of years over which depreciation is spread. Commercial aircraft are usually depreciated over 12–14 years, although they may have a useful life of 20 years or more.

The final element making up the total life-cycle cost concerns "disposal." Obsolete military aircraft are flown one last time to Arizona for "pickling" and storage. The expense of this is not large, so it is frequently ignored in LCC estimation. Civil aircraft have a negative disposal cost because they are worth something on the resale market (typically 10% of purchase price).

18.3 COST-ESTIMATING METHODS

Aircraft, like bologna, are bought by the pound. In 1988, most aircraft cost roughly 150–300 dollars per pound of DCPR weight. (DCPR weight, defined in Chapter 14, typically equals 60–70% of empty weight). The actual cost varies depending upon the maximum speed, avionics sophistication, production rate, and numerous other factors, but weight remains the most important cost-factor within a given class of aircraft.

The cost-estimating methods for a full-scale development proposal are based upon a detailed assessment of the actual tasks to design, test, and produce the aircraft. A "work breakdown structure" (WBS) is prepared. This is an organized tabulation of all of the tasks, and in its most complex form may include hundreds or thousands.

Hours estimates for each task in the WBS are prepared by the appropriate functional groups in the company. This requires estimates for such things as the number of drawings, wind-tunnel tests, tooling fixtures, etc. Other costs such as raw-material purchases, vendor items, computer time, and pur-

chased services are estimated separately. Full-scale-development proposal cost estimation is a massive effort.

Cost estimation during conceptual design is largely statistical. Cost data for a number of aircraft are analyzed using curve-fit programs to prepare "cost estimating relationships" (CER) for the various cost elements.

CER input variables include such factors as aircraft DCPR weight, maximum velocity, and production rate. The output of a CER is either cost or labor hours (engineering, production, etc.), which are converted to cost by multiplying by the appropriate hourly rate.

CERs are developed by the aircraft companies for their own use, and by the various customer organizations for evaluation of proposed aircraft. The Air Force has developed a complex cost model called Modular Life Cycle Cost Model (MLCCM) that is used for detailed cost estimation. The Rand Corporation has published a number of reports featuring simple CERs for conceptual design, some of which are presented later in the chapter.

18.4 RDT&E AND PRODUCTION COSTS

RDT&E and production costs are frequently combined to develop CERs. It is difficult to separate clearly the RDT&E from production costs, especially in the areas of engineering and prototype fabrication.

For example, production of long-lead-time items (e.g., landing-gear forgings) is usually initiated before the prototype has flown. The engineering support of these production items should be considered a part of production. It is difficult for the developer of a CER to determine, years later, how many engineering hours during the RDT&E phase were actually spent in support of production.

It is also common in the development of CERs to assume that the prototype aircraft will have a cost based upon the production-cost CER, with the higher cost of prototypes accounted for by the early position on the learning curve. However, prototypes are usually built virtually by hand, with simplified prototype tooling, and may have labor hour costs much greater than accounted for by the learning curve.

The best CERs are those developed using recent aircraft that are highly similar to the new aircraft being analyzed. Because detailed cost data is usually proprietary, this puts the current producers of aircraft at a great advantage when it comes to estimating the cost of a new aircraft. Boeing has no trouble estimating with great accuracy the costs of a new jetliner, using the costs of their current aircraft.

When a detailed cost baseline for a highly similar aircraft is available, even simple CERs can yield great accuracy. Merely multiplying the component weights of the new aircraft times the dollars per pound or hours per pound for a similar baseline aircraft is probably better than a sophisticated CER based upon a number of not-so-similar aircraft.

For example, the selected cost-baseline aircraft may have required 50 h/lb of manufacturing labor for the fuselage and subsystems and 90 h/lb for the wings and tails. These typical values are multiplied by the appropriate component weights of the new aircraft to determine hours, which are then multiplied times the manufacturing hourly rate to determine cost.

This technique is especially useful for prototype and flight demonstrator (X-series) aircraft, which are poorly estimated by sophisticated CERs based upon production aircraft. However, it may be difficult to find a recent and similar prototype or demonstrator aircraft to use as a cost baseline.

RAND DAPCA IV Model

A set of CERs for conceptual aircraft design developed by the RAND Corporation (Ref. 78) is known as "DAPCA IV." This is the latest version of the Development and Procurement Costs of Aircraft (DAPCA) model.

DAPCA is probably not the very best set of CERs for any one class of aircraft, but is notable in that it seems to provide reasonable results for several classes of aircraft including fighters, bombers, and transports.

DAPCA estimates the hours required for RDT&E and production by the engineering, tooling, manufacturing, and quality control groups. These are multiplied by the appropriate hourly rates to yield costs. Development support, flight-test, and manufacturing material costs are directly estimated by DAPCA.

Engineering hours include the airframe design and analysis, test engineering, configuration control, and system engineering. Engineering hours are primarily expended during RDT&E, but there is some engineering effort throughout production. In the estimating equation presented below, the total engineering effort for a 500-aircraft production run is about three times the engineering effort for a one-aircraft "production run."

The engineering effort performed by the airframe contractor to integrate the propulsion and avionics systems into the aircraft is included under engineering hours. However, the actual engineering effort by the propulsion and avionics contractors is not included. Those items are treated as purchased equipment. Engineering support of tooling and production planning are included in those areas instead of in engineering.

Tooling hours embrace all of the preparation for production: design and fabrication of the tools and fixtures, preparation of molds and dies, programming for numerically-controlled manufacturing, and development and fabrication of production test apparatus. Tooling hours also cover the ongoing tooling support during production.

Manufacturing labor is the direct labor to fabricate the aircraft, including forming, machining, fastening, subassembly fabrication, final assembly, routing (hydraulics, electrics, and pneumatics), and purchased part installation (engines, avionics, subsystems, etc). The equation below includes the manufacturing hours performed by airframe subcontractors, if any.

Quality Control is actually a part of manufacturing, but is estimated separately. It includes receiving inspection, production inspection, and final inspection. Quality Control inspects tools and fixtures as well as aircraft subassemblies and completed aircraft.

The RDT&E phase includes development support and flight-test costs. Development-support costs are the nonrecurring costs of manufacturing support of RDT&E, including fabrication of mockups, iron-bird subsystem simulators, structural test articles, and various other test items used during RDT&E. In DAPCA these costs are estimated directly, although some other

models separately estimate the labor and material costs for development support.

Flight-test costs cover all costs incurred to demonstrate airworthiness for civil certification or Mil-Spec compliance except for the costs of the flight-test aircraft themselves. Costs for the flight-test aircraft are included in the total production-run cost estimation. Flight-test costs include planning, instrumentation, flight operations, data reduction, and engineering and manufacturing support of flight testing.

Manufacturing materials—the raw materials and purchased hardware and equipment from which the aircraft is built—include the structural raw materials, such as aluminum, steel, or prepreg graphite composite, plus the electrical, hydraulic, and pneumatic systems, the environmental control system, fasteners, clamps, and similar standard parts.

These may be contractor-furnished equipment (CFE) or government-furnished equipment (GFE). Manufacturing materials include virtually everything on the aircraft except the engines and avionics.

The following DAPCA equations have been modified to include the quantity term provided in an appendix to Ref. 78.

DAPCA assumes that the engine cost is known. A turbojet-engine cost estimation equation from Ref. 79 has been included for use where the engine cost is unknown. For a turbofan engine, cost should be increased 15–20% higher than predicted with this equation. Note that the equation does not include the cost to develop a new engine.

Modified DAPCA IV Cost Model (*costs in constant 1986 dollars*):

$$\text{Eng hours} = 4.86 W_e^{0.777} V^{0.894} Q^{0.163} = H_E \tag{18.1}$$

$$\text{Tooling hours} = 5.99 W_e^{0.777} V^{0.696} Q^{0.263} = H_T \tag{18.2}$$

$$\text{Mfg hours} = 7.37 W_e^{0.82} V^{0.484} Q^{0.641} = H_M \tag{18.3}$$

$$\left.\begin{aligned} \text{QC hours} &= 0.076\ (\text{mfg hours}) \quad \text{if cargo airplane} \\ &= 0.133\ (\text{mfg hours}) \quad \text{otherwise} \end{aligned}\right\} = H_Q \tag{18.4}$$

$$\text{Devel support cost} = 45.42 W_e^{0.630} V^{1.3} = C_D \tag{18.5}$$

$$\text{Flt test cost} = 1243.03 W_e^{0.325} V^{0.822} FTA^{1.21} = C_F \tag{18.6}$$

$$\text{Mfg materials cost} = 11.0 W_e^{0.921} V^{0.621} Q^{0.799} = C_M \tag{18.7}$$

$$\text{Eng production cost} = 1548[0.043 T_{\max} + 243.25 M_{\max} + 0.969 T_{\text{turbine inlet}} - 2228] = C_{\text{eng}} \tag{18.8}$$

$$\text{RDT\&E + flyaway} = H_E R_E + H_T R_T + H_M R_M + H_Q R_Q + C_D + C_F + C_M + C_{\text{eng}} N_{\text{eng}} + C_{\text{avionics}} \tag{18.9}$$

where

We	= empty weight (lb)
V	= maximum velocity (knots)
Q	= production quantity
FTA	= number of flight test aircraft (typically 2-6)
N_{eng}	= total production quantity times number of engines per aircraft
$T_{\max}$	= engine maximum thrust (lb)
$M_{\max}$	= engine maximum Mach number
$T_{\text{turbine inlet}}$	= turbine inlet temperature (Rankine)
C_{avionics}	= avionics cost

The hours estimated by DAPCA are based upon the design and fabrication of an aluminum aircraft. For aircraft which are largely fabricated from other materials, the hours must be adjusted to account for the more-difficult design and fabrication. Based upon minimal information, the following "fudge factors" are recommended:

aluminum	1.0
graphite-epoxy	1.5–2.0
fiberglass	1.1–1.2
steel	1.5–2.0
titanium	1.7–2.2

The hours estimated with this model are multiplied by the appropriate hourly rates to calculate the labor costs. These hourly rates are called "wrap rates" because they include the direct salaries paid to employees as well as the employee benefits, overhead, and administrative costs. Typically the employee salaries are a little less than half the wrap rate. Average 1986 wrap rates were presented in Ref. 78, as follows:

engineering	\$59.10 = R_E
tooling	\$60.70 = R_T
quality control	\$55.40 = R_Q
manufacturing	\$50.10 = R_M

Predicted costs are then ratioed by some inflation factor to the selected year's constant dollar. Aircraft costs do not all follow the same inflation factor. For example, the salaries of the engineers may increase at a slower rate than the raw-material cost for aluminum.

"Economic escalation factors" for the various cost elements are based upon the actual and predicted cost-inflation for the more important cost-

drivers. One such factor, the "Federal Price Deflator for the Aircraft Industry," is derived from an in-depth analysis of the costs of items used for aircraft production.

For initial estimates and student design projects, the Consumer Price Index (CPI) may be used as an approximate economic escalation-factor. The CPI is the purchasing value of the dollar expressed as a percentage of some chosen base year (changed occasionally to avoid large CPI numbers). The past and projected CPI is published by the government and is readily available.

DAPCA does not estimate avionics costs. They must be estimated from data on similar aircraft or from vendors' quotations. Avionics costs range from roughly 5–25% of flyaway cost depending upon sophistication, or can be approximated as $2000 per pound in 1986 dollars.

Predicted aircraft costs will be multiplied by an "investment cost factor" to determine the purchase price to the customer. The investment cost-factor includes the cost of money and the contractor profit; it is considered highly proprietary by a company. Investment cost-factor may be roughly estimated as 1.1–1.2.

18.5 OPERATIONS AND MAINTENANCE COSTS

O&M costs are determined from assumptions as to how the aircraft will be operated. The main O&M costs are fuel, crew salaries, and maintenance. For a typical military aircraft, the fuel totals about 15% of the O&M costs, the crew salaries about 35%, and the maintenance most of the remaining 50%. Over one-third of U.S. Air Force manpower is dedicated to maintenance.

For commercial aircraft (which fly many more hours per year), the fuel totals about 38% of O&M costs, the crew salaries about 24%, and the maintenance about 25%. The depreciation of the aircraft purchase price is about 12% of total O&M costs, and the insurance is the remaining 1%.

Fuel and Oil Costs

When flying the design mission, the aircraft burns all of the available fuel except what will be required for loiter and for reaching an alternate airport. However, the actual missions will rarely resemble the design mission. Most of the time the aircraft will land with substantial fuel in the tanks which can be used on the next flight.

To estimate yearly fuel usage, a typical mission profile is selected and the total duration and fuel burned are used to determine the average fuel burned per hour. This is multiplied by the average yearly flight hours per aircraft, which must be assumed based upon typical data for that class of aircraft. Table 18.1 provides some rough guidelines for flight hours per year and other LCC parameters.

Finally, the total amount of fuel burned per year of operation is multiplied by the fuel price as obtained from petroleum vendors, ratioed to the appropriate year's dollar. No typical fuel price will be given here because it can change so rapidly. Note that oil costs average less than half a percent of the fuel costs, and can be ignored.

Table 18.1 LCC parameter approximations

Aircraft class	FH/YR/AC	Crew ratio	MMH/FH
Light aircraft	500–1000	–	1/4–1
Business jet	500–2000	–	3–6
Jet trainer	300–500	–	6–10
Fighter (modern)	300–500	1.1	15–20
Bomber	300–500	1.5	25–50
Military transport	700–1400	1.5 if FH/YR < 1200 2.5 if 1200 < FH/YR < 2400 3.5 if 2400 < FH/YR	20–40
Civil transport	2500–4500	–	5–15

Crew Salaries

Crew expenses for military and civil aircraft are calculated differently. The cost of a civil-aircraft crew (including flight and cabin crew) can be statistically estimated based upon the yearly "block hours."

Block hours measure the total time the aircraft is in use, from when the "blocks" are removed from the wheels at the departure airport to when they are placed on the wheels at the destination. Block hours therefore include taxi time, ground hold time, total mission flight time, airborne holding time, extra time for complying with air-traffic-control approach instructions, and time spent on the ground waiting for a gate.

Block speed (V_B)—the average block velocity, i.e., the trip distance divided by the block time—will be substantially less than the actual cruise velocity.

Reference 52 provides detailed formulas prepared by the Airline Transport Association of America for airline block-time estimation. Block time can be approximated by the mission flight time plus 15 min for ground-maneuver and 6 min for air manuever.

Note that the mission distance will not simply be the straight-line distance between the two airports. Airliners must follow federal airways, which may not directly connect the two airports. The additional distance will be approximately 2% of distances over 1400 miles, and $(0.015 + 7/D)\%$ for shorter trips.

The block hours per year can be determined from the ratio between block hours and flight hours for the selected mission, times the total flight hours per year per aircraft (Table 18.1). For a long-range aircraft, the block hours equal approximately the flight hours; but for short-range aircraft with average trip times under an hour, the block time can be substantially greater than the flight time.

Crew cost per block hour can be estimated using Eqs. (18.10) and (18.11). These were provided in Ref. 52 from Boeing data (converted to 1986 dollars). These equations give crew costs of about $705 and $660 per block hour for the B-747 and DC-10 (converted to 1987 dollars). These compare favorably with March 1987 actual crew costs of $748 and $610 (average of four established airlines).

$$\text{Two-man crew cost} = 35\left(V_c \frac{W_0}{10^5}\right)^{0.3} + 84 \tag{18.10}$$

$$\text{Three-man crew cost} = 47\left(V_c \frac{W_0}{10^5}\right)^{0.3} + 118 \tag{18.11}$$

where

V_c = cruise velocity in knots
W_0 = takeoff gross weight

Costs are estimated in 1986 dollars per block hour.

These equations must be viewed as rough approximations only. The current turmoil in the airline industry has created a wide variation in crew costs. The B-747 crew costs per block hour in 1987 ranged from $1013 for an old established airline to $189 for a new low-fare airline!

For military aircraft, crew costs are determined by estimating how many flight-crew members will have to be kept on the active-duty roster to operate the aircraft. This is the number of aircraft times the number of crew members per aircraft, times the "crew ratio."

Military pilots no longer get their own airplane as in the movies. There are always more pilots and other crew members than the number of aircraft. The crew ratio defines the ratio of aircrews per aircraft. It ranges from 1.1 for fighters to 3.5 for transports that are flown frequently. Typical crew ratios are provided in Table 18.1.

The average cost per crewmember, as is obtained from military sources, varies depending upon airplane type. As in civilian life, the cost is much greater than the salaries alone, to cover benefits and overhead. In the absence of better data, the engineering hourly wrap-rates times 2080 hours per year may be used for initial trade studies and student design projects.

Maintenance Expenses

Unscheduled-maintenance costs depend upon how often the aircraft breaks and the average cost to fix it.

Scheduled maintenance depends upon the number of items requiring regularly scheduled maintenance and the frequency and cost of the scheduled maintenance. Maintenance is usually scheduled by accumulated flight hours. For example, light aircraft require a complete inspection every 100 hours. For commercial aircraft, there are also maintenance activities that are scheduled by the number of flights ("cycles").

Maintenance activities are lumped together under Maintenance Man-hours per Flight Hour (MMH/FH). This is the primary measure of maintenance "goodness." MMH/FHs range from well under 1.0 for small private aircraft to over 100 for certain special-purpose aircraft. Typical values are shown in Table 18.1.

Reducing MMH/FH is a key goal of aircraft design, as discussed earlier. MMH/FH is roughly proportional to weight because the parts count and systems complexity go up with weight.

MMH/FH is also strongly affected by the aircraft utilization. An aircraft which is constantly flying will receive more scheduled maintenance per year and will be maintained by more experienced mechanics. For example, the DC-9 has a MMH/FH of about 6.4 in civilian operation. The same plane in military service (C-9), flying only about half as many hours per year, has a MMH/FH of about 12.

From the MMH/FH and flight hours per year, the maintenance man-hours per year can be estimated. The maintenance labor cost can then be determined from the labor wrap-rate obtained from airline or military sources. In the absence of better data, the labor cost can be approximated by the manufacturing wrap-rate presented earlier.

Materials, parts, and supplies used for maintenance will approximately equal the labor costs for military aircraft.

For civil aircraft, Ref. 52 presents the following rough equations for materials cost per flight hour and per cycle. The number of cycles per year is estimated by determining the total yearly block-time divided by the block time per flight. The total materials cost is the cost per flight hour times the flight hours per year, plus the cost per cycle times the cycles per year.

$$\frac{\text{material cost}}{\text{FH}} = 3.3\left(\frac{C_a}{10^6}\right) + 7.04 + \left[58\left(\frac{C_e}{10^6}\right) - 13\right]N_e \tag{18.12}$$

$$\frac{\text{material cost}}{\text{cycle}} = 4.0\left(\frac{C_a}{10^6}\right) + 4.6 + \left[7.5\left(\frac{C_e}{10^6}\right) + 2.8\right]N_e \tag{18.13}$$

where

C_a = aircraft cost less engine
C_e = cost per engine

Resulting costs are in 1986 dollars per flight hour or cycle.

Depreciation

For commercial aircraft, the depreciation is considered a part of the operating expenses. Depreciation is really the allocation of the purchase price over the operating life of the aircraft. While complicated depreciation formulas are used by accountants, a simple straight-line schedule provides a reasonable first estimate. The airframe and engine have different operating lives, and so must be depreciated separately.

The airframe yearly depreciation is the airframe cost less the final resale value, divided by the number of years used for depreciation. If the resale value is 10% of purchase price and the depreciation period is 12 years, the yearly airframe depreciation is the airframe cost times 0.9 divided by 12. (Here airframe cost refers to the total cost minus the total engine costs).

Engine resale value can be neglected for initial analysis. If the engine is depreciated over 4 years, the yearly depreciation cost per engine is the engine purchase price divided by 4.

Insurance

Insurance costs for commercial aircraft add approximately 1% to the cost of operations.

18.6 COST MEASURES OF MERIT (MILITARY)

Once the cost is estimated, it is incorporated into several cost-effectiveness measures of merit. For military aircraft (fighters and bombers), the ultimate measure of merit is the cost to "win the war" (or at least avoid losing it!).

This is determined through parametric variations in sophisticated "campaign models" that simulate in great detail the conduct of a postulated war. The improvement in the outcome of the war is compared to the total LCC to develop the new aircraft and operate it for (typically) 20 years.

Other cost-effectiveness measures of merit in common use include the cost per weapon pound delivered and the cost per target killed. These require detailed analysis of the sortie rate, survivability, and weapons effectiveness that goes beyond the scope of this book.

Trade studies are conducted to determine the variation in these measures of merit with design changes such as payload and turn rate. Conceptual designers in military aircraft companies become very familiar with these measures of merit.

In some military aircraft procurements, cost alone becomes the driving measure of merit. "Design-to-Cost" implies that the aircraft must cost less than some stated value regardless of performance and range requirements.

If the aircraft as designed to meet the stated performance and range requirements costs more than the design-to-cost, then either performance or range must be sacrificed. At this point the designers sincerely hope that no other company has succeeded in designing an aircraft in full compliance with performance, range, and cost requirements.

18.7 AIRLINE ECONOMICS

DOC and IOC

Cost-effectiveness for an airliner is purely economic. The aircraft must generate sufficient revenue in excess of operating costs that the purchase investment is more profitable than investing the same amount of money elsewhere.

Airline operating costs are divided into direct operating costs (DOC) and indirect operating costs (IOC). DOC costs concern flight operations as discussed earlier, namely, fuel, oil, crew, maintenance, depreciation, and insurance.

DOC costs for economic analysis are expressed as cost per seat-mile flown, where the seat-miles are equal to the number of seats on the aircraft times the statute miles flown. DOC per seat-mile is frequently used to compare aircraft and is used as the measure of merit for design trade studies. Currently the wide-body transports average DOC of 2.2 cents per seat-mile (1987).

IOC costs, the remaining costs to run an airline, include the depreciation costs of ground facilities and equipment, the sales and customer service costs, and the administrative and overhead costs.

IOC costs do not lend themselves to statistical analysis. They vary greatly from airline to airline, and depend very little upon the aircraft design. Typically, the yearly IOC costs about equal the DOC costs, but the variation is so great that the only way to obtain reliable IOC costs for economic analysis is from the airlines themselves.

Airline Revenue

Airline revenue comes primarily from ticket sales. Ticket prices are approximately proportional to trip distance, but are higher per mile for shorter distances. Tickets are sold in four classes: first class, business class, coach (tourist) class, and excursion.

Roughly speaking, first class costs twice as much as coach, business class costs 1.5 times coach, and excursion fares are 50–90% of coach fares. However, there is tremendous variation. As this is written, one airline is quoting a higher Los Angeles to Sacramento excursion fare than its coach fare!

For revenue estimation, a phone call to the local airline ticket office will provide current fares over selected routes. For future fares, the current fares can be ratioed by the assumed inflation.

The number of tickets sold in these various classes must be estimated. For the North Atlantic routes, tickets sold are typically 5% in first class, 15% in business class, 10% in coach, and 70% in excursion. If a weighted average of the different fares is calculated, it turns out that the average fare paid is approximately the coach fare.

The remaining parameter to be determined for revenue estimation, the "load factor," measures how full the aircraft is. Load factor equals the seats sold divided by the total seats available. Current load factors range from 60–70%. Load-factor data are provided occasionally in the trade magazine *Aviation Week and Space Technology* (along with other airline operating-cost data).

Thus, the revenue per seat-mile flown can be determined as the average fare sold over that route (approximately the coach fare) times the load factor.

The load factor for breakeven can be calculated as the cost per seat-mile divided by the average fare per seat-mile. The operating-cost breakeven analysis uses the DOC per seat mile. This is the load factor at which the passengers pay just enough to fly the airplane, with no excess for covering indirect costs or to provide the airline any profit.

The total-cost breakeven analysis uses the DOC plus IOC per seat mile. The IOC per seat mile is determined by dividing the airline's total yearly indirect operating costs by the total number of seat miles flown by the airline each year. As a rough approximation, the IOC per seat mile approximately equals the DOC per seat mile.

Investment Cost Analysis

The decision by the airline as to whether or not to buy a particular aircraft is based upon an investment cost-analysis that takes the "net present value" of the revenue minus cost over the useful life of the aircraft and compares it to the investment cost (purchase price).

Net present value (NPV) is an economic valuation based on the concept that money in the hand today is more valuable than money received in the future. At the very least, the money in hand today could be drawing interest in the bank. Even better, money in hand today could be invested in some reasonably safe business venture and draw a higher yearly return.

The "net present value" of future money is the amount of money in hand today which would yield the given future amount of money if invested at a "normal" rate of return. For example, \$110 to be received a year from today would have a net present value of \$100 if a normal investment returns 10% interest per year.

Equation (18.14) determines the future value V_n after n years of an initial investment of value V_0, given an interest rate r. In Eq. (18.15) this is solved for the required investment today to yield a given future value. V_0 is therefore the net present value V_{np} as described above. The interest rate r is known as the "discount factor" in net-present-value calculations.

$$V_n = V_0(1+r)^n \tag{18.14}$$

$$V_0 = V_{np} = \frac{V_n}{(1+r)^n} \tag{18.15}$$

The NPV of an airliner is the total of the net present values of all of the yearly operating profits during the life of the aircraft (usually taken to be the depreciation period). The yearly operating profits are the yearly revenues minus the DOC and IOC, not including depreciation. Depreciation is not included in NPV calculation because it is the yearly apportionment of the purchase price.

The NPV is determined by estimating the revenues and costs for each year of operation, including the effects of the estimated inflation. The yearly operating profit is then converted to NPV using Eq. (18.15). Finally, the NPVs of all of the years of operation are summed. To this is added the NPV of the salvage value of the aircraft at the end of its life (typically equal to 10% of purchase price).

The total NPV must be greater than the purchase price of the aircraft, or the investment will not return the expected normal rate of return, i.e., the discount factor r.

Selection of the appropriate discount factor is critical to the NPV calculation. The selected discount factor should be greater than the interest received from extremely safe investments such as government bonds, but should be less than the return from risky investments such as volatile stocks. The selected discount rate should probably be no less than the real rate of return on the airline company's stock, which equals the yearly dividends plus the increase in stock value, divided by the stock purchase price.

Alternatively, the discount factor can be solved for the value for which the investment just barely breaks even. The discount factor r for which the NPV exactly equals the investment is called the "internal rate of return"; it represents the equivalent interest rate returned by the airline investment. This can be compared to the expected rate of return on other investments to determine if the new airliner is a good buy.

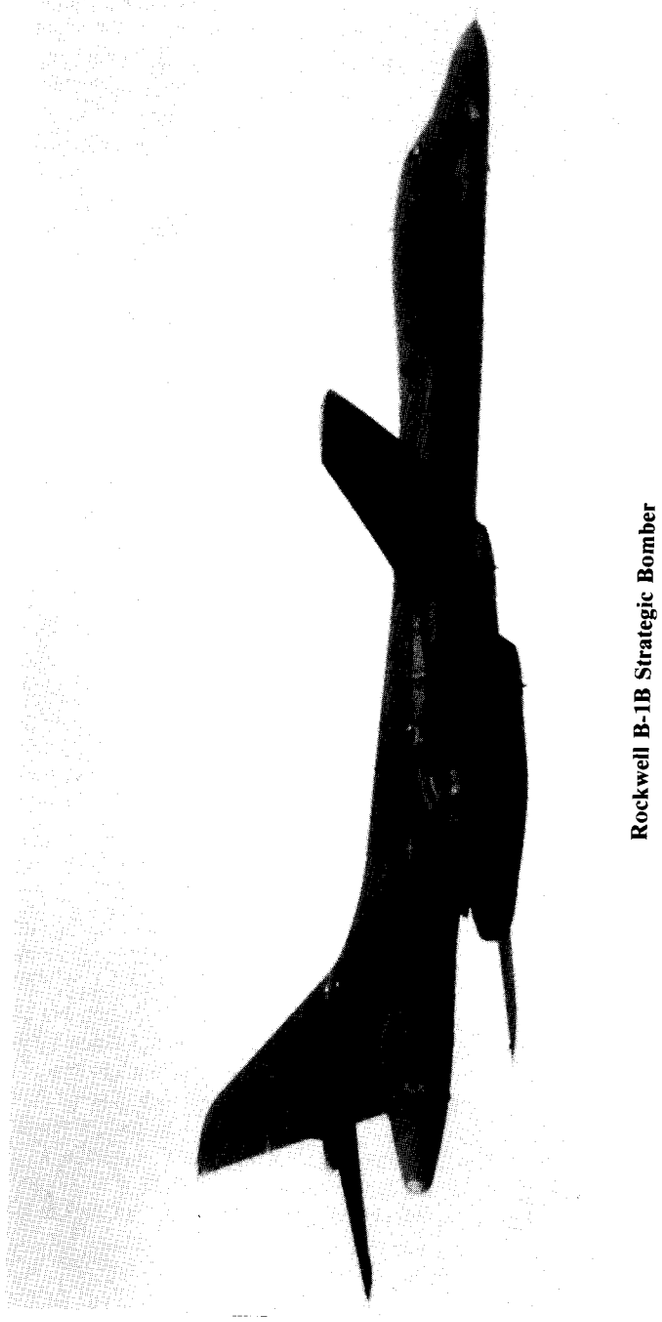

Rockwell B-1B Strategic Bomber

19
SIZING AND TRADE STUDIES

19.1 INTRODUCTION

We have come full circle in the design process. We began with a rough conceptual sketch and a first-order estimation of the T/W and W/S to meet the performance requirements. A "quick and dirty" sizing method was used to estimate the takeoff weight and fuel weight required to meet the mission requirements.

The results of that sizing were used to develop a conceptual design layout that incorporated considerations for the real world, including landing gear, structure, engine installation, etc. The design layout was then analyzed for aerodynamics, weights, installed-engine characteristics, structures, stability, performance, and cost.

The as-drawn aircraft might or might not actually meet all of the performance and mission requirements. The refined estimates for the drags, weights, and installed engine characteristics are all somewhat different from our earlier crude estimates. Therefore, the selected T/W and W/S are probably not optimal. The same is true for the aspect ratio, sweep, taper ratio, and other geometric parameters. Also, the as-drawn weights are probably wrong.

Now we are ready to revisit the sizing analysis using our far-greater knowledge about the aircraft. Refined trade-study methods will allow us to determine the size and characteristics of the optimal aircraft, that meets all performance and mission requirements.

19.2 DETAILED SIZING METHODS

Equations (17.1) and (17.2) [repeated below as Eqs. (19.1) and (19.2)] define the sum of the forces on the aircraft in the X_s and Z_s directions. The resulting accelerations on the aircraft are determined as these force summations divided by the aircraft mass (W/g):

$$\Sigma F_x = T\cos(\alpha + \phi_T) - D - W\sin\gamma \tag{19.1}$$

$$\Sigma F_z = T\sin(\alpha + \phi_T) + L - W\cos\gamma \tag{19.2}$$

$$\dot{W} = -CT \tag{19.3}$$

Equation (19.3) defines the time rate of change in aircraft weight as the specific fuel consumption c times the thrust. Equations (19.4) and (19.5)

determine the equivalent c and thrust for a piston-engine aircraft (see Chapter 5):

$$C = C_{\text{bhp}} \frac{V}{550\ \eta_p} \tag{19.4}$$

$$T = \frac{550_{\text{bhp}}\ \eta_p}{V} \tag{19.5}$$

These equations are the basis of the highly-detailed sizing programs used by the major airframe companies. In these programs the fuel weight is actually calculated by determining the required thrust level and resulting fuel flow during each segment of the mission.

The angle of attack and thrust level are varied to give the required total lift and the required longitudinal acceleration depending upon what maneuver the aircraft must perform (level cruise, climb, accelerate, turn, etc.). Angle of attack and lift are restricted by the maximum lift available. The thrust level is restricted to the available thrust obtained from a table of installed-engine thrust vs altitude and velocity (or Mach number).

To improve the accuracy, the mission is broken into a large number of very short segments that may be less than one minute in duration. The reduction in the aircraft weight during each of these short mission segments is determined by calculating the actual fuel burned based upon the required thrust setting.

The computer iterates for sized takeoff weight by varying the assumed takeoff weight until the ending empty-weight fraction matches the empty-weight fraction determined by the detailed weight estimation. More sophisticated sizing programs will use statistical weights equations to automatically recalculate the allowable empty weight for the sizing variations in takeoff weight, wing area, thrust, aspect ratio, and other trade parameters.

Such methods go beyond the scope of this book. Those who take jobs as sizing and performance specialists in major aircraft companies will find that these computer programs are so large today that they are programmed by a team.

19.3 IMPROVED CONCEPTUAL SIZING METHODS

Review of Sizing Method

For sizing and trade studies during conceptual design, an improved version of the method presented in Chapter 6 is adequate. Remember that the aircraft was sized iteratively by assuming a takeoff weight. A statistical method was used to determine the empty weight for this assumed takeoff weight.

The fuel used was determined by breaking the mission into mission segments, numbered from 1 to x. For each mission segment, the change in aircraft weight was calculated as either a mission-segment weight fraction (W_{i+1}/W_i) due to fuel burned, or as a discrete change in weight due to payload dropped.

Starting with the assumed takeoff weight, the aircraft weight was reduced for each mission segment either by subtracting the discrete weight or by multiplying by the mission-segment weight fraction. The fuel burned during each mission segment was totalled throughout the mission to determine the total fuel burned. A 6% allowance was added to the mission fuel to account for reserve and trapped fuel.

The aircraft takeoff weight was then calculated by summing the payload, crew, fuel, and empty weight. This calculated takeoff weight was compared to the assumed takeoff weight. A new assumed takeoff weight was selected somewhere between the two, and the sizing process was iterated toward a solution.

This same sizing process can be employed for sizing the as-drawn aircraft, but the method can be improved based upon our greater knowledge of the design.

In the initial sizing before the aircraft design layout was prepared, the mission fuel was determined using simplified equations and statistical estimates of the aerodynamic properties and installed-engine characteristics. The empty weight was determined from statistical equations based only upon the takeoff weight.

At this later stage in the design process we can calculate better estimates for the fuel used during each mission segment, and we have a better estimate of the empty weight based upon a detailed analysis of the as-drawn aircraft. These improved methods are presented below.

Many of these methods rely upon calculating, by the methods of the performance chapter, the duration of time to perform the mission segment. The fuel burned during a duration of d at a given thrust T and specific fuel consumption C is then determined by Eq. (19.6). The mission-segment fuel fraction is solved for in Eq. (19.7), where C and $(T/W)_i$ are the average actual values during mission segment i:

$$W_{f_i} = CTd \tag{19.6}$$

$$\frac{W_{i+1}}{W_i} = 1 - Cd\left(\frac{T}{W}\right)_i \tag{19.7}$$

Note that if $(T/W)_i$ remains essentially constant during the iterations for takeoff weight, the result of Eq. (19.7) can be used unchanged for each iteration. This is the case for "rubber engine" sizing.

For "fixed-engine" sizing, Eq. (19.7) would have to be recalculated for each iteration step because the T/W for a fixed thrust changes as the weight is changed. Alternatively, Eq. (19.6) can be used to calculate the actual weight of the fuel burned by that fixed-size engine. The fuel burned is then treated as a weight drop in the sizing iterations.

(A word of caution: Mission-segment weight fractions should range between about 0.9 and 1.0. If a mission-segment weight fraction is less than 0.9, the accuracy should be improved by breaking that mission segment into two or more smaller segments. If the mission-segment weight fraction is calculated to be greater than 1.0, you have probably used the wrong units somewhere or have forgotten the negative sign on an exponent!)

Engine Start, Warmup, and Taxi

In the initial sizing method, the mission-segment weight fraction for engine start, warmup, and taxi was lumped with the takeoff, and assumed to be 0.97–0.99.

A better estimate for the fuel used during engine start, warmup, and taxi uses the actual engine characteristics to calculate the fuel burned by the engine in a certain number of minutes at some thrust setting. Typically this would be 15 min at idle power. Equation (19.7) is used to determine the resulting mission-segment weight fraction.

Takeoff

The takeoff distance was broken into segments and calculated in Chapter 17. The time duration d of those segments is approximately the segment distance divided by the average velocity during the segment. Equation (19.7) can then be used to calculate the mission-segment weight fraction using the appropriate average takeoff thrust and fuel consumption.

Sometimes the design requirements may lump together the engine start, warmup, taxi, and takeoff into a single requirement based upon some amount of time at a given thrust setting. For military combat aircraft this is usually five minutes at maximum dry power. For transports and commercial aircraft, fourteen minutes at ground idle plus one minute at takeoff thrust have often been specified.

Climb and Acceleration

The energy methods of Chapter 17 provided Eq. (17.94), repeated below as Eq. (19.8), for the mission-segment weight fraction for a change in altitude and/or velocity. The average values of C, V, D, and T should be used. A long climb or large change in velocity should be broken into segments such that the quantity $C/[V(1 - D/T)]$ is approximately constant.

$$\frac{W_{i+1}}{W_i} = \exp\left[\frac{-C\Delta h_e}{V(1 - D/T)}\right] \tag{19.8}$$

$$\Delta h_e = \Delta\left(h + \frac{1}{2g} V^2\right) \tag{19.9}$$

The distance travelled during climb is usually "credited" to the cruise segment which follows, i.e., that distance is subtracted from the required cruise range. Distance travelled during climb is calculated as average velocity times the time to climb, which equals $\Delta h_e/P_s$.

Cruise and Loiter

In Chapter 17, methods for determining the optimal velocities and altitudes for cruise and loiter were presented, and the Breguet equations for cruise and loiter were derived. Solving these for mission segment weight fraction yields Eqs. (19.10) and (19.11), where R is the range and E is the endurance time.

$$\text{Cruise:} \quad \frac{W_{i+1}}{W_i} = \exp\left[\frac{-RC}{V(L/D)}\right] \tag{19.10}$$

$$\text{Loiter:} \quad \frac{W_{i+1}}{W_i} = \exp\left[\frac{-EC}{L/D}\right] \tag{19.11}$$

Equation (19.10) provides the mission segment weight fraction for a cruise-climb, as discussed in Chapter 17. For a constant-airspeed, constant-altitude cruise, the cruise must be broken into shorter segments and the L/D revised as the weight changes.

Combat and Maneuver

Fighter aircraft are sized with a requirement for air-combat time. This may be explicitly stated, such as "5 min at maximum thrust at 30,000 ft at 0.9 Mach number." Alternatively, a certain number of turns at combat conditions may be specified. In that case, the time to perform the turns is determined from the performance methods of Chapter 17.

Once the combat time is known, Eq. (19.7) can be used.

Descent

Descent was statistically estimated in the initial sizing method, and no range credit was taken for the horizontal distance travelled during descent. A more accurate calculation will probably yield a small improvement in sized takeoff weight.

$$V_v = V\left(\frac{T}{W}\right) - \frac{\rho V^3 C_{D_0}}{2(W/S)} - \frac{2K}{\rho V}\left(\frac{W}{S}\right) \tag{19.12}$$

Descent is a negative climb, i.e., thrust less than the drag. The climb equation developed in Chapter 17 is repeated as Eq. (19.12), in which V_v is vertical velocity or rate of descent. Descent is usually flown at cruise velocity and idle power setting, unless this produces an extreme descent angle (arcsine V_v/V).

The time to descend is determined from the vertical velocity, and the mission-segment weight fraction is determined from Eq. (19.7). A long descent should be broken into segments for greater accuracy. Also, credit should be taken for the distance travelled unless the mission requirements specifically exclude range credit.

(The detailed calculation of descent fuel is probably more trouble than it is worth for quick studies and student design projects. The earlier statistical method [Eq. (6.22)] is usually good enough.)

Landing

Landing was previously approximated by a small W_{i+1}/W_i fraction (0.992–0.997). This is probably good enough even for more refined sizing.

From obstacle clearance height to full stop takes less than one minute, and is usually flown at idle power. Even if thrust reversers are employed the impact upon total fuel weight is small because the thrust reversers are operated for only about ten seconds.

If more accuracy is desired, the fuel for landing can be calculated by determining the time to land from the distances calculated in Chapter 17, using the average velocity for each landing segment. Then Eq. (19.7) can be employed.

Empty-Weight Estimation and Refined Sizing

Previously the empty weight was estimated statistically using the takeoff weight. Now that we have a design layout, the methods of Chapter 15 can be used to calculate the empty weight for the as-drawn aircraft by a detailed estimation of the weight of each major component of the aircraft.

During the first refined sizing iteration, the assumed takeoff weight is the as-drawn takeoff weight. The empty weight is the as-drawn empty weight. The fuel required is calculated using the refined methods presented above, plus an allowance for reserve and trapped fuel (6%).

Unless the designer has been very lucky, the takeoff weight calculated from the refined estimate of fuel burned and the as-drawn empty weight will not equal the as-drawn takeoff weight. The as-drawn takeoff weight was based upon initial sizing with limited information about the aircraft, and cannot be expected to be very accurate.

Since the calculated takeoff weight does not equal the as-drawn takeoff weight, the designer must iterate by assuming a new takeoff weight. The empty weight must then be determined for the new assumed takeoff weight.

It would be possible to go back to the detailed weight equations of Chapter 15 and recalculate the empty weight by summing the component weights. Without the aid of a sophisticated computer program, however, the time involved would be prohibitive if this were done for each step of the sizing iteration.

An approximate noncomputerized method relies upon the statistical data from Chapter 3 to adjust the as-drawn empty weight based upon the new assumed takeoff weight. Remember that Fig. 3.1 showed the trend of the empty weight ratio W_e/W_0 decreasing with increasing takeoff weight. A good approximation for the new empty weight would be found by adjusting the as-drawn empty weight ratio along the slope shown in Fig. 3.1 for that class of aircraft. The empty weight for the new assumed takeoff weight can therefore be estimated by adjusting the as-drawn empty weight for the new takeoff weight, as shown in Eq. (19.13). The value of C (not to be confused with SFC) represents the slope of the empty-weight-ratio trend line and is taken from Table 3.1.

$$W_e = W_{e_{\text{as drawn}}} \left[\frac{W_0}{W_{0_{\text{as drawn}}}} \right]^{(1+c)} \tag{19.13}$$

C typically equals (-0.1), so $(1 + C)$ equals about 0.9. This indicates that the empty weight as a fraction of takeoff weight will reduce as the assumed takeoff weight is increased.

At this point, sufficient information is available to size the aircraft using the sizing method of Chapter 6 with the improved estimates for fuel burned and empty weight.

If the resulting sized-aircraft weight substantially differs from the as-drawn weight, the results should be considered suspicious and the aircraft redrawn, re-analyzed, and resized. "Substantially different" is a matter of opinion, but this author gets nervous at a takeoff-weight difference greater than about 30% of the as-drawn weight.

19.4 SIZING MATRIX AND CARPET PLOTS

Sizing Matrix

The sizing procedure described above insures that the as-drawn aircraft, scaled to the sized takeoff-weight, will meet the required mission range. However, there is no assurance that it will still meet the numerous performance requirements such as turn rate or takeoff distance.

The configuration geometry was initially selected to meet these requirements based upon assumptions as to lift, drag, thrust, etc. The as-drawn aircraft will have different characteristics and may no longer meet all requirements, or it may exceed all of them, indicating that it has been overdesigned and is not the lightest possible design.

Sufficient information is now available on the as-drawn aircraft to analyze its performance vs the requirements. If it falls short in some performance area, the thrust or wing area could be changed to attain the desired performance. Rather than this time-consuming "hit or miss" method, the designer can apply the "sizing matrix" method.

In the sizing-matrix method, the thrust-to-weight ratio T/W and wing loading W/S are arbitrarily varied from the as-drawn baseline values (typically plus and minus 20%).

Each combination of T/W and W/S produces a different airplane, with different aerodynamics, propulsion, and weights. These different airplanes are separately sized to determine the takeoff weight of each to perform the design mission.

They are also separately analyzed for performance. If the T/W and W/S variations are wide enough, at least one of the aircraft will meet all performance requirements, although it will probably be the heaviest airplane when sized to perform the mission.

Figure 19.1 shows an example of a sizing matrix for a small fighter. Nine T/W-W/S variations of the aircraft have been sized and analyzed for takeoff distance, P_s, and acceleration time. Performance requirements for this example are a takeoff distance under 500 ft, zero P_s at Mach 0.9/5 g/30,000 ft, and an acceleration time under 50 s from Mach 0.9–1.5.

From the data in the matrix it can be seen that the as-drawn baseline (number 5) exceeds the requirements, as do numbers 1, 2, and 6. Number 3 greatly exceeds the requirements but is very heavy. Numbers 4, 7, 8, and 9 are deficient in some requirement but lighter in weight.

The important question becomes: "What combination of T/W and W/S will meet all of the requirements at a minimum weight?"

	$W/S = 50$	$W/S = 60$	$W/S = 70$
$T/W = 1.1$	1 W_0 = 56,000 lb P_s = 700 fps ($M0.9$, 30k ft, 5g's) S_{TO} = 340 ft a = 46 s	2 W_0 = 49,000 lb P_s = 330 fps S_{TO} = 430 ft a = 42 s	3 W_0 = 46,000 lb P_s = 30 fps S_{TO} = 660 ft a = 39 s
$T/W = 1.0$	4 W_0 = 48,500 lb P_s = 430 fps S_{TO} = 450 ft a = 50.5 s	5 RESIZED BASELINE W_0 = 43,700 lb P_s = 30 fps S_{TO} = 595 ft a = 47 s	6 W_0 = 42,000 lb P_s = −190 fps S_{TO} = 800 ft a = 45 s
$T/W = 0.9$	7 W_0 = 44,000 lb P_s = 140 fps S_{TO} = 670 ft a = 56 s	8 W_0 = 39,000 lb P_s = −230 fps S_{TO} = 810 ft a = 53 s	9 W_0 = 36,000 lb P_s = −320 fps S_{TO} = 1070 ft a = 51 s

Require: $P_S \geq 0$ at ($M0.9$, 30k ft, 5g's)
$S_{TO} \leq 500$ ft
$a \leq 50$ s from $M0.9$ to $M1.5$

Fig. 19.1 Sizing matrix.

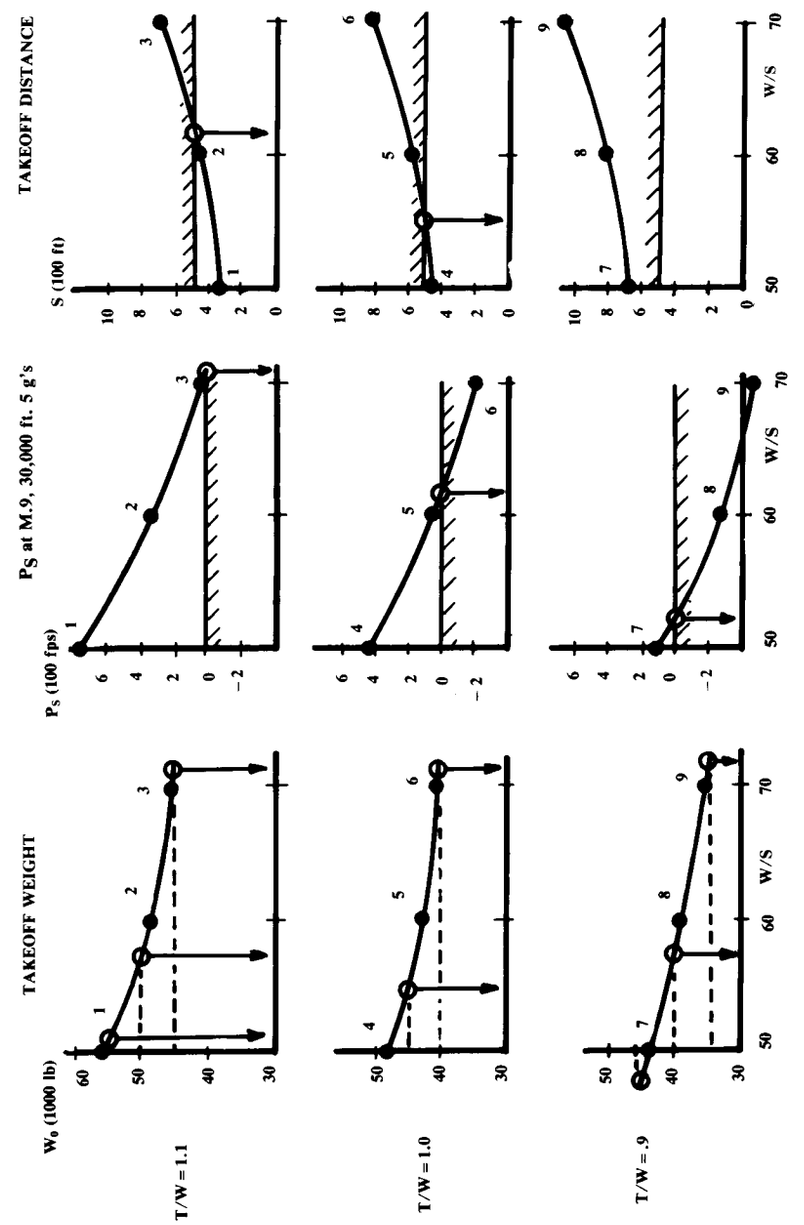

Fig. 19.2 Sizing matrix cross plots.

Sizing Matrix Plot

Optimization of T/W and W/S requires crossplotting the sizing-matrix data, as shown in Fig. 19.2. For each value of thrust-to-weight ratio, the sized takeoff gross weight, P_s, and takeoff distance are plotted vs wing loading. The data points from the sizing matrix in Fig. 19.1 are shown as numbered black dots. (The acceleration data points were plotted in a similar fashion, but not shown.)

From the takeoff-weight graphs in Fig. 19.2, the wing loadings corresponding to regularly spaced arbitrary gross weights are determined. For this example, gross weights at 5,000-lb increments were selected. For these arbitrary weight increments, the corresponding W/S values are shown as circles on Fig. 19.2.

The W/S and T/W values for the arbitrary gross-weight increments are transferred to a T/W-W/S graph as shown in Fig. 19.3. Smooth curves are drawn connecting the various points that have the same gross weight to produce lines of constant-size takeoff gross weight (Fig. 19.3). From these curves one can readily determine the sized takeoff weight for variations of the aircraft with any combination of T/W and W/S.

Next, the W/S values that exactly meet the various performance requirements are obtained from the performance plots for different T/W values (right side of Fig. 19.2). These values are again shown as circles.

These combinations of W/S and T/W that exactly meet a performance requirement are transferred to the T/W-W/S graph and connected by

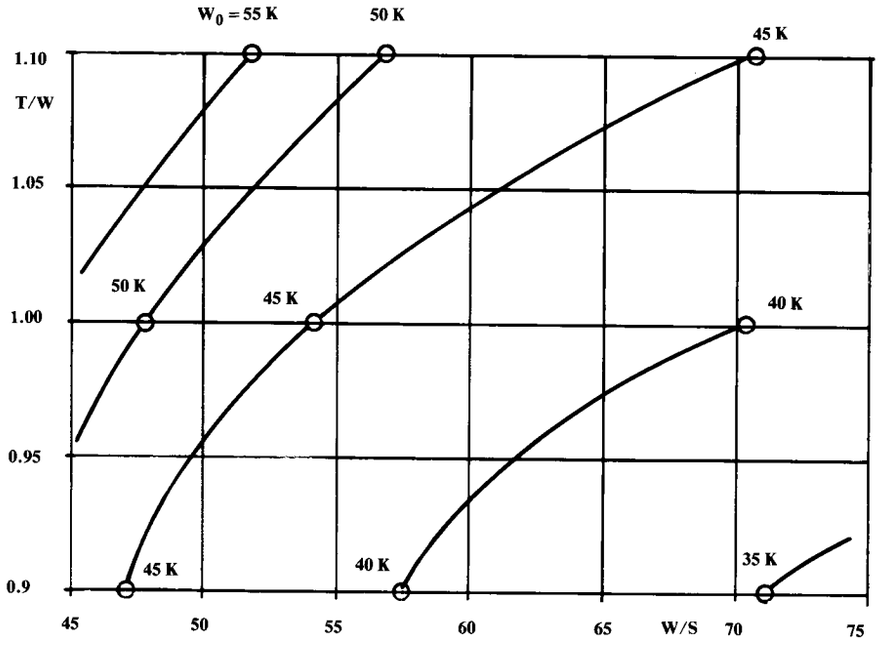

Fig. 19.3 Sizing matrix plot (continued).

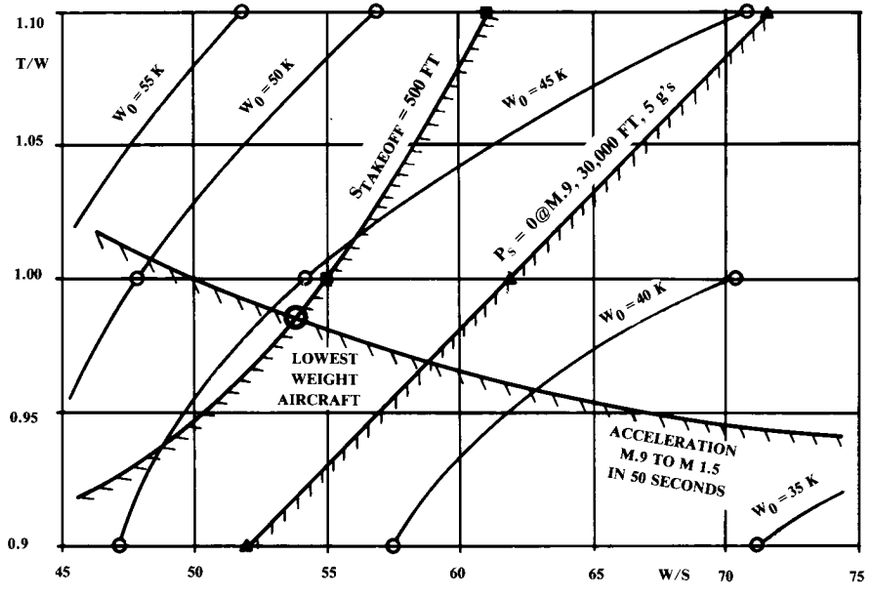

Fig. 19.4 Sizing matrix plot (concluded).

smooth curves, as shown in Fig. 19.4. Shading is used to indicate which side of these "constraint lines" the desired answer must avoid.

The desired solution is the lightest aircraft that meets all performance requirements. The optimum combination of T/W and W/S is found by inspection, as shown in Fig. 19.4, and usually will be located where two constraint lines cross.

This is a simple example with only three performance constraints. In a real optimization, a dozen or more constraint lines may be plotted. While it is not necessary to include every performance requirement in the sizing matrix plot, all those which the baseline aircraft does not handily exceed should be included.

This example showed only a 3×3 sizing matrix. For better accuracy, 5×5 and larger sizing matrices are used at the major aircraft companies.

Carpet Plot

Another presentation format for the sizing matrix, the so-called "carpet plot," is based upon superimposing the takeoff weight plots from Fig. 19.2.

In Fig. 19.5a, the upper-left illustration from Fig. 19.2 is repeated showing a plot of sized takeoff gross weight W_0 vs W/S for a T/W of 1.1. The points labeled 1, 2, and 3—data points from the matrix (Fig. 19.1)—represent wing loadings of 50, 60, and 70.

The next illustration of Fig. 19.5 superimposes the next W_0 vs W/S plot from Fig. 19.2. This plot represents a T/W of 1.0. The data points labeled 4, 5, and 6 again represent wing loadings of 50, 60, and 70.

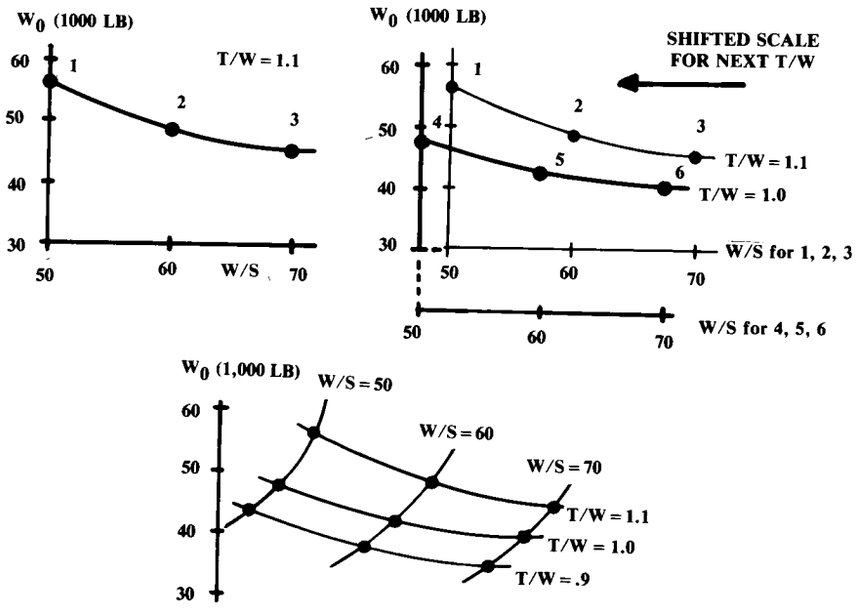

Fig. 19.5 Carpet plot format. (same results!)

To avoid clutter, the horizontal axis has been shifted to the left some arbitrary distance. This shifting of the axis is crucial to the development of the carpet-plot format.

In the lower illustration of Fig. 19.5, the third curve of W_0 vs W/S has been added, again shifting the horizontal axis the same increment. The points labeled 7, 8, and 9 again represent wing loadings of 50, 60, and 70.

Now these regularly spaced wing-loading points on the three curves can be connected, as shown. The resulting curves are said to resemble a carpet; hence the name. The horizontal axis can be removed from the carpet plot because one can now read wing loadings by interpolating between the curves.

In Fig. 19.6, the wing loadings that exactly meet the takeoff, P_s, and acceleration requirements (from Fig. 19.2) have been plotted onto the carpet plot and connected with constraint lines.

The optimal aircraft is found by inspection as the lowest point on the carpet plot that meets all constraints. This usually occurs at the intersection of two constraint curves.

The carpet plot and the sizing-matrix crossplot format give the same answer. Some people prefer the carpet-plot format because the "good" direction for minimum weight is obvious (down). Others prefer the sizing-matrix crossplot format because it is easier to read the optimal thrust-to-weight ratio and wing loading once they are found. Note that both formats are commonly referred to as "carpet plots."

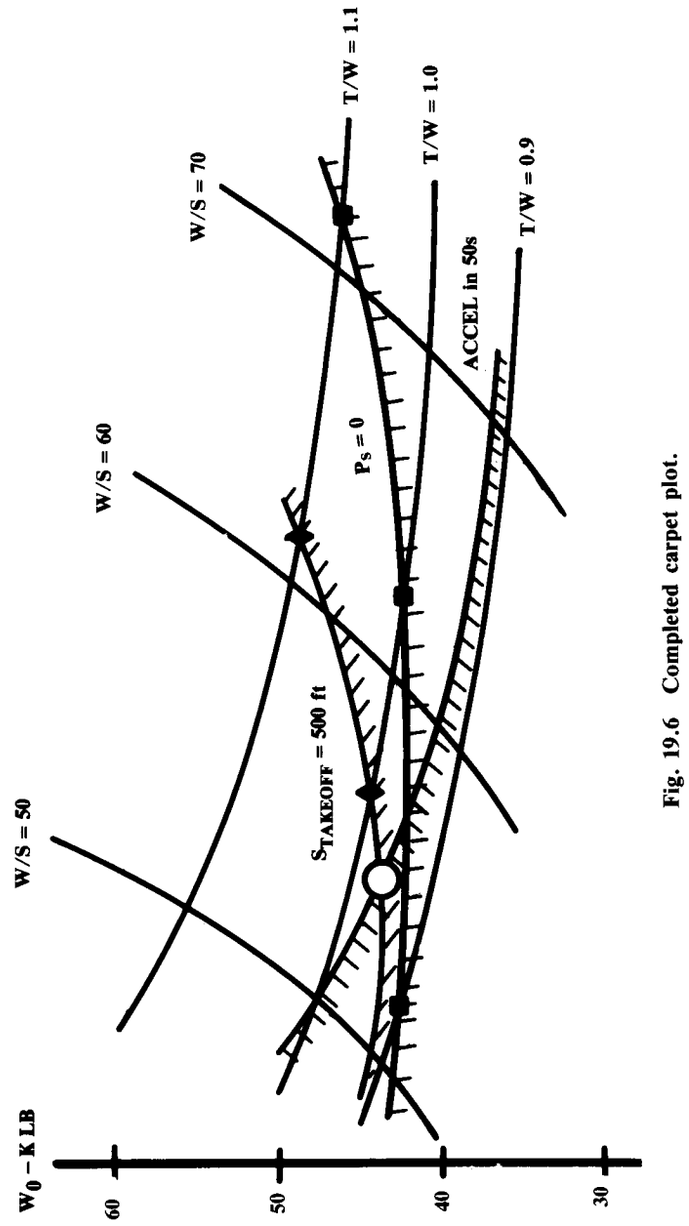

Fig. 19.6 Completed carpet plot.

It is also possible to create sizing plots in which the measure of merit is cost rather than weight. The plotting procedure is the same except that cost values are used rather than weight values in the development of the sizing plot. However, for most aircraft types the minimization of weight will also minimize cost for a given design concept.

Sizing-Matrix Data Approximations

A massive amount of work would be required to analyze fully the impact of variations in T/W and W/S on the aerodynamic, propulsion, and weight data required to develop a carpet plot. A variation in T/W affects the thrust and fuel flow, but also affects the wetted area and wave drag due to the change in nacelle size.

A change in W/S affects the wetted area and wave drag. Additionally, changing W/S affects the drag-due-to-lift (K) factor because the fuselage covers up more or less of the wing span. Note that, while the total parasite drag usually increases as the wing size increases, the drag coefficient may drop because it is referenced to the wing area!

At the major aircraft companies, sophisticated modules for analyzing the effects of the parametric variations of T/W and W/S are incorporated into the sizing programs.

For initial studies and student designs, this analysis can be approximated by ratioing the baseline analysis for the affected parts of the airplane.

The change in zero-lift drag can be assumed to be proportional to the change in wetted area due to the wing-area and nacelle-size variations. Wing wetted area varies approximately directly with wing area. Nacelle wetted area varies roughly with the variation in thrust.

For a supersonic aircraft the wave drag should be recalculated. The wing cross-sectional area varies directly with a change in wing area. This is used to determine the new total cross-sectional area that is used to approximate the wave drag.

The variation in K due to relative fuselage size, being small, may be ignored for initial studies. If the wing area is changed, however, then the aircraft will fly at different lift coefficients.

The statistical equations in Chapter 15 show that the wing and tail component weights vary approximately by the 0.7 power of the change in wing area. The engine itself varies in weight by the 1.1 power of a change in thrust.

Installed propulsion performance can be assumed to ratio directly with the thrust.

These and similar, reasonable approximations can be used to estimate the revisions to aerodynamic, weight, and propulsion data for sizing analysis and carpet plotting.

19.5 TRADE STUDIES

Trade studies produce the answers to design questions beginning with "What if...?" Proper selection and execution of the trade studies is as important in aircraft design as a good configuration layout or a correct

Table 19.1 Typical trade studies

Design trades	Requirements trades	Growth sensitivities
T/W and W/S	Range/payload/passengers	Dead weight
A, Λ	Loiter time	C_{D_0} and K
t/c, λ, airfoil	Speed	$C_{D_{\text{wave}}}$
High-lift devices	Turn-rate, P_s, $n_{\max}$	$C_{L_{\max}}$
BPR, OPR, TIT, etc.	Runway length	Installed thrust and SFC
Materials	Time-to-climb	Fuel price
Configuration	Design-to-cost	
tail type		
variable sweep		
number and type of engines		
maintainability features		
observables		
passenger arrangement		
Advanced technologies		

sizing analysis. Only through the trade studies will the true optimum aircraft emerge.

The "granddaddy" of all trade studies is the *T/W-W/S* carpet plot. This is such an integral part of aircraft analysis that it is not usually even thought of as a trade study. A *T/W-W/S* carpet plot in good measure determines the minimum-weight aircraft that meets all performance requirements.

Table 19.1 shows a number of the trade studies commonly conducted in aircraft design. These are loosely organized into design trades, requirements trades, and growth sensitivities.

Design trades reduce the weight and cost of the aircraft to meet a given set of mission and performance requirements. These include wing-geometry and propulsion variations as well as configuration arrangement trades.

Requirements trades determine the sensitivity of the aircraft to changes in the design requirements. If one requirement forces a large increase in weight or cost, the customer may relax it.

Growth-sensitivity trade studies determine how much the aircraft weight will be impacted if various parameters such as drag or specific fuel consumption should increase. These are typically presented in a single graph, with percent change of the various parameters on the horizontal axis and percent change in takeoff weight on the vertical axis.

Be aware of an important consideration in all of these trade studies: the realism factor. There is an unfortunate tendency to minimize redesign effort, especially for yet another boring trade study! If asked to study the impact of carrying two more internal missiles, the designer may find a way to "stuff them in" without changing the external lines of the aircraft.

This might completely invalidate the results of the trade study. If there was sufficient room in the baseline to fit two more missiles internally, then the baseline was poorly designed. If the baseline was already "tight," then the revised layout must be a fake!

The best way to avoid such problems is to insist that all redesigned layouts used for trade studies be checked to maintain the same internal density as the baseline, calculated as takeoff weight divided by internal volume.

The trade studies shown in Table 19.1 must be calculated using a complete *T/W-W/S* carpet plot for each data point. For example, to determine the optimal aspect ratio the designer might parametrically vary the baseline aspect ratio up and down 20%.

For each aspect ratio, a *T/W-W/S* carpet plot would be used to determine the minimum-weight airplane. These minimum weights would then be plotted vs aspect ratio to find the best aspect ratio.

The workload for trade studies can rapidly exceed manual capabilities. To optimize aspect ratio as described above requires a minimum of $3 \times 3 \times 3$ (27) data points. Each data point requires full analysis for aerodynamics, propulsion, and weights, followed by a sizing iteration.

To truly optimize an aircraft, a large number of the parameters from Table 19.1 should be considered simultaneously. However, the hundreds or thousands of data points required to do this would exceed even computer capabilities.

There is currently great interest in developing optimization procedures that permit such multivariable optimization in a design environment. Two

techniques show promise, "Latin Squares" and "Decomposition," but go beyond the scope of this book.

It has been assumed here that the measure of merit for trade studies will always be takeoff gross weight. Cost, though, will be the final selection measure in a design competition. Using minimum weight as the measure of merit is usually a good approximation to minimum cost because the acquisition cost is so strongly driven by the weight.

However, life-cycle cost is driven largely by fuel cost, which may not be minimized by the minimum-weight airplane. LCC can be estimated and plotted on the sizing matrix, and the best aircraft can then be selected as the lowest LCC point.

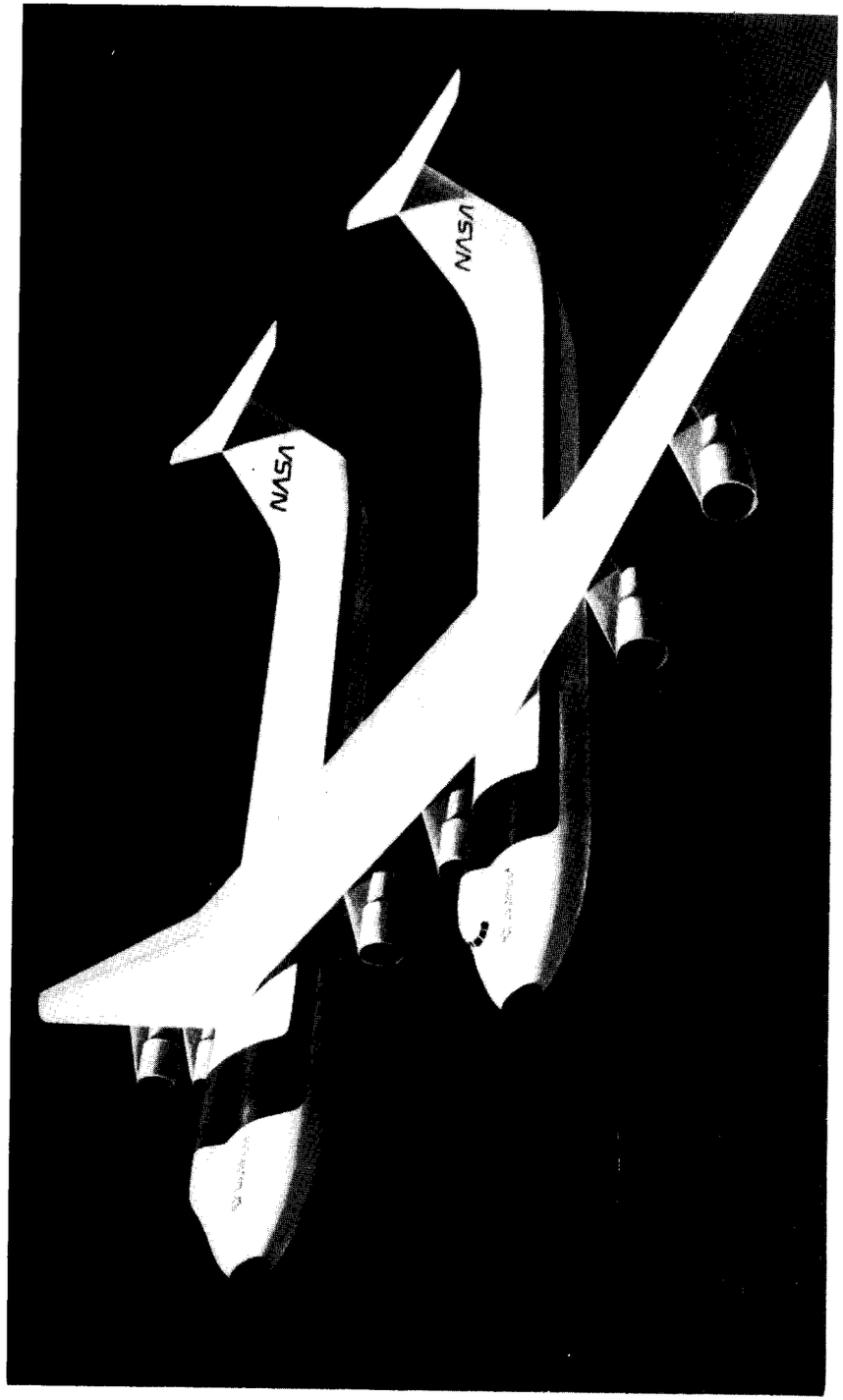

Multibodied-Aircraft Concept

20
VTOL AIRCRAFT DESIGN

20.1 INTRODUCTION

This chapter introduces the essential concepts and technologies of vertical takeoff and landing (VTOL) aircraft design. Although similar in many respects to conventional aircraft design, VTOL presents some key differences and pitfalls to avoid. This chapter emphasizes the differences that affect VTOL vehicle layout and sizing analysis.

The operational benefits of an ability to take off and land vertically are self-evident. Conventional aircraft must operate from a relatively small number of airports or airbases with long paved runways. For commercial transportation, the airport is rarely where you actually wish to go, and is usually crowded, causing delays in the air and on the ground.

The military airbase is highly vulnerable to attack, and during a wartime situation the time expended cruising to and from the in-the-rear airbase increases the required aircraft range and also increases the amount of time it takes for the aircraft to respond to a call for support.

The first type of VTOL heavier-than-air aircraft was the helicopter, which was conceived by Leonardo daVinci but not regularly used until shortly after World War II. The helicopter rapidly proved its worth for rescue operations and short range point-to-point transportation, but its inherent speed and range limitations restricted its application.

For propeller-powered aircraft, the tilt-rotor concept as tested in the Bell XV-15 seems to offer the best compromise between helicopter-like vertical flight and efficient wing-borne cruise. The tilt-rotor concept is the basis of the V-22 Osprey now under development.

Helicopters and tilt-rotors go beyond the scope of this book, but are discussed in Ref. 68.

For jet VTOL aircraft, a clear "best" solution for vertical lift has yet to emerge. Instead, there are a wide variety of alternative vertical-lift concepts, some tested and some not, available for incorporation into a new design. Selection of a "best" concept depends upon the intended mission and operational environment as well as the assumptions made as to the technical details of the selected lift concept.

To date there have only been a few operational jet VTOL designs—the British Harrier and the Russian YAK-36. These are both subsonic aircraft. While at least one supersonic VTOL design has flown (The Mach 2 Mirage III-V back in 1966), there has yet to be an operational supersonic VTOL aircraft.

This is largely due to the increased internal volume required for the vertical-lift apparatus and vertical-flight fuel. Also, most concepts for vertical lift tend to increase the aircraft's cross-sectional area near the aircraft's center of gravity (c.g.), and that increases the supersonic wave drag. Finally, the state of the art in engine thrust-to-weight ratio has imposed an excessive weight penalty on VTOL designs. It has simply not been possible up to now to provide both vertical flight and supersonic forward flight in an operational aircraft of any usable range.

However, the overall level of aircraft/engine technology and VTOL-specific technology is advancing so rapidly that this author expects the next generation of new military jets to include at least one supersonic VTOL concept.

20.2 VTOL TERMINOLOGY

VTOL refers to a capability for Vertical TakeOff and Landing, as opposed to Conventional TakeOff and Landing (CTOL).

An aircraft which has the flexibility to perform either vertical or short takeoffs and landings is said to have Vertical or Short TakeOff and Landing (VSTOL) capability. An aircraft which has insufficient lift for vertical flight at takeoff weight but which can land vertically at landing weight is called a Short TakeOff and Vertical Land (STOVL).

The "tail-sitter" or Vertical Attitude TakeOff and Landing (VATOL) aircraft cannot use its vertical lift capability to shorten a conventional takeoff or landing roll. In contrast, a Horizontal Attitude TakeOff and Land (HATOL) concept can usually deflect part of its thrust downward while in forward flight enabling it to perform a Short TakeOff and Landing (STOL).

20.3 FUNDAMENTAL PROBLEMS OF VTOL DESIGN

A number of unique problems characterize the design and operation of jet VTOL aircraft. Two fundamental problems stand out because they tend to have the greatest impact upon the selection of a VTOL propulsion concept and upon the design and sizing of the aircraft: balance and thrust matching.

Modern supersonic jet fighters have a T/W exceeding 1.0, so it would seem fairly easy to point the jet exhaust downward and attain vertical flight. Unfortunately, this is complicated by the balance problem.

Many subsonic jets and virtually all supersonic jets are designed with the engine at the rear, the cockpit and avionics at the nose, and the payload and fuel near the center of the aircraft. This traditional layout places the expendables on the c.g., co-locates the parts of the aircraft requiring cooling (crew and avionics), and keeps the avionics away from the hot and vibrating engine.

Figure 20.1a illustrates this traditional (and usually optimal) layout. If the aircraft's thrust exceeds its weight, vertical flight could be obtained simply by deflecting the thrust downward, as shown in Fig. 20.1b. However, a "magic finger" must hold up the nose in order to balance the

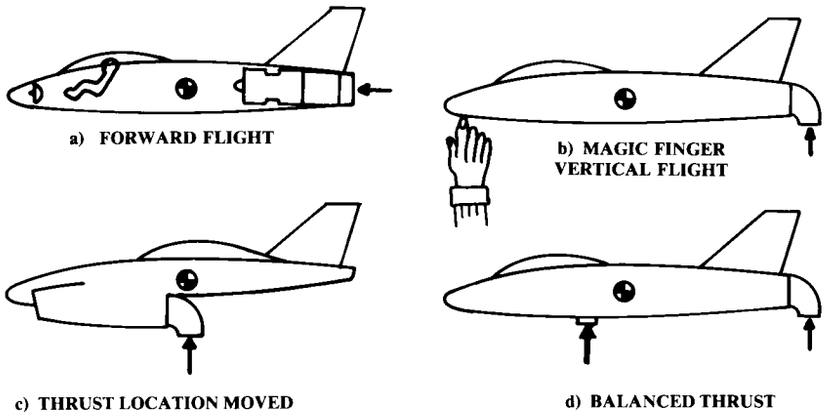

Fig. 20.1 The balance problem.

vertical thrust force at the tail. This balance problem is possibly the single most important driver of the design of the VTOL jet fighter.

There are really only two conceptual approaches to solving the balance problem. Either the thrust can somehow be moved to the c.g. (Fig. 20.1c), or an additional thrust force can be located near the nose (Fig. 20.1d). Both of these approaches will tend to compromise the aircraft away from the traditional and usually optimal layout.

For cruise-dominated VTOL aircraft such as transports, a more severe problem involves thrust matching. If the thrust required for vertical flight is provided by the same engines used for cruise, the engines will be far too large for efficient cruise.

As an example, imagine designing a VTOL transport using four of the TF-39 engines used in the C-5. These produce about 40,000 lb of thrust at sea-level static conditions, or 160,000 lb altogether. If the aircraft is to have a typical 30% thrust surplus for vertical flight ($T/W = 1.3$), then the aircraft can weigh no more than 123,077 lb at takeoff. Note that this is far less than the C-5 at 764,000 lb!

Assuming a typical cruise L/D of 18 yields a required T/W during cruise of about 1/18, or 0.056. If the aircraft weight at the beginning of cruise is about 95% of the takeoff weight, then the total thrust required during cruise is only 6,496 lb ($123{,}077 \times 0.95 \times 0.056$).

This is only 1624 lb of thrust per engine, which is about 18% of the available thrust for that engine at a typical cruise altitude of 35,000 ft. It is doubtful that the engine would even run at that low a thrust setting.

At 35,000 ft and Mach 0.9, the best SFC for this engine would be about 0.73 at a thrust of 9,000 lb per engine. The SFC at the 50% throttle setting is about 1.2—64% worse than the SFC at the higher thrust setting. If the engine would run at only 18% of its available thrust, its SFC would be even worse than the 1.2 value.

Aircraft range is directly proportional to SFC. The mismatch between thrust for vertical flight and thrust for cruise will produce a tremendous fuel

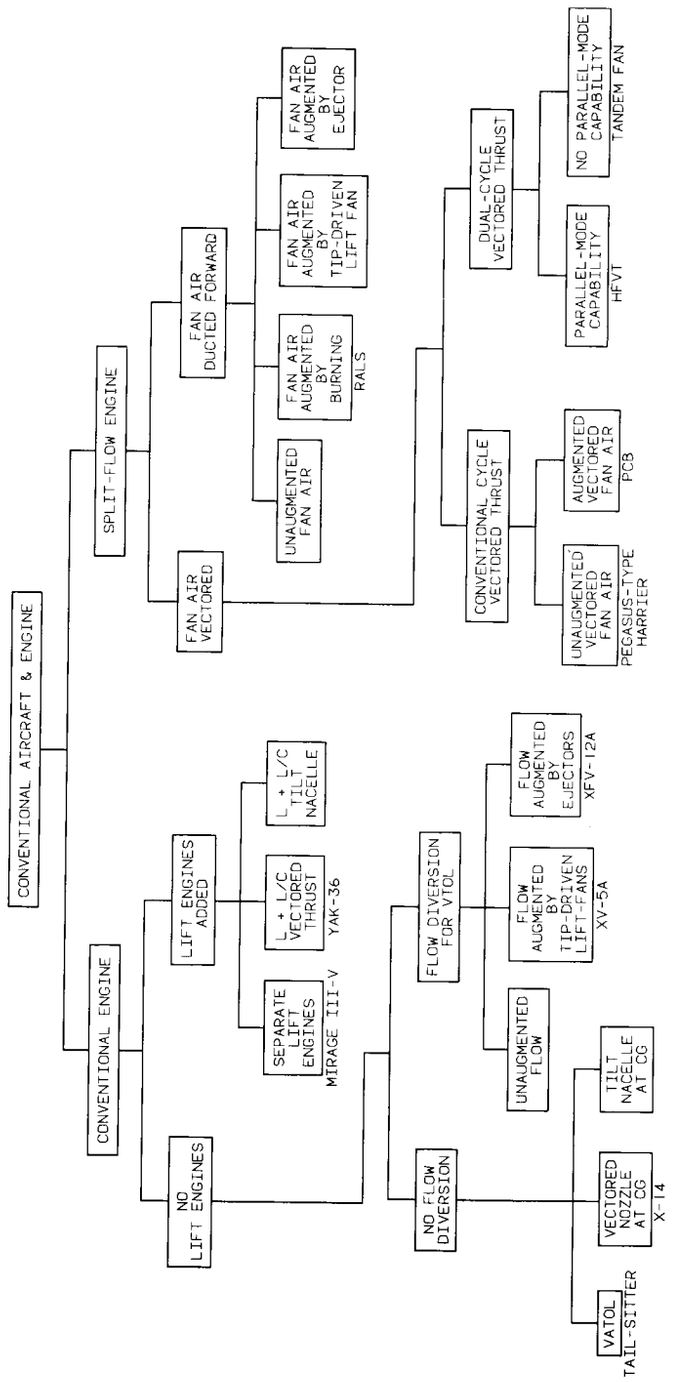

Fig. 20.2 Jet VTOL propulsion options.

consumption and range penalty for a cruise-dominated design that uses only the vectored thrust of its cruise engines for vertical flight. For this reason many conceptual VTOL transport designs incorporate separate "lift engines" used during vertical flight.

If three of the TF-39 engines in the example above could be turned off during cruise (without a drag penalty), the remaining engine could be operated at a 72% thrust setting where it gets an SFC of about 0.8. This is a big improvement over all engines being used for both lift and cruise. However, the use of separate lift engines introduces additional problems, as discussed later.

There are numerous other problems associated with VTOL aircraft design including transition, control, suckdown, hot gas ingestion, FOD, inlet flow matching, and ground erosion. These are discussed below following a brief discussion of the various VTOL jet propulsion options which are currently available to the designer.

20.4 VTOL JET-PROPULSION OPTIONS

The major options for jet VTOL propulsion systems are notionally derived in Fig. 20.2. Broadly speaking, jet VTOL concepts can be divided into those that utilize fairly conventional engines and those that use engines modified so that the fan and core air are split, with the fan air ducted and exhausted from some place separate from the core air.

The conventional-engine VTOL concepts that do not use additional lift engines for vertical flight must have a net takeoff T/W in excess of 1.0. If the jet exhaust is not diverted to some other location for vertical flight, the aircraft must either be a tail sitter (VATOL), or have the engine exhaust at the aircraft c.g. and capable of vectoring downward for vertical flight. This

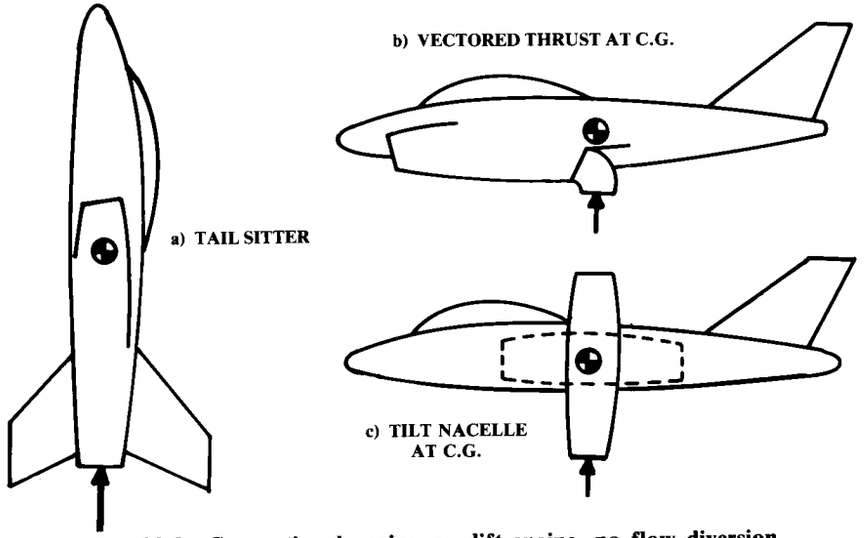

Fig. 20.3 Conventional engine, no lift engine, no flow diversion.

can be accomplished by using a vectoring nozzle or nacelles which tilt (Fig. 20.3).

The X-14 research aircraft had vectoring nozzles at the c.g., with the engines out in front. This is probably not a good arrangement for most applications because the cockpit winds up in back, for balance, and thus does not provide acceptable visibility for the pilot. Also, in forward flight the jet exhaust scrubs alongside the fuselage, causing thermal and acoustic problems.

An alternative approach is to place the nozzles at the center of gravity but put the engine in the rear fuselage as on a regular aircraft, but installed backwards! This "Reverse Installation Vectored Engine Thrust" (RIVET) concept offers design simplicity, reduced weight, ease of transition, and inherent vectoring in forward flight (VIFF). However, inlet duct losses of 5 percent or more will be caused by the 180-deg bend required to supply air to a backwards engine. Sizing studies (Ref. 93) indicate that despite these duct losses, RIVET offers a viable option for supersonic V/STOL.

Tilt nacelles, although heavy, may be the best compromise for some applications. Grumman has been pursuing a tilt-nacelle concept for Naval applications for a number of years.

Some VTOL concepts provide a means of diverting the exhaust flow to gain vertical lift. This is generally done by a retracting blocker device in the engine that shuts off the flow through the rearward-facing nozzle. The flow is then diverted forward through internal ducting (Fig. 20.4).

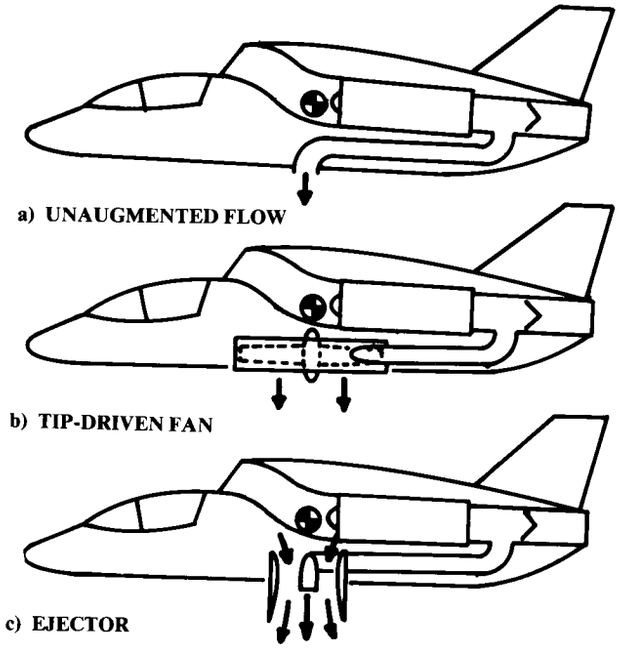

Fig. 20.4 Conventional engine, no lift engines, flow diversion used.

The diverted flow can be exhausted directly downwards, or it can be "augmented" by either a tip-driven fan or an ejector. Both of these can actually increase the thrust obtained from the diverted flow by using the energy of the exhaust flow to accelerate a larger mass of air. This augments thrust by increasing the propulsive efficiency.

The tip-driven fan (a ducted fan) is turned by turbine blades at its tip. The diverted engine exhaust is passed over the turbine blades to spin the fan. The Ryan XV-5A used such fans and attained an "augmentation ratio" of almost three (the lifting thrust attained with the tip-driven fans was almost three times the thrust produced by the jet engines during normal forward flight).

The ejector makes use of the viscosity of the air. Any exhaust jet will "drag" along adjacent air molecules, accelerating the free air in its vicinity. The ejector consists of a short duct with an exhaust stream blowing down it. Additional air is pulled by viscosity into the duct, accelerated, and ejected through a nozzle. This produces thrust greater than the thrust due to the jet exhaust alone.

While ejectors promise theoretical augmentation ratios of 3 or more, a more realistic value ranges from about 1.3 to perhaps 2.2. The Rockwell XFV-12A featured ejectors along the entire span of the wing and canard. It was expected to produce a high value of augmentation ratio, the actual value achieved was only about 1.5, and it never flew.

Both ejectors and tip-driven fans are heavy and tend to chop up the aircraft structure. Also, the internal ducting is bulky and poses a thermal problem. However, ejectors and tip-driven fans tend to reduce the thrust-matching problem since the engines do not have to be sized to lift the aircraft by jet thrust alone. The resulting improvement in cruise fuel consumption may offset the weight of the ejector or tip-driven fan.

One of the simplest ways of providing VTOL capability adds lift engines to an essentially conventional aircraft (Fig. 20.5). This brute-force approach was used in the Mirage III-V. Obviously, the separate lift engines add considerable weight and volume to the design, but the forward-flight engine can be sized for efficient cruise, thus solving the thrust-matching problem.

Since the lift engines are designed for a single operating condition, they can be highly optimized for that condition. Existing lift engines have engine T/W on the order of 15, compared to about 6–8 for a typical forward-flight engine. Future lift engines are expected to have engine T/W of 25 or more.

A more subtle approach than the use of separate engines for lift and cruise is to size the forward-flight engine for efficient cruise, but also provide a means of vectoring its thrust downward for vertical flight. The vertical-thrust shortfall is made up by the addition of lift engines. This is known as a "lift plus lift/cruise ($L + L/C$)" approach.

Since the forward-flight engine is providing some vertical thrust, the thrust required from the lift engines is reduced. The forward-flight thrust can be vectored by a vectoring nozzle as in the YAK-36 or by tilt nacelles.

A major problem with the $L + L/C$ approach is the transition from vertical to forward flight. During the transition period, the lift/cruise engine thrust is being vectored rearward, decreasing the vertical component of

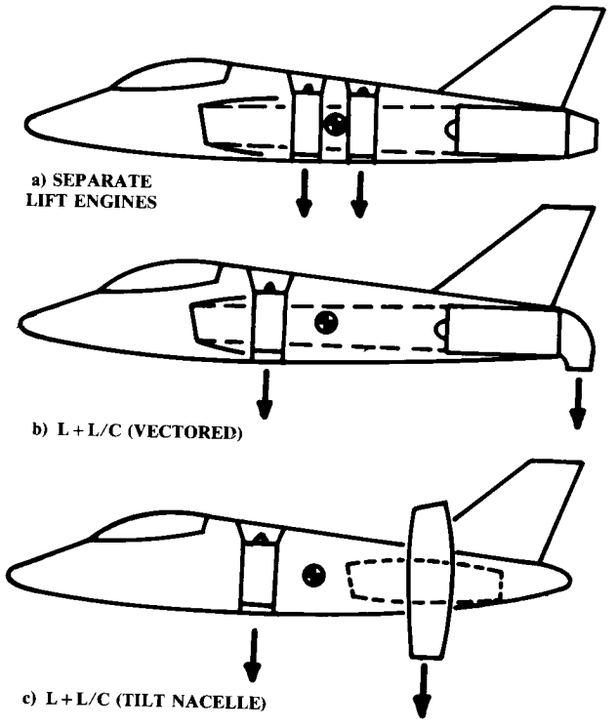

Fig. 20.5 Conventional engine with lift engines.

thrust. Since the lift/cruise engine is at the back of the aircraft, additional thrust is required to avoid a nose-up pitching moment.

If a lift engine should fail during vertical flight or transition, the aircraft would instantly pitch nose-down. It is rumored that the YAK-36 has an automatic ejection seat to save the pilot in this event.

The $L + L/C$ approach is especially poor for providing vectoring in forward flight (VIFF). The pilot must start up the lift engines before the selection of in-flight vectoring.

Another problem is that the aircraft operators would rather not have to provide tools, spare parts, and trained mechanics for two types of engine in one aircraft.

One possible benefit for the $L + L/C$ concept is the ability to use the lift engine to return to base in the event that the cruise engine fails. This requires some aft vectoring ability for the lift engine, which is desirable anyway to aid in transition.

Related to the $L + L/C$ concept is the "shaft-driven lift fan" (SDLF). This offers many of the benefits of $L + L/C$ but without some of the problems. In the SDLF concept, a driveshaft runs from the engine to a separate lift fan positioned where the lift engine on the $L + L/C$ concept is located. The driveshaft is powered by the main engine through a modified

or supplemental turbine, and spins the lift fan to provide vertical thrust. This avoids the need to develop a complete new lift engine, although the fan, driveshaft, gearbox, and turbine must be developed. Also, SDLF has a cooler front exhaust since the forward lift exhaust is not combusted. SDLF does give up the return-to-base capability of the $L + L/C$.

A number of VTOL propulsion concepts are based upon a "split-flow" modification to the turbofan engine. The airflow from the fan is split away from the core airflow and used in some fashion to address the balance and/or thrust-matching problems.

One such approach exhausts the fan air separately and provides a means for vectoring it downward for vertical flight (Fig. 20.6a). The AV-8 Harrier uses the high-bypass Pegasus engine in which the fan air and core air are each separately vectored through "elbow" nozzles (described later). This permits nearly instantaneous vectoring of thrust with no mode changes (such as starting a lift engine or diverting air into an ejector). This approach also simplifies transition and enhances maneuverability.

On the negative side, the Pegasus-type engine suffers the thrust-matching problem since the engine thrust must provide all of the required lifting force. Also, the engine must straddle the aircraft c.g. This increases the aircraft's cross-sectional area right at the wing location, and thus increases supersonic wave drag (the Harrier is subsonic).

It is possible to augment the thrust of such an engine by essentially providing an "afterburner" for the fan and core airflows in so-called plenum-chamber burning (PCB). There is considerable debate about the desirability of such high exhaust temperatures for VTOL operation.

Another means of providing afterburning to the Pegasus-type split flow engine is to duct the fan and core exhausts together during forward flight, and provide a conventional afterburner which is only used in forward flight

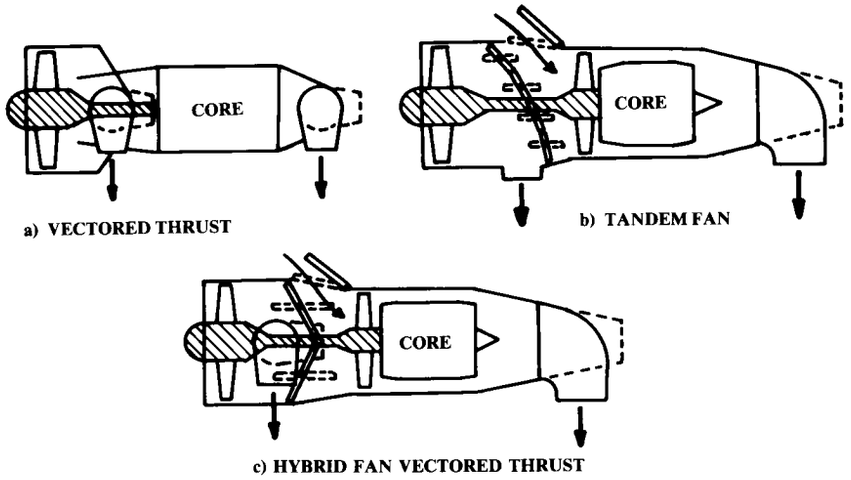

Fig. 20.6 Split-flow engines (vectored fan air).

The vectoring flaps can also be external to the nozzle as a part of the wing flap system. This approach was used on the XC-15 transport prototype. Although this was not a VTOL aircraft, its wing flap system was able to turn the engine flow more than 60 deg for STOL landings. This, combined with a landing gear that permits a 30-deg nose-up position, would provide the required 90 deg of total thrust vectoring for vertical flight.

The bucket vectoring mechanism (Fig. 208b) is similar to the commonly-used clamshell thrust reverser. The great advantage of this concept is that the flow-turning forces are all carried through the hingeline; thus the actuator can be fairly small. Also, the bucket can be designed with a smooth turning surface to raise the turning efficiency. A bucket vectoring nozzle can be designed to have a thrust loss of only about 2–3% when vectored 90 deg.

Figure 20.8c shows an "axisymmetric" vectoring system. The tailpipe is broken along slanted lines into three pieces, as shown. The three pieces are connected with circular rotating-ring bearings so that the middle (shaded) piece can be rotated about its longitudinal axis while the other parts remain unrotated. This causes the middle and end pieces of the tailpipe to vector downward as shown.

The rotating-ring bearings must be circular in shape, so the tailpipe must have a circular cross section along the slanted lines shown. For this to occur the perpendicular cross-sectional shape of the tailpipe must be an ellipse, so

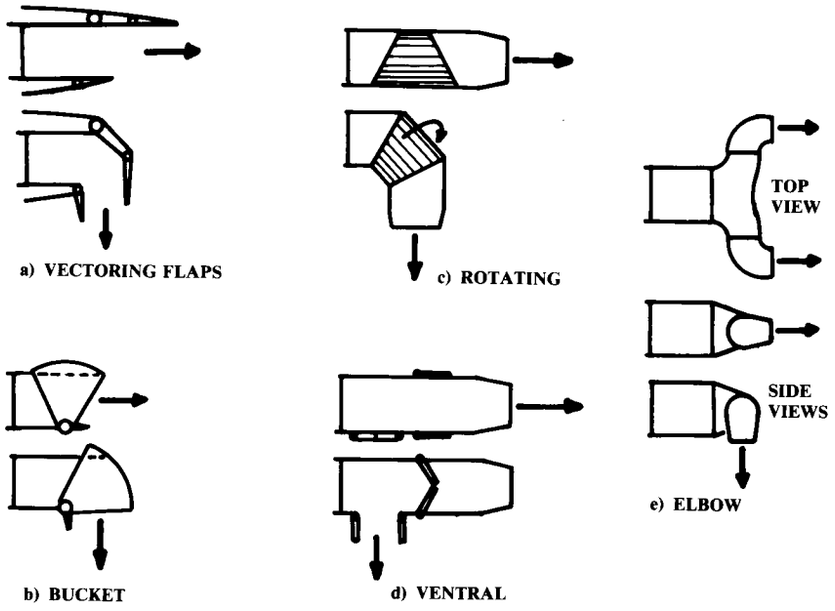

Fig. 20.8 Vectoring nozzles.

this nozzle system is not truly axisymmetric, despite its name. This type of vectoring nozzle has roughly a 3–5% thrust loss when vectored 90 deg.

The ventral nozzle (Fig. 20.8d) is simply a hole in the bottom of the tailpipe leading to a downward-facing nozzle. The flow out the regular nozzle is blocked off with some type of door.

To reduce hot-gas ingestion and damage to the runway, an afterburner is not usually used for vertical lift. A ventral nozzle can therefore be placed upstream (forward) of the afterburner. This moves the vertical thrust substantially forward compared to a vectoring nozzle at the end of the entire engine. That helps the balance problem.

The ventral nozzle has a thrust loss on the order of 3–6% when vectored 90 deg.

The "elbow" nozzle is used on the Pegasus engine in the highly successful AV-8 Harrier. In the elbow nozzle the flow is turned 90 deg outboard (see top view in Fig. 20.8e). A circular ring bearing connects to the movable part of the nozzle which turns the flow 90 deg back to the freestream direction. To vector the flow downward, the ring bearing is rotated 90 deg, as shown.

The elbow nozzle is simple and lightweight, and requires a minimum of actuator force for vectoring. However, the flow is always being turned through a total of 180 deg, even in forward flight. Because of this the engine is always suffering a thrust loss of approximately 6–8%. All the other types of vectoring nozzle only impose a thrust loss during vertical flight.

To reduce this thrust loss, the elbow nozzle can be designed using turns of less than 90 deg by canting the ring bearings downward and rearward. This can reduce the total turning angle to about 110 deg, which reduces the thrust loss to about 4–6%. However, the nozzles will then yaw inward during transition from horizontal to vertical thrust. This reduces the total usable thrust during transition and also increases the exhaust impingement upon the fuselage.

Another alternative is to provide elbow nozzles that are only used during vertical flight. A blocker door like that used for the ventral nozzle can divert the airflow from a conventional nozzle to the elbow nozzles. Like the ventral nozzle, the "part-time" elbow nozzles can be located forward of the afterburner for balance. The use of a conventional nozzle in forward flight saves fuel during cruise. This can more than compensate for the extra nozzle weight.

There is another important factor in the selection of nozzle type. This is the effect of the vectoring mechanism on the resultant thrust magnitude during transition.

For the elbow-type nozzle as used in the Harrier, the vector angle has virtually no effect upon the thrust magnitude. For the vectoring flap, bucket, and rotating segment-type nozzles the only effect is the previously-mentioned loss of thrust due to turning. This thrust loss is zero at zero degrees of deflection and gradually approaches the maximum value as the thrust deflection approaches 90 deg.

For the ventral nozzle, another factor causes a further reduction in thrust during transition. To transition from forward to vertical flight, the flow out the rear nozzle is gradually blocked off and the ventral nozzle is gradually opened.

The net thrust direction during transition is the vector sum of the thrusts produced by the aft and ventral nozzles. For example, if the exhaust massflow out the aft nozzle and the ventral nozzle are equal, then each nozzle has a thrust approximately equal to half the total engine thrust. The direction of the net resultant thrust is therefore 45 deg downward.

The magnitude of the net resultant thrust is found by vector addition to be 0.707 times the total engine thrust (square root of 0.5^2 plus 0.5^2). Thus the magnitude of the thrust is reduced by almost 30% when the net resultant thrust is vectored 45 deg during transition!

Figure 20.9a shows this result. The net resultant thrust for the ventral nozzle drops to about 70% of the total thrust as the thrust is vectored through 45 deg. It returns to full net thrust as the thrust vectoring is continued to 90 deg. By comparison, the elbow-type nozzle has the same thrust at all vector angles.

The reduction in the net resultant thrust of the ventral nozzle can be substantially lessened if the aft and ventral nozzles have vectoring capability. The middle line on Fig. 20.9a shows the net resultant thrust for 20-deg vectoring.

This vectoring ventral nozzle has full net thrust within 20 deg of the zero- and 90-deg vector angles. The worst case 45-deg vector angle, improves to a loss of only 10% of the thrust.

Figure 20.9a ignores the thrust losses due to turning. This reduces the relative advantage of the elbow nozzle. In Fig. 20.9b, the curves of Fig. 20.9a are repeated but with an assumed thrust loss of 3% for each 90-deg turn in the exhaust flow.

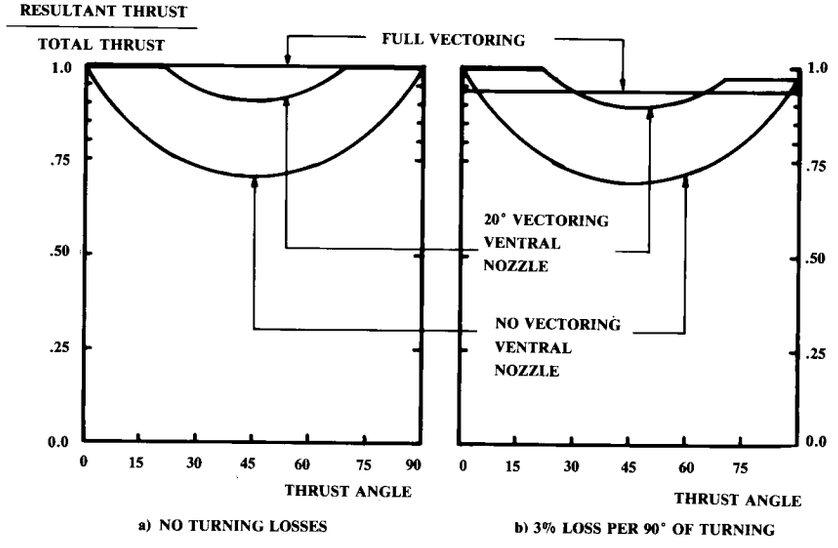

Fig. 20.9 Resultant thrust.

In forward flight, the ventral nozzle has a higher net thrust than the elbow concept due to the two 90-deg turns in the latter. This is also true in vertical flight where the ventral nozzle concept has only one 90-deg turn.

At the 45-deg vector angle, the elbow nozzle has a substantially better net resultant thrust if the ventral nozzle has no vectoring. If the ventral nozzle has a 20-deg vectoring ability, then the difference is negligible.

20.6 SUCKDOWN AND FOUNTAIN LIFT

The VTOL aircraft in hover is not in stagnant air. The jet exhaust that supports the aircraft also accelerates the airmass around it. This entrainment is due to viscosity and is strongest near the exhaust plume, producing a downward flowfield about the aircraft (Fig. 20.10a).

This downward flowfield pushes down on the aircraft with a "vertical drag" force equivalent to a loss of typically 2–6% of the lift thrust. The magnitude of this vertical drag force depends largely upon the relative locations of the exhaust nozzles and the wing. If the nozzles are right under the wing, the entrained airflow will exert a large downward force.

Unfortunately, the nozzles and the wing are both near the c.g. for most VTOL concepts. The use of a tandem wing, forward-swept wing, or joined wing may reduce the entrained download by separating the wing away from nozzles, which are located at the c.g.

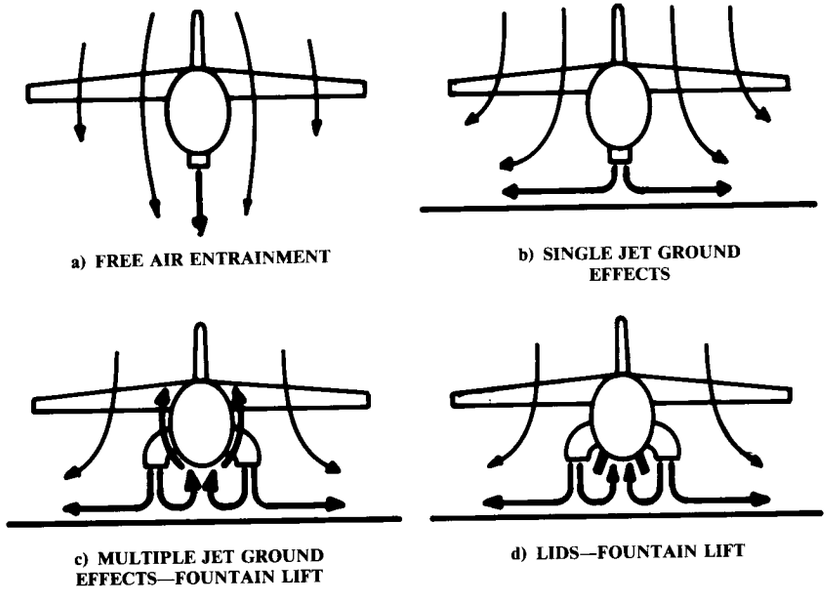

Fig. 20.10 Suckdown and fountain lift.

Figure 20.10b shows the effect of the ground on the entrained flowfield. The jet exhaust strikes the ground and spreads outward. This increases the mixing between the jet exhaust and the adjacent air, which increases the entrainment effect. The entrained download (or "suckdown") therefore increases as the ground is approached.

A single-jet VTOL concept can experience a 30% reduction in effective lift due to suckdown. Furthermore, the suckdown increases as the ground is approached—a very undesirable handling quality!

Figure 20.10c shows a VTOL concept with widely separated multiple nozzles near the ground. The jet exhausts strike the ground and spread outward. The exhausts meet in the middle. Since there is nowhere else to go, they merge and rise upward, forming a "fountain" under the aircraft.

This fountain pushes upward on the aircraft with a magnitude that will often cancel the suckdown force. The strength of the fountain lift depends upon the exact arrangement of the nozzles and the shape of the fuselage. Lower-fuselage shaping that makes it more difficult for the fountain to flow around the fuselage will increase the fountain effect. For example, square lower corners are better than round ones.

Fountain lift increases as the ground is approached. This desirable handling quality counters the undesirable effect of suckdown.

The fountain lift can be increased even more by the use of Lift Improvement Devices (LIDS), (called Cushion Augmentation Devices in Britain). These are longitudinal strakes located along the lower fuselage corners which capture the fountain (Fig. 20.10d). LIDS added to the AV-8B increased the net vertical lift over 6%.

Note that multiple nozzles near to each other may not produce a fountain effect because the exhaust plumes may merge into a single jet, producing a flowfield more like that shown in Fig. 20.10a.

20.7 RECIRCULATION AND HOT-GAS INGESTION

A VTOL aircraft hovering near the ground tends to "drink its own bathwater." The hot exhaust gases find their way back into the inlet, causing a significant reduction in thrust. Also, this "recirculated" air can include dirt and other erosion particles that can damage or destroy the engine. In some cases the dirt kicked up by a hovering VTOL aircraft can completely obscure the pilot's vision.

Figure 20.11 shows the three contributors to exhaust recirculation: bouyancy, fountain, and relative wind. Bouyancy refers to the natural tendancy of hot gases to rise. The jet exhaust mixes with the ambient air and slows down as it moves farther away from the airplane. Eventually it has slowed enough that the outward momentum becomes negligible and the bouyancy effect takes over. The now-warm air rises up around the aircraft and can eventually be drawn back into the inlet.

The bouyancy effect takes time. It takes about 30 seconds in hover for the air around the Harrier to heat up by 5°C. This 5°C increase in air temperature entering the inlet reduces the engine thrust by about 4%.

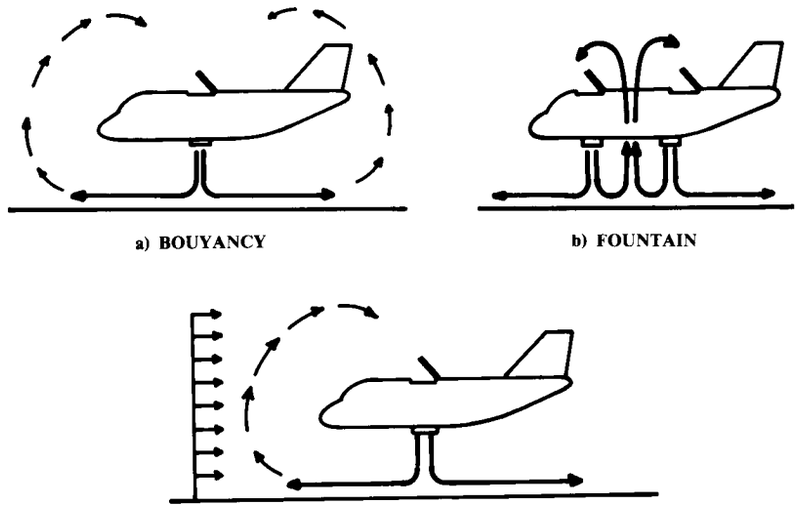

Fig. 20.11 Recirculation.

If the nozzle arrangement produces a fountain, the recirculation will be greatly increased. This causes additional hot-gas ingestion (HGI) in addition to the bouyancy effect. Unlike the bouyancy effect, the fountain effect takes little time to increase the temperature of the air entering the inlet.

The Harrier experiences a 10°C temperature rise due to the fountain effect. This reduces thrust by about 8%.

The third contributor to recirculation, relative wind, can be due to atmospheric wind or to aircraft forward velocity. Essentially, the relative wind pushes back on the spreading exhaust gases, forcing them up. At some combination of relative wind and exhaust velocity the hot gases will wind up back in the inlet.

Hot-gas ingestion is typically limited to speeds below about 50 knots. If the nozzles can rapidly vector from full-aft to a downward angle, a rolling takeoff can be used to minimize HGI problems. The pilot starts the takeoff with the nozzles fully-aft and quickly accelerates to about 50 knots. Then the nozzles are vectored downward and the aircraft takes off.

20.8 VTOL FOOTPRINT

The "footprint" of a VTOL aircraft refers to the effect of the exhaust upon the ground. This is largely determined by the dynamic pressure and temperature of the exhaust flow as it strikes and flows along the ground. Even a helicopter cannot operate from a very loose surface such as fine sand or dust. The exhaust of a turbojet VTOL aircraft can be of such high

pressure and temperature that it can erode a concrete landing pad if the aircraft is hovered in one spot for too long.

No *exact* method exists to determine the acceptable exhaust pressures and temperatures for VTOL operation off of a given surface. Roughly speaking, a turbojet exhaust is marginal for operation off concrete and is too hot and high-pressure for asphalt. The front-fan exhaust of a split-flow turbofan is generally acceptable for concrete, asphalt, and dense sod. However, the core-flow exhaust of the turbofan may be too hot and high-pressure for asphalt and sod.

Ejectors and tip-driven fans substantially reduce the exhaust temperature and pressure, allowing operation from regular sod and perhaps hard-packed soil.

In general, the nozzles should be as far above the ground as possible. The ground temperatures due to a turbofan will be reduced by about 30% if the nozzles are five nozzle diameters above the ground. This suggests that a pair of side-mounted elbow nozzles are preferable to a single ventral nozzle because they are higher off the ground and have less diameter for the same total airflow.

Although Refs. 88 and 89 give some data on footprint, this author does not know any published report that details the suitability of VTOL operation from a variety of surfaces as a function of exhaust pressure, temperature, and nozzle geometry. Such a test report would be a useful data source for the design of jet VTOL aircraft.

20.9 VTOL CONTROL

The VTOL aircraft in hover and transition must be controlled by some form of thrust modulation. Most VTOL concepts use a reaction control system (RCS), in which high-pressure air is ducted to the wing tips and the nose and/or tail. This high-pressure air can be expelled through valve-controlled nozzles to produce yaw, pitch, and roll control moments.

The high-pressure air for the RCS is usually bled off the engine compressor, causing a reduction in thrust. The Harrier loses roughly 10% of its lift thrust due to RCS bleed air.

Bleed-air RCS systems can be light in weight. For the Harrier, the whole system only weighs about 200 lb. However, the RCS ducting occupies a significant volume in the aircraft. Also, RCS ducting is hot and cannot be placed too near the avionics.

If a VTOL concept has three or more lift nozzles placed well away from the c.g., modulation of the lift thrusts can be used for control in vertical flight. For example, if the thrust from the forward nozzle is reduced, the nose will pitch down. Vectoring the left-side nozzles forward and the right-side nozzles rearward will cause the nose to yaw to the left.

In addition to three-axis control (roll, pitch, and yaw), a VTOL needs vertical-velocity control ("heave" control). This is done by varying the lifting thrust. For an aircraft with fixed nozzle-exit area (such as the Harrier), the lifting thrust is varied by engine throttle setting.

An engine with variable nozzle-exit area can change its lifting thrust more rapidly by changing exit area, leaving the throttle setting unchanged. Provision of acceptable heave control generally adds about 5% to the required hover T/W.

A multiengine aircraft should remain under control following the loss of an engine. This common requirement is far more difficult for a VTOL aircraft to meet than for a conventional aircraft. For example, if a VTOL aircraft requires two engines to hover, a third engine of the same thrust would be required to assure hover ability after loss of an engine. Not only that, but the engines must be arranged so that their combined thrust passes through the c.g. with all engines running and with any one engine failed.

The more engines a VTOL concept has, the smaller the impact of adding one extra engine for engine-out hover. However, the increased pilot workload for operating multiple engines and the additional maintenance makes this option less attractive. Also, the more engines, the greater the probability of an engine failure.

Another technique studied for engine-out control involves cross-shafting the engine fans so that the fans of all the engines can be driven from the cores of the other engines. This minimizes the asymmetric thrust loss from the failure of one engine core. However, the weight impact of the cross-shafting mechanisms must be considered.

Some multi-engine VTOL concepts have been designed with several jet engines operating together through some form of augmentation devices. For example, the Ryan XV-5A had two jet engines that were diverted to three tip-driven fans. Either engine could drive all three fans.

20.10 VTOL PROPULSION CONSIDERATIONS

Thrust matching has already been discussed as one of the key problems facing VTOL designers. Inlet matching presents a similar problem. For efficient jet-engine operation at zero airspeed, the inlet should look much like a bellmouth as seen on jet-engine test stands. The inlet should have a large inlet area and generous inlet-lip radii. These features cause unacceptable drag levels during high-speed flight.

As a compromise, inlets can be sized for cruise operations and provided with auxiliary doors for VTOL operation. For reasonable low-speed efficiency these auxiliary doors must be very large compared with typical auxiliary doors as seen on a CTOL aircraft.

Another propulsion consideration is the amount of vertical thrust required for vertical flight. As a minimum, the net T/W for vertical flight must obviously exceed 1.0. For acceptable response in heave (vertical acceleration), the net T/W should equal or exceed 1.05.

The net thrust available for vertical lift will be reduced by suckdown, hot-gas ingestion, and RCS bleed. Because of these factors, the required T/W for vertical flight will greatly exceed the 1.05 value required merely to hold the airplane up and provide heave control.

For most types of VTOL aircraft, the overall installed T/W for vertical flight ranges between about 1.2 and 1.5, with 1.3 being a typical value. Figure 20.12 shows a typical breakdown of contributors to required T/W.

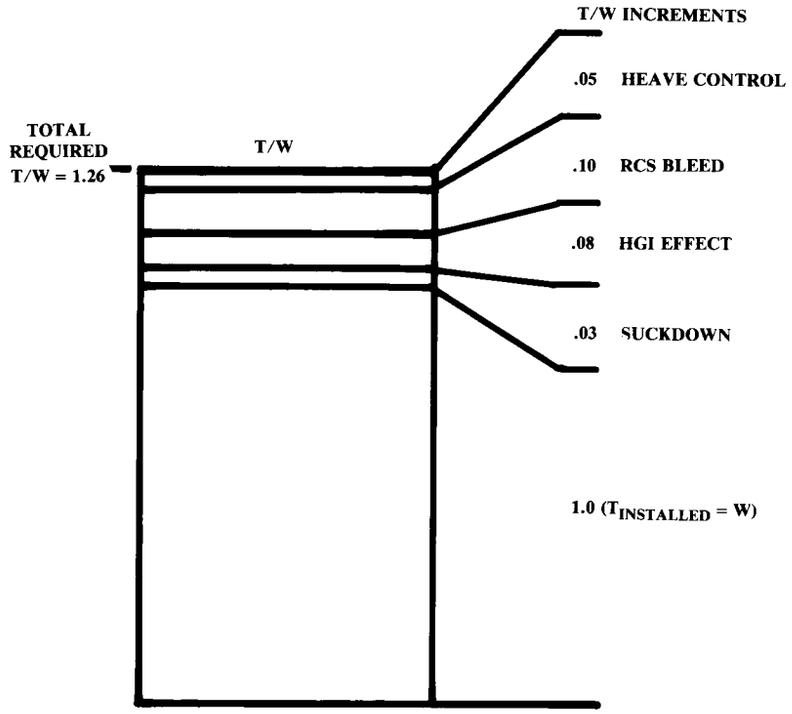

Fig. 20.12 Typical hover T/W breakdown.

20.11 WEIGHT EFFECTS OF VTOL

It is difficult to assess statistically the impact of VTOL on aircraft weights using design data from existing aircraft. VTOL designs are so strongly driven by weight considerations that the designers will push much harder to reduce weight than in a normal CTOL design.

For example, the Harrier was designed so that it requires removing the wing to remove the engine. This would be considered a fatal design flaw in a CTOL aircraft but is tolerated in the Harrier because of the weight savings compared to the immense doors that would otherwise be required to remove the engine.

Because of such design compromises, the Harrier has an empty-weight fraction W_e/W_0 of only 0.48 whereas a statistical approach based upon similar CTOL designs would indicate that the Harrier should have an empty-weight fraction of about 0.55. By way of reference, the A-4M, which performs a similar mission, has an empty-weight fraction of 0.56.

A VTOL aircraft designed to the same ground rules as a CTOL aircraft will always be heavier in two areas, propulsion and control systems.

The propulsion system will be heavier due to the compromises described above for solving the balance and/or thrust-matching problems. The various VTOL propulsion concepts all incorporate some additional features such as vectoring nozzles, extra internal ducting, tilt nacelles, or lift engines. These add weight.

Reference 87 compares CTOL and VTOL versions of a carrier-based utility aircraft (similar to the S-3). The CTOL version's propulsion-system weighs 8% of the takeoff weight. The VTOL version's tilt-nacelle propulsion system weighs 20% of the takeoff weight.

Data from Refs. 87–89 indicate that a typical supersonic CTOL fighter design may have a propulsion-system weight about 16–18% of the takeoff weight. An equivalent VTOL design would have a propulsion-system weight about 18–22% of the takeoff weight.

The far-greater propulsion-system weight for the cruise-dominated utility aircraft reflects the fact that the fighter concept already requires large engines for supersonic flight.

Control-system weights are increased about 50% for most VTOL designs. This is due to the ducting, nozzles, and valves of the typical RCS. However, the total control-system weight is only a small fraction of the takeoff weight (2% for a typical CTOL design) so the impact is slight.

For most VTOL designs the landing gear will weigh the same as for a CTOL design. Carrier-based aircraft may show reduced landing-gear weight with VTOL.

The landing gear of carrier-based aircraft are substantially heavier than the landing gear of other aircraft because of the extremely high sink-rates during landing and because of the catapult and arresting-hook loads. These can increase the landing-gear weight from about 4% to about 6% of the aircraft takeoff gross weight.

A VTOL aircraft designed for carrier operation need not incorporate the heavier landing gear. This represents a weight savings compared to the CTOL carrier-based aircraft.

As mentioned, it is difficult to provide an estimate for the total impact of VTOL on W_e/W_0 based upon statistics. However, data in Refs. 87–89 indicate that a fighter aircraft will experience an increase in W_e/W_0 of roughly 4% if designed to the same groundrules as an equivalent CTOL aircraft. Similarly, a transport/utility aircraft will have an increase in W_e/W_0 of about 7%. These estimates should be considered to be extremely crude.

20.12 SIZING EFFECTS OF VTOL

The final sized weight of a VTOL aircraft will be increased by the empty-weight effects described above. Also, a thrust mismatch between vertical flight and cruise may force the engine to be operated well away from the optimal thrust setting for cruise efficiency. This increases fuel consumption, which increases sized aircraft weight.

These factors will clearly increase the sized aircraft takeoff-weight if a VTOL aircraft is flown over the same mission as an equivalent CTOL. In some cases, though, the mission requirements can be reduced for the VTOL aircraft with no real loss in operational effectiveness.

For example, a Close-Air Support (CAS) aircraft like the A-10 should be based as near as possible to the ground troops being supported. VTOL ability may permit basing literally at the forward lines, thus reducing the mission range requirements while providing better operational effectiveness. The VTOL aircraft can also "loiter" on the ground, unlike the CTOL aircraft, which may have a requirement for a one-hour loiter on a CAS mission.

VTOL greatly simplifies instrument landings. Helicopters can "feel their way around" in foggy conditions that ground all CTOL aircraft. A VTOL capability should therefore reduce landing reserves for loiter or diversion to alternate airports.

On the other hand, the fuel burned by a vertical landing can be substantial whereas a CTOL aircaft uses virtually no fuel in landing.

Another favorable effect of a VTOL capability comes in the optimization of wing loading. For many aircraft the wing loading will be determined by either the takeoff or landing requirements. A VTOL capability removes this consideration, possibly permitting a smaller wing, which in turn reduces weight and fuel usage.

Taken altogether, these factors indicate that the VTOL aircraft will usually be heavier than an equivalent CTOL design. Based upon the data in the references, an increase in sized takeoff weight of about 10–20% can be expected for a fighter design. A transport/utility design will typically size to a weight roughly 30–60% greater than the CTOL design. As before, these are very crude trends, not estimates for any particular design.

21
CONCEPTUAL DESIGN EXAMPLES

21.1 Introduction

This final chapter offers two design examples that illustrate the concepts and methods presented in this book. The design examples are a single-seat aerobatic homebuilt airplane and a lightweight supercruise dogfighter designed to replace the F-16 as the "low" end of a future "high-low" mix of advanced fighters.

These examples illustrate the steps and thought processes used in conceptual design, covering the extremes from propeller-powered, fixed-size-engine design to "rubber-engine" supersonic design. The differences and surprising similarities between these extremes of design are shown.

Design requirements for these aircraft were assumed based upon data for similar aircraft. These design requirements were then treated as if they were mandated by some customer and used as the starting point for the design effort.

The examples are designed and analyzed using the methods presented in the book. Every effort has been made by the author to develop credible, realistic designs and to analyze and optimize them properly. However, no claim is made that these are optimal designs or even good designs or that all calculations are correct!

Furthermore, the examples are incomplete in that only the more important analysis areas are presented due to space limitations. Were the author to grade himself in a college design course, these examples would rate at most a "B." The "A" students would conduct far more analysis (structures, roll rate, c.g. envelopes, etc.) and would ultimately redraw the as-optimized aircraft to insure that the analysis assumptions were realistic.

21.2 Single-Seat Aerobatic

This design represents an aircraft that the author hopes to build and fly some day. It would provide fun weekend aerobatic flying for the occasional pilot and would offer better performance than the Great Lakes Biplane but without the touchy handling qualities of the Pitts Special.

The design is fairly classical in layout but is based around the more recent techniques for quick fabrication using moldless foam-fiberglass sandwich construction. This permits rapid "garage" fabrication of a one-of-a-kind aircraft. Also, the selected engine is already set up for aerobatic flight, which should minimize the installation effort.

One interesting result of the sizing and optimization presented below is that the low-wing loading required for good aerobatic capability has strongly biased the aspect ratio optimization, leading to a lower-than-expected optimal aspect ratio. In fact, without the addition of a maneuver-related performance constraint, the "optimal" aspect ratio approaches zero!

(Special note to homebuilders concerning the first example—DON'T BUILD IT!!! This is a first-pass conceptual design only. It would take at least a man-year of design and analysis effort by an experienced designer before this concept could be built and safely flown.)

DR-1 SINGLE SEAT AEROBATIC HOMEBUILT

ENGINE: LYCOMING O-320-A2B (FROM CITABRIA)

150 Hp AT 2700 RPM, $C_{bhp} = .5$ (Assumed)
272 LBS DRY
30" LENGTH 32" WIDTH 23" HEIGHT

DESIGN GOALS: RAPID FABRICATION (FOAM & FIBERGLASS)

PERFORMANCE: BETWEEN PITTS S-1S AND GREAT LAKES

$V_{max} \geq 130$ KTS $V_{Stall} \leq 50$ KTS

Takeoff ≤ 1000 FT over 50'

Rate of $Climb_{S.L.} \geq 1500$ fpm

RANGE ≥ 280 nm (no reserves) AT $V_{cruise} = 115$ KTS

$n = +9/-6$ g's

$W_{crew} = 220$ Lb (includes parachute)
-Optional open cockpit! (Used for analysis)

HANDLING QUALITIES:

- SLIGHTLY STABLE (LIKE A FIGHTER)
- GOOD SPIN RECOVERY UPRIGHT AND INVERTED

MISSION:

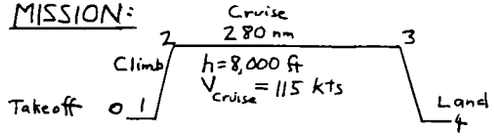

DPR
7/17/87

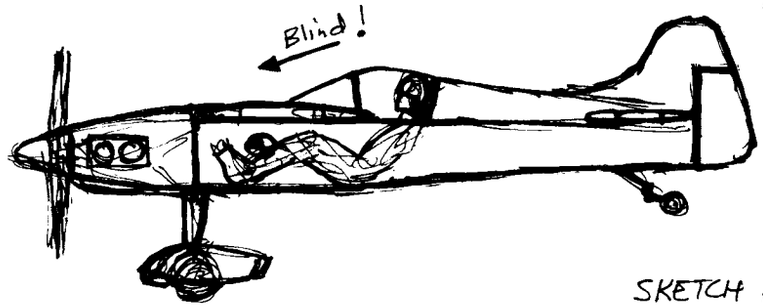

SKETCH #1

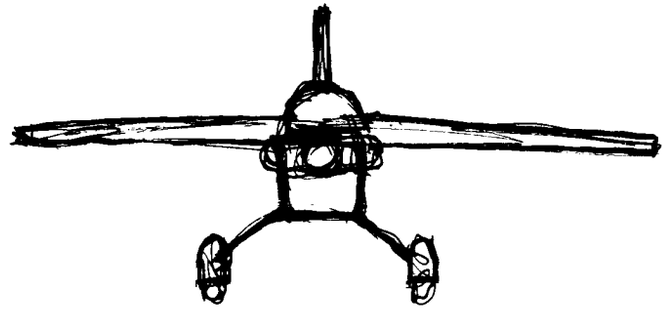

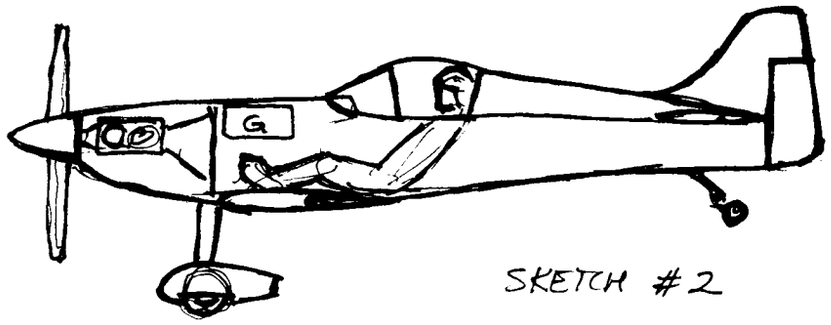

SKETCH #2

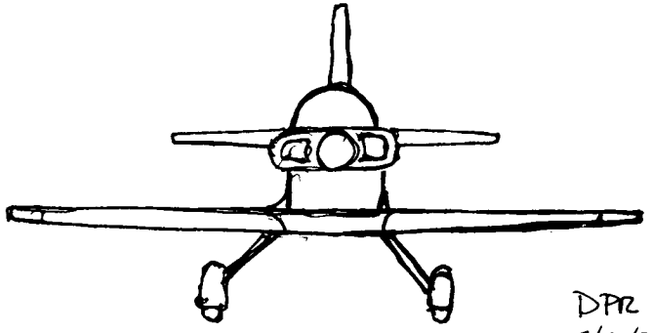

DPR
7/18/87

WING GEOMETRY SELECTION

(From Chapter 4 Charts & Tables)

$A=6$ $\lambda=.4$ $\Lambda_{c/4}=0$ $\Gamma=3°$ (0° Effective)

AIRFOIL : NACA 63_2015 (tip) } Higher t/c at tip to prevent tip stall

NACA 63_2012 (root) }

t/c

No twist (to avoid inverted tip stall)

HORIZONTAL TAIL

$A=4$ $\lambda=.4$ NACA 0012

VERTICAL TAIL

$A=1.5$ $\lambda=.4$ NACA 0012

H_p/W RATIO: PITTS: $W/H_p = 6.4$ } TENTATIVELY SELECT:
GREAT LAKES: $W/H_p = 10$ } $W/H_p = 8$

STATISTICAL (Table 5.4)

$$H_p/W = .004\, V_{max_{mph}}^{.57} = .004(130 \times 1.151)^{.57} = .069$$

or $W/H_p = 14.4$

(but statistics are for cruising aircraft, not aerobatics!)

SO INITIALLY SELECT

★ $W/H_p = 8$ and $W_o = 8 \times 150 = 1200$ Lb

WING LOADING

HISTORICAL: PITTS: $W/S = 11.7$
GREAT LAKES: $W/S = 9.6$
STEVENS ACRO: $W/S = 13.0$

STALL: No flaps, so $C_{L_{max}} \cong .9\, C_{l_{max}} \cong 1.2$

eq 5.6) $W/S \leq \frac{1}{2}(.00238)(50 \times 1.689)^2 (1.2) = 10.2$ Lb/ft²

TAKEOFF: 1,000 Ft. TAKEOFF ⇒ TAKEOFF PARAMETER = 120

$$C_{L_{takeoff}} = C_{L_{max}} \left(\frac{V_{stall}}{V_{takeoff}}\right)^2 = 1.2\left(\frac{1}{1.1}\right)^2 = .99$$

eq 5.8)
$$T.O.P. = 120 = \frac{W/S}{(1)(.99)(1/8)} \; ; \; W/S \leq 14.9$$

CLIMB: Assume climb speed = 70 kts, so $q = 16.6$ Lb/ft²

$$G = \frac{V_v}{V} = \frac{1500/60}{70 \times 1.689} = .212$$

$$T/W = \frac{550 \times 0.8}{70 \times 1.689}\left(\frac{1}{8}\right) = .465$$

Assume $e = .8$

From sketch, $\frac{S_{wet}}{S_{ref}} \cong 3.5$ so $C_{D_o} \cong 3.5 \times .0055 = .02$

eq 5.30) eq 12.23
$$W/S \leq \left[(.465 - .212) + \sqrt{(.465-.212)^2 - \frac{4(.02)}{\pi \times 6 \times .8}}\right] \Big/ \left[\frac{2}{16.6\pi \times 6 \times .8}\right] = 62$$

CRUISE: $q_{cruise} = 35$ Lb/ft²

$$W/S = 35\sqrt{\pi \times 6 \times .8 \times .02} = 20$$

★ SELECT LOWEST: $W/S = 10.2$; $S = \frac{1200}{10.2} = 118$ ft²

INITIAL SIZING

EMPTY WEIGHT FRACTION:

Table 6.2) $\frac{We}{Wo} = .59\, W_o^{-.1} (6)^{.05} (1/8)^{.1} (10.2)^{-.05} (130)^{.17} = 1.093\, W_o^{-.1}$

But this is for cruising, not aerobatic aircraft. We adjust the equation using the Stevens Acro:

Stevens Acro: $W_o = 1300$ $We = 950$ $We/W_o = .73$

Our equation gives: $\frac{We}{Wo} = 1.093(1300)^{-.1} = .533$ (too low!)

Use a fudge-factor to adjust the equation:

$$\frac{We}{Wo} = \left(\frac{.73}{.533}\right) 1.093\, W_o^{-.1} = 1.495\, W_o^{-.1}$$

At $W_o = 1200$ Lb, $We = 883$ Lb

MISSION SEGMENT WEIGHT FRACTIONS

Table 3.2) $\frac{W_1}{W_0} = .97$ $\frac{W_2}{W_1} = .985$

CRUISE: $W/S = (10.2)(.97)(.985) = 9.7$; $q = 35$ LB/FT²

eq 6.13) $$L/D = \frac{1}{\frac{35 \times .02}{9.7} + \frac{9.7}{35 \times \pi \times 6 \times .8}} = 11.04$$

eq 6.12) $$\frac{W_3}{W_2} = e^{\frac{-(2.80 \times 6076)(.5/3600)}{11.04 \times 550 \times 0.8}} = .953$$

Table 3.2) $\frac{W_4}{W_3} = .995$

$$\frac{W_4}{W_0} = .97 \times .985 \times .953 \times .995 = .906$$

eq 3.11) $\frac{W_f}{W_0} = 1.06(1 - .906) = .0997$

$W_f = 1200 \times .0997 = 120$ Lb (total)

$W_{f\,usable} = 120/1.06 = 113$ Lb

INITIAL SIZING (RUBBER ENGINE)

eq 3.4) $$W_o = \frac{220}{1 - .0977 - \frac{We}{Wo}}$$ where $\frac{We}{Wo} = 1.495\, W_o^{-.1}$

```
INPUT  WOdrawn, WEdrawn, We/Wo Exponent:1200,883,-.1
INPUT CREW + PAYLOAD WEIGHT  220

MISSION SEG TYPES
MISSION SEG WT FRACTS    .97   .985   .953   .995

******* SIZING ITERATIONS **********
      WOG        WF        WE        WOCALC
    1200.0     119.6     883.0     1222.6
    1218.1     121.4     895.0     1236.3
    1232.7     122.8     904.6     1247.4
    1244.5     124.0     912.4     1256.4
    1254.0     125.0     918.7     1263.7
    1261.7     125.7     923.8     1269.5
    1268.0     126.4     927.9     1274.2
    1273.0     126.9     931.2     1278.0
    1277.0     127.3     933.9     1281.1
    1280.3     127.6     936.0     1283.6
    1282.9     127.8     937.7     1285.6
    1285.0     128.1     939.1     1287.2
    1286.8     128.2     940.2     1288.5
    1288.1     128.4     941.2     1289.5
    1289.2     128.5     941.9     1290.4
```

BUT THIS HEAVIER W_o WOULD GIVE REDUCED PERFORMANCE WITH A FIXED-SIZE ENGINE!

FIXED-ENGINE SIZING

- Varied $\frac{W_4}{W_0}$ until $W_{o_{calc.}} = W_{o_{drawn}} = 1200$ Lb

```
INPUT  WOdrawn, WEdrawn, We/Wo Exponent:1200,883,-.1
INPUT CREW + PAYLOAD WEIGHT  220

MISSION SEG TYPES
MISSION SEG WT FRACTS   .925

******* SIZING ITERATIONS **********
      WOG          WF          WE         WOCALC
   1200.0         95.4        883.0       1198.4
   1198.7         95.3        882.2       1197.5
   1197.7         95.2        881.5       1196.7
```

- Occurs when $\frac{W_4}{W_0} = .925$
- Solve for W_3/W_2 to determine range:

$$\frac{W_3}{W_2} = \frac{W_4/W_0}{\frac{W_1}{W_0} \times \frac{W_2}{W_1} \times \frac{W_4}{W_3}} = \frac{.925}{(.97)(.985)(.995)} = .973$$

eq 6.12) $\frac{W_3}{W_2} = .973 = e^{\frac{-R\,(.5/3600)}{11.04 \times 550 \times 0.8}}$; $R = 957300$ ft

$R = 158$ nm.

Range of 158 nm. is less than goal of 280 nm. We will lay out design anyway, and use refined sizing methods and optimization techniques to maximize range and performance.

LAYOUT DATA

$W_o = 1200$ Lb $W_e = 883$ Lb $W_f = 120$ Lb (113 Usable)

WING: $S = 118$ Ft^2 $A = 6$ $\lambda = .4$

eq 7.5) $b = 26.6$ ft $= 319.3$ in
eq 7.6) $C_r = 75.6$ in
eq 7.7) $C_t = 30.4$ in
eq 7.8) $\bar{C} = 56$ in
eq 7.9) $\bar{Y} = 68.4$ in

FUSELAGE table 6.3) $L \cong 3.5(1200)^{.23} = 18$ ft
$L_{tail\ arm} \cong 60\%\ L = 10.8$ ft

VERTICAL TAIL eq 6.26) $C_{VT} \cong .04 = \frac{10.8\ S_{VT}}{26.6 \times 118}$; $S_{VT} = 11.6$ ft^2

$A = 1.5$; $\lambda = 0.4$ so $b = 4.1$ ft $C_r = 4.0$ ft $C_t = 1.6$ ft

HORIZONTAL TAIL eq 6.27) $C_{HT} \cong .5 = \frac{10.8\ S_{HT}}{4.7 \times 118}$; $S_{HT} = 25.5$ ft^2

$A = 4.0$; $\lambda = 0.4$ so $b = 10.1$ ft $C_r = 3.6$ ft $C_t = 1.4$ ft

FUEL TANK $W_f = 120$ Lb $= 20$ gallons $= 2.7$ ft^3

TIRE SIZE table 11.1) $D = 11$ in.; $W = 5.3$ in.

PROP DIAMETER eq 10.23) $d = 22\sqrt[4]{150} = 77$ in (?)

Check tip speed: $V = 115$ kts $= 194$ ft/sec
$n = 2700$ rpm $= 45$ rev/sec

eq 10.21 and 10.22) $\sqrt{194^2 + (\pi n d)^2} \leq 850$ ft/sec (Wood Prop.)

so $d \leq 5.85$ ft $= 70$ in

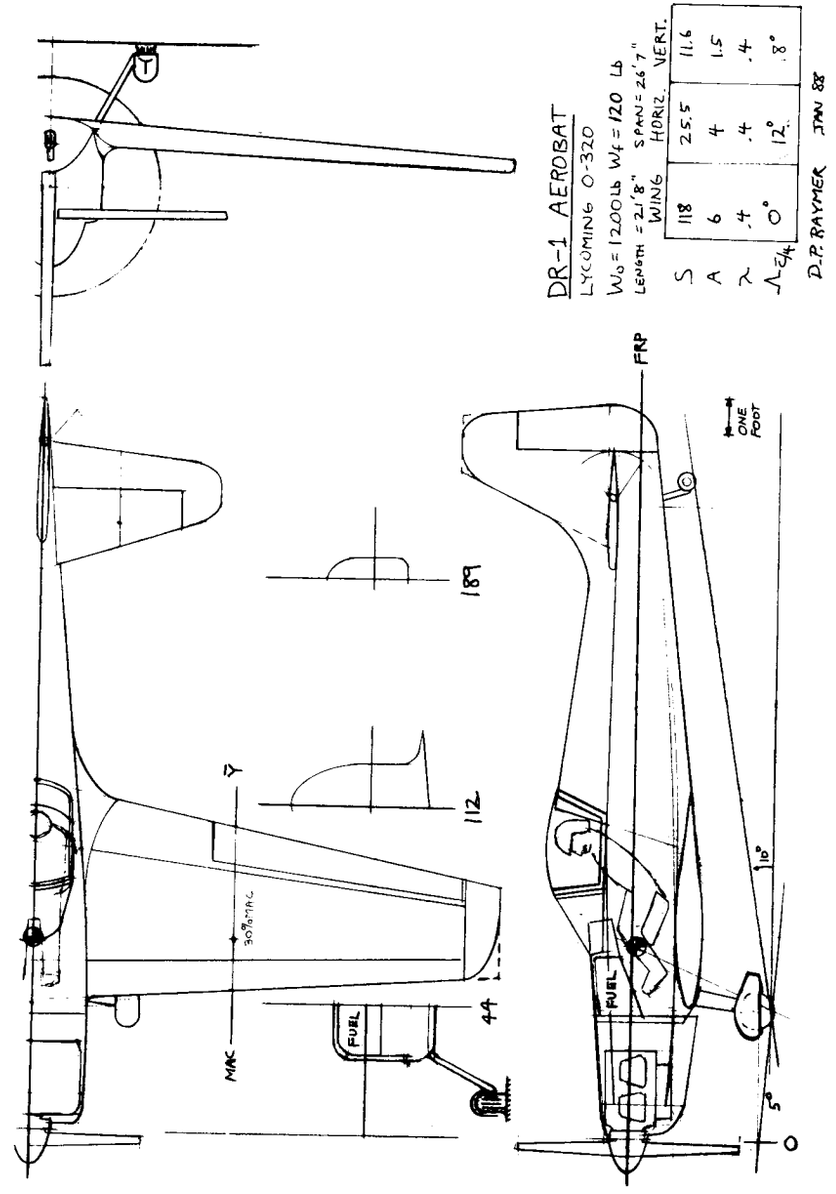

AERODYNAMICS (Wetted and Exposed areas from drawing)

MAXIMUM LIFT: $C_{L_{max}} \cong .9\, C_{\ell_{max}} = (1.35)(0.9) = 1.2$ (eq 12.15)

LIFT CURVE SLOPE:

eq 12.6) $$C_{L_\alpha} = \frac{2\pi \times 6 \times \frac{S_{exp}}{S_{ref}} F}{2 + \sqrt{4 + \frac{6^2}{.95^2}\left(1 + \frac{\tan^2 0}{1}\right)}} = 4.37 \times .837 \times 1.33$$

$C_{L_\alpha} = 4.85$ per radian $= .085$ per degree

PARASITE DRAG (Assuming fully turbulent flow)

Use V = 100 kts = 169 ft/s, h = sea level to determine friction C_f
so M = .15 ; $\mu = 0.37 \times 10^{-6}$

FUSELAGE $\ell = 22$ ft $\quad \ell/d \cong 6.38$

eq 12.26) Reynolds #: R = 23,916,000

eq 12.28) R_{cutoff} = 84,158,000 (using smooth paint)

eq 12.27) $$C_f = \frac{.455}{(\log_{10} 23916{,}000)^{2.58}\left(1 + .144(.15)^2\right)^{.65}} = .0026$$

eq 12.31) $$FF = 1 + \frac{60}{6.38^3} + \frac{6.38}{400} = 1.25$$

$S_{wet} = 164$ ft^2

$$C_{D_{0\,fuselage}} = .0026 \times 1.25 \times 164 / 118 = .0046$$

WING: $\ell = \bar{c} = 4.67$ ft average $t/c = 13.5\%$

eq 12.26) $R = 5 \times 10^6$
eq 12.28) $R_{cutoff} = 16.46 \times 10^6$

eq 12.27) $C_f = .0034$

eq 12.30) $FF = \left[1 + \frac{.6}{.5}(.135) + 100(.135)^4\right]\left[1.34(.15)^{.18}\right] = 1.24$

$S_{wet} = 202.3$ ft^2 $Q \cong 1$ using fillets

$C_{D_{o_{wing}}} = .0034 \times 1.24 \times 202.3/118 = .0071$

TAILS: Since $\bar{c}$'s and t/c's are similar, we can analyze the tails together

$\ell = \bar{c}_{average} = 2.8$ $t/c = 12\%$

$R = 3 \times 10^6$ $R_{cutoff} = 9.6 \times 10^6$

$C_f = .0037$ $S_{wet} = 48.6 + 12 = 60.6$ ft^2

$FF = \left[1 + \frac{.6}{.5}(.12) + 100(.12)^4\right]\left[1.34(.15)^{.18}\right] = 1.20$

$C_{D_{o_{tails}}} = .0037 \times 1.2 \times 60.6/118 = .0023$ (+10% for gaps $\Rightarrow .0025$)

GEAR DRAG: (table 12.4) Tire frontal area $= 1.03$ ft^2; $D/q = 1.03 \times .13 = .134$ ft^2
Strut frontal area $= 0.67$ ft^2; $D/q = 0.67 \times .05 = .033$ ft^2

Add 20% for interference, so $C_{D_{o_{gear}}} = 1.2(.134 + .033)/118 = .0020$

COCKPIT DRAG: (ch 12) Frontal Area $= 1.8$ ft^2; $C_{D_o} = 1.8 \times .5/118 = .0076$ (open cockpit)

TOTAL PARASITE DRAG: $C_{D_o} = 1.05(.0238) = .0250$ (Aero)
(sum plus 5% for leaks & protuberances)

COOLING DRAG:

eq 13.18) $D/q_{cooling} = (4.9 \times 10^{-7})\frac{150(519)^2}{V} = \frac{19.8}{V}$ ft^2

This is for good cowling: triple for light aircraft!

so $C_{D_{o_{cooling}}} \cong .0024$ at $V = 115$ kts (small, so ignore change at other speeds)

MISC. ENGINE DRAG:

eq 13.19) $D/q_{misc} = (2 \times 10^{-4})150 = .03$ ft^2

$C_{D_{o_{misc}}} = .03/118 = .0003$

TOTAL PARASITE AND ENGINE DRAG:

$C_{D_o} = .0250 + .0024 + .0003 = .0277$

INDUCED DRAG:

eq. 12.49) $e = 1.78\left[1 - 0.045(6)^{.68}\right] - 0.64 = 0.87$

$K = \frac{1}{\pi(6)(.87)} = 0.061$

PROPULSION

- Custom-design wooden 2-bladed, fixed-pitch propeller
  D = 70 in

ON-DESIGN:

$$J = \frac{V}{nD} = \frac{115 \times 1.689}{(2700/60)(70/12)} = .74$$

$$C_p = \frac{550(150)}{\rho n^3 D^5} = 0.06$$

From fig. 13.9: $\eta_p = .84$ $\quad \theta_{.75} = 20°$

- But wooden propeller reduces η_p by 10%, while 2-bladed is about 3% better than 3-bladed

data provided by figure 13.9

Thus; $\eta_p = 0.9 \times 1.03 \times (.84) = .78$ (on-design at 115 kts)

OFF-DESIGN: Use figure 13.10 to adjust η_p (see plot)

STATIC THRUST: From fig. 13.8; $C_T/C_p = 2.5$

eq 13.16) $T_{static} = 2.5 \frac{550(150)}{nD} = 786$ Lb (assuming 3-bladed)

- 2-bladed propeller has 5% less static thrust, thus:

$$T_{static} = .95 \times 786 = 747 \text{ Lb}$$

- But this is for a variable pitch propeller, which changes to a flat blade angle at static conditions.
- Instead, assume the static thrust equals the highest forward thrust value found above (see plot)

(Crude assumption - better to use fixed-pitch data!)

THRUST v.s. VELOCITY

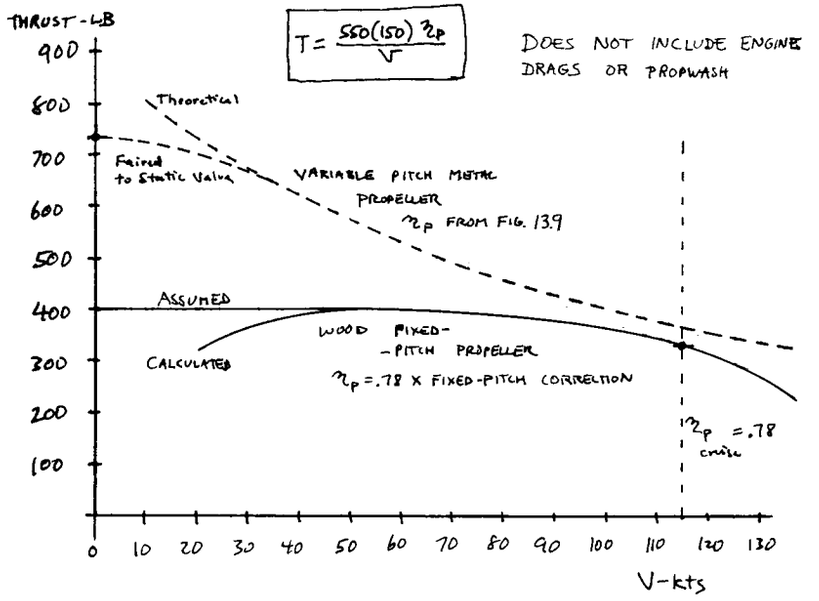

CORRECTION FOR PROPWASH DRAG EFFECT:

Washed Area ≅ 265 ft²

eq 13.17) $$\eta_{P_{effective}} = \eta_p \left[1 - \frac{1.558}{(70/12)^2}(.004)(265)\right] = .95\,\eta_p$$

Thus; $\text{Thrust}_{actual} = .95 \times \text{Thrust}_{\text{calculated above}}$

WEIGHTS

eq 15.46) $W_{wing} = .036(118)^{.758}\left(\frac{6}{\cos 0}\right)^{.6}(45)^{.006}(.4)^{.04}\left(\frac{100(.138)}{\cos 0}\right)^{-.3}(9\times1200)^{.49} = 168$ Lb

eq 15.47) $W_{ht} = .016(9\times1200)^{.414}(45)^{.168}(25.5)^{.896}\left(\frac{100(.12)}{\cos 10}\right)^{-.12}\left(\frac{4}{\cos^2 10}\right)^{.043}(.4)^{-.02} = 20$ Lb

eq 15.48) $W_{vt} = .073(1+.2(0))(9\times1200)^{.376}(45)^{-.122}(166)^{.873}\left(\frac{100(.12)}{\cos 15}\right)^{-.49}\left(\frac{4}{\cos^2 15}\right)^{-.357}$
$\times(.4)^{.039} = 15$ Lb

eq 15.49) $W_{fus} = .052(164)^{1.086}(9\times1200)^{.177}(140)^{-.051}\left(\frac{190}{25}\right)^{-.072}(45)^{.241} = 115$ Lb

eq 15.50) $W_{\substack{main\\gear}} = .095(3\times1200)^{.768}\left(\frac{25}{12}\right)^{.409} = 69$ Lb

eq 15.52) $W_{\substack{installed\\engine}} = 2.575(272)^{.922} = 452$ Lb – This seems too high; table 15.2 gives $W_{\substack{inst.\\eng}} = 1.3(272) = 380$ Lb

eq 15.53) $W_{\substack{fuel\\system}} = 2.49(20)^{.726}\left(\frac{1}{1+0/1}\right)^{.363} = 22$ Lb

eq 15.54) $W_{\substack{flight\\controls}} = .053\left(\frac{190}{12}\right)^{1.536}\left(\frac{26.6}{12}\right)^{.371}(9\times1200\times10^{-4})^{.8} = 5$ Lb

eq 15.56) $W_{electrical} = 12.57(22+W_{av})^{.51} = 73$ Lb
↳ from next equation

eq 15.57) $W_{av} = 2.117\,W_{uav}^{.933} = 2.117(5)^{.933} = 9.5$ Lb
↳ From data in Ref. 11

$W_{furnishings} \cong 20$ Lb (From data in Ref. 11)

WEIGHTS BY OTHER METHODS

CESSNA METHODS (Ref. 11)

$W_{wing} = .047\,W_o^{.397}\,S^{.36}\,n^{.397}\,A^{1.712} = 225$ Lb

$W_{ht} = .055\,W_o^{.887}\,S_h^{.101}\,A_h^{.138}\,t_{root}^{-.223} = 60$ Lb

$W_{vt} = .108\,W_o^{.567}\,S_v^{.125}\,A_v^{.482}\,t_{root}^{-.747}(\cos\Lambda_{c/4})^{-.882} = 17.7$ Lb

Ref 10 METHOD

$W_{\substack{fus\\w/o\ nacelle}} = 200\left[\left(\frac{W_o n}{10^5}\right)^{.286}\left(\frac{L}{10}\right)^{.857}\left(\frac{W+D}{10}\right)\left(\frac{Ve}{100}\right)^{.338}\right]^{1.1} = 114$ Lb

$W_{nacelle} = 2.5\sqrt{H_p} = 31$ Lb

COMPARISON TO ACTUAL DATA (Ref. 11)

$W_{electrical} \cong 40$ Lb

$W_{gear} = \left(\frac{W_{gear}}{W_o}\right)W_o \cong .054(1200) = 64$ Lb
↳ Average of C-180 and L-19A values

WEIGHTS ADJUSTMENTS & BALANCE

As discussed in Chapter 3, fiberglass homebuilts have reduced weight due to design differences, not due to composite construction. Nonetheless, we will use the factors in table 15.4 to estimate the weight savings for each component.

COMPONENT	FUDGE FACTOR	ADJUSTED WEIGHT: Ch 15 / Other Methods	SELECTED WEIGHT	DISTANCE TO DATUM *
FUSELAGE	.90	104 / 128	130 Lb	115 in
WING	.85	143 / 175	160	70
HOR. TAIL	.83	17 / 45	40	210
VERT. TAIL	.83	12 / 13	15	225
ENGINE	—	452 / 380	380	16
GEAR	.95	66 / 57	60	45
FUEL SYS.	—	22	22	50
FL. CONTROLS	—	5	5	80
ELECTRICAL	—	73 / 40	40	40
AVIONICS	—	9.5	10	60
FURNISHINGS	—	20	20	100
		Σ We =	882 Lb @	59.5 in
PILOT & CHUTE			220	85
FUEL (Available, if W_o = 1200 Lb)			98	50
		Σ W_o =	1200 Lb @	63.3 in

MOST-AFT C.G IS NO-FUEL: $W_{e+PILOT}$ = 1102 Lb @ 64.5 in

* Measured from back of spinner - see drawing

STABILITY & CONTROL

$\bar{c}$ = 56 in

MOST-AFT C.G. IS AT 64.5 in } $\bar{X}_{cg} = \frac{64.5}{56} = 1.15$

WING AERO. CENTER AT 62 in so $\bar{X}_{acw} = \frac{62}{56} = 1.107$

eq 12.6) $C_{L_\alpha} = 4.85$ per radian

$C_{m_w} = 0$ (since airfoil is symmetric)

FUSELAGE

eq 16.22) $C_{m_{\alpha_{fus}}} = \frac{(.008)(35^2)(234)}{(56)(118 \times 12^2)} = .002$ per deg.

$= .12$ per rad.

TAIL AERO. CENTER AT 206 in so $\bar{X}_{ach} = \frac{206}{56} = 3.68$

eq 12.6) $C_{L_{\alpha_h}} = 3.77$ per radian

DOWNWASH (fig 16.12)

$r = \frac{144}{319.3/2} = .9$

$m = \frac{28}{319.3/2} = .2$ } $\frac{d\epsilon}{d\alpha} = .38$

eq 16.20) $\frac{d\alpha_h}{d\alpha} = 1 - .38 = .62$

Assume: $\eta_h = q_h/q = .9$ (eq 16.6)

POWER-OFF NEUTRAL POINT (STICK-FIXED)

eq 16.9) $\bar{X}_{np} = \dfrac{(4.85)(1.107) - .12 + .9\left(\frac{11.6}{118}\right)(3.77)(.62)(3.68)}{4.85 + .9\left(\frac{11.6}{118}\right)(3.77)(.62)} = 1.188$

So $X_{np} = 1.188 \times 56 = 66.6$ in. ; which is at 32% of $\bar{c}_{wing}$

STATIC MARGIN $= \dfrac{66.6 - 64.5}{56} = .04$ (ie, 4% STABLE)

eq 16.10) $C_{m_\alpha} = -4.85\left(\dfrac{66.6 - 64.5}{56}\right) = -.182$ (like an F-4 !!)

STICK-FREE (Ch. 16.5) Elevator area $\cong$ 40% of Tail area,

so $C_{L_{\alpha_h}} \cong .8\, C_{L_{\alpha_h}}$ (fixed)

eq 16.9) $\bar{X}_{np} = \dfrac{(4.85)(1.107) - .12 + .8\left[.9\left(\frac{11.6}{118}\right)(3.77)(.62)(3.68)\right]}{4.85 + .8\left[.9\left(\frac{11.6}{118}\right)(3.77)(.62)\right]} = 1.168$

$X_{np} = 1.168 \times 56 = 65.4$ in

STATIC MARGIN $= \dfrac{65.4 - 64.5}{56} = .016$ (1.6% STABLE)

eq 6.10) $C_{m_\alpha} = -4.85\left(\dfrac{65.4 - 64.5}{56}\right) = -.08$ (near-neutral !)

Prop effects will further destabilize ! Must move wing aft in next design iteration.

TRIM ANALYSIS

MOMENTS:

eq 16.7) $C_{m_{cg}} = 0 = 4.85\alpha(1.15 - 1.107) + 0 + 0 + 0.12\alpha - \left[.9\left(\frac{11.6}{118}\right)C_{L_h}(3.68 - 1.15)\right]$

or $C_{m_{cg}} = 0 = .329\alpha - .224\, C_{L_h}$

eq 16.29) $C_{L_h} = C_{L_{\alpha_h}}\left[.62\alpha + (0-0) - \Delta\alpha_{OL}\right]$

↳ due to flap (ie, elevator)

eq 16.14 & 16.15) $\Delta\alpha_{OL} = -\frac{.9}{3.77}(5.3)(.4)(1)\, K_\zeta \delta_e = -.51\,\delta_e$ (small δ_e)

so $C_{m_{cg}} = .329\alpha - .224\left[3.77\right]\left[.62\alpha + .51\,\delta_e\right]$

or $\underline{C_{m_{cg}} = -0.195\alpha - 0.43\,\delta_e}$

LIFT:

eq 16.29 & 16.30) $\underline{C_{L_{total}} = 4.85\alpha + .9\left(\frac{11.6}{118}\right)(3.77)\left[.62\alpha + .51\,\delta_e\right]}$

(Note: α and δ_e in radians !)

TRIM PLOT

Vary α and δe, find C_m and C_L

α	δ_e 0°	-2°	-4°	-6°
0°	0 ; 0	.015 ; -.006	.030 ; -.01	.045 ; -.018
2°	-.007 ; .18	.008 ; .179	.023 ; .170	.038 ; .16
4°	-.014 ; .35	.001 ; .344	.016 ; .34	.031 ; .33
6°	-.021 ; .53	-.006 ; .52	.009 ; .515	.024 ; .51
8°	-.028 ; .71	-.012 ; .70	.002 ; .695	.017 ; .69
10°	-.034 ; .89	-.019 ; .88	-.004 ; .875	.011 ; .87

Values are $\{C_{m_{cg}} ; C_{L_{total}}\}$

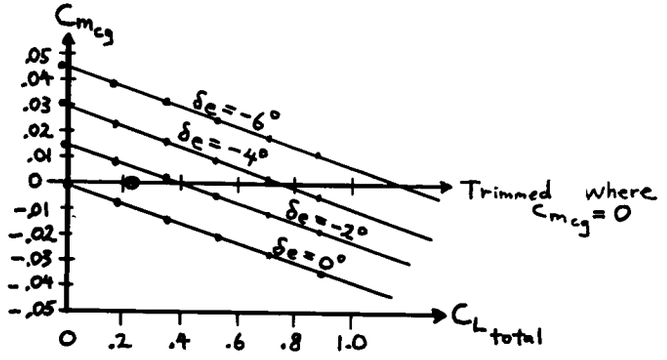

CRUISE TRIM $q = 35$ lb/ft² so $C_L = \frac{W/S}{q} = \frac{9.7}{35} = .278$

At $C_L = .278$ and $C_{m_{cg}} = 0$, $\delta_e \cong -1.2°$ (Circled point above)

TRIM VIA TAIL INCIDENCE ONLY

Required $i_h = -\Delta\alpha_{OL} = -(-.51\,\delta_e) = -(-.51)(-1.2°) = -.61°$

SPIN RECOVERY

(fig 16.30)

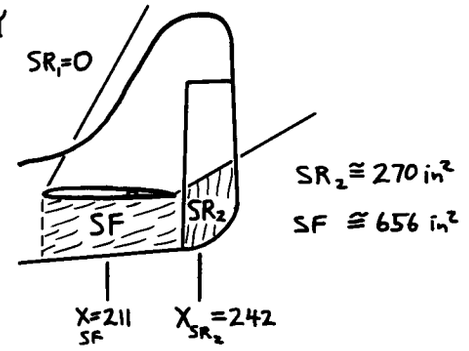

MOST-AFT C.G. AT X = 64.5, so $\begin{cases} L = 211 - 64.5 = 146.5 \text{ in} \\ L_2 = 242 - 64.5 = 177.5 \text{ in} \end{cases}$

eq 16.65) $TDR = \frac{656(146.5)^2}{(118\times12^2)(319.3/2)^2} = 0.0325$

eq 16.66) $URVC = \frac{0 + 270(177.5)}{(118\times12^2)(319.3/2)} = 0.0177$

eq 16.64) $TDPF = .0325 \times .0177 = .00057 = \underline{5.7\times10^{-4}}$ (Actual)

eq 16.49) $I_{xx} \cong (26.6)^2(1200)(.25)^2/4g = 412$ slug-ft²

eq 16.50) $I_{yy} \cong (19.2)^2(1200)(.38)^2/4g = 496$ slug-ft²

eq 16.67) $\mu = \frac{10.2}{(.00238)g(26.6)} = 5.004$

fig 16.31) $\frac{I_{xx} - I_{yy}}{b^2\, W/g} = -31\times10^{-4}$

From fig 16.31 for Rudder-alone recovery, must have $\underline{TDPF > 14\times10^{-4}}$

- SO NO PROBLEM IN UPRIGHT SPIN, AND INVERTED WE HAVE EVEN MORE RUDDER AREA

AS-DRAWN PERFORMANCE

STALL: $V_{Stall} = \sqrt{\frac{2\,W/S}{\rho\, C_{L_{max}}}} = 84.5$ ft/sec $= 50$ kts

TAKEOFF:
from eq 5.8) $TOP = \frac{10.2}{(.99)(1/8)} = 82.4$ Fig 5.4) $S_{TO} \cong 900$ ft

V_{max} and RATE OF CLIMB: Use a graph

HORSEPOWER (AND THRUST) ADJUSTMENT FOR ALTITUDE:

eq 13.9) $bhp = bhp_{SL}\left(\sigma/\sigma_0 - \frac{1-\sigma/\sigma_0}{7.55}\right) = 0.76\, bhp_{SL}$ $(h = 8000$ ft$)$

EQUATIONS: $C_L = \frac{W/S}{q} = \frac{10.2}{q}$

$C_D = 0.0277 + 0.061\, C_L^2$ $\quad D = 118\, q\, C_D$

eq 17.37) $V_V = V\left(\frac{T-D}{W}\right)$; where T is from Thrust graph prepared earlier, times 0.95 for Propwash effect

V_{KTS}	q - Lb/ft² S.L./8000 ft	C_L S.L./8000	C_D S.L./8000	D-Lb SL/8000	V_V - ft/s SL/8000
60	12/9.4	.85/1.09	.07/.10	99/111	23/15
80	22/17	.46/.60	.04/.05	104/100	30/22
100	34/27	.30/.38	.033/.036	132/115	20/18
120	49/38	.21/.27	.030/.032	173/143	9/15
140	67/53	.15/.19	.029/.03	230/187	—

MAXIMUM SPEED

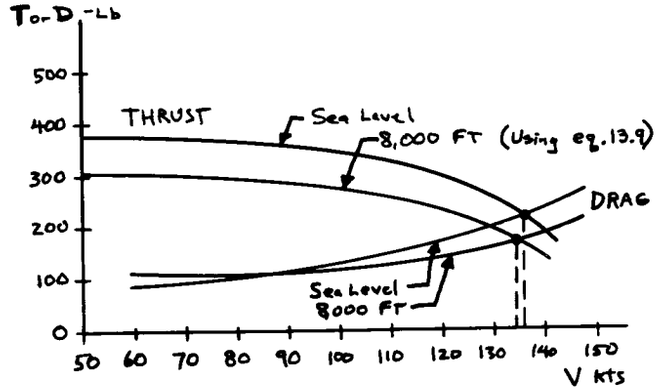

So $V_{max} = 136$ kts @ Sea Level
$= 134$ kts @ 8,000 ft

RATE OF CLIMB

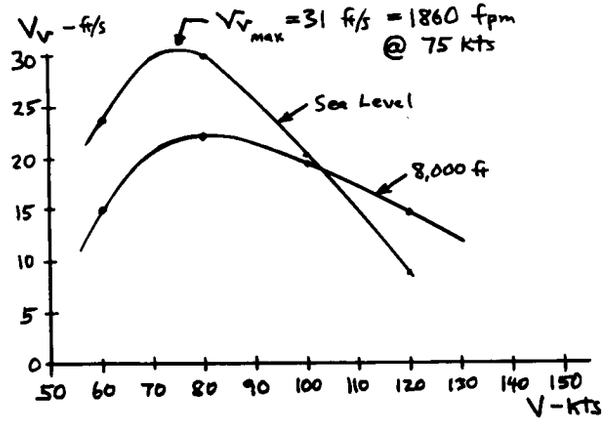

REFINED SIZING

$C_{bhp} = .5$ per hour

$C_{D_0} = .0277$ $\quad e = 0.87$ $\quad T = .95\,T_{(from\ graph)}$ (sea level)

$W_{o_{as\ drawn}} = 1200$ $\quad W_{e_{as\ drawn}} = 883$ Lb $\quad W_{crew} = 220$ Lb

MISSION SEGMENT WEIGHT FRACTIONS

Warmup & Takeoff: Previously-used $\{\frac{W_1}{W_0} = .97\}$ seems excessive compared to cruise fraction $\{\frac{W_3}{W_2} = .953\}$!

Try assuming 5 minutes at maximum power:

$W_f = C_{bhp}(Bhp)(5/60) = .5 \times 150 \times 5/60 = 6.25$ Lb

At $W_0 = 1200$; $\frac{W_1}{W_0} = \frac{1200 - 6.25}{1200} = \underline{.995}$

Use $\frac{W_1}{W_0} = .995$, ignore small change as W_0 changes

Climb & Acceleration: Based on climb chart, climb at 80 kts to 8,000 ft then accelerate to 115 kts for cruise.

eq 19.9) $\Delta h_e = (8000 + \frac{1}{2g}(115 \times 1.689)^2) - (0 + \frac{1}{2g}(80 \times 1.689)^2) = 8302$ ft

equiv. $C = (.5)\frac{80 \times 1.689}{550(.78 \times .95)} = .17$ per hr

From chart; $D/T = 100/360 = .278$ at sea level; $D/T = 105/290 = .362$ at 8,000 ft } Average $D/T = .32$

eq 19.8) $\frac{W_2}{W_1} = e^{\frac{-(.17/3600)(8302)}{(80 \times 1.689)(1 - .32)}} = \underline{.996}$

REFINED SIZING, Cont.

Cruise: 280 nm at 115 kts at 8000 ft, so $q = 35$

$(W/S)_{cruise} = (W/S)_{Takeoff} \times .995 \times .996 = 10.1$

$(L/D)_{cruise} = \frac{1}{\frac{35(.0277)}{10.1} + \frac{10.1}{35\pi(6)(.87)}} = 8.8$

$\frac{W_3}{W_2} = e^{\frac{-(280 \times 6076)(.5/3600)}{(8.8)(550)(.78 \times .95)}} = \underline{.936}$

Descent & Land: Use $\frac{W_4}{W_3} = \underline{.995}$

FUEL FRACTION

$\frac{W_4}{W_0} = .995 \times .996 \times .936 \times .995 = .923$

$\frac{W_f}{W_0} = 1.06(1 - .923) = .0817$

At $W_0 = 1200$ Lb, $W_{f_{required}} = 1200 \times .0817 = 98$ Lb

★ BY PURE LUCK, THIS EQUALS THE AS-DRAWN FUEL AVAILABLE! NORMALLY THE $W_{f_{required}}$ FOR THE DESIGN MISSION IS ABOVE OR BELOW THE $W_{f_{as\text{-}drawn}}$, REQUIRING RESIZING.

W/S - ASPECT RATIO OPTIMIZATION

Since Hp is fixed, we cannot perform Hp/W − W/S optimization. Instead we will optimize W/S and A, holding Range = 280nm.

- Vary W/S ±20%, so W/S = 8.16; 10.2; and 12.24
- Vary A ±33%, so A = 4; 6; and 8

This defines 9 different aircraft, as follows:

A: \ W/S:	8.16	10.2	12.24
4	①	②	③
6	④	⑤	⑥
8	⑦	⑧	⑨

⑤ IS THE AS-DRAWN BASELINE

EFFECTS OF (W/S) AND (A) VARIATIONS

WING AREA: $S_w \propto \left(\frac{1}{W/S}\right)$ {"$\propto$" indicates "proportional to"}

TAIL AREA: $S_{tails} \propto \left(\frac{1}{W/S}\right)^{3/2}$ Holding Volume Coefficient constant

(ignore effect of (A) on tail size since $\propto \sqrt{A}$)

WEIGHTS: eq 15.46) $W_w \propto S_w^{.758} A^{.6}$
eq 15.47) $W_{ht} \propto S_{ht}^{.896}$
eq 15.48) $W_{vt} \propto S_{vt}^{.873}$
} Use these to ratio the selected as-drawn component weights.

AERO:
- eq 12.49 used to recompute (e) for each (A)
- Assume wetted areas vary by wing/tail areas
- Must ratio resulting C_{D_0} to new reference area, where needed.

① $W/S = .8 \times 10.2 = 8.16$ $\quad A = .66 \times 6 = 4$

$S'_{tails} = \left(\frac{1}{.8}\right)^{3/2} S_{tails} = \frac{1}{.72} S_{tails}$

$W_w = 130\left(\frac{1}{.8}\right)^{.758}(.666)^{.6} = 121$ Lb $\quad \Delta = -9$ Lb

$W_{ht} = 40\left(\frac{1}{.72}\right)^{.896} = 54$ Lb $\quad \Delta = 14$ Lb

$W_{vt} = 15\left(\frac{1}{.72}\right)^{.873} = 20$ Lb $\quad \Delta = 5$ Lb

$\Delta = 10$ Lb

So $W_e = 882 + 10 = \underline{892}$ Lb

Wing: $C_{D_{0_w}} = \left(\frac{1}{.8}\right).0092 = .0115$ $\quad \Delta = .0023$

tails: $C_{D_{0_t}} = \left(\frac{1}{.72}\right).0033 = .0045$ $\quad \Delta = .0012$

so $C_{D_0} = .0277 + .0023 + .0012 = .0312$ (ref. to old S_{ref})

$C_{D_0} = .0312(.8) = \underline{.0250}$ (ref. to new S_{ref})

$e = \underline{.93}$ for A = 4

MISSION SEGMENT WEIGHT FRACTIONS:

Cruise: $W/S = 8.16(.995)(.996) = 8.09$

$$L/D = \frac{1}{\frac{35(.0250)}{8.09} + \frac{8.09}{35\pi(4)(.93)}} = 7.8$$

$$\frac{W_3}{W_2} = e^{\frac{-(280 \times 6076)(.5/3600)}{(7.8)(550)(.78 \times .95)}} = \underline{.928}$$

ALL OTHER MISSION SEGMENT WEIGHT FRACTIONS ARE ESSENTIALLY UNCHANGED

① Continued

SIZING : USING SAME METHOD BUT WITH

$We_{as\text{-}drawn} = 892$ and $\frac{W_3}{W_2} = .928$

```
INPUT  WOdrawn, WEdrawn, We/Wo Exponent:1200,892,-.1
INPUT CREW + PAYLOAD WEIGHT  220

MISSION SEG TYPES        1   1   1   1
MISSION SEG WT FRACTS    .995   .996   .928   .995

******* SIZING ITERATIONS **********
        WOG          WF          WE          WOCALC
     1200.0       108.0       892.0       1220.0
     1216.0       109.5       902.7       1232.2
     1229.0       110.6       911.3       1242.0
     1239.4       111.6       918.3       1249.9
     1247.8       112.3       923.9       1256.2
     1254.5       112.9       928.4       1261.4
     1260.0       113.4       932.0       1265.5
     1264.4       113.8       935.0       1268.8
     1267.9       114.1       937.3       1271.4
     1270.7       114.4       939.2       1273.6
     1273.0       114.6       940.7       1275.3
     1274.9       114.8       941.9       1276.7
     1276.3       114.9       942.9       1277.8
     1277.5       115.0       943.7       1278.7
```

SO THE MODIFIED AIRCRAFT WITH $(W/S) = 8.16$ AND ASPECT RATIO $= 4$ MUST BE SIZED UP TO $W_0 = 1278$ LB TO PERFORM THE DESIGN MISSION

② $W/S = 10.2$ $A = .66 \times 6 = 4$

$W_W = 130(.666)^{.6} = 102$ $\Delta = -28$ Lb

No change in tail sizes, so $We = 882 - 28 = \underline{854}$ Lb

No change in wing/tail areas, so $C_{D_0} = .0277$

$e = .93$ for $A = 4$

Cruise: $W/S = 10.1$ (Same as baseline)

$$L/D = \frac{1}{\frac{35(.0277)}{10.1} + \frac{10.1}{35\pi(4)(.93)}} = 8.29$$

$$\frac{W_3}{W_2} = e^{-\frac{(280 \times 6076)(.5/3600)}{(8.29)(550)(.78 \times .95)}} = \underline{.932}$$

```
INPUT  WOdrawn, WEdrawn, We/Wo Exponent:1200,854,-.1
INPUT CREW + PAYLOAD WEIGHT  220

MISSION SEG TYPES        1   1   1   1
MISSION SEG WT FRACTS    .995   .996   .932   .995

******* SIZING ITERATIONS **********
        WOG          WF          WE          WOCALC
     1200.0       103.0       854.0       1177.0
     1181.6       101.4       842.2       1163.7
     1167.2       100.2       833.0       1153.2
     1156.0        99.2       825.8       1145.0
     1147.2        98.5       820.1       1138.6
     1140.3        97.9       815.7       1133.6
     1134.9        97.4       812.2       1129.6
     1130.7        97.1       809.5       1126.5
     1127.4        96.8       807.3       1124.1
     1124.8        96.6       805.7       1122.2
     1122.7        96.4       804.3       1120.7
     1121.1        96.2       803.3       1119.6
     1119.9        96.1       802.5       1118.6
     1118.9        96.1       801.9       1117.9
```

③ $W/S = 1.2 \times 10.2 = 12.24$ $\quad A = .666 \times 6 = 4$

$S'_{tails} = \left(\frac{1}{1.2}\right)^{3/2} S_{tails} = \left(\frac{1}{1.31}\right) S_{tails}$

$W_w = 130\left(\frac{1}{1.2}\right)^{.758}(.666)^{.6} = 89$ Lb $\quad \Delta = -41$ Lb

$W_{ht} = 40\left(\frac{1}{1.31}\right)^{.896} = 31 \quad \Delta = -9$

$W_{vt} = 15\left(\frac{1}{1.31}\right)^{.893} = 12 \quad \Delta = -3$

$\Delta = -53$ Lb

so $W_e = 882 - 53 = \underline{829}$ Lb

Wing: $C_{D_{o_w}} = \left(\frac{1}{1.2}\right).0092 = .0077 \quad \Delta = -.0015$

tails: $C_{D_{o_t}} = \left(\frac{1}{1.31}\right).0033 = .0025 \quad \Delta = -.0008$

so $C_{D_o} = .0277 - .0015 - .0008 = .0254$ (old S_{ref})

$C_{D_o} = .0254\,(1.2) = \underline{.0305}$ (new S_{ref})

$e = .93$ for $A = 4$

Cruise: $W/S = 12.24\,(.995)(.996) = 12.13 \quad L/D = 8.5 \quad \frac{W_3}{W_2} = .934$

```
INPUT  WOdrawn, WEdrawn, We/Wo Exponent:1200,829,-.1
INPUT CREW + PAYLOAD WEIGHT  220

MISSION SEG TYPES        1   1   1   1
MISSION SEG WT FRACTS    .995  .996  .934  .995

******* SIZING ITERATIONS **********
        WOG          WF          WE          WOCALC
      1200.0       100.5       829.0       1149.5
      1159.6        97.1       803.8       1121.0
      1128.7        94.5       784.5       1099.1
      1105.0        92.5       769.7       1082.2
      1086.8        91.0       758.3       1069.3
      1072.8        89.9       749.5       1059.3
      1062.0        89.0       742.7       1051.6
      1053.7        88.3       737.5       1045.7
      1047.3        87.7       733.4       1041.2
      1042.4        87.3       730.3       1037.6
      1038.6        87.0       727.9       1034.9
      1035.7        86.7       726.1       1032.8
      1033.4        86.6       724.7       1031.2
      1031.6        86.4       723.5       1030.0
      1030.3        86.3       722.7       1029.0
```


④ $W/S = .8 \times 10.2 = 8.16 \quad A = 6$

$S'_{tails} = \left(\frac{1}{.72}\right) S_{tails}$

$W_w = 130\left(\frac{1}{.8}\right)^{.758} = 154$ Lb $\quad \Delta = 24$ Lb

$W_{ht} = 40\left(\frac{1}{.72}\right)^{.896} = 54 \quad \Delta = 14$

$W_{vt} = 15\left(\frac{1}{.72}\right)^{.873} = 20 \quad \Delta = 5$

$\Delta = 45$

so $W_e = 882 + 45 = 927$ Lb

$C_{D_o} = .0250$ (same as ①)

$e = .87$ for $A = 6$

Cruise: $W/S = 8.09$ (same as ①) $\quad L/D = 8.18 \quad \frac{W_3}{W_2} = .9316$

```
INPUT  WOdrawn, WEdrawn, We/Wo Exponent:1200,927,-.1
INPUT CREW + PAYLOAD WEIGHT  220

MISSION SEG TYPES        1   1   1   1
MISSION SEG WT FRACTS    .995  .996  .9316  .995

******* SIZING ITERATIONS **********
        WOG          WF          WE          WOCALC
      1200.0       103.5       927.0       1250.5
      1240.4       107.0       955.1       1282.1
      1273.7       109.9       978.1       1308.0
      1301.1       112.2       997.0       1329.3
      1323.6       114.2      1012.5       1346.7
      1342.1       115.8      1025.2       1361.0
      1357.2       117.1      1035.6       1372.7
      1369.6       118.1      1044.1       1382.3
      1379.7       119.0      1051.1       1390.1
      1388.0       119.7      1056.8       1396.5
      1394.8       120.3      1061.4       1401.7
      1400.3       120.8      1065.2       1406.0
      1404.9       121.2      1068.3       1409.5
      1408.5       121.5      1070.8       1412.3
      1411.6       121.8      1072.9       1414.6
      1414.0       122.0      1074.6       1416.5
      1416.0       122.2      1075.9       1418.1
      1417.7       122.3      1077.0       1419.3
      1419.0       122.4      1078.0       1420.4
```

⑤ IS THE BASELINE, SO $W_o = 1200$ Lb.

⑥ $W/S = 1.2 \times 10.2 = 12.24$ $\quad A = 6$

$S'_{tails} = \left(\frac{1}{1.31}\right) S_{tails}$ (Same as ③)

$W_w = 130\left(\frac{1}{1.2}\right)^{.758}$	=	113 Lb	$\Delta = -17$ Lb
W_{ht} = (Same as ③)	=	31	$\Delta = -9$
W_{vt} = " " "	=	12	$\Delta = -3$
			$\Delta = -29$ Lb
			$W_e = 853$ Lb

Cruise: $C_{D_o} = .0305$, $W/S = 12.13$ } (Same as ③)

$L/D = 9.16$ $\quad \frac{W_3}{W_2} = .939$

```
INPUT  WOdrawn, WEdrawn, We/Wo Exponent:1200,853,-.1
INPUT CREW + PAYLOAD WEIGHT  220

MISSION SEG TYPES        1   1   1   1
MISSION SEG WT FRACTS   .995   .996  .939  .995

******* SIZING ITERATIONS **********
      WOG          WF          WE          WOCALC
    1200.0        94.2       853.0        1167.2
    1173.8        92.2       836.2        1148.4
    1153.5        90.6       823.2        1133.8
    1137.7        89.3       813.0        1122.4
    1125.4        88.4       805.2        1113.5
    1115.9        87.6       799.0        1106.6
    1108.5        87.1       794.2        1101.3
    1102.7        86.6       790.5        1097.1
    1098.2        86.2       787.6        1093.9
    1094.7        86.0       785.3        1091.3
    1092.0        85.8       783.6        1089.3
    1089.9        85.6       782.2        1087.8
    1088.2        85.5       781.1        1086.6
    1086.9        85.4       780.3        1085.7
    1085.9        85.3       779.7        1084.9
```


⑦ $W/S = .8 \times 10.2 = 8.16$, $S'_{tails} = \left(\frac{1}{.72}\right) S_{tails}$ } Same as ① $\quad A = 1.333 \times 6 = 8$

$W_w = 130\left(\frac{1}{.8}\right)^{.758}(1.333)^{.6}$	=	183 Lb	$\Delta = 53$ Lb
W_{ht} = (Same as ①)	=	54	$\Delta = 14$
W_{vt} = " " "	=	20	$\Delta = 5$
			$\Delta = 72$ Lb
			$W_e = 954$ Lb

Cruise: $C_{D_o} = .0250$ (Same as ①)

$W/S = 8.09$ $\quad L/D = 8.37$ $\quad \frac{W_3}{W_2} = .933$

```
INPUT  WOdrawn, WEdrawn, We/Wo Exponent:1200,954,-.1
INPUT CREW + PAYLOAD WEIGHT  220

MISSION SEG TYPES        1   1   1   1
MISSION SEG WT FRACTS   .995   .996  .933  .995

******* SIZING ITERATIONS **********
      WOG          WF          WE          WOCALC
    1200.0       101.8       954.0        1275.8
    1260.6       106.9       997.3        1324.2
    1311.4       111.2      1033.4        1364.6
    1354.0       114.8      1063.5        1398.3
    1389.4       117.8      1088.5        1426.4
    1419.0       120.3      1109.3        1449.7
    1443.5       122.4      1126.6        1469.0
    1463.9       124.1      1140.9        1485.0
    1480.8       125.6      1152.8        1498.3
    1494.8       126.8      1162.6        1509.3
    1506.4       127.7      1170.7        1518.4
    1516.0       128.6      1177.4        1526.0
    1524.0       129.2      1182.9        1532.2
    1530.5       129.8      1187.5        1537.3
    1536.0       130.3      1191.3        1541.6
    1540.5       130.6      1194.5        1545.1
    1544.2       130.9      1197.0        1548.0
    1547.2       131.2      1199.2        1550.4
    1549.7       131.4      1200.9        1552.4
    1551.8       131.6      1202.4        1554.0
    1553.6       131.7      1203.6        1555.3
    1555.0       131.9      1204.6        1556.5
```

⑧ $W/S = 10.2$ $A = 1.33 \times 6 = 8$

$W_w = 130(1.333)^{.6} = 155$ $\Delta = 25$

$W_e = 907$

Cruise:

$C_{D_0} = .0277$ } (Same as ⑤)

$W/S = 10.1$ }

$e = .81$ for $A = 8$

$L/D = 9.08$ $\frac{W_3}{W_2} = .938$

```
INPUT  WOdrawn, WEdrawn, We/Wo Exponent:1200,907,-.1
INPUT CREW + PAYLOAD WEIGHT  220

MISSION SEG TYPES        1   1   1   1
MISSION SEG WT FRACTS   .995  .996  .938  .995

******* SIZING ITERATIONS **********
        WOG          WF          WE          WOCALC
     1200.0        95.5       907.0        1222.5
     1218.0        96.9       919.2        1236.2
     1232.5        98.1       929.1        1247.2
     1244.2        99.0       937.0        1256.1
     1253.7        99.8       943.4        1263.2
     1261.3       100.4       948.6        1269.0
     1267.4       100.9       952.7        1273.6
     1272.4       101.2       956.1        1277.3
     1276.3       101.6       958.8        1280.3
     1279.5       101.8       960.9        1282.7
     1282.1       102.0       962.7        1284.7
     1284.2       102.2       964.1        1286.2
     1285.8       102.3       965.2        1287.5
     1287.2       102.4       966.1        1288.5
     1288.2       102.5       966.8        1289.3
```


⑨ $W/S = 1.2 \times 10.2 = 12.24$ $A = 1.333 \times 6 = 8$

$S'_{tails} = \frac{1}{1.31} S_{tails}$

$W_w = 130\left(\frac{1}{1.2}\right)^{.758}(1.333)^{.6} = 135$ Lb $\Delta = 5$ Lb

$W_{ht} =$ (same as ③) $= 31$ $\Delta = -9$

$W_{vt} =$ " " " $= 12$ $\Delta = -3$

$\Delta = -7$

$W_e = 875$

Cruise:

$C_{D_0} = .0305$ } (Same as ③)

$W/S = 12.13$ }

$e = .81$

$L/D = 9.52$ $\frac{W_3}{W_2} = .941$

```
INPUT  WOdrawn, WEdrawn, We/Wo Exponent:1200,875,-.1
INPUT CREW + PAYLOAD WEIGHT  220

MISSION SEG TYPES        1   1   1   1
MISSION SEG WT FRACTS   .995  .996  .941  .995

******* SIZING ITERATIONS **********
        WOG          WF          WE          WOCALC
     1200.0        91.7       875.0        1186.7
     1189.4        90.9       868.0        1178.9
     1181.0        90.3       862.5        1172.8
     1174.5        89.8       858.2        1168.0
     1169.3        89.4       854.8        1164.2
     1165.2        89.1       852.1        1161.2
     1162.0        88.8       850.0        1158.9
     1159.5        88.6       848.4        1157.0
     1157.5        88.5       847.1        1155.5
     1155.9        88.4       846.0        1154.4
     1154.7        88.3       845.2        1153.5
     1153.7        88.2       844.6        1152.8
```

SIZING MATRIX RESULTS (W_o)

A:	W/S: 8.16	10.2	12.24
4	① 1278 Lb	② 1117 Lb	③ 1030 Lb
6	④ 1420 Lb	⑤ 1200 Lb	⑥ 1085 Lb
8	⑦ 1556 Lb	⑧ 1289 Lb	⑨ 1153 Lb

CROSSPLOT AS IN Fig 19.2 TO YIELD THE FOLLOWING:

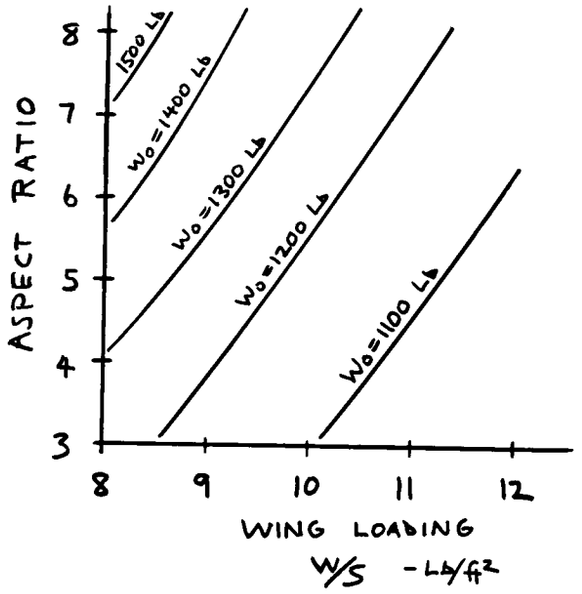

PERFORMANCE CONSTRAINT LINES

STALL: As before, $V_{STALL}=50$ requires $W/S \leq 10.2$

RATE OF CLIMB: $V_v \geq 1500$ ft/min at Sea Level

Assume $V=75$ kts (best R.O.C. for baseline)

so $q=19.1$ $\quad T=360$ Lb (from graph)

$$D = qS\left(C_{D_o} + \frac{(W/S/q)^2}{\pi A e}\right) \qquad V_v = \left(\frac{T-D}{W}\right)V$$

① $W=1278$ Lb $\quad S=1278/8.16=156.6$ ft²

$$D = 156.6 \times 19.1\left(.0250 + \frac{(8.16/19.1)^2}{\pi\, 4\,(.93)}\right) = 122 \text{ Lb}$$

$$V_v = 75 \times 1.689\left(\frac{360-122}{1278}\right) = 23.6 \text{ ft/sec} = 1415 \text{ ft/min}$$

② $W=1117$ Lb $\quad S=1117/10.2=109$ ft²

$$D = 109 \times 19.1\left(.0277 + \frac{(10.2/19.1)^2}{\pi\, 4\,(.93)}\right) = 108.5 \text{ Lb}$$

$$V_v = 75 \times 1.689\left(\frac{360-108.5}{1117}\right) = 28.5 \text{ ft/sec} = 1711 \text{ ft/min}$$

③ $W=1030$ Lb $\quad S=1030/12.24=84.1$

$$D = 84.1 \times 19.1\left(.0305 + \frac{(12.24/19.1)^2}{\pi\, 4\,(.93)}\right) = 105.4 \text{ Lb}$$

$$V_v = 75 \times 1.689\left(\frac{360-105.4}{1030}\right) = 31.3 \text{ ft/sec} = 1878 \text{ ft/min}$$

SIMILARLY:

④ $V_v = 1284$ ft/min
⑤ $V_v = 1636$ ft/min
⑥ $V_v = 1863$ ft/min
⑦ $V_v = 1154$ ft/min
⑧ $V_v = 1529$ ft/min
⑨ $V_v = 1774$ ft/min

MAXIMUM SPEED: $V_{max} \geq 130$ kts at 8,000 ft

- QUICK METHOD: CALCULATE DRAG AT 130 kts, USE TO SHIFT PREVIOUS DRAG CURVE UP OR DOWN, THEN FIND INTERSECTION WITH THRUST CURVE.

①	D = 196 Lb	V_{max} = 130 kts
②	D = 157 Lb	V_{max} = 136 kts
③	D = 139 Lb	V_{max} = 138 kts
④	D = 211 Lb	V_{max} = 127 kts
⑤	D = 163 Lb	V_{max} = 134 kts
⑥	D = 139 Lb	V_{max} = 138 kts
⑦	D = 228 Lb	V_{max} = 125 kts
⑧	D = 172 Lb	V_{max} = 133 kts
⑨	D = 145 Lb	V_{max} = 137 kts

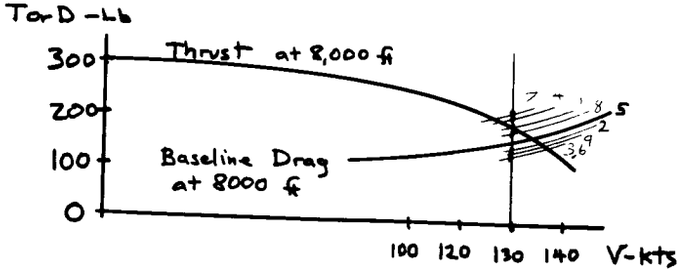

CROSSPLOTTING THE STALL, RATE-OF-CLIMB, AND V_{max} REQUIREMENTS ONTO THE SIZING GRAPH GIVES NO LOWER LIMIT ON ASPECT RATIO! AT VERY LOW ASPECT RATIOS, THE INDUCED DRAG WOULD BECOME EXCESSIVE DURING MANEUVERS. THEREFORE, WE NEED SOME REQUIREMENT BASED ON MANEUVERING.

DEFINE A NEW PERFORMANCE REQUIREMENT BASED ON SUSTAINED TURN:

$\dot{\psi} \geq 30$ °/sec SUSTAINED, AT 100 kts, S.L.

eq 17.50) $\dot{\psi} = 30\,°/sec = .5236$ rad/sec $= \dfrac{g\sqrt{n^2-1}}{100 \times 1.689}$

so $n \geq 2.92$

T = 345 Lb, from graph

eq 17.52) $n = \sqrt{\dfrac{3\pi AE}{W/S}\left(\dfrac{345}{W} - \dfrac{3}{W/S}C_{D_0}\right)}$

Check if we are close to stall (which reduces e):

$C_L = \dfrac{nW/S}{q_0} = .88$ for baseline
$= 1.056$ for $W/S = 12,24$

} Prior e estimates should be approximately correct.

USING PRIOR DATA:

①	n = 2.8		
②	n = 2.9	⑥	n = 3.3
③	n = 2.8	⑦	n = 3.2
④	n = 3.1	⑧	n = 3.4
⑤	n = 3.3	⑨	n = 3.5

NOTE: Large values of n are incorrect because they imply $C_L > C_{L_{stall}}$. However, we can use those values to crossplot for n = 2.92 which is below stall.

AIRCRAFT DESIGN

SIZING GRAPH WITH CONSTRAINTS

USING THE METHODS OF CHAPTER 19, WE CROSSPLOT THE CONSTRAINT DATA AS SHOWN:

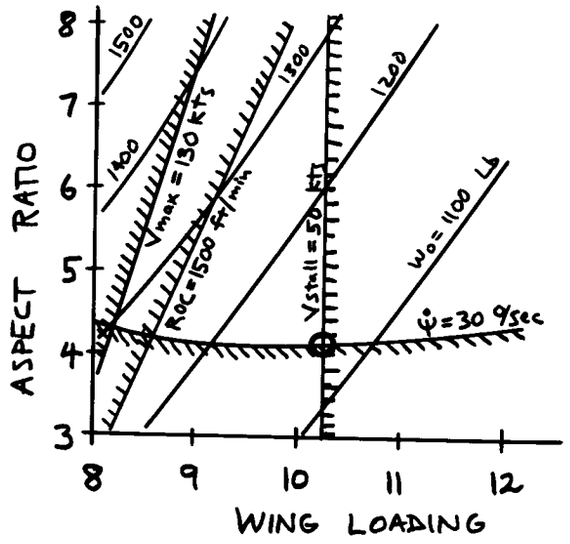

SO THE OPTIMAL AIRCRAFT FOR THE GIVEN REQUIREMENTS OCCURS AT {W/S = 10.2} AND {A = 4.2} AND HAS W_o = 1130 LB. THE NEXT STEP IN THE DESIGN PROCESS IS TO REDRAW THE AIRCRAFT AND ANALYZE IT IN DETAIL FOR STRUCTURES.

A Conceptual Approach

21.3 Lightweight Supercruise Fighter

The U.S. Air Force currently operates the F-15 and F-16 as a "high-low" mix of dogfighters. The F-15 has greater range, avionics, and weaponry but is too costly to fill the entire inventory requirement. The F-16, with less capability and cost, rounds out the total required dogfighter inventory and also serves in an air-to-ground role.

The U.S. Air Force is developing the Advanced Tactical Fighter (ATF) as a replacement for the F-15. The next fighter after ATF is then likely to be a replacement for the F-16, which is almost as old as the F-15. This new fighter would be the "low" end of a "high-low" mix with ATF.

This design example presents such an F-16 follow-on design. Design requirements are based upon assumed improvements to published F-16 capabilities, with the addition of a required capability for sustained supersonic cruise ("supercruise") on dry power. Also, relatively short takeoff and landing requirements are imposed.

The selected design incorporates one unproven technology, the variable dihedral vertical tail. This patented concept purports to control the rearward shift in aerodynamic center as the aircraft accelerates to supersonic flight by converting from a "V" tail subsonically to upright vertical tails supersonically. This should reduce trim drag and enhance maneuverability.

Such a technology study is very common in early conceptual design. As will be seen, the impact of such a technology on aerodynamics, weights, propulsion, etc., is estimated as best as possible, and the aircraft is sized and optimized. The resulting aircraft is then compared to a baseline design that doesn't incorporate the new technology to determine if the new idea should be pursued.

(Homebuilders: don't build this one either!)

DR-3 LIGHTWEIGHT SUPERCRUISE FIGHTER

- F-16 REPLACEMENT ; POST-2000 TIME FRAME
- SINGLE - SEAT ; SINGLE -ENGINE (NEW, ie, "RUBBER")

PRIMARY MISSION : AIR-TO-AIR

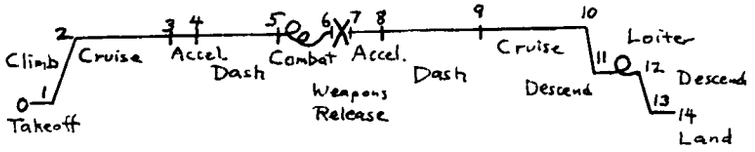

3&10 (Cruise): 200 nm at Best Cruise Mach and Altitude (BCA/BCM)
5&9 (Dash) : 50 nm at M1.4 at 35,000 ft.
6 (Combat): 3 min at Maximum Thrust, M0.9 at 20,000 ft
12 (Loiter): 20 min at Sea Level, Best Loiter Speed
7 (Weapons Release): 400 Lb (Missiles only)

PAYLOAD : 2 ADVANCED MISSILES (200 Lb, 5in x92in)
ADVANCED GUN (400 Lb), 750 ROUNDS AMMO (440 Lb)
PILOT (220 LB)

PERFORMANCE REQUIREMENTS

- TAKEOFF AND LANDING: 1,000 ft GROUND ROLL
- APPROACH SPEED ≤ 130 kts
- MAXIMUM MACH ≥ 1.8 (A/B) ; ≥ M1.4 (Dry)
- ACCELERATE M0.9 to M1.4 in 30 sec at 35,000 ft.
- $P_S = 0$ at 5g at 30,000 ft. at M0.9 and M1.4
- $\dot{\psi} \geq 20°/sec$ at 350 kts at 20,000 ft.

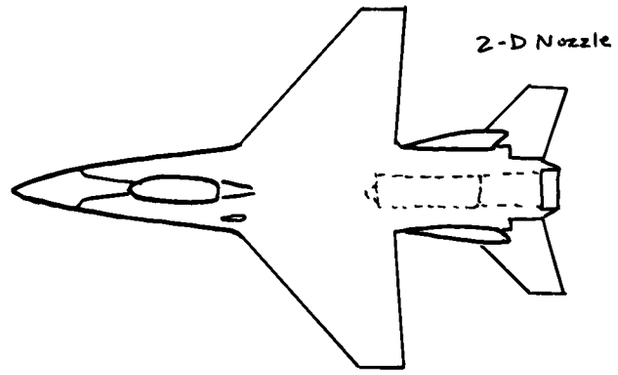

Sketch 1 - CONVENTIONAL CONCEPT
DPR 1/15/88

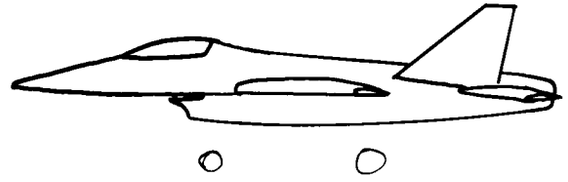

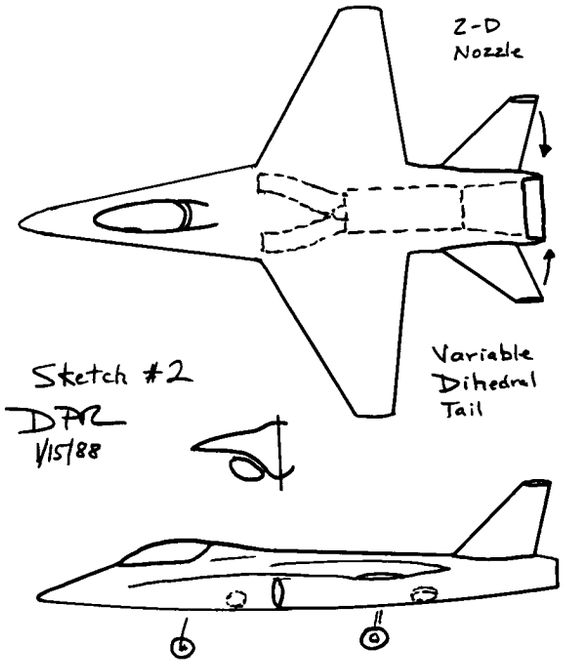

Sketch #2
DPR
1/15/88

WING GEOMETRY

$A = 5.416\,(1.8)^{-.622} = 3.8$

$\Lambda_{LE} = 48^\circ \quad (\Lambda_{c/4} \cong 40^\circ)$

} CHECK V.S. FIG. INDICATES TRANSONIC PITCHUP ! CHANGE TO: $\{A = 3.5,\ \Lambda_{c/4} = 30^\circ\}$ (so $\Lambda_{LE} \cong 40^\circ$)

SELECT: $\lambda = 0.25$

$t/c = 6\%$

Airfoil: 64A006 (Initially)

ENGINE : POST-2000 "RUBBER" ENGINE, APPROXIMATE WITH APPEN. A.4-1 ENGINE WITH 20% SFC REDUCTION.

T/W

table 5.3) $T/W_{takeoff} = 0.648\,(1.8)^{.594} = .92$ (Use Initially)

W/S

Stall: $V_{approach} \leq 130$ KTS $= 220$ ft/sec

$V_{stall} \leq V_{approach}/1.2 = 183$ ft/sec

$W/S \leq q_0 C_{L_{max}}$ at stall

fig 5.3) $C_{L_{max}} \cong 1.5 + .3$ (L.E. FLAP) $\cong 1.8$

so $W/S \leq 72$ Lb/ft^2 (at Sea Level)

W/S (continued)

Landing:

from eq $S_{\substack{\text{landing}\\ \text{ground}\\ \text{roll}}} = 80\frac{W}{S}\left(\frac{1}{\sigma C_{L_{max}}}\right) \leq 1{,}000$

so $W/S \leq 22.5$ (!)

(MUCH TOO LOW FOR A FIGHTER! WE WILL IGNORE THIS INITIALLY AND USE THRUST REVERSING TO LAND.)

Takeoff:

fig 5.4) TOP ≅ 80

eq 5.9) $W/S = TOP\left(\frac{C_{L_{max}}}{1.21}\right)T/W = 80\left(\frac{1.8}{1.21}\right)(.92) = 109$

Cruise: table 12.2) $C_{f_e} = .0035$

assume $S_{wet}/S_{ref} \cong 4$, so $C_{D_o} \cong .014$ (eq 12.23)

eq 12.50) $e = 4.61\left(1-.045(3.5)^{.68}\right)(\cos 40°) - 3.1 = 0.86$

At M.9 and 35,000 ft (assumed BCM/BCA), $q = 284$ lb/ft²

so

$$(W/S)_{\substack{\text{opt.}\\ \text{cruise}}} = 284\sqrt{\frac{\pi \times 3.5 \times 0.86 \times 0.014}{3}} = 59.6$$

$$(W/S)_{takeoff} \cong \frac{59.6}{.97 \times .977} = 62.9$$

(Using typical values for $\frac{W_1}{W_0}$ and $\frac{W_2}{W_1}$)

W/S (continued)

Instantaneous Turn: At 350 kts and 20,000 ft, $q = 222$ lb/ft²

$$\dot{\psi} = \frac{20}{57.3} \geq \frac{32.2\sqrt{n^2-1}}{350 \times 1.689}\ ;\ \text{so}\ n \geq 6.5\ g\text{'s}\ \left(= q C_L/(W/S)\right)$$

Assume $C_{L_{\substack{max\\ maneuver}}} \cong 1.4$

then $(W/S)_{combat} = \frac{222 \times 1.4}{6.5} = 48$

$(W/S)_{takeoff} \cong 48/.85 = \underline{56}$

Sustained Turn: At M.9 and 30,000 ft; V = 895 ft/s; $q = 357$ lb/ft²

$C_{D_o} = .014$; assume $e = .6$ (reduced during high-g turns)

$(T/W)_{combat} = 0.92\left(\frac{1}{.85}\right)\left(\frac{16000}{30000}\right) = .58$

↑ Actual and S.L.S. values from A.4-1

↑ Typical (W_{combat}/W_0)

$$(W/S)_{combat} = \left[.58 + \sqrt{.58^2 - \frac{4 \times 5^2 \times .014}{\pi \times 3.5 \times .6}}\right] \Big/ \left[\frac{2 \times 5^2}{357 \times \pi \times 3.5 \times .6}\right] = 44$$

$(W/S)_{takeoff} = 44/.85 = 52$

Question: What T/W could permit use of W/S = 56

$(W/S)_{combat} = .85 \times 56 = 48$

eq. 5.24) $(T/W)_{combat} = \frac{357 \times .014}{48} + 48\left(\frac{5^2}{357 \times \pi \times 3.5 \times .6}\right) = .614$

$(T/W)_{takeoff} = .614(.85)\left(\frac{30000}{16000}\right) = \underline{.98}$ (Use This)

INITIAL SIZING

Empty Weight Fraction: (Assume composite structure)

table 6.1) $\frac{We}{Wo} = \left[-.02 + 2.16\, W_o^{-.1} \times 3.5^{.2} \times .98^{.04} \times 56^{-.1} \times 1.8^{.08}\right] \times 0.9$

$$\frac{We}{Wo} = 1.75\, W_o^{-.1} - .018$$

Mission Segment Weight Fractions:

Warmup & Takeoff: eq 6.8) $\frac{W_1}{W_0} = .98$

Climb: eq 6.9) $\frac{W_2}{W_1} = 1.0065 - .0325(.9) = .977$

Cruise: (Assume M.9 at 35,000 ft. for BCA/BCM)
V = 876 ft/sec ; q = 283 Lb/ft²

$$W/S = 56 \times .98 \times .977 = 54$$

eq 6.13) $$L/D = \frac{1}{\frac{283 \times .014}{54} + \frac{54}{283\pi \times 3.5 \times .86}} = 10.7$$

SFC:
- A.4-1, Partial Power at M.9 ; 36,000 ft gives: C = 1.07
- Increase this 10% to approximate installation: C = 1.18
- Reduce this 20% for advanced technology: C = 0.94

so;

eq 6.11) $$\frac{W_3}{W_2} = e^{-\frac{(200 \times 6076)(.94/3600)}{876 \times 10.7}} = .967$$

Acceleration:

eq 6.10) $\left(\frac{W_4}{W_3}\right)_{M.1 \to 1.4} = .9616$

eq 6.9) $\left(\frac{W_4}{W_3}\right)_{M.1 \to .9} = .9773$

$$\left(\frac{W_4}{W_3}\right)_{M.9 \to 1.4} = \frac{.9616}{.9773} = .984$$

Dash: M1.4 at 35,000 ft. ; V = 1362 ft/sec ; q = 685 Lb/ft²

$$W/S = 56 \times .98 \times .977 \times .967 \times .984 = 51$$

Looking at fig. 12.31, we roughly estimate;

$$(C_{D_o})_{M1.4} \cong 2 \times (C_{D_o})_{subsonic} = .028 \quad \text{(crude !)}$$

eq 12.52) $$(K)_{M1.4} \cong \left(\frac{3.5\,(1.4^2 - 1)}{4 \times 3.5\sqrt{1.4^2 - 1} - 2}\right)\cos 40^\circ = .22$$

or $$e = \frac{1}{\pi A K} = .414$$

$$L/D = \frac{1}{\frac{685 \times .028}{51} + \frac{51 \times .22}{685}} = 2.55 \quad (!)$$

SFC:
A.4-1, Military (Max. Dry) Power — C = 1.2
Increase 10% (Installation)
Reduce 20% (Advanced Technology) — C = 1.06

eq 6.11) $$\frac{W_5}{W_4} = e^{-\frac{(50 \times 6076)(1.06/3600)}{1362 \times 2.55}} = .975$$

Combat d = 3 min.

$$(T/W)_{combat} = .98 \times \left(\frac{16000}{30000}\right) \Big/ (.98 \times .977 \times .967 \times .984 \times .975) = .588$$

SFC: A.4-1 for Max. thrust at M.9 at 20,000 ft : C = 1.78
Increase 10% for installation
Reduce 20% for advanced technology } C = 1.57

$$\frac{W_6}{W_5} = 1 - [(1.57/3600)(.588)(3 \times 60)] = .954$$

Weight Drop: Ignore for initial sizing

Accelerate: $\frac{W_8}{W_7} \cong \frac{W_4}{W_3} = .984$

Dash: $\frac{W_9}{W_8} \cong \frac{W_5}{W_4} = .975$

Cruise: $\frac{W_{10}}{W_9} \cong \frac{W_3}{W_2} = .967$

Descent: Ignore, assuming range credit

Loiter: E = 20 min ; Sea Level

$$(W/S)_{loiter} = 56 \times .98 \times .977 \times .967 \times .984 \times .975 \times .954 \times .984 \times .975 \times .967 = 44$$

eq 17.13) $$V_{best\ loiter} = \sqrt{\frac{2 \times 44}{\rho}} \sqrt{\frac{1}{.014 \times \pi \times 3.5 \times .86}} = 319 \text{ ft/sec}$$

so $q = 121 \text{ lb/ft}^2$

$$L/D = \frac{1}{\frac{121 \times .014}{44} + \frac{44}{121 \pi \times 3.5 \times .86}} = 13$$

SFC: Adjusted from A.4-1 : C = .906

$$\frac{W_{12}}{W_{11}} = e^{-\frac{(20 \times 60)(.906/3600)}{13}} = .977$$

Descent for Landing: $\frac{W_{13}}{W_{12}} = .993$

Land: $\frac{W_{14}}{W_{13}} = .995$ (eq 6.23)

TOTAL MISSION WEIGHT FRACTION

$$\frac{W_{14}}{W_0} = .98 \times .977 \times .967 \times .984 \times .975 \times .954 \times .984 \times .975 \times .967 \times .977 \times .993 \times .995 = .7586$$

FUEL FRACTION

$$\frac{W_f}{W_0} = 1.06(1 - .7586) = .256$$

SIZING

Need to adjust Empty Weight equation for impact of variable dihedral tails. Assume $\Delta We = 200$ Lb at initial guess $W_0 = 20{,}000$.

Then $We = \left[\left[1.75\,(20{,}000)^{-.1} - .018\right]20{,}000\right] + 200 = 12{,}841$ Lb

At other W_0 guess values, use;

eq 19.13) $We = 12841\left[\frac{W_0}{20000}\right]^{.9}$

SIZING ITERATIONS

$W_{crew+payload} = 220 + (2\times200) + 400 + 440 = 1460$ Lb

***** SIZING ITERATIONS **********

WOG	WF	WE	WOCALC
20000.0	5117.7	12841.0	19418.7
19534.9	4998.7	12572.0	19030.6
19131.5	4895.4	12338.0	18693.5
18781.1	4805.8	12134.5	18400.2
18476.4	4727.8	11957.1	18145.0
18211.3	4660.0	11802.6	17922.6
17980.3	4600.9	11667.8	17728.7
17779.0	4549.4	11550.2	17559.5
17603.4	4504.4	11447.5	17411.9
17450.2	4465.2	11357.8	17283.0
17316.4	4431.0	11279.4	17170.4
17199.6	4401.1	11210.8	17071.9
17097.4	4375.0	11150.9	16985.9
17008.2	4352.1	11098.5	16910.6
16930.1	4332.1	11052.6	16844.8
16861.9	4314.7	11012.5	16787.2
16802.1	4299.4	10977.4	16736.8
16749.9	4286.0	10946.7	16692.7
16704.1	4274.3	10919.8	16654.1
16664.1	4264.1	10896.2	16620.3
16629.0	4255.1	10875.6	16590.7
16598.4	4247.3	10857.5	16564.8
16571.5	4240.4	10841.7	16542.1
16548.0	4234.4	10827.8	16522.2
16527.4	4229.1	10815.7	16504.8
16509.3	4224.5	10805.1	16489.5
16493.5	4220.4	10795.8	16476.2
16479.6	4216.9	10787.6	16464.5

LAYOUT DATA

$W_0 \cong 16480$ Lb. $\quad W_f = .256 \times W_0 \cong 4220$ Lb $= 94$ ft^3

Fuselage: table 6.3) $L \cong .93\,(16480)^{.39} = 41$ ft $= 492$ in

Wing: $S = 16480/56 = 294$ ft^2

$A = 3.5 \qquad \lambda = 0.25 \qquad \Lambda_{c/4} = 30^\circ$

eq 7.5) $b = \sqrt{3.5 \times 294} = 32$ ft $= 384$ in

eq 7.6) $C_{root} = \frac{2 \times 294}{32\,(1+.25)} = 14.7$ ft $= 176$ in

eq 7.7) $C_{tip} = 176 \times .25 = 44$ in

eq 7.8) $\bar{c} = 123$ in

eq 7.9) $\bar{y} = 76.8$ in

Tails: (see ch.4) Lay out "V" tail such that the total tail area equals the sum of the required vertical and horizontal tail areas determined by the volume coefficient method. (Assume $L_t \cong 200$ in)

Vertical Tail: $S_{vt} = .07\frac{b_w S_w}{L_t} = 39$ ft^2

Horizontal Tail: $S_{ht} = .4\frac{\bar{c}_w S_w}{L_t} = 72$ ft^2

} Sum $= 111$ ft^2

- If the tails met at the aircraft centerline, $\Gamma_t = \tan^{-1}\left(\frac{39}{72}\right) = 28.4^\circ$
- We will lay out the projected planform for top view as a horizontal equivalent, using $\Gamma_t = 28.4^\circ$ and $S_{t_{true}} = 111$ ft^2.

$(S_{ht})_{projected} = 111\cos 28 = 97.6$ ft^2

Using $A = 3.5$; $\lambda = .25$; $\Lambda_{c/4} = 30^\circ$

} $b_h = 18.5$ ft $= 222$ in; $C_{root} = 8.4$ ft $= 101$ in; $C_{tip} = 25.3$ in

- True tail geometry will be graphically determined.

ENGINE: $T=(T/W)W_0 = .98 \times 16480 = 16150.4$ Lb (SLS)

A.4-1 ; 100%-Sized Engine: $T = 30{,}000$ Lb
$L = 160$ in
$D = 44$ in
$W = 3{,}000$ Lb

So Scale Factor: $SF = \frac{16150.4}{30{,}000} = .538$

$L = 160\,(.538)^{.4} = 125$ in
$D = 44\,(.538)^{.5} = 32$ in
$W = 3000\,(.538)^{1.1} = 1517$ Lb
} Engine with conventional nozzle

TO PROVIDE PITCH CONTROL AT SUPERSONIC SPEEDS (WHEN THE TAILS ARE NEAR-VERTICAL), WE WILL USE A TWO-DIMENSIONAL VECTORING NOZZLE WITH THRUST REVERSING TO SHORTEN THE LANDING. THIS REQUIRES A CIRCLE-TO-SQUARE ADAPTER WHICH LENGTHENS THE ENGINE.

CAPTURE AREA SIZING

From A.4-1 at M1.8 at 30,000 ft, $\dot{m} = 270$ Lbm/s (mass flow)
Scale by Scale Factor: $\dot{m} = .538 \times 270 = 145.3$ Lbm/s

Fig 10.13) $A_c/\dot{m} = 3.8$ at M1.8, so $A_c = 3.8 \times 145.3 = \underline{552\ in^2}$

LANDING GEAR $W_w \cong .9 \times \frac{16480}{2} = 7416$

MAIN: $D = 1.59\,(7416)^{.302} = 23$ in
$W = .098\,(7416)^{.467} = 6.3$ in

NOSE: $D = 18$ in, $W = 5$ in } 80% of main gear

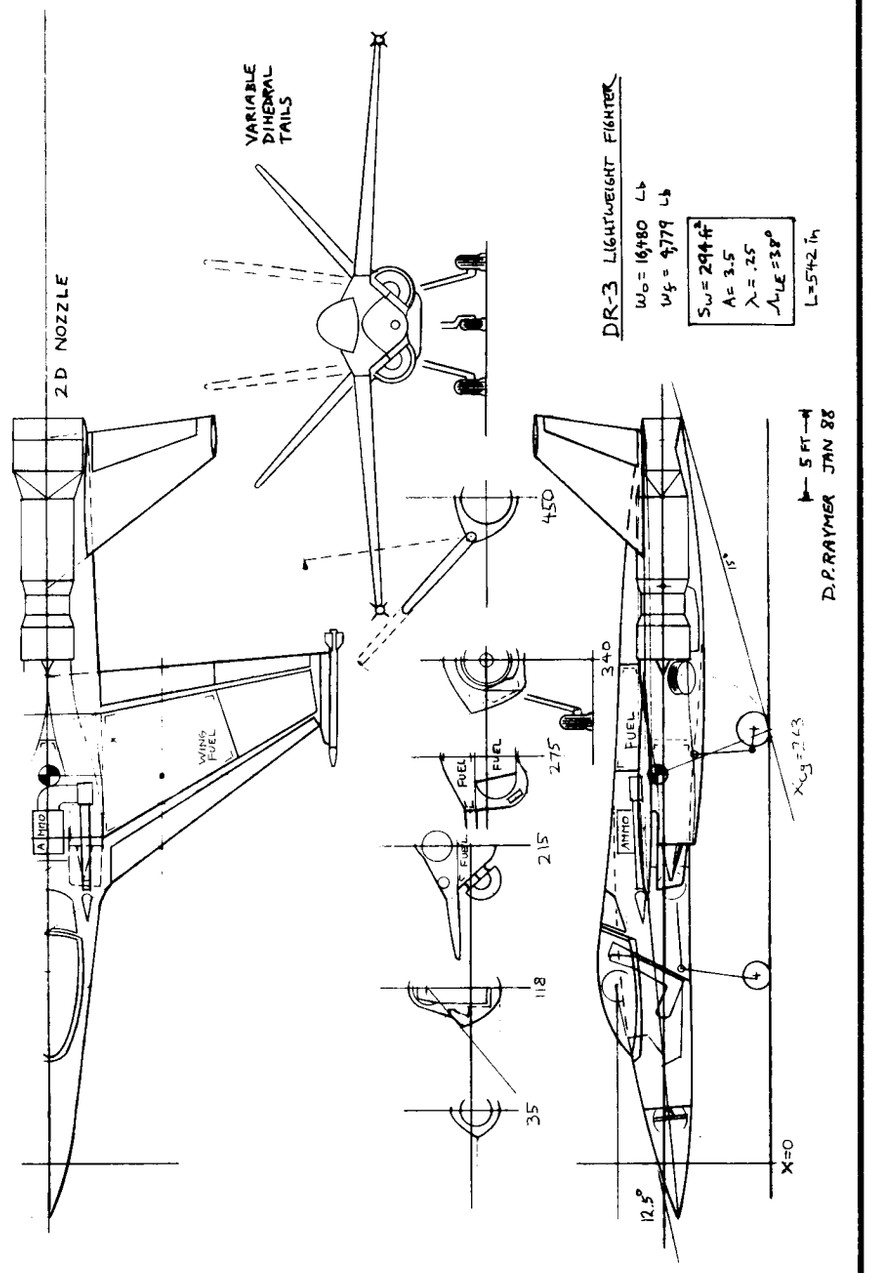

FUEL TANKS

Required: $W_f = .256 \times 16480 \cong 4220$ Lb

Assume: Integral wing tanks (85% Usable Volume)

Bladder fuselage tanks (83% Usable Volume)

Volumes Measured from Drawing:

WING { Total: 61 ft³ at X = 275 in
Usable: 61 x .85 = 52 ft³ = 2334 Lb

FORWARD FUSELAGE { Total: 38 ft³ at X = 240 in
Usable: 38 x .83 = 28 ft³ = 1257 Lb

AFT FUSELAGE { Total: 32 ft³ at X = 295 in
Usable: 32 x .83 = 26.5 ft³ = 1189 Lb

Fuel C.G. (desire near aircraft $X_{cg} = 265$ in)

Wing	2334	@	275 in
Fwd fus.	1257	@	240 in
Aft fus.	1189	@	295 in
Total:	4780 Lb	@	271 in

Too much! Too far aft!

Reduce fuel in Aft fuselage tank:

Wing	2334 Lb	@	275 in
Fwd fus.	1257	@	240 in
Aft fus.	629	@	295 in
Total:	4220 Lb	@	267 in

(Good!)

AERO DATA FROM DRAWING

Wetted Areas:

Wing: $A_{exp} = 215$ ft²; $S_{wet} = 215(1.977 + (.52 \times .06)) = 432$ ft²

Tails: $A_{exp} = 90$ ft²; $S_{wet} = 90(1.977 + (.52 \times .06)) = 181$ ft²

Fuselage Wetted Area Plot:

Perimeters measured from drawing:

X	Perimeter	Notes
-37	0 (in)	
35	114	Canopy starts at X=73
118	184 *	Wing starts at X = 185
215	174 (222 with inlet)	
275	216	Canopy ends at X = 240
340	212	Wing ends at X = 370
450	164	
505	150	

(* 125 not including canopy)

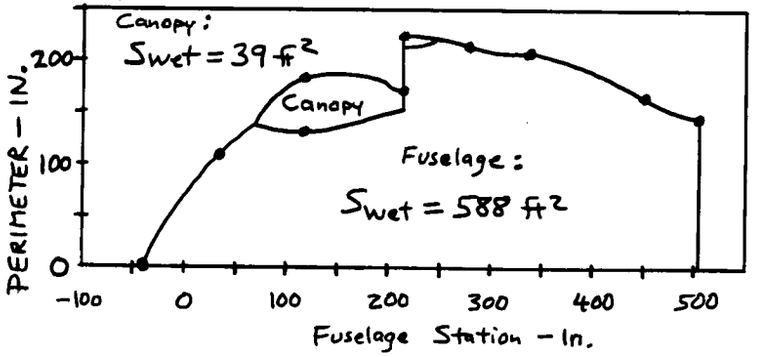

DESIGN ANALYSIS

From the design layout, the aircraft was analyzed using the methods presented in this book. The author-prepared computer code 'RDS' was used, which automates the number-crunching of these methods. RDS is available from AIAA along with this textbook, and the RDS program disk includes the complete DR-3 sample design files as described below.

Lift and Drag

Drag analysis was based upon fully turbulent flow over camouflage paint. Areas and geometric information for wings, tails, fuselage, canopy, and boundary-layer diverter were determined from the drawing and input as shown on the next page. Fuselage and canopy equivalent diameters were determined from maximum cross-section areas. D/q for the missile was input based upon the AIM-9 data in fig. 12.22, and a cannon port D/q of 0.2 was input as a constant value from zero to Mach 2. Leakage and protuberance drag of six percent was assumed.

For wave drag analysis, the maximum total cross section area was estimated at 20.9 square feet, less 3.83 for capture area, or a net of 17.07 square feet. As this is intended to be a supersonic-cruise aircraft and was designed with low wave drag in mind, an Ewd of 2.0 was assumed.

Maximum lift was estimated by adjusting the airfoil maximum lift for the effects of the assumed automatic leading- and trailing-edge maneuver flaps. For a 64-series airfoil, Cl-max is about 0.82, and from table 12.1, delta-Y is about 1.28. Using table 12.2 the lift adjustment for trailing-edge plain flaps is about 0.9, and for leading-edge flaps, about 0.3. With hinge line angles of 10 and 39 degrees, equation 12.21 gives a delta CL-max of about 0.82, so as a first approximation, the wing was analyzed using an adjusted airfoil Cl-max of 1.64.

For landing, a historical CL-max value of 1.8 was used.

The following pages include a sample of the parasite drag calculation for one altitude and velocity, the total parasite drag as a function of speed and altitude, the parameters determined for calculation of drag-due-to-lift factor ('K'), a plot of K versus speed and lift coefficient, and drag polars and L/D ratios for the DR-3.

AERODYNAMIC INPUTS

AIRCRAFT TYPE : SUPERSONIC, THIN WING

KEY AERODYNAMIC DATA

Max V or M#	=	2.000
Max Altitude	=	50000.000
% Laminar	=	0.000
k/10^5 (ft)	=	3.330
%Leak&Protub	=	6.000
Amax-aircrft	=	17.070
length-eff	=	45.200
Ewd	=	2.000
CL-cruise	=	0.210

WING

# Comonts	=	1.000
Sref-wing	=	294.000
Sexp-wing	=	215.000
A true	=	3.500
A effective	=	3.500
Lambda=Ct/Cr	=	0.250
Sweep-LE	=	38.000
t/c average	=	0.060
Delta Y	=	1.280
Q (interfer)	=	1.000
CL-design	=	0.400
CLmx-airfoil	=	1.640
Drag Fudge	=	1.000

HORIZONTAL TAIL

# Comonts	=	1.000
S-tail	=	92.000
Sexp-tail	=	92.000
A true	=	4.000
A effective	=	4.000
Lambda=Ct/Cr	=	0.340
Sweep-LE	=	30.000
t/c average	=	0.060
Delta Y	=	1.280
Q (interfer)	=	1.000
Drag Fudge	=	1.000

FUSELAGE

# Comonts	=	1.000
Swet	=	588.000
length	=	45.200
diam-effctiv	=	5.500
Q (interfer)	=	1.000
Upsweep-deg	=	0.000
Abase	=	0.000
Drag Fudge	=	1.000

SMOOTH CANOPY or BLISTER or FAIRING

# Componts	=	1.000
Swet	=	39.000
length	=	13.900
diam-effctiv	=	2.000
Q (interfer)	=	1.000
Drag Fudge	=	1.000

BOUNDARY LAYER DIVERTER

# Componts	=	1.000
# Wedges	=	2.000
l	=	4.200
d	=	2.830
width	=	0.330
Drag Fudge	=	1.000

MISC D/q v.s. MACH #

Mach Number	D/q
0.000	0.120
0.980	0.120
1.100	0.270
1.200	0.290
2.000	0.300
0.000	0.000
0.000	0.000
0.000	0.000
0.000	0.000
0.000	0.000
0.000	0.000

MISC D/q v.s. MACH #

Mach Number	D/q
0.000	0.200
2.000	0.200
0.000	0.000
0.000	0.000
0.000	0.000
0.000	0.000
0.000	0.000
0.000	0.000
0.000	0.000
0.000	0.000
0.000	0.000

ALTITUDE = 0 VELOCITY OR MACH = 1.4

	R#	Cf -flat plate	FF	Q	Fudge	S-wet	Cdo-component
WING	39.696 million	20.678 counts	1.000	1.000	1.000	431.8	32.190 counts
HORZ TAIL	19.333 million	23.044 counts	1.000	1.000	1.000	184.8	15.350 counts
FUSBLAGE	189.132 million	16.586 counts	1.000	1.000	1.000	588.0	35.163 counts
		Base drag =	0.000	counts	Upsweep drag =	0.000	counts
CNPY/FAIR	54.638 million	19.735 counts	1.000	1.000	1.000	39.0	2.775 counts
BL DIVRTR	15.495 million	23.847 counts	1.000	1.000	1.000	2.8	0.238 counts
D/q vs M				10.546 counts			
D/q vs M				7.211 counts			

Drag rise or Wave Drag coeff. Cdw = 126.949 counts
TOTAL PARASITE DRAG COEFFICIENT Cdo = 230.422 counts

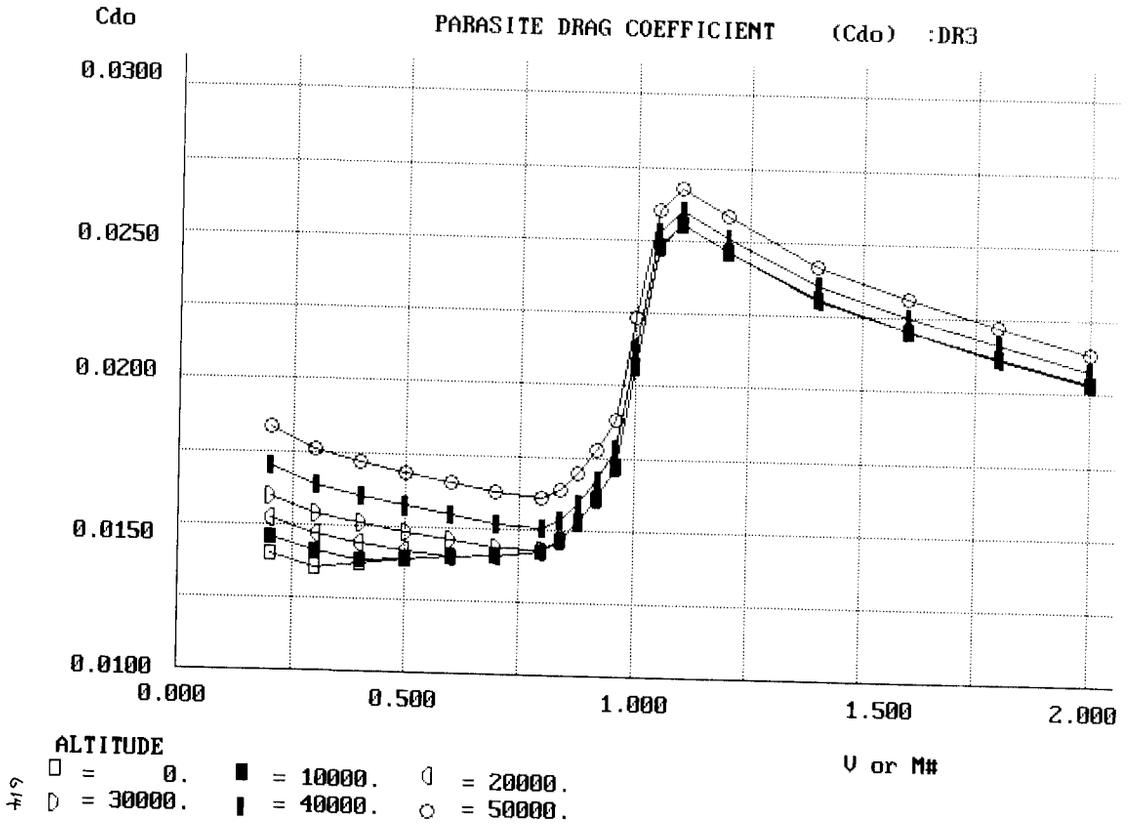

DRAG-DUE-TO-LIFT (K) FACTOR CALCULATION

Aspect Ratio =	3.50
Effective Aspect Ratio =	3.50
Leading edge sweep =	38.00
Sweep of max t/c line =	23.67
Fuselage lift factor F =	1.47
Sexposed/Sref =	0.73
K-100% = 1/PIxAspect Ratio =	0.09
M# for Sonic leading edge =	1.27
CLmax at Mach 0.2 =	1.79

Lift Coeff.	% Suction
0.1500	0.6100
0.2500	0.8100
0.3500	0.9400
0.4500	0.9400
0.5500	0.8700
0.6500	0.7200
0.8000	0.5100
1.0000	0.3300
1.2000	0.2400
1.4000	0.0000

Mach number	CL-ALPHA	1/CL-ALPHA
0.2000	3.6717	0.2724
0.3000	3.7163	0.2691
0.4000	3.7821	0.2644
0.5000	3.8729	0.2582
0.6000	3.9951	0.2503
0.7000	4.1587	0.2405
0.8000	4.3809	0.2283
0.8400	4.4925	0.2226
0.8800	4.6215	0.2164
0.9200	4.7722	0.2095
0.9600	4.9507	0.2020
1.0000	5.9154	0.1690
1.0500	6.1744	0.1620
1.1000	5.7853	0.1729
1.2000	5.2005	0.1923
1.4000	4.1591	0.2404
1.6000	3.3519	0.2983
1.8000	2.8183	0.3548
2.0000	2.4413	0.4096
2.2000	2.1628	0.4624

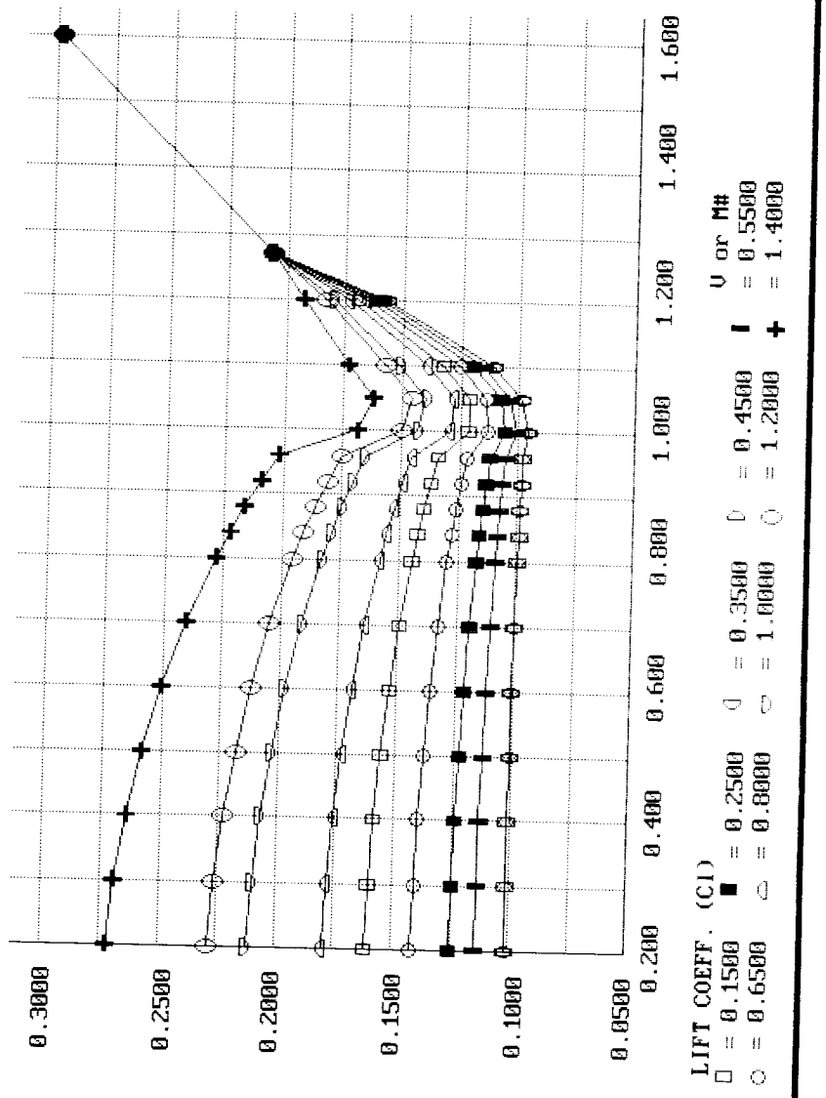
INDUCED DRAG FACTOR (K) :DR3
K
0.3000
0.2500
0.2000
0.1500
0.1000
0.0500
0.200
0.400
0.600
0.800
1.000
1.200
1.400
1.600
LIFT COEFF. (CL)
□ = 0.1500 ■ = 0.2500 ◁ = 0.3500 ▷ = 0.4500 ▮ = 0.5500
○ = 0.6500 ⬭ = 0.8000 ⬭ = 1.0000 ◯ = 1.2000 ✚ = 1.4000
V or M#

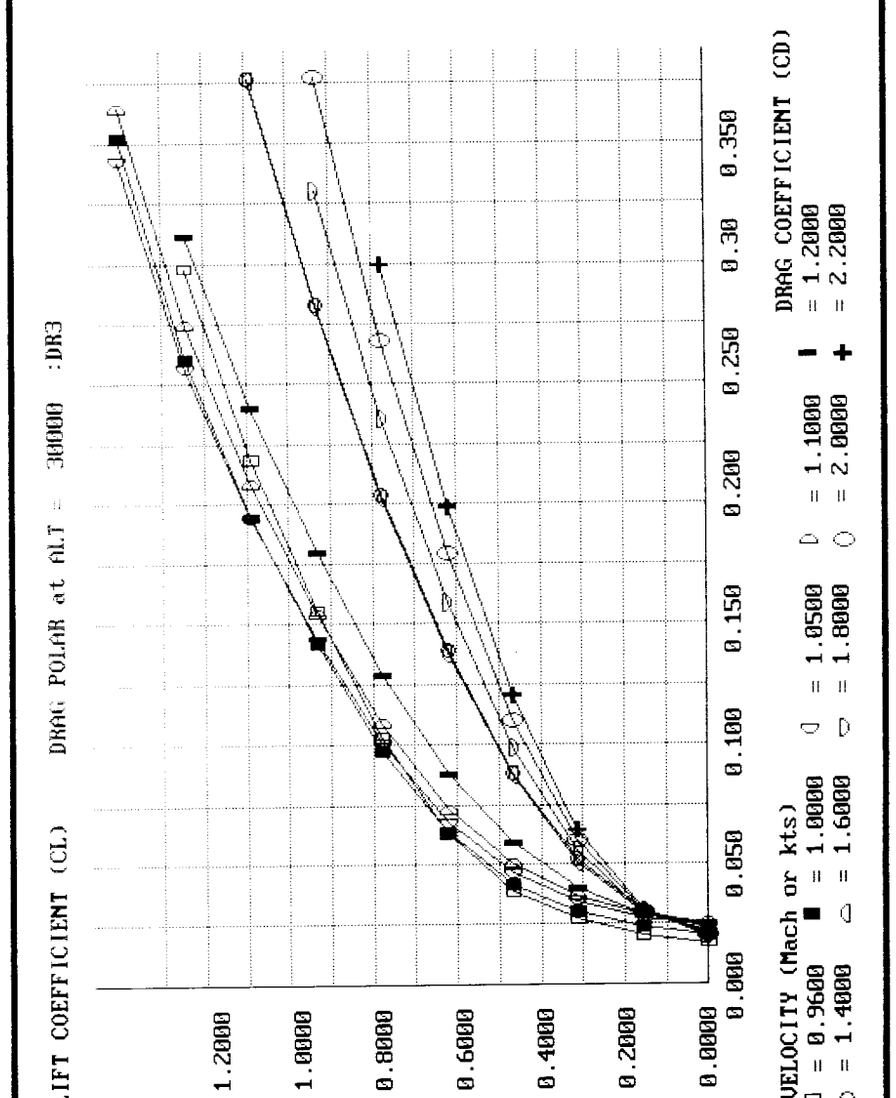
LIFT COEFFICIENT (CL) DRAG POLAR at ALT = 30000 :DR3
1.2000
1.0000
0.8000
0.6000
0.4000
0.2000
0.0000
0.000
0.050
0.100
0.150
0.200
0.250
0.30
0.350
DRAG COEFFICIENT (CD)
VELOCITY (Mach or kts)
□ = 0.9600 ■ = 1.0000 ◁ = 1.0500 ▷ = 1.1000 ▮ = 1.2000
○ = 1.4000 ⬭ = 1.6000 ⬭ = 1.8000 ◯ = 2.0000 ✚ = 2.2000

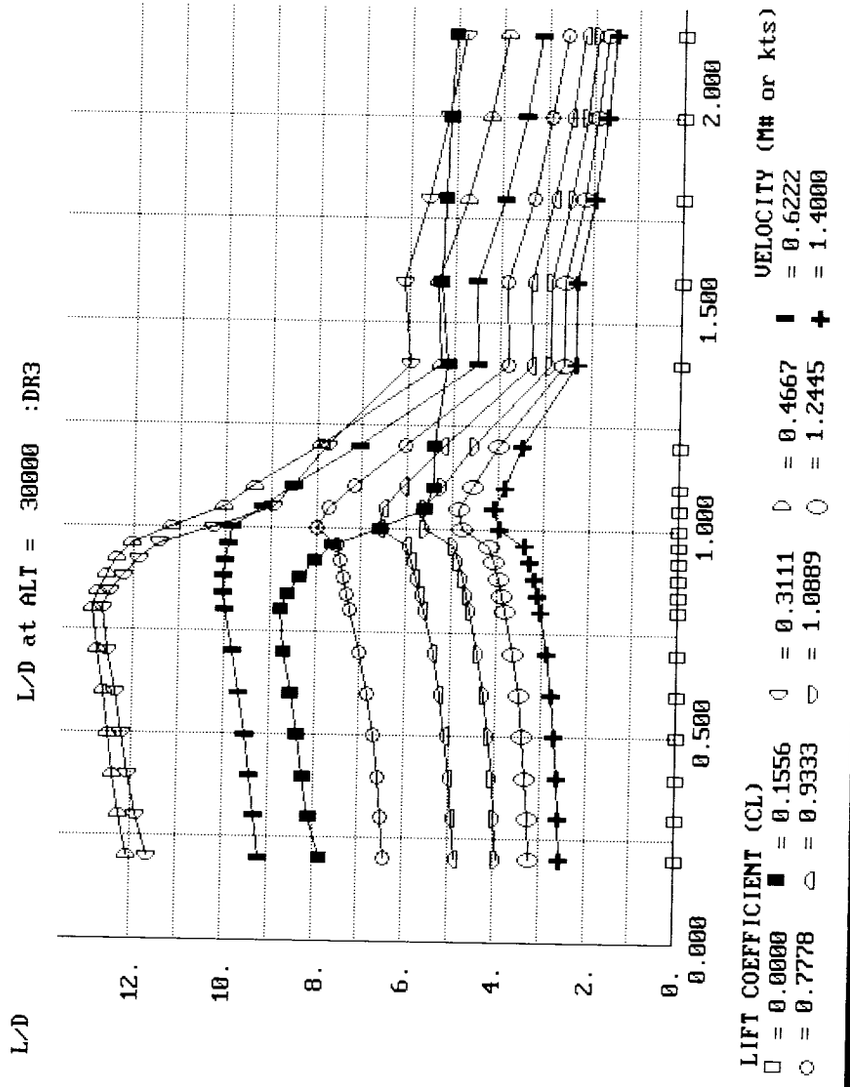

ADDITIONAL DRAGS FOR TAKEOFF AND LANDING

FLAPS: (Only used for landing)

- Assume $\delta_{flap} = 60°$; from drawing $\left\{\frac{\text{flap span}}{\text{wing span}} = .43\right\}$
- Assume aileron used as flap also with $\delta_a = 30°$ from drawing $\left\{\frac{\text{aileron span}}{\text{wing span}} = .35\right\}$

eq 12.37) $\Delta C_{D_0} = .0023\left((.43 \times 60) + (.35 \times 30)\right) = .0835$

LANDING GEAR: (Using values from table 12.4)

	Frontal Area	× Table 12.4 factor	= D/q
Main Wheels:	2.1 ft²	.25	.53
Main Struts:	5.8 ft²	.30	1.74
Nose Wheel:	.7 ft²	.25	.18
Nose Strut:	3.2 ft²	.30	.96
		Subtotal	3.41

Increase 20% for interference
Increase 7% for open wheelwells
} $D/q = 4.38$

$$\Delta C_{D_{0_{gear}}} = \frac{4.38}{294} = .0149$$

Weights

Weights analysis was based upon the fighter equations in chapter 15, with adjustments for composite material usage as in table 15.4. The as-drawn takeoff weight of 16,480 lb. was used throughout, with ultimate load factor of Nz=7.33x1.5, or 11. Required dimensions and areas, such as the control surface area for the wing, were measured from the drawing.

The V-tail was analyzed as a "horizontal" tail using the true area and aspect ratio of the surface (90 sq. ft., and 11). A 200 lb. weight penalty for the variable dihedral mechanism was added as a part of the miscellaneous empty weight.

For the landing gear, it was assumed that landing weight equals takeoff weight, and gear load factor was assumed to be 4.

For engine cooling it was assumed that a shroud covers the entire engine, so the shroud length is 14 ft. Engine control length was estimated from the drawing as 18.3 ft. To allow for the extra weight of the 2-D vectoring nozzle, an additional 400 lb. was added to the misc. empty weight.

In the absence of better data, installed avionics weight of 990 lb. was guessed using table 11.6. However, the RDS program requires uninstalled avionics weight which it uses to estimate installed avionics weight, so equation 15.21 was used to back out an uninstalled weight of 727 lb.!

The gun was assumed to always stay with the aircraft and so was treated as an addition to the misc. empty weight of 400 lbs.

The following pages provide the complete weights assumptions and inputs, followed by the resulting summary weights statement. The empty weight for the as-drawn takeoff weight of 16,480 lbs. was determined to be 10947.2 lbs., somewhat above the preliminary prediction of 10788 used for initial sizing.

WEIGHTS INPUTS

AIRCRAFT TYPE : FIGHTER/ATTACK

KEY AIRCRAFT DATA		(Nz(ult) = 1.5 x Nz(design limit))
Wdg	=	16480.000
Nz (ultimate)	=	11.000
Sw	=	294.000
M	=	1.800
Nen	=	1.000
WING		
X-Location	=	280.000
Kdw	=	1.000
Kvs	=	1.000
A	=	3.500
t/c	=	0.060
lambda=Ct/Cr	=	0.250
sweep c/4	=	30.000
Scsw	=	72.000
Fudge Factor	=	0.850
HORIZONTAL TAIL		
X-Location	=	470.000
Fw	=	4.700
Ah	=	6.500
Sht	=	90.000
Fudge Factor	=	0.830
VERTICAL TAIL		
X-Location	=	0.000
Krht	=	0.000
Ht/Hv	=	0.000
Svt	=	0.000
Lt	=	0.000
Sr	=	0.000
A(vt)	=	0.000
tail lambda	=	0.000
tail sweep	=	0.000
# vert tails	=	0.000
Fudge Factor	=	0.000

FUSELAGE

X-Location	=	260.000
Kdwf	=	1.000
L	=	39.000
D	=	4.000
W	=	5.400
Fudge Factor	=	0.900

LANDING GEAR

X-Location	=	285.000
Kcb	=	1.000
Ktpg	=	1.000
Wl	=	16480.000
Nl	=	4.000
Lm (in)	=	46.000
Ln (in)	=	52.000
Nnw	=	1.000
NoseGear Loc	=	155.000
Fudge Factor	=	0.950

NACELLE

X-Location	=	400.000
T per engine	=	16150.400
Sfw	=	52.000
Wen	=	1517.000
Kvg (inlet)	=	1.000
Ld	=	10.700
Kd	=	1.310
Ls	=	2.000
De	=	2.700
Inlet X-Loc	=	270.000
Fudge Factor	=	0.900

ENGINE INSTALLATION

X-Location	=	400.000
Ltp	=	0.000
Lsh	=	14.000
Lec	=	18.300
Wt-Oil	=	50.000
Fudge Factor	=	0.000

FUEL SYSTEM

X-Location	=	267.000
Vt	=	703.300
Vi	=	389.000
Vp	=	314.300
Nt	=	3.000
SFC (max T)	=	1.900
Fudge Factor	=	0.000

CONTROLS & INSTRUMENTS

X-Location	=	260.000
Scs	=	94.000
Ns	=	4.000
Nc	=	1.000
Nci	=	1.000
Fudge Factor	=	0.000

HYDRAULICS & ELECTRICS

X-Location	=	260.000
Kvsh	=	1.000
Nu	=	10.000
Kmc	=	1.450
Rkva	=	120.000
La	=	25.000
Ngen	=	1.000
Fudge Factor	=	0.000

AIR CONDITIONING & FURNISHINGS

X-Location	=	100.000
(no inputs)	=	0.000
Fudge Factor	=	0.000

LOADS; MISC WT; & AVIONICS

Wuav	=	727.000
-Location	=	120.000
Wcrew	=	220.000
-Location	=	120.000
Wcargo	=	840.000
-Location	=	260.000
Wpassengers	=	0.000
-Location	=	0.000
Wmisc(empty)	=	1000.000
-Location	=	382.000
Wmisc(load)	=	0.000
-Location	=	0.000

```
------ FIGHTER/ATTACK GROUP WEIGHT STATEMENT : FILE   DR3.DWT ------
STRUCTURES GROUP :    4526.2          EQUIPMENT GROUP     :    3066.7
  Wing           :    1459.4            Flight Controls   :     655.7
  Horiz. Tail    :     280.4            Instruments       :     122.8
  Vert. Tail     :       0.0            Hydraulics        :     171.7
  Fuselage       :    1574.0            Electrical        :     713.2
  Main Lndg Gear :     631.5            Avionics          :     989.8
  Nose Lndg Gear :     171.1            Furnishings       :     217.6
  Engine Mounts  :      39.1            Air Conditioning  :     190.7
  Firewall       :      58.8            Handling Gear     :       5.3
  Engine Section :      21.0          MISC EMPTY WEIGHT   :    1000.0
  Air Induction  :     291.1          TOTAL WEIGHT EMPTY  :   10947.2

PROPULSION GROUP :    2354.3          USEFUL LOAD GROUP   :    5532.8
  Engine(s)      :    1517.0            Crew              :     220.0
  Tailpipe       :       0.0            Fuel              :    4422.8
  Engine Cooling :     172.0            Oil               :      50.0
  Oil Cooling    :      37.8            Cargo             :     840.0
  Engine Controls:      20.0            Passengers        :       0.0
  Starter        :      39.5            Misc Useful Load  :       0.0
  Fuel System    :     568.0          DESIGN GROSS WEIGHT:   16480.0

EMPTY CG= 285.3 LOADED-NO FUEL CG= 281.0 GROSS WT CG= 277.2
```


Propulsion

The DR-3 uses the engine in appendix A.4-1, with an assumed reduction in SFC of 20 percent due to advanced technology. The uninstalled engine, which already includes reasonable allowances for the installation effects of bleed and power extraction, was loaded into data arrays for maximum afterburning thrust and SFC, and maximum dry power thrust and SFC. Then installation values for inlet recovery, inlet drag, and nozzle drag were input and used to calculate installed thrust and SFC throughout the flight envelope.

Following are the input assumptions, analysis calculations, and graphs of the installed thrust and SFC.

INLET RECOVERY

- A.4-1 incorporates $\{P_1/P_o = .97\}$ subsonic, and $\{.97\}$ times the recovery schedule of Mil E 5008B for supersonic operation. Our inlet is F-104-like, but we assume advanced technology and auxiliary intakes to improve performance at lower speeds.

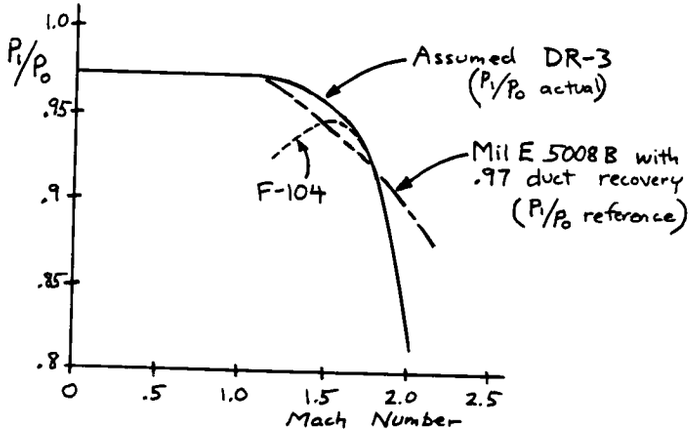

INLET DRAG (fig. 13.6, axisymmetric inlet)

$A_c = 552\ in^2 = 3.83\ ft^2$
$S_{ref} = 294\ ft^2$
$\Big\}\ D_{inlet} = 3.83\, q_o \left(\frac{D/q}{A_c}\right)$ fig. 13.6

PROPULSION INPUTS

AIRCRAFT TYPE : JET PROPELLED

KEY PROPULSION DATA

SLS Thrust	=	16150.400
SFC Fudge	=	0.800
Acapture	=	3.830
C-bleed	=	0.000
bleed ratio	=	0.000
Nozzle Cd	=	0.015
Amax-fuslage	=	16.900

Mach Number	P1/PoREF	Mach Number	Ram Factor
0.400	1.000	0.400	1.350
0.600	1.000	0.600	1.350
0.800	1.000	0.800	1.350
1.000	0.970	1.000	1.350
1.200	0.962	1.200	1.320
1.400	0.949	1.400	1.290
1.600	0.933	1.600	1.260
1.800	0.916	1.800	1.230
2.000	0.897	2.000	1.200
2.200	0.877	2.200	1.170
2.400	0.855	2.400	1.140

Mach Number	P1/PoACT	Mach Number	InletDrag
0.400	0.970	0.400	0.025
0.600	0.970	0.600	0.040
0.800	0.970	0.800	0.070
1.000	0.970	1.000	0.110
1.200	0.968	1.200	0.140
1.400	0.960	1.400	0.145
1.600	0.945	1.600	0.135
1.800	0.912	1.800	0.120
2.000	0.830	2.000	0.080
2.200	0.720	2.200	0.060
2.400	0.600	2.400	0.040

PROPULSION ANALYSIS : TURBOJET/TURBOFAN

M#	Inlet loss	Bleed loss	Inlet D/q	Nozzle D/q
0.4	0.0000	0.0000	0.0957	0.2535
0.6	0.0000	0.0000	0.1532	0.2535
0.8	0.0000	0.0000	0.2681	0.2535
1.0	-0.0393	0.0000	0.4213	0.2535
1.2	-0.0464	0.0000	0.5362	0.2535
1.4	-0.0511	0.0000	0.5553	0.2535
1.6	-0.0498	0.0000	0.5171	0.2535
1.8	-0.0287	0.0000	0.4596	0.2535
2.0	0.0484	0.0000	0.3064	0.2535
2.2	0.1528	0.0000	0.2298	0.2535
2.4	0.2619	0.0000	0.1532	0.2535

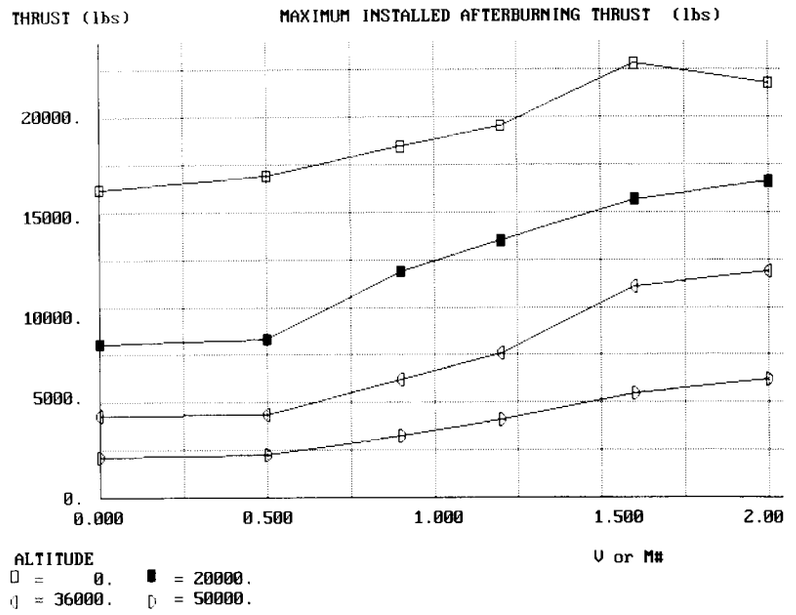

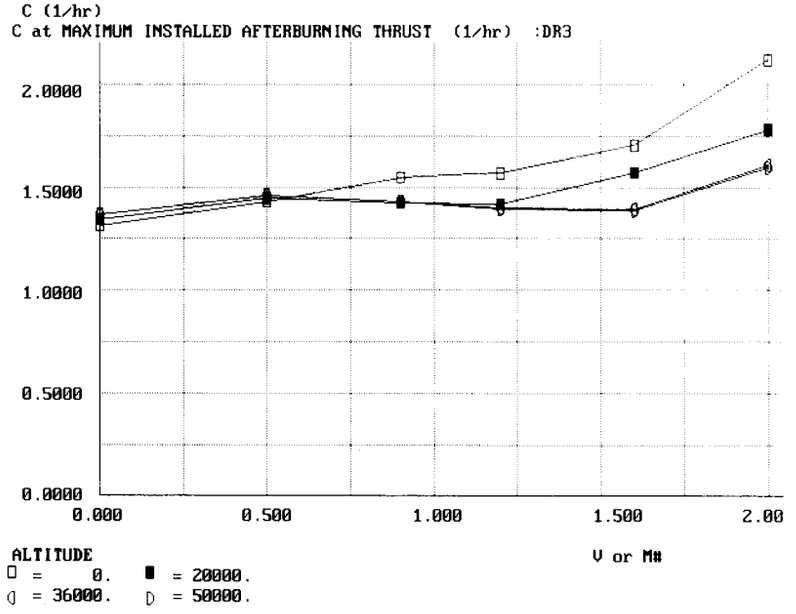

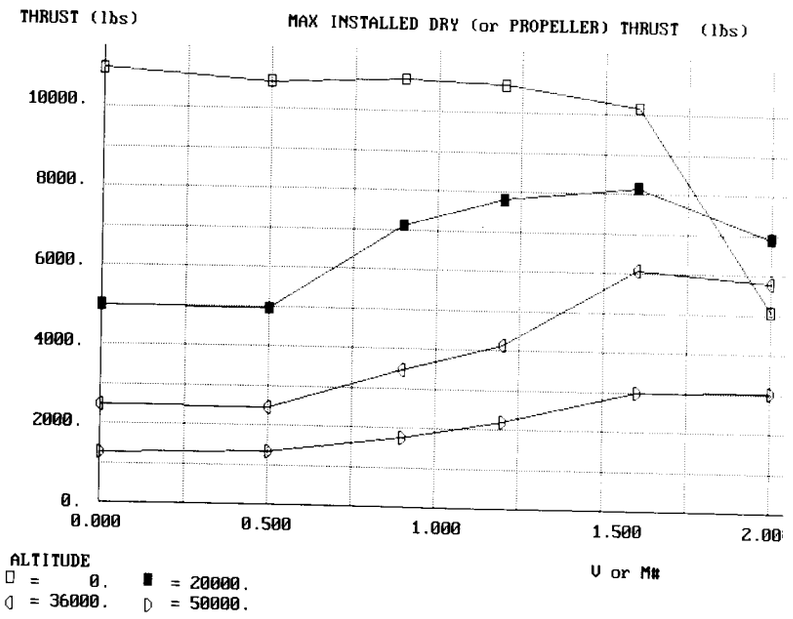

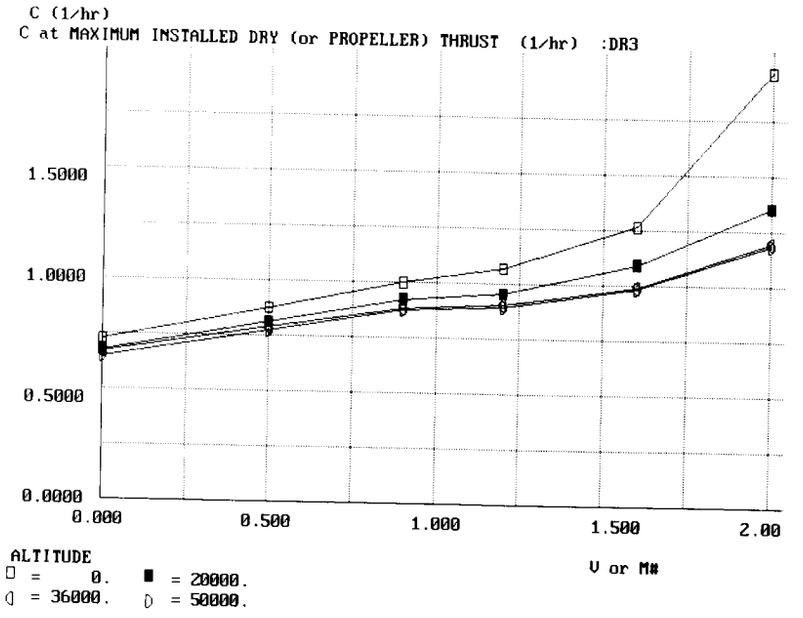

STABILITY AND CONTROL

Our advanced fighter concept does not lend itself to any first-order stability and controls analysis. Such a fighter would use relaxed static stability with a fully-computerized flight control system. This would automatically operate the 2-D vectoring nozzle, variable dihedral tail surfaces, and conventional aerodynamic control surfaces to provide the desired control authority as well as handling qualities.

We have sized the tails using the historical volume coefficient method, and have located the center of gravity at about the 40 percent of mean chord location. These should provide some assurance that the design is workable. However, to determine the exact stability, control, and handling qualities characteristics of such an advanced fighter will require a full 6-DOF simulation analysis using detailed aerodynamic data, preferably from the wind tunnel.

Thus, in early conceptual design of advanced aircraft with computerized flight control systems it is not uncommon to virtually ignore stability and control during the very early sizing studies, and to bring in the S&C experts only when an initial baseline is selected.

Refined Sizing and Performance

The RDS computer program was then used to calculate refined sizing and performance of the DR-3 using the methods of the book. A detailed mission model was developed, using several assumptions. Takeoff was assumed to consist of five minutes at Military (dry) power. Cruise was performed at M0.9 at 45,000 ft., determined from the range optimization plot to be approximately best cruise speed and altitude (see below).

Best loiter speed at sea level was determined to be 176 kts. This was found using the range optimization plot, which indicated that the velocity for best range at sea level was about Mach .35. Comparing equations 17.13 and 17.25 it can be seen that the velocity for best loiter is about one over the fourth root of three, or 0.76 times the velocity for best range. This yields Mach .266, or 176 kts.

Mission sizing, as detailed below, resulted in a sized takeoff gross weight of 17301.5 lbs., versus our as-drawn weight of 16480 lbs.

Performance calculations were done at a combat weight of .87 times takeoff weight, which is the weight at the end of cruise (beginning of combat).

Following are the inputs and results of the refined sizing and performance calculations, including takeoff, landing, Ps, turn rate, and acceleration. Also included are plots of flight envelope, specific range, rate of climb, Ps, and turn rate.

MISSION INPUTS: FILE DR3.DMS

SEGMENT 1 IS A TAKEOFF SEGMENT
THRUST SETTING = 100.000 ALTITUDE = 0.000 TIME = 0.083

SEGMENT 2 IS A CLIMB and/or ACCELERATE SEGMENT
THRUST SETTING = 100.000 STARTING ALT = 0.000 END ALT = 45000.000 START VEL = 0.200
END VEL = 0.900

SEGMENT 3 IS A CRUISE SEGMENT
THRUST SETTING = 100.000 ALTITUDE = 45000.000 VELOCITY = 0.900 RANGE = 200.000

SEGMENT 4 IS A CLIMB and/or ACCELERATE SEGMENT
THRUST SETTING = 999.000 STARTING ALT = 35000.000 END ALT = 35000.000 START VEL = 0.900
END VEL = 1.400

SEGMENT 5 IS A CRUISE SEGMENT
THRUST SETTING = 100.000 ALTITUDE = 35000.000 VELOCITY = 1.400 RANGE = 50.000

SEGMENT 6 IS A KNOWN TIME FUEL BURN SEGMENT
THRUST SETTING = 999.000 ALTITUDE = 20000.000 VELOCITY = 0.900 TIME = 0.050 FIX
BD/RUBBER = 0.000

SEGMENT 7 IS A WEIGHT DROP SEGMENT
Wt. DROPPED = 0.000

SEGMENT 8 IS A CLIMB and/or ACCELERATE SEGMENT
THRUST SETTING = 999.000 STARTING ALT = 20000.000 END ALT = 35000.000 START VEL = 0.900
END VEL = 1.400

SEGMENT 9 IS A CRUISE SEGMENT
THRUST SETTING = 100.000 ALTITUDE = 35000.000 VELOCITY = 1.400 RANGE = 50.000

SEGMENT 10 IS A CRUISE SEGMENT
THRUST SETTING = 100.000 ALTITUDE = 45000.000 VELOCITY = 0.900 RANGE = 200.000

SEGMENT 11 IS A LOITER SEGMENT
ALTITUDE = 0.000 VELOCITY = 176.000 TIME = 0.333

SEGMENT 12 IS A LANDING SEGMENT
Wi/Wi-1 = 0.995

SIZING ANALYSIS RESULTS

SEGMENT 1 IS A TAKEOFF SEGMENT
W/S = 56.00 T/W = 0.666 C = 0.7280 E = 0.0830
MISSION SEGMENT WEIGHT FRACTION = 0.960

SEGMENT 2 IS A CLIMB/ACCELERATE SEGMENT
W/S = 53.75 T/W = 0.414 C = 0.9185 CL = 0.2901 CD0 = 0.0142 K = 0.1129 L/D = 12.2521
DELTA ENERGY HEIGHT = 57599.3789
MISSION SEGMENT WEIGHT FRACTION = 0.968

SEGMENT 3 IS A CRUISE SEGMENT
CLIMB/DESCENT RANGE CREDIT = 28.49
W/S = 52.03 T/W AVAILABLE = 0.155 T/W REQUIRED = 0.089 THRUST SETTING USED = 57.6 %
CL = 0.2979 CD0 = 0.0172 K = 0.1061 L/D = 11.1762 C = 0.9461
MISSION SEGMENT WEIGHT FRACTION = 0.972

SEGMENT 4 IS A CLIMB/ACCELERATE SEGMENT
W/S = 50.59 T/W = 0.533 C = 1.3988 CL = 0.1097 CD0 = 0.0249 K = 0.1694 L/D = 4.0753
DELTA ENERGY HEIGHT = 16904.1094
MISSION SEGMENT WEIGHT FRACTION = 0.989

SEGMENT 5 IS A CRUISE SEGMENT
CLIMB/DESCENT RANGE CREDIT = 9.66
W/S = 50.04 T/W AVAILABLE = 0.422 T/W REQUIRED = 0.340 THRUST SETTING USED = 80.5 %
CL = 0.0732 CD0 = 0.0233 K = 0.2983 L/D = 2.9411 C = 1.0238
MISSION SEGMENT WEIGHT FRACTION = 0.983

SEGMENT 6 IS A KNOWN TIME FUEL BURN SEGMENT
W/S = 49.18 T/W AVAILABLE = 0.822 THRUST SETTING USED = 100.0 %
C = 1.4254 E = 0.0500
MISSION SEGMENT FRACTION OR FUEL BURNED IS 0.941

SEGMENT 7 IS A WEIGHT DROP SEGMENT
WEIGHT DROPPED IS 0.0

SEGMENT 8 IS A CLIMB/ACCELERATE SEGMENT
W/S = 46.30 T/W = 0.787 C = 1.4087 CL = 0.0711 CD0 = 0.0246 K = 0.1694 L/D = 2.7889
DELTA ENERGY HEIGHT = 33051.9961
MISSION SEGMENT WEIGHT FRACTION = 0.980

SEGMENT 9 IS A CRUISE SEGMENT
CLIMB/DESCENT RANGE CREDIT = 12.70
W/S = 45.35 T/W AVAILABLE = 0.466 T/W REQUIRED = 0.371 THRUST SETTING USED = 79.6 %
CL = 0.0664 CD0 = 0.0233 K = 0.2983 L/D = 2.6965 C = 1.0261
MISSION SEGMENT WEIGHT FRACTION = 0.983

SEGMENT 10 IS A CRUISE SEGMENT
CLIMB/DESCENT RANGE CREDIT = 0.00
W/S = 44.56 T/W AVAILABLE = 0.181 T/W REQUIRED = 0.096 THRUST SETTING USED = 53.1 %
CL = 0.2552 CD0 = 0.0172 K = 0.1127 L/D = 10.3823 C = 0.9728
MISSION SEGMENT WEIGHT FRACTION = 0.954

SEGMENT 11 IS A LOITER SEGMENT
W/S = 42.97 T/W AVAILABLE = 0.856 T/W REQUIRED = 0.075 THRUST SETTING USED = 8.8 %
CL = 0.4092 CD0 = 0.0137 K = 0.1017 L/D = 13.3050 C = 1.2119
MISSION SEGMENT WEIGHT FRACTION = 0.970

SEGMENT 12 IS A LANDING SEGMENT
MISSION SEGMENT WEIGHT FRACTION = 0.995

MISSION SEGMENT		MISSION SEGMENT WEIGHT FRACTION OR DROPPED WEIGHT	Wi/WO
1	TAKEOFF SEGMENT	0.9597	0.9597
2	CLIMB and/or ACCELERATE	0.9681	0.9291
3	CRUISE SEGMENT	0.9723	0.9034
4	CLIMB and/or ACCELERATE	0.9892	0.8936
5	CRUISE SEGMENT	0.9827	0.8782
6	KNOWN TIME FUEL BURN SEGMENT	0.9414	0.8267
7	WEIGHT DROP SEGMENT	0.0000	0.8267
8	CLIMB and/or ACCELERATE	0.9797	0.8099
9	CRUISE SEGMENT	0.9826	0.7958
10	CRUISE SEGMENT	0.9644	0.7674
11	LOITER SEGMENT	0.9701	0.7445
12	LANDING SEGMENT	0.9950	0.7408

PROJECT DR3: SIZING/MISSION ANALYSIS RESULTS

MISSION FILE : DR3.DMS
T/W = 0.980 W/S = 56.00

CRUISE SEGMENT # 3 RANGE (nmi) = 200.0
CRUISE SEGMENT # 5 RANGE (nmi) = 50.0
CRUISE SEGMENT # 9 RANGE (nmi) = 50.0
CRUISE SEGMENT # 10 RANGE (nmi) = 200.0
LOITER SEGMENT # 11 TIME (hrs) = 0.33
(Ranges are reduced during analysis for climb/descent range credit)

TOTAL RANGE = 500.0 TOTAL LOITER TIME = 0.33
FUEL WEIGHT = 4754.4 EMPTY WEIGHT = 11437.1
USEFUL LOAD (less Wf)= 1110.0 AIRCRAFT GROSS WEIGHT = 17301.5

```
---------------------------- TAKEOFF ----------------------------
  AIRCRAFT OPERATING WEIGHT RATIO  (Wi/WO) = 1.000
  TAKEOFF  THRUST-TO-WEIGHT RATIO    (T/W) = 0.995
                      TAKEOFF  THRUST  =  16393.5
                TAKEOFF WINGLOADING  (W/S) =  56.00
                Vstall =  99.75  (kts)
             Vtakeoff = 109.73  (kts)
CLIMB ANGLE = 35.68  (deg)  CLIMB  CD0 =  0.1124
       CL =  1.49           K =  0.2724
                CLIMB  L/D =  2.43
-----------------------------------------------------------------

         GROUND ROLL DISTANCE =    577.8
             ROTATE DISTANCE =    185.3
         TRANSITION DISTANCE =    761.2
             CLIMB DISTANCE =      0.0
      TOTAL TAKEOFF DISTANCE =   1524.3
FAR PART 25 TAKEOFF DISTANCE =   1752.9




---------------------------- LANDING ----------------------------

  AIRCRAFT OPERATING WEIGHT RATIO  (Wi/WO) = 1.000
  ROLLOUT  THRUST-TO-WEIGHT RATIO    (T/W) = -0.392
              LANDING WINGLOADING  (W/S) =  56.00
            Vstall =  95.79  (kts)
         Vtouchdown = 114.95  (kts)

           APPROACH ANGLE = -3.00  (deg)
            APPROACH  CD0 =  0.1124
                       CL =  1.62
                        K =  0.2724
              APPROACH L/D =  2.53
-----------------------------------------------------------------

        APPROACH DISTANCE =    773.7
           FLARE DISTANCE =   2730.5
    FREE GROUND ROLL DIST =    194.2
         BRAKING DISTANCE =    795.3
    TOTAL LANDING DISTANCE =   4493.6
FAR PART 25 LANDING DISTANCE =   7489.4
```



```
------------------------- Ps AND TURN RATE -------------------------
VELOCITY or MACH # =     0.90                ALTITUDE = 30000.00
          Afps =  994.66    rho =0.000889          q =  356.32
Wi/WO = 0.872  W/S =  48.83              T/W = 0.581       THRUST =   8353.2

         MAXIMUM INSTANTANEOUS TURN RATE =  14.97 (deg/sec)
AT LOAD FACTOR  N =  1     CD0 =  0.0161    K =  0.1372   CL =  0.14
         Ps(fps) =   +398.35       TURN RATE =  0.00 (deg/sec)
AT LOAD FACTOR  N =  2     CD0 =  0.0161    K =  0.1098   CL =  0.27
         Ps(fps) =   +361.32       TURN RATE =  3.57 (deg/sec)
AT LOAD FACTOR  N =  3     CD0 =  0.0161    K =  0.0981   CL =  0.41
         Ps(fps) =   +306.91       TURN RATE =  5.83 (deg/sec)
AT LOAD FACTOR  N =  4     CD0 =  0.0161    K =  0.1062   CL =  0.55
         Ps(fps) =   +206.70       TURN RATE =  7.98 (deg/sec)
AT LOAD FACTOR  N =  5     CD0 =  0.0161    K =  0.1300   CL =  0.69
         Ps(fps) =    +16.47       TURN RATE = 10.10 (deg/sec)
AT LOAD FACTOR  N =  6     CD0 =  0.0161    K =  0.1514   CL =  0.82
         Ps(fps) =   -253.64       TURN RATE = 12.19 (deg/sec)
AT LOAD FACTOR  N =  7     CD0 =  0.0161    K =  0.1661   CL =  0.96
         Ps(fps) =   -583.09       TURN RATE = 14.28 (deg/sec)




---------------------- ACCELERATION ----------------------

  AIRCRAFT OPERATING WEIGHT RATIO  (Wi/WO) = 0.872
                WINGLOADING  (W/S) =  48.83

AT VELOCITY (average) =  532.84   T/W =0.553   THRUST =   7940.7
   CD0 = 0.0175      K = 0.1312     CL = 0.1637 Ps(fps)=   +381.75
             dV/dt = 13.6593  DELTA TIME =   3.56
AT VELOCITY (average) =  561.64   T/W =0.553   THRUST =   7940.7
   CD0 = 0.0210      K = 0.1214     CL = 0.1474 Ps(fps)=   +372.00
             dV/dt = 12.6280  DELTA TIME =   3.85
AT VELOCITY (average) =  590.45   T/W =0.553   THRUST =   7940.7
   CD0 = 0.0250      K = 0.1211     CL = 0.1333 Ps(fps)=   +347.62
             dV/dt = 11.2248  DELTA TIME =   4.33
AT VELOCITY (average) =  619.25   T/W =0.553   THRUST =   7940.7
   CD0 = 0.0258      K = 0.1326     CL = 0.1212 Ps(fps)=   +338.49
             dV/dt = 10.4215  DELTA TIME =   4.67
AT VELOCITY (average) =  648.05   T/W =0.553   THRUST =   7940.7
   CD0 = 0.0249      K = 0.1694     CL = 0.1107 Ps(fps)=   +338.17
             dV/dt =  9.9490  DELTA TIME =   4.89
AT VELOCITY (average) =  676.85   T/W =0.553   THRUST =   7940.7
   CD0 = 0.0249      K = 0.1694     CL = 0.1015 Ps(fps)=   +331.63
             dV/dt =  9.3415  DELTA TIME =   5.21
AT VELOCITY (average) =  705.66   T/W =0.794   THRUST =  11403.7
   CD0 = 0.0233      K = 0.2066     CL = 0.0934 Ps(fps)=   +625.26
             dV/dt = 16.8934  DELTA TIME =   2.88
AT VELOCITY (average) =  734.46   T/W =0.794   THRUST =  11403.7
   CD0 = 0.0233      K = 0.2983     CL = 0.0862 Ps(fps)=   +617.02
             dV/dt = 16.0170  DELTA TIME =   3.04
AT VELOCITY (average) =  763.26   T/W =0.794   THRUST =  11403.7
   CD0 = 0.0233      K = 0.2983     CL = 0.0798 Ps(fps)=   +615.79
             dV/dt = 15.3820  DELTA TIME =   3.16
AT VELOCITY (average) =  792.06   T/W =0.794   THRUST =  11403.7
   CD0 = 0.0233      K = 0.2983     CL = 0.0741 Ps(fps)=   +611.26
             dV/dt = 14.7136  DELTA TIME =   3.31
-----------------------------------------------------------------
TIME TO ACCELERATE FROM    0.900 TO    1.400 IS     38.9 sec
DISTANCE TRAVELED IS     7.1 (nmi)
-----------------------------------------------------------------
```

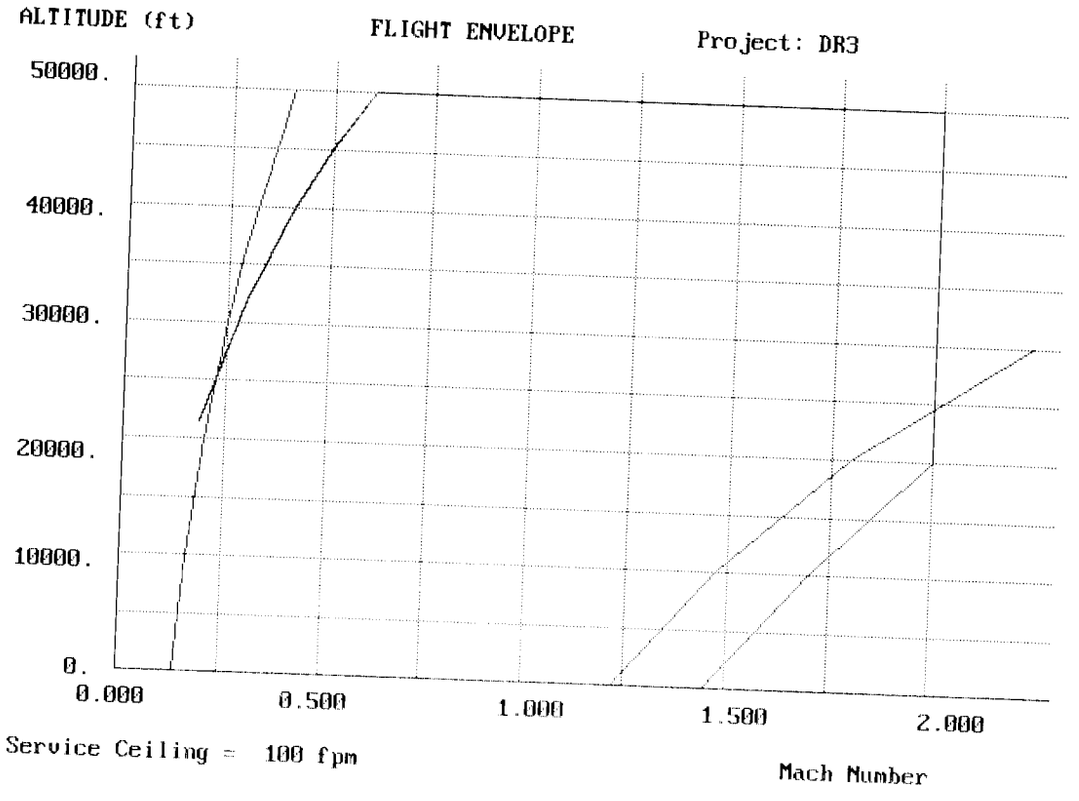
ALTITUDE (ft)
FLIGHT ENVELOPE
Project: DR3
50000.
40000.
30000.
20000.
10000.
0.
0.000
0.500
1.000
1.500
2.000
Service Ceiling = 100 fpm
Mach Number

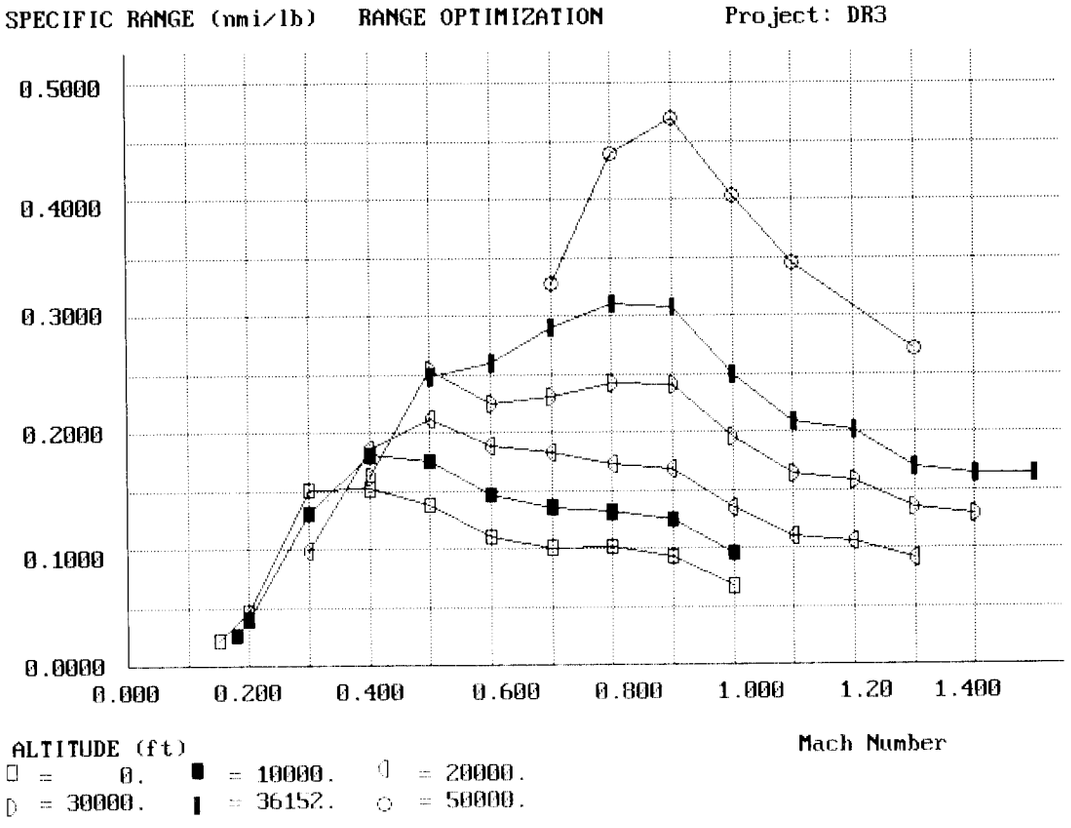
SPECIFIC RANGE (nmi/lb)
RANGE OPTIMIZATION
Project: DR3
0.5000
0.4000
0.3000
0.2000
0.1000
0.0000
0.000
0.200
0.400
0.600
0.800
1.000
1.20
1.400
Mach Number
ALTITUDE (ft)
= 0.
= 10000.
= 20000.
= 30000.
= 36152.
= 50000.

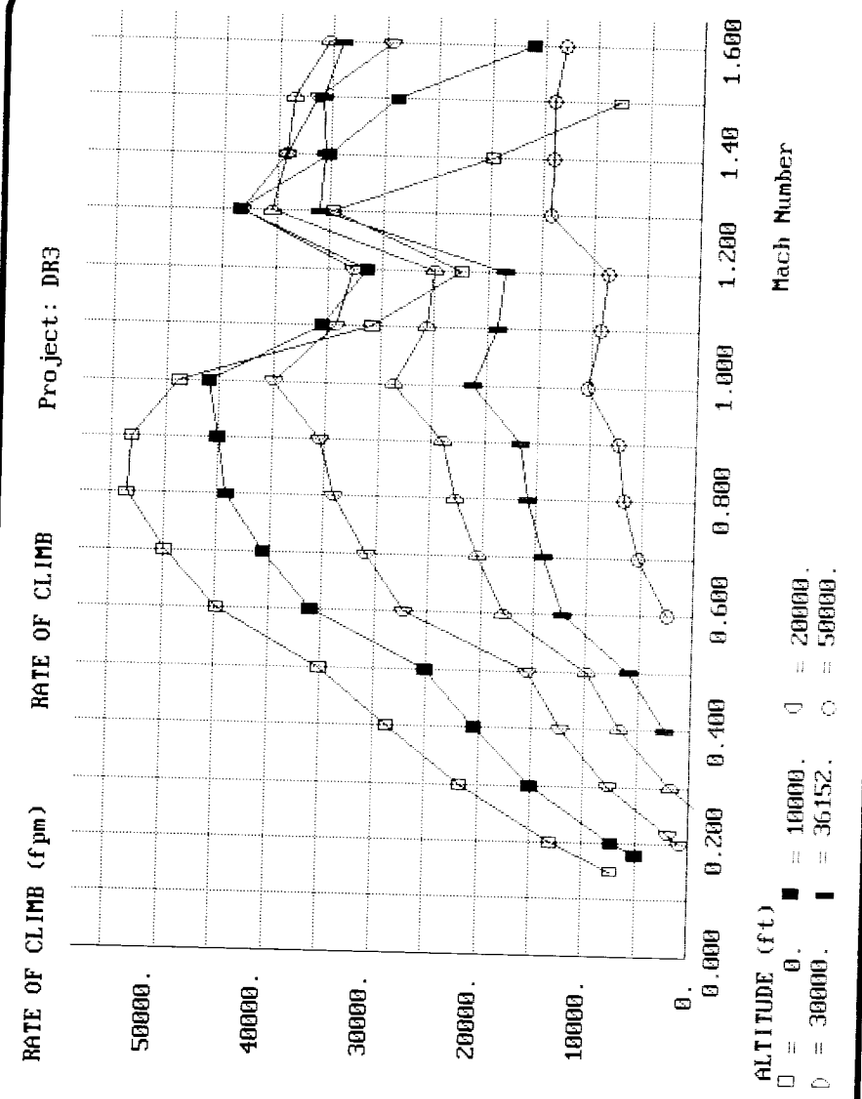
RATE OF CLIMB (fpm)
RATE OF CLIMB
Project: DR3
50000.
40000.
30000.
20000.
10000.
0.
0.000
0.200
0.400
0.600
0.800
1.000
1.200
1.40
1.600
Mach Number
ALTITUDE (ft)
□ = 0. ■ = 10000. ◁ = 20000.
▷ = 30000. ▮ = 36152. ○ = 50000.

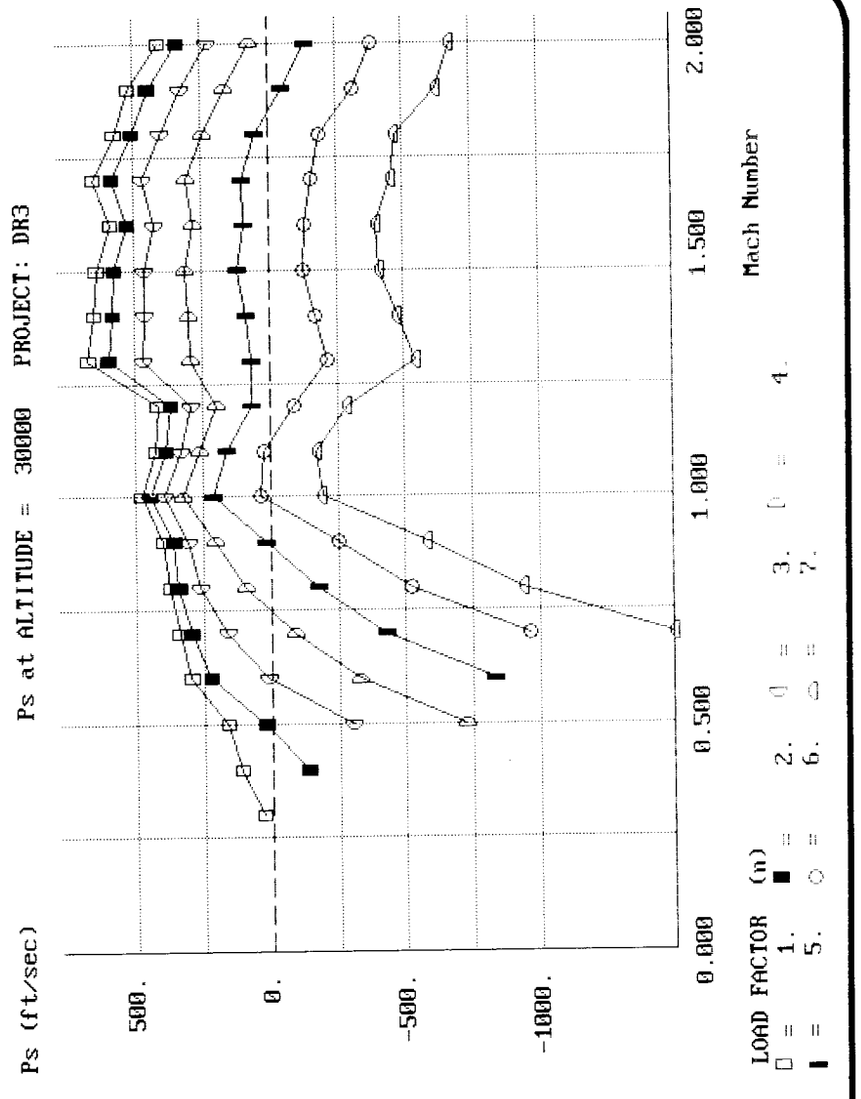
Ps (ft/sec)
Ps at ALTITUDE = 30000 PROJECT: DR3
500.
0.
-500.
-1000.
0.000
0.500
1.000
1.500
2.000
Mach Number
LOAD FACTOR (n)
□ = 1. ■ = 2. ◁ = 3. ▷ = 4.
▮ = 5. ○ = 6. ⊃ = 7.

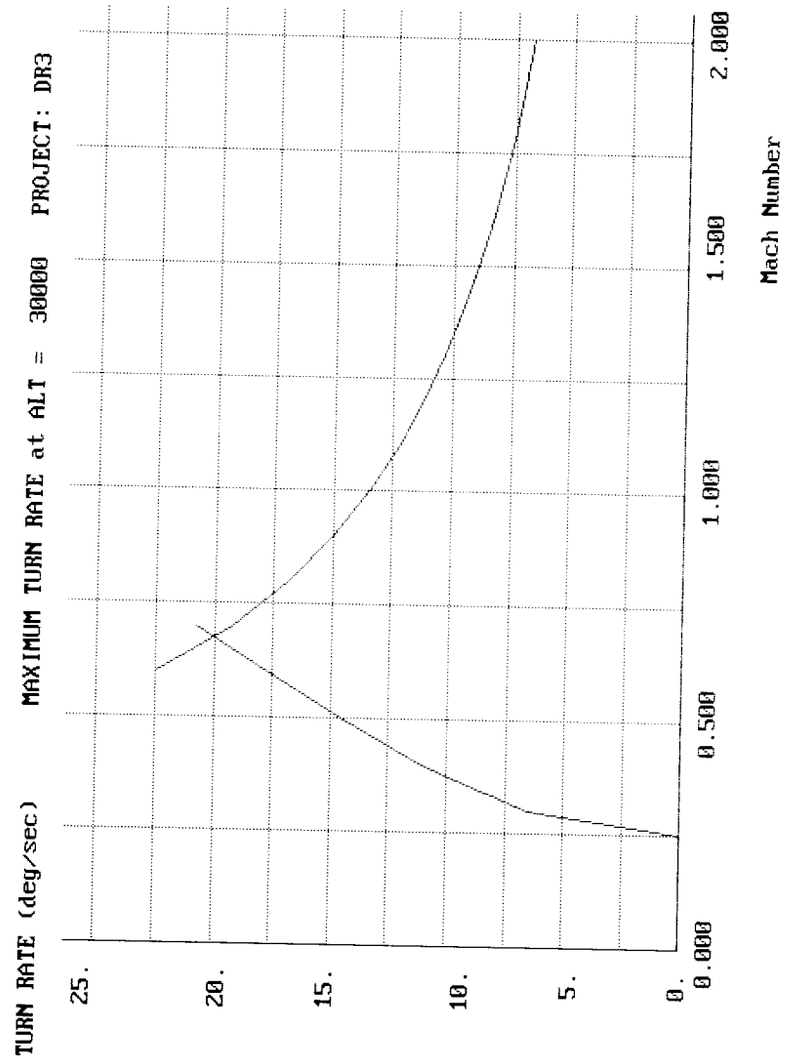

T/W-W/S Optimization

Optimization of the DR-3 for thrust-to-weight ratio and wing loading was done by parametric variations about the as-drawn baseline of T/W=.98 and W/S=56. Variations of plus-and-minus 20 percent were chosen, and appropriate modifications to the RDS inputs were made.

For variations in T/W, the impact on weight was accounted for by inputting the new engine thrust and weight in the weight input matrix, and by inputting the new T/W in the aircraft data matrix. Uninstalled engine weight was assumed to vary by the 1.1 power of the relative change in thrust (see eq. 10.3).

For variations in W/S, the weight impact was calculated by inputting the new wing and tail areas. Note that tail area must vary by the 3/2 power of the relative change in wing area to keep tail volume constant (see eq. 6.28 and 6.29).

The aerodynamic impact of the change in W/S was determined by inputting the new wing and tail areas, both reference and exposed. Also, the change in wave drag due to the change in wing size was approximated by changing the maximum cross sectional area of the design (Amax). This was "eyeball-estimated" as a one square foot difference.

Using these input revisions, mission sizing and performance analysis was completely rerun for all parametric variations, with results as shown in the following table and carpet plot. The optimum airplane which meets all requirements is shown by the upper circle. It weighs about 22,000 lbs., and has a T/W of 1.11 and a W/S of 60.5. However, by relaxing the acceleration requirement from 30 seconds to about 47 seconds (Mach 0.9 to 1.4), the weight of an optimal aircraft fully meeting all other requirements drops to about 17,000 lbs.!

DR-3 Sizing and Performance Results

T/W	W/S	W_e* as drawn, lb	W_0 resized, lb	Takeoff groundroll, ft	Landing groundroll, ft	Ps M.9 $n=5$	Ps M1.4 $n=5$	Ps M1.8 $n=1$	Ps M1.4 $n=1$	Accel time, s
1.18	44.8	11,647	31,688	546	749	243	376	794	146	30.6
1.18	56	11,324	25,188	659	914	122	341	922	210	29.2
1.18	67.2	11,102	22,060	771	1071	−13	302	1027	261	28
0.98	44.8	11,271	21,232	629	811	137	122	446	11	41.5
0.98	56	10,947	17,302	763	990	16.5	87	573	74	39.0
0.98	67.2	10,725	15,396	896	1168	−120	48	680	127	37
0.784	44.8	10,896	15,548	756	888	33	−126	106	−122	64.3
0.784	56	10,572	12,854	922	1086	−88	−161	234	−58	58
0.784	67.2	10,350	11,560	1087	1281	−224	−200	340	−6	54
Required:				1000	1000	0	0	0	0	30

*where $W_0 = 16{,}480$ lb

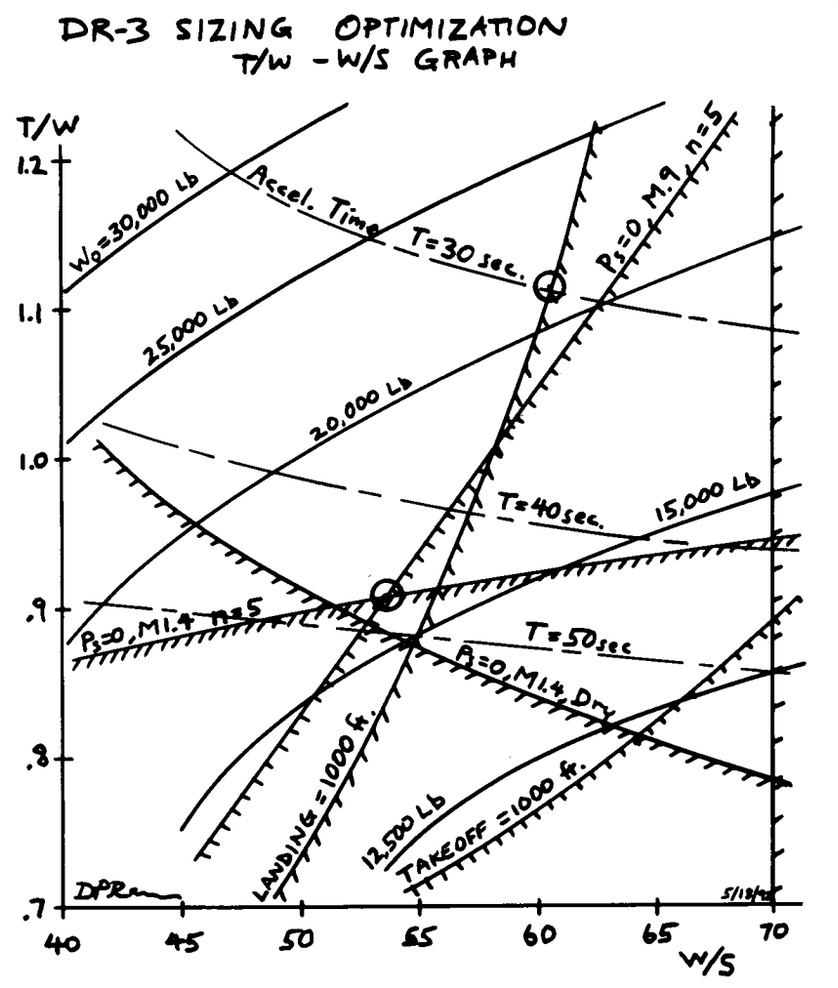

APPENDIX A

A.1 Conversion Factors

Multiply	By	To Obtain
British Thermal Unit/ Minute (BTU/min)	3.969×10^{6}	calories/second
	1.297×10	foot-pounds/second
	2.357×10^{-2}	horsepower
	2.987×10^{-2}	kilogram meters/second
Centimeter (cm)	3.281×10^{-2}	feet
	3.938×10^{-1}	inches
	1.000×10^{-5}	kilometers
	1.000×10^{-2}	meters
Cubic Foot (ft^3)	28.317	liters
	7.481	gallons
Foot (ft)	3.048×10	centimeters
	1.200×10	inches
	3.048×10^{-4}	kilometers
	3.048×10^{-1}	meters
	1.894×10^{-4}	miles
Foot-Pound/Second (ft-lb/s)	7.713×10^{-2}	BTU/min
	3.239×10^{-1}	calories/second
	1.818×10^{-3}	horsepower
	1.383×10^{-1}	kilogram meters/second
Foot/Second (ft/s)	1.097	kilometers/hour
	5.921×10^{-1}	knots
	3.048×10^{-1}	meters/second
	6.818×10^{-1}	miles/hour
Gallon (U.S.) (gal)	1.3368×10^{-1}	cubic feet
	3.78542	liters
	3.785×10^{-3}	cubic meters
	231	cubic inches
	128	fluid ounces
Gram (g)	3.528×10^{-2}	ounces
	2.205×10^{-3}	pounds
Horsepower (hp)	4.242×10	BTU/min
	550	foot-pounds/second
	7.604×10	kilogram meters/second
	745.7	watt
Imperial Gallon	2.774×10^{2}	cubic inches
	1.201	gallons (U.S.)
	4.546	liters
Inch (in.)	2.540	centimeters
	8.333×10^{-2}	feet
	2.540×10^{-2}	meters

(continued)

A.1 (cont'd) Conversion Factors

Multiply	By	To Obtain
Kilogram (kg)	1.000×10^{3}	grams
	6.854×10^{-2}	slugs
	2.205	pounds
	9.807	newtons
Kilogram-Meter/Second (kg-m/s)	3.347×10	BTU/min
	7.233	foot-pounds/second
Kilometer/Hour (km/h)	9.113×10^{-1}	feet/second
	5.396×10^{-1}	knots
	6.214×10^{-1}	miles/hour
Knot	1.689	feet/second
	1.151	miles/hour
	1.852	kilometers/hour
Liter (l)	3.532×10^{-2}	cubic feet
	2.6417×10^{-1}	gallons
	1.000×10^{-3}	cubic meters
	33.8142	fluid ounces
Meter (m)	1.000×10^{2}	centimeters
	3.281	feet
	3.937×10	inches
	1.000×10^{-3}	kilometers
	6.214×10^{-4}	miles
Meter/Second (m/s)	3.281	feet/second
	3.600	kilometers/hour
	1.943	knots
	2.237	miles/hour
Mile/Hour (mph)	1.467	feet/second
	1.609	kilometers/hour
	0.8684	knots
	0.4470	meters/second
Nautical Mile (nmi)	6.076×10^{3}	feet
	1.852×10^{3}	meters
	1.15078	mile
Pound (lb)	4.536×10^{2}	grams
	16	ounces
Slug	1.459×10^{4}	grams
	1.459×10	kilograms
	32.174	Lb_{mass}
Statute Mile (mi)	5.280×10^{3}	feet
	1.609	kilometers
	1.760×10^{3}	yards
	0.868976	nautical mile

A.2-1 Characteristics of the standard atmosphere

h (ft/10³)	T (°R)	p (psf)	ρ (sl/ft³)	μ (sl/ft/s)	a (ft/s)	ν (ft²/s)
0	518.69	2116.2	.23769 −2	.37373 −6	1116.4	.15723 −3
1	515.1	2041	.2308	.3717	1112.6	.1611
2	511.6	1963	.2241	.3697	1108.7	.1650
3	508.0	1897	.2175	.3677	1104.9	.1691
4	504.4	1828	.2111	.3657	1101.0	.1732
5	500.9	1761	.2043	.3637	1097.1	.1776
6	497.3	1696	.1987 −2	.3616 −6	1093.2	.1820 −3
7	493.7	1633	.1927	.3596	1089.3	.1866
8	490.2	1572	.1869	.3576	1085.3	.1914
9	486.6	1513	.1811	.3555	1081.4	.1963
10	483.1	1456	.1756	.3534	1077.4	.2013
11	479.5	1400	.1701 −2	.3514 −6	1073.4	.2066 −3
12	475.9	1346	.1648	.3493	1069.4	.2120
13	472.4	1294	.1596	.3472	1065.4	.2175
14	468.8	1244	.1546	.3451	1061.4	.2233
15	465.2	1195	.1496	.3430	1057.4	.2293
16	461.7	1148	.1448 −2	.3409 −6	1053.3	.2354 −3
17	458.1	1102	.1401	.3388	1049.2	.2418
18	454.6	1058	.1355	.3367	1045.1	.2484
19	451.0	1015	.1311	.3346	1041.0	.2553
20	447.4	9733 −1	.1267	.3325	1036.9	.2623
21	443.9	9333 −1	.1225 −2	.3303 −6	1032.8	.2697 −3
22	440.3	8946	.1184	.3282	1028.6	.2772
23	436.8	8572	.1144	.3260	1024.5	.2851
24	433.2	8212	.1104	.3238	1020.3	.2932
25	429.6	7863	.1066	.3217	1016.1	.3017
26	426.1	7527 −1	.1029 −2	.3195 −6	1011.9	.3104 −3
27	422.5	7203	.9931 −3	.3173	1007.7	.3195
28	419.0	6890	.9580	.3151	1003.4	.3289
29	415.4	6588	.9239	.3129	999.1	.3387
30	411.9	6297	.8907	.3107	994.8	.3488
31	408.3	6016 −1	.8584 −3	.3085 −6	990.5	.3594 −3
32	404.8	5746	.8270	.3063	986.2	.3703
33	401.2	5485	.7966	.3040	981.9	.3817
34	397.6	5235	.7670	.3018	977.5	.3935
35	394.1	4993	.7382	.2995	973.1	.4058
36	390.5	4761 −1	.7103 −3	.2973 −6	968.7	.4185 −3
(a)	390.0	4727	.7061	.2969	968.1	.4205
37	390.0	4539	.6780	.2969	968.1	.4379
38	390.0	4326	.6463	.2969	968.1	.4594
39	390.0	4124	.6161	.2969	968.1	.4820
40	390.0	3931	.5873	.2969	968.1	.5056

(continued)

h (ft/10³)	T (°R)	p (psf)	ρ (sl/ft³)	μ (sl/ft/s)	a (ft/s)	ν (ft²/s)
41	390.0	3743 −1	.5598 −3	.2969 −6	968.1	.5304 −3
42	390.0	3572	.5337	.2969	968.1	.5564
43	390.0	3405	.5087	.2969	968.1	.5837
44	390.0	3246	.4849	.2969	965.1	.6123
45	390.0	3095	.4623	.2969	968.1	.6423
46	390.0	2950 −1	.4407 −3	.2969 −6	968.1	.6738 −3
47	390.0	2812	.4201	.2969	968.1	.7068
48	390.0	2681	.4005	.2969	968.1	.7415
49	390.0	2556	.3818	.2969	968.1	.7778
50	390.0	2436	.3639	.2969	968.1	.8159
51	390.0	2214 −1	.3307 −3	.2969 −6	968.1	.8978 −3
54	390.0	2012	.3006	.2969	968.1	.9879
56	390.0	1829	.2732	.2969	968.1	.1087 −2
58	390.0	1662	.2482	.2969	968.1	.1196
60	390.0	1510	.2256	.2969	968.1	.1316
62	390.0	1373 −1	.2051 −3	.2969 −6	968.1	.1448 −2
64	390.0	1243	.1864	.2969	968.1	.1593
66	390.0	1134	.1694	.2969	968.1	.1753
68	390.0	1031	.1540	.2969	968.1	.1929
70	390.0	9367 −2	.1399	.2969	968.1	.2122
72	390.0	8514 −2	.1272 −3	.2969 −6	968.1	.2335 −2
74	390.0	7739	.1156	.2969	968.1	.2568
76	390.0	7035	.1051	.2969	968.1	.2826
78	390.0	6394	.9552 −4	.2969	968.1	.3108
80	390.0	5813	.6683	.2969	968.1	.3420
(b)	390.0	5193 −2	.7764 −4	.2969 −6	968.1	.3824 −2
85	394.3	4533	.6771	.2997	973.4	.4426
90	402.5	3629	.5253	.3048	983.5	.5803
95	410.6	2888	.4097	.3099	993.4	.7565
100	418.8	2309	.3211	.3150	1003.2	.9809
110	435.1	1495 −2	.2001 −4	.3250 −6	1022.5	.1624 −1
120	451.4	9837 −3	.1270	.3348	1041.5	.2637
130	467.6	6574	.8190 −5	.3444	1060.1	.4206
140	483.9	4455	.5364	.3539	1078.3	.6598
150	500.1	3060	.3564	.3632	1096.3	.1019 +0
(c)	508.8	2515 −3	.2880 −5	.3682 −6	1105.7	.1278 +0
160	508.8	2125	.2433	.3682	1105.7	.1513
170	508.8	1479	.1693	.3682	1105.7	.2175
(d)	508.8	1218	.1395	.3682	1105.7	.2640
180	499.0	1027	.1200	.3626	1095.0	.3023
190	473.0	7047 −4	.8589 −6	.3505	1071.7	.4081
200	457.0	4754	.6061	.3381	1047.9	.5580

Symbols— h = geo. altitude; T = temperature; ρ = density; μ = viscosity; a = sound speed; p = pressure; ν = kinematic viscosity

Single digit preceded by plus or minus sign indicates power of 10 (i.e., .23769 −2 = .0023769)

Altitudes of Temperature Profile Discontinuity—
(a) 36,152 ft (b) 82,346 ft (c) 155,348 ft (d) 175,344 ft

Data from "US Extension of the ICAO Standard Atmosphere," 1958.

A.2-2 Compressible Flow Tables (NACA TR-1135;1953)

NOTATIONS

M or M_1 local Mach number or Mach number upstream of a normal shock wave

$\frac{p}{p_t}$ ratio of static pressure to total pressure

$\frac{\rho}{\rho_t}$ ratio of static density to total density

$\frac{T}{T_t}$ ratio of static temperature to total temperature

β $\sqrt{M^2-1}$

$\frac{q}{p_t}$ ratio of dynamic pressure, $\frac{1}{2}\rho V^2$, to total pressure

$\frac{A}{A_*}$ ratio of local cross-sectional area of an isentropic stream tube to cross-sectional area at the point where $M=1$

$\frac{V}{a_*}$ ratio of local speed to speed of sound at the point where $M=1$

ν Prandtl-Meyer angle (angle through which a supersonic stream is turned to expand from $M=1$ to $M>1$), deg

μ Mach angle, $\sin^{-1}\frac{1}{M}$, deg

M_2 Mach number downstream of a normal shock wave

$\frac{p_2}{p_1}$ static pressure ratio across a normal shock wave

$\frac{\rho_2}{\rho_1}$ static density ratio across a normal shock wave

$\frac{T_2}{T_1}$ static temperature ratio across a normal shock wave

$\frac{p_{t_2}}{p_{t_1}}$ total pressure ratio across a normal shock wave

$\frac{p_1}{p_{t_2}}$ ratio of static pressure upstream of a normal shock wave to total pressure downstream

A.2-2 Compressible Flow Tables

SUBSONIC FLOW

$\gamma=7/5$

M	$\frac{p}{p_t}$	$\frac{\rho}{\rho_t}$	$\frac{T}{T_t}$	β	$\frac{q}{p_t}$	$\frac{A}{A_*}$	$\frac{V}{a_*}$
0	1.0000	1.0000	1.0000	1.0000	0	∞	0
.01	.9999	1.0000	1.0000	1.0000	.7000 $^{-4}$	57.8738	.01095
.02	.9997	.9998	.9999	.9998	.2799 $^{-3}$	28.9421	.02191
.03	.9994	.9996	.9998	.9995	.6296 $^{-3}$	19.3005	.03286
.04	.9989	.9992	.9997	.9992	.1119 $^{-2}$	14.4815	.04381
.05	.9983	.9988	.9995	.9987	.1747 $^{-2}$	11.5914	.05476
.06	.9975	.9982	.9993	.9982	.2514 $^{-2}$	9.6659	.06570
.07	.9966	.9976	.9990	.9975	.3418 $^{-2}$	8.2915	.07664
.08	.9955	.9968	.9987	.9968	.4460 $^{-2}$	7.2616	.08758
.09	.9944	.9960	.9984	.9959	.5638 $^{-2}$	6.4613	.09851
.10	.9930	.9950	.9980	.9950	.6951 $^{-2}$	5.8218	.10944
.11	.9916	.9940	.9976	.9939	.8399 $^{-2}$	5.2992	.12035
.12	.9900	.9928	.9971	.9928	.9979 $^{-2}$	4.8643	.13126
.13	.9883	.9916	.9966	.9915	.1169 $^{-1}$	4.4969	.14217
.14	.9864	.9903	.9961	.9902	.1353 $^{-1}$	4.1824	.15306
.15	.9844	.9888	.9955	.9887	.1550 $^{-1}$	3.9103	.16395
.16	.9823	.9873	.9949	.9871	.1760 $^{-1}$	3.6727	.17482
.17	.9800	.9857	.9943	.9854	.1983 $^{-1}$	3.4635	.18569
.18	.9776	.9840	.9936	.9837	.2217 $^{-1}$	3.2779	.19654
.19	.9751	.9822	.9928	.9818	.2464 $^{-1}$	3.1123	.20739
.20	.9725	.9803	.9921	.9798	.2723 $^{-1}$	2.9635	.21822
.21	.9697	.9783	.9913	.9777	.2994 $^{-1}$	2.8293	.22904
.22	.9668	.9762	.9904	.9755	.3276 $^{-1}$	2.7076	.23984
.23	.9638	.9740	.9895	.9732	.3569 $^{-1}$	2.5968	.25063
.24	.9607	.9718	.9886	.9708	.3874 $^{-1}$	2.4956	.26141
.25	.9575	.9694	.9877	.9682	.4189 $^{-1}$	2.4027	.27217
.26	.9541	.9670	.9867	.9656	.4515 $^{-1}$	2.3173	.28291
.27	.9506	.9645	.9856	.9629	.4851 $^{-1}$	2.2385	.29364
.28	.9470	.9619	.9846	.9600	.5197 $^{-1}$	2.1656	.30435
.29	.9433	.9592	.9835	.9570	.5553 $^{-1}$	2.0979	.31504
.30	.9395	.9564	.9823	.9539	.5919 $^{-1}$	2.0351	.32572
.31	.9355	.9535	.9811	.9507	.6293 $^{-1}$	1.9765	.33637
.32	.9315	.9506	.9799	.9474	.6677 $^{-1}$	1.9219	.34701
.33	.9274	.9476	.9787	.9440	.7069 $^{-1}$	1.8707	.35762
.34	.9231	.9445	.9774	.9404	.7470 $^{-1}$	1.8229	.36822
.35	.9188	.9413	.9761	.9367	.7879 $^{-1}$	1.7780	.37879
.36	.9143	.9380	.9747	.9330	.8295 $^{-1}$	1.7358	.38935
.37	.9098	.9347	.9733	.9290	.8719 $^{-1}$	1.6961	.39988
.38	.9052	.9313	.9719	.9250	.9149 $^{-1}$	1.6587	.41039
.39	.9004	.9278	.9705	.9208	.9587 $^{-1}$	1.6234	.42087
.40	.8956	.9243	.9690	.9165	.1003	1.5901	.43133
.41	.8907	.9207	.9675	.9121	.1048	1.5587	.44177
.42	.8857	.9170	.9659	.9075	.1094	1.5289	.45218
.43	.8807	.9132	.9643	.9028	.1140	1.5007	.46257
.44	.8755	.9094	.9627	.8980	.1187	1.4740	.47293
.45	.8703	.9055	.9611	.8930	.1234	1.4487	.48326
.46	.8650	.9016	.9594	.8879	.1281	1.4246	.49357
.47	.8596	.8976	.9577	.8827	.1329	1.4018	.50385
.48	.8541	.8935	.9560	.8773	.1378	1.3801	.51410
.49	.8486	.8894	.9542	.8717	.1426	1.3595	.52433

A.2-2 Compressible Flow Tables

SUBSONIC FLOW

$\gamma = 7/5$

M	$\frac{p}{p_t}$	$\frac{\rho}{\rho_t}$	$\frac{T}{T_t}$	β	$\frac{q}{p_t}$	$\frac{A}{A_*}$	$\frac{V}{a_*}$
0.50	0.8430	0.8852	0.9524	0.8660	0.1475	1.3398	0.53452
.51	.8374	.8809	.9506	.8602	.1525	1.3212	.54469
.52	.8317	.8766	.9487	.8542	.1574	1.3034	.55483
.53	.8259	.8723	.9468	.8480	.1624	1.2865	.56493
.54	.8201	.8679	.9449	.8417	.1674	1.2703	.57501
.55	.8142	.8634	.9430	.8352	.1724	1.2550	.58506
.56	.8082	.8589	.9410	.8285	.1774	1.2403	.59507
.57	.8022	.8544	.9390	.8216	.1825	1.2263	.60505
.58	.7962	.8498	.9370	.8146	.1875	1.2130	.61501
.59	.7901	.8451	.9349	.8074	.1925	1.2003	.62492
.60	.7840	.8405	.9328	.8000	.1976	1.1882	.63481
.61	.7778	.8357	.9307	.7924	.2026	1.1767	.64466
.62	.7716	.8310	.9286	.7846	.2076	1.1657	.65448
.63	.7654	.8262	.9265	.7766	.2127	1.1552	.66427
.64	.7591	.8213	.9243	.7684	.2177	1.1452	.67402
.65	.7528	.8164	.9221	.7599	.2227	1.1356	.68374
.66	.7465	.8115	.9199	.7513	.2276	1.1265	.69342
.67	.7401	.8066	.9176	.7424	.2326	1.1179	.70307
.68	.7338	.8016	.9153	.7332	.2375	1.1097	.71268
.69	.7274	.7966	.9131	.7238	.2424	1.1018	.72225
.70	.7209	.7916	.9107	.7141	.2473	1.0944	.73179
.71	.7145	.7865	.9084	.7042	.2521	1.0873	.74129
.72	.7080	.7814	.9061	.6940	.2569	1.0806	.75076
.73	.7016	.7763	.9037	.6834	.2617	1.0742	.76019
.74	.6951	.7712	.9013	.6726	.2664	1.0681	.76958
.75	.6886	.7660	.8989	.6614	.2711	1.0624	.77894
.76	.6821	.7609	.8964	.6499	.2758	1.0570	.78825
.77	.6756	.7557	.8940	.6380	.2804	1.0519	.79753
.78	.6691	.7505	.8915	.6258	.2849	1.0471	.80677
.79	.6625	.7452	.8890	.6131	.2894	1.0425	.81597
.80	.6560	.7400	.8865	.6000	.2939	1.0382	.82514
.81	.6495	.7347	.8840	.5864	.2983	1.0342	.83426
.82	.6430	.7295	.8815	.5724	.3027	1.0305	.84335
.83	.6365	.7242	.8789	.5578	.3069	1.0270	.85239
.84	.6300	.7189	.8763	.5426	.3112	1.0237	.86140
.85	.6235	.7136	.8737	.5268	.3153	1.0207	.87037
.86	.6170	.7083	.8711	.5103	.3195	1.0179	.87929
.87	.6106	.7030	.8685	.4931	.3235	1.0153	.88818
.88	.6041	.6977	.8659	.4750	.3275	1.0129	.89703
.89	.5977	.6924	.8632	.4560	.3314	1.0108	.90583
.90	.5913	.6870	.8606	.4359	.3352	1.0089	.91460
.91	.5849	.6817	.8579	.4146	.3390	1.0071	.92332
.92	.5785	.6764	.8552	.3919	.3427	1.0056	.93201
.93	.5721	.6711	.8525	.3676	.3464	1.0043	.94065
.94	.5658	.6658	.8498	.3412	.3500	1.0031	.94925
.95	.5595	.6604	.8471	.3122	.3534	1.0022	.95781
.96	.5532	.6551	.8444	.2800	.3569	1.0014	.96633
.97	.5469	.6498	.8416	.2431	.3602	1.0008	.97481
.98	.5407	.6445	.8389	.1990	.3635	1.0003	.98325
.99	.5345	.6392	.8361	.1411	.3667	1.0001	.99165
1.00	.5283	.6339	.8333	.0000	.3698	1.0000	1.00000

A.2-2 Compressible Flow Tables

SUPERSONIC FLOW

$\gamma = 7/5$

M or M_1	$\frac{p}{p_t}$	$\frac{\rho}{\rho_t}$	$\frac{T}{T_t}$	β	$\frac{q}{p_t}$	$\frac{A}{A_*}$	$\frac{V}{a_*}$	ν	μ	M_2	$\frac{p_2}{p_1}$	$\frac{\rho_2}{\rho_1}$	$\frac{T_2}{T_1}$	$\frac{p_{t_2}}{p_{t_1}}$	$\frac{p_1}{p_{t_2}}$
1.00	0.5283	0.6339	0.8333	0	0.3698	1.000	1.00000	0	90.00	1.000	1.000	1.000	1.000	1.000	0.5283
1.01	.5221	.6287	.8306	.1418	.3728	1.000	1.00351	.04473	81.93	.9901	1.023	1.017	1.007	1.000	.5221
1.02	.5160	.6234	.8278	.2010	.3758	1.000	1.01058	.1257	78.64	.9805	1.047	1.033	1.013	1.000	.5160
1.03	.5099	.6181	.8250	.2468	.3787	1.001	1.02481	.2294	76.14	.9712	1.071	1.050	1.020	1.000	.5100
1.04	.5039	.6129	.8222	.2857	.3815	1.001	1.03300	.3510	74.06	.9620	1.095	1.067	1.026	.9999	.5039
1.05	.4979	.6077	.8193	.3202	.3842	1.002	1.04114	.4874	72.25	.9531	1.120	1.084	1.033	.9999	.4980
1.06	.4919	.6024	.8165	.3516	.3869	1.003	1.04925	.6367	70.63	.9444	1.144	1.101	1.039	.9997	.4920
1.07	.4860	.5972	.8137	.3807	.3895	1.004	1.05731	.7973	69.16	.9360	1.169	1.118	1.046	.9996	.4861
1.08	.4800	.5920	.8108	.4079	.3919	1.005	1.06533	.9680	67.81	.9277	1.194	1.135	1.052	.9994	.4803
1.09	.4742	.5869	.8080	.4337	.3944	1.006	1.07331	1.148	66.55	.9196	1.219	1.152	1.059	.9992	.4746
1.10	.4684	.5817	.8052	.4583	.3967	1.008	1.08124	1.336	65.38	.9118	1.245	1.169	1.065	.9989	.4689
1.11	.4626	.5766	.8023	.4818	.3990	1.010	1.08913	1.532	64.28	.9041	1.271	1.186	1.071	.9986	.4632
1.12	.4568	.5714	.7994	.5044	.4011	1.011	1.09699	1.735	63.23	.8966	1.297	1.203	1.078	.9982	.4576
1.13	.4511	.5663	.7966	.5262	.4032	1.013	1.10479	1.944	62.25	.8892	1.323	1.221	1.084	.9978	.4521
1.14	.4455	.5612	.7937	.5474	.4052	1.015	1.11256	2.160	61.31	.8820	1.350	1.238	1.090	.9973	.4467
1.15	.4398	.5562	.7908	.5679	.4072	1.017	1.12029	2.381	60.41	.8750	1.376	1.255	1.097	.9967	.4413
1.16	.4343	.5511	.7879	.5879	.4090	1.020	1.12797	2.607	59.55	.8682	1.403	1.272	1.103	.9961	.4360
1.17	.4287	.5461	.7851	.6074	.4108	1.022	1.13561	2.839	58.73	.8615	1.430	1.290	1.109	.9953	.4307
1.18	.4232	.5411	.7822	.6264	.4125	1.025	1.14321	3.074	57.94	.8549	1.458	1.307	1.115	.9946	.4255
1.19	.4178	.5361	.7793	.6451	.4141	1.026	1.15077	3.314	57.18	.9485	1.485	1.324	1.122	.9937	.4204
1.20	.4124	.5311	.7764	.6633	.4157	1.030	1.15828	3.558	56.44	.8422	1.513	1.342	1.128	.9928	.4154
1.21	.4070	.5262	.7735	.6812	.4171	1.033	1.16575	3.806	55.74	.8360	1.541	1.359	1.134	.9918	.4104
1.22	.4017	.5213	.7706	.6989	.4185	1.037	1.17319	4.057	55.05	.8300	1.570	1.376	1.141	.9907	.4055
1.23	.3964	.5164	.7677	.7162	.4198	1.040	1.18057	4.312	54.39	.8241	1.598	1.394	1.147	.9896	.4006
1.24	.3912	.5115	.7648	.7332	.4211	1.043	1.18792	4.569	53.75	.8183	1.627	1.411	1.155	.9884	.3958

317913—54——4

A.2-2 Compressible Flow Tables

SUPERSONIC FLOW—Continued

$\gamma = 7/5$

M or M_1	$\frac{p}{p_t}$	$\frac{\rho}{\rho_t}$	$\frac{T}{T_t}$	β	$\frac{q}{p_t}$	$\frac{A}{A_*}$	$\frac{V}{a_*}$	ν	μ	M_2	$\frac{p_2}{p_1}$	$\frac{\rho_2}{\rho_1}$	$\frac{T_2}{T_1}$	$\frac{p_{t_2}}{p_{t_1}}$	$\frac{p_1}{p_{t_2}}$
1.25	.3861	.5067	.7619	.7500	.4223	1.047	1.19523	4.830	53.13	.8126	1.656	1.429	1.159	.9871	.3911
1.26	.3809	.5019	.7590	.7666	.4233	1.050	1.20249	5.093	52.53	.8071	1.686	1.446	1.166	.9857	.3865
1.27	.3759	.4971	.7561	.7829	.4244	1.054	1.20972	5.359	51.94	.8016	1.715	1.463	1.172	.9842	.3819
1.28	.3708	.4923	.7532	.7990	.4253	1.058	1.21690	5.627	51.38	.7963	1.745	1.481	1.178	.9827	.3774
1.29	.3658	.4876	.7503	.8149	.4262	1.062	1.22404	5.898	50.82	.7911	1.775	1.498	1.185	.9811	.3729
1.30	.3609	.4829	.7474	.8307	.4270	1.066	1.23114	6.170	50.28	.7860	1.805	1.516	1.191	.9794	.3685
1.31	.3560	.4782	.7445	.8462	.4277	1.071	1.23819	6.445	49.76	.7809	1.835	1.533	1.197	.9776	.3642
1.32	.3512	.4736	.7416	.8616	.4283	1.075	1.24521	6.721	49.25	.7760	1.866	1.551	1.204	.9758	.3599
1.33	.3464	.4690	.7387	.8769	.4289	1.080	1.25218	7.000	48.75	.7712	1.897	1.568	1.210	.9738	.3557
1.34	.3417	.4644	.7358	.8920	.4294	1.084	1.25912	7.280	48.27	.7664	1.928	1.585	1.216	.9718	.3516
1.35	.3370	.4598	.7329	.9069	.4299	1.089	1.26601	7.561	47.79	.7618	1.960	1.603	1.223	.9697	.3475
1.36	.3323	.4553	.7300	.9217	.4303	1.094	1.27286	7.844	47.33	.7572	1.991	1.620	1.229	.9676	.3435
1.37	.3277	.4508	.7271	.9364	.4306	1.099	1.27968	8.128	46.88	.7527	2.023	1.638	1.235	.9653	.3395
1.38	.3232	.4463	.7242	.9510	.4308	1.104	1.28645	8.413	46.44	.7483	2.055	1.655	1.242	.9630	.3356
1.39	.3187	.4418	.7213	.9655	.4310	1.109	1.29318	8.699	46.01	.7440	2.087	1.672	1.248	.9607	.3317
1.40	.3142	.4374	.7184	.9798	.4311	1.115	1.29987	8.987	45.58	.7397	2.120	1.690	1.255	.9582	.3280
1.41	.3098	.4330	.7155	.9940	.4312	1.120	1.30652	9.276	45.17	.7355	2.153	1.707	1.261	.9557	.3242
1.42	.3055	.4287	.7126	1.008	.4312	1.126	1.31313	9.565	44.77	.7314	2.186	1.724	1.268	.9531	.3205
1.43	.3012	.4244	.7097	1.022	.4311	1.132	1.31970	9.855	44.37	.7274	2.219	1.742	1.274	.9504	.3169
1.44	.2969	.4201	.7069	1.036	.4310	1.138	1.32623	10.146	43.98	.7235	2.253	1.759	1.281	.9476	.3133
1.45	.2927	.4158	.7040	1.050	.4308	1.144	1.33272	10.438	43.60	.7196	2.286	1.776	1.287	.9448	.3098
1.46	.2886	.4116	.7011	1.064	.4306	1.150	1.33917	10.731	43.23	.7157	2.320	1.793	1.294	.9420	.3063
1.47	.2845	.4074	.6982	1.077	.4303	1.156	1.34558	11.023	42.86	.7120	2.354	1.811	1.300	.9390	.3029
1.48	.2804	.4032	.6954	1.091	.4299	1.163	1.35195	11.317	42.51	.7083	2.389	1.828	1.307	.9360	.2996
1.49	.2764	.3991	.6925	1.105	.4295	1.169	1.35828	11.611	42.16	.7047	2.423	1.845	1.314	.9329	.2962
1.50	.2724	.3950	.6897	1.118	.4290	1.176	1.36458	11.905	41.81	.7011	2.458	1.862	1.320	.9298	.2930
1.51	.2685	.3909	.6868	1.131	.4285	1.183	1.37083	12.200	41.47	.6976	2.493	1.879	1.327	.9266	.2898
1.52	.2646	.3869	.6840	1.145	.4279	1.190	1.37705	12.495	41.14	.6941	2.529	1.896	1.334	.9233	.2866
1.53	.2608	.3829	.6811	1.158	.4273	1.197	1.38322	12.790	40.81	.6907	2.564	1.913	1.340	.9200	.2835
1.54	.2570	.3789	.6783	1.171	.4266	1.204	1.38936	13.086	40.49	.6874	2.600	1.930	1.347	.9166	.2804

A.2-2 Compressible Flow Tables

SUPERSONIC FLOW—Continued

$\gamma = 7/5$

M or M_1	$\frac{p}{p_t}$	$\frac{\rho}{\rho_t}$	$\frac{T}{T_t}$	β	$\frac{q}{p_t}$	$\frac{A}{A_*}$	$\frac{V}{a_*}$	ν	μ	M_2	$\frac{p_2}{p_1}$	$\frac{\rho_2}{\rho_1}$	$\frac{T_2}{T_1}$	$\frac{p_{t_2}}{p_{t_1}}$	$\frac{p_1}{p_{t_2}}$
1.55	.2533	.3750	.6754	1.184	.4259	1.212	1.39546	13.381	40.18	.6841	2.636	1.947	1.354	.9132	.2773
1.56	.2496	.3710	.6726	1.197	.4252	1.219	1.40152	13.677	39.87	.6809	2.673	1.964	1.361	.9097	.2744
1.57	.2459	.3672	.6698	1.210	.4243	1.227	1.40755	13.973	39.56	.6777	2.709	1.981	1.367	.9061	.2714
1.58	.2423	.3633	.6670	1.223	.4235	1.234	1.41353	14.269	39.27	.6746	2.746	1.998	1.374	.9026	.2685
1.59	.2388	.3595	.6642	1.236	.4226	1.242	1.41948	14.564	38.97	.6715	2.783	2.015	1.381	.8989	.2656
1.60	.2353	.3557	.6614	1.249	.4216	1.250	1.42539	14.861	38.68	.6684	2.820	2.032	1.388	.8952	.2628
1.61	.2318	.3520	.6586	1.262	.4206	1.258	1.43127	15.156	38.40	.6655	2.857	2.049	1.395	.8915	.2600
1.62	.2284	.3483	.6558	1.275	.4196	1.267	1.43710	15.452	38.12	.6625	2.895	2.065	1.402	.8877	.2573
1.63	.2250	.3446	.6530	1.287	.4185	1.275	1.44290	15.747	37.84	.6596	2.933	2.082	1.409	.8838	.2546
1.64	.2217	.3409	.6502	1.300	.4174	1.284	1.44866	16.043	37.57	.6568	2.971	2.099	1.416	.8799	.2519
1.65	.2184	.3373	.6475	1.312	.4162	1.292	1.45439	16.338	37.31	.6540	3.010	2.115	1.423	.8760	.2493
1.66	.2151	.3337	.6447	1.325	.4150	1.301	1.46008	16.633	37.04	.6512	3.048	2.132	1.430	.8720	.2467
1.67	.2119	.3302	.6419	1.337	.4138	1.310	1.46573	16.928	36.78	.6485	3.087	2.148	1.437	.8680	.2442
1.68	.2088	.3266	.6392	1.350	.4125	1.319	1.47135	17.222	36.53	.6458	3.126	2.165	1.444	.8640	.2417
1.69	.2057	.3232	.6364	1.362	.4112	1.328	1.47693	17.516	36.28	.6431	3.165	2.181	1.451	.8598	.2392
1.70	.2026	.3197	.6337	1.375	.4098	1.338	1.48247	17.810	36.03	.6405	3.205	2.198	1.458	.8557	.2368
1.71	.1996	.3163	.6310	1.387	.4085	1.347	1.48798	18.103	35.79	.6380	3.245	2.214	1.466	.8516	.2344
1.72	.1966	.3129	.6283	1.399	.4071	1.357	1.49345	18.397	35.55	.6355	3.285	2.230	1.473	.8474	.2320
1.73	.1936	.3095	.6256	1.412	.4056	1.367	1.49889	18.689	35.31	.6330	3.325	2.247	1.480	.8431	.2296
1.74	.1907	.3062	.6229	1.424	.4041	1.376	1.50429	18.981	35.08	.6305	3.366	2.263	1.487	.8389	.2273
1.75	.1878	.3029	.6202	1.436	.4026	1.386	1.50966	19.273	34.85	.6281	3.406	2.279	1.495	.8346	.2251
1.76	.1850	.2996	.6175	1.448	.4011	1.397	1.51499	19.565	34.62	.6257	3.447	2.295	1.502	.8302	.2228
1.77	.1822	.2964	.6148	1.460	.3996	1.407	1.52029	19.855	34.40	.6234	3.488	2.311	1.509	.8259	.2206
1.78	.1794	.2931	.6121	1.473	.3980	1.418	1.52555	20.146	34.18	.6210	3.530	2.327	1.517	.8215	.2184
1.79	.1767	.2900	.6095	1.485	.3964	1.428	1.53078	20.436	33.96	.6188	3.571	2.343	1.524	.8171	.2163
1.80	.1740	.2868	.6068	1.497	.3947	1.439	1.53598	20.725	33.75	.6165	3.613	2.359	1.532	.8127	.2142
1.81	.1714	.2837	.6041	1.509	.3931	1.450	1.54114	21.014	33.54	.6143	3.655	2.375	1.539	.8082	.2121
1.82	.1688	.2806	.6015	1.521	.3914	1.461	1.54626	21.302	33.33	.6121	3.698	2.391	1.547	.8038	.2100
1.83	.1662	.2776	.5989	1.533	.3897	1.472	1.55136	21.590	33.12	.6099	3.740	2.407	1.554	.7993	.2080
1.84	.1637	.2745	.5963	1.545	.3879	1.484	1.55642	21.877	32.92	.6078	3.783	2.422	1.562	.7948	.2060
1.85	.1612	.2715	.5936	1.556	.3862	1.495	1.56145	22.163	32.72	.6057	3.826	2.438	1.569	.7902	.2040
1.86	.1587	.2686	.5910	1.568	.3844	1.507	1.56644	22.449	32.52	.6036	3.870	2.454	1.577	.7857	.2020
1.87	.1563	.2656	.5884	1.580	.3826	1.519	1.57140	22.735	32.33	.6016	3.913	2.469	1.585	.7811	.2001
1.88	.1539	.2627	.5859	1.592	.3808	1.531	1.57633	23.019	32.13	.5996	3.957	2.485	1.592	.7765	.1982
1.89	.1516	.2598	.5833	1.604	.3790	1.543	1.58123	23.303	31.94	.5976	4.001	2.500	1.600	.7720	.1963
1.90	.1492	.2570	.5807	1.616	.3771	1.555	1.58609	23.586	31.76	.5956	4.045	2.516	1.608	.7674	.1945
1.91	.1470	.2542	.5782	1.627	.3753	1.568	1.59092	23.869	31.57	.5937	4.089	2.531	1.616	.7627	.1927
1.92	.1447	.2514	.5756	1.639	.3734	1.580	1.59572	24.151	31.39	.5918	4.134	2.546	1.624	.7581	.1909
1.93	.1425	.2486	.5731	1.651	.3715	1.593	1.60049	24.432	31.21	.5899	4.179	2.562	1.631	.7535	.1891
1.94	.1403	.2459	.5705	1.662	.3696	1.606	1.60523	24.712	31.03	.5880	4.224	2.577	1.639	.7488	.1873

A.2-2 Compressible Flow Tables

SUPERSONIC FLOW—Continued

$\gamma = 7/5$

M or M_1	$\frac{p}{p_t}$	$\frac{\rho}{\rho_t}$	$\frac{T}{T_t}$	β	$\frac{q}{p_t}$	$\frac{A}{A_*}$	$\frac{V}{a_*}$	ν	μ	M_2	$\frac{p_2}{p_1}$	$\frac{\rho_2}{\rho_1}$	$\frac{T_2}{T_1}$	$\frac{p_{t_2}}{p_{t_1}}$	$\frac{p_1}{p_{t_2}}$
1.95	.1381	.2432	.5680	1.674	.3677	1.619	1.60993	24.992	30.85	.5862	4.270	2.592	1.647	.7442	.1856
1.96	.1360	.2405	.5655	1.686	.3657	1.633	1.61460	25.271	30.68	.5844	4.315	2.607	1.655	.7395	.1839
1.97	.1339	.2378	.5630	1.697	.3638	1.646	1.61925	25.549	30.51	.5826	4.361	2.622	1.663	.7349	.1822
1.98	.1318	.2352	.5605	1.709	.3618	1.660	1.62386	25.827	30.33	.5808	4.407	2.637	1.671	.7302	.1806
1.99	.1298	.2326	.5580	1.720	.3598	1.674	1.62844	26.104	30.17	.5791	4.453	2.652	1.679	.7255	.1789
2.00	.1278	.2300	.5556	1.732	.3579	1.688	1.63299	26.380	30.00	.5774	4.500	2.667	1.688	.7209	.1773
2.01	.1258	.2275	.5531	1.744	.3559	1.702	1.63751	26.655	29.84	.5757	4.547	2.681	1.696	.7162	.1757
2.02	.1239	.2250	.5506	1.755	.3539	1.716	1.64201	26.929	29.67	.5740	4.594	2.696	1.704	.7115	.1741
2.03	.1220	.2225	.5482	1.767	.3518	1.730	1.64647	27.203	29.51	.5723	4.641	2.711	1.712	.7069	.1726
2.04	.1201	.2200	.5458	1.778	.3498	1.745	1.65090	27.476	29.35	.5707	4.689	2.725	1.720	.7022	.1710
2.05	.1182	.2176	.5433	1.790	.3478	1.760	1.65530	27.748	29.20	.5691	4.736	2.740	1.729	.6975	.1695
2.06	.1164	.2152	.5409	1.801	.3458	1.775	1.65967	28.020	29.04	.5675	4.784	2.755	1.737	.6928	.1680
2.07	.1146	.2128	.5385	1.812	.3437	1.790	1.66402	28.290	28.89	.5659	4.832	2.769	1.745	.6882	.1665
2.08	.1128	.2104	.5361	1.824	.3417	1.806	1.66833	28.560	28.74	.5643	4.881	2.783	1.754	.6835	.1651
2.09	.1111	.2081	.5337	1.835	.3396	1.821	1.67262	28.829	28.59	.5628	4.929	2.798	1.762	.6789	.1636
2.10	.1094	.2058	.5313	1.847	.3376	1.837	1.67687	29.097	28.44	.5613	4.978	2.812	1.770	.6742	.1622
2.11	.1077	.2035	.5290	1.858	.3355	1.853	1.68110	29.364	28.29	.5598	5.027	2.826	1.779	.6696	.1608
2.12	.1060	.2013	.5266	1.869	.3334	1.869	1.68530	29.631	28.14	.5583	5.077	2.840	1.787	.6649	.1594
2.13	.1043	.1990	.5243	1.881	.3314	1.885	1.68947	29.897	28.00	.5568	5.126	2.854	1.796	.6603	.1580
2.14	.1027	.1968	.5219	1.892	.3293	1.902	1.69362	30.161	27.86	.5554	5.176	2.868	1.805	.6557	.1567
2.15	.1011	.1946	.5196	1.903	.3272	1.919	1.69774	30.425	27.72	.5540	5.226	2.882	1.813	.6511	.1553
2.16	.9956 −1	.1925	.5173	1.915	.3252	1.935	1.70183	30.689	27.58	.5525	5.277	2.896	1.822	.6464	.1540
2.17	.9802 −1	.1903	.5150	1.926	.3231	1.953	1.70589	30.951	27.44	.5511	5.327	2.910	1.831	.6419	.1527
2.18	.9649 −1	.1882	.5127	1.937	.3210	1.970	1.70992	31.212	27.30	.5498	5.378	2.924	1.839	.6373	.1514
2.19	.9500 −1	.1861	.5104	1.948	.3189	1.987	1.71393	31.473	27.17	.5484	5.429	2.938	1.848	.6327	.1502
2.20	.9352 −1	.1841	.5081	1.960	.3169	2.005	1.71791	31.732	27.04	.5471	5.480	2.951	1.857	.6281	.1489
2.21	.9207 −1	.1820	.5059	1.971	.3148	2.023	1.72187	31.991	26.90	.5457	5.531	2.965	1.866	.6236	.1476
2.22	.9064 −1	.1800	.5036	1.982	.3127	2.041	1.72579	32.250	26.77	.5444	5.583	2.978	1.875	.6191	.1464
2.23	.8923 −1	.1780	.5014	1.993	.3106	2.059	1.72970	32.507	26.64	.5431	5.636	2.992	1.883	.6145	.1452
2.24	.8785 −1	.1760	.4991	2.004	.3085	2.078	1.73357	32.763	26.51	.5418	5.687	3.005	1.892	.6100	.1440
2.25	.8648 −1	.1740	.4969	2.016	.3065	2.096	1.73742	33.018	26.39	.5406	5.740	3.019	1.901	.6055	.1428
2.26	.8514 −1	.1721	.4947	2.027	.3044	2.115	1.74125	33.273	26.26	.5393	5.792	3.032	1.910	.6011	.1417
2.27	.8382 −1	.1702	.4925	2.038	.3023	2.134	1.74504	33.527	26.14	.5381	5.845	3.045	1.919	.5966	.1405
2.28	.8251 −1	.1683	.4903	2.049	.3003	2.154	1.74882	33.780	26.01	.5368	5.898	3.058	1.929	.5921	.1394
2.29	.8123 −1	.1664	.4881	2.060	.2982	2.173	1.75257	34.032	25.89	.5356	5.951	3.071	1.938	.5877	.1382

A.2-2 Compressible Flow Tables

SUPERSONIC FLOW—Continued

$\gamma = 7/5$

M or M_1	$\frac{p}{p_t}$	$\frac{\rho}{\rho_t}$	$\frac{T}{T_t}$	β	$\frac{q}{p_t}$	$\frac{A}{A_*}$	$\frac{V}{a_*}$	ν	μ	M_2	$\frac{p_2}{p_1}$	$\frac{\rho_2}{\rho_1}$	$\frac{T_2}{T_1}$	$\frac{p_{t_2}}{p_{t_1}}$	$\frac{p_1}{p_{t_2}}$
2.30	.7997 −1	.1646	.4859	2.071	.2961	2.193	1.75629	34.283	25.77	.5344	6.005	3.085	1.947	.5833	.1371
2.31	.7873 −1	.1628	.4837	2.082	.2941	2.213	1.75999	34.533	25.65	.5332	6.059	3.098	1.956	.5789	.1360
2.32	.7751 −1	.1609	.4816	2.093	.2920	2.233	1.76366	34.783	25.53	.5321	6.113	3.110	1.965	.5745	.1349
2.33	.7631 −1	.1592	.4794	2.104	.2900	2.254	1.76731	35.031	25.42	.5309	6.167	3.123	1.974	.5702	.1338
2.34	.7512 −1	.1574	.4773	2.116	.2879	2.274	1.77093	35.279	25.30	.5297	6.222	3.136	1.984	.5658	.1328
2.35	.7396 −1	.1556	.4752	2.127	.2859	2.295	1.77453	35.526	25.18	.5286	6.276	3.149	1.993	.5615	.1317
2.36	.7281 −1	.1539	.4731	2.138	.2839	2.316	1.77811	35.771	25.07	.5275	6.331	3.162	2.002	.5572	.1307
2.37	.7168 −1	.1522	.4709	2.149	.2818	2.338	1.78166	36.017	24.96	.5264	6.386	3.174	2.012	.5529	.1297
2.38	.7057 −1	.1505	.4688	2.160	.2798	2.359	1.78519	36.261	24.85	.5253	6.442	3.187	2.021	.5486	.1286
2.39	.6948 −1	.1488	.4668	2.171	.2778	2.381	1.78869	36.504	24.73	.5242	6.497	3.199	2.031	.5444	.1276
2.40	.6840 −1	.1472	.4647	2.182	.2758	2.403	1.79218	36.746	24.62	.5231	6.553	3.212	2.040	.5401	.1266
2.41	.6734 −1	.1456	.4626	2.193	.2738	2.425	1.79563	36.988	24.52	.5221	6.609	3.224	2.050	.5359	.1257
2.42	.6630 −1	.1439	.4606	2.204	.2718	2.448	1.79907	37.229	24.41	.5210	6.666	3.237	2.059	.5317	.1247
2.43	.6527 −1	.1424	.4585	2.215	.2698	2.471	1.80248	37.469	24.30	.5200	6.722	3.249	2.069	.5276	.1237
2.44	.6426 −1	.1408	.4565	2.226	.2678	2.494	1.80587	37.708	24.19	.5189	6.779	3.261	2.079	.5234	.1228
2.45	.6327 −1	.1392	.4544	2.237	.2658	2.517	1.80924	37.946	24.09	.5179	6.836	3.273	2.088	.5193	.1218
2.46	.6229 −1	.1377	.4524	2.248	.2639	2.540	1.81258	38.183	23.99	.5169	6.894	3.285	2.098	.5152	.1209
2.47	.6133 −1	.1362	.4504	2.259	.2619	2.564	1.81591	38.420	23.88	.5159	6.951	3.298	2.108	.5111	.1200
2.48	.6038 −1	.1346	.4484	2.269	.2599	2.588	1.81921	38.655	23.78	.5149	7.009	3.310	2.118	.5071	.1191
2.49	.5945 −1	.1332	.4464	2.280	.2580	2.612	1.82249	38.890	23.68	.5140	7.067	3.321	2.128	.5030	.1182
2.50	.5853 −1	.1317	.4444	2.291	.2561	2.637	1.82574	39.124	23.58	.5130	7.125	3.333	2.138	.4990	.1173
2.51	.5762 −1	.1302	.4425	2.302	.2541	2.661	1.82898	39.357	23.48	.5120	7.183	3.345	2.147	.4950	.1164
2.52	.5674 −1	.1288	.4405	2.313	.2522	2.686	1.83219	39.589	23.38	.5111	7.242	3.357	2.157	.4911	.1155
2.53	.5586 −1	.1274	.4386	2.324	.2503	2.712	1.83538	39.820	23.28	.5102	7.301	3.369	2.167	.4871	.1147
2.54	.5500 −1	.1260	.4366	2.335	.2484	2.737	1.83855	40.050	23.18	.5092	7.360	3.380	2.177	.4832	.1138
2.55	.5415 −1	.1246	.4347	2.346	.2465	2.763	1.84170	40.280	23.09	.5083	7.420	3.392	2.187	.4793	.1130
2.56	.5332 −1	.1232	.4328	2.357	.2446	2.789	1.84483	40.509	22.99	.5074	7.479	3.403	2.198	.4754	.1122
2.57	.5250 −1	.1218	.4309	2.367	.2427	2.815	1.84794	40.736	22.91	.5065	7.539	3.415	2.208	.4715	.1113
2.58	.5169 −1	.1205	.4289	2.378	.2409	2.842	1.85103	40.963	22.81	.5056	7.599	3.426	2.218	.4677	.1105
2.59	.5090 −1	.1192	.4271	2.389	.2390	2.869	1.85410	41.189	22.71	.5047	7.659	3.438	2.228	.4639	.1097
2.60	.5012 −1	.1179	.4252	2.400	.2371	2.896	1.85714	41.415	22.62	.5039	7.720	3.449	2.238	.4601	.1089
2.61	.4935 −1	.1166	.4233	2.411	.2353	2.923	1.86017	41.639	22.53	.5030	7.781	3.460	2.249	.4564	.1081
2.62	.4859 −1	.1153	.4214	2.422	.2335	2.951	1.86318	41.863	22.44	.5022	7.842	3.471	2.259	.4526	.1074
2.63	.4784 −1	.1140	.4196	2.432	.2317	2.979	1.86616	42.086	22.35	.5013	7.903	3.483	2.269	.4489	.1066
2.64	.4711 −1	.1128	.4177	2.443	.2298	3.007	1.86913	42.307	22.26	.5005	7.965	3.494	2.280	.4452	.1058

A.2-2 Compressible Flow Tables

SUPERSONIC FLOW—Continued

$\gamma = 7/5$

M or M_1	$\frac{p}{p_t}$	$\frac{\rho}{\rho_t}$	$\frac{T}{T_t}$	β	$\frac{q}{p_t}$	$\frac{A}{A_*}$	$\frac{V}{a_*}$	ν	μ	M_2	$\frac{p_2}{p_1}$	$\frac{\rho_2}{\rho_1}$	$\frac{T_2}{T_1}$	$\frac{p_{t_2}}{p_{t_1}}$	$\frac{p_1}{p_{t_2}}$
2.65	.4639 −1	.1115	.4159	2.454	.2280	3.036	1.87208	42.529	22.17	.4996	8.026	3.505	2.290	.4416	.1051
2.66	.4568 −1	.1103	.4141	2.465	.2262	3.065	1.87501	42.749	22.08	.4988	8.088	3.516	2.301	.4379	.1043
2.67	.4498 −1	.1091	.4122	2.476	.2245	3.094	1.87792	42.968	22.00	.4980	8.150	3.527	2.311	.4343	.1036
2.68	.4429 −1	.1079	.4104	2.486	.2227	3.123	1.88081	43.187	21.91	.4972	8.213	3.537	2.322	.4307	.1028
2.69	.4362 −1	.1067	.4086	2.497	.2209	3.153	1.88368	43.405	21.82	.4964	8.275	3.548	2.332	.4271	.1021
2.70	.4295 −1	.1056	.4068	2.508	.2192	3.183	1.88653	43.621	21.74	.4956	8.338	3.559	2.343	.4236	.1014
2.71	.4229 −1	.1044	.4051	2.519	.2174	3.213	1.88936	43.838	21.65	.4949	8.401	3.570	2.354	.4201	.1007
2.72	.4165 −1	.1033	.4033	2.530	.2157	3.244	1.89218	44.053	21.57	.4941	8.465	3.580	2.364	.4166	.9998 −1
2.73	.4102 −1	.1022	.4015	2.540	.2140	3.275	1.89497	44.267	21.49	.4933	8.528	3.591	2.375	.4131	.9929 −1
2.74	.4039 −1	.1010	.3998	2.551	.2123	3.306	1.89775	44.481	21.41	.4926	8.592	3.601	2.386	.4097	.9860 −1
2.75	.3978 −1	.9994 −1	.3980	2.562	.2106	3.338	1.90051	44.694	21.32	.4918	8.656	3.612	2.397	.4062	.9792 −1
2.76	.3917 −1	.9885 −1	.3963	2.572	.2089	3.370	1.90325	44.906	21.24	.4911	8.721	3.622	2.407	.4028	.9724 −1
2.77	.3858 −1	.9778 −1	.3945	2.583	.2072	3.402	1.90598	45.117	21.16	.4903	8.785	3.633	2.418	.3994	.9658 −1
2.78	.3799 −1	.9671 −1	.3928	2.594	.2055	3.434	1.90868	45.327	21.08	.4896	8.850	3.643	2.429	.3961	.9591 −1
2.79	.3742 −1	.9566 −1	.3911	2.605	.2039	3.467	1.91137	45.537	21.00	.4889	8.915	3.653	2.440	.3928	.9526 −1
2.80	.3685 −1	.9463 −1	.3894	2.615	.2022	3.500	1.91404	45.746	20.92	.4882	8.980	3.664	2.451	.3895	.9461 −1
2.81	.3629 −1	.9360 −1	.3877	2.626	.2006	3.534	1.91669	45.954	20.85	.4875	9.045	3.674	2.462	.3862	.9397 −1
2.82	.3574 −1	.9259 −1	.3860	2.637	.1990	3.567	1.91933	46.161	20.77	.4868	9.111	3.684	2.473	.3829	.9334 −1
2.83	.3520 −1	.9158 −1	.3844	2.647	.1973	3.601	1.92195	46.368	20.69	.4861	9.177	3.694	2.484	.3797	.9271 −1
2.84	.3467 −1	.9059 −1	.3827	2.658	.1957	3.636	1.92455	46.573	20.62	.4854	9.243	3.704	2.496	.3765	.9209 −1
2.85	.3415 −1	.8962 −1	.3810	2.669	.1941	3.671	1.92714	46.778	20.54	.4847	9.310	3.714	2.507	.3733	.9147 −1
2.86	.3363 −1	.8865 −1	.3794	2.679	.1926	3.706	1.92970	46.982	20.47	.4840	9.376	3.724	2.518	.3701	.9086 −1
2.87	.3312 −1	.8769 −1	.3777	2.690	.1910	3.741	1.93225	47.185	20.39	.4833	9.443	3.734	2.529	.3670	.9026 −1
2.88	.3263 −1	.8675 −1	.3761	2.701	.1894	3.777	1.93479	47.388	20.32	.4827	9.510	3.743	2.540	.3639	.8966 −1
2.89	.3213 −1	.8581 −1	.3745	2.711	.1879	3.813	1.93731	47.589	20.24	.4820	9.577	3.753	2.552	.3608	.8906 −1
2.90	.3165 −1	.8489 −1	.3729	2.722	.1863	3.850	1.93981	47.790	20.17	.4814	9.645	3.763	2.563	.3577	.8848 −1
2.91	.3118 −1	.8398 −1	.3712	2.733	.1848	3.887	1.94230	47.990	20.10	.4807	9.713	3.773	2.575	.3547	.8790 −1
2.92	.3071 −1	.8307 −1	.3696	2.743	.1833	3.924	1.94477	48.190	20.03	.4801	9.781	3.782	2.586	.3517	.8732 −1
2.93	.3025 −1	.8218 −1	.3681	2.754	.1818	3.961	1.94722	48.388	19.96	.4795	9.849	3.792	2.598	.3487	.8675 −1
2.94	.2980 −1	.8130 −1	.3665	2.765	.1803	3.999	1.94966	48.586	19.89	.4788	9.918	3.801	2.609	.3457	.8619 −1
2.95	.2935 −1	.8043 −1	.3649	2.775	.1788	4.038	1.95208	48.783	19.81	.4782	9.986	3.811	2.621	.3428	.8563 −1
2.96	.2891 −1	.7957 −1	.3633	2.786	.1773	4.076	1.95449	48.980	19.75	.4776	10.06	3.820	2.632	.3398	.8507 −1
2.97	.2848 −1	.7872 −1	.3618	2.797	.1758	4.115	1.95688	49.175	19.68	.4770	10.12	3.829	2.644	.3369	.8453 −1
2.98	.2805 −1	.7788 −1	.3602	2.807	.1744	4.155	1.95925	49.370	19.61	.4764	10.19	3.839	2.656	.3340	.8398 −1
2.99	.2764 −1	.7705 −1	.3587	2.818	.1729	4.194	1.96162	49.564	19.54	.4758	10.26	3.848	2.667	.3312	.8345 −1
3.00	.2722 −1	.7623 −1	.3571	2.828	.1715	4.235	1.96396	49.757	19.47	.4752	10.33	3.857	2.679	.3283	.8291 −1
3.01	.2682 −1	.7541 −1	.3556	2.839	.1701	4.275	1.96629	49.950	19.40	.4746	10.40	3.866	2.691	.3255	.8238 −1
3.02	.2642 −1	.7461 −1	.3541	2.850	.1687	4.316	1.96861	50.142	19.34	.4740	10.47	3.875	2.703	.3227	.8186 −1
3.03	.2603 −1	.7382 −1	.3526	2.860	.1673	4.357	1.97091	50.333	19.27	.4734	10.54	3.884	2.714	.3200	.8134 −1
3.04	.2564 −1	.7303 −1	.3511	2.871	.1659	4.399	1.97319	50.523	19.20	.4729	10.62	3.893	2.726	.3172	.8083 −1

A.2-2 Compressible Flow Tables

SUPERSONIC FLOW—Continued

$\gamma = 7/5$

M or M_1	$\frac{p}{p_t}$	$\frac{\rho}{\rho_t}$	$\frac{T}{T_t}$	β	$\frac{q}{p_t}$	$\frac{A}{A_*}$	$\frac{V}{a_*}$	ν	μ	M_2	$\frac{p_2}{p_1}$	$\frac{\rho_2}{\rho_1}$	$\frac{T_2}{T_1}$	$\frac{p_{t_2}}{p_{t_1}}$	$\frac{p_1}{p_{t_2}}$
3.05	.2526 −1	.7226 −1	.3496	2.881	.1645	4.441	1.97547	50.713	19.14	.4723	10.69	3.962	2.738	.3145	.8032 −1
3.06	.2489 −1	.7149 −1	.3481	2.892	.1631	4.483	1.97772	50.902	19.07	.4717	10.76	3.911	2.750	.3118	.7982 −1
3.07	.2452 −1	.7074 −1	.3466	2.903	.1618	4.526	1.97997	51.090	19.01	.4712	10.83	3.920	2.762	.3091	.7932 −1
3.08	.2416 −1	.6999 −1	.3452	2.913	.1604	4.570	1.98219	51.277	18.95	.4706	10.90	3.929	2.774	.3065	.7882 −1
3.09	.2380 −1	.6925 −1	.3437	2.924	.1591	4.613	1.98441	51.464	18.88	.4701	10.97	3.938	2.786	.3038	.7833 −1
3.10	.2345 −1	.6852 −1	.3422	2.934	.1577	4.657	1.98661	51.650	18.82	.4695	11.05	3.947	2.799	.3012	.7785 −1
3.11	.2310 −1	.6779 −1	.3408	2.945	.1564	4.702	1.98879	51.835	18.76	.4690	11.12	3.955	2.811	.2986	.7737 −1
3.12	.2276 −1	.6708 −1	.3393	2.955	.1551	4.747	1.99097	52.020	18.69	.4685	11.19	3.964	2.823	.2960	.7689 −1
3.13	.2243 −1	.6637 −1	.3379	2.966	.1538	4.792	1.99313	52.203	18.63	.4679	11.26	3.973	2.835	.2935	.7642 −1
3.14	.2210 −1	.6568 −1	.3365	2.977	.1525	4.838	1.99527	52.386	18.57	.4674	11.34	3.981	2.848	.2910	.7595 −1
3.15	.2177 −1	.6499 −1	.3351	2.987	.1512	4.884	1.99740	52.569	18.51	.4669	11.41	3.990	2.860	.2885	.7549 −1
3.16	.2146 −1	.6430 −1	.3337	2.998	.1500	4.930	1.99952	52.751	18.45	.4664	11.48	3.998	2.872	.2860	.7503 −1
3.17	.2114 −1	.6363 −1	.3323	3.008	.1487	4.977	2.00162	52.931	18.39	.4659	11.56	4.006	2.885	.2835	.7457 −1
3.18	.2083 −1	.6296 −1	.3309	3.019	.1475	5.025	2.00372	53.112	18.33	.4654	11.63	4.015	2.897	.2811	.7412 −1
3.19	.2053 −1	.6231 −1	.3295	3.029	.1462	5.073	2.00579	53.292	18.27	.4648	11.71	4.023	2.909	.2786	.7367 −1
3.20	.2023 −1	.6165 −1	.3281	3.040	.1450	5.121	2.00786	53.470	18.21	.4643	11.78	4.031	2.922	.2762	.7323 −1
3.21	.1993 −1	.6101 −1	.3267	3.050	.1438	5.170	2.00991	53.648	18.15	.4639	11.85	4.040	2.935	.2738	.7279 −1
3.22	.1964 −1	.6037 −1	.3253	3.061	.1426	5.219	2.01195	53.826	18.09	.4634	11.93	4.048	2.947	.2715	.7235 −1
3.23	.1936 −1	.5975 −1	.3240	3.071	.1414	5.268	2.01398	54.003	18.03	.4629	12.01	4.056	2.960	.2691	.7192 −1
3.24	.1908 −1	.5912 −1	.3226	3.082	.1402	5.319	2.01599	54.179	17.98	.4624	12.08	4.064	2.972	.2668	.7149 −1
3.25	.1880 −1	.5851 −1	.3213	3.092	.1390	5.369	2.01799	54.355	17.92	.4619	12.16	4.072	2.985	.2645	.7107 −1
3.26	.1853 −1	.5790 −1	.3199	3.103	.1378	5.420	2.01998	54.529	17.86	.4614	12.23	4.080	2.998	.2622	.7065 −1
3.27	.1826 −1	.5730 −1	.3186	3.113	.1367	5.472	2.02196	54.703	17.81	.4610	12.31	4.088	3.011	.2600	.7023 −1
3.28	.1799 −1	.5671 −1	.3173	3.124	.1355	5.523	2.02392	54.877	17.75	.4605	12.38	4.096	3.023	.2577	.6982 −1
3.29	.1773 −1	.5612 −1	.3160	3.134	.1344	5.576	2.02587	55.050	17.70	.4600	12.46	4.104	3.036	.2555	.6941 −1
3.30	.1748 −1	.5554 −1	.3147	3.145	.1332	5.629	2.02781	55.222	17.64	.4596	12.54	4.112	3.049	.2533	.6900 −1
3.31	.1722 −1	.5497 −1	.3134	3.155	.1321	5.682	2.02974	55.393	17.58	.4591	12.62	4.120	3.062	.2511	.6860 −1
3.32	.1698 −1	.5440 −1	.3121	3.166	.1310	5.736	2.03165	55.564	17.53	.4587	12.69	4.128	3.075	.2489	.6820 −1
3.33	.1673 −1	.5384 −1	.3108	3.176	.1299	5.790	2.03356	55.734	17.48	.4582	12.77	4.135	3.088	.2468	.6781 −1
3.34	.1649 −1	.5329 −1	.3095	3.187	.1288	5.845	2.03545	55.904	17.42	.4578	12.85	4.143	3.101	.2446	.6741 −1
3.35	.1625 −1	.5274 −1	.3082	3.197	.1277	5.900	2.03733	56.073	17.37	.4573	12.93	4.151	3.114	.2425	.6702 −1
3.36	.1602 −1	.5220 −1	.3069	3.208	.1266	5.956	2.03920	56.241	17.31	.4569	13.00	4.158	3.127	.2404	.6664 −1
3.37	.1579 −1	.5166 −1	.3057	3.218	.1255	6.012	2.04106	56.409	17.26	.4565	13.08	4.166	3.141	.2383	.6626 −1
3.38	.1557 −1	.5113 −1	.3044	3.229	.1245	6.069	2.04290	56.576	17.21	.4560	13.16	4.173	3.154	.2363	.6588 −1
3.39	.1534 −1	.5061 −1	.3032	3.239	.1234	6.126	2.04474	56.742	17.16	.4556	13.24	4.181	3.167	.2342	.6550 −1

A.2-2 Compressible Flow Tables

SUPERSONIC FLOW—Continued

$\gamma = 7/5$

M or M_1	$\frac{p}{p_t}$	$\frac{\rho}{\rho_t}$	$\frac{T}{T_t}$	β	$\frac{q}{p_t}$	$\frac{A}{A_*}$	$\frac{V}{a_*}$	ν	μ	M_2	$\frac{p_2}{p_1}$	$\frac{\rho_2}{\rho_1}$	$\frac{T_2}{T_1}$	$\frac{p_{t_2}}{p_{t_1}}$	$\frac{p_1}{p_{t_2}}$
3.40	.1512 −1	.5009 −1	.3019	3.250	.1224	6.184	2.04656	56.907	17.10	.4552	13.32	4.188	3.180	.2322	.6513 −1
3.41	.1491 −1	.4958 −1	.3007	3.260	.1214	6.242	2.04837	57.073	17.05	.4548	13.40	4.196	3.194	.2302	.6476 −1
3.42	.1470 −1	.4908 −1	.2995	3.271	.1203	6.301	2.05017	57.237	17.00	.4544	13.48	4.203	3.207	.2282	.6439 −1
3.43	.1449 −1	.4858 −1	.2982	3.281	.1193	6.360	2.05196	57.401	16.95	.4540	13.56	4.211	3.220	.2263	.6403 −1
3.44	.1428 −1	.4808 −1	.2970	3.291	.1183	6.420	2.05374	57.564	16.90	.4535	13.64	4.218	3.234	.2243	.6367 −1
3.45	.1408 −1	.4759 −1	.2958	3.302	.1173	6.480	2.05551	57.726	16.85	.4531	13.72	4.225	3.247	.2224	.6331 −1
3.46	.1388 −1	.4711 −1	.2946	3.312	.1163	6.541	2.05727	57.888	16.80	.4527	13.80	4.232	3.261	.2205	.6296 −1
3.47	.1368 −1	.4663 −1	.2934	3.323	.1153	6.602	2.05901	58.050	16.75	.4523	13.88	4.240	3.274	.2186	.6261 −1
3.48	.1349 −1	.4616 −1	.2922	3.333	.1144	6.664	2.06075	58.210	16.70	.4519	13.96	4.247	3.288	.2167	.6226 −1
3.49	.1330 −1	.4569 −1	.2910	3.344	.1134	6.727	2.06247	58.370	16.65	.4515	14.04	4.254	3.301	.2148	.6191 −1
3.50	.1311 −1	.4523 −1	.2899	3.354	.1124	6.790	2.06419	58.530	16.60	.4512	14.13	4.261	3.315	.2129	.6157 −1
3.51	.1293 −1	.4478 −1	.2887	3.365	.1115	6.853	2.06589	58.689	16.55	.4508	14.21	4.268	3.329	.2111	.6123 −1
3.52	.1274 −1	.4433 −1	.2875	3.375	.1105	6.917	2.06759	58.847	16.51	.4504	14.29	4.275	3.343	.2093	.6089 −1
3.53	.1256 −1	.4388 −1	.2864	3.385	.1096	6.982	2.06927	59.004	16.46	.4500	14.37	4.282	3.356	.2075	.6056 −1
3.54	.1239 −1	.4344 −1	.2852	3.396	.1087	7.047	2.07094	59.162	16.41	.4496	14.45	4.289	3.370	.2057	.6023 −1
3.55	.1221 −1	.4300 −1	.2841	3.406	.1078	7.113	2.07261	59.318	16.36	.4492	14.54	4.296	3.384	.2039	.5990 −1
3.56	.1204 −1	.4257 −1	.2829	3.417	.1069	7.179	2.07426	59.474	16.31	.4489	14.62	4.303	3.398	.2022	.5957 −1
3.57	.1188 −1	.4214 −1	.2818	3.427	.1059	7.246	2.07590	59.629	16.27	.4485	14.70	4.309	3.412	.2004	.5925 −1
3.58	.1171 −1	.4172 −1	.2806	3.437	.1051	7.313	2.07754	59.784	16.22	.4481	14.79	4.316	3.426	.1987	.5892 −1
3.59	.1155 −1	.4131 −1	.2795	3.448	.1042	7.382	2.07916	59.938	16.17	.4478	14.87	4.323	3.440	.1970	.5861 −1
3.60	.1138 −1	.4089 −1	.2784	3.458	.1033	7.450	2.08077	60.091	16.13	.4474	14.95	4.330	3.454	.1953	.5829 −1
3.61	.1123 −1	.4049 −1	.2773	3.469	.1024	7.519	2.08238	60.244	16.08	.4471	15.04	4.336	3.468	.1936	.5798 −1
3.62	.1107 −1	.4008 −1	.2762	3.479	.1016	7.589	2.08397	60.397	16.04	.4467	15.12	4.343	3.482	.1920	.5767 −1
3.63	.1092 −1	.3968 −1	.2751	3.490	.1007	7.659	2.08556	60.549	15.99	.4463	15.21	4.350	3.496	.1903	.5736 −1
3.64	.1076 −1	.3929 −1	.2740	3.500	.9984 −1	7.730	2.08713	60.700	15.95	.4460	15.29	4.356	3.510	.1887	.5705 −1
3.65	.1062 −1	.3890 −1	.2729	3.510	.9900 −1	7.802	2.08870	60.851	15.90	.4456	15.38	4.363	3.525	.1871	.5675 −1
3.66	.1047 −1	.3852 −1	.2718	3.521	.9817 −1	7.874	2.09026	61.000	15.86	.4453	15.46	4.369	3.539	.1855	.5645 −1
3.67	.1032 −1	.3813 −1	.2707	3.531	.9734 −1	7.947	2.09180	61.150	15.81	.4450	15.55	4.376	3.553	.1839	.5615 −1
3.68	.1018 −1	.3776 −1	.2697	3.542	.9652 −1	8.020	2.09334	61.299	15.77	.4446	15.63	4.382	3.568	.1823	.5585 −1
3.69	.1004 −1	.3739 −1	.2686	3.552	.9570 −1	8.094	2.09487	61.447	15.72	.4443	15.72	4.388	3.582	.1807	.5556 −1
3.70	.9903 −2	.3702 −1	.2675	3.562	.9490 −1	8.169	2.09639	61.595	15.68	.4439	15.81	4.395	3.596	.1792	.5526 −1
3.71	.9767 −2	.3665 −1	.2665	3.573	.9410 −1	8.244	2.09790	61.743	15.64	.4436	15.89	4.401	3.611	.1777	.5497 −1
3.72	.9633 −2	.3629 −1	.2654	3.583	.9331 −1	8.320	2.09941	61.889	15.59	.4433	15.98	4.408	3.625	.1761	.5469 −1
3.73	.9500 −2	.3594 −1	.2644	3.593	.9253 −1	8.397	2.10090	62.036	15.55	.4430	16.07	4.414	3.640	.1746	.5440 −1
3.74	.9370 −2	.3558 −1	.2633	3.604	.9175 −1	8.474	2.10238	62.181	15.51	.4426	16.15	4.420	3.654	.1731	.5412 −1

A.2-2 Compressible Flow Tables

SUPERSONIC FLOW—Continued

$\gamma = 7/5$

M or M_1	$\frac{p}{p_t}$	$\frac{\rho}{\rho_t}$	$\frac{T}{T_t}$	β	$\frac{q}{p_t}$	$\frac{A}{A_*}$	$\frac{V}{a_*}$	ν	μ	M_2	$\frac{p_2}{p_1}$	$\frac{\rho_2}{\rho_1}$	$\frac{T_2}{T_1}$	$\frac{p_{t_2}}{p_{t_1}}$	$\frac{p_1}{p_{t_2}}$
3.75	.9242 −2	.3524 −1	.2623	3.614	.9098 −1	8.552	2.10386	62.326	15.47	.4423	16.24	4.426	3.669	.1717	.5384 −1
3.76	.9116 −2	.3489 −1	.2613	3.625	.9021 −1	8.630	2.10533	62.471	15.42	.4420	16.33	4.432	3.684	.1702	.5356 −1
3.77	.8991 −2	.3455 −1	.2602	3.635	.8945 −1	8.709	2.10679	62.615	15.38	.4417	16.42	4.439	3.698	.1687	.5328 −1
3.78	.8869 −2	.3421 −1	.2592	3.645	.8870 −1	8.789	2.10824	62.758	15.34	.4414	16.50	4.445	3.713	.1673	.5301 −1
3.79	.8748 −2	.3388 −1	.2582	3.656	.8796 −1	8.870	2.10968	62.901	15.30	.4410	16.59	4.451	3.728	.1659	.5274 −1
3.80	.8629 −2	.3355 −1	.2572	3.666	.8722 −1	8.951	2.11111	63.044	15.26	.4407	16.68	4.457	3.743	.1645	.5247 −1
3.81	.8512 −2	.3322 −1	.2562	3.676	.8649 −1	9.032	2.11254	63.186	15.22	.4404	16.77	4.463	3.758	.1631	.5220 −1
3.82	.8396 −2	.3290 −1	.2552	3.687	.8577 −1	9.115	2.11395	63.327	15.18	.4401	16.86	4.469	3.772	.1617	.5193 −1
3.83	.8283 −2	.3258 −1	.2542	3.697	.8505 −1	9.198	2.11536	63.468	15.14	.4398	16.95	4.475	3.787	.1603	.5167 −1
3.84	.8171 −2	.3227 −1	.2532	3.708	.8434 −1	9.282	2.11676	63.608	15.10	.4395	17.04	4.481	3.802	.1589	.5140 −1
3.85	.8060 −2	.3195 −1	.2522	3.718	.8363 −1	9.366	2.11815	63.748	15.06	.4392	17.13	4.487	3.817	.1576	.5114 −1
3.86	.7951 −2	.3165 −1	.2513	3.728	.8293 −1	9.451	2.11954	63.887	15.02	.4389	17.22	4.492	3.832	.1563	.5089 −1
3.87	.7844 −2	.3134 −1	.2503	3.739	.8224 −1	9.537	2.12091	64.026	14.98	.4386	17.31	4.498	3.847	.1549	.5063 −1
3.88	.7739 −2	.3104 −1	.2493	3.749	.8155 −1	9.624	2.12228	64.164	14.94	.4383	17.40	4.504	3.863	.1536	.5038 −1
3.89	.7635 −2	.3074 −1	.2484	3.759	.8087 −1	9.711	2.12364	64.302	14.90	.4380	17.49	4.510	3.878	.1523	.5012 −1
3.90	.7532 −2	.3044 −1	.2474	3.770	.8019 −1	9.799	2.12499	64.440	14.86	.4377	17.58	4.516	3.893	.1510	.4987 −1
3.91	.7431 −2	.3015 −1	.2464	3.780	.7952 −1	9.888	2.12634	64.576	14.82	.4375	17.67	4.521	3.908	.1497	.4962 −1
3.92	.7332 −2	.2986 −1	.2455	3.790	.7886 −1	9.977	2.12767	64.713	14.78	.4372	17.76	4.527	3.923	.1485	.4938 −1
3.93	.7233 −2	.2958 −1	.2446	3.801	.7820 −1	10.07	2.12900	64.848	14.74	.4369	17.85	4.533	3.939	.1472	.4913 −1
3.94	.7137 −2	.2929 −1	.2436	3.811	.7755 −1	10.16	2.13032	64.983	14.70	.4366	17.94	4.538	3.954	.1460	.4889 −1

(concluded)

A.2-3 Shock Charts

REPORT 1135—NATIONAL ADVISORY COMMITTEE FOR AERONAUTICS

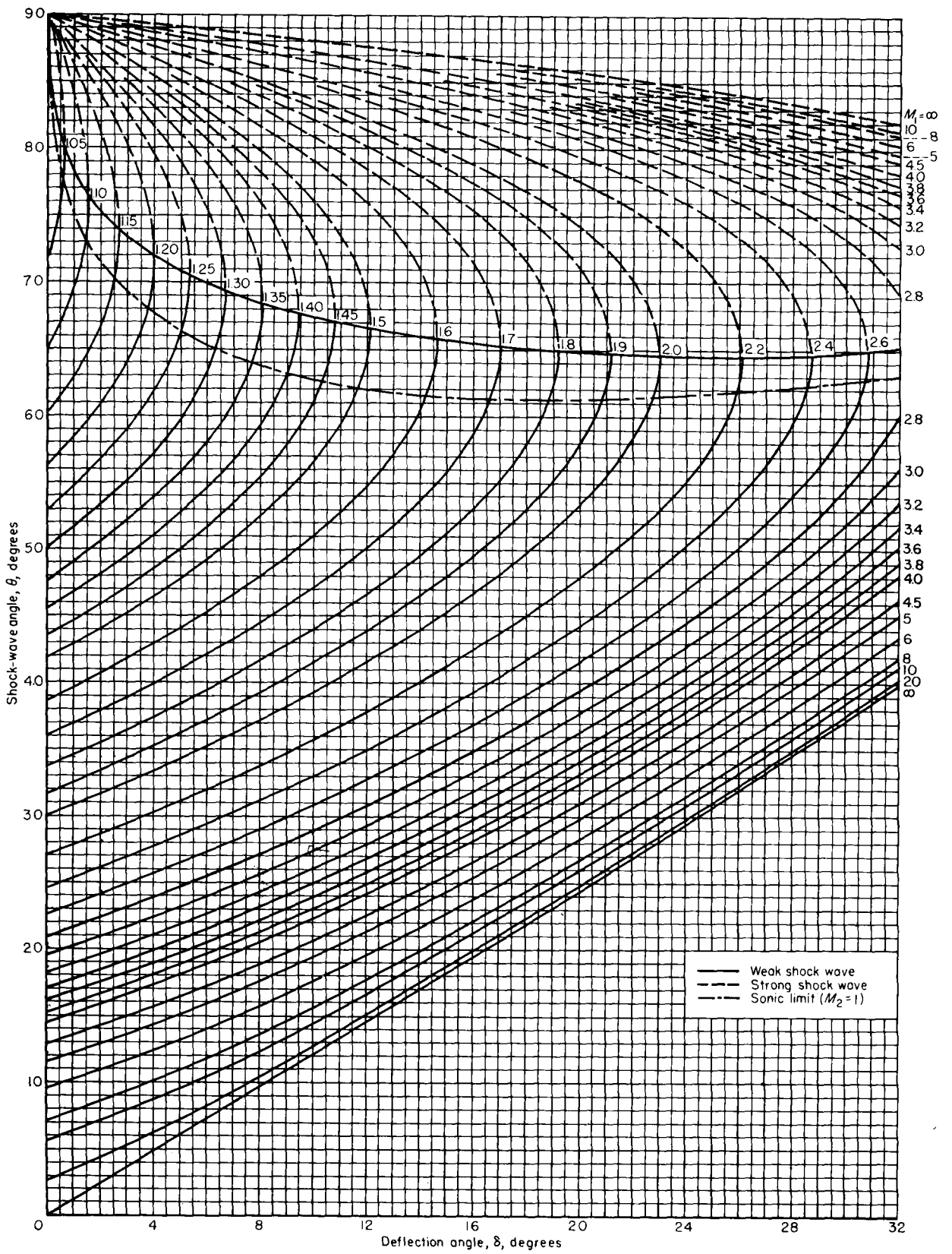

Variation of shock-wave angle with flow-deflection angle for various upstream Mach numbers. Perfect gas, $\gamma = 7/5$.

A.2-3 Shock Charts

REPORT 1135—NATIONAL ADVISORY COMMITTEE FOR AERONAUTICS

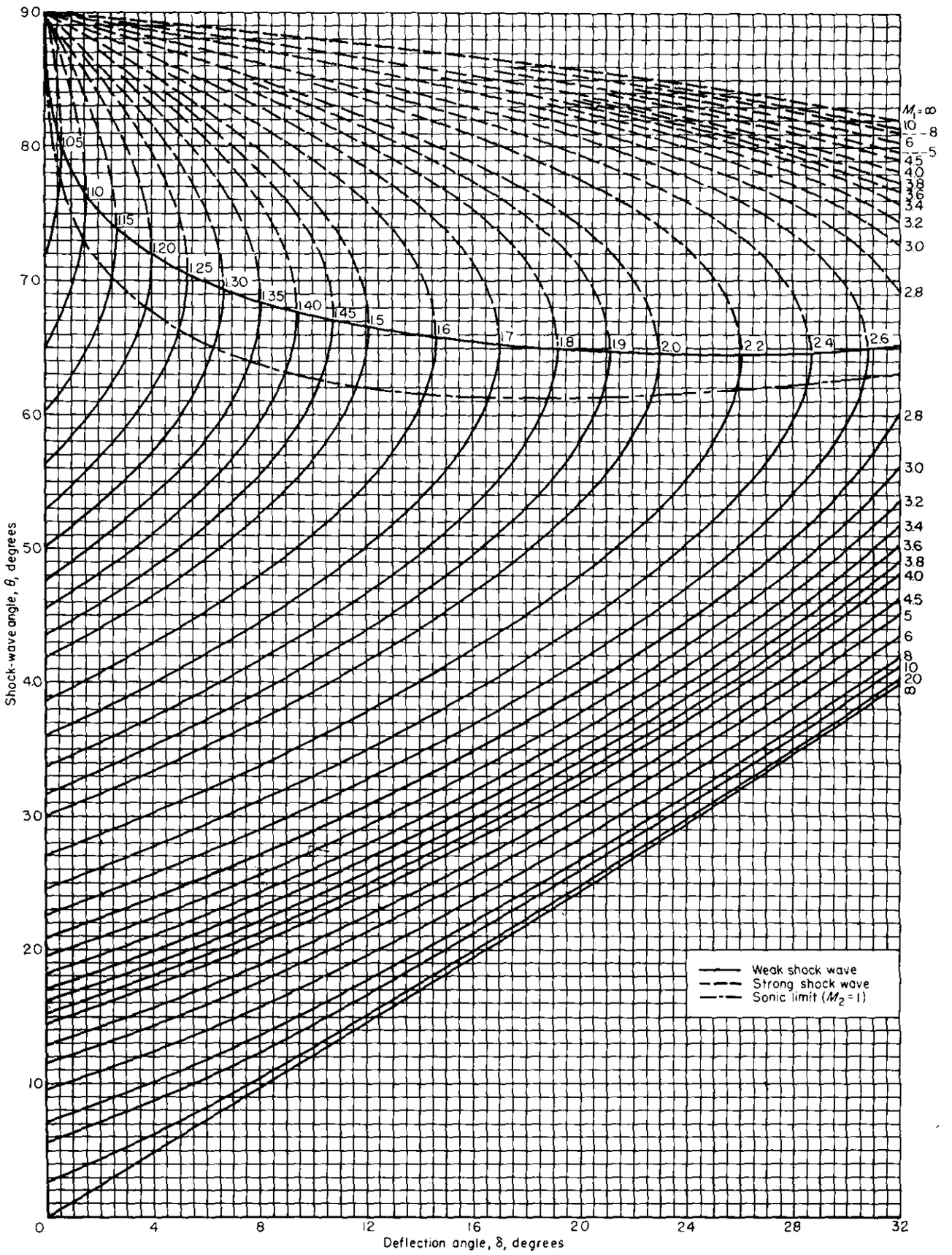

Variation of shock-wave angle with flow-deflection angle for various upstream Mach numbers. Perfect gas, $\gamma = 7/5$.

A.2-3 Shock Charts

EQUATIONS, TABLES, AND CHARTS FOR COMPRESSIBLE FLOW

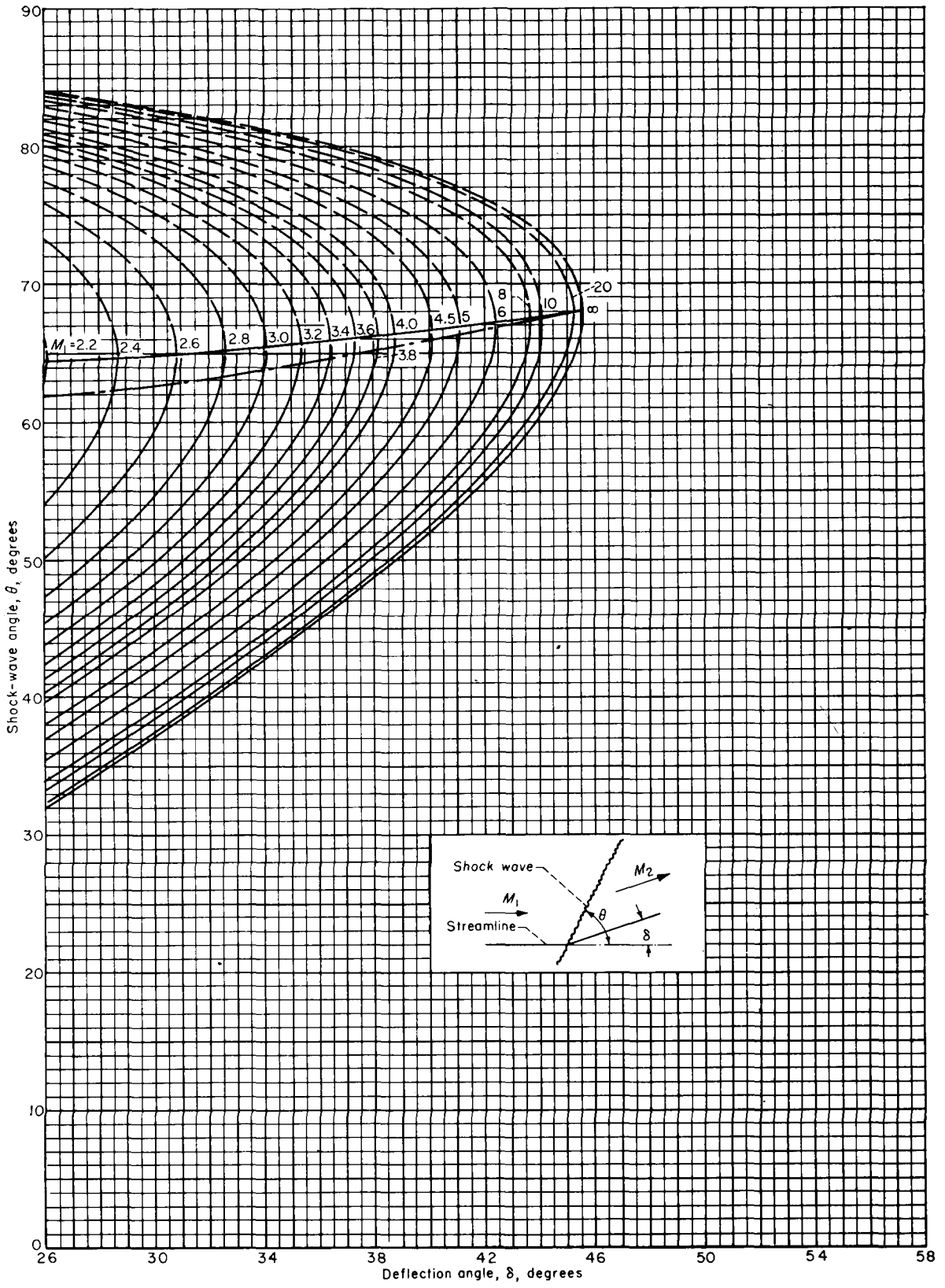

Concluded

A.2-3 Shock Charts

EQUATIONS, TABLES, AND CHARTS FOR COMPRESSIBLE FLOW

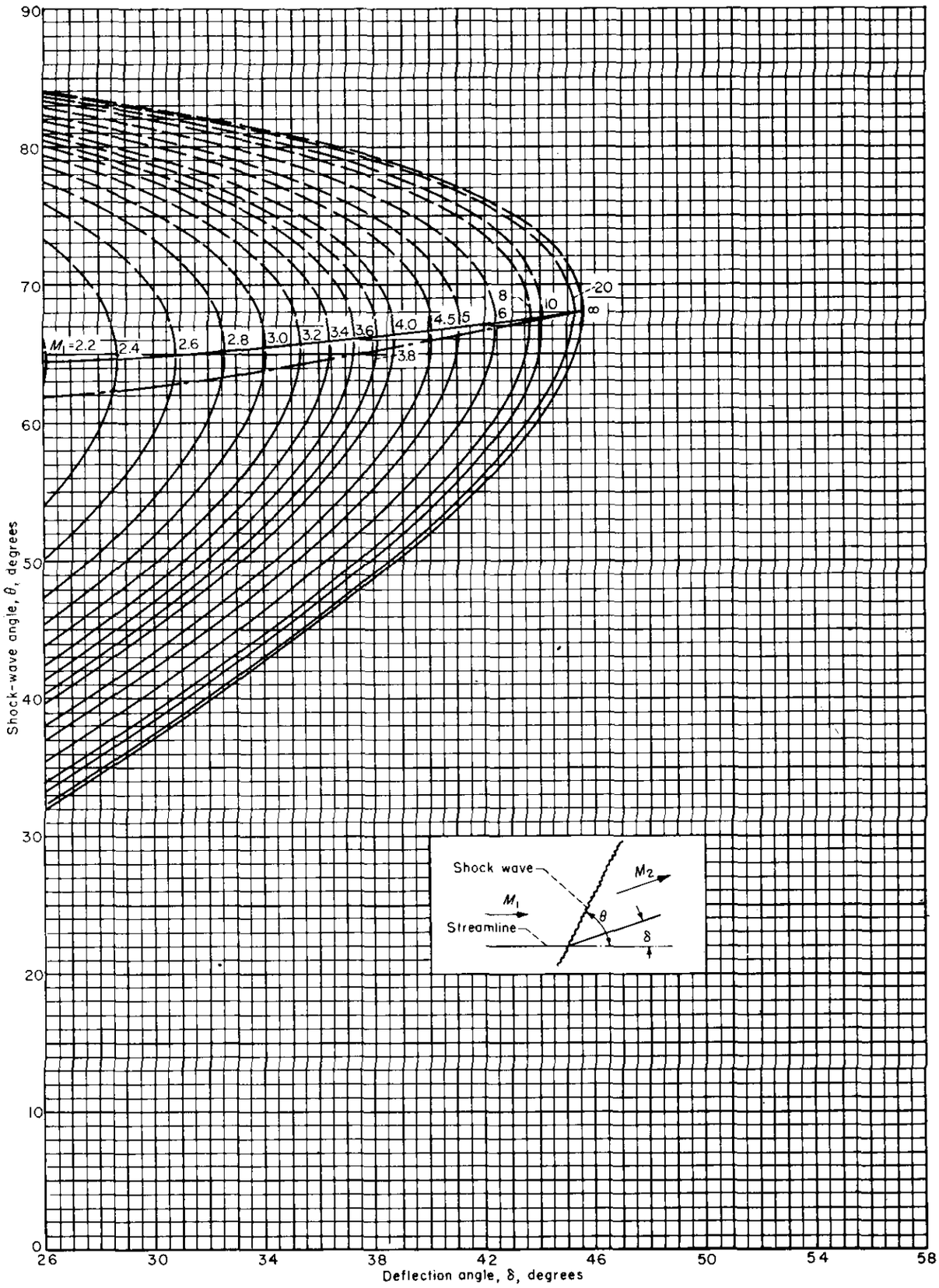

Concluded

A.2-3 Shock Charts

REPORT 1135—NATIONAL ADVISORY COMMITTEE FOR AERONAUTICS

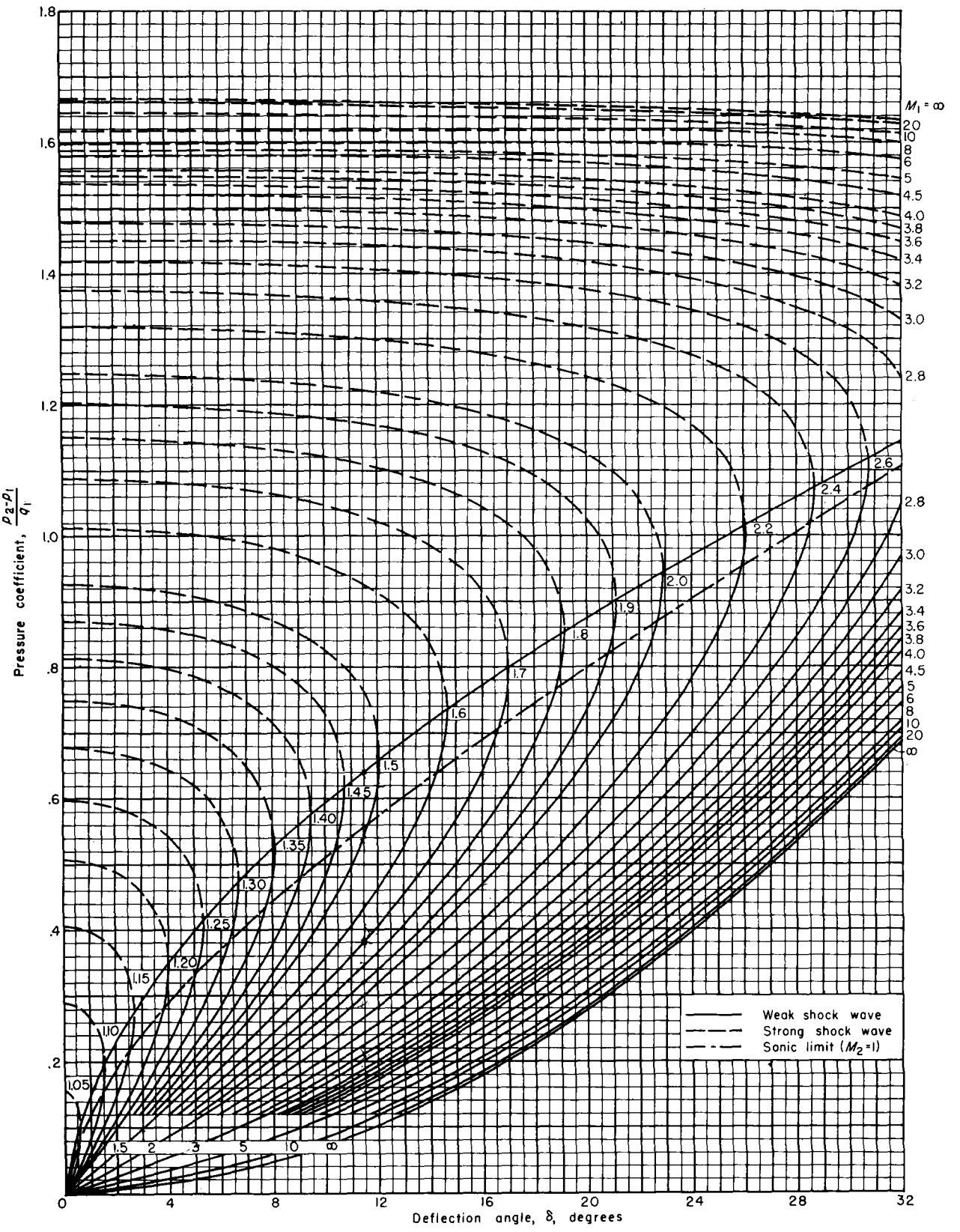

Variation of pressure coefficient across shock waves with flow-deflection angle for various upstream Mach numbers. Perfect gas, $\gamma = 1.4$

A.2-3 Shock Charts

EQUATIONS, TABLES, AND CHARTS FOR COMPRESSIBLE FLOW

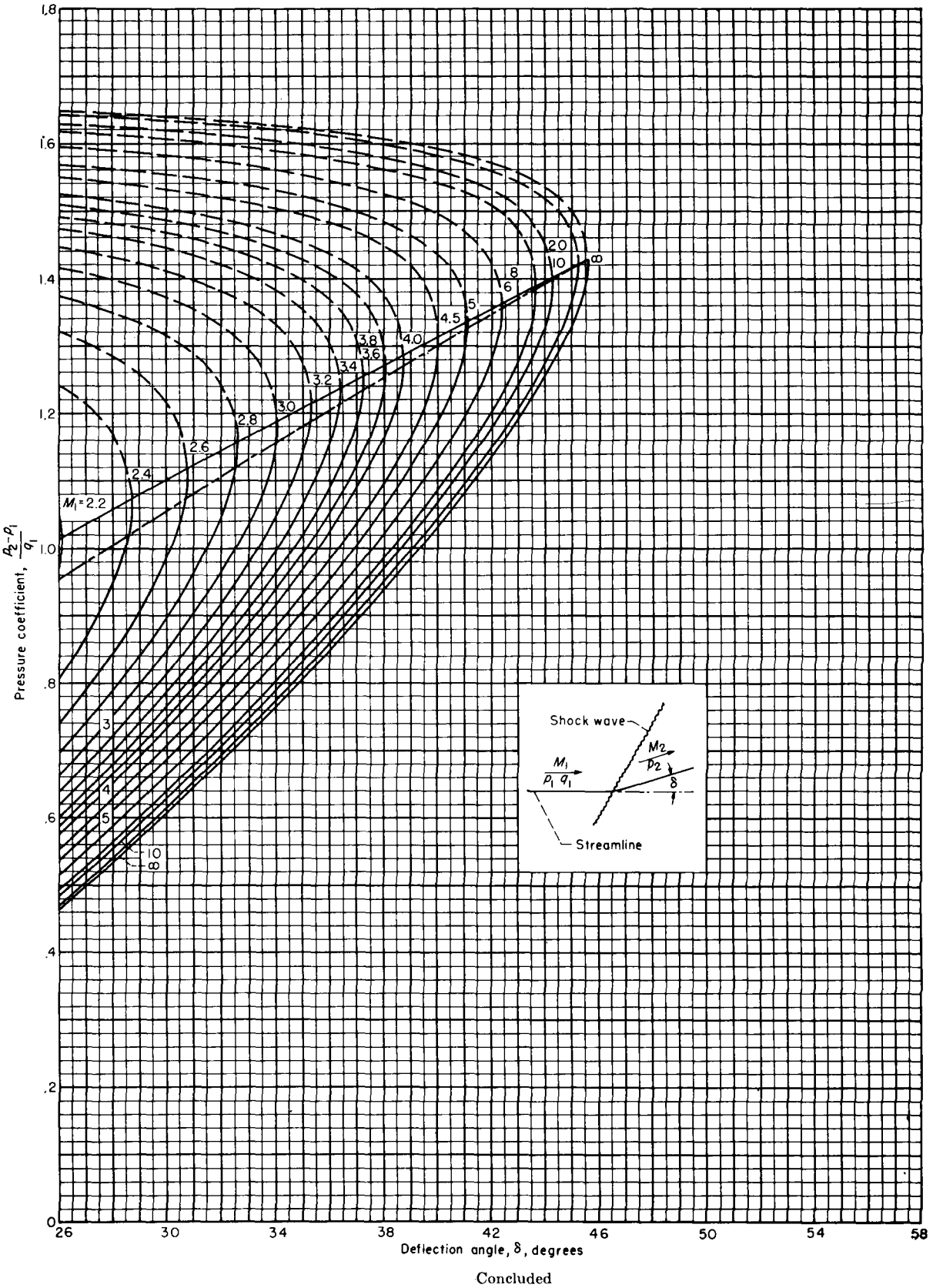

Concluded

A.2-3 Shock Charts

REPORT 1135—NATIONAL ADVISORY COMMITTEE FOR AERONAUTICS

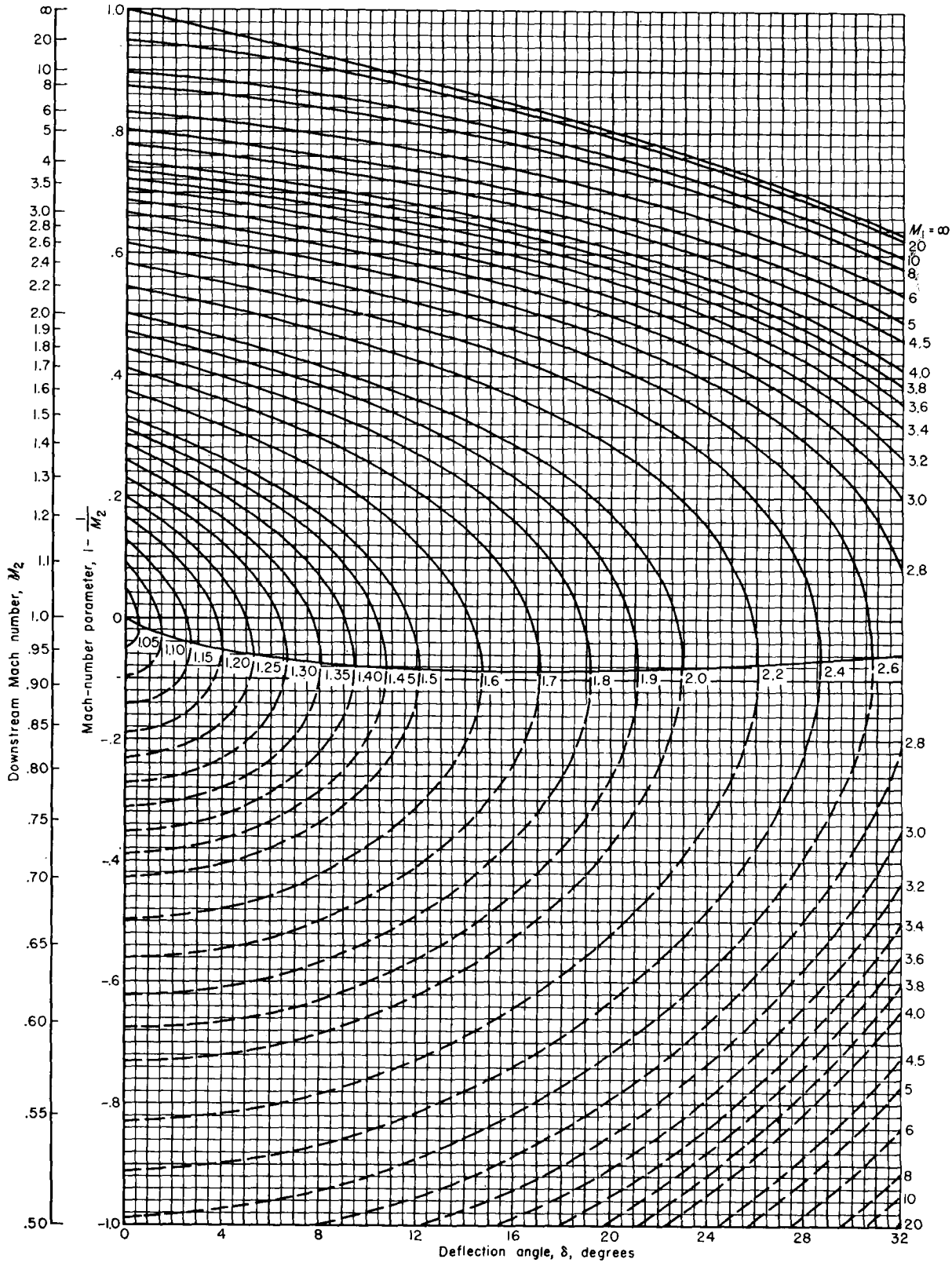

Variation of Mach number downstream of a shock wave with flow-deflection angle for various upstream Mach numbers. Perfect gas, $\gamma=7/5$.

A.2-3 Shock Charts

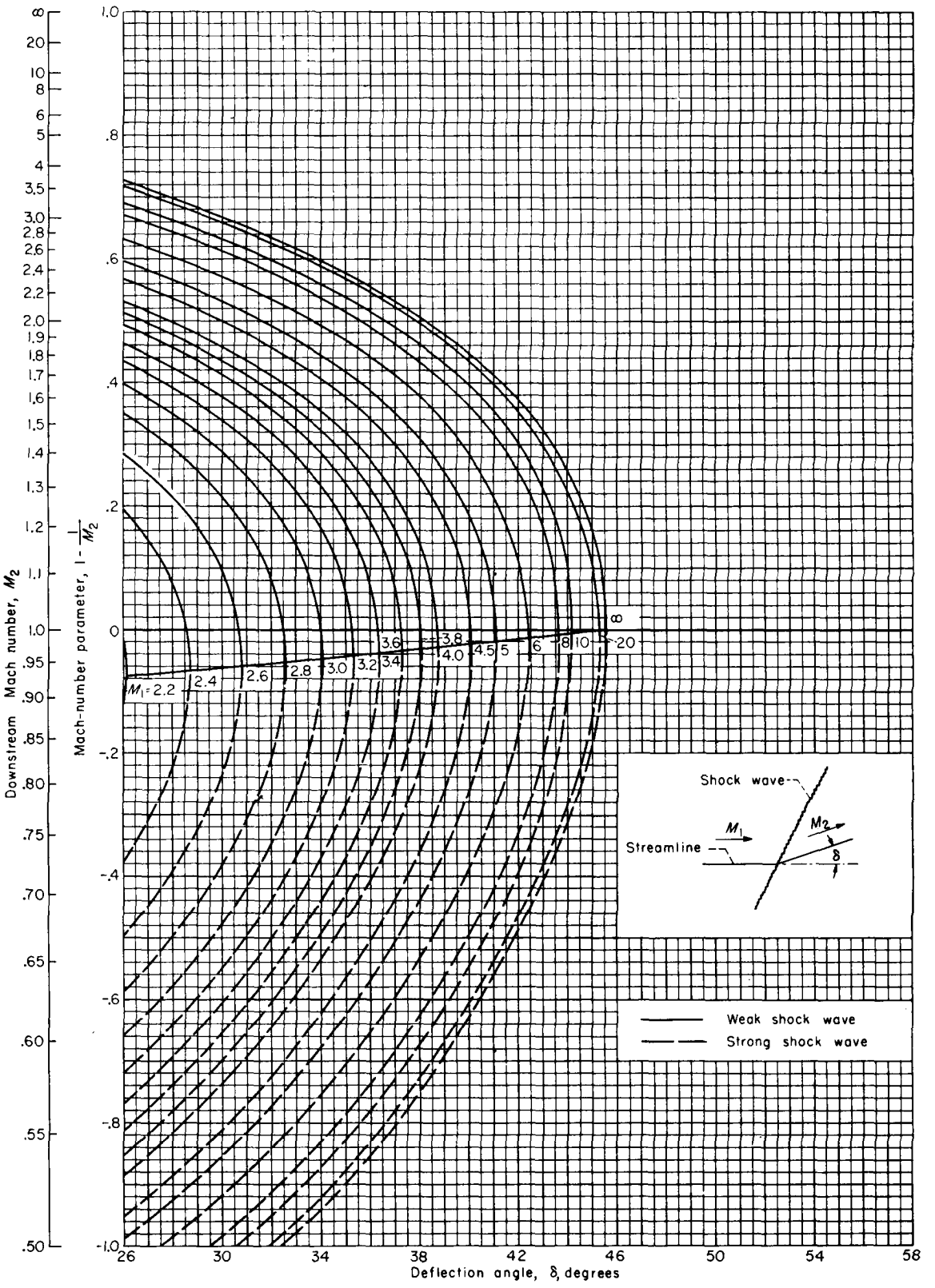

Concluded

A.2-3 Shock Charts

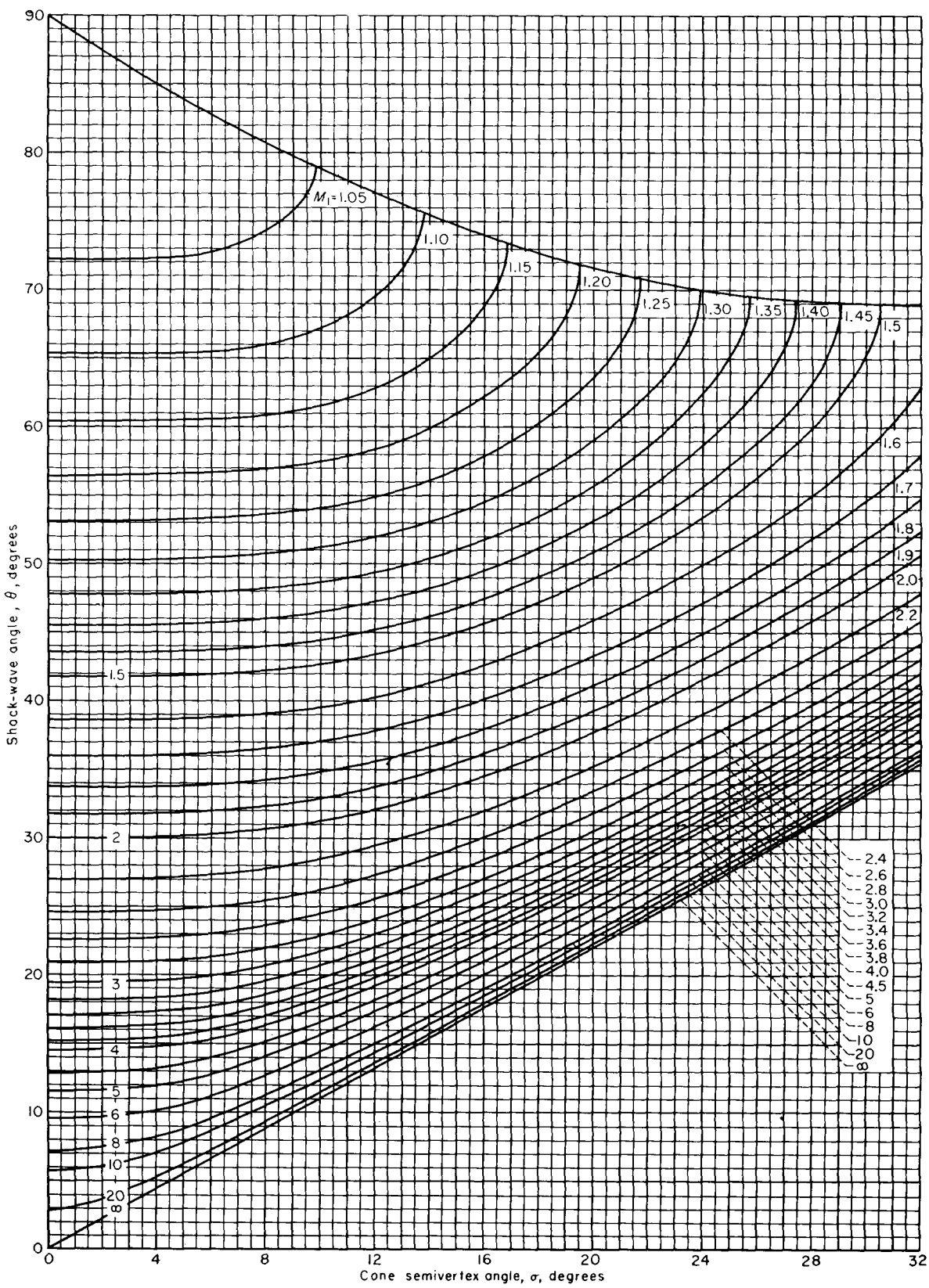

Variation of shock-wave angle with cone semivertex angle for various upstream Mach numbers. Perfect gas, $\gamma = 1.405$.

A.2-3 Shock Charts

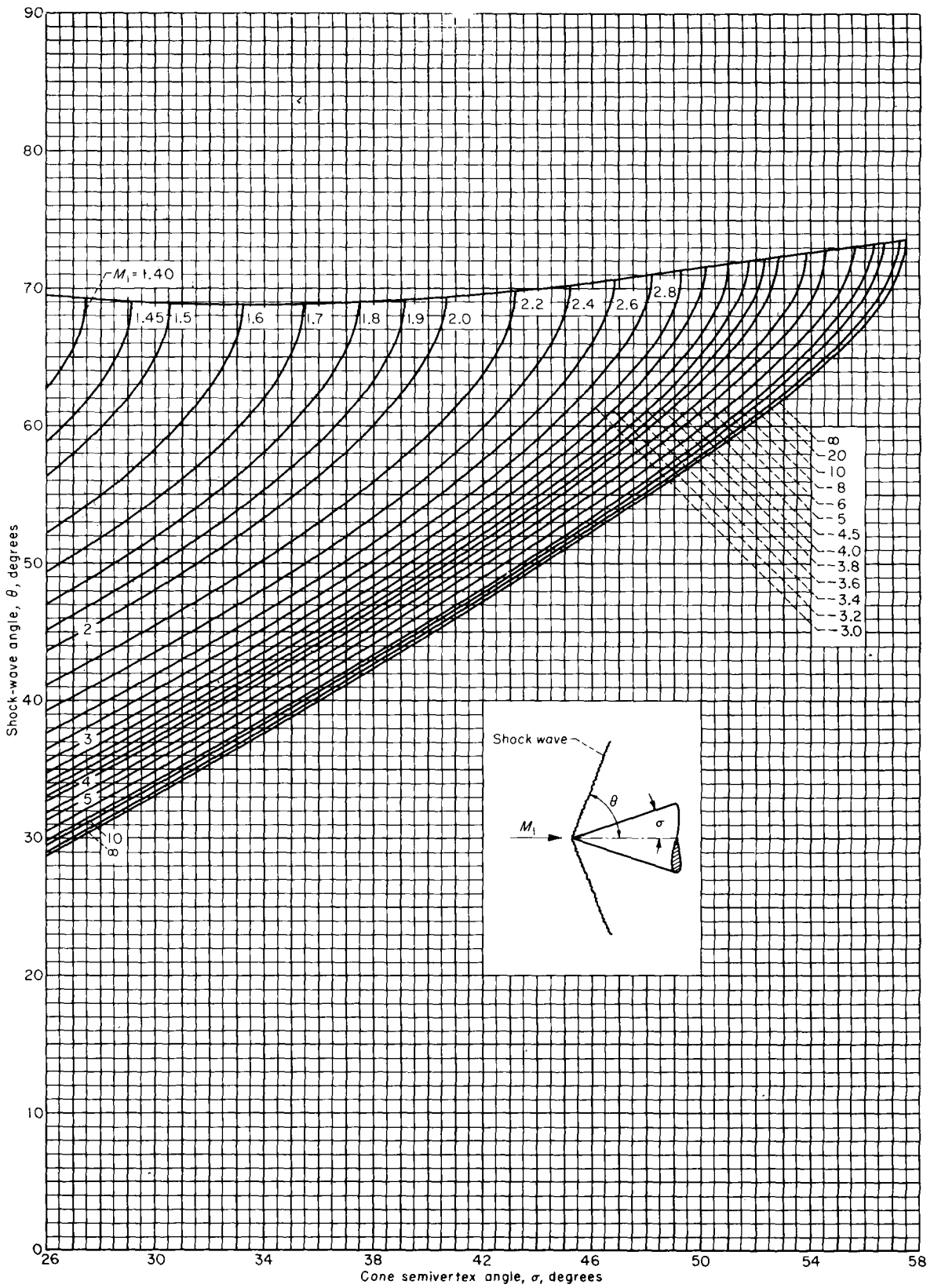

Concluded

A.2-3 Shock Charts

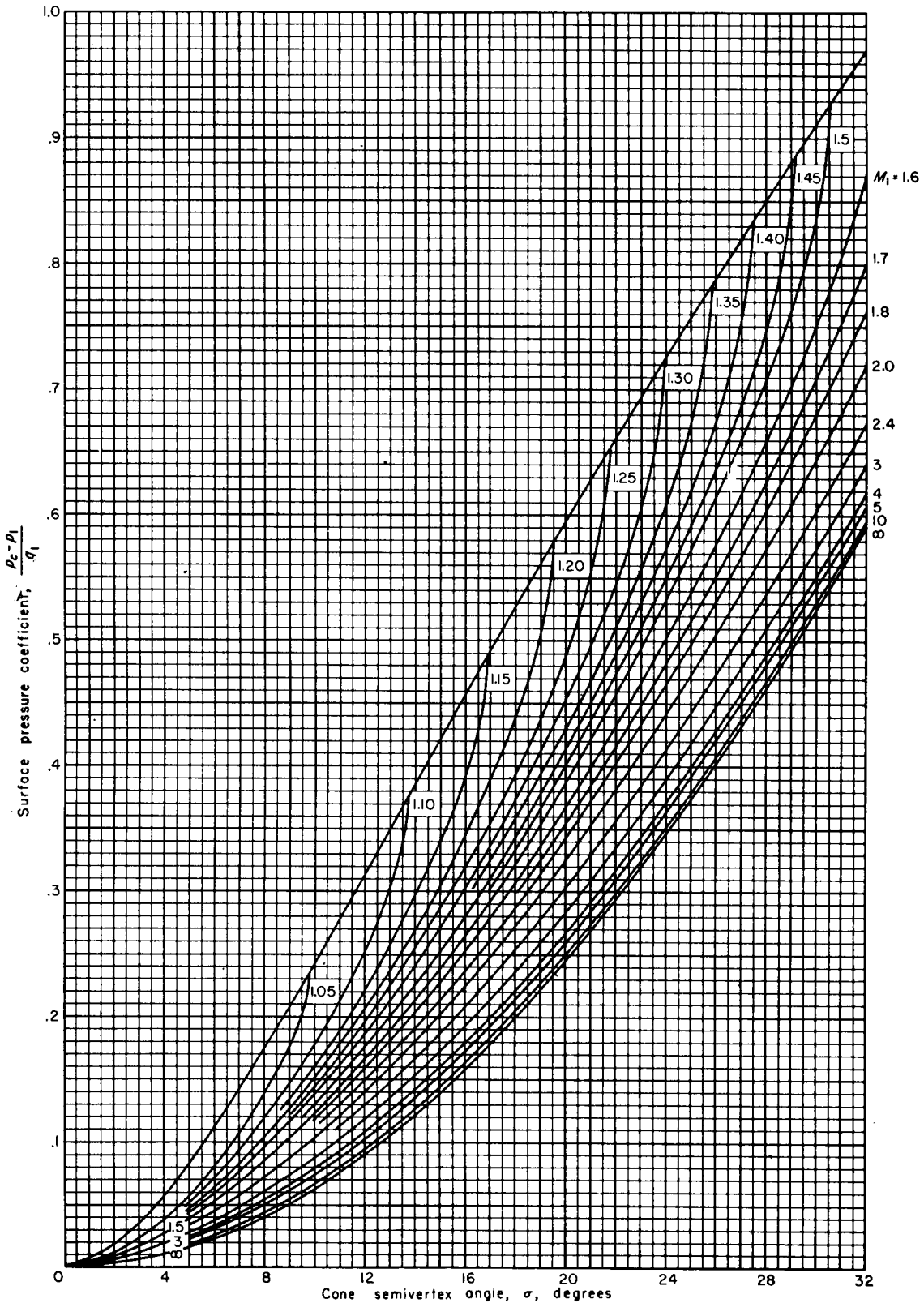

Variation of surface pressure coefficient with cone semivertex angle for various upstream Mach numbers. Perfect gas, $\gamma = 1.405$.

A.2-3 Shock Charts

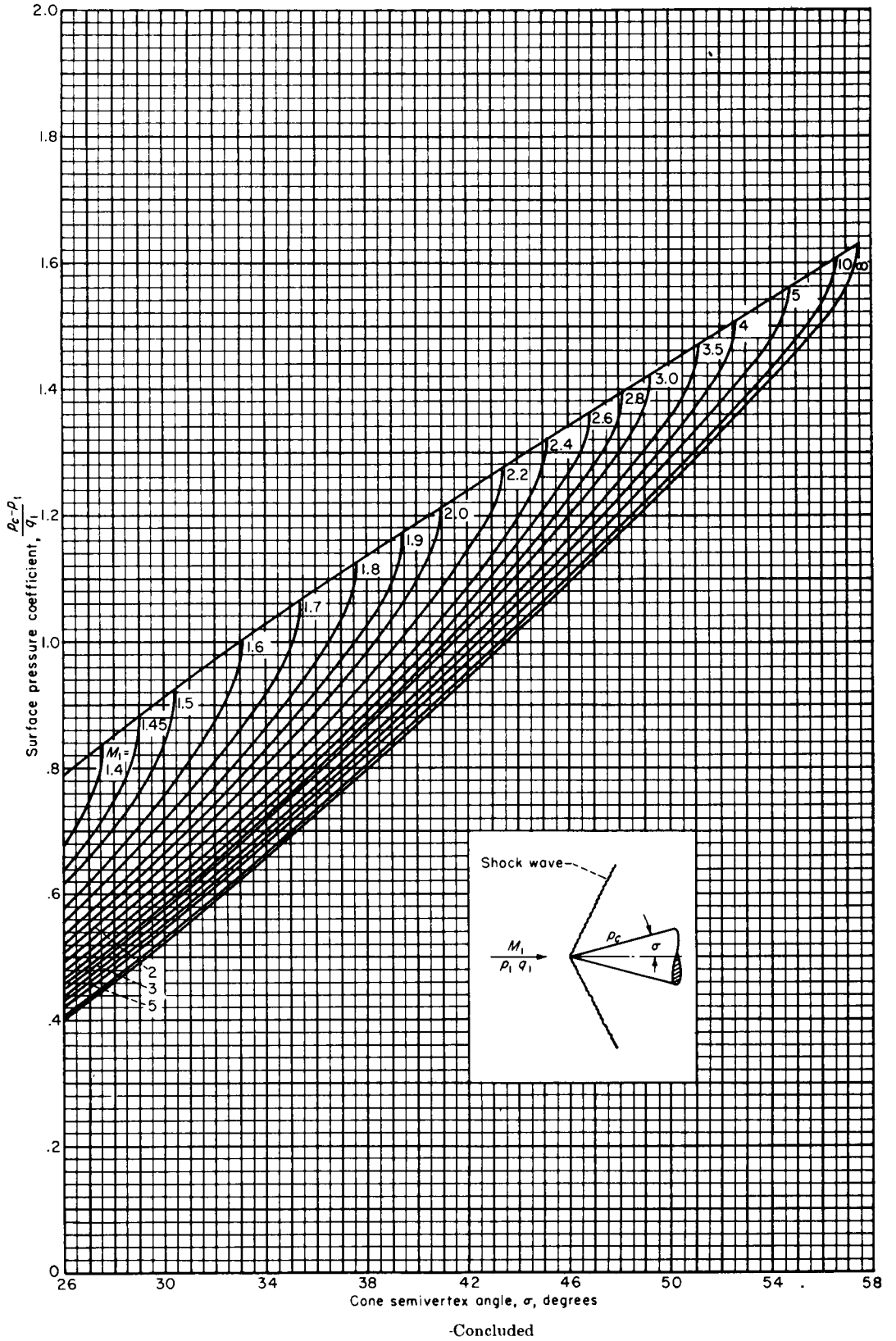

-Concluded

A.2-3 Shock Charts

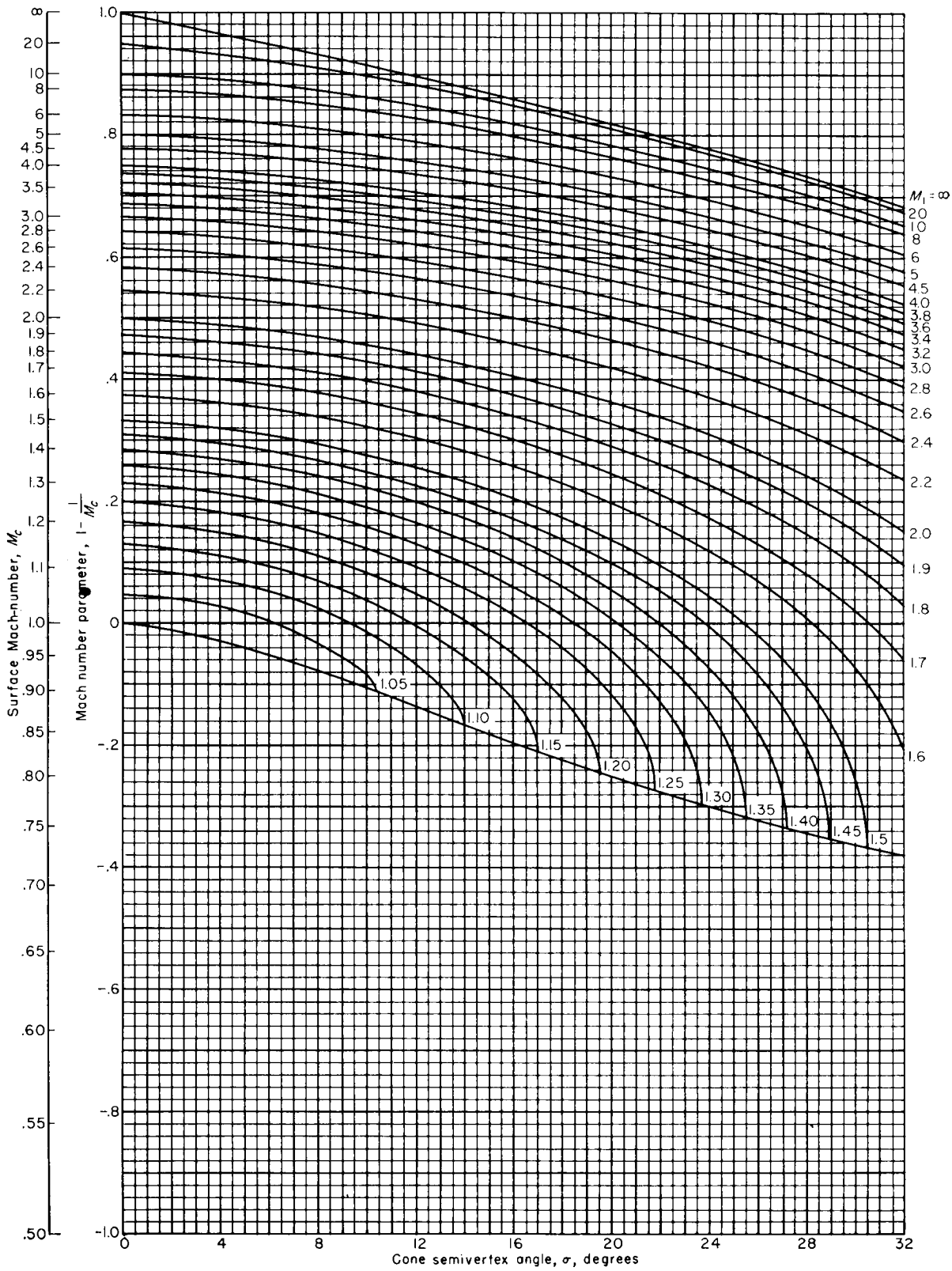

Variation of Mach number at the surface of a cone with cone semivertex angle for various upstream Mach numbers. Perfect gas, $\gamma = 1.405$.

A.2-3 Shock Charts

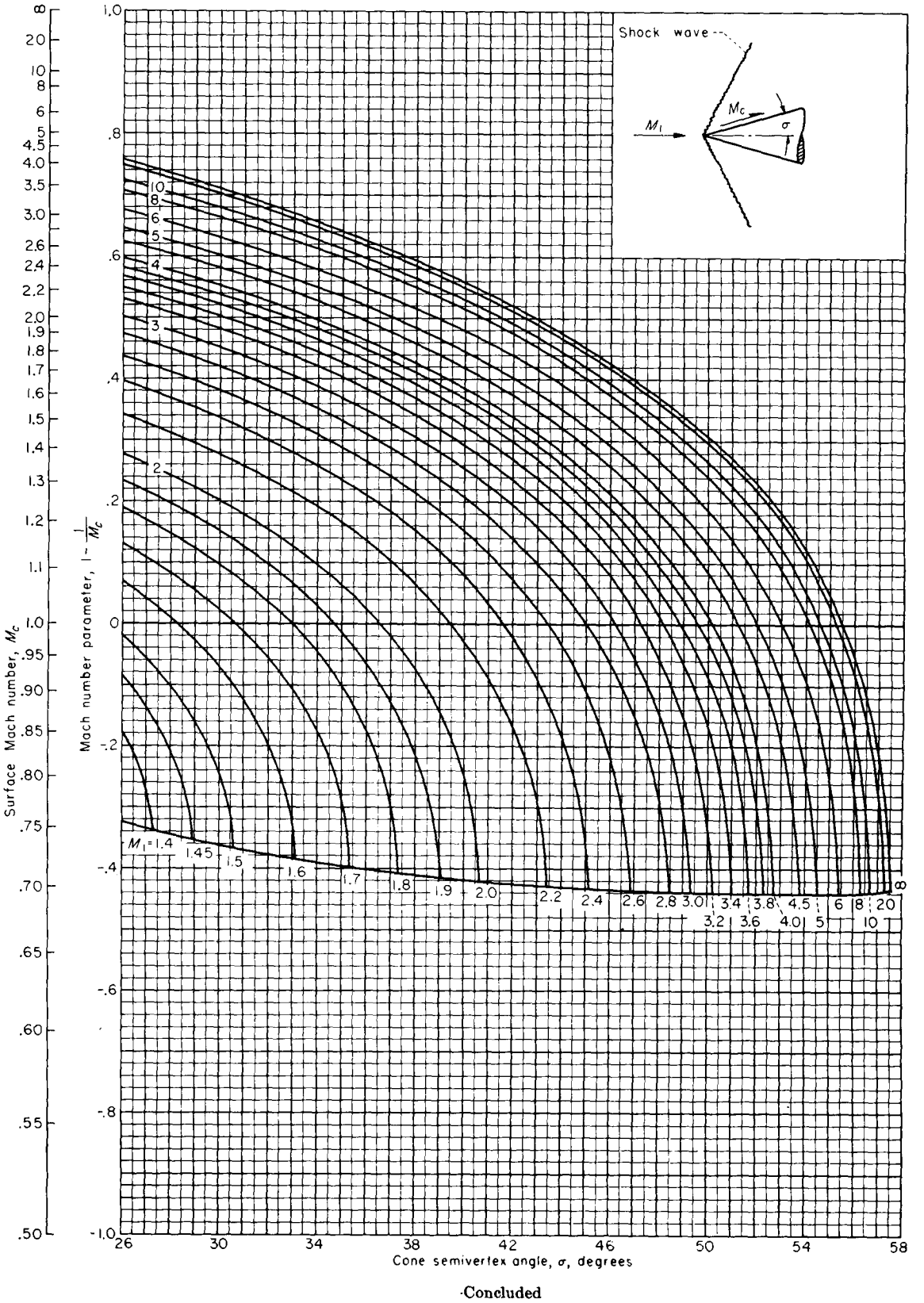

Concluded

A.2-3 Shock Charts

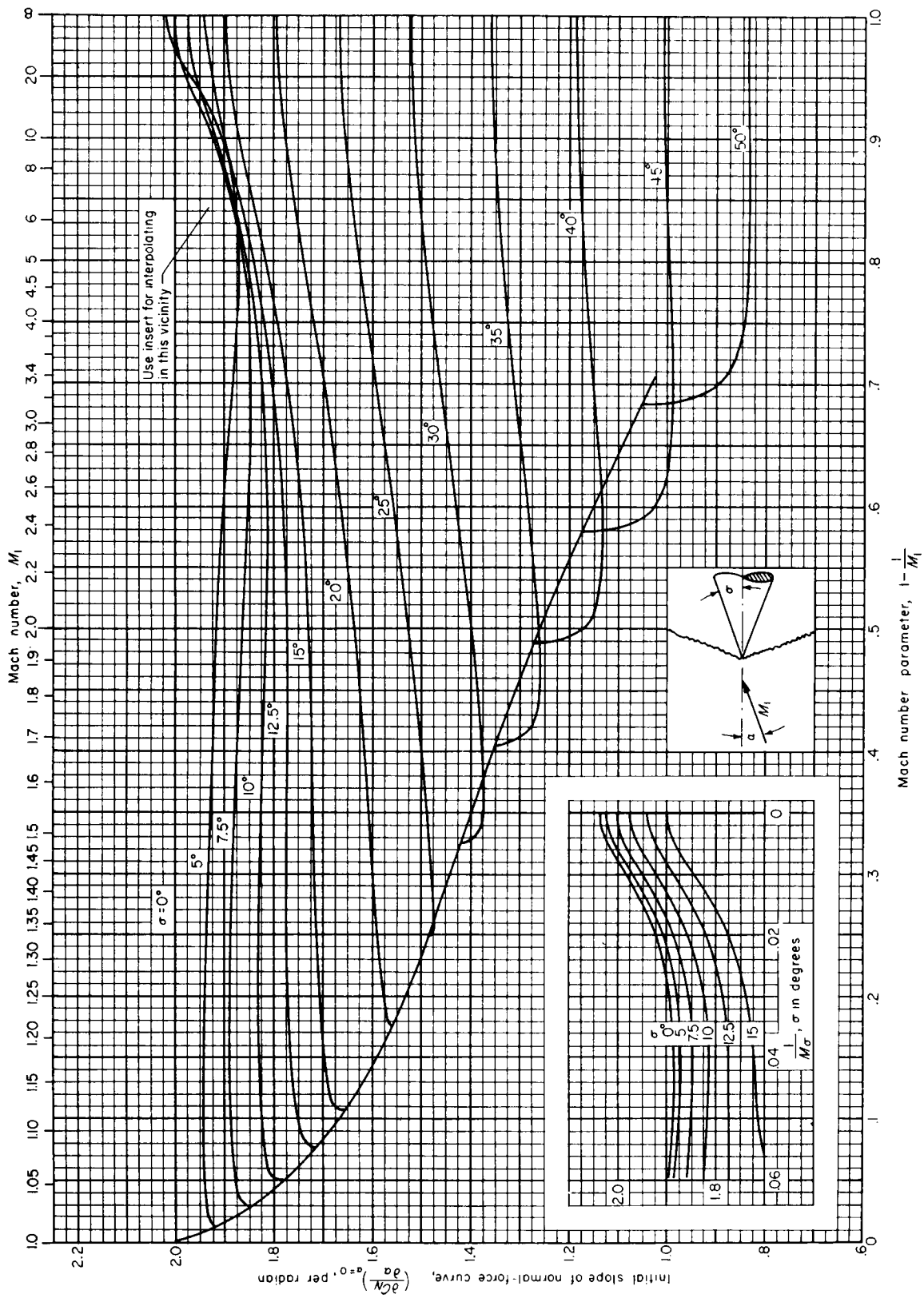

Variation of the initial slope of the normal-force curve with upstream Mach number for various cone semivertex angles. Perfect gas, $\gamma = 1.405$.

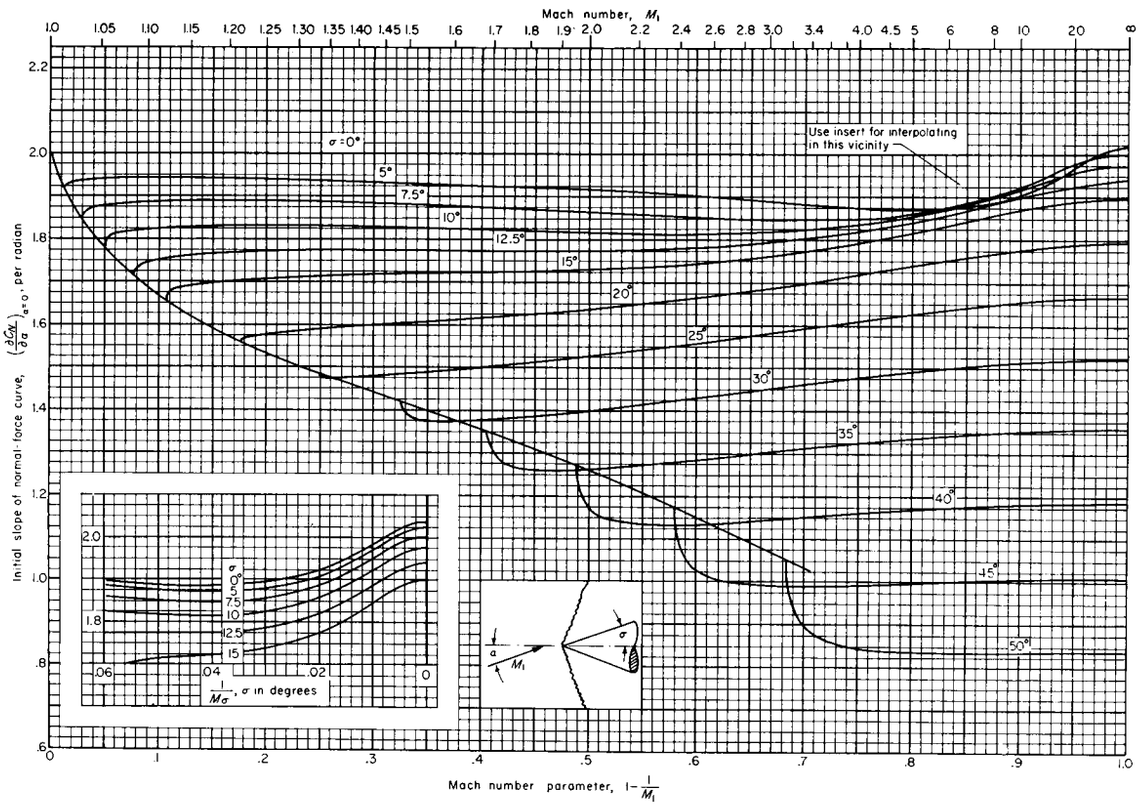

Variation of the initial slope of the normal-force curve with upstream Mach number for various cone semivertex angles. Perfect gas, $\gamma = 1.405$.

NACA 0006

Stations and ordinates given in percent of airfoil chord]

Upper surface		Lower surface	
Station	Ordinate	Station	Ordinate
0	0	0	0
1.25	.95	1.25	−.95
2.5	1.31	2.5	−1.31
5.0	1.78	5.0	−1.78
7.5	2.10	7.5	−2.10
10	2.34	10	−2.34
15	2.67	15	−2.67
20	2.87	20	−2.87
25	2.97	25	−2.97
30	3.00	30	−3.00
40	2.90	40	−2.90
50	2.65	50	−2.65
60	2.28	60	−2.28
70	1.83	70	−1.83
80	1.31	80	−1.31
90	.72	90	−.72
95	.40	95	−.40
100	(.06)	100	(−.06)
100	0	100	0

L. E. radius: 0.40

NACA 0009

[Stations and ordinates given in percent of airfoil chord]

Upper surface		Lower surface	
Station	Ordinate	Station	Ordinate
0	0	0	0
1.25	1.42	1.25	−1.42
2.5	1.96	2.5	−1.96
5.0	2.67	5.0	−2.67
7.5	3.15	7.5	−3.15
10	3.51	10	−3.51
15	4.01	15	−4.01
20	4.30	20	−4.30
25	4.46	25	−4.46
30	4.50	30	−4.50
40	4.35	40	−4.35
50	3.97	50	−3.97
60	3.42	60	−3.42
70	2.75	70	−2.75
80	1.97	80	−1.97
90	1.09	90	−1.09
95	.60	95	−.60
100	(.10)	100	(−.10)
100	0	100	0

L. E. radius: 0.89

NACA 2415

[Stations and ordinates given in percent of airfoil chord]

Upper surface		Lower surface	
Station	Ordinate	Station	Ordinate
0	-----	0	0
1.25	2.71	1.25	−2.06
2.5	3.71	2.5	−2.86
5.0	5.07	5.0	−3.84
7.5	6.06	7.5	−4.47
10	6.83	10	−4.90
15	7.97	15	−5.42
20	8.70	20	−5.66
25	9.17	25	−5.70
30	9.38	30	−5.62
40	9.25	40	−5.25
50	8.57	50	−4.67
60	7.50	60	−3.90
70	6.10	70	−3.05
80	4.41	80	−2.15
90	2.45	90	−1.17
95	1.34	95	−.68
100	(.16)	100	(−.16)
100	-----	100	0

L. E. radius: 2.48
Slope of radius through L. E.: 0.10

NACA 4415

[Stations and ordinates given in percent of airfoil chord]

Upper surface		Lower surface	
Station	Ordinate	Station	Ordinate
0	-------	0	0
1.25	3.07	1.25	−1 79
2.5	4.17	2.5	−2.48
5.0	5.74	5.0	−3.27
7.5	6.91	7.5	−3.71
10	7.84	10	−3.98
15	9.27	15	−4.18
20	10.25	20	−4.15
25	10.92	25	−3.98
30	11.25	30	−3.75
40	11.25	40	−3.25
50	10.53	50	−2.72
60	9.30	60	−2.14
70	7.63	70	−1.55
80	5.55	80	−1.03
90	3.08	90	−.57
95	1.67	95	−.36
100	(.16)	100	(−.16)
100	-------	100	0

L. E. radius: 2.48
Slope of radius through L. E.: 0.20

NACA 23015

[Stations and ordinates given in percent of airfoil chord]

Upper surface		Lower surface	
Station	Ordinate	Station	Ordinate
0	-----	0	0
1.25	3.34	1.25	−1.54
2.5	4.44	2.5	−2.25
5.0	5.89	5.0	−3.04
7.5	6.90	7.5	−3.61
10	7.64	10	−4.09
15	8.52	15	−4.84
20	8.92	20	−5.41
25	9.08	25	−5.78
30	9.05	30	−5.96
40	8.59	40	−5.92
50	7.74	50	−5.50
60	6.61	60	−4.81
70	5.25	70	−3.91
80	3.73	80	−2.83
90	2.04	90	−1.59
95	1.12	95	−.90
100	(.16)	100	(−.16)
100	-----	100	0

L. E. radius: 2.48
Slope of radius through L. E.: 0.305

NACA 64-006

[Stations and ordinates given in percent of airfoil chord]

Upper surface		Lower surface	
Station	Ordinate	Station	Ordinate
0	0	0	0
.50	.494	.50	−.494
.75	.596	.75	−.596
1.25	.754	1.25	−.754
2.5	1.024	2.5	−1.024
5.0	1.405	5.0	−1.405
7.5	1.692	7.5	−1.692
10	1.928	10	−1.928
15	2.298	15	−2.298
20	2.572	20	−2.572
25	2.772	25	−2.772
30	2.907	30	−2.907
35	2.981	35	−2.981
40	2.995	40	−2.995
45	2.919	45	−2.919
50	2.775	50	−2.775
55	2.575	55	−2.575
60	2.331	60	−2.331
65	2.050	65	−2.050
70	1.740	70	−1.740
75	1.412	75	−1.412
80	1.072	80	−1.072
85	.737	85	−.737
90	.423	90	−.423
95	.157	95	−.157
100	0	100	0

L. E. radius: 0.256

NACA 65(216)-415
$a = 0.5$

[Stations and ordinates given in percent of airfoil chord]

Upper surface		Lower surface	
Station	Ordinate	Station	Ordinate
0	0	0	0
.244	1.236	.756	−.960
.469	1.498	1.031	−1.110
.930	1.947	1.570	−1.359
2.121	2.837	2.879	−1.801
4.564	4.175	5.436	−2.411
7.044	5.208	7.956	−2.832
9.540	6.073	10.460	−3.169
14.561	7.465	15.439	−3.673
19.608	8.518	20.392	−4.022
24.669	9.315	25.331	−4.267
29.742	9.900	30.258	−4.428
34.825	10.279	35.175	−4.507
30.916	10.467	40.084	−4.523
45.019	10.438	44.981	−4.446
50.153	10.131	49.847	−4.251
55.263	9.512	54.737	−3.940
60.305	8.645	59.695	−3.521
65.308	7.575	64.692	−2.995
70.281	6.373	69.719	−2.409
75.237	5.152	74.763	−1.848
80.180	3.890	79.820	−1.278
85.117	2.639	84.883	−.723
90.062	1.533	89.938	−.305
95.020	.606	94.980	−.030
100.000	0	100.000	0

L. E. radius: 1.498
Slope of radius through L. E.: 0.233

A.3 Airfoil Data

NACA 0006

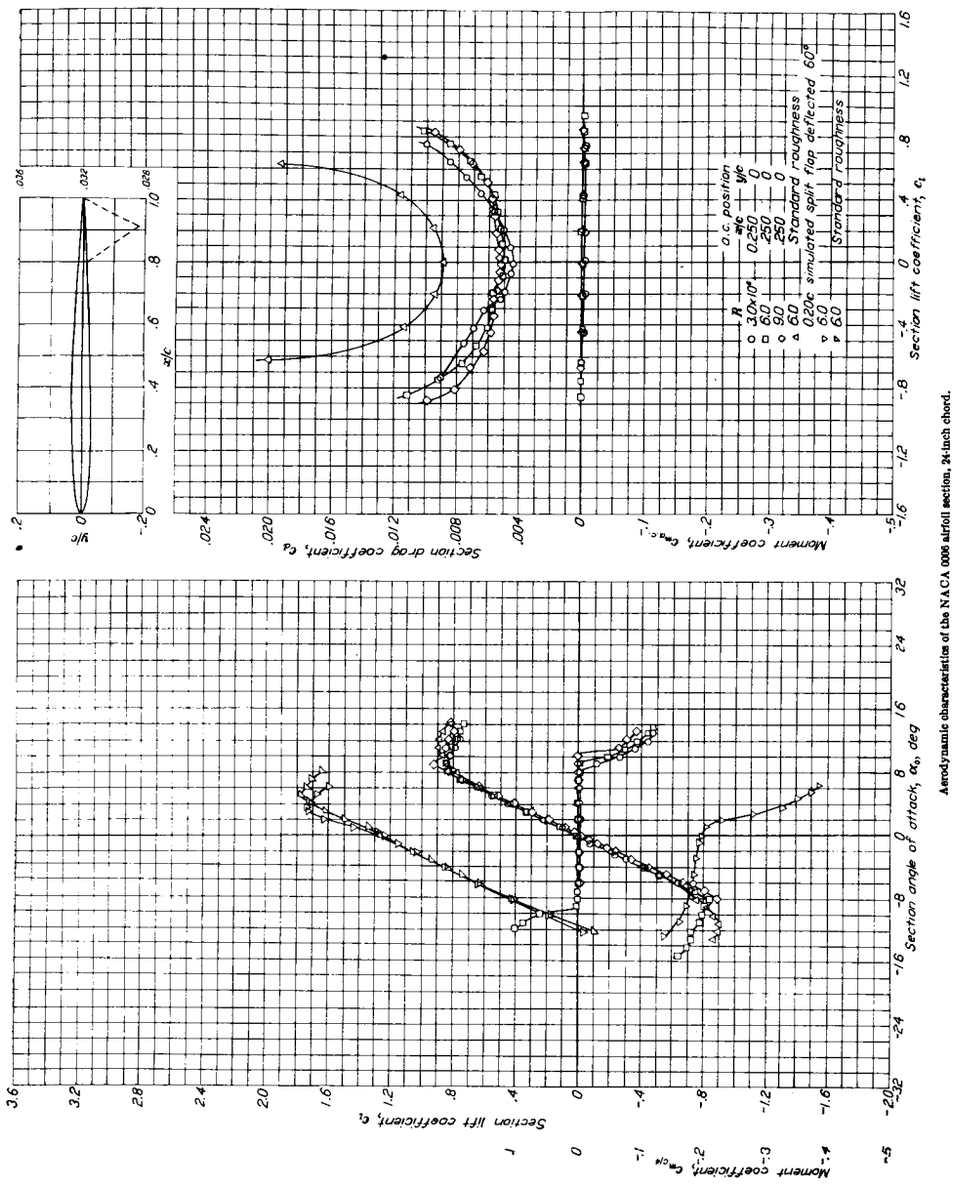

Aerodynamic characteristics of the NACA 0006 airfoil section, 24-inch chord.

A.3 Airfoil Data

NACA 0009

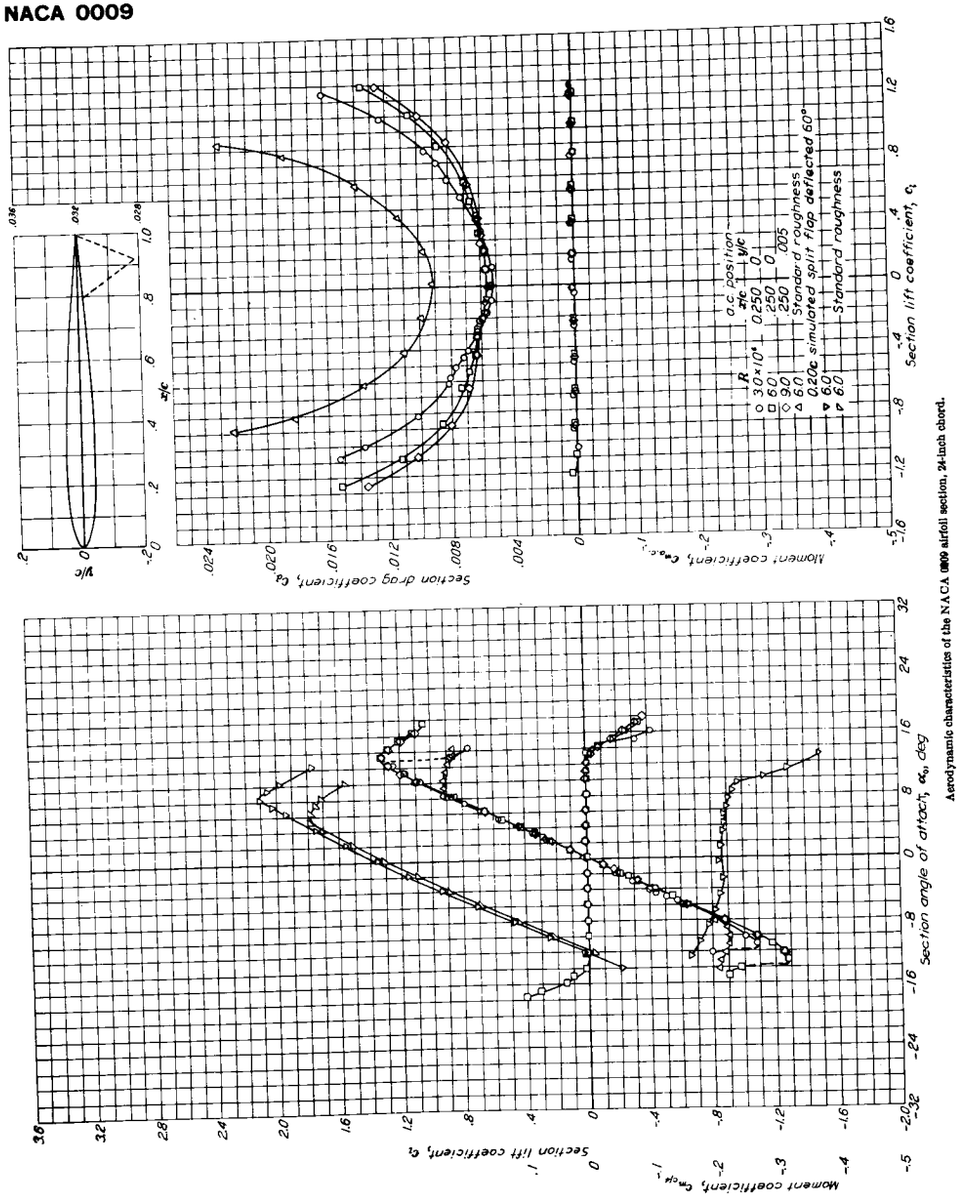

Aerodynamic characteristics of the NACA 0009 airfoil section, 24-inch chord.

A.3 Airfoil Data

NACA 0006

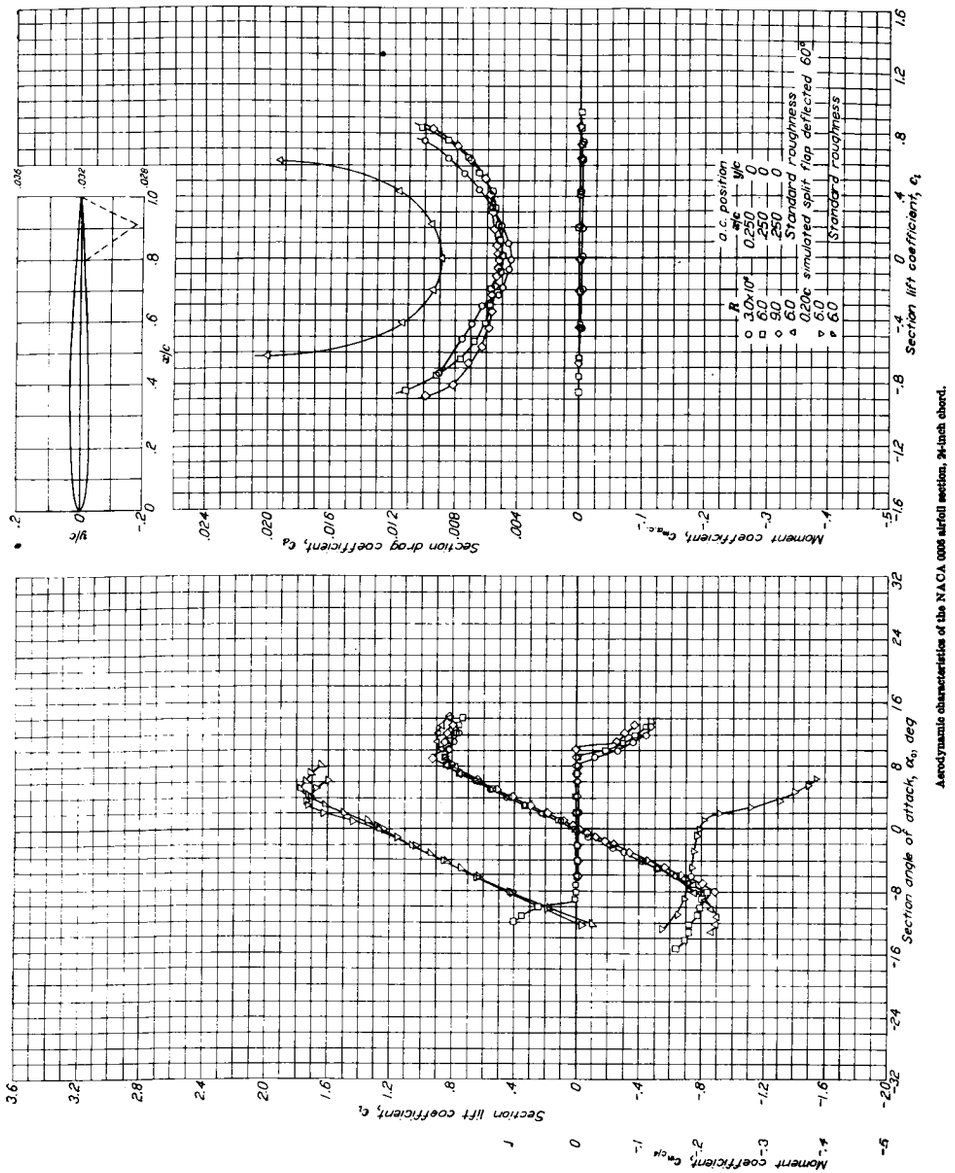

Aerodynamic characteristics of the NACA 0006 airfoil section, 24-inch chord.

A.3 Airfoil Data

NACA 0009

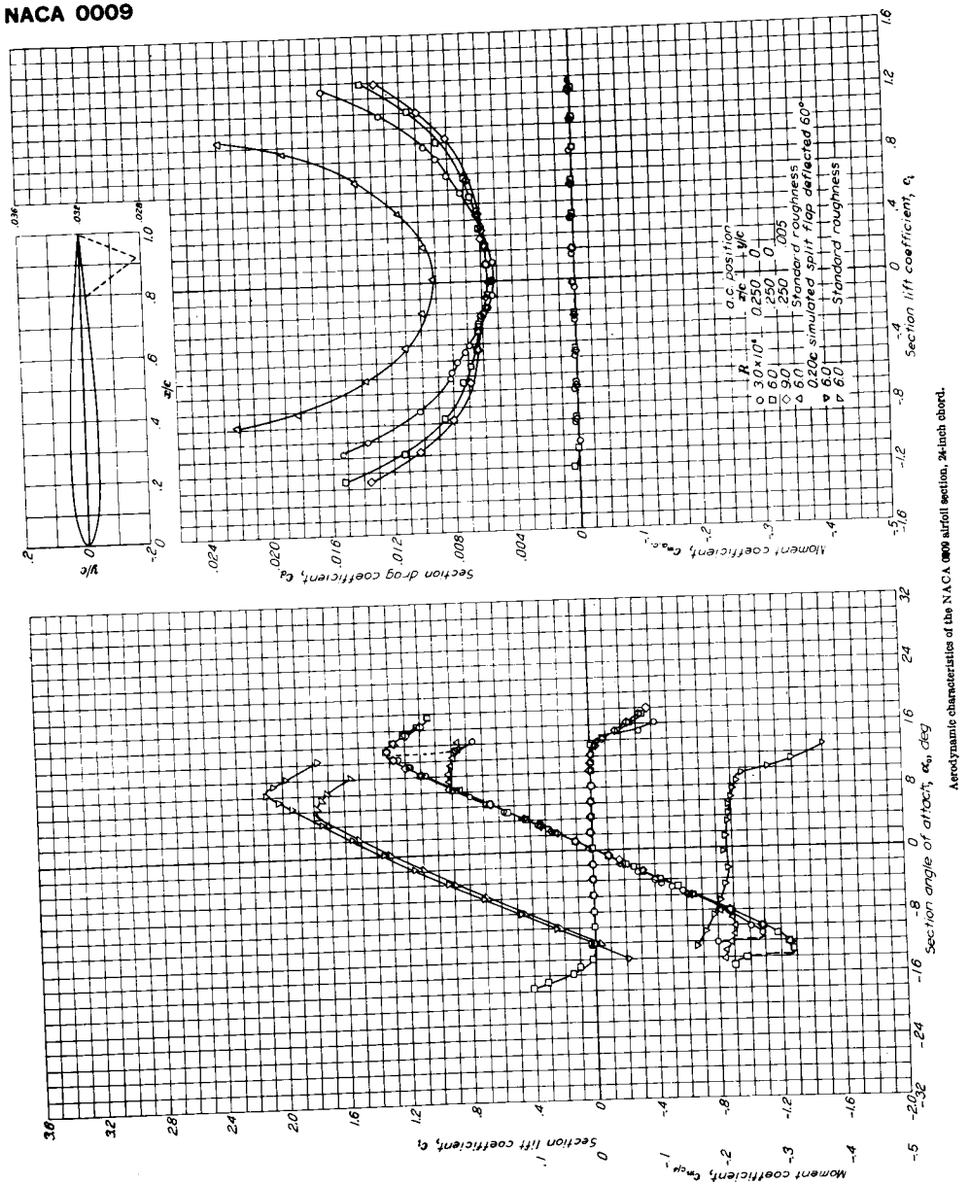

Aerodynamic characteristics of the NACA 0009 airfoil section, 24-inch chord.

A.3 Airfoil Data

NACA 2415

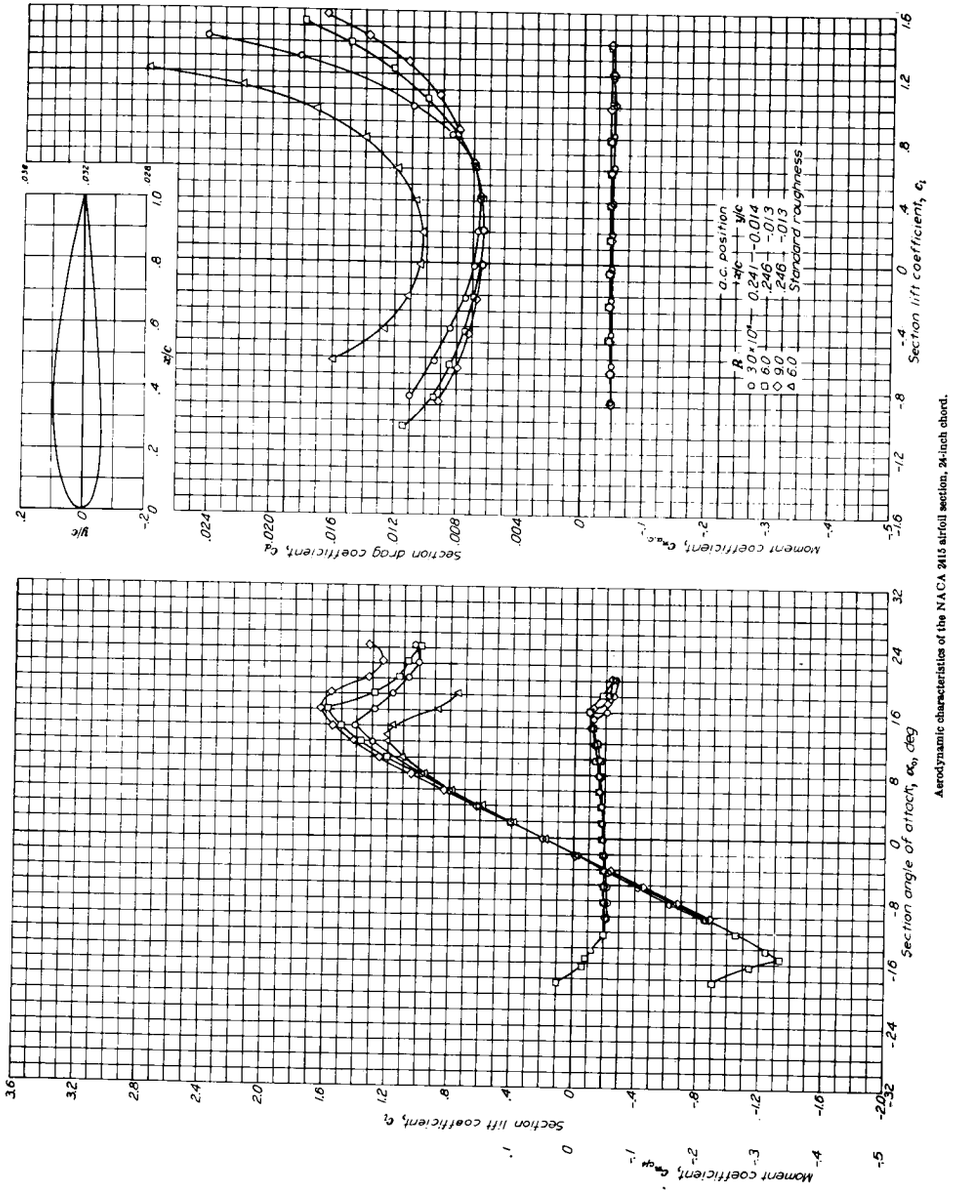

Aerodynamic characteristics of the NACA 2415 airfoil section, 24-inch chord.

A.3 Airfoil Data

NACA 4415

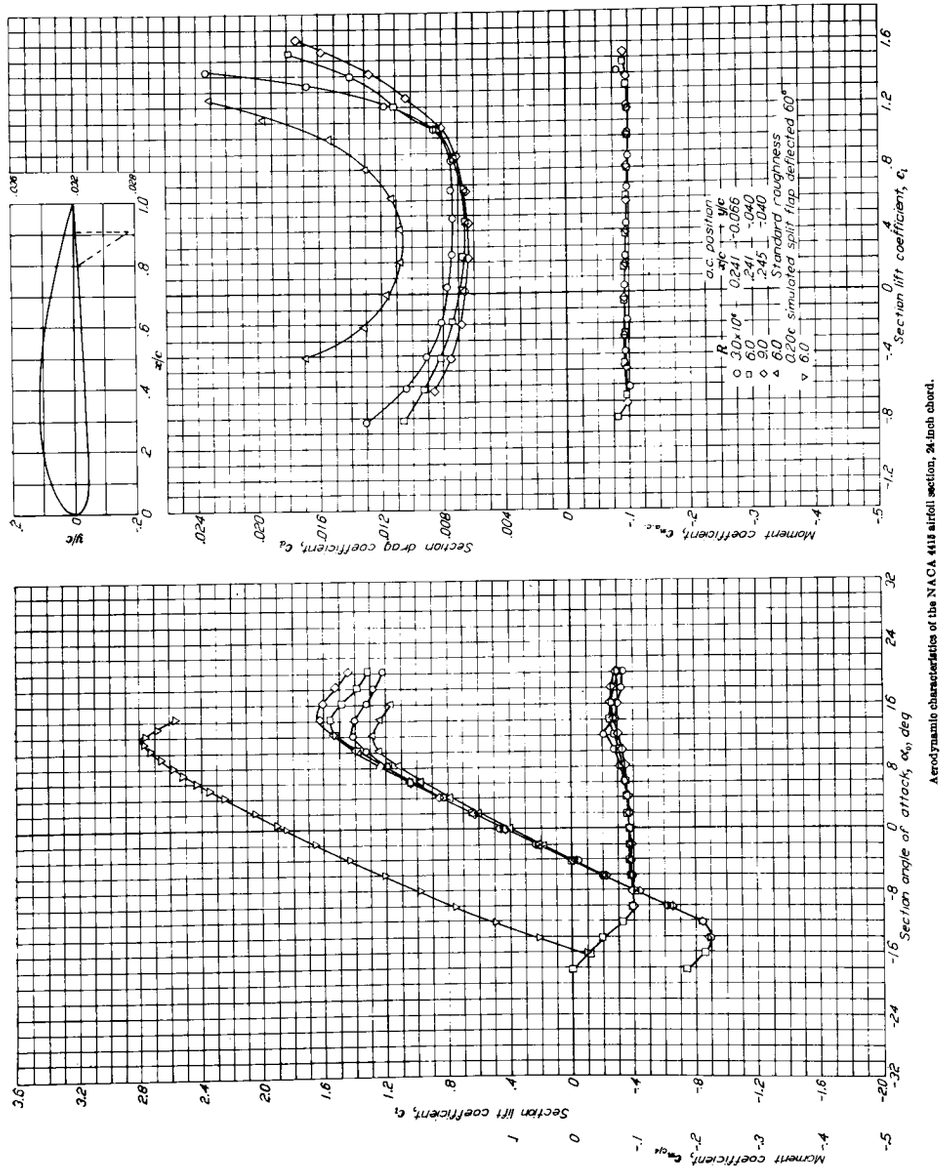

Aerodynamic characteristics of the NACA 4415 airfoil section, 24-inch chord.

A.3 Airfoil Data

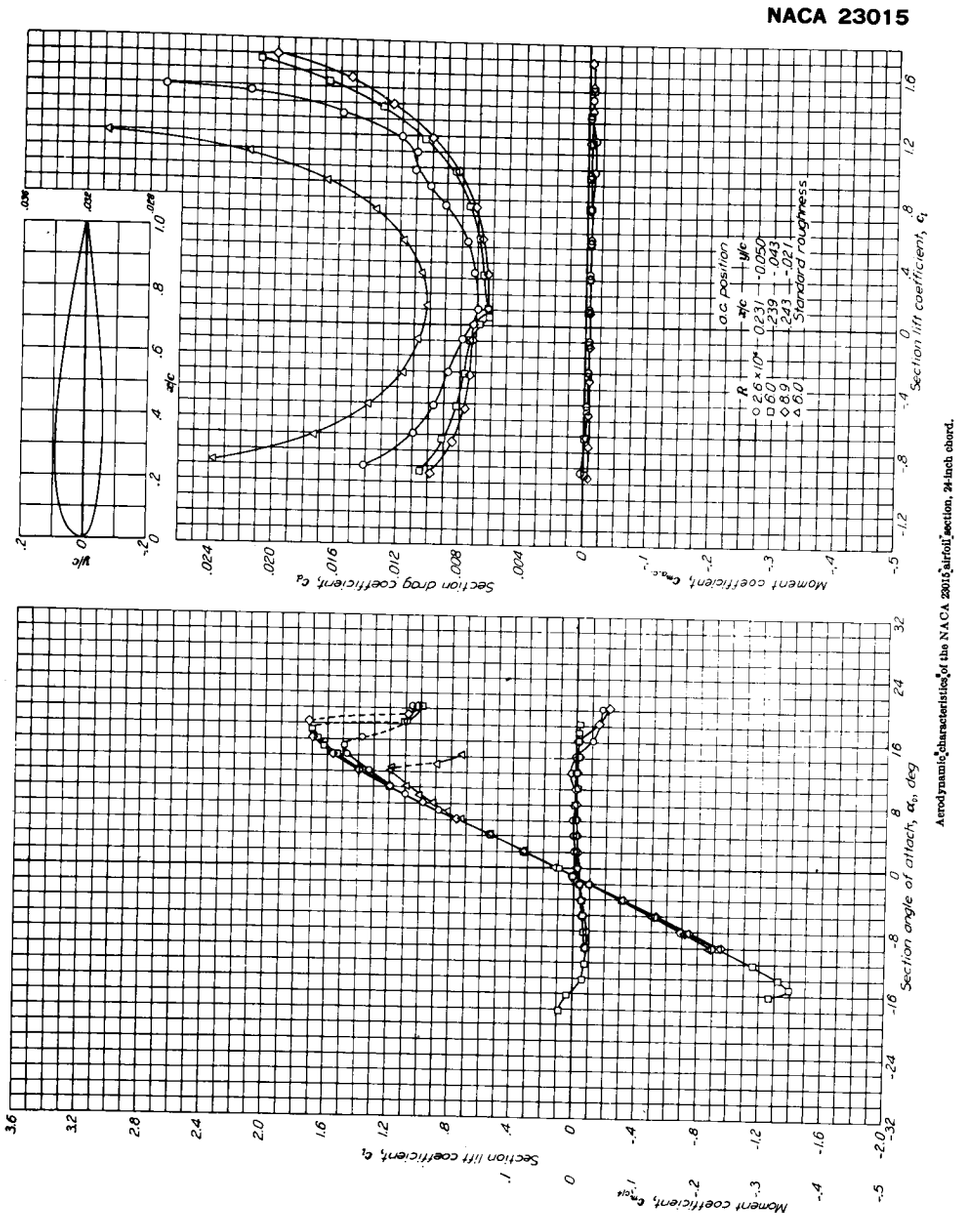

Aerodynamic characteristics of the NACA 23015 airfoil section, 24-inch chord.

A.3 Airfoil Data

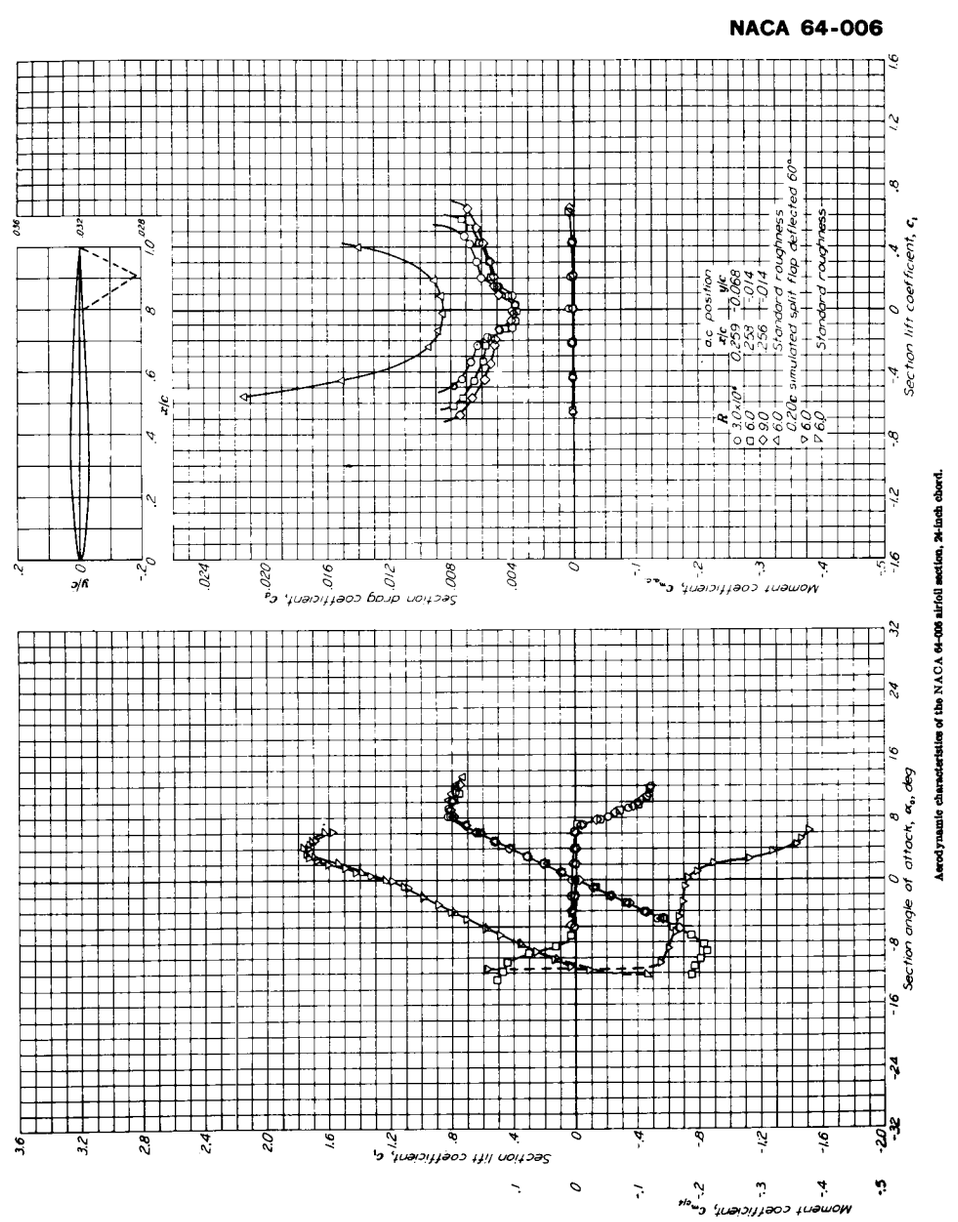

Aerodynamic characteristics of the NACA 64-006 airfoil section, 24-inch chord.

A.3 Airfoil Data

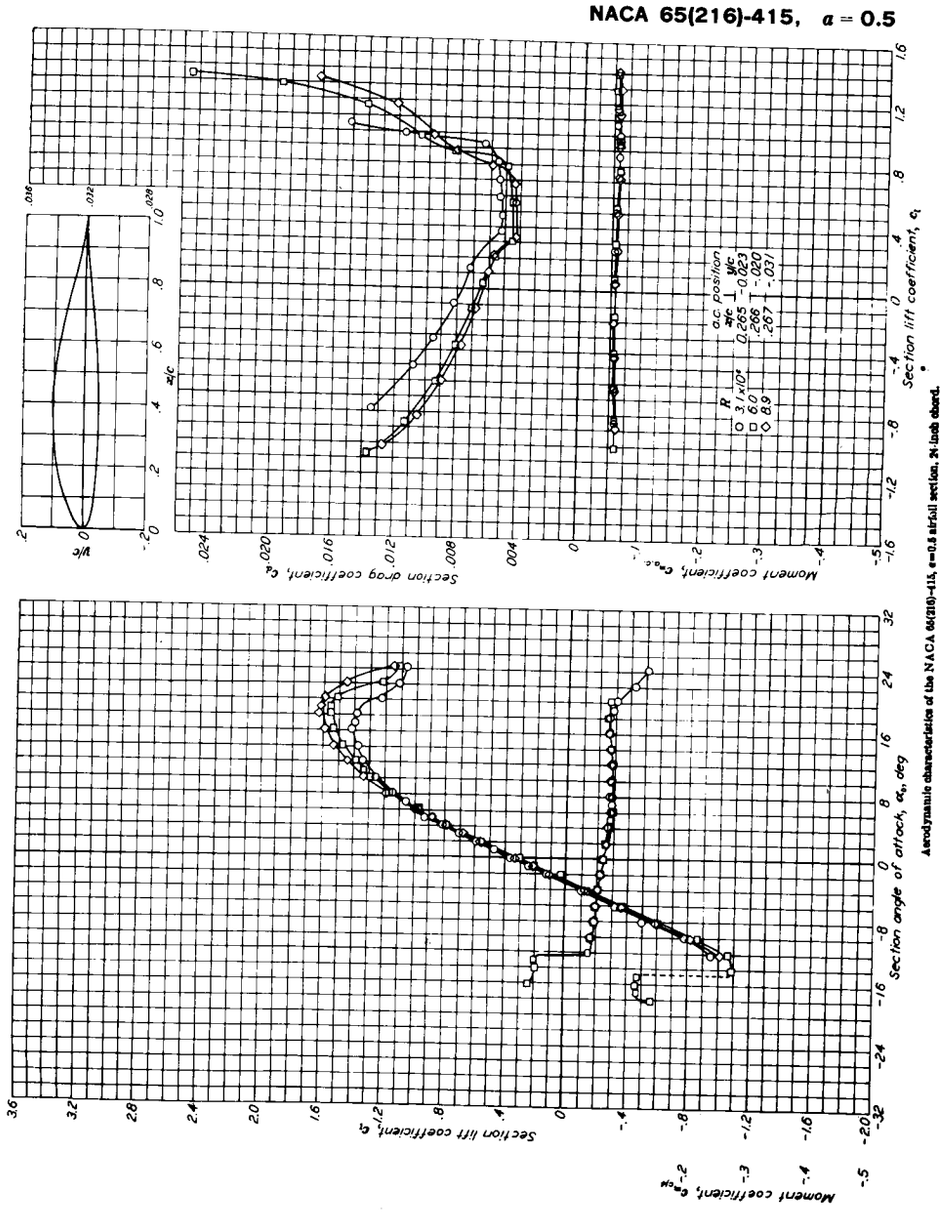

A.3 Airfoil Data

Airfoil Coordinates
Eppler 662

PROFIL N	662 15.02% X	Y
0	100.000	0.000
1	99.642	.118
2	98.640	.483
3	97.117	1.056
4	95.113	1.745
5	92.609	2.516
6	89.626	3.395
7	86.231	4.390
8	82.500	5.493
9	78.528	6.682
10	74.435	7.890
11	70.276	8.968
12	65.983	9.824
13	61.519	10.489
14	56.922	10.988
15	52.232	11.331
16	47.501	11.525
17	42.776	11.570
18	38.108	11.470
19	33.541	11.225
20	29.121	10.841
21	24.891	10.324
22	20.891	9.681
23	17.159	8.923
24	13.729	8.062
25	10.631	7.113
26	7.892	6.094
27	5.535	5.024
28	3.578	3.926
29	2.037	2.828
30	.921	1.761

PROFIL N	662 15.02% X	Y
31	.239	.770
32	.003	-.074
33	.351	-.733
34	1.336	-1.289
35	2.879	-1.785
36	4.966	-2.210
37	7.571	-2.567
38	10.668	-2.858
39	14.221	-3.088
40	18.189	-3.264
41	22.522	-3.392
42	27.165	-3.474
43	32.061	-3.512
44	37.148	-3.506
45	42.363	-3.456
46	47.642	-3.357
47	52.919	-3.206
48	58.130	-2.993
49	63.214	-2.702
50	68.116	-2.302
51	72.841	-1.742
52	77.449	-1.061
53	81.940	-.382
54	86.229	.169
55	90.177	.509
56	93.628	.611
57	96.423	.500
58	98.431	.276
59	99.613	.077
60	100.000	-.000

CM= -.1497 β= 5.92°

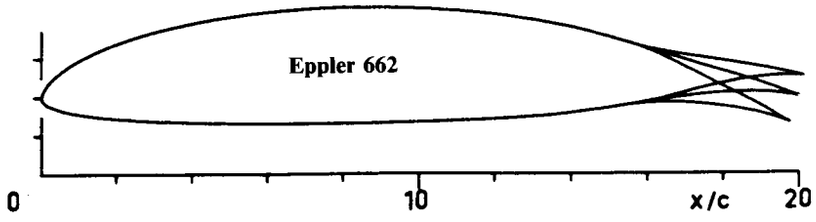

Eppler 662 – Flapped sailplane airfoil. (Ref. = NACA C.P. 2085)

A.3 Airfoil Data

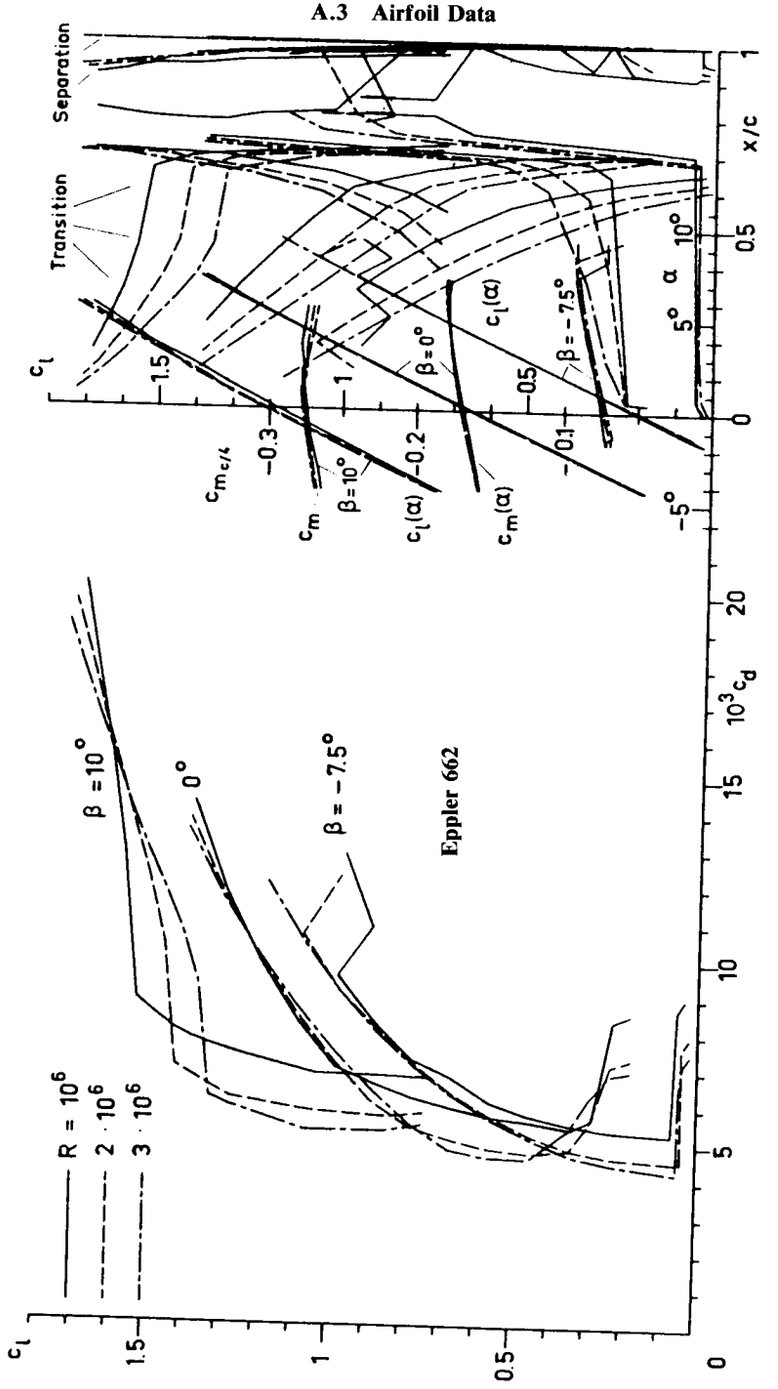

Theoretical section characteristics for airfoil 662.

A.3 Airfoil Data

Airfoil Coordinates
Eppler 748

PROFIL 748 19.73%		
N	X	Y
0	100.000	0.000
1	99.641	.122
2	98.632	.505
3	97.102	1.131
4	95.133	1.899
5	92.723	2.711
6	89.835	3.545
7	86.485	4.425
8	82.726	5.357
9	78.615	6.330
10	74.212	7.330
11	69.581	8.340
12	64.785	9.335
13	59.887	10.290
14	54.948	11.177
15	50.028	11.967
16	45.180	12.630
17	40.456	13.136
18	35.901	13.453
19	31.541	13.546
20	27.392	13.402
21	23.468	13.018
22	19.779	12.401
23	16.337	11.577
24	13.164	10.572
25	10.282	9.417
26	7.714	8.142
27	5.482	6.781
28	3.606	5.368
29	2.104	3.939
30	.992	2.534

PROFIL 748 19.73%		
N	X	Y
31	.284	1.201
32	.000	.006
33	.275	-.985
34	1.174	-1.865
35	2.614	-2.728
36	4.542	-3.540
37	6.925	-4.279
38	9.731	-4.932
39	12.923	-5.485
40	16.454	-5.923
41	20.278	-6.224
42	24.342	-6.362
43	28.592	-6.284
44	33.026	-5.899
45	37.743	-5.174
46	42.826	-4.217
47	48.237	-3.189
48	53.855	-2.189
49	59.567	-1.259
50	65.278	-.434
51	70.888	.248
52	76.292	.759
53	81.380	1.084
54	86.044	1.220
55	90.181	1.180
56	93.695	.984
57	96.483	.673
58	98.462	.338
59	99.621	.090
60	100.000	-.000

CM= -.1732 β= 6.65°

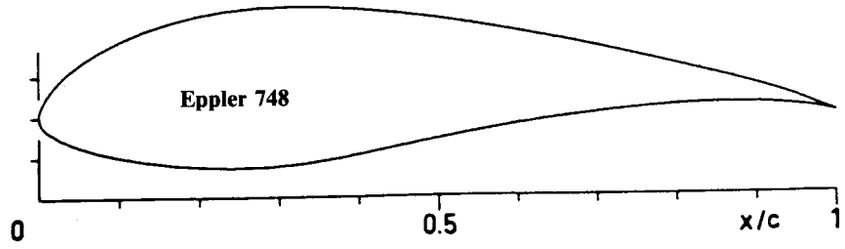

Eppler 748 for foot-launched sailplanes. (Ref. = NACA C.P. 2085)

A.3 Airfoil Data

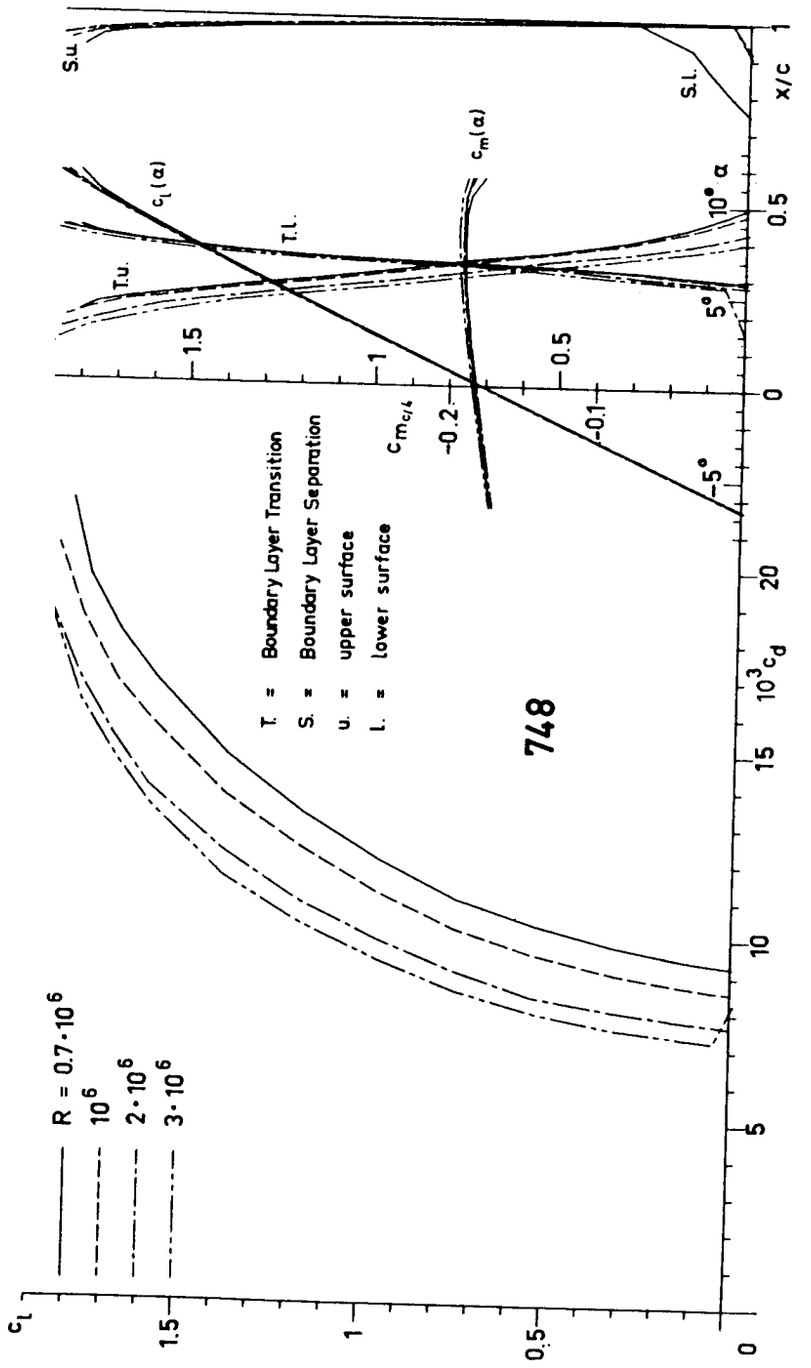

Theoretical section characteristics for airfoil 748.

A.3 Airfoil Data

TABLE I.- NLF(1)-0215F AIRFOIL COORDINATES ($\delta_f = 0^o$)

[c = 60.960 cm (24.000 in.)]

UPPER SURFACE		LOWER SURFACE	
X/C	Z/C	X/C	Z/C
.00240	.00917	.00000	-.00006
.00909	.01947	.00245	-.00704
.02004	.03027	.01099	-.01211
.03527	.04120	.02592	-.01656
.05469	.05201	.04653	-.02052
.07816	.06250	.07242	-.02399
.10546	.07247	.10324	-.02699
.13635	.08175	.13854	-.02954
.17050	.09019	.17788	-.03166
.20758	.09761	.22073	-.03334
.24720	.10389	.26654	-.03456
.28894	.10887	.31473	-.03531
.33237	.11240	.36468	-.03554
.37702	.11428	.41576	-.03519
.42253	.11427	.46731	-.03415
.46864	.11219	.51867	-.03225
.51524	.10784	.56920	-.02925
.56247	.10147	.61825	-.02441
.61010	.09373	.66662	-.01663
.65752	.08513	.71614	-.00705
.70408	.07603	.76645	.00167
.74914	.06673	.81565	.00804
.79206	.05746	.86198	.01155
.83222	.04844	.90359	.01198
.86902	.03983	.93862	.00990
.90193	.03175	.96588	.00655
.93044	.02428	.98504	.00323
.95409	.01737	.99630	.00086
.97285	.01082	1.00000	.00000
.98710	.00507		
.99658	.00126		
1.00000	.00000		

A.3 Airfoil Data

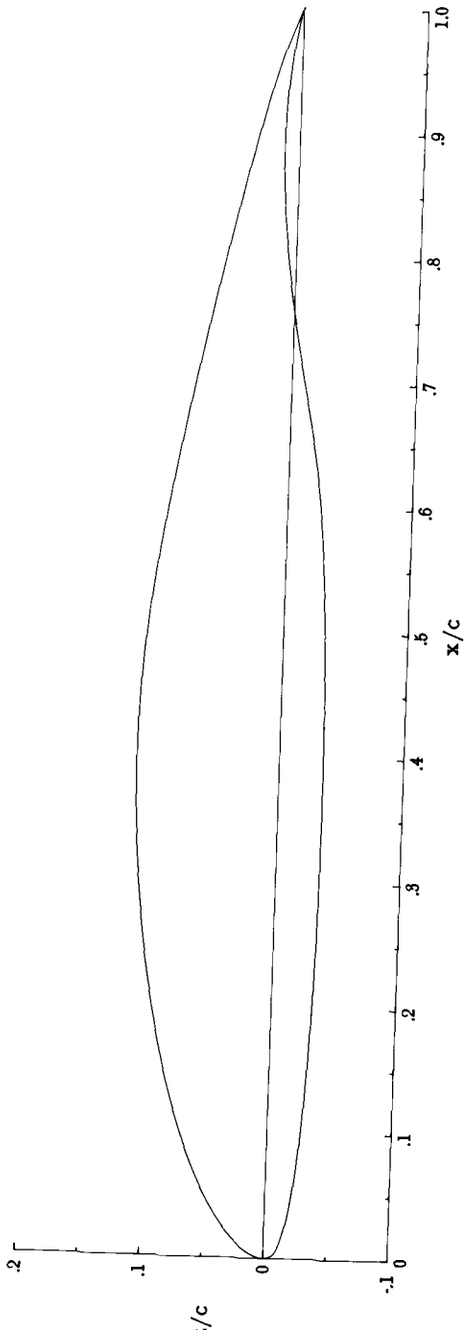

(a) $\delta_f = 0°$.

NLF(1)-0215F airfoil shape.

A.3 Airfoil Data

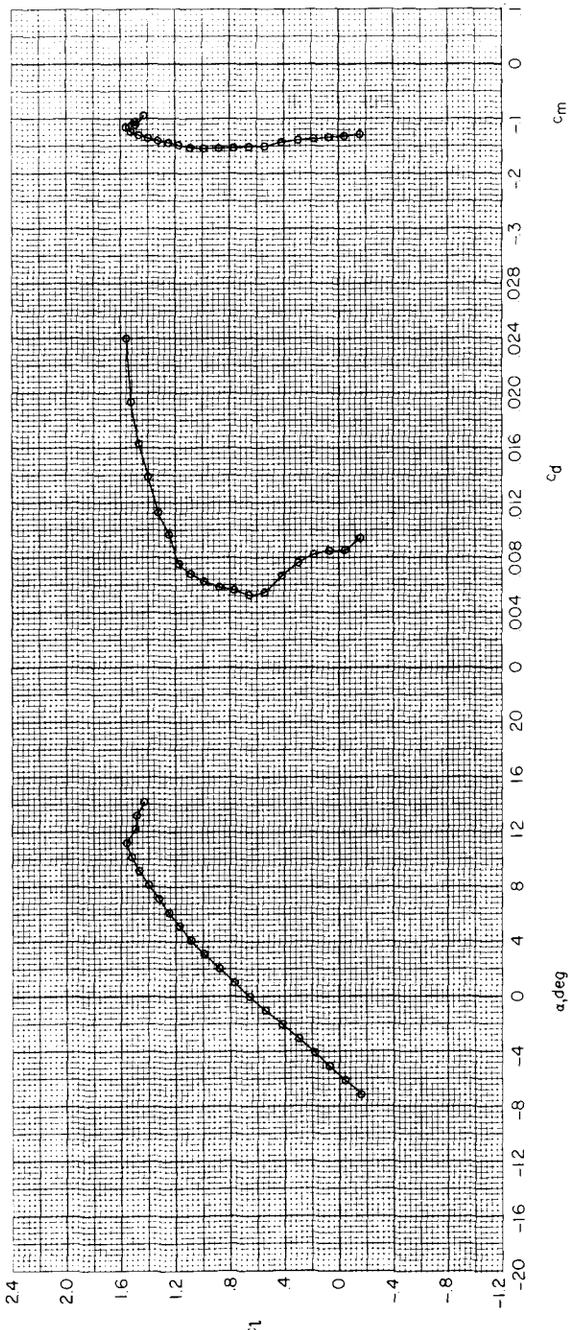

(a) R = 3.0×10^6.

Section characteristics with $\delta_f = 0°$ at M = 0.10.

A.3 Airfoil Data

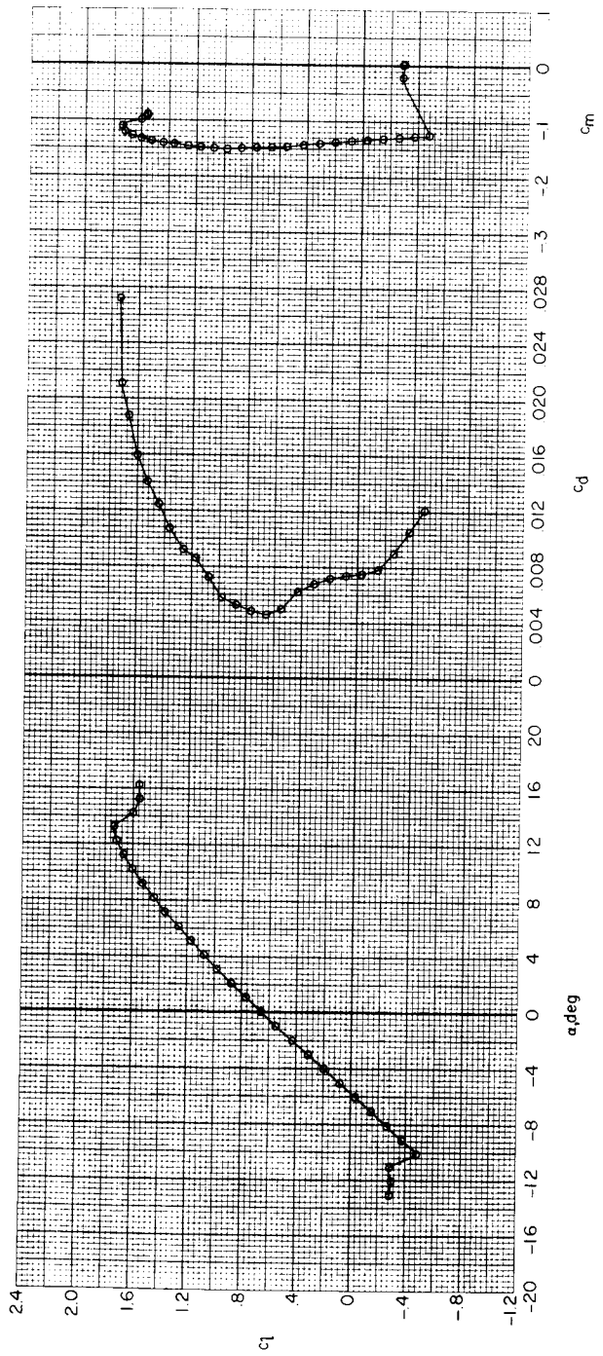

(b) R = 6.0 × 10^6. Continued.

A.3 Airfoil Data

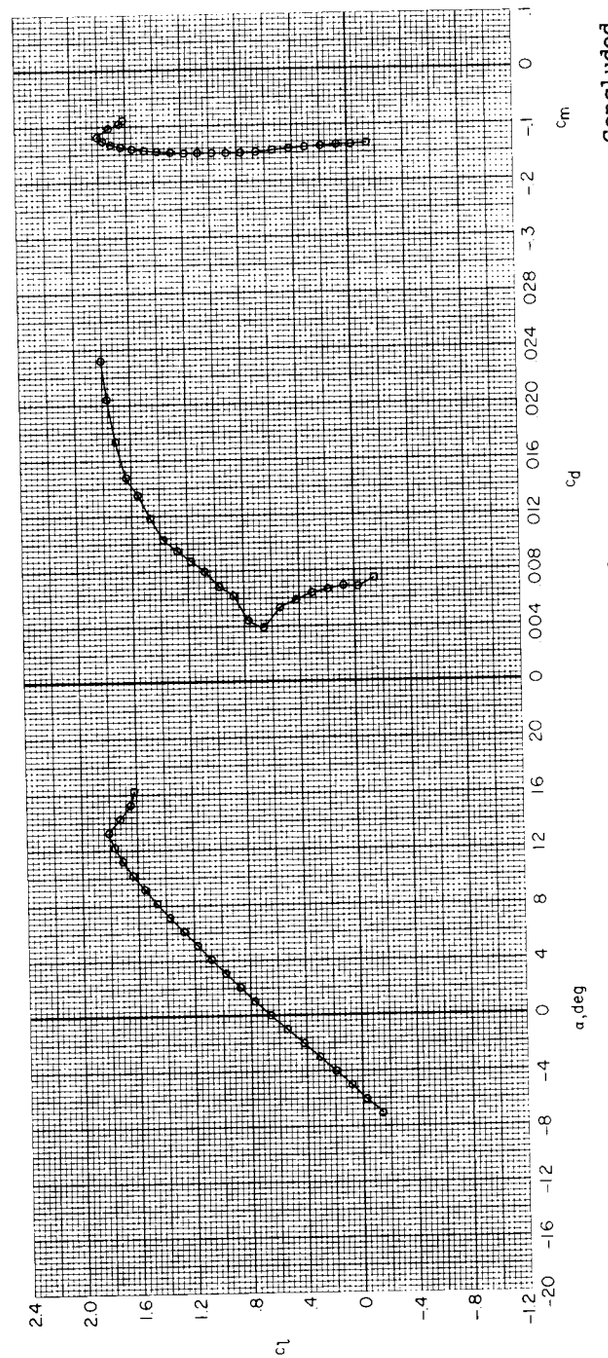

(c) R = 9.0 × 10^6. Concluded.

A.3 Airfoil Data

Airfoil Coordinates
NLF(2)-0415

UPPER SURFACE		LOWER SURFACE	
X/C	Z/C	X/C	Z/C
.00004	.00076	.00212	-.00519
.00339	.00805	.01042	-.01028
.01157	.01578	.02481	-.01556
.02457	.02348	.04468	-.02100
.04251	.03097	.06956	-.02654
.06534	.03820	.09906	-.03210
.09285	.04519	.13268	-.03762
.12474	.05196	.16994	-.04297
.16059	.05850	.21025	-.04804
.19991	.06475	.25308	-.05261
.24219	.07063	.29785	-.05649
.28688	.07600	.34399	-.05945
.33346	.08075	.39094	-.06122
.38139	.08473	.43810	-.06148
.43013	.08784	.48486	-.05953
.47913	.08996	.53165	-.05421
.52787	.09096	.57997	-.04592
.57580	.09075	.63002	-.03644
.62242	.08919	.68079	-.02708
.66720	.08616	.73118	-.01850
.70961	.08126	.78007	-.01121
.74985	.07382	.82636	-.00546
.78883	.06416	.86897	-.00139
.82663	.05364	.90692	.00107
.86248	.04325	.93928	.00210
.89552	.03349	.96529	.00204
.92495	.02470	.98436	.00133
.95000	.01698	.99605	.00043
.97030	.01015	1.00000	0.00000
.98592	.00455		
.99628	.00109		
1.00000	0.00000		

A.3 Airfoil Data

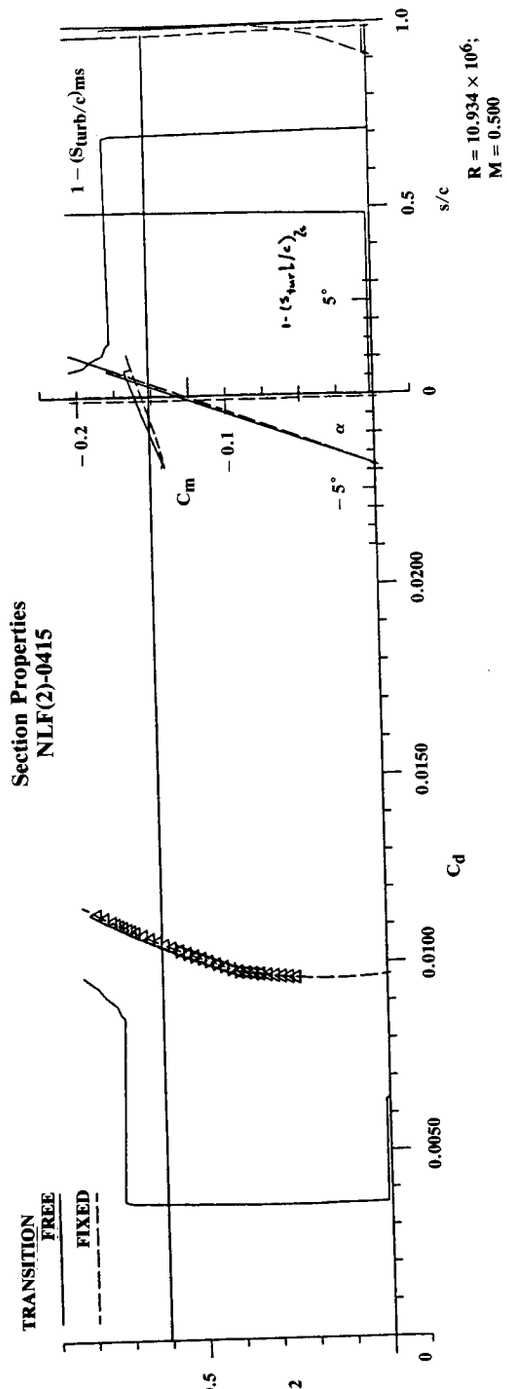

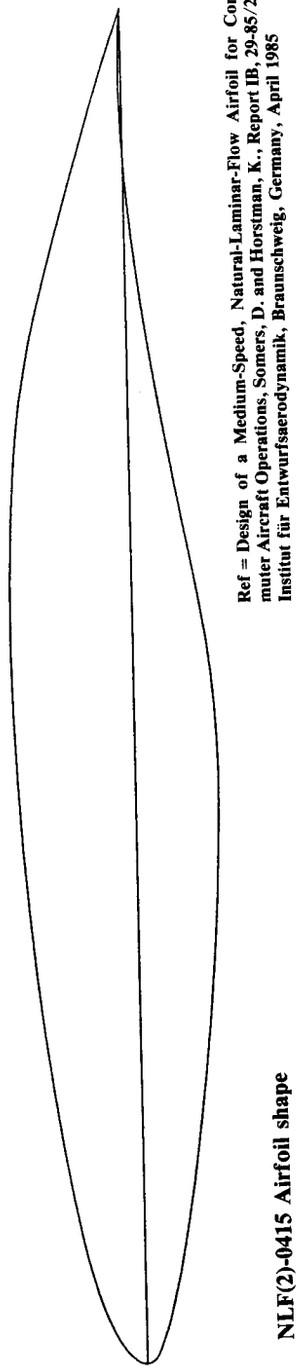

Ref = Design of a Medium-Speed, Natural-Laminar-Flow Airfoil for Commuter Aircraft Operations, Somers, D. and Horstman, K., Report IB, 29-85/26, Institut für Entwurfsaerodynamik, Braunschweig, Germany, April 1985

NLF(2)-0415 Airfoil shape

A.3 Airfoil Data

Table I. Coordinates for the NASA SC(2)-0714 Airfoil

Upper surface		Lower surface	
x/c	z/c	x/c	z/c
0.0000	0.0000	0.0000	0.0000
.0020	.0095	.0020	−.0093
.0050	.0158	.0050	−.0160
.0100	.0219	.0100	−.0221
.0200	.0293	.0200	−.0295
.0300	.0343	.0300	−.0344
.0400	.0381	.0400	−.0381
.0500	.0411	.0500	−.0412
.0700	.0462	.0700	−.0462
.1000	.0518	.1000	−.0517
.1200	.0548	.1200	−.0547
.1500	.0585	.1500	−.0585
.1700	.0606	.1700	−.0606
.2000	.0632	.2000	−.0633
.2200	.0646	.2200	−.0647
.2500	.0664	.2500	−.0666
.2700	.0673	.2800	−.0680
.3000	.0685	.3000	−.0687
.3300	.0692	.3200	−.0692
.3500	.0696	.3500	−.0696
.3800	.0698	.3700	−.0696
.4000	.0697	.4000	−.0692
.4300	.0695	.4200	−.0688
.4500	.0692	.4500	−.0676
.4800	.0684	.4800	−.0657
.5000	.0678	.5000	−.0644
.5300	.0666	.5300	−.0614
.5500	.0656	.5500	−.0588
.5700	.0645	.5800	−.0643
.6000	.0625	.6000	−.0509
.6200	.0610	.6300	−.0451
.6500	.0585	.6500	−.0410
.6800	.0555	.6800	−.0346
.7000	.0533	.7000	−.0302
.7200	.0509	.7300	−.0235
.7500	.0469	.7500	−.0192
.7700	.0439	.7700	−.0150
.8000	.0389	.8000	−.0093
.8200	.0353	.8300	−.0048
.8500	.0294	.8500	−.0027
.8700	.0251	.8700	−.0013
.9000	.0181	.8900	−.0008
.9200	.0131	.9200	−.0016
.9500	.0049	.9400	−.0035
.9700	−.0009	.9500	−.0049
.9800	−.0039	.9600	−.0066
.9900	−.0071	.9700	−.0085
1.0000	−.0104	.9800	−.0109
		.9900	−.0137
		1.0000	−.0163

NASA SC(2)-0714 Airfoil (NASA TP-2890).

A.3 Airfoil Data

Figure 10. Profile-drag coefficient versus Reynolds number at various normal-force coefficients.

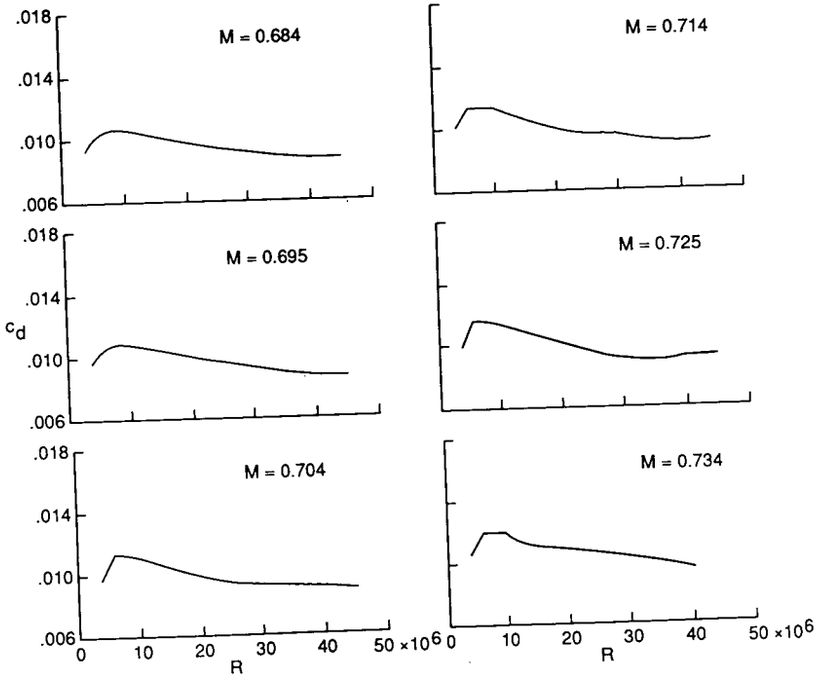

(a) $c_n = 0.51$.

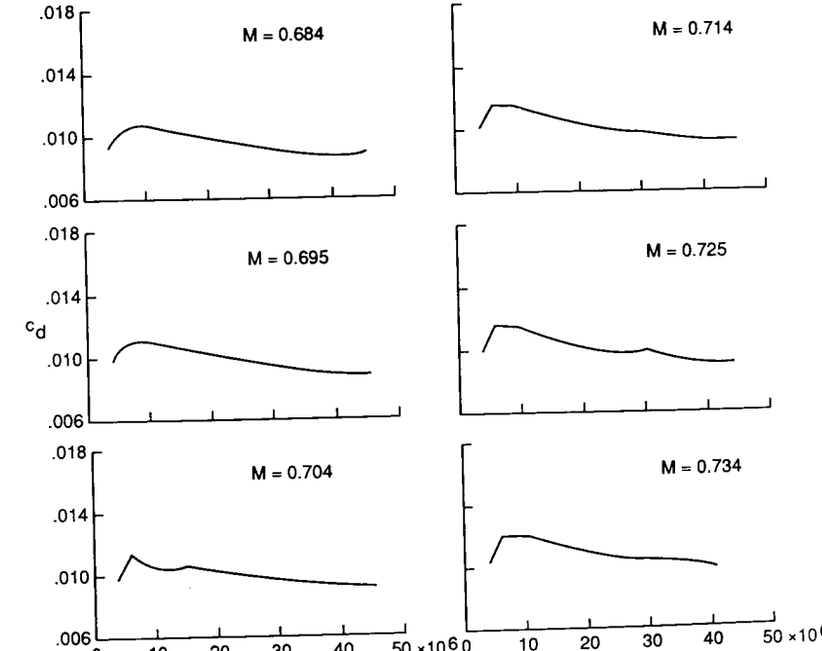

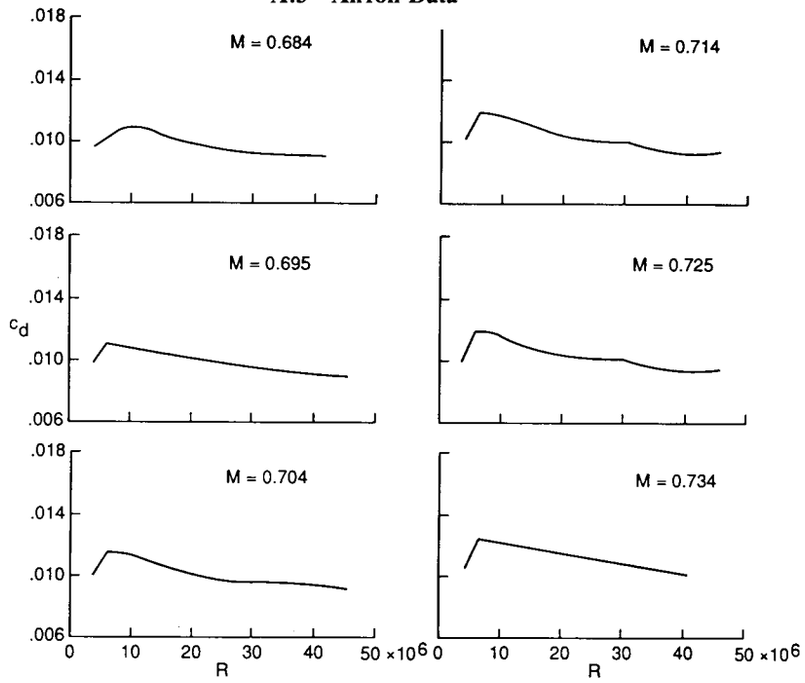

(c) $c_n = 0.61$.

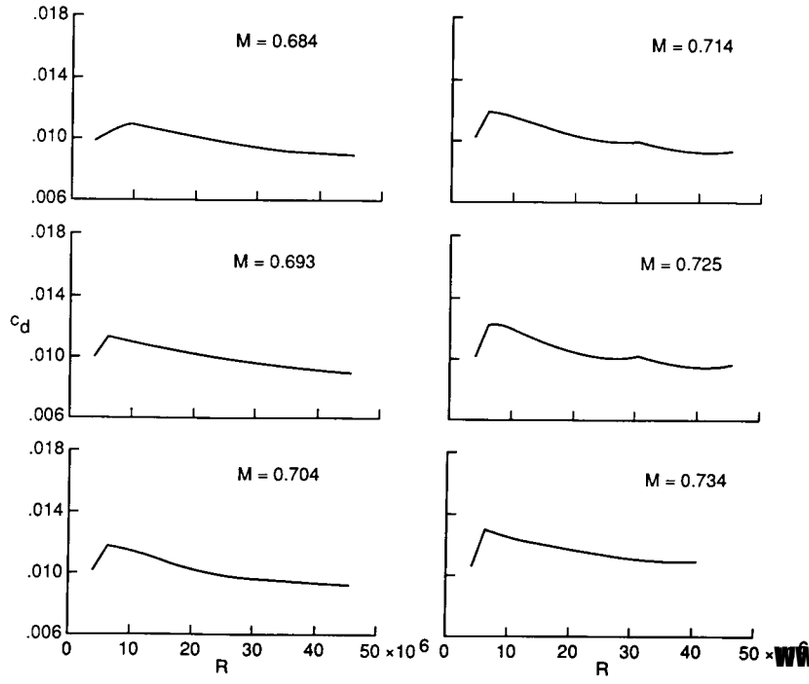

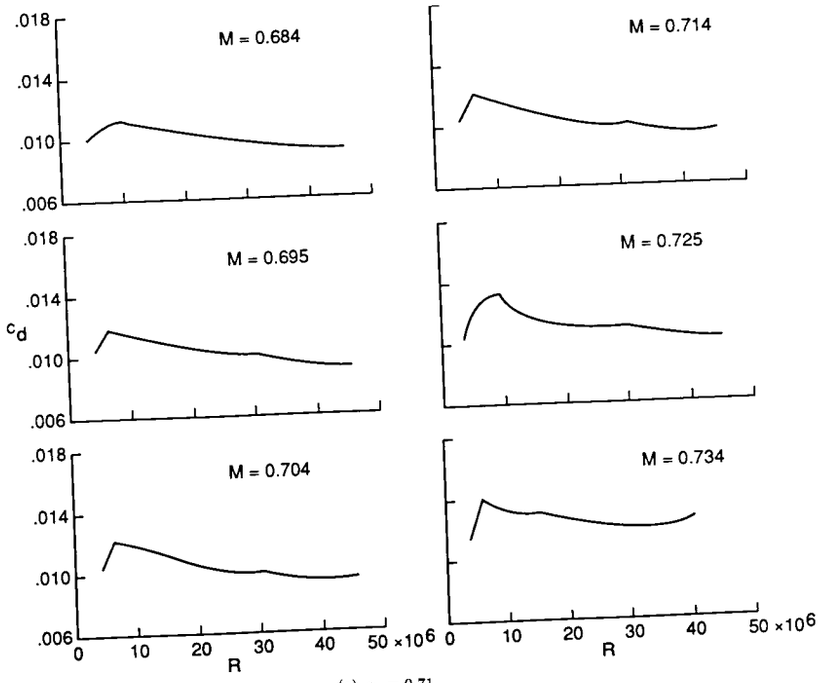

(e) $c_n = 0.71$.

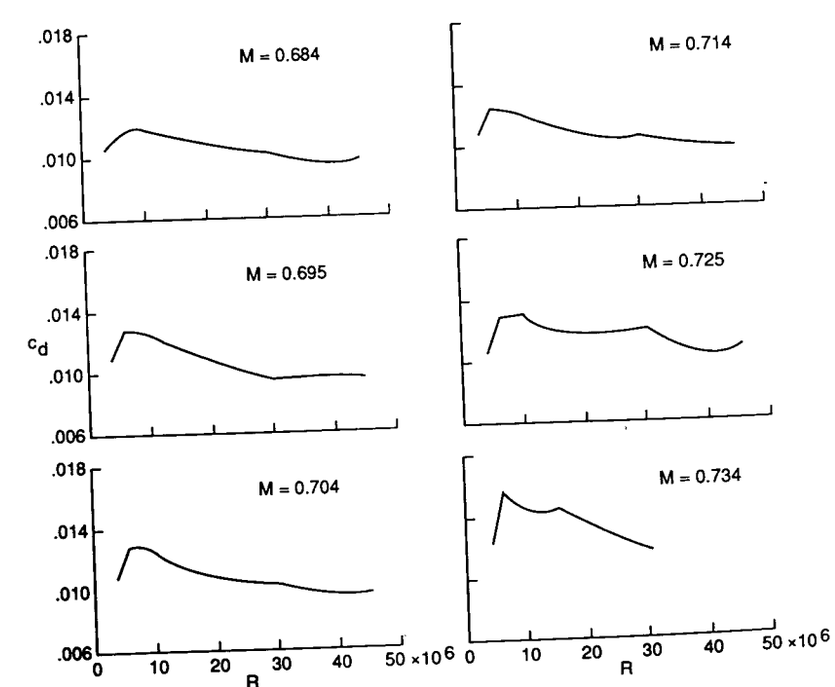

A.3 Airfoil Data

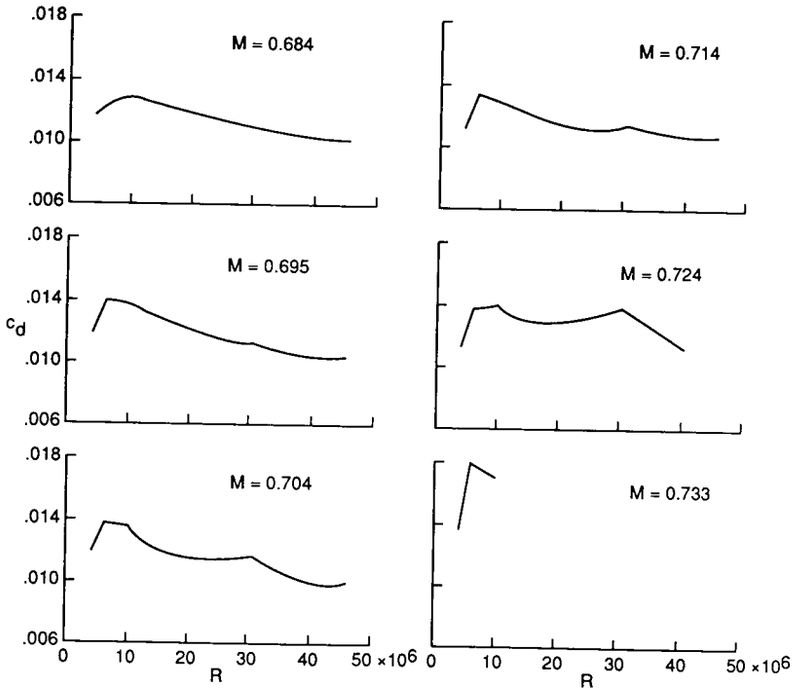

(g) $c_n = 0.81$.

A.3 Airfoil Data

Figure 11. Quarter-chord pitching-moment coefficient versus Reynolds number at various normal-force coefficients

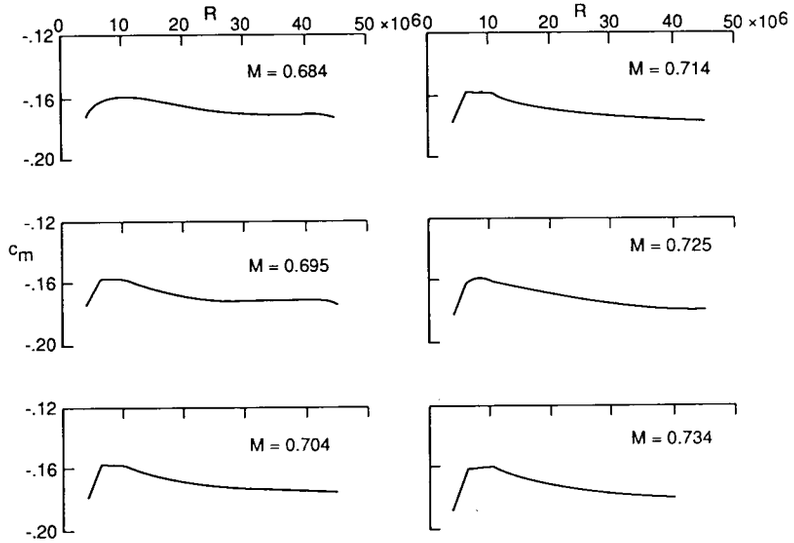

(a) $c_n = 0.51$.

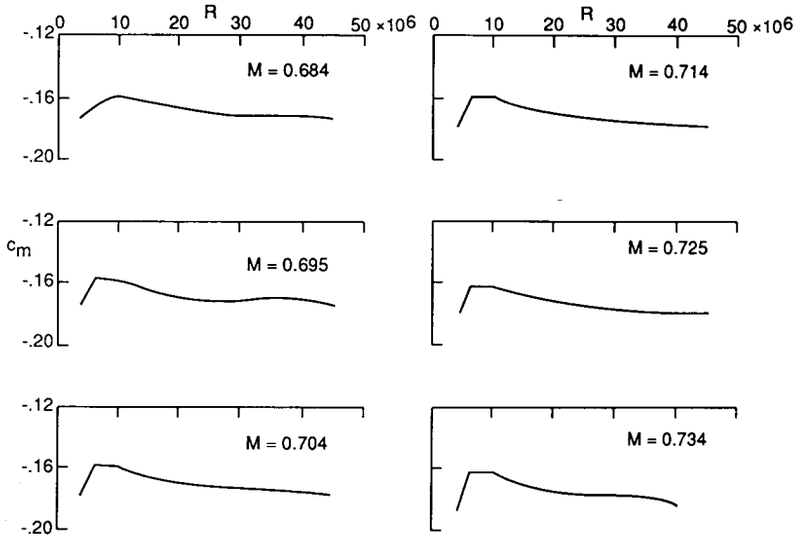

(b) $c_n = 0.56$.

A.3 Airfoil Data

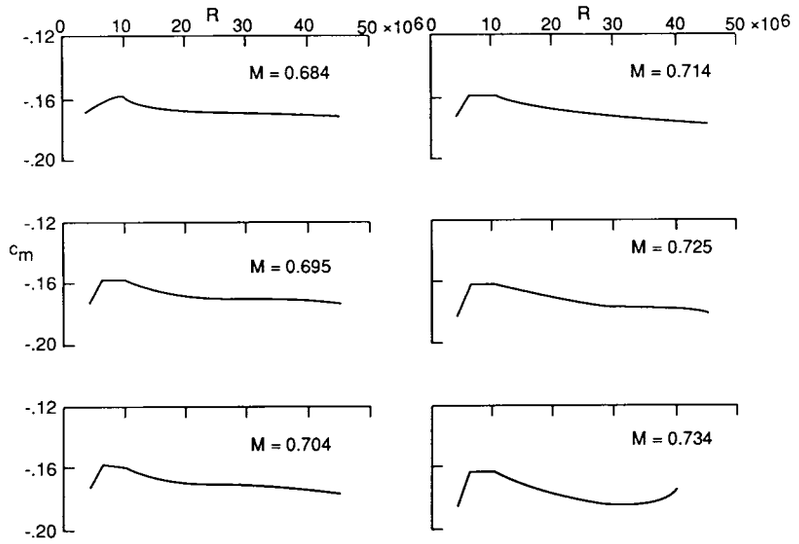

(c) $c_n = 0.61$.

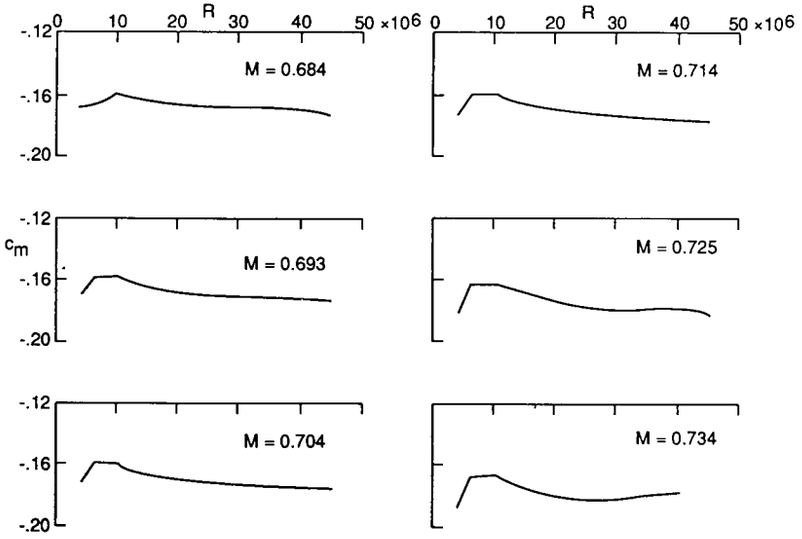

(d) $c_n = 0.66$.

A.3 Airfoil Data

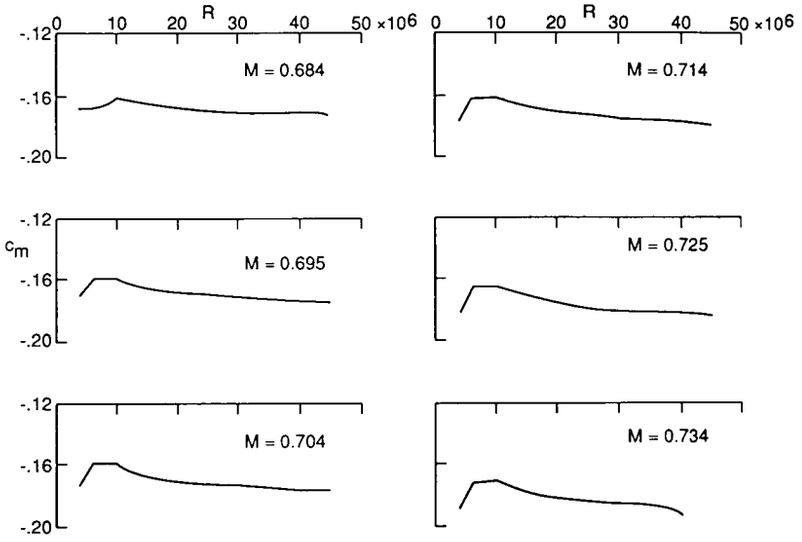

(e) $c_n = 0.71$.

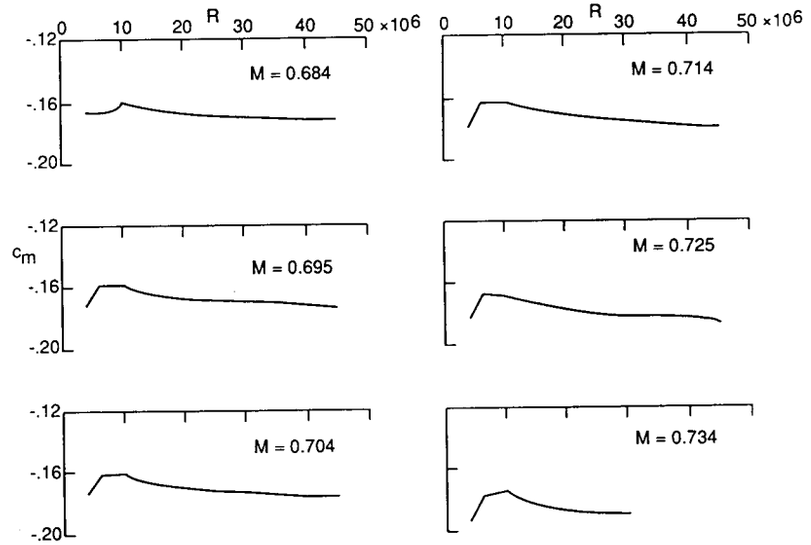

(f) $c_n = 0.76$.

A.3 Airfoil Data

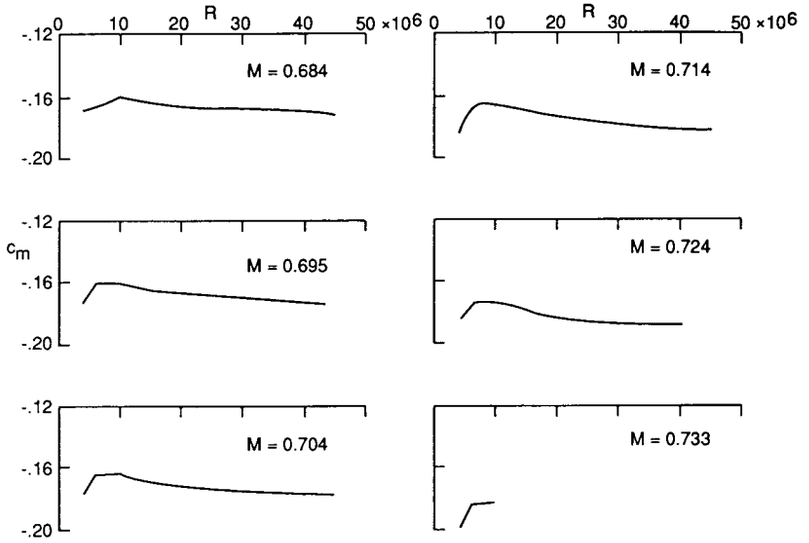

(g) $c_n = 0.81$.

APPENDIX A.4
TYPICAL ENGINE PERFORMANCE CURVES

This Appendix contains performance curves for three different types of aircraft engines: an afterburning turbofan, a high-bypass-ratio turbofan, and a turboprop. Although not identical to any currently in production, these engines are representative of advanced technology suitable for use in aircraft design studies. The engines may be scaled using the scaling laws presented in Chapter 10.

These curves were generated using Version 2.0 of the engine-cycle analysis programs ONX and OFFX that are based on the methods contained in the AIAA Education Series textbook, *Aircraft Engine Design,* by Jack D. Mattingly, William H. Heiser, and Daniel H. Daley. Both the textbook and the programs with their user guide are available from the American Institute of Aeronautics and Astronautics, 370 L'Enfant Promenade, SW, Washington, DC 20024. The author would like to thank Dr. Mattingly for preparation of these engine performance curves.

Note: All altitudes are in feet.

A.4-1 Afterburning turbofan characteristics

Sea-level static thrust, lb	30,000
Sea-level static TSFC, 1/hr	1.64
Sea-level static airflow, lbm/s	246
Bare-engine weight, lb	3,000
Engine length (including axisymmetric nozzle), in.	160
Maximum diameter, in.	44
Fan-face diameter, in.	40
Overall pressure ratio	22
Fan pressure ratio	4.3
Bypass ratio	0.41

The following installed engine data reflects these assumptions:

1) Mil. Spec. MIL-E-5008B inlet pressure recovery and inlet duct total pressure ratio of 0.97.

2) Power extraction of 320 kW to drive electric generators and auxiliary equipment at all power settings and flight conditions.

3) High-pressure bleed airflow at rate of 1.7 lb/s.

A.4 Typical Engine Performance Curves

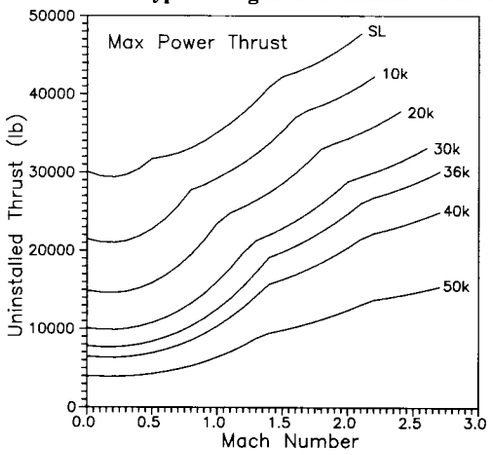

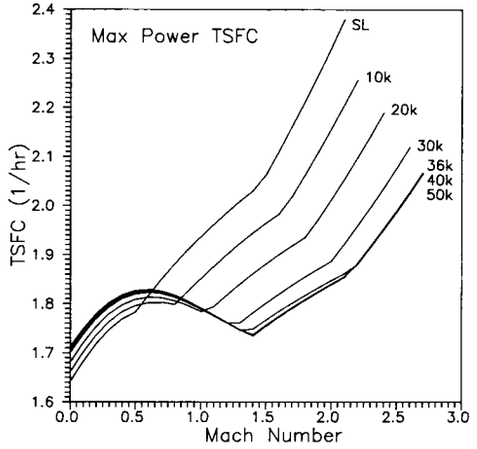

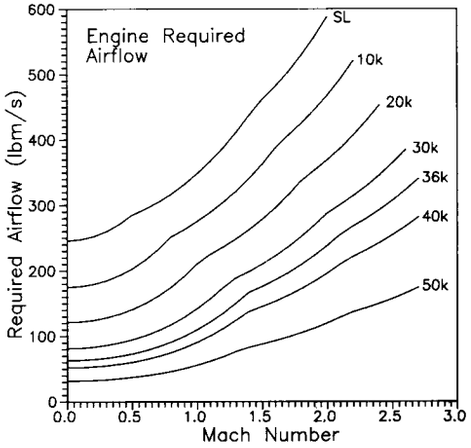

A.4 Typical Engine Performance Curves

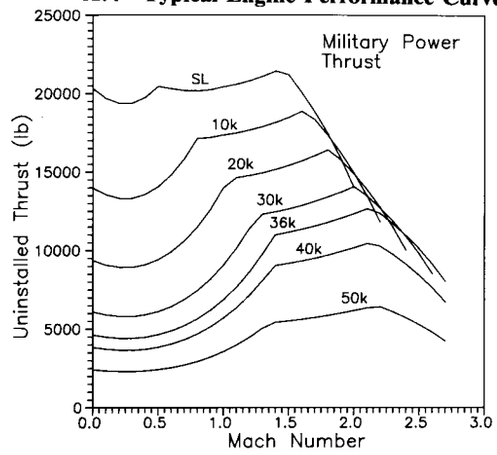

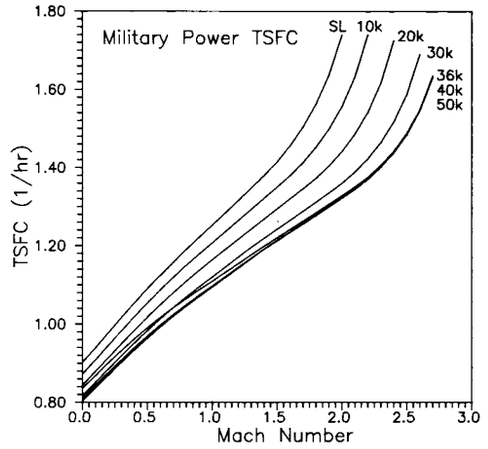

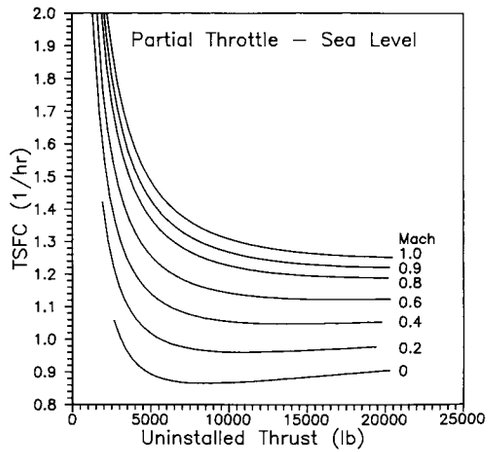

A.4 Typical Engine Performance Curves

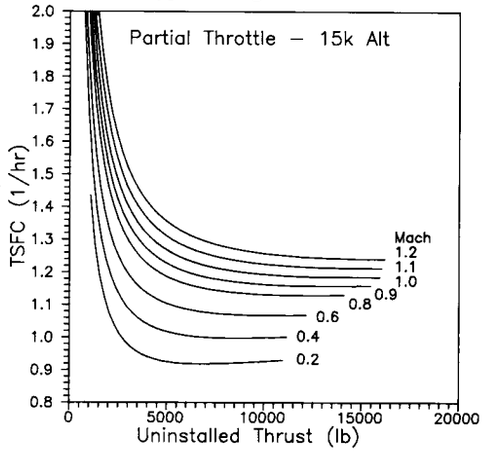

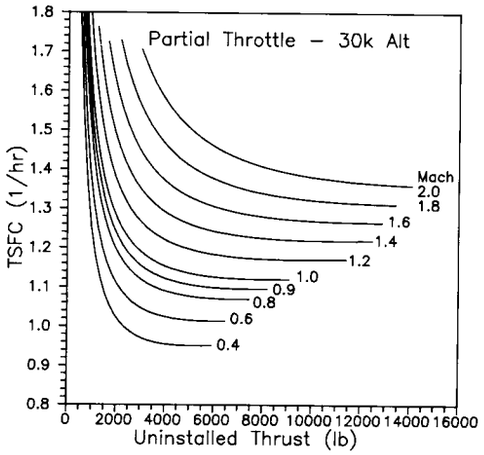

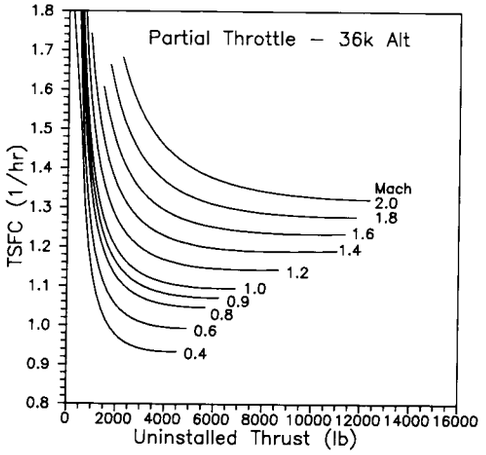

A.4 Typical Engine Performance Curves

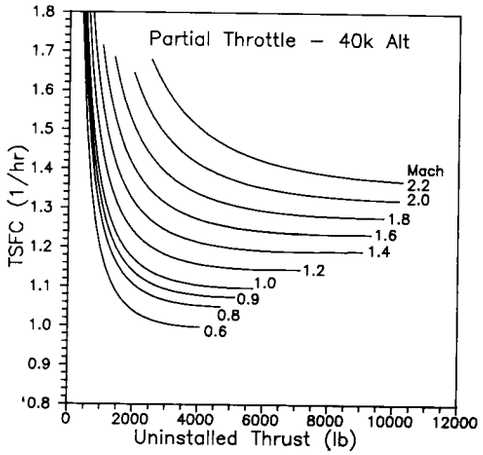

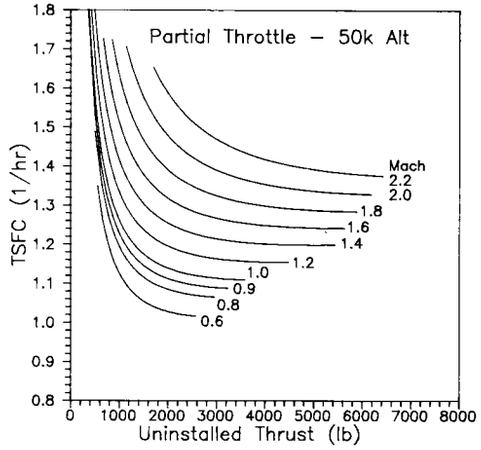

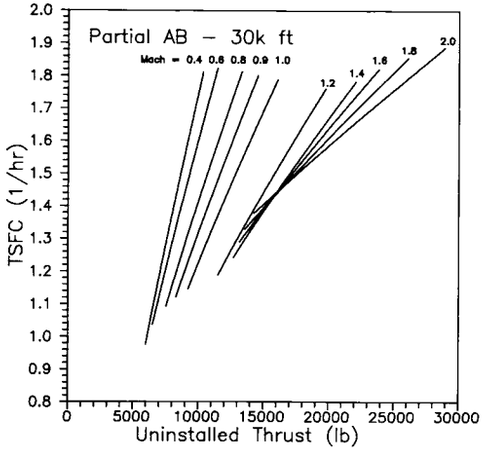

A.4 Typical Engine Performance Curves

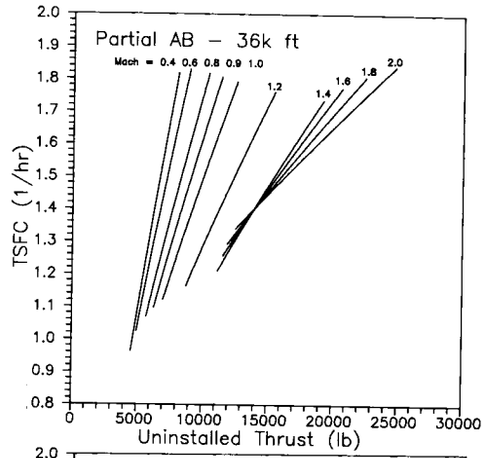

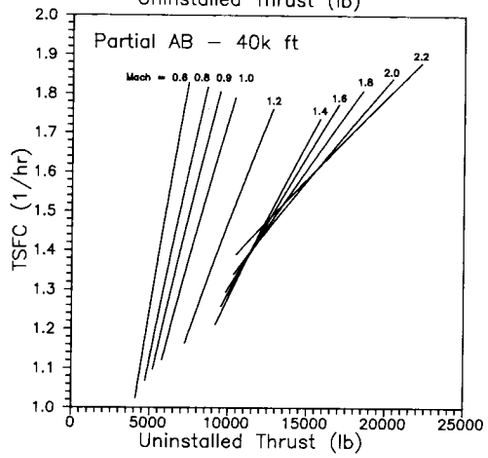

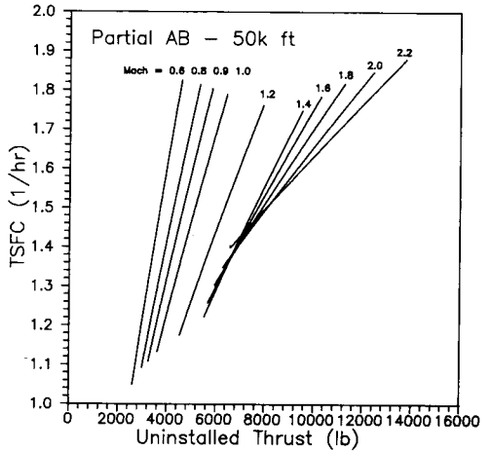

A.4-2 High-bypass turbofan characteristics

Sea-level static thrust, lb	50,000
Sea-level static TSFC, 1/hr	0.40
Sea-level static airflow, lb/s	1,680
Bare-engine weight, lb	7,700
Engine length, in.	150
Maximum engine diameter, in.	100
Overall pressure ratio	30
Fan pressure ratio	1.6
Bypass ratio	8.0

The following installed-engine data reflects these assumptions:

1) Inlet total pressure ratio of 0.97.

2) Power extraction of 650 kW to drive electric generators and auxiliary equipment at all power settings and flight conditions.

3) High-pressure bleed airflow at rate of 2.0 lb/s.

Maximum rated performance is plotted with dashes.

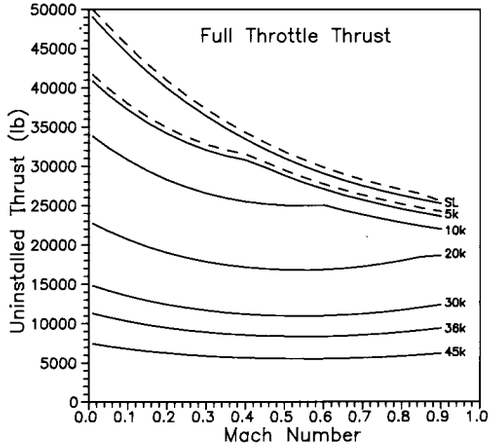

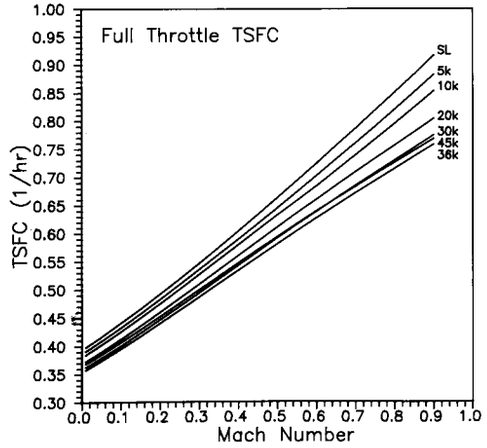

A.4 Typical Engine Performance Curves

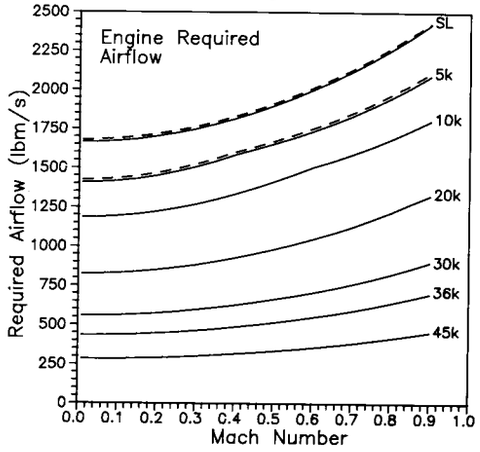

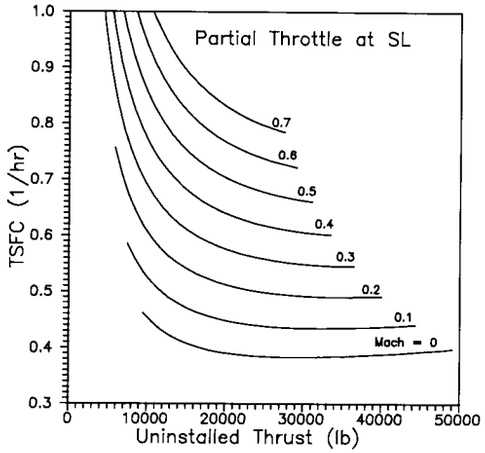

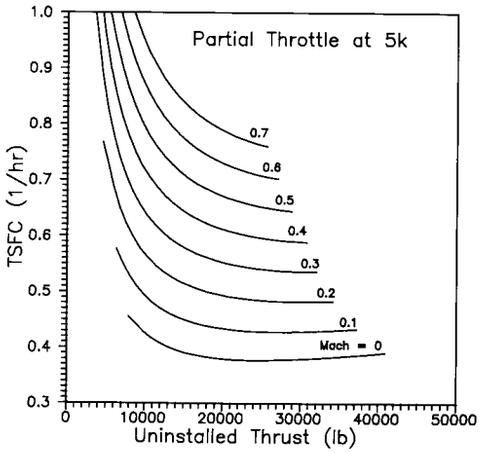

A.4 Typical Engine Performance Curves

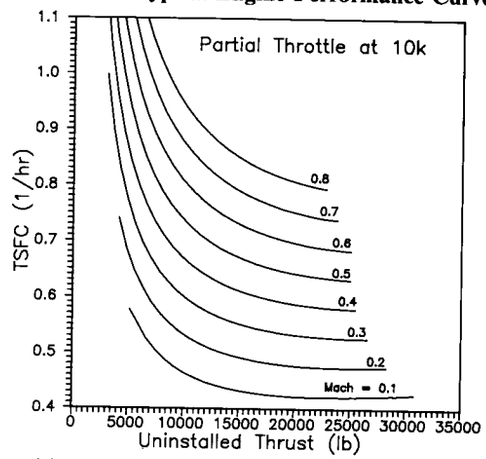

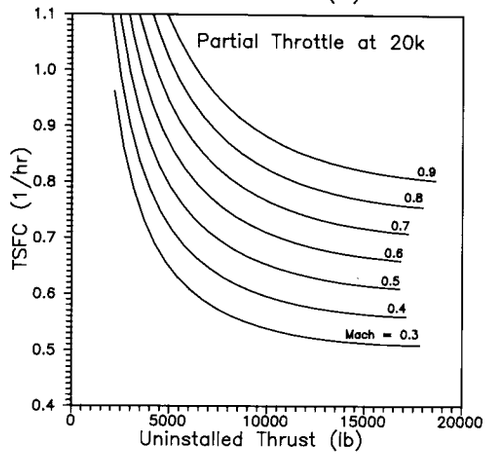

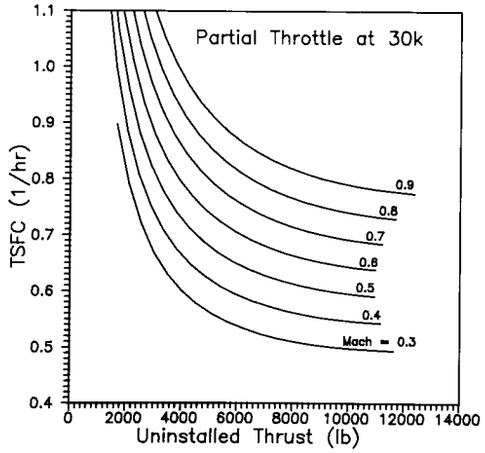

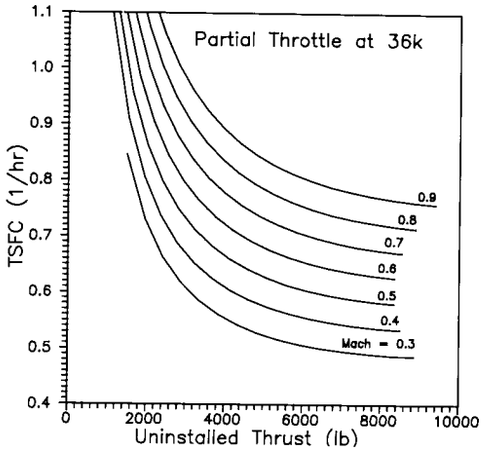

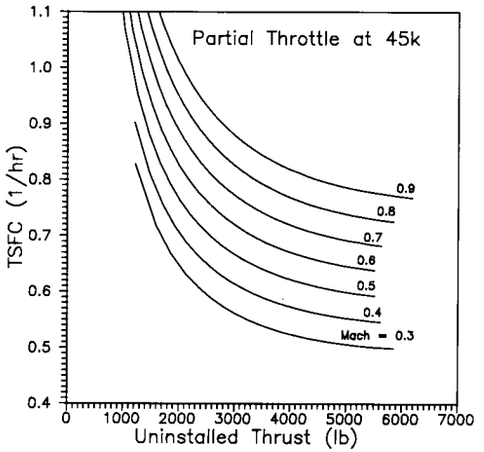

A.4-3 Turboprop characteristics

Sea-level static thrust, lb	32,000
Sea-level static power, hp	6,500
Sea-level static TSFC, 1/hr	0.14
Sea-level static airflow, lbm/s	42.3
Bare-engine weight (including gear box and propeller), lb	2,600
Diameter of four-bladed, two-row propeller, ft	20.5
Engine length (propeller to exhaust), in.	200
Engine diameter, in.	46
Overall pressure ratio	30

The following uninstalled-engine data reflects these assumptions:

1) Inlet total pressure ratio of 0.97.

2) Power extraction of 54 kW to drive electric generators and auxiliary equipment at all power settings and flight conditions.

3) High-pressure bleed airflow at rate of 0.8 lb/s.

Maximum rated performance is plotted with dashes.

A.4 Typical Engine Performance Curves

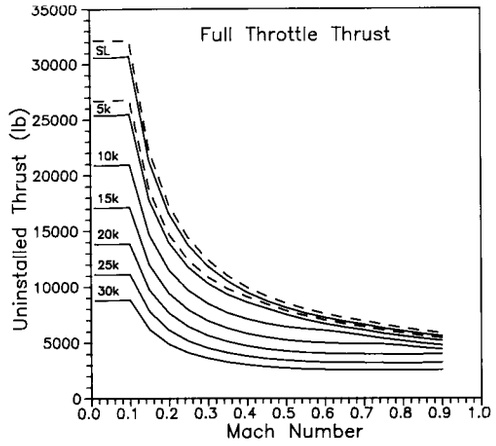

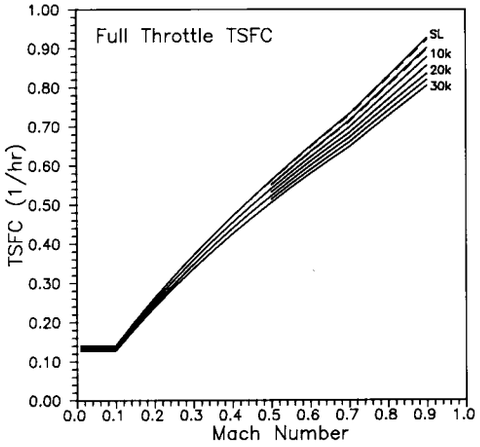

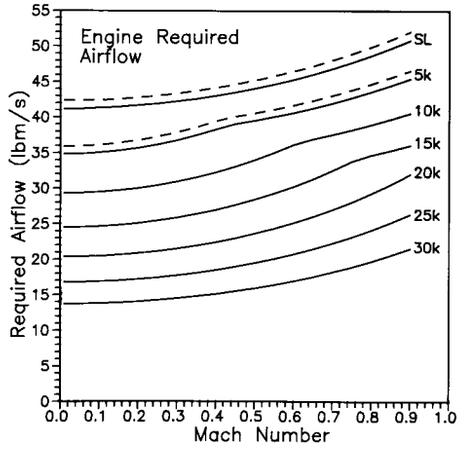

A.4 Typical Engine Performance Curves

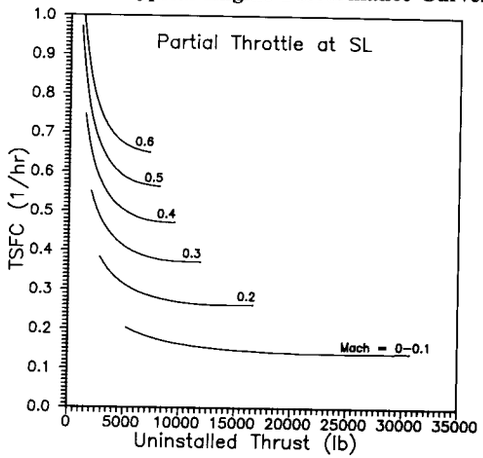

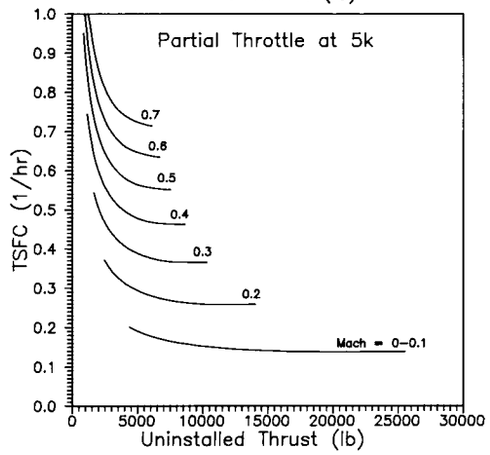

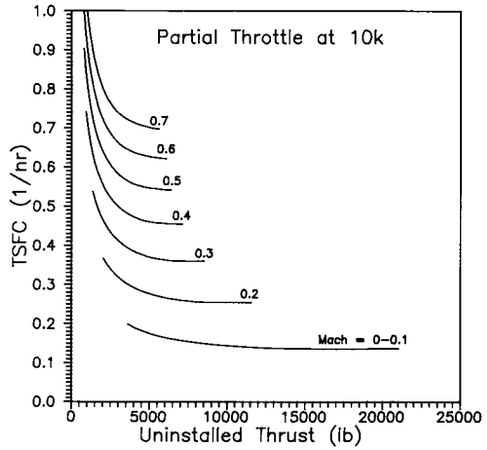

A.4 Typical Engine Performance Curves

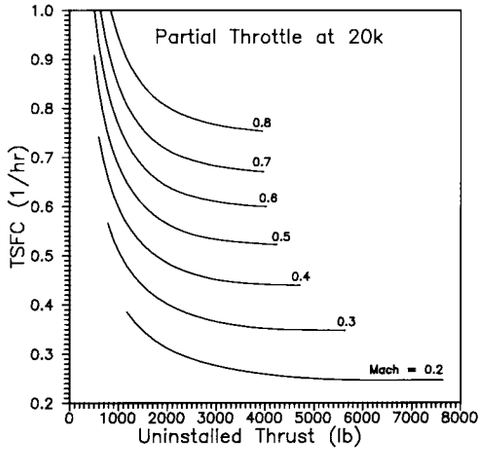

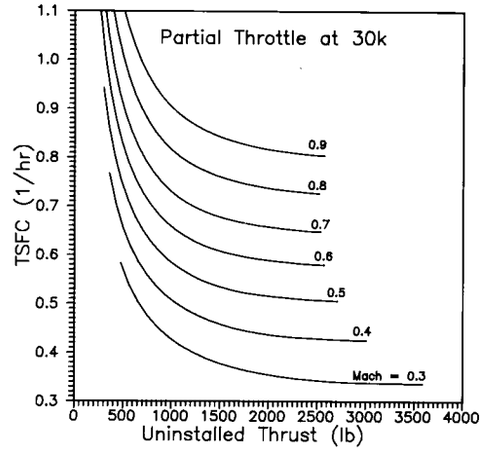

APPENDIX A.5
DESIGN REQUIREMENTS AND SPECIFICATIONS

A.5-1 Federal Aviation Regulations (FAR)—Applicability[a]

Category	Various[b]	Normal	Transport
A) Characteristics.			
Maximum takeoff weight, lb	≤ 12,500	≤ 12,500	—
Number of engines	One or more	Two or more	Two or more
Type of engine	All	Propeller engines only	All
Minimum crew:			
Flight crew	One or more	Two	Two or more
Cabin attendants	None	< 20 Pass.: None ≥ 20 Pass.: One	< 10 Pass.: None ≥ 10 Pass.: One or more
Maximum number of occupants	10	11–23	Not restricted
Maximum operating altitude, ft	25,000	25,000	Not restricted
B) FAR Applicability.			
Airworthiness standards airplanes	Part 23	Part 23	Part 25
Airworthiness standards engines	Part 33	Part 33	Part 33
Airworthiness standards propellers	Part 35	Part 35	Part 35
Noise standards	Part 36: Prop-Driven, Appendix F		Part 36
General operating and flight rules	Part 91	Part 91	Part 91
Operations:			
Domestic, flag and supplemental comm. operators of large aircraft	—	—	Part 121
Air travel clubs using large aircraft	—	—	Part 123
Air taxi and comm. operators	—	Part 135	—
Agricultural aircraft	Part 137	—	—

[a]After E. Torenbeck (Ref. 23).
[b]Normal, utility, acrobatic, and agricultural.

A.5-2 Takeoff specifications[a]

Item	MIL-C5011A (Military)	FAR Part 23 (Civil)	FAR Part 25 (Commercial)
Velocity	$V_{TO} \geq 1.1\ V_s$ $V_{CL} \geq 1.2\ V_s$	$V_{TO} \geq 1.1\ V_s$ $V_{CL} \geq 1.2\ V_s$	$V_{TO} \geq 1.1\ V_s$ $V_{CL} \geq 1.2\ V_s$
Climb	Gear up: 500 fpm @ S.L. (AEO) 100 fpm @ S.L. (OEI)	Gear up: 300 fpm @ S.L. (AEO)	Gear down: ½% @ V_{TO} Gear up: 3% @ V_{CL} (OEI)
Field-length definition	Takeoff distance over 50-ft obstacle	Takeoff distance over 50-ft obstacle	115% of takeoff distance with AEO over 35 ft or balanced field length
Rolling coefficient	$\mu = 0.025$	Not defined	Not defined

AEO = all engines operating; OEI = one engine inoperative.
[a](After L. Nicolai, Ref. 10)

A.5-3 Landing specifications[a]

Item	MIL-C5011A	FAR Part 23	FAR Part 25
Velocity	$V_A \geq 1.2\ V_s$ $V_{TD} \geq 1.1\ V_s$	$V_A \geq 1.3\ V_s$ $V_{TD} \geq 1.15\ V_s$	$V_A \geq 1.3\ V_s$ $V_{TD} \geq 1.15\ V_s$
Field-length definition	Landing distance over 50-ft obstacle	Landing distance over 50-ft obstacle	Landing distance over 50 ft obstacle divided by 0.6
Braking coefficient	$\mu = 0.30$	Not defined	Not defined

[a](After L. Nicolai, Ref. 10)

A.5-4 FAR climb requirements for multiengine aircraft

Adapted from Refs. 23 and 49 and FAR parts 23 and 25.
V_{s_0} = stall speed in landing configuration for reciprocating-engine-powered airplanes.
V_{s_1} = stall speed in a specified configuration for reciprocating-engine-powered airplanes.
V_2 = climbout speed over 35-ft obstacle. LOF: liftoff.

Turbine-Engine Aircraft: FAR 25

All segments with one engine stopped, except go-around in landing configuration, which has all engines operating. Engine power or thrust set at "maximum rated", except being "maximum continuous" for third-segment climb. Maximum thrust attained after 8 s from flight idle for go-around. AEO: all engines operating.

Operation	Speed	Flaps	Landing gear	Minimum climb gradient for aircraft with n engines, %		
				$n = 2$	$n = 3$	$n = 4$
Takeoff Climb						
First-segment	LOF	Takeoff	Down	≥ 0	0.3	0.5
Second-segment	V_2[a]	Takeoff	Up	2.4	2.7	3.0
Third-segment	$\geq 1.25 V_s$[b]	Up	Up	1.2	1.4	1.5
Landing						
Go-around in approach configuration	$\leq 1.5 V_s$[b]	Approach	Up	2.1	2.4	2.7
Go-around in landing configuration	$\leq 1.3 V_s$[b] AEO	Landing	Down	3.2	3.2	3.2

[a]Over 35-ft obstacle. [b]Stall speed in the pertinent condition.

Reciprocating-Engine Aircraft: FAR 25

Power or thrust for operating engines set for takeoff on first and second segments and go-around and for "maximum continuous" during cruise and third segment. One engine windmilling propeller for first and second segments. If plane has automatic feathering, the propeller on an inoperative engine assumed to be feathered. One engine stopped (may be feathered) for third segment and go-around.

Operation	Speed	Flap setting	Landing gear	Minimum steady-climb rate, ft/min
Takeoff climb				
First-segment	V_2[a]	Takeoff	Down	≥ 50
Second-segment	V_2[a]	Takeoff	Up	$\geq 0.046 V_{s_1}^2$[b]
Third-segment	Best	Up[c]	Up	$\geq \left(0.079 - \frac{0.106}{n}\right) V_{s_0}^2$[d]
Landing go-around (approach configuration)	$\leq 1.5 V_{s_1}$	Approach[e]	Up	$\geq 0.053 V_{s_0}^2$[f]

[a]Out of ground effect. [b]V_{s_1} in knots. [c]Or most favorable. [d]At 5000-ft altitude. [e]But $V_{s_1} \leq 1.1 V_{s_0}$. [f]V_{s_0} in knots.

A.5-4 (cont'd.) FAR climb requirements for multiengine aircraft

FAR 23 (Turbine or Reciprocating)

Multiengine power at maximum continuous except for $W < 6000$ lb.
AEO: All engines operating.

Aircraft status	Speed	Flaps	Landing gear	Minimum steady-climb rate, ft/min
One engine out (prop feathered)[a]	Most favorable	Most favorable	Up	$\geq 0.027 V_{s_0}^{2}$ [b]
AEO, $W > 6000$ lb	Most favorable	Takeoff	Up	$\geq$ 300-ft/min climb gradient ≥ 0.0833 land plane ≥ 0.0667 seaplane
$W < 6000$ lb	Most favorable	Takeoff	Down	$\geq$ 300 ft/min and $\geq 11.5 V_{s_1}$ [c]

[a]If $W < 6000$ lb and $V_{s_0} < 61$ knots, there is no engine-out climb requirement.
[b]V_{s_0} in knots at 5000 ft. [c]V_{s_1} in knots.

A.5-5 Special carrier suitability requirements (USN)

1) Minimum rate of climb (at design landing weight and approach speed) of 500 ft/min at intermediate thrust (non-AB) with one engine inoperative.
2) Minimum longitudinal acceleration at end of catapult stroke of 0.065 g (at maximum catapult weight; all engines operating).
3) Aircraft to fit on 70- by 52-ft aircraft elevator.
4) Landing-gear width not to exceed 22 ft.
5) Folded height of the aircraft not to exceed 18 ft 6 in. Height while folding not to exceed 24 ft 6 in. (18 ft 6 in. desirable).
6) Aircraft maximum weight (loaded and fueled) not to exceed 80,000 lb (elevator limit).
7) Wingspan not to exceed 82 ft (64 ft desired).
8) Design landing weight to include high-value stores, empty external fuel-tanks, and associated suspension equipment (pylons, ejectors, etc.)

REFERENCES

[1]Taylor, J., *Jane's All the World Aircraft,* Jane's, London, England, UK, 1976.
[2]Abbott, I. and von Doenhoff, A., *Theory of Wing Sections,* McGraw-Hill, New York, 1949.
[3]Purser, P. and Campbell, J., "Experimental Verification of a Simplified Vee-Tail Theory and Analysis of Available Data on Complete Models with Vee Tails," NACA 823, 1945.
[4]Perkins, C. and Hage, R., "Airplane Performance, Stability, and Control," Wiley, New York, 1949.
[5]Loffin, L., "Subsonic Aircraft: Evolution and the Matching of Size to Performance," NASA Ref. 1060, 1980.
[6]Sheridan, H., "Aircraft Preliminary Design Methods Used in the Weapons System Analysis Division," Navy Department Weapons Systems Analysis Div., Rept. R-5-62-13, 1962.
[7]Roskam, J., *Methods for Estimating Drag Polars of Subsonic Airplanes,* Published by Author, 1971.
[8]Hoerner, S., *Fluid Dynamic Drag,* Published by Author, 1958.
[9]Wallner, L., "Generalization of Turbojet and Turbine-Propeller Engine Performance in Windmilling Condition," NACA RM-2267, 1951.
[10]Nicolai, L., *Fundamentals of Aircraft Design,* Univ. of Dayton, Dayton, OH, 1975.
[11]Roskam, J., *Airplane Design,* Roskam Aviation and Engineering Corp., Ottawa, KS, 1985.
[12]Diehl, W., *Engineering Aerodynamics,* Ronald, New York, 1928.
[13]Raymer, D., "Supercruise for a STOL Dogfighter," *Aerospace America,* Aug. 1985, pp. 72–75.
[14]Raymer, D., "CDS Grows New Muscles," *Astronautics & Aeronautics,* June 1982, pp. 22–31.
[15]Liming, R., *Practical Analytic Geometry with Applications to Aircraft,* Macmillan, New York, 1944.
[16]Sears, W., "On Projectiles of Minimum Wave Drag," *Quarterly of Applied Mathematics,* Vol. IV, No. 4, Jan. 1947.
[17]Whitcomb, R., "A Study of the Zero-Lift Drag Rise Characteristics of Wing-Body Combinations Near the Speed of Sound," NACA RM-L-52H08, 1952.
[18]Ball, R., *Fundamentals of Aircraft Combat Survivability Analysis and Design,* AIAA Education Series, New York, 1985.
[19]Stadmore, H., "Radar Cross Section Fundamentals for the Aircraft Designer," AIAA Paper 79-1818, AIAA Aircraft Systems and Technology Meeting, New York, Aug. 1979.
[20]Fuhs, A. E., *Radar Cross Section Lectures,* AIAA, New York, 1984.
[21]Ruck, G., et al., "Radar Cross Section Handbook, Vols. I and II, Plenum, New York, 1970.
[22]Anonymous, "Anthropometry of Flying Personnel," Wright Air Development Center, TR 52-321, 1954.

[23]Torenbeek, E., *Synthesis of Subsonic Airplane Design,* Delft Univ. Press, Delft, The Netherlands, 1982.
[24]Smyth, S. and Raymer, G., "Aircraft Conceptual Design," Course Notes, Lockheed Corp., 1980.
[25]Seddon, J. and Goldsmith, E. L., *Intake Aerodynamics,* AIAA Education Series, New York, 1985.
[26]Crosthwait, E., Kennon, I., and Roland, H., "Preliminary Design Methodology for Air Induction Systems," U.S. Air Force SEG-TR-67-1, Wright-Patterson AFB, OH, 1967.
[27]Ball, W., "Propulsion System Installation Corrections," AFFDL TR-72-147, Air Force Flight Dynamics Lab., Wright-Patterson AFB, OH, 1972.
[28]Stinton, D., *The Design of the Aeroplane,* Granada, London, England, UK, 1983.
[29]Bingelis, T., *Firewall Forward,* Published by Author, Austin, TX, 1983.
[30]Anonymous, *Aircraft Tire Data,* Goodyear Corp.
[31]Anonymous, NASA Rept. TR-R-64.
[32]Currey, N., *Aircraft Landing Gear Design: Principles and Practices,* AIAA Education Series, Washington, DC, 1988.
[33]Conway, H., *Landing Gear Design,* Chapman & Hall, London, England, UK, 1958.
[34]Tomkins, F., "Installation *Handbook-Airborne Gas Turbine* Auxiliary Power Units," Garrett Corp., 1983.
[35]Covert, E. E., James, C. R., Kimzey, W. F., Richey, G. K., and Rooney, E. C., (eds.), *Progress in Astronautics and Aeronautics: Thrust and Drag: Its Prediction and Verification,* Vol. 98, AIAA, New York, 1985.
[36]Lowry, J. and Polhamus, E., "A Method for Predicting Lift Increments Due to Flap Deflection at Low Angles of Attack in Incompressible Flow," NASA TN-3911, 1957.
[37]Hoak, D., Ellison, D., et al., "USAF DATCOM," Air Force Flight Dynamics Lab., Wright-Patterson AFB, OH.
[38]Proceedings of "Evolution of Aircraft Wing Design Symposium," AIAA, Dayton, OH, 1980.
[39]Dillner, B., May, F., and McMasters, J., "Aerodynamic Issues in the Design of High-Lift Systems for Transport Aircraft," *AGARD Fluid Dynamics Panel Symposium,* Brussels, Belgium, May 1984.
[40]Bonner, E., Clever, W., and Dunn, K., "Aerodynamic Preliminary Analysis System II—Part I—Theory," NASA Contractor Rept. 165627, 1981.
[41]Jones, R. T., "Theory of Wing-Body Drag at Supersonic Speeds," NACA Rept. 1284, 1956.
[42]Harris, R., "An Analysis and Correlation of Aircraft Wave Drag," NASA TM-X-947, 1964.
[43]Jumper, E., "Wave Drag Prediction Using a Simplified Supersonic Area Rule," *Journal of Aircraft,* Vol. 20, Oct. 1983, pp. 893–895.
[44]O'Conner, W., "Lift and Drag Prediction in Computer-Aided Design," U.S. Air Force ASD/XR-73-8, 1973.
[45]Cavallo, B., "Subsonic Drag Estimation Methods," U.S. Naval Air Development Center Rept. NADC-AW-6604, 1966.
[46]Mattingly, J. D., Heiser, W., and Daley, D. H., *Aircraft Engine Design,* AIAA Education Series, New York, 1987.
[47]Cawthon, J., Truax, P., and Steenkin, W., "Supersonic Inlet Design and Airframe—Inlet Integration Program (Project Tailor-Mate)," AFFDL TR-71-124, Air Force Flight Dynamics Lab., Wright-Patterson AFB, OH, 1973.
[48]Fraas, A., *Aircraft Power Plants,* McGraw-Hill, New York, 1943.

[49]Lan, C. and Roskam, J., *Airplane Aerodynamics and Performance,* Roskam Aviation and Engineering Corp., Ottawa, KS, 1980.
[50]Anonymous, "Generalized Method of Propeller Performance Estimation," Hamilton Standard Rept. PDB 6101A, United Aircraft Corp., 1963.
[51]Cardinale, S., "Basic Loads—General Information for Designers," Lockheed Corp., 1982.
[52]Corning, G., "Supersonic and Subsonic, CTOL and VTOL, Airplane Design," Published by Author, 1976.
[53]Schrenk, O., "A Simple Approximation Method for Obtaining the Spanwise Lift Distribution," NACA TM-948, 1940.
[54]Peery, D., *Aircraft Structures,* McGraw-Hill, New York, 1950.
[55]Timoshenko, S., *Strength of Materials,* Van Nostand, New York, 1930.
[56]Neubert, H. and Kiger, R., "Modern Composite Aircraft Technology," *Sport Aviation,* Experimental Aircraft Association, July 1976.
[57]Crossley, F. A., "Aircraft Applications of Titanium: A Review of the Past and Potential for the Future," *Journal of Aircraft,* Vol. 18, Dec. 1981, pp. 993–1002.
[58]Tsai, S., *Composites Design—1985,* Think Composites, Dayton, OH, 1985.
[59]Hoskin, B. and Baker, A., (eds.), *Composite Materials for Aircraft Structures,* AIAA Education Series, New York, 1986.
[60]Bruhn, E., *Analysis and Design of Flight Vehicle Structures,* Tri-State Offsett, 1973.
[61]Anonymous, "Military Standardization Handbook—Metallic Materials and Elements for Aerospace Vehicle Structures," Mil-Hdbk-5B, Sept. 1971.
[62]Staton, R., "Statistical Weight Estimation Methods for Fighter/Attack Aircraft," Vought Aircraft Rept. 2-59320/8R-50475, 1968.
[63]Staton, R., "Cargo/Transport Statistical Weight Estimation Equations," Vought Aircraft Rept. 2-59320/9R-50549, 1969.
[64]Jackson, A., "Preliminary Design Weight Estimation Program," AeroCommander Div., Rept. 511-009, 1971.
[65]Toll, T., et al., "Summary of Lateral-Control Research," NACA 868.
[66]Phillips, W., "Appreciation and Prediction of Flying Qualities," NACA 927, 1949.
[67]Roskam, J., "Airplane Flight Dynamics—Part I," Roskam Aviation and Engineering Corp., Ottawa, KS, 1979.
[68]Seckel, E., "Stability and Control of Airplanes and Helicopters," Academic, New York, 1964.
[69]Lockenour, J., "Flying Qualities Considerations in Initial Design," Air Force Flight Dynamics Lab., Wright-Patterson AFB, OH, AFFDL/FGC-TM-74-222, 1978.
[70]Hoerner, S. and Borst, H., *Fluid Dynamic Lift,* Hoerner Fluid Dynamics, Bricktown, NJ, 1975.
[71]Tallman, F., *Flying the Old Planes,* Doubleday, Garden City, New York, 1973.
[72]Harper, R. P., Jr. and Cooper, G. E., "Handling Qualities and Pilot Evaluation," *Journal of Guidance, Control, and Dynamics,* Vol. 9, Sept./Oct. 1986, pp. 515–529.
[73]Rhodeside, G., "Investigation of Aircraft Departure Susceptibility Using a Total-G Simulator," AIAA Paper 86-0492, AIAA 24th Aerospace Sciences Meeting, Reno, NV, 1986.
[74]NACA Rept. TN-1045.
[75]Herbst, W. B. and Krogull, B., "Design for Air Combat," AIAA Paper 72-749, AIAA 4th Aircraft Design, Flight Test, and Operations Meeting, Los Angeles, CA, Aug. 1972.
[76]Skow, A., "Advanced Fighter Agility Metrics," TR 84-05, Eidetics International, Torrance, CA, 1984.

[77]Marx, H., "Comparative Costs of Military Aircraft—Fiction vs Fact," AIAA Paper 83-2565, AIAA Aircraft Design, Systems, and Technology Meeting, Fort Worth, TX, 1983.
[78]Hess, R. W. and Romanoff, H. P., "Aircraft Airframe Cost Estimating Relationships," Rand Corp., Rept. R-3255-AF, Santa Monica, CA, 1987.
[79]Birkler, J. L., Garfinkle, J. B., and Marks, K. E., "Development and Production Cost Estimating Relationships for Aircraft Turbine Engines," Rand Corp., Rept. N-1882-AF, Santa Monica, CA, 1982.
[80]Bengelink, R. L., "The Integration of CFD and Experiment: An Industry Viewpoint," AIAA Paper 88-2043, AIAA 15th Aerodynamic Testing Conf., San Diego, CA, 1988.
[81]Raj, P., Keen, J., and Singer, S., "Application of an Euler Aerodynamic Method to Free-Vortex Flow Simulation," AIAA Paper 88-2517, AIAA 6th Applied Aerodynamics Conf., Williamsburg, VA, 1988.
[82]Miranda, L. R., "Transonics and Fighter Aircraft: Challenges and Opportunities for CFD," NASA Transonic Symposium, NASA Langley Research Center, Hampton, VA, 1988.
[83]Niu, M., *Airframe Structural Design,* Conmilit, Hong Kong, 1988. (Distributed by Technical Book Company, Los Angeles, CA).
[84]Hughes, T., *The Finite Element Method,* Prentice-Hall, Englewood Cliffs, New York, 1987.
[85]Desai, C. and Abel, J., *Introduction to the Finite Element Method,* Von Nostrand Reinhold, New York, 1971.
[86]Prziemienecki, J., "Finite Element Analysis," (unpublished Notes), 1988.
[87]Kalemaris, S., "Weight Impact of VTOL," SAWE Paper 1326, SAWE, New York, 1979.
[88]Kohlman, D., "Introduction to V/STOL Aircraft," Iowa State Univ. Press, Ames, Iowa, 1981.
[89]Proceedings of "Special Course on V/STOL Aerodynamics," AGARD-R-710, Advisory Group for Aerospace Research and Development, 1984.
[90]Raymer, D. P., "The Impact of VTOL on the Conceptual Design Process," AIAA Paper 88-4479, AIAA/AHS/ASEE Aircraft Design, Systems, and Operations Meeting, Atlanta, GA, Sept. 1988.
[91]Hoblit, F. M., *Gust Loads on Aircraft: Concepts and Applications*, AIAA Education Series, Washington, DC, 1988.
[92]DeMeis, R., "F-117A: First in Stealth," *Aerospace America*, Feb. 1991, pp. 32–42.
[93]Raymer, D. et al., "Supersonic STOVL; The Future is Now," *Aerospace America*, Aug. 1990, pp. 18–22.
[94]Raymer, D., "Post-Stall Maneuver and the Classic Turn Rate Plot," AIAA Paper 91-3170, Sept. 1991.

INDEX